STUDIES OF THE PROPERTIES OF PARTICULATE MATTER IN THE UK ATMOSPHERE

by

BUNTHOON LAONGSRI

A thesis submitted to the
University of Birmingham for the degree of
DOCTOR OF PHILOSOPHY

Division of Environmental Health and Risk Management
School of Geography, Earth and Environmental Sciences
College of Life and Environmental Sciences
The University of Birmingham

May 2012

ABSTRACT

Studies of the physical and chemical properties of airborne particulate matter were carried out in the UK atmosphere. Aerosol samples were collected at the Elms Road observatory site (500 daily samples) and Harwell (100 daily samples) site representing urban background and rural area, respectively. The chemical components of both $PM_{2.5}$ and $PM_{2.5-10}$ were mainly analysed for carbonaceous compounds, sulphate, nitrate, chloride and oxalate. Size distributions of aerosol components were also investigated by size-segregated air samplers in conjunction with the study of ammonia gas to stabilise semi-volatile species such as NH_4NO_3 and NH_4Cl in atmospheric particles. Concentrations and composition of carbonaceous compounds (organic (OC) and elemental (EC) carbon) in particulate matter clearly showed higher value in the urban background than those in the rural area. An OC/EC minimum ratio of 0.35 was used to distinguish between primary and secondary OC, as EC was a good indicator of primary sources. Sulphate and nitrate showed a close relationship, indicating that these two species undergo similar formation and removal processes in the atmosphere. Chloride in coarse particles is mainly originated from marine aerosol with a weak correlation observed with other major species. Additionally, chloride was also observed significantly in the fine fraction, suggesting the importance of anthropogenic sources, as indicated also by air mass trajectory analysis.

Oxalate is reported as one of the major components of organic aerosol and average concentrations sampled over different intervals in PM_{10} were 0.04 ± 0.03 µg m^{-3} at the rural site and 0.06 ± 0.05 at the urban background site. Similarity between oxalate concentrations during a period of simultaneous sampling at the urban and rural sites was observed. A good correlation and similar pattern of size distribution between oxalate and sulphate was found, suggesting formation from the same atmospheric processes such as in-cloud formation or cloud processing of oxalate and sulphate formed in homogeneous reaction processes. Clustering of air mass trajectories showed important sources of oxalate in continental areas associated with the high levels of other atmospheric pollutants. Excess ammonia gas supplied during a size-segregated air sampling experiment revealed higher concentrations of nitrate and chloride particles, indicating that ammonia could stabilise semi-volatile aerosol species such as nitrate and chloride which are expected in form of ammonium salts.

ACKNOWLEDGEMENTS

First, I am sincerely grateful to my supervisor, Professor Roy M. Harrison for his invaluable advice, encouragement and support during my time for PhD study. Under his guidance, I learned a lot about measurement and characteristic of airborne particulate matter since I started this research course. I wish to acknowledge the Royal Thai Government for providing the full scholarship for this PhD course through the National Institute of Metrology (Thailand), Ministry of Science and Technology.

My special thanks go to Dr. Gillian Kingston, for helping me to set up air sampling experiment and training to operate air samplers, ion chromatograph, carbon analyser including assistance during laboratory work, Dr. Jianxin Yin, for her suggestions and providing some information of analytical technique, Dr. Johanna Gietl, for her help to exchange filters when air sampling was conducted at Harwell site.

Last but not least, I would like to thank my wife, Sukanya and daughter, Nicharee for their company and moral support.

TABLE OF CONTENTS

Chapter		Page
LIST OF TABLES		
LIST OF FIGURES		
ABBREVIATIONS		
1	**Introduction**	**1**
	1.1 Background	1
	1.2 Physical properties of airborne particulate matter	5
	1.3 Chemical properties of airborne particulate matter	7
	1.4 Oxalate in ambient air	14
	1.4.1 Occurrence of oxalic acid and/or oxalate	15
	1.4.2 Source of oxalic acid and/or oxalate	16
	1.4.2.1 Biogenic sources	16
	1.4.2.2 Anthropogenic sources	16
	1.4.2.3 Photochemical oxidation	17
	1.4.3 Concentration of atmospheric oxalate	18
	1.4.4 The studies of the sources and production of atmospheric oxalate	21
	1.4.4.1 Sampling and extraction methods	21
	1.4.4.2 Analytical methods	22
	1.4.4.3 Seasonal variation of oxalate	22
	1.4.4.4 Spatial variation of oxalate	23
	1.4.4.5 Size distributions of oxalate	25
	1.4.4.6 Correlation studies of oxalate to identify primary and secondary sources	27
	1.4.4.7 Conclusions of oxalate in ambient air from literature data	31
	1.5 Objectives of this study	32
2	**Aerosol sampling devices and analytical methodology**	**33**
	2.1 Synopsis	33

Chapter **Page**

2.2 Aerosol sampling devices 33

2.2.1 Partisol plus air samplers 33

2.2.2 Micro-orifice uniform-deposit impactors (MOUDI) 35

2.3 Aerosol sampling 37

2.4 Extraction from filters 38

2.5 Chemical analysis 38

2.5.1 Determination of organic carbon, elemental carbon and total carbon with carbon aerosol analyser 38

2.5.2 Determination of water-soluble organic carbon with carbon aerosol analyser 43

2.5.3 Determination of anion components with ion chromatography 44

2.5.4 Determination of cation components with ion chromatography 47

2.5.5 Determination of mass of particulate matter with gravimetry 48

2.6 Data and statistical analysis 49

3 Interpretation of carbonaceous aerosol concentrations in particulate matter 53

3.1 Synopsis 53

3.2 Sampling locations 53

3.3 Summary of atmospheric aerosol concentrations 55

3.3.1 Carbonaceous aerosol concentrations in urban background and rural sites 59

3.3.2 Relationships between organic and elemental carbon 65

3.3.3 Interpretation of carbonaceous aerosol between sites 78

3.4 Conclusions 87

4 Interpretation of ion component composition of particulate matter 89

4.1 Synopsis 89

4.2 Particulate matter chemical components 89

4.3 Atmospheric aerosol concentrations in urban background and rural sites 95

4.3.1 Relationships between major component composition in PM 98

Chapter **Page**

4.3.2 Relationships between oxalate and major component composition in PM 102

4.3.3 The ratios calculated between major component composition in PM 111

4.4 Interpretation of ion species in PM between sites 113

4.4.1 Seasonal behaviour of ion species 121

4.4.2 Implication of relationships between oxalate and major component composition between sites 124

4.5 Conclusions 130

5 A trajectory analysis of long-range transport of major aerosol species at EROS and Harwell sites 132

5.1 Synopsis 132

5.2 Overview of air mass back trajectories 132

5.2.1 Meteorological data 134

5.3 Calculation of trajectories and cluster analysis 134

5.4 Atmospheric boundary layer 136

5.5 Results and discussion 138

5.5.1 Whole data set at EROS 138

5.5.2 Seasonal variation 148

5.5.3 Cluster analysis for simultaneous data between EROS and Harwell 152

5.6 Conclusions 168

6 Interpretation of size distributions of major components in airborne particulate matter 170

6.1 Synopsis 170

6.2 Size distributions of ionic species in atmospheric aerosols 171

6.3 Measurement of aerosol size distributions at EROS 173

6.3.1 Contribution of aerosol particles by ammonia experiment 181

6.4 Size distributions of inorganic ions 187

6.5 Size distribution of oxalate 206

6.6 Conclusions 212

Chapter **Page**

7 Conclusions and recommendations for further work 214

7.1 Conclusions 214

7.2 Recommendations for further work 221

REFERENCES 223

APPENDIX A Estimation of measurement uncertainty 240

APPENDIX B Calculation of concentration of ammonia gas supply 248

APPENDIX C Air mass back trajectories 250

APPENDIX D Box-whisker plots of major components in $PM_{2.5}$ by clusters in each season at EROS 271

APPENDIX E The Kolmogrov-Smirnov test 275

LIST OF TABLES

Table	Title	Page
	CHAPTER 1	
Table 1.1	Limit values of PM for the protection of human health	2
Table 1.2	Characteristics of airborne particulate matter; fine (ultrafine plus accumulation- mode) and coarse mode particles	7
Table 1.3	Chemical composition (%) of airborne particulate matter around the world	10
Table 1.4	Relative contributions (%) of chemical composition to PM mass by site types in Europe	11
Table 1.5	Chemical properties of oxalic acid and experimental data	15
Table 1.6	Literature data of oxalic acid (oxalate) in the aerosol samples	19
	CHAPTER 2	
Table 2.1	The detection limits and precision study of OC/EC analysis	43
Table 2.2	The detection limits and recoveries study of ionic analysis by IC	47
	CHAPTER 3	
Table 3.1	Summary of chemical composition statistics ($\mu g\ m^{-3}$) in $PM_{2.5}$, $PM_{2.5-10}$ and PM_{10} at EROS and Harwell sites for the entire period	55
Table 3.2	Correlation coefficients (r) calculated between OC and EC concentration in $PM_{2.5}$, $PM_{2.5-10}$ and PM_{10} at EROS and Harwell sites	66
Table 3.3	Primary and secondary OC concentrations ($\mu g\ m^{-3}$) based on the common minimum OC/EC ratio in $PM_{2.5}$ and PM_{10} at EROS and HAR sites	71
Table 3.4	Primary and secondary OC concentrations ($\mu g\ m^{-3}$) based on the minimum OC/EC ratio in $PM_{2.5}$ and PM_{10}, $(OC/EC)_{min} = 0.35$	73
Table 3.5	Statistical data of EC, OC, OC_{prim} and OC_{sec} ($\mu g\ m^{-3}$) at EROS and Harwell sites during the simultaneous period, $(OC/EC)_{min} = 0.35$	80
Table 3.6	The local contributions of carbonaceous materials, sulphate and nitrate in $PM_{2.5}$, $PM_{2.5-10}$ and PM_{10}	80
Table 3.7	Results of regression analysis of EROS (urban background) and Harwell (rural) concentrations in $PM_{2.5}$	84
Table 3.8	Inter-site correlation coefficients (r) calculated between carbonaceous species concentrations in $PM_{2.5}$, $PM_{2.5-10}$ and PM_{10}	86

Table **Title** **Page**

CHAPTER 4

Table 4.1 Correlations (*r*) calculated between analysed species in $PM_{2.5}$, $PM_{2.5-10}$ and PM_{10} at EROS during the period from November 2008 to April 2011 99

Table 4.2 Mean SO_4^{2-}/NO_3^-, Cl^-/NO_3^-, $C_2O_4^{2-}/SO_4^{2-}$ and $C_2O_4^{2-}/NO_3^-$ ratios at the two sampling sites 112

Table 4.3 Statistical data of sulphate, nitrate, chloride, oxalate, secondary OC and WSOC ($\mu g\ m^{-3}$) concentrations including the ratio of $WSOC/OC_{sec}$ at EROS and Harwell sites measured simultaneously 116

Table 4.4 The local contributions of sulphate, nitrate, chloride, oxalate, OC_{sec} and WSOC in $PM_{2.5}$, $PM_{2.5-10}$ and PM_{10} calculated based on mean differences concentration between EROS and Harwell during the simultaneous period (EROS conc. – HAR conc.) 117

Table 4.5 Results of regression analysis of EROS (urban background) and Harwell (rural) concentrations of ion components in $PM_{2.5}$ 120

Table 4.6 Intra- and inter-site correlation coefficients of aerosol species in $PM_{2.5}$, $PM_{2.5-10}$ and PM_{10} calculated from samples measured simultaneously 126

CHAPTER 5

Table 5.1 Comparison between the boundary layer and the free troposphere Characteristics 137

Table 5.2 Average concentrations (± S.D.) of major chemical components in $PM_{2.5}$ by trajectory clusters at EROS for the entire dataset 142

Table 5.3 Average ratios of SO_4^{2-}/NO_3^-, Cl^-/NO_3^-, $C_2O_4^{2-}/SO_4^{2-}$, $C_2O_4^{2-}/NO_3^-$ and $C_2O_4^{2-}/OC_{sec}$ by trajectory clusters including meteorological data (± S.D.) at EROS for the entire dataset 142

Table 5.4 Average concentrations (± S.D.) of major chemical components in $PM_{2.5}$ by trajectory clusters in each season at EROS 151

Table 5.5 Average concentrations (± S.D.) of major chemical components in $PM_{2.5}$ by trajectory clusters arriving at EROS and Harwell during the period of simultaneous air sampling 156

CHAPTER 6

Table 6.1 Summary of air sampling conditions by MOUDI and chemical analysis of aerosol samples at EROS 175

Table 6.2 Four modes of size distribution in concentrations of anions, cations, TC and PM_{mass} of aerosol at EROS 179

Table 6.3 Mean fraction contributions of aerosol species in different size modes for the whole and simultaneous datasets 181

Table	Title	Page
Table 6.4	Contributions of major components in aerosol as the difference between air samples collected with and without ammonia atmosphere ($conc._{with} - conc._{without}$)	185

LIST OF FIGURES

Figure	Title	Page
CHAPTER 1		
Figure 1.1	Sources of particulate matter	4
Figure 1.2	Possible photochemical production of oxalic (C_2), malonic (C_3), succinic (C_4) and azelaic (C_4) acids in the atmosphere	18
CHAPTER 2		
Figure 2.1	The Partisol Plus Model 2025 Sequential air sampler and operating diagram	35
Figure 2.2	Air sampling by the MOUDI with ammonia experiment	37
Figure 2.3	Schematic diagram of the Thermal-Optical Carbon Aerosol Analyser (Sunset Laboratory analyser)	40
Figure 2.4	Thermogram obtained by thermal-optical transmission (TOT) analysis with EUSAAR_2 temperature programme for sucrose standard	41
Figure 2.5	Diagram of water extraction of aerosol samples collected onto QMA filters	44
Figure 2.6	Ion analysis process	45
CHAPTER 3		
Figure 3.1	Locations of the two sampling sites in the UK; EROS and Harwell	54
Figure 3.2	Time series of OC, EC concentrations in $PM_{2.5}$ measured at EROS and Harwell sites	60
Figure 3.3	Box-whisker plots of monthly major component concentration in $PM_{2.5}$ at EROS and Harwell sites	61
Figure 3.4	Comparison of monthly average chemical concentrations in PM_{10} at Harwell with network data	63
Figure 3.5	Seasonal average concentrations at EROS and Harwell site; (a) $PM_{2.5}$; (b) PM_{10}	64
Figure 3.6	Relationships of organic carbon to elemental carbon in $PM_{2.5}$ and PM_{10} at EROS and HAR sites	69
Figure 3.7	Secondary organic carbon in $PM_{2.5}$ at EROS estimated using the OC/EC ratio of 0.75, while the error bars represent a range of the OC/EC ration from 0.70 to 0.80	71
Figure 3.8	Plots of EC, OC_{prim}, OC_{sec}, sulphate and nitrate in $PM_{2.5}$ versus daily mean temperature (1/K) at EROS and HAR sites collected simultaneously	75

Figure **Title** **Page**

Figure 3.9 Monthly average of primary and secondary OC calculated based on OC/EC minimum ratio of 0.35 and secondary OC/OC ratio in $PM_{2.5}$ at EROS 78

Figure 3.10 Relationships between EROS and Harwell concentrations of EC, OC, primary and secondary OC calculated by the OC/EC minimum ratio of 0.35 82

Figure 3.11 Plot of OC difference ($\Delta OC = OC_{EROS} - OC_{HAR}$) versus EC difference ($\Delta EC = EC_{EROS} - EC_{HAR}$) data taken simultaneously between EROS and Harwell 84

Figure 3.12 Time series of OC_{prim}, OC_{sec} concentrations in $PM_{2.5}$ measured at EROS and Harwell sites during the simultaneous period 85

CHAPTER 4

Figure 4.1 Time series of (a) sulphate, (b) nitrate, (c) chloride and (d) oxalate concentrations in $PM_{2.5}$ measured at EROS and Harwell sites 96

Figure 4.2 Relationship between oxalate and sulphate concentrations in $PM_{2.5}$ measured at EROS 104

Figure 4.3 Relationship between oxalate and sulphate concentrations in $PM_{2.5}$ measured at Harwell 105

Figure 4.4 Relationship between oxalate and nitrate concentrations in $PM_{2.5}$ measured at EROS 106

Figure 4.5 Relationship between oxalate and nitrate concentrations in $PM_{2.5}$ measured at Harwell 107

Figure 4.6 Relationship between oxalate and secondary OC concentrations in $PM_{2.5}$ measured at EROS 109

Figure 4.7 Relationship between oxalate and secondary OC concentrations in $PM_{2.5}$ measured at Harwell 110

Figure 4.8 Plot of all data of WSOC versus organic carbon concentrations measured at EROS and Harwell 114

Figure 4.9 Relationships between WSOC and secondary organic carbon concentrations in $PM_{2.5}$ measured at EROS and Harwell 114

Figure 4.10 Relationships between EROS and Harwell concentrations of (a) sulphate, (b) nitrate, (c) chloride, (d) oxalate and (e) WSOC during the simultaneous period 118

Figure 4.11 Time series of (a) sulphate, (b) nitrate, (c) chloride, (d) oxalate and (e) WSOC concentrations in $PM_{2.5}$ measured simultaneously at EROS and Harwell sites. 121

Figure 4.12 Relationship between oxalate and WSOC concentrations in $PM_{2.5}$ measured simultaneously at EROS and Harwell 125

Figure 4.13 Relationship between oxalate and secondary OC concentrations in $PM_{2.5}$ measured simultaneously at EROS and Harwell 125

Figure **Title** **Page**

Figure 4.14 In-cloud isoprene chemistry for the formation of hygroscopic organic acids: glycolic acid, glyoxylic acid, pyruvic acid, and oxalic acid 128

Figure 4.15 Flow chart for the in-cloud formation of oxalic acid from acetylene and ethene as precursors 129

CHAPTER 5

Figure 5.1 The percent change in total spatial variance with cluster number for the clustering of trajectories arriving at EROS from November 2008 to April 2011 139

Figure 5.2 Average 3-day back trajectory for the main trajectory clusters arriving at EROS from November 2008 to April 2011 140

Figure 5.3 Seasonal number of trajectories analysed for each cluster at EROS 140

Figure 5.4 Box-whisker plots of major components in $PM_{2.5}$ at EROS by clusters for the whole dataset; (a) sulphate, (b) nitrate, (c) chloride, (d) oxalate, (e) OC, (f) EC, (g) OC_{prim} and (h) OC_{sec} 144

Figure 5.5 Average 3-day back trajectories for the main trajectory clusters in each season arriving at EROS 149

Figure 5.6 The percent changes in total spatial variance with cluster number for the clustering of trajectories arriving at EROS and Harwell during the period of simultaneous air sampling (12 July 2010 to December 2010) 153

Figure 5.7 Average 3-day back trajectories for the main trajectory clusters arriving at EROS and Harwell during the period of simultaneous air sampling (12 July 2010 to December 2010) 154

Figure 5.8 Box-whisker plots of major components in $PM_{2.5}$ at EROS by clusters during the simultaneous air sampling with Harwell; (a) sulphate, (b) nitrate, (c) chloride, (d) oxalate, (e) OC, (f) EC, (g) OC_{prim}, (h) OC_{sec}, (i) WSOC and (j) $WSOC/OC_{sec}$ 158

Figure 5.9 Box-whisker plots of major components in $PM_{2.5}$ at Harwell by clusters during the simultaneous air sampling with EROS; (a) sulphate, (b) nitrate, (c) chloride, (d) oxalate, (e) OC, (f) EC, (g) OC_{prim}, (h) OC_{sec}, (i) WSOC and (j) $WSOC/OC_{sec}$ 163

CHAPTER 6

Figure 6.1 Mass size distribution of airborne particulate matter in urban atmosphere 172

Figure 6.2 Major component composition by modes during the periods of samples collected simultaneously with (P1, P2 and P6) and without (P9, P10 and P14) NH_3 gas supply 186

Figure 6.3 Size distributions of chemical species in aerosol samples collected with MOUDI operated under normal conditions for all periods 195

Figure **Title** **Page**

Figure 6.4(a) Comparisons of mean size distributions of sulphate during the air sampling with and without NH_3 supply for (a) the whole period and (b) the simultaneous period (with NH_3 – mean of P1, P2 and P6; without NH_3 – mean of P9, P10 and P14) 198

Figure 6.4 (b) Comparisons of mean size distributions of nitrate during the air sampling with and without NH_3 supply for (a) the whole period and (b) the simultaneous period (with NH_3 – mean of P1, P2 and P6; without NH_3 – mean of P9, P10 and P14) 199

Figure 6.4(c) Comparisons of mean size distributions of chloride during the air sampling with and without NH_3 supply for (a) the whole period and (b) the simultaneous period (with NH_3 – mean of P1, P2 and P6; without NH_3 – mean of P9, P10 and P14) 200

Figure 6.4(d) Comparisons of mean size distributions of sodium during the air sampling with and without NH_3 supply for (a) the whole period and (b) the simultaneous period (with NH_3 – mean of P1, P2 and P6; without NH_3 – mean of P9, P10 and P14) 201

Figure 6.4(e) Mean size distributions of sodium and potassium during the air sampling without NH_3 supply for the whole period 202

Figure 6.5 Mean size distributions of (a) sulphate, (b) nitrate, (c) chloride and (d) oxalate measure at Marylebone road (MR) and Regents College (RC) sites during March 2007 203

Figure 6.6 Correlation coefficient matrix among the measured ionic components by modes of size distribution 205

Figure 6.7 Size distributions of oxalate in aerosol samples collected with MOUDI operated under normal conditions for all period 208

Figure 6.8 Size distributions of sulphate and oxalate in aerosol samples collected during the simultaneous period 208

Figure 6.9 Comparison of mean size distributions of oxalate during the air sampling with and without NH_3 supply for (a) the whole period and (b) the simultaneous period (with NH_3 – mean of P1, P2 and P6; without NH_3 – mean of P9, P10 and P14) 209

ABBREVIATIONS

ACA	Aerosol carbon analyser
AQEG	Air Quality Expert Group
ARL	Air Resources Laboratory
CA	Carboxylic acid
CCN	Cloud condensation nuclei
COMEAP	Committee on Medical Effects of Air Pollution
CSV	Cluster spatial variance
DCA	Dicarboxylic acid
DDW	Distilled deionised water
DMS	Dimethyl sulphide
D_p	Aerodynamic diameter
EC	Elemental carbon
EN	European Standard
EPA	Environmental Protection Agency
EROS	Elms road observatory site
EU	European Union
EUSAAR	European Super-sites for Atmospheric Aerosol Research project
FID	Flame ionisation detector
GC	Gas chromatography
GDAS	Global data assimilation system
GMT	Greenwich Mean Time
HAR	Harwell
HDPE	High-density polyethylene
HYSPLIT	HYbrid Single-Particle Lagrangian Integrated Trajectory
IC	Ion chromatography
LRT	Long-range transport
MCA	Monocarboxylic acid
MMAD	Mass median aerodynamic diameter
MOUDI	Micro-Orifice Uniform-Deposit Impactor
MR	Marylebone road
MSA	Methanesulfonic acid
NCEP	National Centers for Environmental Prediction

NO	Nitric oxide
NOAA	National Oceanic and Atmospheric Administration
OC	Organic carbon
OM	Organic matter
PAH	Polycyclic Aromatic Hydrocarbon
PM	Particulate matter
PM_{10}	Particulate matter with aerodynamic diameter less than or equal to 10 μm
PM_{15}	Particulate matter with aerodynamic diameter less than or equal to 15 μm
$PM_{2.5}$	Particulate matter with aerodynamic diameter less than or equal to 2.5 μm
$PM_{2.5-10}$	Particulate matter with aerodynamic diameter between 2.5 μm and 10 μm
PMF	Positive matrix factorization
POA	Primary organic aerosol
PTFE	Polytetrafluoroethylene
QA	Quality assurance
QC	Quality control
QUARG	Quality of Urban Air Review Group
RC	Regent college
RH	Relative humidity
RMA	Reduced major axis
RSD	Relative standard deviation
RSP	Respirable suspended particulate
SOA	Secondary organic aerosol
SV	Spatial variance
TC	Total carbon
TOC	Total organic carbon
TOT	Thermal optical transmission
TSV	Total spatial variance
UK	United Kingdom
US	United States
VOC	Volatile organic compound
WISOC	Water-insoluble organic carbon
WSOC	Water-soluble organic carbon

CHAPTER 1
INTRODUCTION

1.1 Background

An aerosol consists of tiny liquid or solid particles which are suspended in a gaseous medium long enough to enable observation and measurement. The aerosol particle samples are generally called particulate matter (PM). PM covers a very wide size range from a few nanometres (nm) to tens of micrometres (μm). With reference to the Air Quality Standards Regulations 2010 for the United Kingdom, PM_{10} defines as particulate matter which passes through a size-selective inlet as defined in the reference method for the sampling and measurement of PM_{10}, EN 12341, with a 50% efficiency cut-off at 10 μm aerodynamic diameter, whilst $PM_{2.5}$ means particulate matter which passes through a size-selective inlet as defined in the reference method for the sampling and measurement of $PM_{2.5}$, EN 14907, with a 50% efficiency cut-off at 2.5 μm aerodynamic diameter. The concentrations of particulate matter in ambient air are measured and recorded in term of the mass of particulate matter in one cubic metre of air, mostly using the units of microgram per cubic metre, $\mu g\ m^{-3}$. Atmospheric aerosols are of interest mainly because of their effects on health and climate. PM affects the climate by absorbing and scattering solar radiation, and by altering the properties and lifetime of clouds (Solomon et al., 2007). Scattering and absorbing the solar radiation is known as the "direct" effect of aerosols on the global climate, which can lead either cooling or warming of the atmosphere depending on the proportion of light scattered to that absorbed. Atmospheric particles also have an "indirect" effect on climate by altering the properties of clouds, resulting in a change of their scattering properties and longevity.

Concerning human health, many epidemiological studies have shown a link between increased mortality and/or morbidity with increased PM_{10} or $PM_{2.5}$ (Laden et al., 2006 and references therein). An increase of 1.3% in the total daily mortality with an increase of 10 $\mu g\ m^{-3}$ in 2-day mean $PM_{2.5}$ concentration has been reported. For PM_{10} or PM_{15}, the estimated association of 10 $\mu g\ m^{-3}$ increase in 2-day mean particulate matter on total mortality was 0.4%. This value calculated based on the reconstruction of data reported in six U.S. cities and replication of the original analysis (Schwartz et al., 1996; Rebecca et al, 2000). UK estimates indicate that short-term exposure to the level of PM_{10} which they experienced in 2002 led to

6500 deaths and 6400 hospital admissions (AQEG, 2005). In addition, the report by the Committee on Medical Effects of Air Pollution (COMEAP) in 2001 showed that for each 1 μg m^{-3} decrease in $PM_{2.5}$ over the lifetime of the current population of England and Wales, between 0.2 and 0.5 million years of life will be gained. This is equivalent, on average, to 1.5 – 3.5 days or much more for every individual. The UK Air Quality Standards Regulations have released the standards of PM_{10} and $PM_{2.5}$ in ambient air as shown in Table 1.1 in order to set the limit values for the protection of human health (Statutory Instruments, 2010). In addition, Table 1.1 also shows the EU directive 2008/50/EC on ambient air quality and cleaner air concerning PM_{10} limit values for the protection of human health (Official Journal, 2008).

All effects are influenced by the chemical and physical properties of airborne particulate matter, which make these properties very important to be analysed and monitored. In addition, the study of the properties of particulate matter including their chemical composition and size distributions will provide invaluable data in order to understanding about the sources and formation mechanisms of the atmospheric aerosols.

Table 1.1 Limit values of PM for the protection of human health

The UK Air Quality Standards Regulations 2010 which come into force on 11th June 2010			
PM_{10}			
Average period		*Limit value*	
One day		50 μg m^{-3}, not to be exceeded more than 35 times a calendar year	
Calendar year		40 μg m^{-3}	
$PM_{2.5}$			
Average period	*Limit value*	*Margin of tolerance*	*Date by which limit value is to be met*
Calendar year	25 μg m^{-3}	20% on 11th June 2008, decreasing on the next 1st January and every 12 months thereafter by equal annual percentages to reach 0% by 1st January 2015	1st January 2015
The EU directive 2008/50/EC			
PM_{10}			
Average period		*Limit value*	*Margin of tolerance*
One day		50 μg m^{-3}, not to be exceeded more than 35 times a calendar year	50%
Calendar year		40 μg m^{-3}	20%

Particulate matter in ambient air

Particles or particulate matter consist of both primary constituents, which are directly emitted from the source into the ambient air, and secondary constituents, which are produced in the atmosphere by chemical reactions. The relative importance of primary and secondary constituent depends mainly on geographical region, with its particular mix of emissions, and on atmospheric chemistry. For example, in the UK, Harrison et al. (2012) reported that $PM_{2.5}$:PM_{10} ratios declined from around 0.8 in southeast England to below 0.6 in Scotland consistent with a higher contribution of secondary particulate matter southeast England. Significant gradients of particulate matter were observed between rural, urban background and roadside sites, especially the high increment for heavily trafficked street canyon locations. In addition, their studies showed that concentrations of $PM_{2.5}$ were highest in the winter months and lowest in the summer consistent with better mixing and volatilization of semi-volatile compounds in the high temperature condition. Regionally, PM can be transported from areas of high emissions to relatively clean remote regions.

Primary particles

Primary particles are emitted cover a wide size ranges. The particles with aerodynamic diameter of less than 1 μm commonly found from combustion sources when fuels are burned. The particles with larger than 1 μm in aerodynamic diameter were from dust sources. Particles larger than 10 μm in aerodynamic diameter, which of less concern in atmospheric aerosols, usually deposit to the surface within a short period after being emitted and do not have a large effect on light scattering, unless strong winds and turbulence re-suspend the particles. There are significant sources of primary particles such as mobile source and stationary source. The major mobile source is road transport which produces both fine (from fuel burning) and coarse (from tyres and brake wear) primary particles. Stationary sources are the burning of fuels for industrial, commercial and domestic purposes. Primary particles also emitted from natural sources such as sea spray, biogenic sources (pollen fragments and particulate abrasion products from leaf surfaces).

Secondary particles

Secondary particulate matter is produced from chemical reactions of the gas precursors released into the atmosphere. The important primary emissions of precursors also include motor vehicles, residential wood combustion, meat cooking etc., which contain very complex mixtures of organic and inorganic substances to be released in the gas and particulate phases. The formation of secondary particles takes time according to their properties of precursors under the meteorology conditions. During the hours or even days over which this happens, the air containing the pollution can transport to other areas.

Figure 1.1 shows the sources of particulate matter with the contribution of primary and secondary particles. On the right side of the figure, there are urban background site located away from specific emission sources and roadside site located between busy road and the pavement. People live and work in both sites. On the left of the figure, the sources of secondary particulate matter are seen and the secondary particles take time before arriving the mainland area. The sources of primary particulate matter are demonstrated in the centre of the figure.

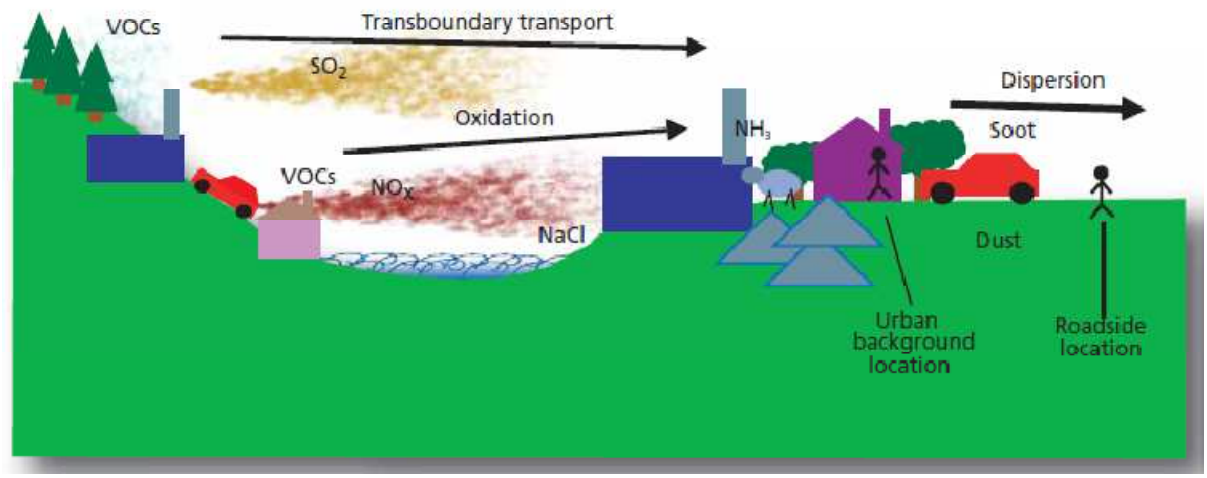

Figure 1.1 Sources of particulate matter (source: AQEG, 2005)

1.2 Physical properties of airborne particulate matter

There are various properties of airborne particulate matter which are important to their role in atmospheric process. These include their number concentration, their mass, size, chemical composition, and aerodynamic and optical properties (Finlayson-Pitts and Pitts, 1986). The most important physical property is size of particle. Particle size reflects the nature of source of the particles and relates to their health effects including to their aesthetic and climatic effects via their light scattering properties. Size of particulate matter covers a wide range between approximately 0.002 μm to 100 μm, however the most important particles with respect to atmospheric chemistry and physics are in the 0.001 – 10 μm. Size is often expressed in terms of effective diameter, which depends on a physical rather than a geometric property. The most commonly used effective diameter is the aerodynamic diameter, D_p, which is defined as the diameter of the unit density (ρ_p = 1 g cm^{-3}) sphere that has the same settling velocity as the particle being measured (Hinds, 1999).

With regard to the current atmospheric measurements, particulate matter can be classified as PM_{10} (50% cut-off aerodynamic diameter of 10 μm), $PM_{2.5}$ (fine particles, 50% cut-off aerodynamic diameter of 2.5 μm) and $PM_{2.5-10}$ (coarse particles with aerodynamic diameter between 2.5 μm – 10 μm) including $PM_{0.1}$ (ultrafine particles, 50% cut-off aerodynamic diameter of 0.1 μm). The latter is a recent focus because these small particles might penetrate the issue in the deep lung, leading to the respiratory health effects (Hughes et al., 1998; Pakkanen et al., 2001). Due to the mechanism of formation, Whitby (2007) produced a simplified size distribution model called the Whitby trimodal model. This model showed that transforming atmospheric aerosol number distributions to volumer distributions revealed three distinct size modes, which he labeled the nuclei, accumulation and coarse modes. Each of particle modes consisted of the size range of D_p less than 0.1μm for a nucleation mode, D_p from 0.1 μm to 1.0 or 2.0 μm for an accumulation mode, and D_p more than 1.0 or 2.0 μm for a coarse mode. Each mode was fitted by a lognormal function. The nucleation mode may be divided into two modes that are a nucleation and Aitken mode. Most studies regard the nucleation mode as being smaller than the Aitken mode, so the nucleation mode has an upper limit of around 0.02 or 0.03 μm whereas the Aitken mode is significantly larger (Jaffrezo, et al., 2005; Kerminen, et al., 1999; Pakkanen et al., 2001). Whitby separated the particles into two main fractions; fine particle with diameters less than 1.0 or 2.0 μm and coarse particles

with diameters of more than 1.0 or 2.0 μm. Currently, legislative air quality objectives are defined in term of PM_{10} and $PM_{2.5}$ that fractions of particles with an aerodynamic diameter below 10 μm and 2.5 μm, respectively. Therefore, the trimodal size distribution is represented and modified as; nucleation or Aitken mode, below approximately 0.1 μm in diameter; accumulation mode (0.1 μm < D_p < 2.5 μm), and the coarse mode (2.5 μm < D_p < 10 μm). With regard to fine fraction, the particle size classification is also divided into the fine (D_p < 2.5 μm) and ultrafine (D_p < 0.1 μm) fractions.

The size distribution of aerosol particle is changed in the atmosphere by the processes of new particle formation (gas to particle by photochemical oxidation of precursors), following by growth (coagulation and condensation), evaporation and removal (diffusion, settling, impaction, washout and rainout) (Hinds, 2001). An increase in the particle size occurs through coagulation and condensation of aerosol particles. Coagulation is the growth process of aerosol from the collision of particles whilst particle condensation occurs when more vapor molecules arrive on their particle's surface. Evaporation is the reverse process changing the size and results in a net loss of molecules and reduction of airborne particles.

Fine mode and coarse mode particles differ not only in size but also in formation mechanism, sources, removal, and chemical, physical and biological properties (Table 1.2). The fine mode particles are often directly emitted as primary particles from combustion sources or formed by condensation of gaseous compounds via gas to particle conversion processes, or by coagulation and adsorption mechanisms (secondary particles). Particles in find mode are often related to long-range transport, while large particles may be formed locally by mechanical demolition, disintegration processes (sea spray), industrial activities or re-suspension of surface material, especially during drier conditions. In the UK urban areas, fine particles are mainly produced by vehicle exhaust emissions from road traffic. The major sources of coarse particles are from re-suspended road dusts, windblown soils and sea spray particles (QUARG, 1996).

Table 1.2 Characteristics of airborne particulate matter; fine (ultrafine plus accumulation- mode) and coarse mode particles (source: U.S. EPA, 2009)

	Fine		Coarse
	Ultrafine	Accumulation	
Formation Processes	Combustion, high-temperature processes, and atmospheric reactions		Break-up of large solids/droplets
Formed by	Nucleation of atmospheric gases including H_2SO_4, NH_3 and some organic compounds Condensation of gases	Condensation of gases Coagulation of smaller particles Reactions of gases in or on particles Evaporation of fog and cloud droplets in which gases have dissolved and reacted	Mechanical disruption (crushing, grinding, abrasion of surfaces) Evaporation of sprays Suspension of dusts Reactions of gases in or on particles
Composed of	Sulphate EC Metal compounds Organic compounds with very low saturation vapor pressure at ambient temperature	Sulphate, nitrate, ammonium, and hydrogen ions EC Large variety of organic compounds Metals: compounds of Pb, Cd, V, Ni, Cu, Zn, Mn, Fe, etc. Particle-bound water Bacteria, viruses	Nitrates/chlorides/sulfates from HNO_3/HCl/SO_2 reactions with coarse particles Oxides of crustal elements (Si, Al, Ti, Fe) $CaCO_3$, $CaSO_4$, NaCl, sea salt Bacteria, pollen, mold, fungal spores, plant and animal debris
Solubility	Not well characterized	Largely soluble, hygroscopic, and deliquescent	Largely insoluble and nonhygroscopic
Sources	High temperature combustion Atmospheric reactions of primary gaseous compounds.	Combustion of fossil and biomass fuels, and high temperature industrial processes, smelters, refineries, steel mills etc. Atmospheric oxidation of NO_2, SO_2, and organic compounds, including biogenic organic species (e.g., terpenes)	Resuspension of particles deposited onto roads Tire, brake pad, and road wear debris Suspension from disturbed soil (e.g., farming, mining, unpaved roads) Construction and demolition Fly ash from uncontrolled combustion of coal, oil, and wood Ocean spray
Atmospheric half-life	Minutes to hours	Days to weeks	Minutes to hours
Removal Processes	Grows into accumulation mode Diffuses to raindrops and other surfaces	Forms cloud droplets and rains out Dry deposition	Dry deposition by fallout Scavenging by falling rain drops
Travel Distance	<1 to 10s of km	100s to 1000s of km	<1 to 10s of km (100s to 1,000s of km in dust storms for the small size tail)

1.3 Chemical properties of airborne particulate matter

Measurement of chemical composition in $PM_{2.5}$ is required under the directive on ambient air quality and cleaner air for Europe (Directive 2008/50/EC of the European Parliament and of the Council of 21 May 2008). According to the directive, the measurements are to ensure that adequate information is made available on levels in the background locations. Measurement

of $PM_{2.5}$ must include at least the total mass concentration and concentrations of appropriate compounds to characterise its chemical composition. Chemical species should be analysed and list at least SO_4^{2-}, NO_3^-, Na^+, K^+, NH_4^+, Cl^-, Ca^{2+}, Mg^{2+}, elemental (EC) and organic carbon (OC). The data is necessary to judge the enhanced levels in more polluted locations, assess the possible contribution from long-rang transport of air pollution, support source apportionment analysis and for the understanding of specific pollutants.

Many previous studies reported the chemical composition of airborne particulate matter (Chow et al., 1994; Harrison and Jones, 1995; Eldred et al., 1997; Muller, 1999; Harrison and Yin, 2000; Yin and Harrison, 2008). Those results indicate that the composition of PM showed various components which are influenced by pollution sources, chemical reactions in the atmosphere, long-range transport effect and meteorological conditions. In the UK, the recent study by Yin and Harrison (2008) reports that typical overall aerosol particle composition in an urban location (City Centre, Birmingham) obtained from application of a mass closure model are expressed as follows; $(NH_4)_2SO_4$ ~16.0%, $NH_4NO_3/NaNO_3$ ~18.5%, Organics ~23.7%, EC ~8.0%, NaCl ~9.3%, Calcium salts ~7.4%, Iron-rich dusts ~13.4%, other ~ 3.7% for PM_{10}; $(NH_4)_2SO_4$ ~24.0%, $NH_4NO_3/NaNO_3$ ~21.2%, Organics ~26.1%, EC ~11.2%, NaCl ~4.0%, Calcium salts ~2.5%, Iron-rich dusts ~5.9%, other ~ 5.2% for $PM_{2.5}$.

Airborne particles contain both major and minor components. The relative abundance of the major chemical components, termed as ‘bulk chemical composition’ was reviewed in the study of Harrison and Yin (2000) for urban areas in the UK and around the world. These major components include sulphate, nitrate, ammonium, chloride, elemental and organic carbon, crustal materials and biological materials. There are many minor chemical components present in airborne particles depending on the detection limit, sensitivity of the analytical procedure to determine their concentrations. Minor components comprise the following; trace metals (lead, cadmium, mercury, nickel, chromium, zinc and manganese) which are used in metallurgical processes or in industrial products, trace organic compounds as presented at a very low concentration even though the total mass of organic compounds comprise a significant part of the overall mass of particles. Table 1.3 shows the measurements of chemical composition in PM and the results indicate the variation of component concentrations at different locations around the world including substantial temporal variability in chemical concentrations of PM. In Europe, Putaud et al. (2010) have summarized the data on chemical characteristics of PM obtained in the European aerosol

research activities at rural, urban and kerbside sites over the past decade. The results show in Table 1.4 for $PM_{2.5}$, $PM_{2.5-10}$ and PM_{10}.

Table 1.3 Chemical composition (%) of airborne particulate matter around the world (modified from Harrison and Yin, 2000)

Sampling site	PM	Total Mass ($\mu g\ m^{-3}$)	EC	OC	Organics	TC	SO_4^{2-}	NO_3^-	Cl^-	NH_4^+	Crustal	Minerals	Other	Reference
Birmingham, UK	$PM_{2.5}$	15.8	11.2	-	26.1	-	24.0	21.2	4.0	-	8.4	-	5.2	Yin and Harrison,
	PM_{10}	23.9	8.0	-	23.7	-	16.0	18.5	9.3	-	20.8	-	3.7	2008
Birmingham, UK	PM_{10}	25.7	18.0	20.0	-	38.0	17.0	6.0	2.0	6.0	-	-	31.0	Harrison et al., 1997
	$PM_{2.5}$	22.5	-	-	-	50.0	26.1	6.6	1.8	9.9	-	5.6	0.0	
Leeds, UK	$PM_{2.5\text{-}15}$	13.3	-	-	-	13.3	7.4	5.8	8.2	2.5	-	62.8	0.0	Clarke et al., 1984
	PM_{15}	35.5	-	-	-	33.8	19.2	7.9	4.2	6.8	-	28.1	0.0	
Southern California	$PM_{2.5}$	37.0	5.0	-	26.5		20.9	9.8	0.4	9.0	2.5	-	23.9	Chow et al., 1994
(urban)	PM_{10}	37.0	3.5		20.0		13.2	12.7	1.3	5.7	18.2	-	19.3	
Edison California	$PM_{2.5}$	49.6	6.0	31.4	44.0	37.4	6.0	3.0	-	2.0	35.0	-	0.0	Chow et al., 1996
	PM_{10}	52.5	5.7	19.7	27.6	25.4	6.3	3.0	-	2.0	46.1	-	4.3	
	$PM_{2.5}$	-	3.9	14.9	20.9	18.8	34.1	1.1	-	13.0	-	4.3	22.8	
Eastern U.S.	$PM_{2.5\text{-}10}$	-	-	-	-	-	4.9	-	-	1.8	-	51.8	41.5	U.S. EPA, 1996
	PM_{10}	-	3.3	6.1	8.5	9.4	27.8	1.2	-	10.7	-	19.6	18.9	
	$PM_{2.5}$	-	14.7	27.8	38.9	42.5	10.8	15.7	-	7.5	-	14.6	0.0	
Western U.S.	$PM_{2.5\text{-}10}$	-	-	-	-	-	3.1	-	-	0.8	-	69.3	26.8	U.S. EPA, 1996
	PM_{10}	-	5.1	21.4	30.0	26.5	4.6	24.0	-	6.7	-	36.3	0.0	
Lahore Parkistan	TSP	607	2.9	13.1	-	16.0	3.0	2.1	-	1.2	-	16.4	61.3	Smith et al. 1996
Hong Kong	RSP	66.2	-	-	-	57.1	14.4	2.8	2.3	3.3	-	6.1	14.0	Qin et al., 1997
Beijing China	$PM_{2.5}$	66	4.7	-	24.2	-	24.9	9.7	0.3	14.3	1.7	-	20.1	Huang et al., 2005
Nanjing,(urban) China	$PM_{2.5}$	-	5.0	-	37.3	-	20.9	12.0	3.9	12.5	3.8	-	-	Yang et al., 2005

Table 1.4 Relative contributions (%) of major chemical composition to PM mass by site types in Europe (source: Putaud et al., 2010)

		PM_{10}			$PM_{2.5}$			$PM_{2.5-10}$		
		Rural*	Urban*	Kerbside*	Rural*	Urban*	Kerbside*	Rural*	Urban*	Kerbside*
N-western Europe	Min.dust	4%	12%			5%	1%		26%	
	Sea salt	12%	10%	7%		4%	1%		15%	
	SO_4^{2-}	13%	14%	8%		21%	18%		6%	
	NO_3^-	16%	14%	12%		16%			20%	
	OM	15%	18%	16%		25%			14%	
	EC	4%	5%	9%		7%			1%	
	TC	14%	18%	20%		25%			12%	
Southern Europe	Min.dust	15%	21%	28%		11%	14%		42%	69%
	Sea salt	3%	12%	5%		6%	2%		22%	11%
	SO_4^{2-}	16%	12%	12%		15%	15%		4%	5%
	NO_3^-	14%	9%	8%		7%	7%		11%	9%
	OM		26%			23%			13%	
	EC		6%			8%			2%	
	TC	13%	21%	28%		30%	38%		11%	
Central Europe	Min.dust	9%	12%	15%	3%	5%	6%	22%	25%	29%
	Sea salt	2%	2%	2%	1%	1%	1%	2%	3%	5%
	SO_4^{2-}	19%	15%	9%	17%	19%	12%	5%	4%	4%
	NO_3^-	13%	12%	8%	6%	13%	10%	10%	7%	6%
	OM	23%	21%	21%	15%	22%	26%	5%	15%	13%
	EC	6%	10%	17%	5%	14%	21%	3%	3%	10%
	TC	32%	32%	38%	19%	31%	35%	6%	14%	19%

***** Rural background represents the distance of area from large pollution sources 10 – 50 km
Urban background represents the area of <2500 vehicals/day with a radius of 50 km
Kerbside represents area located by traffic lanes

Sulphate is mainly formed within the atmosphere by oxidation of SO_2, which is itself directly emitted from i.e. fossil fuel combustion, industrial processes, and volcanoes or produced within the atmosphere by oxidation of reduced sulphur species such as dimethyl sulphide (DMS) emitted by oceanic phytoplankton. Sulphate is expected to be found mostly in the fine fraction as ammonium sulphate and may be present as sodium sulphate of marine origin (Harrison and Pio, 1983). The oxidation of SO_2 can be found both in gas phase (homogeneous processes) (Calvert and Stockwell, 1983) and in the aqueous phase (heterogeneous processes) in the presence of cloud, fog or aerosol droplets (Schwartz, 1987). In practice, hydroxyl radical usually plays an important oxidant in homogeneous gas phase oxidation of SO_2 and dissolved ozone and hydrogen peroxide rapidly reacted with dissolved SO_2 in aqueous phase.

Nitrate occurs in the atmosphere due to the formation of nitric acid (HNO_3), which can then form particles by reacting with ammonia or sodium chloride. It is mainly found as ammonium nitrate (NH_4NO_3) produced via the reaction between gaseous nitric acid and ammonia, which is a major component in the fine particle fraction. In some environment, particulate nitrate is also observed in the coarse particle fraction in association with sodium. This is expected to be sodium nitrate ($NaNO_3$) produced from the reaction between nitric acid and sodium chloride (NaCl). Nitric oxide (NO) directly emitted converts to nitrogen dioxide (NO_2), primarily through reaction with ozone. The major pathway to nitric acid is reaction with the same hydroxyl radicals that transform sulphur dioxide to sulphuric acid (Calvert and Stochkwell, 1983). Ammonium sulphate is a fairly stable compound in atmosphere but ammonium nitrate does not exhibit the same behaviour. The atmospheric equilibrium of gaseous ammonia and nitric acid is strongly influenced by temperature and relative humidity (Russell et al., 1983). Under the lower temperature and higher relative humidity, ammonium nitrate favours in the particulate phase.

Ammonium is usually produced via the neutralisation of aerosol acids (i.e. H_2SO_4, HNO_3 and HCl) by atmospheric ammonia forming ammonium salts (Harrison and Kitto, 1992). Ammonium is almost entirely confined to the fine fraction where it is present in forms of chlorides, sulphates and nitrates.

Chloride mainly contributes by primary emissions from sea salt and possible associates in PM during the winter months by the grit used for de-icing road. These contribute mostly to the coarse fraction. Chloride may be found as secondary particle in the form of ammonium chloride derived from the reaction between ammonia and hydrochloric acid (HCl) vapour emitted from combustion sources such as incinerators and power plants. In the UK, it is likely to be of modest importance due to low concentration of its precursor, HCl. Under normal atmospheric conditions, ammonium nitrate and ammonium chloride are unstable existing in the reversible phase equilibrium with the gaseous precursors. These equilibriums are largely controlled by temperature and relative humidity.

Elemental carbon (EC) and organic carbon (OC) are the atmospheric particulate carbons with a complex mixture of substances containing carbon atoms. These compounds make up a major contribution to airborne particulate matter. Carbon compounds, sometimes called "carbonaceous materials" consist mainly of elemental carbon (EC) and organic carbon (OC). The total carbon (TC) term is defined as the sum of all carbon in particulate matter (OC and EC). EC is essentially a primary pollutant originated mainly from the incomplete combustion of fossil fuels and the pyrolysis of biological material during combustion. These particles are predominately less than 1 μm in size and are found in fine fraction. OC is a mixture of hydrocarbons and oxygenates, constituting most of the remaining particulate carbon. It has been divided into water-soluble organic carbon (WSOC) and water-insoluble organic carbon (WISOC), or into primary organic aerosol (POA) and secondary organic aerosol (SOA) (Seinfeld and Pankow, 2003). POA emitted directly into the atmosphere, for example as products of fossil fuel combustion or biomass burning. On the contrary, particulate organic carbon formed in the atmosphere by the photochemical oxidation of volatile organic compounds (VOC) is referred to as SOA. The contribution of POA and SOA to particulate matter can vary greatly, depending on the distance and strength of the sources, the photochemical processes and the age of the aerosol. In order to estimate the concentrations of primary and secondary OC, however, there is no direct measurement method to quantify the distinction between these OC. One of the estimation methods is to use the EC as the tracer of primary OC and consequently the secondary OC is calculated based on the OC/EC minimum ratios. This method describes and details in Chapter 3.

Crustal materials include soil dusts and windblown rock-derived minerals. The main sources of dust are unpaved roads, agricultural tilling and construction. Harrison et al. (1997) reported that largely crustal minerals were mostly associated with coarse particulate matter in Birmingham, UK. Soil-related material is composed mainly of silicon, calcium, iron, aluminium, potassium and titanium compounds; additionally, road dust includes the elements associated with vehicular emissions such as Cu, Zn and Pb (Swietlicki et al., 1996). However, the composition and concentrations for this particulate fraction could be variable due to local geology, surface conditions, meteorology and human activities including construction and traffic.

Biological materials consist of both small organisms like bacteria as well as spores of fungi, myxomycetes, bryophytes and pteridophytes and larger particles such as pollen grains of flowering plants, moss gemmae and fragments of cellulose plant materials (Matthias-Maser and Jaenicke, 1994; Morris, 1995). Particles of biological origin usually vary in size from below 1 μm to approximately 50 μm or larger. They are generally in coarse sizes except viruses, which range from 0.005 to 0.05 μm. Many studies have been characterized as organic carbon instead of as individual constituents (Ion et al., 2005; Sun and Ariya, 2006). Furthermore, the biological viability of any given species in the ambient air will depend upon its tolerance of UV radiation, impact of rainfall, high wind speeds, relative humidity and temperature fluctuations.

1.4 Oxalate in ambient air

Aerosol particles are known to contain organic carbon material in variable concentrations, depending on their locations. Organic compounds which include soluble and insoluble species account for a significant fraction of the fine particulate mass in the atmosphere (Jacobson, et al., 2000; Zhang et al., 2007). The most important compounds which contribute a significant fraction to organic aerosol mass are WSOC. WSOC represented a significant water-soluble component of the atmospheric aerosol (Zappoli et al., 1999; Krivacsy et al., 2001; Yang et al. 2003; Wang et al., 2005; Fosco and Schmeling, 2007). Much of the research work found that WSOC had potential to act as cloud condensation nuclei (CCN) (Novakov and Penner, 1993; Yu, 2000; Mircea et al., 2002; Yao et al., 2002; Sun and Ariya, 2006) and also reduced surface tension of CCN, which is one of the parameters determining cloud formation (Facchini et al., 1999).

Among the different types of WSOC, monocarboxylic acids (MCA) and dicarboxylic acids (DCA) are currently significant group of interest in the chemical characterisation of PM (Chebbi and Carlier, 1996; Cecinato et al., 1999; Zlotorzynska and McGranth, 2000; Limbeck et al., 2001; Falkovich et al., 2004; Karthikeyan and Balasubramanian, 2005; Wang et al., 2007). Formic and acetic acids are ubiquitous components in aerosol particles (Chebbi and Carlier, 1996). Oxalic acid is the dominant dicarboxylic acids followed by malonic and succinic acids (Kawamura and Ikushima, 1993; Kawamura and Usukura, 1993; Yao et al., 2002) and it constituents up to 50 - 70% of total atmospheric DCA (Sempere and Kawamura, 1994; 1996). In the real atmospheric particles, oxalate was found as a mixture of various inorganic and organic compounds but the previous studies have provided its chemical properties and experimental data shown in Table 1.5.

Table 1.5 Chemical properties of oxalic acid and experimental data (source: Sun and Ariya, 2006)

Compound	Oxalic acid
Formula	$C_2H_2O_4$
Molecular weight	90.03
Solubility in water	2.2×10^5 mg L^{-1} at 25 ^oC
Density	1.900 g cm^{-3} at 25 ^oC
Vapour pressure	3.5×10^{-5} mmHg at 30 ^oC

1.4.1 Occurrence of oxalic acid and/or oxalate

Chebbi and Carlier (1996) state that carboxylic acids have been detected in atmospheric aqueous and gas phases since the seventies. To the author's knowledge, the occurrence of oxalate measured in aerosols and in precipitation have been demonstrated using ion chromatography by Norton et al. (1983). Thereafter, Kawamura and Kaplan (1987) found that the diacids (C_2-C_{10}) were mainly associated with particles but a minor fraction of these compounds have been sampled in vapour phase. They suggested the possibility of low molecular weight diacids (i.e. oxalic) presented in the vapour phase under elevated temperature conditions. Oxalic acid is mostly present in particulate phase in the ambient atmosphere due to the less volatile comparing with formic and acetic acids, which are the main monocarboxylic acids present in the gas phase (Chebbi and Carlier, 1996). Limbeck et al. (2001) measured the gas/aerosol distribution of oxalic acid and reported a gas phase concentration of 23 ± 15 ng m^{-3} and aerosol concentration of 68 ± 40 ng m^{-3}. Concentration

of oxalic acid shows seasonal variation with a maximum in summer (Kawamura and Ikushima, 1993; Sempere and Kawamura, 1994).

1.4.2 Source of oxalic acid and/or oxalate

The main sources of oxalic acid in the atmosphere comprise primary biogenic and anthropogenic emission and photochemical transformations of precursors in aqueous, gaseous, and particulate phases (Chebbi and Carlier, 1996).

1.4.2.1 Biogenic sources

DCAs are common metabolic products, therefore oxalic acid is a major metabolic product of fungi in natural environments and is present in soils as calcium oxalate. The concentration of oxalic acid in the soil (156-166 nmol g^{-1}) is less abundant than its (2330-2510 nmol g^{-1}) in urban dust, which is originated from the dry deposition of aerosols (Kawamura and Kaplan., 1987). Kawamura and Kaplan also point out that DCAs in the bog sediment are metabolic or alteration products of plant debris. The distribution of DCAs in bogs is similar to that of soil samples but different from that of atmospheric DCAs, suggesting the formation process in soil would be considered. It should be noted that if the soil was the source of atmospheric DCAs, there would inevitably be some fractionation during the evaporation process. On the other hand, if the atmosphere was the source of the DCAs in soils, then soil degradation processes might be important.

1.4.2.2 Anthropogenic sources

Motor exhaust emission have been suggested as a source of low molecular weight DCAs (C_2-C_{10}). The measurement results show a similar distribution of DCAs to that found in the ambient air, indicating that incomplete combustion of aromatic hydrocarbons i.e. benzene, toluene and naphthalenes in gasoline and diesel engines could be the potential sources of atmospheric DCAs with oxalic acid concentrations range between 25% - 50% of the total DCA (Kawamura and Kaplan., 1987, Kawamura and Ikushima, 1993). Oxalic acid is the dominant species, followed by succinic, malonic, maleic, glutaric, adipic, and phthalic acids. The concentration of oxalic acid in motor exhausts is 30 – 60 times higher than the average atmospheric concentrations. On the other hand, Yao et al. (2004), Yu et al. (2005), Huang

and Yu (2007) concluded that vehicle exhaust is not expected to be a significant primary source of oxalic acid in atmosphere.

Biomass burning can be a significant process for the emission of oxalic acid and its precursors in the atmosphere. Jaffrezo et al. (1998) indicate that biomass burning plumes contributed the very high concentration of oxalate. Yamasoe et al. (2000) reported that oxalate accounted for about 0.1% of the total aerosol mass emitted during the burning processes. Schmidl et al. (2008) showed that the mean oxalate concentration in smoke from the burning of wood was around 0.1% - 0.3% of the total emitted mass. In addition, Kundu et al. (2010a,b) measured the aerosols in Amazonian during biomass burning season and reported high concentrations of oxalic acid in range 0.7 $\mu g\ m^{-3}$ – 2.1 $\mu g\ m^{-3}$.

1.4.2.3 Photochemical oxidation

DCAs generally agree that their sources are produced by the photooxidation of precursors in aqueous, gaseous and particulate phases (Dabek-Zlotorzynska and McGrath, 2000). Precursors include cycloolefins, aliphatic diolefins (Chebbi and Carlier, 1996) and aromatic hydrocarbons such as benzene and toluene (Kawamura et al., 1996). The atmospheric chemical sources of DCAs are not quantitatively well known but the possible qualitative picture of photochemical production shows in Figure 1.2. Oxalic acid can be formed by glyoxal and methylglyoxal, which are the oxidation products of aromatic hydrocarbons. With regard to the modeling study by Myriokefalitakis et al. (2011), anthropogenic hydrocarbons contribute by about 21% to the global oxalate chemical production. Alkenes (ethene and propene), acetylene and aromatics (benzene, toluene and xylene) contribute 3%, 10% and 8%, respectively to global oxalate production. The formation pathway of oxalate by anthropogenic hydrocarbons is through glyoxal, glycolaldehyde and methylglyoxal intermediates.

The oxidation of biogenic volatile organic compound is responsible for 79% of the global oxalate chemical production (Myriokefalitakis et al., 2011). Isoprene is the major organic compound emitted by plants and trees (Taalman, 1996; Borbon et al., 2001). Global emission of isoprene estimated at 175 billion to 503 billion kilograms per annum (386 billion to 1,109 billion pounds) and account for an estimated 57% of total emission of natural volatile organic compounds (NTP, 2011). It has been shown that intermediate products from the oxidation of

isoprene i.e. glyoxal, glycolaldehyde and methylglyoxal can be transformed into oxalic acid (Lim et al., 2005; Ervens et al., 2004). This pathway could contribute to about 70% (~ 22 Tg yr^{-1}) to the global oxalate production (Myriokefalitakis et al., 2011).

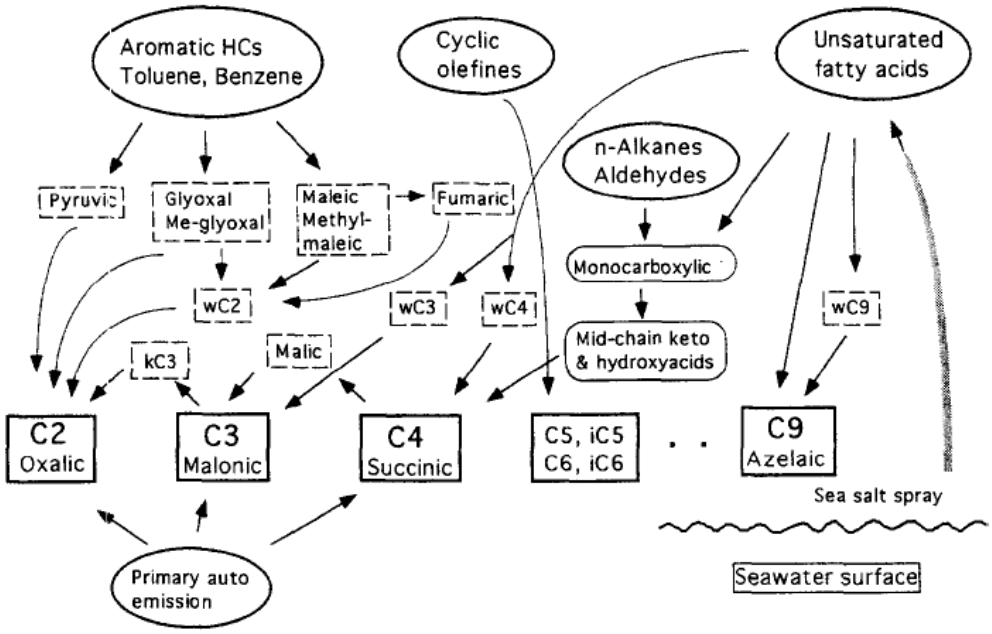

Figure 1.2 Possible photochemical production of oxalic (C_2), malonic (C_3), succinic (C_4) and azelaic (C_4) acids in the atmosphere (source: Kawamura et al., 1996)

1.4.3 Concentration of atmospheric oxalate

The concentrations of oxalate range from several ng m^{-3} up to a thousand ng m^{-3} (or a few tens of pmol m^{-3} to a few tens of nmol m^{-3}) depending on location. Table 1.6 lists the published oxalic/oxalate concentrations in ambient air by locations, sampling types and time. Among the different types of atmospheric pollutants, oxalic acid which is a major dicarboxylic acids has been a target of interest in the chemical characterization of the atmosphere. Aerosols samples in many research works were collected at the sampling location across a wide range of ambient environments, from coastal to rural to urban. The oxalate concentrations changed in different atmosphere because of their possible sources associated with anthropogenic and biogenic emissions, their temporal and geographical variability and the several mechanisms for their productions.

Table 1.6 Literature data of oxalic acid (oxalate) in the aerosol samples

Sampling site	Site type	Date	Concentration of oxalic acid (oxalate) (ng m^{-3})	Reference
Japan	Urban	April 1988 – February 1989	279 ± 190	Kawamura and Ikushima, 1993
New York	Semiurban	October 1991	58 – 360	Khwaja, 1995
Hungary		September 1995 – February 1996	130.9	Kiss et al., 1997
Brazil	Urban	July 1996	1140 ± 1200	Souza et al., 1999
Northwest Pacific Ocean	Marine	December 1994 – January 1997	89.4	Matsumoto et al., 1998
Sonnblick	Continental background	May 1997	153	Limbeck and Puxbaum, 1999
South Africa	Savanna	May 1997	193	Limbeck and Puxbaum, 1999
Las Vegas	Urban	April – June 1997	0 – 800	Tran et al., 2000
Vienna	Urban	June 1997	340	Limbeck and Puxbaum, 1999
Italy	Urban	May – December 1997	19	Cecinato et al., 1999
South Africa	Rural background	October 1997 – February 1998	14.8 – 179.5	Limbeck et al., 2001
California	Marine	June 1999	(8 – 59)	Hegg et al., 2002
Germany	One coastal rural, two rural, two urban	February 1998 – August 1999	16 – 637	Rohrl and Lammel, 2001
Brazil	Rainforest	September – October 1999	329 – 619	Graham et al., 2002
China	Urban	1999 – 2000	(300 – 500)	Yao et al., 2002a
Alert	Arctic	Feb – May 2000	13.2 – 40.9	Narukawa et al., 2002
Hong Kong	Urban	June 2000 – May 2001	350	Yao et al., 2002b
Nanjing	Urban	February – May 2001	178 – 1423	Wang et al., 2002
Nanjing	Urban, suburban	February – September 2001	(220 – 299)	Yang et al., 2005
Chicago	Urban and lake shore	July – August 2002	(186 ± 81)	Fosco and Schmeling, 2007

Table 1.6 *(continued)*

Sampling site	Site type	Date	Concentration of oxalic acid (oxalate) (ng m^{-3})	Reference
Brazil	Amazonia	September - November 2002	22 – 1340	Falkovich et al., 2004
Chicago	Urban and lake shore	June – July 2003	(193 ± 86)	Fosco and Schmeling, 2007
Beijing, China	Three urban, one rural	March 2002 – October 2003	(353 ± 259 - 377 ± 320)	Wang et al., 2007
Beijing	Three urban, one rural	2001 – 2003	(350)	Wang et al., 2005
Singapore	n.a.	May 2004	32.7 - 34.2 (361.4 – 481.4)	Yang and Yu, 2008
Chicago	Urban and lake shore	June – August 2004	(99 ± 44)	Fosco and Schmeling, 2007
Shenzhen, China	Coastal urban	July 2004 – January 2005	(47 ± 28 – 220 ± 140)	Huang et al., 2006
Indonesia	Urban, semirural, rural	March 2005	(1300 ± 500 – 2900 ± 170)	See et al.,2007
Mexico	Urban	March 2006	1330 ± 620	Stone et al., 2010
Baoji, China	Urban	February 2008	816 ± 172	Wang et al., 2010
Baoji, China	Urban	April 2008	532 ± 247	Wang et al., 2010
Helsinki, Finland	Urban	April –May 2006	(91 ± 110)	Saarnio et al., 2010
Helsinki, Finland	Urban	July and September 2006	(50 ± 37)	Saarnio et al., 2010
Chennai, India	Urban	January 2007	472.4 ± 136.9	Pavuluri et al., 2010
New Delhi, India	Urban	November 2006 – February 2007	1431	Miyazaki et al., 2009
Mt. Rax, Austria	Urban background	April 1999	52	Limbeck et al., 2005
Mangsham, China	Rural	September – October 2007	607 - 806	He and Kawamura, 2010
Jesu Island, Korea	Marine	April 2003 – April 2004	458	Kundu et al., 2010
Hyytiala, Finland	Rural	2001 – 2005	(91 – 204)	Niemi et al., 2009
Lahore, Pakistan	Urban	December 2005 – February 2006	(970 ± 400)	Biswas et al., 2008
PRD, China	Urban Semi-rural Urban/roadside Rural	December 2006 – January 2007; July – August 2007	199 261 278 274	Ho et al., 2011

Table 1.6 *(continued)*

Sampling site	Site type	Date	Concentration of oxalic acid (oxalate) (ng m^{-3})	Reference
Lasi, Romania	Urban background	January 2007 – March 2008	(35 – 109)	Arsene et al., 2011
Mountain Tai, China	Mountain	March – June 2006; March – May 2007	(100 – 480)	Deng et al., 2010

1.4.4 The studies of the sources and production of atmospheric oxalate

1.4.4.1 Sampling and extraction methods

In general, airborne particulate matters could be collected on Teflon membrane, quartz fiber filters and aluminium foils to characterise the chemical composition and the particle sizes. All the quartz filters were baked at a minimum of 500 ^{o}C for a period of time before sampling to reduce organic residues. Filter samplers include high-volume or low-volume dichotomous samplers which utilize a virtual impactor. The high-volume samplers are commonly used to collect particles with aerodynamic diameters less than 10 μm (PM_{10}) at flow rate of 1.1 to 1.4 m^3 min^{-1}. The low-volume dichotomous sampler separates particle into fine $PM_{2.5}$ and coarse ($PM_{2.5}$ – PM_{10}) size fractions at flow rate of approximately 16.7 L min^{-1}. Size distribution measurements were made using a cascade impactor (e.g. a Micro-Orifice Uniform Deposit Impactor). This sampler operates several impactors in series, arranged in order of decreasing cutoff size with the largest cutoff size first. In its operation, each stage is assumed to capture all particles reaching it that are larger than its cut off size. Because the aerosol flows in sequence through successive stages, the particles captured on the impaction plate of a given stage represent all particles smaller than the cutoff size of the previous stage and larger than the cutoff size of the given stage. The sequential separation divides the entire distribution of particles into a series of contiguous groups according to their aerodynamic diameters.

DCAs collected onto filters are polar compounds. The low molecular weight DCAs are miscible with water, so water extraction technique is the commonly used for extraction of aerosol samples. Ultrasonication was frequently employed during extraction for the filter-collected acids. Other extraction methods reported, especially for gas chromatography determination of DCAs in particulate matter, are sequential extraction by the Soxhlet

technique or shaking with organic solvents. This procedure utilized evaporation of organic solvent resulting in preconcentration of trace organic acids before analysis.

1.4.4.2 Analytical methods

Much of the research work used the ion chromatography technique to determine the ionic concentrations of the aqueous extracted air samples (Zlotorzynska and McGrath, 2000). It has been shown that ion chromatography continues to be a reliable and effective method for ionic species identification. This technique is very attractive for the monitoring of atmospheric pollution because it shows the good separation of many similar species, the provision of reliable information on the presence or absence of a wide variety of ions including its versatility and high sensitivity. Ion chromatography typically does not require extensive sample preparation and is an effective method for the separation of low-molecular-weight carboxylic acids, so why a number of research workers have performed this in their study.

Kawamura et al. (2010) studied for the intercomparison of the measurements of oxalate in aerosol samples by gas chromatography (GC) and ion chromatography (IC). The air samples were collected by a high volume virtual impactor sampler and extracted to be analysed following the reference methods. Practically, this bifunctional species has been analysed by GC after derivatization to butyl ester and by IC without derivatization. The results indicate that oxalate concentrations obtained by GC method and IC technique were consistent and the two data sets could be used for the comparison of the concentrations. It should be noted that the recovery of oxalic acid measurements would be reported, especially by the GC method in order to obtain the best and reliable results.

1.4.4.3 Seasonal variation of oxalate

Kerminen et al. (2000) investigated the chemistry of low molecular weight dicarboxylic acids at urban and rural conditions and at a site intermediate between these two in Finland. The behavior of fine-particle (< 2.3 μm) oxalate, malonate and succinate had a clear winter minimum, with especially low for malonate. Concentrations of malonate and succinate were of similar magnitude over most of the time and roughly ten times lower than that of oxalate. Both oxalate and malonate display high concentrations during the spring and autumn. The ratio of malonate to oxalate is relatively stable outside the winter period, being suggestive of

similarities in their sources and/or atmospheric formation processes. On the contrary, Wang et al. (2007) indicate that the concentration of oxalic acid shown higher concentration at traffic urban site in the winter season (spring, winter>summer, autumn). This variation implied that road transportation might be the significant sources of oxalic acid in the urban environment, however the traffic emissions could be constant all the year round, the seasonal variation might be related to other emission sources and the meteorological conditions. For example, at Beijing in winter, the high value of oxalic acid in atmosphere suggested that coal burning for heating might be a major source of particulate oxalate. A weak source of coal burning or rainy season during summer and autumn contribute low levels of oxalate causing from the efficient scavenging of soluble aerosol species. Moreover, summer and autumn are also the favorable seasons for atmospheric diffusion and pollutant dispersion. The data from industrial and residential sites do not show the seasonal variation of oxalic acid.

1.4.4.4 Spatial variation of oxalate

Observations of oxalic acid in motor exhaust have been found so that the speculations of direct emission from combustion could be sources of it in urban areas, which are exposed to traffic (Kawamura and Kaplan, 1987). The concentrations of oxalate were clearly higher at the urban site compared to the rural site. The concentrations of oxalate and malonate were roughly 1.3 – 1.6 times higher at urban site compared to rural site (Kerminen et al., 2000). This result supports the significant role of local traffic as a source of oxalate in urban conditions. Kerminen et al. (2000) indicate that both oxalate and malonate mostly produced via photochemical reactions in the atmosphere but their nature in local traffic emissions is quite difficult to estimate based on their data. Furthermore, Yao et al. (2002) studied the concentrations of dicarboxylic acids in $PM_{2.5}$ in Hong Kong. The aerosol samples were collected from Tsim Sha Tsui (TST) East in Kowloon. TST is a commercial area with many high-rise commercial buildings and many restaurants at the street level. The sampling site was located around 40m from a heavily trafficked road. The gas–phase oxalate concentrations were found more than twice the concentrations of the field blanks and were about 6 - 12% of the total oxalate found in the samples. Overall, oxalate principally partitioned in the particulate phase. The oxalate concentration (0.35 $\mu g.m^{-3}$) was large than the malonate (0.09 $\mu g.m^{-3}$) and succinate (0.05 $\mu g.m^{-3}$) concentration. In their study, the sum of the concentration of these three dicarboxylic acids (oxalate, malonate and succinate) was 4-7% of the sulphate concentration in $PM_{2.5}$. The spatial variation also investigated in the

measurement by Wang et al. (2007). The results indicate that the concentration of oxalic acid shown higher concentration at traffic urban in the winter. It seems the traffic activities might be the major source of oxalic acid in the urban area. The study of correlation coefficients of oxalic acid between different sites was evaluated and the result shown that oxalic acid has also regional sources in the urban scale. In addition to those data, oxalate only shown strong correlation with NO_2, which is a traffic source indicator, so motor exhaust hydrocarbon emissions might be its major source.

On the other hand, Yu et al. (2005) reported that among some of the measurement made in Hong Kong which the aerosol samples were collected at three locations at the same time throughout a year. Two of the locations, one in a rural environment and the other in a roadside environment with heavy vehicular traffic, were contrasting in relation to influence from vehicular emissions; however, the levels of oxalic acids were similar at the two locations in all four seasons. This data and that of Yao et al. (2004) data clearly indicate that vehicular emissions contribute little to ambient oxalic acid. The weak correlations between oxalate and elemental carbon, a tracer for primary emissions from incomplete combustion, provided additional supporting evidence for this. Yu et al. (2005) also mention that oxalic acid was at or near the end of many oxidation chains of hydrocarbon compounds. The most immediate precursors were conceivably C_2 difunctional compounds such as glyoxylic acid, glycolic acid, glycoaldehyde and glyoxal. Among them, glyoxal had the most abundant gas-phase source. Model calculation of an urban scenario was able to generate an oxalate concentration of 180 ng. m^{-3} from in-cloud oxidation of glyoxal derived from a gas-phase concentration of 0.1 ppbv of glyoxal. This level of oxalate was of the same order of magnitude found in aerosol samples from field measurements made in polluted environments. This demonstrates that in-cloud formation pathways were capable of producing a significant portion of observed oxalate concentrations in urban environments.

In marine atmosphere, Warneck (2003) presented a chemical mechanism that offered a natural route to the production of oxalic acid in marine clouds. The formation pathways leading to oxalic acid in atmosphere were from acetylene proceeding via glyoxal as intermediate and from ethene proceeding via glycolaldehyde intermediate.

1.4.4.5 Size distributions of oxalate

The size distribution of aerosols is modified in the atmosphere by the processes of new particle formation (gas-to-particle conversion and photochemical reactions), growth (coagulation and condensation), evaporation and removal (diffusion, settling, impaction, washout and rainout). The knowledge of the size distributions provides important information about their sources, formation and growth mechanism. Size distribution data of dicarboxylic acids are also useful understanding of their potential contributions to CCN. The typical modes in the mass size distributions of ambient aerosols include nuclei, accumulation and coarse modes (Hinds, 1999). The nuclei mode consists of gases and vapors emitted directly into atmosphere and particles produced in the atmosphere by gas-to-particle conversion. This mode is usually found near the sources because of their high number concentration. These particles coagulate rapidly with each other and in particular with the accumulation mode particles. Nuclei particles may provide as site for the formation of cloud droplet and may be removed from the atmosphere as rain droplet. The accumulation mode comprises combustion particles, smog particles and nuclei-mode particles that have coagulated with accumulation-mode particles. The nuclei and accumulation modes together constitute fine particles. The accumulation mode may have two submodes: a condensation mode with the mass median aerodynamic diameters (MMAD) of 0.2 – 0.3 μm and a droplet mode with MMAD of 0.5 – 0.8 μm. The droplets are formed by the growth of hygroscopic condensation-mode particles. Coarse particles included sea salts or particles generated through abrasion mechanisms (e.g. dust from the wind-driven erosion of soils or released plant fragments). The separation of particle size between coarse and fine particles is the point between 1 and 3 μm. Each mode has different chemical composition, source, size range and formation mechanism.

The size distributions of oxalate were dominated by the large droplet mode while the condensation mode and the coarse mode were both small. The droplet mode oxalate and sulphate were found to be highly correlated (Huang et al., 2006). In this study, the sample collected at coastal city in southern China and size distribution measured in the range of 0.056 – 18 μm. The diameter of 1.8 μm was used at the split size between fine and coarse particles. The results shown the three modes as resolved by positive matrix factorization (PMF) with the mass medium aerodynamic diameters (MMAD) at 0.4, 1.0 and 5.5 μm corresponding to the condensation, droplet and coarse modes, respectively. Oxalate had a dominant droplet mode, a minor condensation mode, and a minor coarse mode. The

contribution of individual identified sources to oxalate was examined in the size bin of 1.0 – 1.8 μm. The results found that in-cloud processing had a dominant contribution of 79% in the summer and 73% in the winter. In general, the condensation mode at 0.2 ± 0.1 μm is attributed to gas-particle condensation and the droplet mode at 0.7 ± 0.2 μm is attributed to in-cloud processes including cloud droplet activation, physical transferring and chemical transformation in cloud droplets and evaporation of cloud droplets (Yao et al., 2003). Oxalate was dominant in the fine mode with MMAD of 0.7 ± 0.1 μm so it is possibly a droplet mode formed by in-cloud processes. Moreover, in the 0.54 – 1.0 μm particles, oxalate was highly correlated with sulphate with a correlation coefficient of 0.99 similar to the study of Huang et al. (2006). Since sulphate in the droplet mode has been attributed to in-cloud processes, oxalate in the droplet mode can also be produced by similar processes. Yao et al. (2002) found that the condensation mode of oxalate was usually observed at 0.177 – 0.32 μm. The droplet mode of oxalate was slightly shift from 0.32 – 0.54 to 0.54 – 1.0 μm and from 0.54 – 1.0 to 1.0 – 1.8 μm, suggesting that the minor oxalate evaporation after in-cloud formation could be considered. Yao et al. (2002) also conclude that in-cloud processes were the principal pathways to form dicarboxlic acids including oxalate in aerosol particles and sometimes result in shifting the oxalate peak to slightly larger particles due to oxalate evaporation after in-cloud formation. The more explanation about this behaviour is that oxalate form in particulate phase is stable during the cloud evaporation stage and remains in the aerosol phase. Species like nitrate or chloride that may have existed as ammonium salt particles can be displaced by the oxalate produced and forced them to return to the gas phase. The result of these aqueous-phase processes usually causes an overall increase in particle mass and size (Seinfeld and Pandis, 1998).

Kerminen et al. (2000) state that oxalate size distributions displayed a dominant in accumulation mode and the minor two supermicron modes. As the presence of oxalate peak in coarse mode (two supermicron modes), oxalate was associated with sea-salt and crustal particles. Sodium had typically a single coarse mode peaking between 2 and 3 μm and non-sea-salt calcium, a tracer for crustal material, peaked between 3 and 10 μm. The larger mean size of non-sea-salt calcium compared with sodium was indicative of more local sources for crustal particles compared with sea-salt. Contribution of sea-salt to oxalate particle was supported by the reasonably good correlation between the sodium to non-sea-salt calcium ratio and the relative magnitude of oxalate in two coarse modes. The mean diameter of

oxalate in the lower supermicron mode was usually smaller than that of sodium, indicating a surface reaction of gaseous oxalic acid or its precursor with sea-salt particles.

1.4.4.6 Correlation studies of oxalate to identify primary and secondary sources

Sources of oxalic acid in atmosphere associated with anthropogenic and biogenic emissions and several photochemical reactions. A number of research works have studied the possible sources and formation mechanism of oxalic acid in the aerosol by correlation analysis between oxalic acid and several source indicators including within their category (low-molecular weight dicarboxylic acids). These source indicators are selected in some measurements such as Al and Ca^{2+} for crustal material, K^+ for biomass burning, Cl^- for waste or coal burning, NO_2 for traffic emission, SO_4^{2-} and methanesulfonate (MSA) for secondary formation of different mechanism (Wang et al., 2007; Yao et al.,2004; Yu et al.,2005; Yamasoe et al., 2000). Kerminen et al. (2000) found that the ratio of malonate to oxalate was relatively stable outside the winter period and the correlation between the oxalate and malonate was high at both rural (R^2 = 0.63) and urban site (R^2 = 0.75), being suggestive of similarities in their sources and/or atmospheric formation processes. Correlation of succinate with oxalate (R^2 = 0.67) and malonate (R^2 = 0.80) was high at urban environment but not so at rural environment. At urban site, Yao et al. (2002) also reported on the moderate correlations between succinate and malonate (R^2 = 0.78) and between malonate and oxalate (R^2 = 0.78). This result suggests that malonate was an intermediate in the transformation of succinate to oxalate which is stated by Kawamura et al. (1996). Furthermore, relationships study of low molecular weight dicarboxylic acid between sulphate and oxalate, sulphate and malonate and sulphate and succinate showed the correlation coefficients of R^2 = 0.73, R^2 = 0.85 and R^2 = 0.88, respectively. Yao et al. (2003) studied the size distribution and formation of oxalate in the summer in Beijing representing an urban area. The results found that in the fine particle samples (0.54 – 1.0 μm), oxalate was highly correlated with sulphate with a correlation coefficient of 0.99, suggesting that oxalate and sulphate originated from similar atmospheric processes.

The researches on sulphate and oxalate collected across a wide geographical span in the East Asia region up to Beijing in the north and down to Hong Kong in the south, indicate that the two species were highly correlated among samples (Yu et al., 2005). Sulphate and oxalate concentrations at each location or at multiple locations in the same region showed good

correlation with the correlation coefficients from R^2 = 0.69 to R^2 = 0.95. To estimate the production of oxalate in atmosphere, the production rate of sulphate can be used as the model because of the good correlation between their species. The production rate of sulphate from the in-cloud processes can be demonstrated as the equation below

$$P_{sulphate} = fk_{cloud}k_{SO_2}^{H}[O_x][SO_2] \qquad \text{(Equation 1.1)}$$

Where f is the frequency of cloud events, k_{cloud} is the rate constant of SO_2 oxidation, $k_{SO_2}^{H}$ is the Henry's law constant of SO_2, $[O_x]$ is the oxidant concentration in the cloud that is responsible for oxidation of aqueous S(IV) into sulphate, $[SO_2]$ is the gaseous SO_2 concentration

Then, the production rate of oxalate via in-cloud mechanisms can be approximated as

$$P_{oxalate} = fk'_{cloud}k_X^{H}[O'_X][X] \qquad \text{(Equation 1.2)}$$

Where f is the frequency of cloud events, k'_{cloud} is the oxidation rate constant leading to oxalate formation, k_X^{H} is the Henry's law constant of precursor X, $[O'_X]$ is the oxidant concentration in the cloud that is responsible for oxidation of X to oxalate, $[X]$ is the gaseous concentration of precursor X

Sulphate and MSA have been used as reference to investigate the major formation pathways of dicarboxylic acids (Huang et al., 2005; Yuan et al., 2004). Since sulphate has been well understood that its formation pathway is the most effective and predominant by in-cloud processes, and MSA is generally believed to be produced via gas-phase oxidation of dimethylsulfide (DMS) by OH and NO_3 radicals, followed by condensation on particles (Kerminen et al., 1997). Previous studies shown that in-cloud and heterogeneous formation can yield a good correlation between sulphate and oxalate, whilst gas-phase oxidation followed by gas-particle condensation can observe a high correlation between MSA and oxalate in atmosphere. For example, Huang et al. (2006) reported the high correlation of droplet mode oxalate and sulphate (R^2 = 0.92), a strong indication of a common in-cloud formation mechanism. On the contrary, in Beijing, Wang et al. (2007) indicate that oxalate

was found moderate correlation with MSA but weak correlation with sulphate, suggesting that gas-phase formation is important for the formation of oxalic acid in atmosphere. This result was in total disagreement with the studies of Yao et al. (2003), Yu et al. (2005) and Huang et al. (2006).

Ammonium in general also had a similar positive correlation with oxalate. It is know that ammonium tracks sulphate since it is mainly produced by the reaction between gaseous NH_3 and acidic sulphate particles. Consequently, the positive correlation between ammonium and oxalate is linked with that between sulphate and oxalate. This correlation coefficient between ammonium and oxalate reported in the measurement of aerosol samples by Yu et al. (2005) with R^2 from 0.44 to 0.91.

Primary emissions of oxalic acid from biomass burning were analysed by the correlation analysis of oxalate with K^+. To study the contribution of biomass burning, the ratio of carboxylic acid CA to K^+ (CA/ K^+) indicated the different sources between biomass burning and other sources of CA (Wang et al., 2007). The calculation of contribution of the biomass burning to CA is detailed in Wang et al. (2007). In Beijing, the biomass burning contributed about 30 – 60% to formic and oxalic acid. The seasonal variation of the contribution followed the order of autumn > summer > winter, which was consistent with the land farming activities. The contribution of biomass burning was higher in PM_{10} than in $PM_{2.5}$, suggesting that coarse CAs were more from this primary source. The correlation coefficients (R^2) between oxalate and K^+ were 0.77 – 0.91 and 0.71 – 0.86 for PM_{10} and $PM_{2.5}$, respectively. Huang et al. (2006) reported that oxalate shown approximately the same moderate correlation with K^+ (R^2 = 0.75) as that between sulphate and K^+ (R^2 = 0.74). The significant relationship between the droplet oxalate and K^+ was from biomass burning particles acting as effective CCN to promote in-cloud sulphate and oxalate production. For the condensation mode of oxalate, it was found that biomass burning unlikely appear to be a significant primary source, as its poor correlation with the condensation mode K^+ (R^2 = 0.10). Huang et al. (2006) concluded that oxalate in condensation mode was mainly produced by photochemical processes in the gas phase after that it was condensed onto existing particles in the condensation mode. On the contrary, in the study of biomass burning, the result of Yao et al., (2003) shown poor correlation between oxalate and K^+ (R^2 = 0.58), therefore, primary biomass burning was not a major source of the oxalate in atmosphere.

The other research works try to determine the correlation between oxalate with other important source indicators. For example, Yao et al. (2003) also mentioned that their previous work on the measurement of oxalate and organic carbon (OC) showing low correlation coefficient ($R^2 < 0.1$) in $PM_{2.5}$ in Beijing, so non-cloud heterogeneous reactions of particulate organic carbon were not a major process for the formation of oxalate. Yu et al. (2005) states that oxalate had poor correlations with elemental carbon (EC), a tracer for primary emissions from incomplete combustion of fuels in transportation, heating, power generation, and wood in residential heating, and agriculture. Sulphate also had poor correlations with EC, which was anticipated as a result of their different production sources. Moreover, sources of dicarboxylic acids can be identified by correlation study of the ubiquitous monocarboxylic acids, acetic and formic acid, in the ambient air. Wang et al. (2007) determined the ratio of acetic to formic acid (A/F) in or order to investigate CA sources. In that study, acetic acid was mainly from primary emissions, whilst formic acid was largely from secondary formation. Therefore, the high A/F ratio indicate the important of direct emission and low A/R ratio imply the photochemical processes accounting for CA in ambient air. Wang et al. (2007) have proved that A/F ratio was a suitable indicator to study the relative contribution of primary and secondary sources to CA. It shows significant difference between primary (A/F > 1) and secondary (A/F < 1) sources. The annual average A/F ratio was 0.71 in $PM_{2.5}$ in Beijing indicating that secondary formation was the dominant source of dicarboxylic acids in urban environments. The relationship of oxalic acids in $PM_{2.5}$ with those in PM_{10} was also investigated by Wang et al. (2007). It can be seen that the concentration of oxalic acid in $PM_{2.5}$ shown strong correlations with those in PM_{10}. The results indicate that oxalic acid mainly presented in the fine mode with the linear regression equations as $PM_{2.5} = 0.767 \times PM_{10}$ in summer and $PM_{2.5} = 0.869 \times PM_{10}$ in winter.

With regard to oxalate in coarse fraction, Huang et al. (2006) indicate that oxalate in coarse particle shown a moderate correlation with the coarse mode Ca^{2+} ($R^2 = 0.56$) and Na^+ ($R^2 = 0.37$), suggesting an association with soil particles and sea salt particles. The correlation coefficient between the coarse mode NO_3^- and oxalate found a high value ($R^2 = 0.68$), supporting the suggestion of coarse oxalate producing from adsorption by coarse particles. This is because oxalic acid and other acidic species in the gas phase could be adsorbed onto alkaline coarse particles similar to the formation pathway of NO_3^- in coarse mode (Mochida et al., 2003).

1.4.4.7 Conclusions of oxalate in ambient air from literature data

- Oxalic acid is typically the single most abundant DCA in aerosols in both rural and urban environments. Its concentration ranges from several ng m^{-3} up to a thousand ng m^{-3} depending on location.
- Ion chromatography is the main analytical technique in the analysis of oxalic acid in atmospheric aerosol. This technique shows the good separation of low molecular weight carboxylic acid and typically does not require extensive sample preparation. The measurement results obtained from IC technique were consistent with those from GC method.
- To date, a limited number of studies have investigated the seasonal variations of oxalic acid in the atmosphere and some results showed the different patterns. For example, in Bejing representing the urban condition, the concentration of oxalic acid shown higher in winter but in Finland at urban condition, it clearly had a winter minimum.
- Concentration level of oxalate was clearly higher at urban site compared to rural site. The estimation of photochemical reactions in causing elevated oxalate concentration in local traffic emission is quite difficult to demonstrate clearly and needs more experimental data.
- Size distribution data of oxalate in aerosol provide important data about its sources and formation pathway. Oxalate was dominantly in size distributions by the large droplet mode while the condensation mode and the coarse mode were both small. Oxalate was highly correlated with sulphate in many research works. Since sulphate in the droplet mode has been attributed to in-cloud processes, oxalate in the droplet mode can also be formed by similar processes.
- The correlation study between oxalic acid in aerosol and source indicators can be used to identify the possible sources and formation mechanism of oxalic acid.
- Due to the lack and uncertain information on sources and formation pathway of oxalate in aerosol, the comprehensive study on the measurement and source apportionment of airborne particulate matter to better understanding and accurate measurement of oxalate component is very interesting.

1.5 Objectives of this study

The purpose of this thesis is to study the properties of airborne particulate matter in the UK atmosphere both physical and chemical properties. The specific objectives are shown as the following;

- To analyse the major chemical components of airborne particulate matter both fine ($PM_{2.5}$) and coarse ($PM_{2.5-10}$) fractions at selected locations (EROS representing urban background site and Harwell representing rural site). The aerosol samplers and chemical measurement methods are shown in Chapter 2.
- To quantify the carbonaceous material in particulate matter including identify their sources by the relationship studies between carbonaceous material with major chemical composition (Chapter 3).
- To measure the ionic components in airborne particulate matter and examine their sources affecting concentrations via the relationship studies of interested species both inter- and intra-site concentrations (Chapter 4).
- To estimate the local contribution of air pollution by comparison the concentration difference between both sites when aerosol samples taken simultaneously (Chapter 3 – 4).
- To determine the air mass trajectories of major aerosol species in particulate matter in order to investigate their sources by long-range transport (Chapter 5).
- To study the mass size distributions of major aerosol species in particulate matter in order to better understanding their formation pathways (Chapter 6).
- To examine whether ammonia would stabilise the semi-volatile species in atmospheric aerosol by experiment designed with direct comparison between the air sampling under ammonia gas atmosphere and normal conditions (Chapter 6).
- To focus on the particulate oxalate in the UK atmosphere not only concentrations in ambient air but also its sources and formation mechanisms (Chapter 4 – 6).

CHAPTER 2

AEROSOL SAMPLING DEVICES AND ANALYTICAL METHODOLOGY

2.1 Synopsis

The principles of aerosol collection devices used in this study are shown in this chapter including sampling method, filter extraction and chemical analysis of aerosol samples. The quality control (QC) and quality assurance (QA) procedures are also described in the experiment to achieve an accurate and reliable measurement results. In addition, a brief summary of data and statistical analysis is given at the end of the chapter.

2.2 Aerosol sampling devices

In this work, the low-volume Partisol Plus samplers and the cascade impactors were employed in order to collect airborne particulate matter for bulk chemical analysis. Bulk chemical composition refers to the relative abundance of the major chemical components in aerosol samples (Harrison and Yin, 2000).

2.2.1 Partisol Plus air samplers

The Partisol Plus Model 2025 Sequential Air Sampler combined the unit of automatic filter exchange capabilities with well-established dichotomous splitting methodology developed by the US EPA. The system contained two supply and two storage magazines, each with a capacity of up to 16 filter cassettes, as well as a filter exchange mechanism that replaced two filter cassettes at the same time. The Partisol fitted with PM_{10} inlet and can separate particles into fine ($PM_{2.5}$) and coarse ($PM_{2.5-10}$) size fractions at a flow rate of 16.7 l min^{-1} (Figure 2.1). The device maintained the fine and coarse particle stream by the separated flow controllers at 15.0 and 1.7 l min^{-1}, respectively. It is important to maintain a constant flow rate during the sampling period so precise flow control is essential to its operation. The particle size discrimination characterietics of both the inlet and the virtual impactor depend critically on specified air velocities. A change in velocity will result in a change in the nominal particle size collected. The air stream containing PM_{10} is forced into the virtual impactor where the air flow is split. Most or the fine particles make a sharp turn to follow the higher velocity

flow stream and pass onto the fine filter whilst the coarse particles are collected onto the coarse filter. Electronic flow controllers maintain their calibrated settings well, but must be occasionally checked for dust build-up on the sensor that would change heat transfer characteristics. Furthermore, accurate air flow is needed because the mass concentration of atmospheric particles is computed as mass of component species divided by the actual volume of air samples. In this study, Partisol is regularly sent to company for the calibration of the system and for maintaining the consistent operation of the hardware. The routine check for air flow in order to verify the calibration of the Partisol is performed using the sampler's Audit screen, which is accessed via the Service Mode when the sampler is in the Stop Mode. The current flow should be read within ±5% of set flow. The coarse particle sample was corrected for the collection of fine particles in the carrier flow. Because a small proportion of the fine particles are collected on coarse particle filter. The calculation of coarse PM is achieved by the correction of fine particles in the carrier flow using the formula, $C_c = M_c/V_t - V_c/V_t.C_f$ (where C_c is the mass concentration of the coarse particle fraction, M_c is the mass collection on coarse particle fraction filter, V_c and V_t are the volumes of air samples through the coarse fraction filters and the sum of coarse and fine fraction filters, respectively, and C_f is the mass concentration of the fine particle fraction). The system collected particulate matter onto 47 mm diameter filters. The quartz fibre filters, Whatman Grade QM-A Circles, were used in this study. All the quartz filters were baked for 4 h at 500 ^{o}C before sampling to reduce organic residues (Harrison *et al.*, 2003).

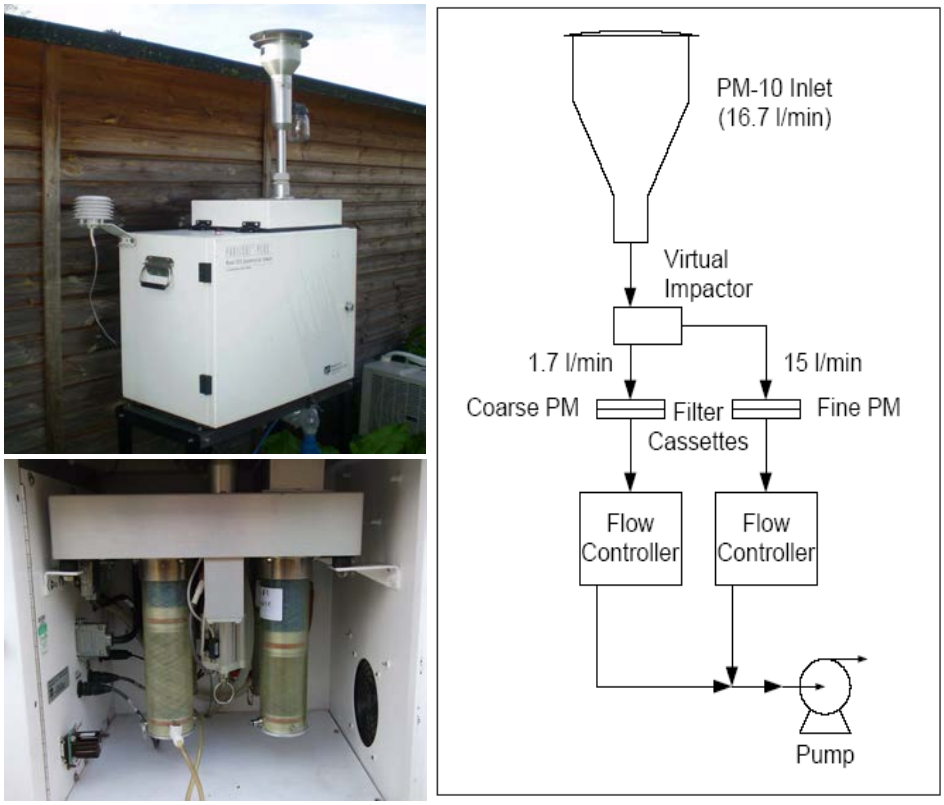

Figure 2.1 The Partisol Plus Model 2025 Sequential air sampler and operating diagram

2.2.2 Micro-Orifice Uniform-Deposit Impactors (MOUDI)

In the study of mass size distribution and form of chemical components, 10-stage micro-orifice uniform-deposit impactors (MOUDI) were employed in order to collect the various size fractions of particulate matter. Basically, the MOUDI is designed such that as the aerosol stream flows through each stage, particles having sufficient inertia will deposit on that particular stage collection plate, whilst smaller particles with insufficient inertia will associate with the stream lines and pass to the next collection stage. The stages are assembled in a stack in order of reducing particle size until the smallest particles are collected at an after filter. Total nozzle area decreases with increasing stage number, so providing that the volumetric flow rate remains constant, the air velocity increases at each stage. Significant variation in the air flow rate leads to incorrect particle size measurement. The cascade impactors give basically well-defined stage cut-off diameters, which are the aerodynamic diameter of particles that accumulate on any given collection surface, at given inlet air flow rates. The impactor plates in this model were able to rotate for spreading out the particle deposit uniformly over the stage. This minimised particle build up under each nozzle and reduced possible particle blow off by the jets. The calibrated cut-points (d_{50} –values) at 30 l min^{-1} for

the inlet and 10 stages of the MOUDI were 18, 9.9, 6.2, 3.1, 1.8, 1, 0.55, 0.325, 0.175, 0.099 and 0.054 μm. Aluminium foil and Teflon filters (1 μm pore size PTFE) with 47 mm diameter were used as the collection substrates in the impaction stages. The MOUDI was equipped with a back-up filter stage, which contained 37 mm diameter filter. The quartz fibre filters, Whatman Grade QM-A Circles, were used in this stage. In this experiment, the back-up filter stage collected the particulate matter smaller than 0.175 μm.

The system was designed for the injection of ammonia gas into aerosol stream during the sampling as shown in Figure 2.2. The ammonia gas cylinder with concentration of 50 ppm (NH_3 in synthetic air) was supplied by Teflon tube and connected to the MOUDI inlet. The gas flow controller was used to adjust and control the flow rate of ammonia gas to the desire value based on the total air flow rate of the MOUDI. Calibrated rotameters were used to measure the air and ammonia gas flow rate before starting and at the end of air sampling. The inline filter which contained Teflon filter (1 μm) was connected between the gas flow controller and the MOUDI inlet to minimise the impurities of ammonia gas. To ensure that the ammonia is reasonably well mixed with the air coming into the MOUDI, the flow Reynolds number, a dimensionless number, that characterised gas flow through a pipe was also calculated as shown in Appendix B.

Even though concentration of ammonia gas nearby the MOUDI system did not monitor, the dispersion of ammonia gas coming from exhaust stream of MOUDI's pump might not have any influence on each other. This was because the air samplers were set separately around 5 metres. Additionally, this experiment was operated with the relative low ammonia gas concentration (50 ppb in total air flow).

Figure 2.2 Air sampling by the MOUDI with ammonia experiment

2.3 Aerosol sampling

Airborne particulate matter both fine ($PM_{2.5}$) and coarse ($PM_{2.5\text{-}10}$) fractions have been collected daily with filter changing normally taking place at 1200 noon over the period November 2008 to April 2011 using Partisol samplers. The exposed filters were stored in filter cassettes within the storage magazines inside of the instrument and then transferred to small sealed polyethylene bags. The filters were then kept in a freezer until being analysed to prevent loss of volatile compounds.

As mentioned above in ammonia experiment, a set of size-segregated samples were collected for 72 h during November 2010 to January 2011. Then the filters were transferred to plastic Petri dish and stored in a freezer. To obtain the mass concentrations of aerosol particles, the filters were weighed before and after sampling under the same conditions as described more detail in 2.5.5.

2.4 Extraction from filters

The aerosol quartz fibre filters remaining from carbon analysis, which detailed in section 2.5.1, were transferred from their bags to a narrow neck 15 ml of HDPE bottles. Vinyl gloves and tweezers were used when handling the filters throughout the extraction process and the filters were extracted the same day as removed from the freezer. The distilled deionised water (DDW) (10 ml) were added and the bottles were extracted in an ultrasonic bath for 30 min at room temperature. After ultrasonication, the filter extracts were filtered through a syringe filter (0.2 μm) and then kept in a cold room until analysis. For particulate matter collected onto aluminium foil and PTFE filters in ammonia experiment, the filters were wetted with propan-2-ol (0.5 ml) to eliminate the natural hydrophobicity of filters. Then, 15 ml of ddw were added and ultrasonication performed for 30 min. The leachate was filtered and kept in the same manner until being analysed.

2.5 Chemical analysis

2.5.1 Determination of organic carbon, elemental carbon and total carbon with carbon aerosol analyser

For the determination of organic (OC), elemental (EC) and total carbon (TC = OC + EC) concentration, a Sunset Laboratory Thermal-Optical Carbon Aerosol Analyser was used in this study. It uses thermal desorption in combination with optical transmission of laser light through the sample to speciate carbon collected on a quartz fibre filter (Sunset Laboratory Inc., 2004). All carbon evolving from the filter is oxidised to carbon dioxide, the carbon dioxide is reduced to methane, and the methane is measured using a flame ionisation detector (FID). A red-light laser and photocell are used to monitor transmittance of the filter, which typically darkens as refractory OC chars during a non-oxidising heat ramp and then lightens as the char burns off during an oxidizing heat ramp. The calculation software divides TC into OC and EC by setting the split time between the two as the time in the analysis when the transmittance of the filter returns to its original value at the beginning of the analysis.

The schematic diagram of the Sunset Laboratory is shown in Figure 2.3. A punch (a nominal area of 1.5 or 1.0 cm^2) from a quartz filter sample was placed on a quartz boat and put in the main oven positioned in the path of a red light diode laser. A thermocouple at the end of the boat was used to monitor sample temperature during analysis. All carbon species evolved

from the filter were converted to carbon dioxide in an oxidation oven immediately downstream from the primary oven, and the carbon dioxide was reduced to methane before passing into a flame ionization detector (FID). The parameter file or the temperature program for this work used a protocol recently developed for the European Super-sites for Atmospheric Aerosol Research project (EUSAAR_2) (Cavalli *et al.*, 2010). The analysis started in a non-oxidising atmosphere (helium) with a 10-second purge followed by four temperature ramps to a maximum of 650 ^{o}C. The temperatures in He steps were at He 200 ^{o}C for 120s, at He 300 ^{o}C for 150s; at He 450 ^{o}C for 180s and at He 650 ^{o}C for 180s. A cooling blower then came on and the temperature dropped below 500 ^{o}C. Approximately 10 seconds before the temperature reached 500 ^{o}C, an electronic gas valve switched to 10% oxygen in He, which arrived at the sample about the time of the temperature dropped below 500 ^{o}C. A series of four heating ramps, this time with the sample in an oxidizing atmosphere, then brought the sample to a temperature of 850 ^{o}C. The temperatures in this step were at O_2/He 500 ^{o}C for 120s; at O_2/He 550 ^{o}C for 120s; at O_2/He 700 ^{o}C for 70s and at O_2/He 850 ^{o}C for 80s. Any carbon remaining on the filter was burned off during these final heat ramps. Approximately 2 minutes after 850 ^{o}C set point was initiated, a gas valve switched to flush a standard gas of 5% methane in He from the loop and into the analyser and the heater was switched off. An example of the temperature programme run by sucrose standard is shown in Figure 2.4.

Two software programmes, namely the instrument programme and the calculation programme, were used in this instrument. The instrument programme set up and maintained control of the system during operation according to the preset temperature programme and stored the raw data (output signals from the FID, laser detector, thermocouple, and flow sensors) into a text format output file for subsequent calculation of the results. The instrument program also displayed the thermogram for the analyses sample; this included the time signals, the front oven temperature, the laser transmittance, the oven pressure, and the FID detector. After the analysis of a series of samples, the calculation programme was run to obtain quantitative data (in μgC cm^{-2} of filter) for OC, EC and TC. The data were saved into a spreadsheet format for further calculation (i.e., multi-point sucrose standard correction and conversion of OC, EC and TC concentrations to unit of μgC m^{-3} for fine and coarse particles).

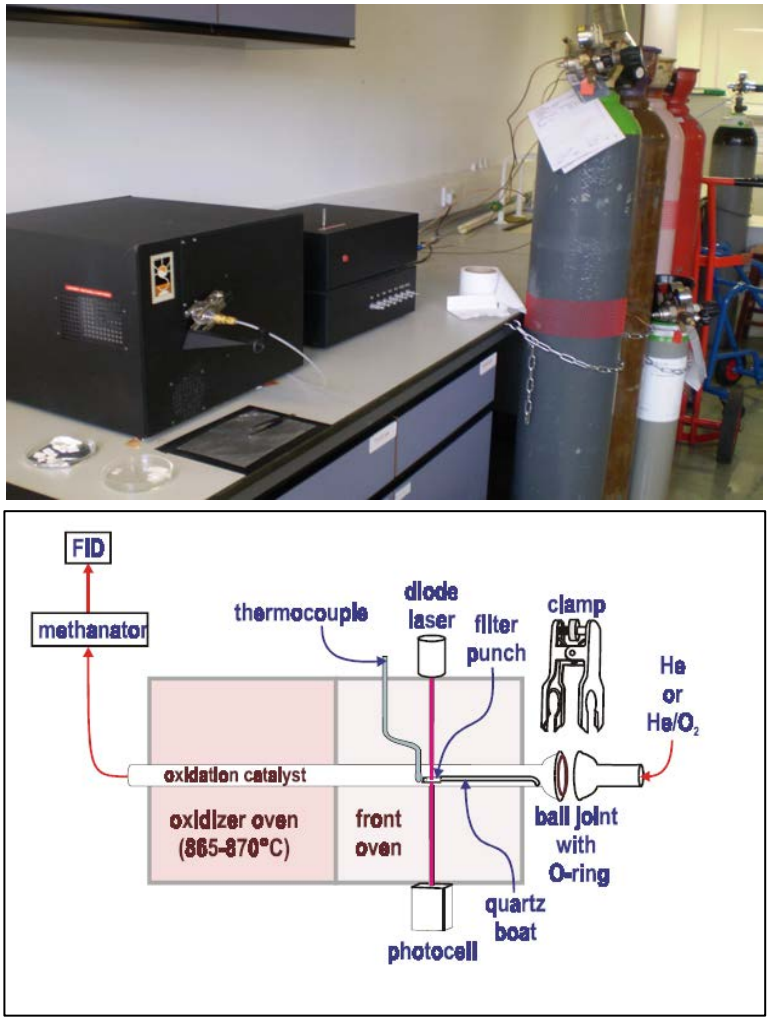

Figure 2.3 Schematic diagram of the Thermal-Optical Carbon Aerosol Analyser (Sunset Laboratory analyser)

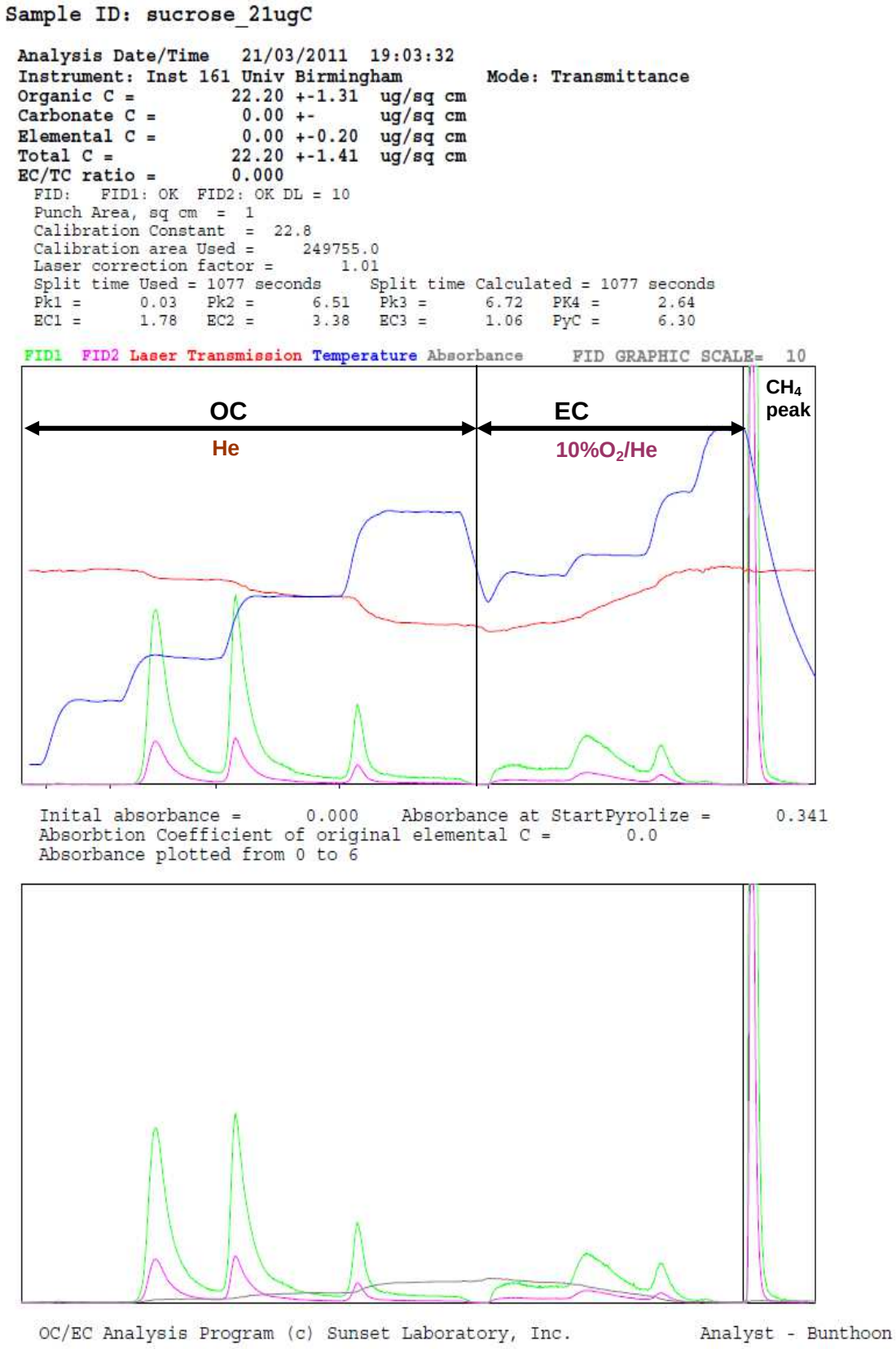

Figure 2.4 Thermogram obtained by thermal-optical transmission (TOT) analysis with EUSAAR_2 temperature programme for sucrose standard

The quality control experiment of the OC/EC analysis is an essential parameter to achieve the reliable results. As mentioned above, an injection loop in the analyser was used to inject a fixed volume of nominal 5% methane in He standard at the end of each analysis. The standard was treated as an internal standard for calculation of OC, EC and TC concentrations. The mass of carbon in the loop was determined by running a three-point calibration using standard aqueous solutions of sucrose, calculating an average FID response factor for the calibration runs, and applying that average calibration response factor to the average FID response to the internal standard for the calibration runs to calculate the average measured mass of carbon (as methane) in the loop. For analysis of a filter sample, the FID response to the known mass of carbon (as methane) in the loop was used by the software to determine the FID response factor (counts μgC^{-1}) for the methane standard for a given analysis, and this FID response factor was then used to calculate OC, EC, and TC loading for the filter portion used in the analysis. For quality assurance, daily checks were performed by running instrument blanks and a single sucrose standard. Instrument blank, which was analysed by pre-fired quartz fibre filter, was used to verify that the inside of the carbon analyser over and sample transfer lines were clean. It should be less than 0.2 $\mu gC\ cm^{-2}$. The first blank analysis also used to observe that the laser, the pressure of oven, the FID signal and the heating programme behaved correctly throughout the analysis. A single calibration check by applied sucrose solution onto blank quartz filter was used to confirm that the FID response had not shifted substantially since the late three-point calibration. The acceptance criterion for the accuracy was calculated within 5%.

The method detection limits of OC/EC analysis were determined by measuring of ten pre-fired quartz fibre filters. The detection limits, which were estimated as three times the standard deviation shown in equation 2.1, were 0.83, 0.11 and 0.83 $\mu g\ m^{-3}$ for OC, EC and TC, respectively. In this work, the detection limit for EC was calculated on the order of instrument blanks acceptance criterion of 0.2 $\mu gC\ cm^{-2}$.

$$Detection\ limit = 3 \times SD\ of\ component\ in\ blank\ filter \qquad \text{(Equation 2.1)}$$

The precision of this method was also evaluated by analysis of six replicate punches from the same filter to determine the uniformity of the deposit on filter. The relative standard deviations for OC, EC and TC were 3.7%, 13.8% and 1.5%, respectively (Table 2.1). In addition, the inter-laboratory comparison on the analysis of OC/EC was also run for further

assurance of analyses. The programme of GGD/LO 09-1117 was conducted by GGD Amsterdam in 2009 and the test was carried out by four participants.

Table 2.1 The detection limits and precision study of OC/EC analysis

	Concentration ($\mu g\ m^{-3}$)[a]		
	OC	EC	TC
Pre-fired QMA			
1	0.2	0.0	0.2
2	0.3	0.0	0.3
3	0.2	0.0	0.2
4	0.8	0.0	0.8
5	0.7	0.0	0.7
6	0.9	0.0	0.9
7	0.1	0.0	0.1
8	0.6	0.0	0.6
9	0.7	0.0	0.7
10	0.7	0.0	0.7
Mean	0.53	0.00	0.53
S.D.	0.28	0.00	0.28
Detection limit (3*S.D.)	0.83	0.11[b]	0.83
$PM_{2.5}$ (18/05/10)			
1	3.4	0.9	4.3
2	3.3	1.0	4.3
3	3.5	0.9	4.4
4	3.4	1.1	4.5
5	3.3	1.0	4.4
6	3.6	0.8	4.4
Mean	3.41	0.96	4.37
S.D.	0.13	0.13	0.07
RSD	3.7	13.8	1.5

[a] air volume based on a nominal PM fine fraction collected 24h sampling period.
[b] calculated based on instrument blank acceptance of 0.2 $\mu gC\ cm^{-2}$.

2.5.2 Determination of water-soluble organic carbon with carbon aerosol analyser

Measurement of the water-soluble organic carbon (WSOC) is a relatively simple extension of the total carbon measurement and supplies valuable clues regarding the chemistry of organic aerosol. In practice, the two instruments for trace analysis of carbon in environmental samples are total organic carbon (TOC) analyser and aerosol carbon analyser (Sunset Laboratory). TOC mostly used for water samples and Sunset Laboratory is designed for determing particulate matter collected on filter substrates. Yang *et al* (2003) indicate that the two methods gave equivalent results by measuring of standards compounds and aerosol

samples. In this work, a Sunset Laboratory was chosen as the simplest way of determining this fraction by measuring OC before and after treatment with water.

The collected aerosol quartz fibre filters were cut into two 1.5 cm^2 pieces by using a filter punch in laminar flow fume-hood. One portion was analysed for OC/EC and the other portion used for water extraction process before being analysed into ACA. The extraction method was applied by using Buchner filtration to separate the wsoc in the samples as shown in Figure 2.5. The ddw (2.5 ml) were gently and slowly dropped onto the filters to minimise the loss of EC and water insoluble organic carbon. The filtration process took place around 10 min for each sample and then the filters were left over night in laminar flow fume-hood. The extracted filters were kept in freezer until being analysed by ACA. For the quality control, the pre-fired quartz fibre filters were water extracted in the same manner as aerosol sample. The results of OC/EC analysis were corrected by the controlled samples.

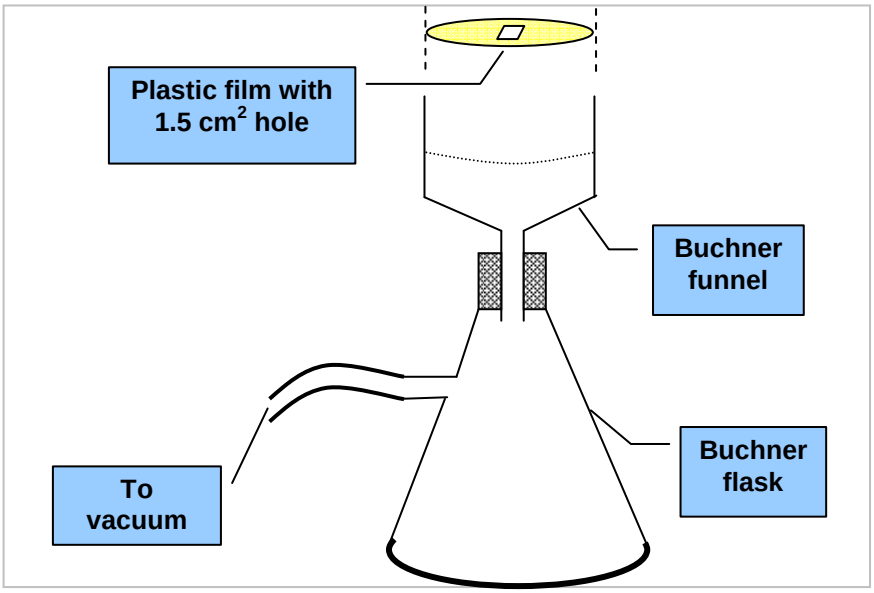

Figure 2.5 Diagram of water extraction of aerosol samples collected onto QMA filters

2.5.3 Determination of anion components with ion chromatography

Ion chromatography (IC) was selected as the analysis of choice for the determination of anion components in airborne PM samples. The advantage of using IC analysis is to minimise the samples preparation and the instrument has a good separation and high sensitivity for multiple ion analysis (Zlotorzynska and McGrath, 2000). In this work, inorganic anions (sulphate-SO_4^{2-}, nitrate-NO_3^- and chloride-Cl^-) including dicarboxylic acid (oxalate, $C_2O_4^{2-}$)

were analysed by using Dionex ICS2000 Ion Chromatography System (ICS-2000). An IC system typically consists of a liquid eluent, a high-pressure pump, a sample injector, a guard and separator column, a chemical suppressor, a conductivity cell, and a data collection system as shown in Figure 2.6.

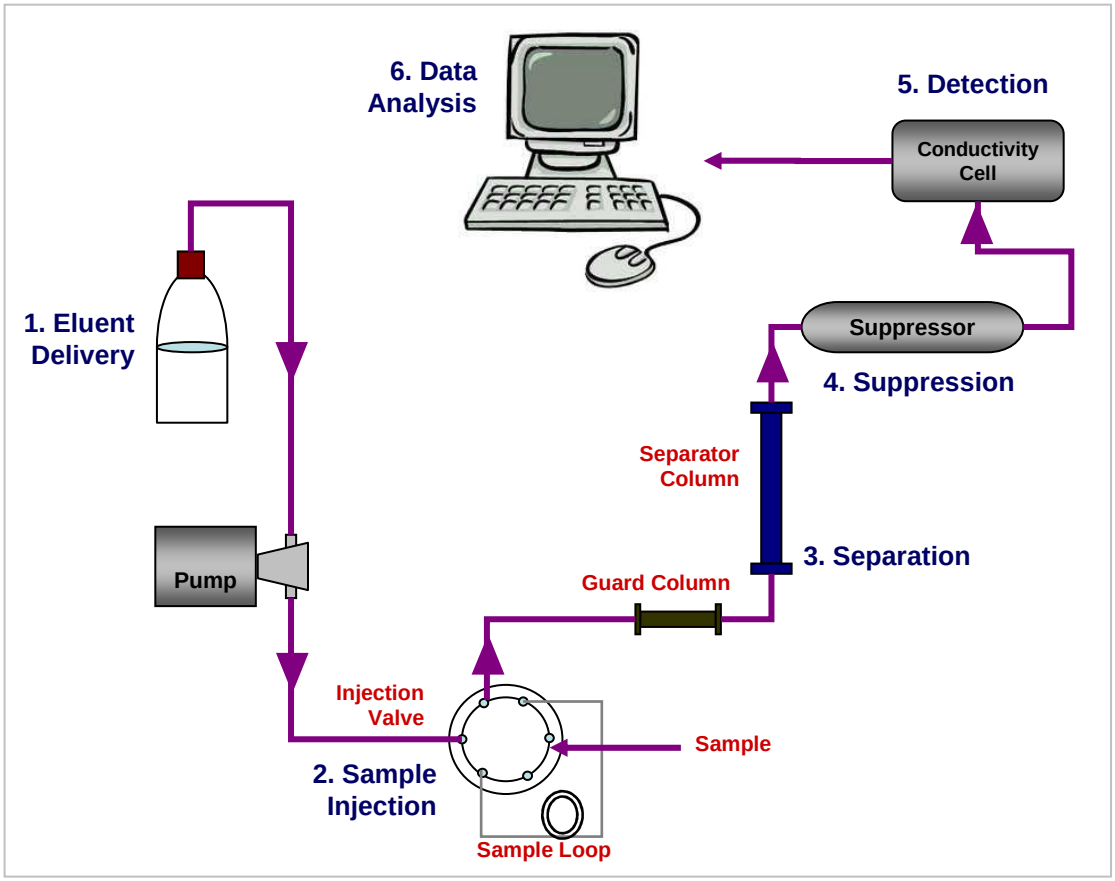

Figure 2.6 Ion analysis process

The ICS-2000 is an integrated ion chromatography system containing an analytical column (IonPac AS11HC with 2 × 250 mm) with a guard column (IonPac AG11HC with 2 × 50 mm). The eluent for these samples was the potassium hydroxide (gradient) and its flow rate during the analyses was equal to 0.38 ml min^{-1}. The injection sample volume of 200 µl was loaded into the eluent stream and 5 ml sample vials were used with the auto sampler. The ICS-2000 was controlled by Chromeleon software which also provided data acquisition and data processing functions. The data collection system identified the ions based on retention time and quantified each analyte by integrating the peak area or peak height. IC system was calibrated using a series of mixed anion standards of known concentration (0.2 – 20 ppm) before running a sample. The mixed standard solutions containing SO_4^{2-}, NO_3^-, Cl^- and $C_2O_4^{2-}$ were prepared and kept in the cold room to avoid losses of volatile species. By comparing the

data obtained from a sample to that obtained from the standards, the ions component concentrations were to be identified and quantified. In this analysis, samples were filtered with syringe filters (0.2 μm) before loading into IC to avoid blockages or damage to connecting tubing, column end frits, and other hardware components of IC system as detailed in section 2.4.

For quality control and quality assurance, fresh mixed standard solutions were prepared and used in every analysis before running the samples. These standards were made from stock standard solutions which were prepared every six months. The detection limits of IC technique were determined for anion components as three times the standard deviation from the analysis of ten blank filters. Pre-fired quartz fibre filters were allowed to equilibrate to room temperature and then placed in polyethylene bottle. Filters were water extracted following the procedure in section 2.4. The method detection limits as calculated according to equation 2.1 were 0.007, 0.044, 0.011 and 0.002 μg m^{-3} for SO_4^{2-}, NO_3^-, Cl^- and $C_2O_4^{2-}$, respectively, at a nominal volume of 21.6 m^{-3} for a typical 24h sample period of fine fraction (Table 2.2). The recovery determination was performed by the analysis of spiked filters. The mixed calibration solutions of 500 μl with ions concentration range 5-120 ppm were spiked onto pre-fired filters and then kept the samples dry overnight in the laminar flow fume-hood. The samples were then water extracted and kept in the cold room until IC anlaysis. The control blank filters were also performed in the same procedure in order to use for correction of recovery calculation. The recovery is calculated according to the following equation;

$$\text{Recovery}(\%) = \frac{\textit{average measurement concentration}}{\textit{true concentration}} \times 100 \qquad \text{(Equation 2.2)}$$

Average recovery efficiency for anionic species appeared at 95%, 99%, 100% and 81% for SO_4^{2-}, NO_3^-, Cl^- and $C_2O_4^{2-}$, respectively. To determine the method repeatability, which assesses the precision of the IC analysis, ionic components analysed on multiple filters were compared. The relative standard deviations of ten spiked samples were calculated and the results showed good repeatability with RSDs less than 2.5%.

2.5.4 Determination of cation components with ion chromatography

The IC technique was also used to determine the major cation components by using a Dionex DX 500. The samples were analysed for sodium (Na^+), ammonium (NH_4^+) and potassium (K^+). A GP40 gradient pump was used to deliver eluent to Dionex system. A 1000 μl sample loop was loaded via an AS40 Automated Sampler, using 5 ml sample vials. A CD20 Conductivity Detector was used as the detection for measuring the electrical conductance of the sample ions based on a chemical or physical property of the analyte. The analytical column used was an IonPac CS12A (4 × 250 mm) and a guard column IonPac CG12A (4 × 50 mm) with an eluent of 20 mM methanesulfonic acid (MSA, CH_4O_3S). This eluent was freshly prepared by dissolving 0.9 ml of MSA in distilled deionised water (l000 ml). A personal computer associated with Dionex PeakNet software was used for instrument control, data collection and data processing. Only samples collected by MOUDI were be analysed for cation species. Method detection limits for analysis of cation components were determined by water extracted of ten blank aluminium foil substrates. The detection limits of Na^+, NH_4^+ and K^+ were 0.095, 0.078 and 0.030 μg m^{-3} respectively, at a nominal volume of 123.5 m^{-3} for a typical 72h sample period of MOUDI experiment (Table 2.2). Due to the hydrophobicity of Teflon and aluminium foil surface, the standard solutions were not be able to spike onto their surfaces hence the recoveries of cations anlaysis were not studied in this work. To ensure the accuracy of measurement results, a series of mixed cation standards in concentration range 0.2 – 20 ppm was used for calibrating of IC system prior to sample analysis.

Table 2.2 The detection limits and recoveries study of ionic analysis by IC

	Concentration (μg m^{-3})[a]						
	SO_4^{2-}	NO_3^-	Cl^-	$C_2O_4^{2-}$	Na^+	NH_4^+	K^+
Blank filters[b]							
1	0.01	0.01	0.01	0.001	0.06	0.00	0.03
2	0.01	0.03	0.01	0.000	0.00	0.00	0.00
3	0.01	0.00	0.01	0.002	0.00	0.07	0.00
4	0.01	0.00	0.01	0.000	0.06	0.03	0.00
5	0.01	0.02	0.01	0.000	0.00	0.00	0.00
6	0.01	0.00	0.01	0.000	0.02	0.00	0.01
7	0.02	0.03	0.01	0.000	0.00	0.00	0.00
8	0.01	0.00	0.01	0.001	0.00	0.00	0.00
9	0.01	0.03	0.02	0.000	0.00	0.00	0.00
10	0.01	0.00	0.01	0.000	0.08	0.04	0.02
Mean	0.011	0.012	0.010	0.000	0.022	0.015	0.006
S.D.	0.002	0.015	0.004	0.001	0.032	0.026	0.010
*Detection limit (3*S.D.)*	*0.007*	*0.044*	*0.011*	*0.002*	0.095	0.078	*0.030*

Table 2.2 *(continued)*

	Concentration (μg m^{-3})[a]						
	SO_4^{2-}	NO_3^-	Cl^-	$C_2O_4^{2-}$	Na^+	NH_4^+	K^+
Spiked filters[c]					n.a.	n.a.	n.a.
1	2.63	2.82	2.32	0.098	-	-	-
2	2.63	2.77	2.32	0.097	-	-	-
3	2.64	2.80	2.32	0.101	-	-	-
4	2.65	2.86	2.32	0.103	-	-	-
5	2.65	2.84	2.33	0.102	-	-	-
6	2.66	2.82	2.33	0.102	-	-	-
7	2.65	2.85	2.33	0.099	-	-	-
8	2.65	2.81	2.32	0.100	-	-	-
9	2.66	2.88	2.33	0.095	-	-	-
10	2.69	2.90	2.35	0.099	-	-	-
Mean	2.651	2.834	2.326	0.100	-	-	-
S.D.	0.015	0.040	0.011	0.002	-	-	-
RSD	*0.6*	*1.4*	*0.5*	*2.4*	-	-	-
After blank correction	2.637	2.757	2.315	0.094	-	-	-
Spiked conc.	2.778	2.778	2.315	0.116	-	-	-
Recovery (%)	*95*	*99*	*100*	*81*	-	-	-

[a] air volume based on a nominal PM fine fraction collected 24h sampling period for anions and 72h in MOUDI experiment for cations.
[b] quartz fibre filters and aluminium foil substrates were used as blank analysis for anions and cations analysis, respectively.
[c] the standards could not be spiked onto Teflon filters or aluminium foils due to hydrophoblic surface hence there were no data available for recoveries of cations analysis in MOUDI experiment.

The blank concentrations of ionic species were typically found with a very small (~1%) of the field measurements. Therefore, the data presented in this study were not corrected for the blank concentrations. Recoveries were studied as for QA/QC purpose and associated with the calculation of measurement uncertainty as detailed in Appendix A. The recovery values of ionic species were not used to correct values in the rest of the thesis. Additionally, the detection limits were analysed as the lowest levels at which those concentrations may be quantified with confidence (Harrison and Mora, 1996). In this study, the samples which were present below detection limits were calculated as half of detection to obtain the best and reliable data.

2.5.5 Determination of mass of particulate matter with gravimetry

Particulate matter mass concentration was measured by weighing of aluminium foil and the Teflon filters using a Sartorius model MC5 microbalance before and after air sampling. These filters were used as the collected substrates in MOUDI experiment. All filters were equilibrated at a relative humidity of 45-55% and a temperature of 20±2 ^oC in the weighing room for at least 24h before weighing commenced. An ionising blower and alpha particle

source were used to eliminate the effects of static electricity on the weighing process. The filters were weighed three or more times to ensure reliability and sample mass concentrations were subsequently calculated using the net filter weight gain after air sampling.

2.6 Data and statistical analysis

All datasets obtained in the study were used to analyse and evaluate the sources and formation pathways of major chemical components in airborne particulate matter. In principle, the two most common practices to analyse datasets are nonparametric and parametric analysis. Nonparametric statistical procedures are used to evaluate research data which do not require and restrict the assumptions about the distribution of the data. On the contrary, parametric method strongly requires that the form of the population distribution be completely specified as normal distribution. This makes nonparametric statistical methods more flexible and appropriate in this study since the data observed tend to be heterogeneous, and the heterogeneity is not well described. The Kolmogorov-Smirnov test was applied to dataset to investigate the sample distribution. These nonparametric tests used mostly for testing hypotheses of data comparison such as the Mann-Whitney test and Kruskal-Wallis test. However, nonparametric procedures are less suited for the estimation of association for this datasets. The following are the details of methods of data analysis.

Determination of association

The measurements of levels of association or the relationships between chemical components in air samples were determined both inter- and intra-sites in order to investigate their origins as well as formation pathways. The Pearson (product-moment) correlation should be the first choice (Belle, 2008) to measure the correlation coefficients (r). This test measures the strength of the linear relationship between two variables. Because of all concentrations data (raw data) used without removing outlier in this study, Peason correlation test is appropriate and higher sensitive than rank correlation analysis (nonparametric method). A linear association implies that as one variable increases, the other increases or decreases linearly. The correlation coefficient does not imply cause and effect. Test results between two variables should report as high correlation or strong relationship. The values of these correlation coefficients usually range from -1.00 to +1.00. Values of the correlation coefficient close to +1.00 indicate that as one variable increases, the other increases nearly linearly. On the contrary, a correlation coefficient close to -1.00 indicates that as one variable

increases, the other decrease nearly linearly. Values close to 0 imply little correlation between the variables. A rough guide to the degree of the association given by some statistical references (Yin, 2002) indicates that *r*, in the range 0.00 - 0.19, represents a very weak correlation, 0.20 - 0.39 a weak correlation, 0.40 - 0.69 a modest correlation, 0.70 - 0.89 a strong correlation and 0.90 - 1.00 a very strong correlation. In order to know whether the correlation is significant between two variables, the null hypothesis, a hypothesis of no correlation, was tested consulting a table for Pearson product moment correlation values at the 0.05 levels of significance, with the number of degrees of freedom $n - 2$ (n is the number of observations). The distributions of both variables should be analysed because a skewed distribution produces a smaller *r* than a normal distribution. The Kolmogorov-Smirnov was used to determine the distribution of datasets and reported in Appendix E. Test results, however, indicate that ionic species analysed in air samples deviate significantly from a normal distribution. Thus, smaller *r* values might be observed and reported for the determination of association. In this thesis, the "good" correlations of chemical components in aerosol samples denote strong and very strong correlations. The "poor" correlations of chemical components denote weak and very weak correlations.

Regression analysis

The correlation analysis is always used in conjunction with regression analysis. When data of two variables are plotted on a graph, they are said to have a linear relationship if the points tend to fall in a straight line. The strength of the association between the variables can be estimated by judging how close the points are to the line. The correlation between the variables is high when the points are very near the line and low when the line is a poor summary of the positions of the points. The position of the line shows how a change in one variable is expected to affect the other. The reduced major axis (RMA) regression was applied in this study (Ayers, 2001). The best linear fitting line is achieved by minimising the deviations of both variables. The coefficients of determination or coefficients of regression were reported as R^2. If there is a perfect relationship, the coefficient of determination is 1.00. This means all the points on the graph lie on the regression line and all the variation in one variable is explained by the other one. RMA regression was applied to the dataset in order to determine the relationship between rural and urban background concentration during the samples collected simultaneously (chapter 3.3.3, 4.4).

Measures of central tendency

The measures of central tendency of samples were estimated by the sample mean in this study. In case of mean value higher than 75^{th} percentile of the observations, the discussion still based on this value with special cautions and data also presented the sample median as reported in Table 3.1. The reasons of this case mostly come from the measurement data observed outliers. Outliers result commonly from transcription errors, data-coding errors, or measurement system problems. However, outliers may also represent true extreme values of a distribution and indicate more variability in the population than was expected. Not removing true outliers and removing false outliers both lead to a distortion of calculates of population parameters. Rejecting an outlier from a dataset should be done with extreme caution, particularly for environmental data sets, which often contain legitimate extreme values (U.S. EPA, 2006).

Data below the limits of detection

As mentioned about the method of determination of detection limits of chemical analysis, some data obtained from this study fell below the detection limit of the analytical procedure. These measurement data are generally reported as non-detects (<dl). In these cases, the concentrations of analysed species are unknown although they lie somewhere between zero and the detection limits. There are a variety ways to evaluate data that includes values below the detection limit. However, there are no general procedures that are applicable in all cases (U.S. EPA, 2006). In this thesis, data below the limits of detection are replaced with dl/2 and the usual analysis performed.

Comparision of two populations

Generally, it is difficult to obtain a truly random sample in the environmental sciences (Watts and Halliwell, 1996). Many of statistical tests described are based on the assumption that the observations being tested have a normal or almost normal distribution. When this condition cannot be met, a range of distribution-free or nonparametric statistical tests are appropriate. In this study, Kolmogorov-Smirnov test was applied to datasets and test results indicated that chemical components analysed in air samples deviate significantly from a normal distribution as shown Appendix E. Therefore, nonparametric tests were used in all hypothesis tests of significant differences. The Mann-Whitney U test is a nonparametric test that can be used to analyse data from two-group independent groups design when measurement can at least be ranked or be ordered. This test makes no assumptions about data distribution. It does assume

that the two distributions are similar in shape but the distributions need not be symmetric. The two datasets need not be drawn from normal distributions. This test evaluates the null hypothesis that two groups of sample come from the same population.

Comparison of several populations

The Kruskal-Wallis nonparametric test can be used to assess whether any significant differences between *k* independent samples. It is used for comparing more than two samples. The test assumes that the measurements under study are at least on an ordinal scale and that underlying variable has a continuous distribution. The null hypothesis is that the *k* samples come from the same population, or that their underlying distributions have the same average. This test was performed to investigate the significant differences for component concentrations between clusters of air back trajectories (chapter 5.5). For trajectory analysis, cluster method was used for classifying air mass backward trajectories generated from the HYSPLIT4 (HYbrid Single-Particle Lagrangian Integrated Trajectory) model as detailed in Chapter 5.

Lastly, estimation of measurement uncertainty associated with analysed data was also evaluated in order to achieve the reliability and traceability of measurement results as described in Appendix A.

CHAPTER 3

INTERPRETATION OF CARBONACEOUS AEROSOL CONCENTRATIONS IN PARTICULATE MATTER

3.1 Synopsis

In this chapter, concentration composition data of aerosol collected at urban background (EROS) and rural (HAR) are presented in all particle size ranges ($PM_{2.5}$, $PM_{2.5-10}$, PM_{10}) with basic statistical characteristic. Carbonaceous material, which is commonly divided into an organic carbon (OC) and elemental carbon (EC) fraction, are mainly discussed. The data set presented here compares with the other important components such as sulphate, nitrate and nitrogen oxides in order to investigate their sources of particles at both sites. The commonly used method to distinguish primary organic carbon (OC_{prim}) from secondary organic carbon (OC_{sec}) on the basis of the OE/EC minimum ratios of individual samples is determined. The OE/EC ratio used in this calculation is considered carefully following the recently published paper. Relationship between OC and EC including graphical presentation of their concentrations will also be explored. Furthermore, this chapter reports and discusses the interpretation of inter-site difference of carbonaceous aerosol data collected simultaneously.

3.2 Sampling locations

- The Elms Road Observatory Site (EROS)

EROS was located within the ‘‘green space’’ of the University of Birmingham campus. This is an urban background site located in an open field within the university. The site is about 3.5 km southwest of the centre of Birmingham, which has a population of over one million and is part of a conurbation of 2.5 million population. The nearest anthropogenic sources are a nearby railway, some moderately trafficked roads about 500 m and other surrounding activities from the university and local residents.

- Harwell (HAR)

This rural site is located within the grounds of the Harwell Science Centre, Didcot, Oxfordshire. The Partisol air sampler was installed outside the monitoring station which is a self-contained, air conditioned housing and located within the grounds. The surrounding area is generally open with agricultural fields. There is limited activity in the area and the nearest road about 400 metres from the monitoring site is used only for access to buildings within the Science Park. The nearest trees are at a distance of 200 - 300 metres from the monitoring station. Distant sources include the busy A34 dual carriageway about 2 km to the east and the Didcot Power Station about 5 km to the north-east.

The sampling locations are shown in Figure 3.1. At both sites, the PM samples were collected daily onto quartz fibre filters by using the Partisol Plus samplers as mentioned in section 2.2.1. The sampling periods were from November 2008 to April 2011 and from July 2010 to December 2010 for EROS and Harwell, respectively.

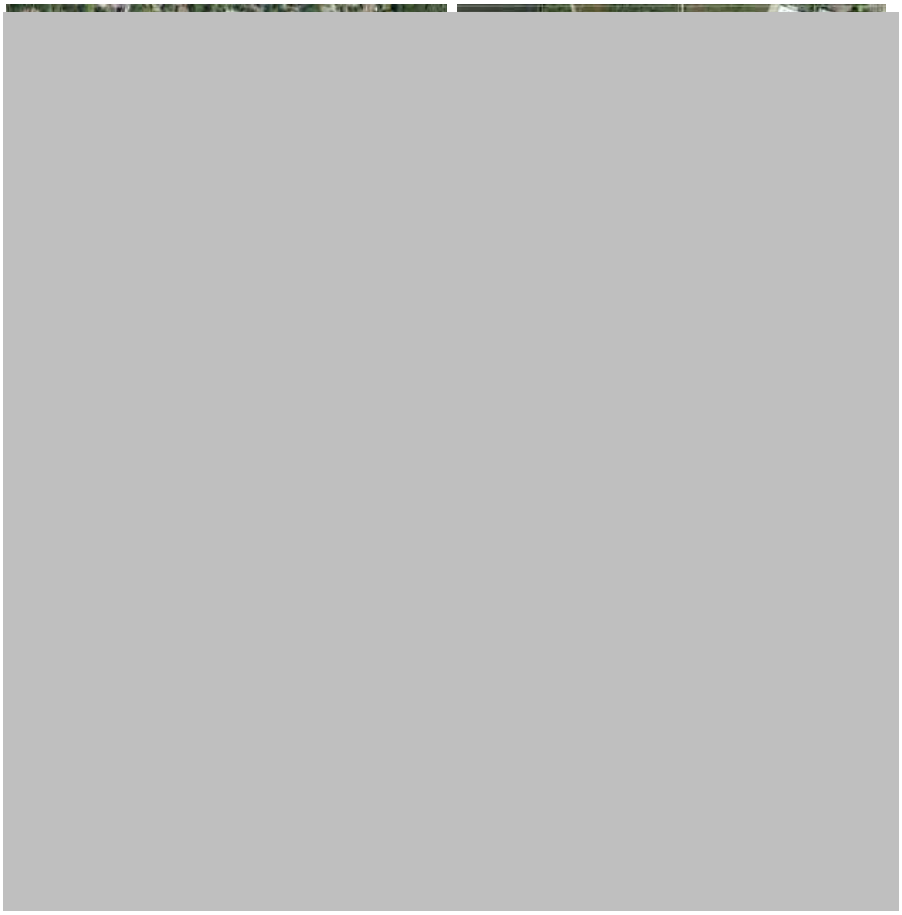

Figure 3.1 Locations of the two sampling sites in the UK; EROS and Harwell

3.3 Summary of atmospheric aerosol concentrations

A summary of the concentration data of oxalate, nitrate, sulphate, chloride, organic (OC) and elemental carbon (EC) in the $PM_{2.5}$, $PM_{2.5-10}$ and PM_{10} appears in Table 3.1. The sampling periods were split into four seasons as follow — summer is defined to comprise the months of June, July and August; autumn is September, October and November; winter is December, January and February; and spring is March, April and May. Basic statistical characteristics are shown in term of mean, median, minimum, maximum, percentile and sampling number. It needs to be noted that the data obtained from Harwell were mainly used for comparison with EROS data collected simultaneously. This interpretation will be described later in section 3.3.3. For the quality assurance, comparison of ionic species in PM collected for the thesis at Harwell with national data shows in Figure 3.4. Since 24 h aerosol samples did not collect at the same time, individual data comparison cannot be evaluated. Only monthly mean concentratios of chemical components were determined and presented.

Table 3.1 Summary of chemical composition statistics ($\mu g\ m^{-3}$) in $PM_{2.5}$, $PM_{2.5-10}$ and PM_{10} at EROS and Harwell sites for the entire period (EROS – from November 2008 to April 2011 and Harwell – from July 2010 to December 2010)

	Sampling period	N	Maximun	75%ile	Median	25%ile	Minimum	Mean
EROS								
$PM_{2.5}$								
Oxalate	Whole	500	0.34	0.06	0.03	0.01	<dl	0.05
	Summer	116	0.14	0.04	0.02	0.02	<dl	0.03
	Autumn	165	0.16	0.03	0.02	0.01	<dl	0.03
	Winter	101	0.30	0.10	0.02	0.01	<dl	0.05
	Spring	118	0.34	0.12	0.05	0.02	<dl	0.07
Nitrate	Whole	500	25.51	3.45	1.24	0.56	<dl	2.72
	Summer	116	6.83	0.86	0.56	0.41	0.19	0.92
	Autumn	165	10.88	2.33	0.99	0.54	<dl	1.75
	Winter	101	13.26	5.49	3.47	1.41	0.15	3.97
	Spring	118	25.51	5.84	2.29	0.88	0.16	4.80
Sulphate	Whole	500	9.63	2.46	1.44	0.90	0.17	1.86
	Summer	116	4.44	1.71	1.22	0.91	0.44	1.45
	Autumn	165	6.48	1.98	1.11	0.79	0.24	1.57
	Winter	101	7.49	2.88	2.00	1.02	0.31	2.25
	Spring	118	9.63	2.92	1.80	1.17	0.17	2.32
Chloride	Whole	500	4.07	0.98	0.46	0.21	<dl	0.73
	Summer	116	2.37	0.38	0.20	0.11	0.04	0.37
	Autumn	165	4.07	0.60	0.40	0.22	<dl	0.53
	Winter	101	3.29	1.86	1.17	0.50	0.09	1.25
	Spring	118	3.92	1.32	0.69	0.28	<dl	0.93

Table 3.1 *(continued)*

	Sampling period	N	Maximun	75%ile	Median	25%ile	Minimum	Mean
OC	Whole	500	18.8	3.7	2.5	1.6	<dl	3.0
	Summer	116	7.0	2.1	1.7	1.4	0.9	1.9
	Autumn	165	18.8	3.4	2.4	1.7	0.9	3.0
	Winter	101	12.1	5.9	4.3	3.1	2.0	4.9
	Spring	118	6.4	3.4	2.4	1.5	<dl	2.6
EC	Whole	500	8.2	1.4	0.8	0.5	<dl	1.1
	Summer	116	2.8	0.6	0.5	0.4	0.2	0.6
	Autumn	165	8.2	1.5	1.0	0.7	0.2	1.4
	Winter	101	8.2	2.4	1.3	0.7	<dl	1.7
	Spring	118	4.0	1.1	0.6	0.4	<dl	0.9
$PM_{2.5-10}$								
Oxalate	Whole	500	0.058	0.021	0.010	0.002	<dl	0.013
	Summer	116	0.058	0.027	0.020	0.008	<dl	0.019
	Autumn	165	0.054	0.020	0.010	0.002	<dl	0.012
	Winter	101	0.021	0.003	0.001	0.001	<dl	0.003
	Spring	118	0.049	0.023	0.016	0.008	<dl	0.016
Nitrate	Whole	500	5.27	0.90	0.53	0.33	<dl	0.73
	Summer	116	2.56	0.74	0.48	0.37	0.04	0.62
	Autumn	165	3.29	0.78	0.47	0.32	<dl	0.70
	Winter	101	1.70	0.66	0.42	0.25	<dl	0.52
	Spring	118	5.27	1.48	0.80	0.49	<dl	1.08
Sulphate	Whole	500	1.89	0.34	0.24	0.16	<dl	0.27
	Summer	116	0.55	0.26	0.20	0.15	<dl	0.21
	Autumn	165	0.89	0.34	0.22	0.15	<dl	0.26
	Winter	101	1.11	0.33	0.24	0.15	<dl	0.27
	Spring	118	1.89	0.41	0.30	0.23	<dl	0.36
Chloride	Whole	500	3.70	1.17	0.63	0.24	<dl	0.82
	Summer	116	2.37	0.77	0.37	0.19	<dl	0.53
	Autumn	165	3.52	1.26	0.78	0.35	<dl	0.92
	Winter	101	2.96	1.24	0.65	0.32	<dl	0.87
	Spring	118	3.70	1.48	0.73	0.23	<dl	0.94
OC	Whole	500	6.6	1.5	1.2	0.9	<dl	1.3
	Summer	116	5.3	1.5	1.1	0.9	<dl	1.3
	Autumn	165	6.6	1.5	1.2	1.0	<dl	1.4
	Winter	101	5.7	1.3	1.0	0.8	<dl	1.1
	Spring	118	3.8	1.5	1.2	0.8	<dl	1.2
EC	Whole	500	0.96	0.13	0.05	0.05	<dl	0.11
	Summer	116	0.23	0.08	0.05	0.05	<dl	0.07
	Autumn	165	0.86	0.17	0.05	0.05	<dl	0.14
	Winter	101	0.96	0.15	0.05	0.05	<dl	0.13
	Spring	118	0.62	0.12	0.05	0.05	<dl	0.11
PM_{10}								
Oxalate	Whole	500	0.38	0.08	0.04	0.02	0.01	0.06
	Summer	116	0.20	0.07	0.04	0.02	0.01	0.05
	Autumn	165	0.16	0.05	0.03	0.02	0.01	0.04

Table 3.1 *(continued)*

	Sampling period	N	Maximun	75%ile	Median	25%ile	Minimum	Mean
	Winter	101	0.30	0.10	0.02	0.01	0.01	0.05
	Spring	118	0.38	0.14	0.07	0.04	0.01	0.09
Nitrate	Whole	500	29.27	4.53	1.92	0.97	<dl	3.46
	Summer	116	8.35	1.69	1.09	0.82	0.28	1.54
	Autumn	165	12.49	3.37	1.48	0.95	<dl	2.44
	Winter	101	14.67	6.06	4.05	2.02	0.15	4.48
	Spring	118	29.27	7.51	3.49	1.54	0.46	5.88
Sulphate	Whole	500	11.18	2.72	1.69	1.13	0.31	2.13
	Summer	116	4.68	1.91	1.42	1.11	0.55	1.67
	Autumn	165	7.37	2.24	1.32	0.96	0.50	1.82
	Winter	101	8.11	3.27	2.21	1.32	0.31	2.52
	Spring	118	11.18	3.35	2.13	1.49	0.55	2.67
Chloride	Whole	500	7.03	2.14	1.23	0.68	0.06	1.56
	Summer	116	3.46	1.21	0.73	0.35	0.10	0.90
	Autumn	165	5.01	1.88	1.24	0.79	0.19	1.45
	Winter	101	5.40	2.72	1.95	1.17	0.21	2.12
	Spring	118	7.03				0.06	1.87
OC	Whole	500	20.9	5.3	3.6	2.7	0.9	4.3
	Summer	116	8.1	3.5	2.9	2.3	1.6	3.2
	Autumn	165	20.9	5.1	3.7	2.8	2.1	4.4
	Winter	101	16.5	7.0	5.3	4.1	2.5	6.0
	Spring	118	8.4	5.1	3.4	2.4	0.9	3.8
EC	Whole	500	8.3	1.5	0.8	0.5	0.1	1.2
	Summer	116	3.0	0.7	0.5	0.4	0.2	0.6
	Autumn	165	8.2	1.7	1.1	0.8	0.2	1.5
	Winter	101	8.3	2.5	1.4	0.8	0.1	1.8
	Spring	118	4.3	1.2	0.7	0.5	0.1	0.9
Harwell								
$PM_{2.5}$								
Oxalate	Whole	107	0.18	0.03	0.01	0.01	0.01	0.02
	Summer	57	0.11	0.03	0.02	0.01	0.01	0.02
	Autumn	50	0.18	0.02	0.01	0.01	0.01	0.02
Nitrate	Whole	107	11.65	1.21	0.58	0.35	<dl	1.29
	Summer	57	3.45	0.64	0.42	0.30	<dl	0.57
	Autumn	50	11.65	2.75	1.17	0.50	0.15	2.10
Sulphate	Whole	107	6.76	1.63	1.01	0.72	0.05	1.40
	Summer	57	3.98	1.54	0.95	0.77	0.30	1.20
	Autumn	50	6.76	2.15	1.02	0.61	0.05	1.62
Chloride	Whole	107	0.87	0.32	0.17	0.09	0.01	0.23
	Summer	57	0.82	0.20	0.11	0.08	0.01	0.17
	Autumn	50	0.87	0.43	0.23	0.16	0.01	0.30

Table 3.1 *(continued)*

	Sampling period	N	Maximun	75%ile	Median	25%ile	Minimum	Mean
OC	Whole	107	4.8	1.9	1.5	1.2	0.5	1.7
	Summer	57	2.7	1.6	1.4	1.1	0.5	1.4
	Autumn	50	4.8	2.6	1.7	1.2	0.7	2.1
EC	Whole	107	1.9	0.5	0.2	0.1	<dl	0.4
	Summer	57	0.7	0.3	0.2	0.1	<dl	0.2
	Autumn	50	1.9	0.8	0.5	0.2	0.1	0.6
$PM_{2.5-10}$								
Oxalate	Whole	107	0.05	0.03	0.02	<dl	<dl	0.02
	Summer	57	0.05	0.04	0.03	0.018	<dl	0.03
	Autumn	50	0.03	0.01	<dl	<dl	<dl	0.01
Nitrate	Whole	107	3.40	0.84	0.60	0.26	<dl	0.71
	Summer	57	1.96	0.67	0.43	0.25	<dl	0.52
	Autumn	50	3.40	1.22	0.74	0.33	<dl	0.93
Sulphate	Whole	107	2.08	0.29	0.21	0.15	<dl	0.29
	Summer	57	0.42	0.21	0.17	0.13	<dl	0.18
	Autumn	50	2.08	0.51	0.26	0.21	<dl	0.42
Chloride	Whole	107	2.60	0.85	0.46	0.21	0.04	0.61
	Summer	57	2.60	0.63	0.29	0.17	0.04	0.50
	Autumn	50	2.21	0.94	0.63	0.41	0.09	0.74
OC	Whole	107	3.3	1.2	0.9	0.8	<dl	1.0
	Summer	57	3.3	1.3	1.0	0.8	<dl	1.1
	Autumn	50	2.2	1.0	0.8	0.8	<dl	1.0
EC	Whole	107	0.5	<dl	<dl	<dl	<dl	0.1
	Summer	57	<dl	<dl	<dl	<dl	<dl	<dl
	Autumn	50	0.5	<dl	<dl	<dl	<dl	0.1
PM_{10}								
Oxalate	Whole	107	0.18	0.05	0.03	0.02	<dl	0.04
	Summer	57	0.14	0.06	0.05	0.03	<dl	0.05
	Autumn	50	0.18	0.03	0.02	0.01	<dl	0.03
Nitrate	Whole	107	14.75	2.00	1.21	0.70	0.16	2.00
	Summer	57	4.76	1.28	0.81	0.59	0.24	1.10
	Autumn	50	14.75	3.83	1.82	0.86	0.16	3.02
Sulphate	Whole	107	7.53	1.97	1.24	0.95	0.36	1.69
	Summer	57	4.14	1.76	1.13	0.96	0.40	1.38
	Autumn	50	7.53	2.55	1.33	0.94	0.36	2.04
Chloride	Whole	107	3.33	1.17	0.68	0.30	0.09	0.84
	Summer	57	3.33	0.85	0.39	0.23	0.09	0.67
	Autumn	50	3.08	1.26	0.87	0.63	0.15	1.04
OC	Whole	107	7.0	3.2	2.5	2.0	1.0	2.8
	Summer	57	4.7	2.8	2.5	2.1	1.0	2.5
	Autumn	50	7.0	3.7	2.8	2.0	1.5	3.1

Table 3.1 *(continued)*

	Sampling period	N	Maximun	75%ile	Median	25%ile	Minimum	Mean
EC	Whole	107	2.2	0.5	0.2	0.1	<dl	0.4
	Summer	57	0.7	0.3	0.2	0.1	<dl	0.2
	Autumn	50	2.2	0.9	0.5	0.2	<dl	0.6

3.3.1 Carbonaceous aerosol concentrations in urban background and rural sites

Carbonaceous aerosol consists of both EC and OC, which were also the major species of interest in this study. In the case of EC at EROS, as shown in Table 3.1, the average concentrations with estimated uncertainties of measurement were 1.1 ± 0.08 μg m^{-3}, 0.2 ± 0.01 μg m^{-3} and 1.2 ± 0.09 μg m^{-3} in $PM_{2.5}$, $PM_{2.5-10}$ and PM_{10}, respectively. For EC at HAR, the average concentrations with estimated uncertainties of measurement were 0.4 ± 0.03 μg m^{-3}, 0.2 ± 0.01 μg m^{-3} and 0.4 ± 0.03 μg m^{-3} in $PM_{2.5}$, $PM_{2.5-10}$ and PM_{10}, respectively. There is a clear higher concentration at urban background site comparing to rural site both in $PM_{2.5}$ and PM_{10} indicating that the impact of local sources contribution is very appreciable and would be expected for pollutants with anthropogenic sources. A similar EC concentration in $PM_{2.5}$ at EROS was observed in this study when compared with the previous study (Yin *et al*., 2010), showing the EC concentration at 1.41 ± 0.44 μg m^{-3}. EC observed in $PM_{2.5}$ and PM_{10} at EROS are lower than the previous results obtained in Birmingham City Centre Site (BCCS) which is a central urban background site within the city of Birmingham (Harrison and Yin, 2008). Those EC reported at 1.6 ± 1.1 μg m^{-3} and 1.7 ± 1.1 μg m^{-3} in $PM_{2.5}$ and PM_{10}, respectively. The time series, mean monthly concentrations and seasonal patterns of organic and elemental carbon at EROS and HAR are shown in Figures 3.2, 3.3 and 3.5, respectively. According to quality assurance, comparisons of mean monthly concentrations of chemical components with national network data at Harwell present in Figure 3.4.

Given the current regulatory focus on $PM_{2.5}$ and the dominant proportion of OC and EC in fine fraction (21 – 78 %) rather than in the coarse fraction, the major discussions in this section focus upon $PM_{2.5}$ (Na et al., 2004). In addition to the low level of EC in coarse fractions, the proportion of EC in $PM_{2.5-10}$ to PM_{10} contains around 17% but a rather greater proportion of the EC appeared at 92% in $PM_{2.5}$ to PM_{10}. The EC concentration measured at EROS over a year period showed the highest concentration in the winter as same as OC concentration. From the time series, it further appears that the EC levels during the summer were low as well at both sites. As EC is a primary source emission, derived from ground-

level of the incomplete combustion of fossil fuels and the pyrolysis of biological material during combustion, this behaviour is expected due to less effective dispersion processes in the colder months of the year. The NO_x data obtained from the adjacent Birmingham Tyburn site, which represents as urban background site, showed well correlated with EC concentration(*r* = 0.61). This correlations support the suggestion that at EROS, the EC derives mainly from transportation as NO_x to be a good tracer of road traffic emissions in the atmosphere of Birmingham (Harrison et al, 1997)

With regard to OC at EROS, the average concentrations with measurement uncertainties were 3.0 ± 0.22 μg m^{-3}, 1.3 ± 0.09 μg m^{-3} and 4.3 ± 0.31 μg m^{-3} in $PM_{2.5}$, $PM_{2.5-10}$ and PM_{10}, respectively. For OC at HAR, the average concentrations were 1.7 ± 0.12 μg m^{-3}, 1.0 ± 0.07 μg m^{-3} and 2.8 ± 0.20 μg m^{-3} in $PM_{2.5}$, $PM_{2.5-10}$ and PM_{10}, respectively. In the case of $PM_{2.5}$ and PM_{10}, the urban background site clearly exceeds the rural site. On the contrary, the difference is quite small between both sites for OC in coarse fractions ($PM_{2.5-10}$).

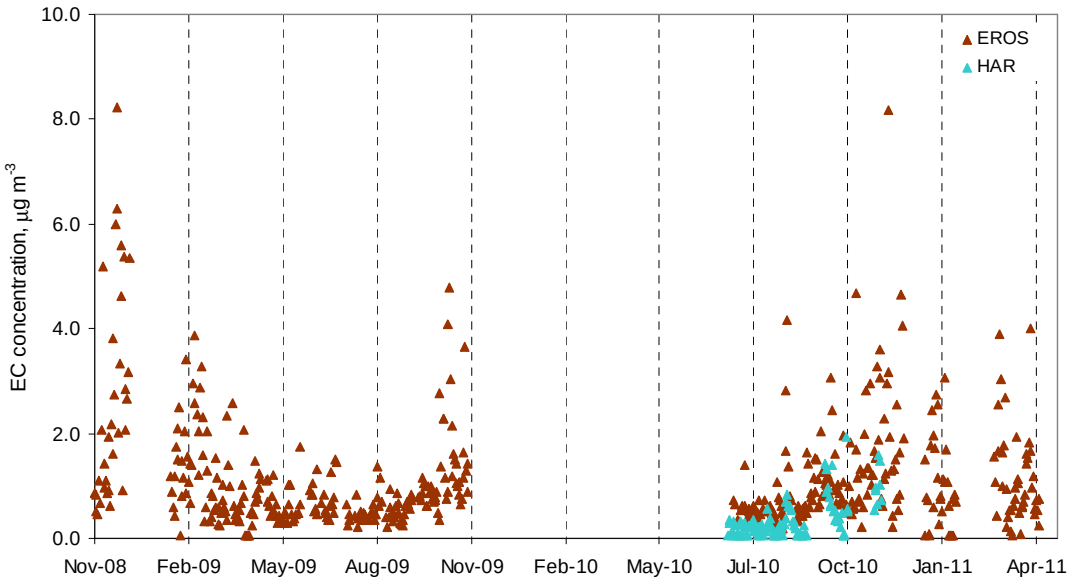

Figure 3.2 Time series of OC, EC concentrations in $PM_{2.5}$ measured at EROS and Harwell sites

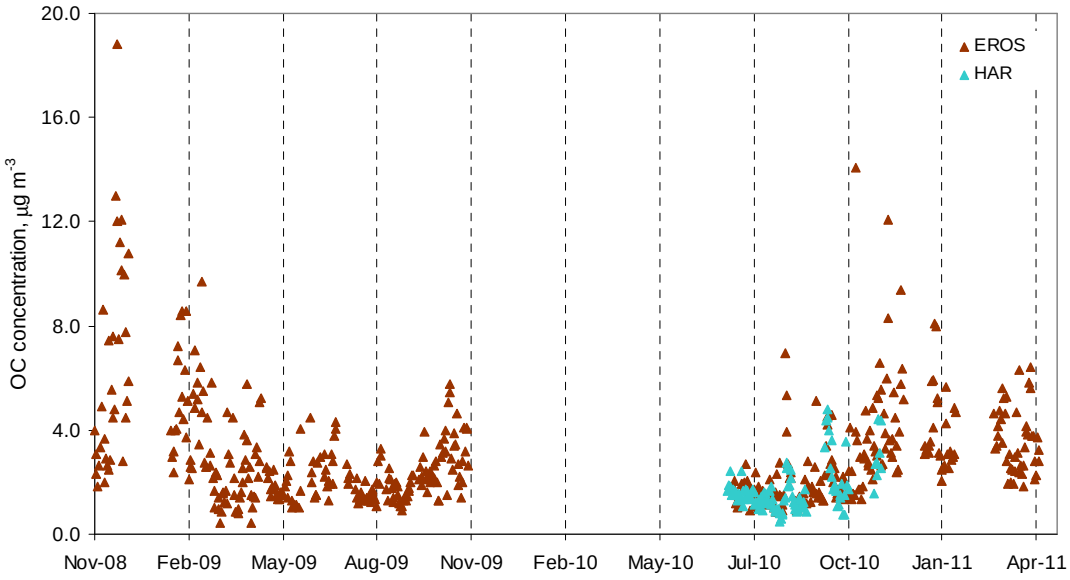

Figure 3.2 *(continued)*

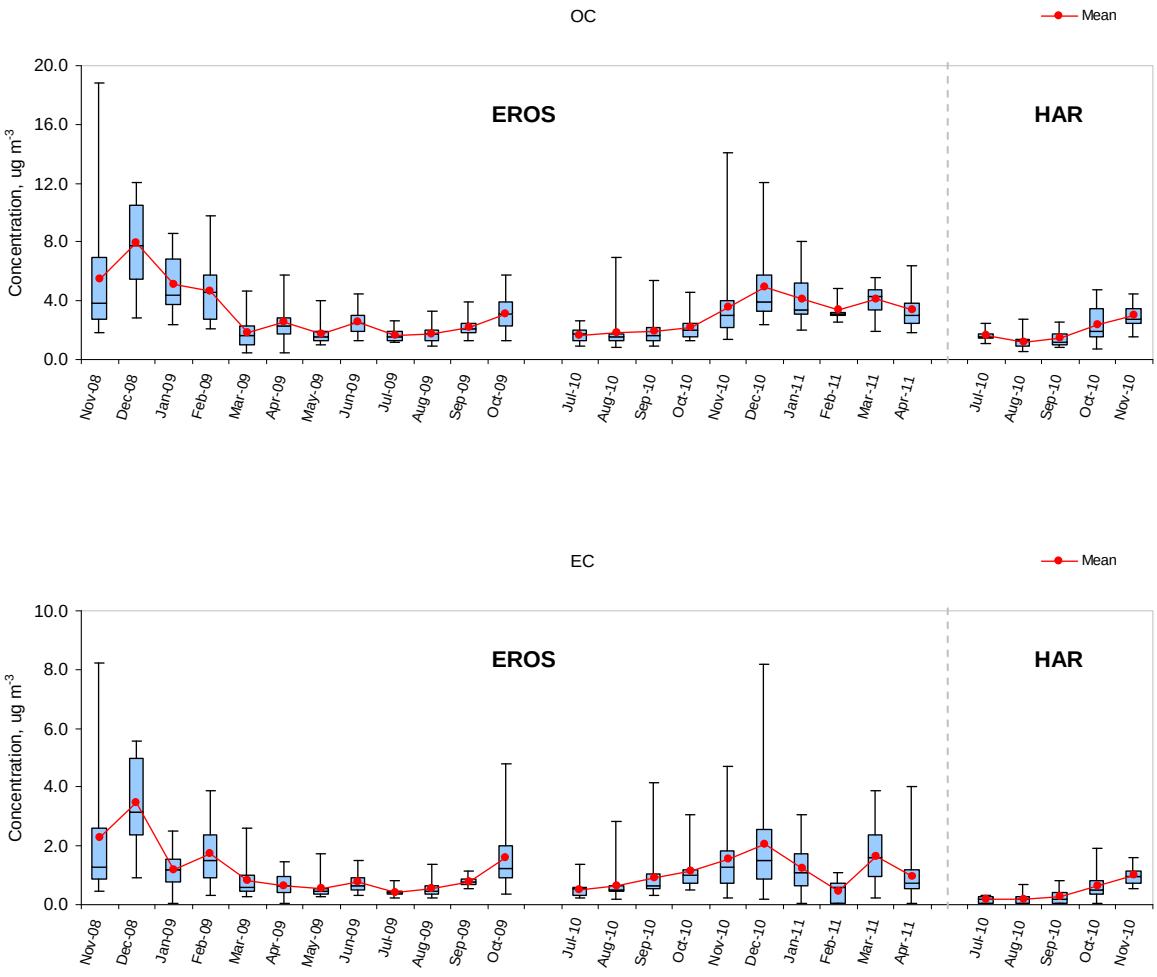

Figure 3.3 Box-whisker plots of monthly major component concentrations in $PM_{2.5}$ at EROS and Harwell sites

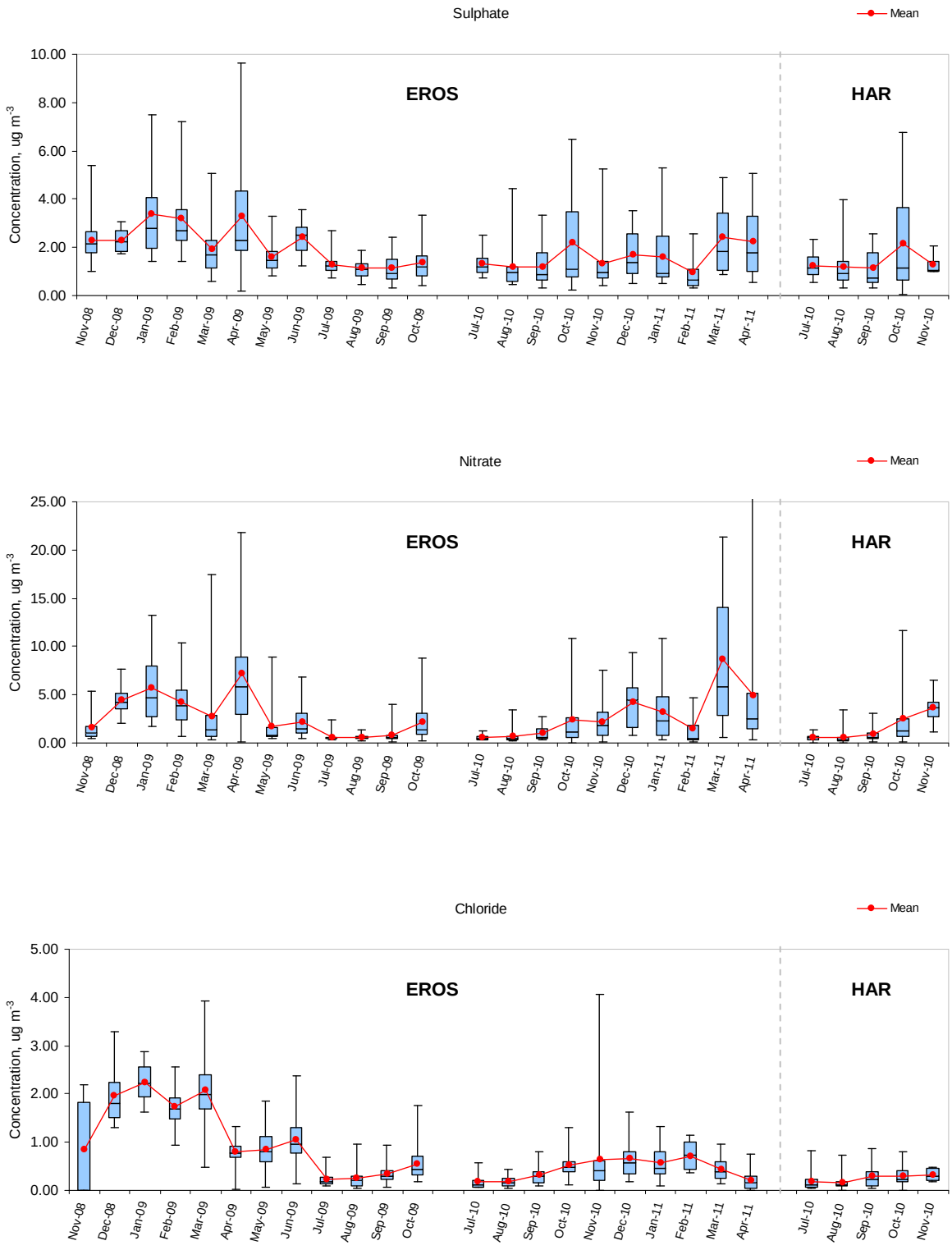

Figure 3.3 *(continued)*

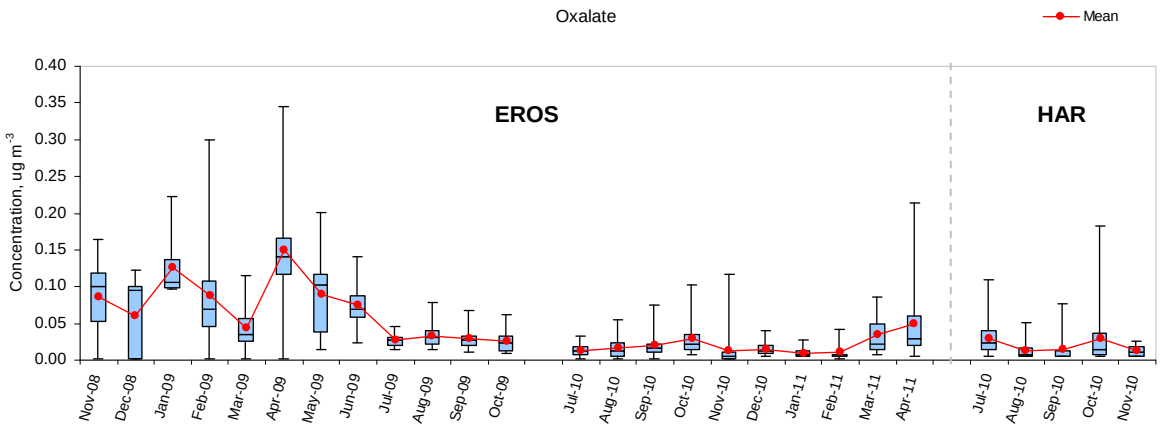

Figure 3.3 *(continued)*

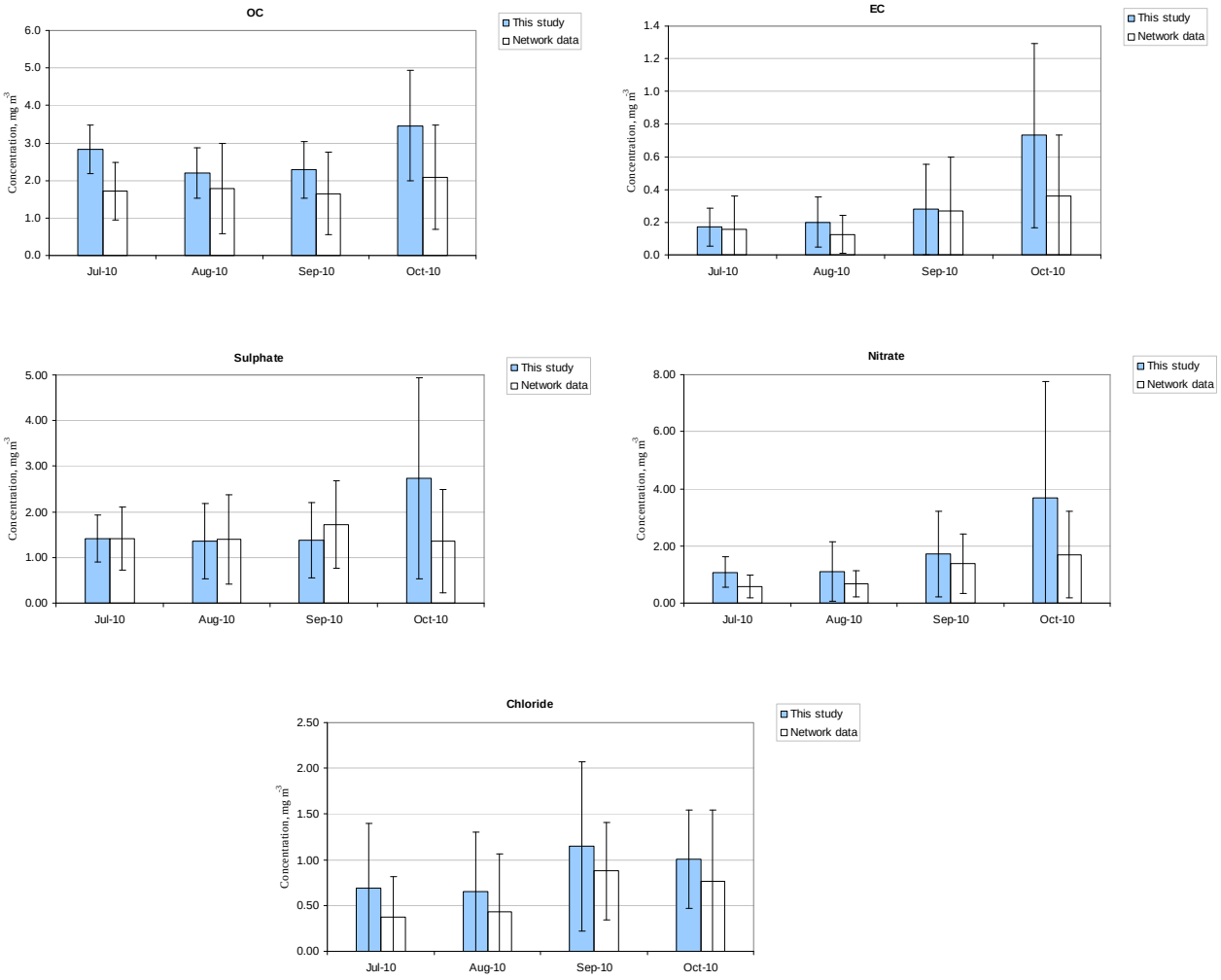

Figure 3.4 Comparisons of monthly average chemical concentrations in PM_{10} at Harwell with network data. Error bars denote standard deviations (Each individual data cannot be compared because 24h air samples did not collect at the same time)

(a)

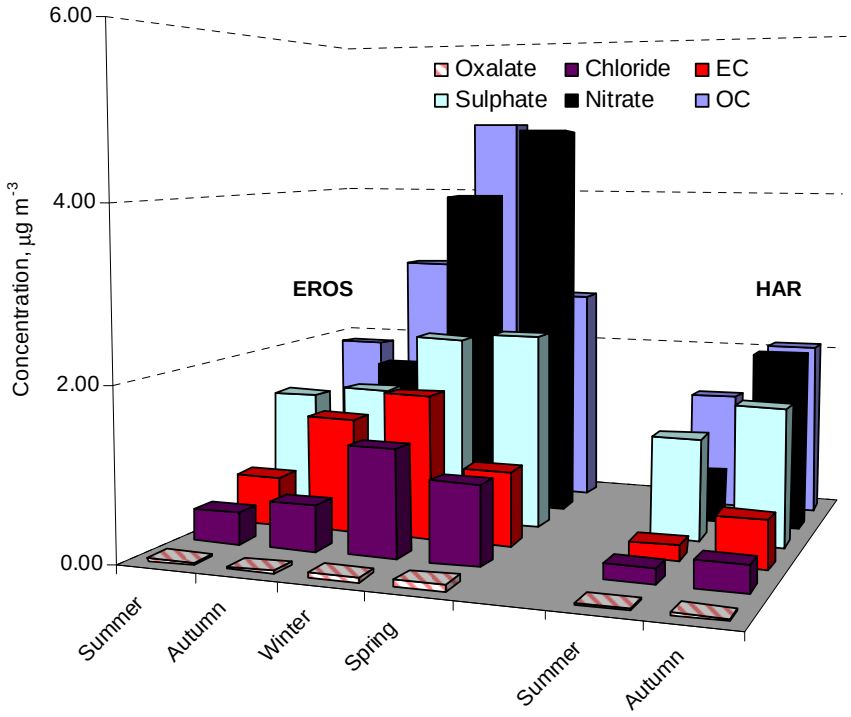

(b)

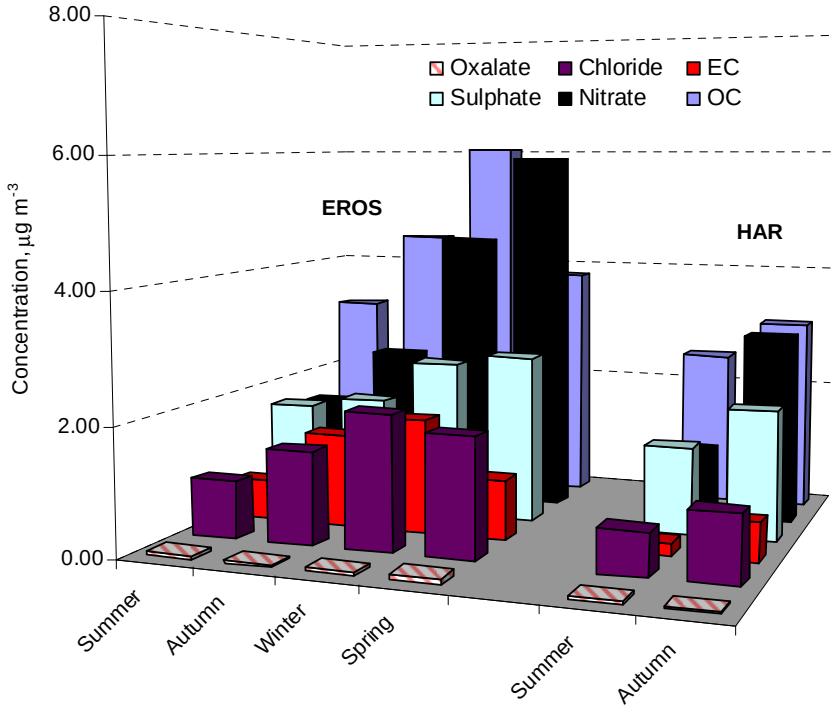

Figure 3.5 Seasonal average concentrations at EROS and Harwell site; (a) $PM_{2.5}$; (b) PM_{10}

3.3.2 Relationships between organic and elemental carbon

As mentioned in 3.3.1 that EC has only a primary origin from the burning of carbonaceous matter and is a good tracer for emissions from fossil fuel combustion namely urban emissions from road transport (EC_{ff}), OC may be emitted directly to the atmosphere in many ways (OC_{prim}) including from fossil fuel emissions (OC_{ff}), biomass burning (OC_{bb}) or biological particles or plant debris (OC_{bio}). Secondary OC (OC_{sec}) is formed when organic carbon gases are oxidised in the atmosphere to form higher polarity and therefore lower volatility reaction products that then condense and increase the mass concentration of particulate matter (Seinfeld and Pankow, 2003). The sources of carbonaceous particles can be qualitatively evaluated by finding the relationship between OC and EC concentrations. If major fractions of OC and EC are emitted by a dominant primary source, for example, road transport emission, meat cooking and biomass burning, the good correlation between OC and EC concentrations should be observed because the relative rates of EC and OC emission would be proportional to each other (Na et al., 2004). In this study, the correlations between OC and EC in $PM_{2.5}$, $PM_{2.5-10}$ and PM_{10} at EROS and Harwell sites present in Table 3.2. The good correlation relationships are found for whole data both in $PM_{2.5}$ (r = 0.83 and r = 0.86 for EROS and Harwell, respectively) and PM_{10} (r = 0.83 and r = 0.76 for EROS and Harwell, respectively). These findings suggest that OC and EC fractions at EROS and Harwell may be impacted from local vehicular emission. If the data are sorted by season, it can be seen that a poor correlation between OC and EC concentrations are observed in summer at Harwell (r = 0.48 and r = 0.33 for $PM_{2.5}$ and PM_{10}, respectively). Similar lower correlation coefficient values are seen at EROS for $PM_{2.5}$ and PM_{10} in summer comparing to winter. These indicate that the influence of other significant primary sources or OC_{sec}, which are formed in higher photochemical activity on summer days, may be related source (Strader et al., 1999).

With regard to coarse fractions ($PM_{2.5-10}$), weak correlation coefficients are observed at both sites. It is likely that the coarse OC has arisen largely from processes other than fossil fuel combustion for example, in urban areas, the mechanical wear of tyres known as a source of supermicrometer OC particles to the atmosphere (Thorpe and Harrison, 2008) including particles of biological origin like plant debris, pollen, fungal spores also accumulated in the aerosol coarse fraction (Bauer et al., 2002; Matthias-Maser and Jaenicke, 2000).

Table 3.2 Correlation coefficients (*r*) calculated between OC and EC concentration in $PM_{2.5}$, $PM_{2.5-10}$ and PM_{10} at EROS and Harwell sites

	$PM_{2.5}$	$PM_{2.5-10}$	PM_{10}
EROS			
Whole	0.83	0.50	0.83
Summer	0.75	0.37	0.60
Autumn	0.88	0.50	0.86
Winter	0.81	0.65	0.82
Spring	0.67	0.45	0.72
HAR			
Whole	0.86	0.57	0.76
Summer	0.48	n.a	0.33
Autumn	0.88	0.52	0.85

The study of relationship between OC and EC mainly used to distinguish OC_{prim} from OC_{sec} in atmospheric particles. This classical method is based on the minimum values of OC/EC ratios and the concentration of OC_{sec} is estimated from the following equation;

$$OC_{\text{sec}} = OC_{total} - (OC/EC)_{\min} \times EC \qquad \text{(Equation 3.1)}$$

where

$$OC = OC_{\text{sec}} + OC_{ff} + OC_{bb} + OC_{bio} \qquad \text{(Equation 3.2)}$$

and

$$EC = EC_{ff} + EC_{bb} \qquad \text{(Equation 3.3)}$$

As recently studied by Pio *et al*. (2011), the OC/EC ratio could be represented as

$$(OC/EC)_{\min} \approx OC_{ff} / EC_{ff} \qquad \text{(Equation 3.4)}$$

Under this assumption, the urban areas, principally during winter and the periods of low photochemical activity, the contributions of OC_{bb}, OC_{bio}, and the OC_{sec} to the OC aerosol fraction may be unimportant, allowing the following simplification; $OC \approx OC_{ff}$ and $EC \approx EC_{ff}$.

In this study, aerosol samples were collected onto quartz filter and it is found that OC concentration measured at both sites did not show zero value as presented in Figure 3.6. This is probably because there will always be some secondary OC present in atmosphere, even when EC concentration are zero. The OC/EC minimum ratio calculated by this method is also

influenced by sampling artifacts as well as variability of sampling location, meteorology and uncertainty of OC and EC measurement. The adsorption of organic gases referred to a positive artefact could result in the overestimation of particulate OC concentrations because the adsorbed organics contribute to the total carbon in samples during filter analysis. On the contrary, a negative artefact is due to evaporation of organic particles during sample collection. The evaporation of collected particles may result in the underestimation of OC concentrations (Kirchstetter et al., 2001; Fitz, D.R., 1990). Since the OC/EC minimum lines estimated passed through the origin, the artefacts would be negligible and only the analytical uncertainty was evaluated in this study. This is because if there is an OC artifact, the minimum line would not go through the origin as there would always be OC in samples with no EC. The uncertainty of OC/EC minimum ratios was estimated based on propagation of error and calculated by the square root of the sum of the squares of individual measurement uncertainty of OC and EC. These uncertainties were from repeatability, sensitivity, calibration of OC/EC analyser by standard solutions and uncertainty in the volume of particle steam. The measurement uncertainties for OC and EC analysis are calculated and estimated approximately 7.2% as detailed in Appendix A, then each data points has uncertainty, u_i, of

$$u_i = \sqrt{u(OC)^2 + u(EC)^2} \qquad \text{(Equation 3.5)}$$

where, $u(OC)$ and $u(EC)$ are the uncertainties of OC and EC analysis, respectively. Therefore, uncertainty of OC/EC line, $u(\frac{OC}{EC})$, calculated as;

$$u\left(\frac{OC}{EC}\right) = \sqrt{\sum_{i=1}^{n} u_i^2} \qquad \text{(Equation 3.6)}$$

where, *n* is the number of samples

The plots of OC versus EC at EROS give the OC/EC minimum ratio with uncertainties of 0.75 ± 0.05 for $PM_{2.5}$ and 1.20 ± 0.10 for PM_{10} (Figure 3.6). These observed OC/EC ratios are consistent with results reported by Pio *et al*. (2011) for urban background conditions of large urban areas (0.6 – 0.8 in $PM_{2.5}$) but a higher OC/EC ratio estimated for PM_{10} (0.8 – 1.1). The OC/EC ratio observed in PM_{10} was higher than those in $PM_{2.5}$ indicate that EC was only associated with incomplete combustion processes, which released into the atmosphere carbonaceous compounds mainly in the form of submicron particles (Smekens et al., 2005).

On the contrary, the OC/EC ratio at HAR showed very high values (1.80 ± 0.03 and 2.15 ± 0.05 for $PM_{2.5}$ and PM_{10}, respectively) as normally observed with the samples from remote and rural areas. In order to determine primary and secondary OC, the minimum OC/EC ratio value of 0.7 was used for $PM_{2.5}$ at HAR and 1.0 for PM_{10} at both sites as giving higher confidence because those ratios derived from many data located in different sites across Europe. Those results concluded that the pattern of the OC/EC minimum ratio decreased and represented by the best fit line of a minimum stable value at high EC median concentration (0.7 and 1.0 for $PM_{2.5}$ and PM_{10}, respectively) (Pio et al., 2011). The results of OC_{prim} and OC_{sec} for all data and seasonal calculated based on these minimum OC/EC ratios for $PM_{2.5}$ and PM_{10} appear in Table 3.3. Changes of OC/EC minimum ratio affect the estimation of OC_{sec} as shown in Figure 3.7. Positive and negative sampling artifacts observed for the OC concentration introduce additional uncertainty in the estimation of secondary OC. There may be other possibility to obtain a higher OC/EC ratio such as the contribution of OC from primary sources other than fossil fuel combustions in urban environment. Unfortunately, there were no measurement data for positive artefacts in this study. However, the influence of OC artefacts on the estimates of primary and secondary OC were evaluated based on the measurement uncertainty associated with OC/EC ratio. OC artefacts affected the concentration of primary and secondary OC in $PM_{2.5}$ around 7% and 3%, respectively. At EROS site, the whole mean secondary OC concentrations were 2.2 ± 0.8 μg m^{-3} and 3.1 ± 1.6 μg m^{-3} for $PM_{2.5}$ and PM_{10}, respectively. As expected in rural area, the OC_{sec} concentrations were observed lower at Harwell sits (1.5 ± 0.7 μg m^{-3} for $PM_{2.5}$ and 2.4 ± 0.8 μg m^{-3} for PM_{10}).

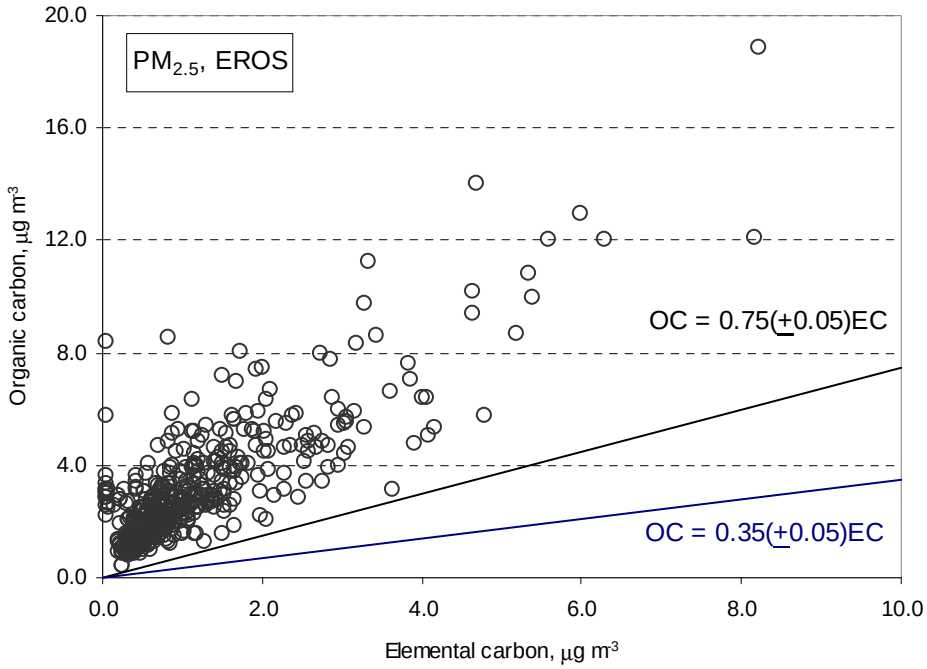

Figure 3.6 Relationships of organic carbon to elemental carbon in $PM_{2.5}$ and PM_{10} at EROS and HAR sites

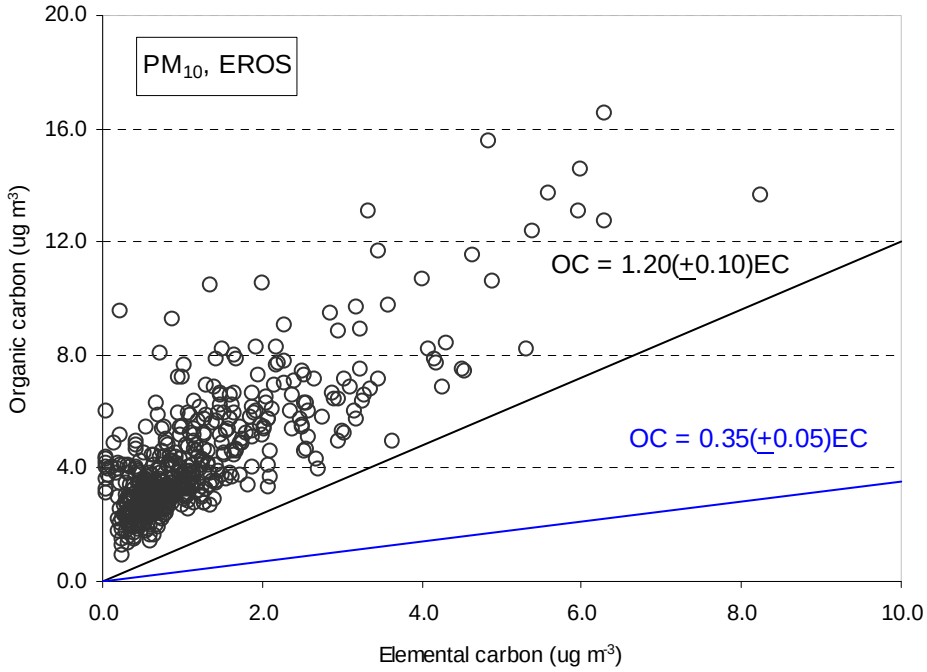

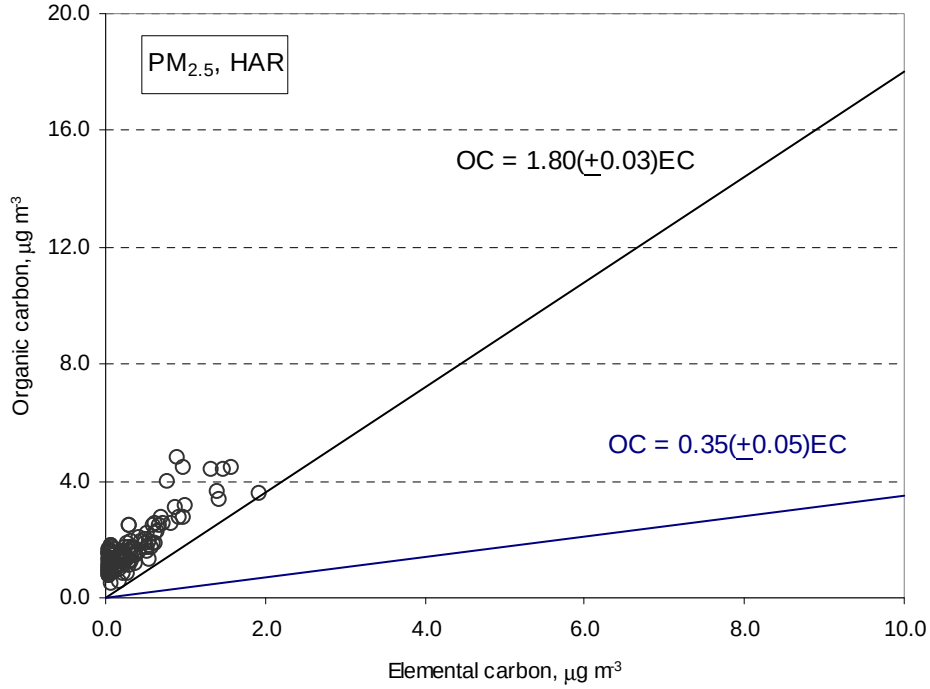

Figure 3.6 *(continued)*

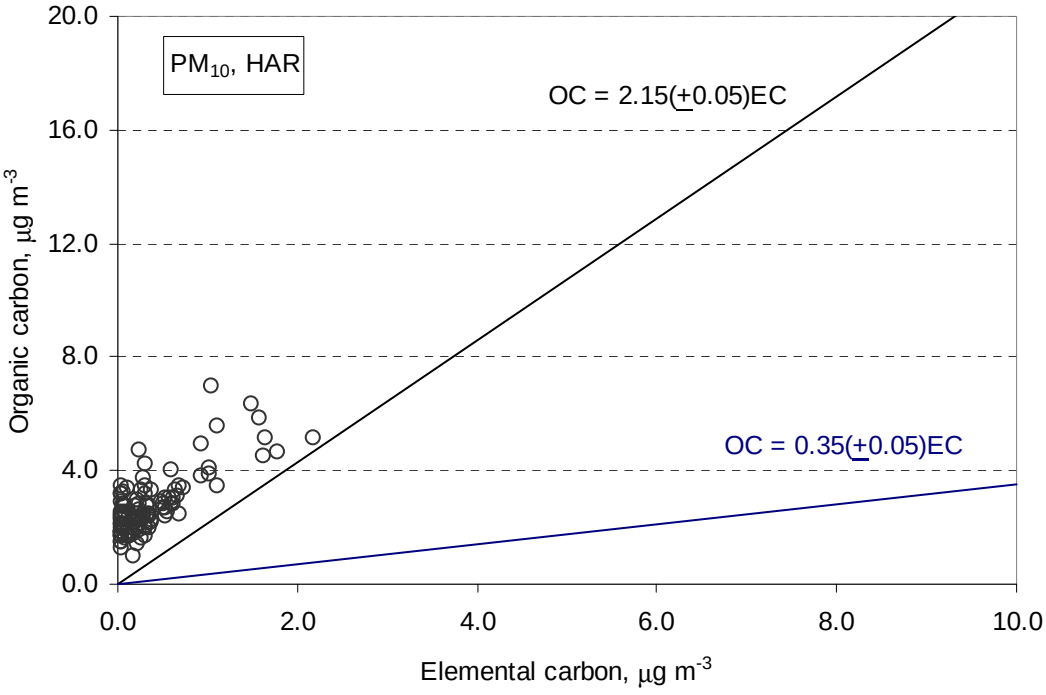

Figure 3.6 *(continued)*

Table 3.3 Primary and secondary OC concentrations (μg m^{-3}) based on the common minimum OC/EC ratio in $PM_{2.5}$ and PM_{10} at EROS and HAR sites

Sampling site	Season	N	Secondary OC		Primary OC	
			Mean ± S.D.	Range	Mean ± S.D.	Range
$PM_{2.5}$*						
EROS	Whole	500	2.2 ± 0.8 (71)	0.2 – 12.7	0.9 ± 0.8	<dl – 6.2
	Summer	116	1.4 ± 0.7 (78)	0.6 – 5.7	0.4 ± 0.3	0.1 – 2.1
	Autumn	165	2.0 ± 1.6 (67)	0.3 – 12.7	1.0 ± 0.9	0.2 – 6.2
	Winter	101	3.6 ± 1.7 (73)	1.3 – 8.7	1.3 ± 1.1	<dl – 6.1
	Spring	118	2.0 ± 1.1 (74)	0.2 – 5.7	0.7 ± 0.5	<dl – 3.0
HAR	Whole	107	1.5 ± 0.7 (83)	0.5 – 4.2	0.3 ± 0.3	<dl – 1.3
	Summer	57	1.3 ± 0.4 (93)	0.5 – 2.2	0.1 ± 0.1	<dl – 0.5
	Autumn	50	1.7 ± 0.9 (81)	0.7 – 4.2	0.4 ± 0.3	<dl – 1.3
PM_{10}**						
EROS	Whole	500	3.1 ± 1.6 (72)	0.6 – 12.7	1.2 ± 1.1	0.1 – 8.3
	Summer	116	2.5 ± 1.0 (81)	1.2 – 7.3	0.6 ± 0.4	0.2 – 3.0
	Autumn	165	3.0 ± 1.6 (67)	1.2 – 12.7	1.5 ± 1.2	0.2 – 8.2
	Winter	101	4.2 ± 1.8 (70)	1.5 – 10.2	1.8 ± 1.5	0.1 – 8.3
	Spring	118	2.9 ± 1.3 (76)	0.6 – 6.5	0.9 ± 0.8	0.1 – 4.3
HAR	Whole	107	2.4 ± 0.8 (86)	0.8 – 5.9	0.4 ± 0.4	<dl – 2.2
	Summer	57	2.3 ± 0.7 (92)	0.8 – 4.5	0.2 ± 0.1	<dl – 0.7
	Autumn	50	2.5 ± 0.9 (81)	1.4 – 5.9	0.6 ± 0.5	0.1 – 2.2

Note : Percentage of secondary OC in brackets.
* $(OC/EC)_{min}$ = 0.75 for EROS and $(OC/EC)_{min}$ = 0.70 for Harwell
** $(OC/EC)_{min}$ = 1.0 at both sites

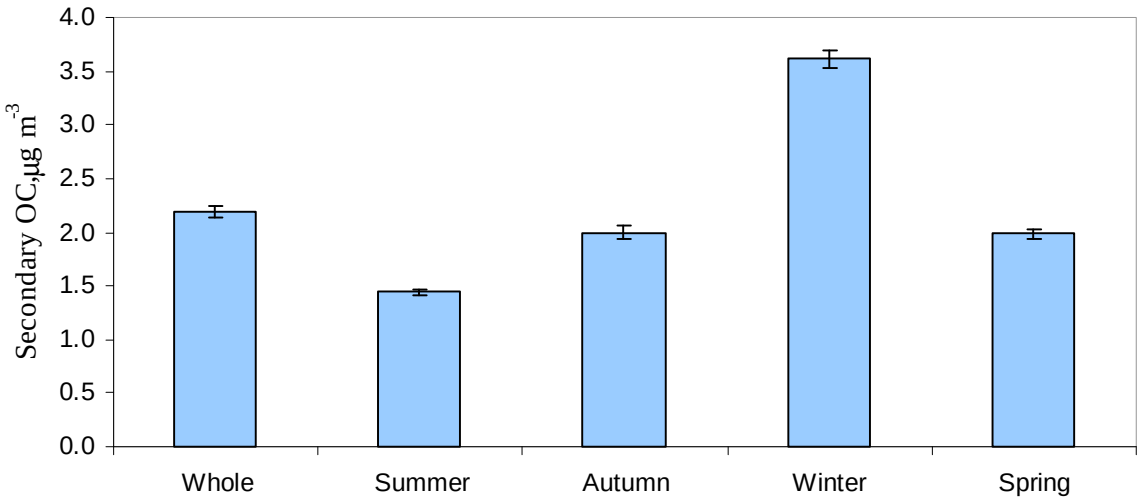

Figure 3.7 Secondary organic carbon in $PM_{2.5}$ at EROS estimated using the OC/EC ratio of 0.75, while the error bars represent a range of the OC/EC ratio from 0.70 to 0.80

However, secondary OC concentration estimates by EC/OC ratio remained uncertain. Pio et al. (2011) investigated by setting further experiment to evaluate and compare the represent of OC/EC minimum ratio obtained from these parameters. The results indicate that the OC/EC minimum ratios by this method overestimated the direct emissions of OC_{ff} from road

transport. This additional OC may be contributed from OC_{sec}, other OC_{prim} sources than fossil fuel combustion and biomass burning; and evaporation, oxidation and condensation processes affecting organic aerosol loadings and composition in the atmosphere. Therefore, the recommended OC/EC minimum ratio, which reflected the composition of vehicle combustion emissions, was in the range of 0.3 – 0.4. Table 3.4 summarises the OC_{prim} and OC_{sec} in $PM_{2.5}$ and PM_{10} calculated based on the OC/EC ratio of 0.35 (±0.05). As appeared in this study, the calculated OC_{sec} concentrations in $PM_{2.5}$ slightly increased about 18% and 7% at EROS and HAR sites, respectively. In consistent with the higher OC_{sec} concentrations in PM_{10} were observed about 26% and 8% at EROS and HAR sites, respectively. These suggest that there are a few more organic compounds from other sources mainly occurred by secondary formation in the atmosphere and the impact of sources unrelated to local vehicular emissions. The discussions on OC_{prim} and OC_{sec} in following section mainly refer to the concentration calculated based on the OC/EC ratio of 0.35. As application of this method of OC/EC minimum ratio, OC_{prim} anticipated the same marked inter-seasonal as those in EC. The winter showed the highest OC_{prim} concentration in $PM_{2.5}$ at 0.6 ± 0.5 μg m^{-3} and the lowest in summer at 0.2 ± 0.1 μg m^{-3} for EROS. This behaviour was consistent with the relationship between EC and OC_{prim} and the inverse of the daily mean temperature as plotted in Figure 3.8. There is some scatter but EC and OC_{prim} show more a good fit to a linear regression especially at EROS (R^2 = 0.37). This temperature dependence could be explained by greater atmospheric stability and lower mixing depths at lower temperatures leading to poorer dispersion characteristics for the primary pollutants. Referring to the sampling in cold months, atmospheric stability was evaluated following Pasquill stability classes (Pasquill, 1961). The Pasquill stability categories originally defined as extremely unstable (A), moderately unstable (B), slightly unstable (C), neutral (D), slightly stable (E) and stable (F) conditions. These categories are deteminded from wind speed (at 10 m height above ground) and incoming insolation as controlling parameters. The Pasquill stability classes were roughly estimated during air sampling in midwinter (22 samples in January 2011). The results show that most stability classes appeared in neutral condition (D) during night time and in slightly unstable condition (C) during daytime with the wind speed range 1.4 – 6.7 m s^{-1}, suggesting a good atmospheric stability and poor dispersion of pollutants in lower temperature. The plots of sulphate and nitrate versus mean temperature also include in Figure 3.6 in order to support the assumption of volatile loss during the high temperature. Nitrate shows the better correlation with inverse temperature than suphate at both sites as the loss of ammonium nitrate in the high temperature condition and the relative low temperature favouring

ammonium nitrate formation (Allen et al., 1989). It is likely that OC_{sec} and nitrate appear to increase as temperature decreases (for EROS, $R^2 = 0.39$ and $R^2 = 0.24$, respectively). OC_{sec} concentration data presented much higher in winter at EROS (4.3 ± 2.0 μg m^{-3} and 5.4 ± 2.4 μg $m^{-3}$for $PM_{2.5}$ and PM_{10}, respectively) than those in summer (1.7 ± 0.8 μg m^{-3} and 3.0 ± 1.1 μg m^{-3} for $PM_{2.5}$ and PM_{10}, respectively). These results are against the assumption of the contribution of lower photochemical reaction in the atmosphere during winter. The atmospheric mixing depths are also used to explain as the lower mixing depth during the winter may contribute to the higher concentrations of OC_{sec}. The accumulation of OC_{sec} precursors and the acceleration of OC_{sec} formation could be observed in the low mixing depth conditions especially in the winter (low temperature). In the previous study by Strader et al. (1999) on modeling the secondary organic aerosol formation, decreasing the mixing depth by a factor of 2 resulted in an increase in the maximum OC_{sec} concentration by 60%. On the other hand, increasing the mixing depth by a factor of 2 resulted in a decrease in maximum OC_{sec} concentration by 45%. The behaviour of OC_{sec} is closer to nitrate than that of sulphate so that it is probably the temperature dependence equilibrium between particulate and vapour phase which is driving the temperature dependence of concentration. These results are strongly supportive of the previous conclusion reported by Harrison and Yin (2008).

Table 3.4 Primary and secondary OC concentrations (μg m^{-3}) based on the minimum OC/EC ratio in $PM_{2.5}$ and PM_{10}, $(OC/EC)_{min} = 0.35$

Sampling site	Season	N	Secondary OC		Primary OC	
			Mean ± S.D.	Range	Mean ± S.D.	Range
$PM_{2.5}$ *						
EROS	Whole	500	2.6 ± 1.8 (87)	0.3 – 16.0	0.4 ± 0.4	<dl – 2.9
	Summer	116	1.7 ± 0.8 (89)	0.7 – 6.4	0.2 ± 0.1	0.1 – 1.0
	Autumn	165	2.5 ± 0.8 (83)	0.8 – 16.0	0.5 ± 0.8	0.1 – 2.9
	Winter	101	4.3 ± 2.0 (88)	1.7 – 10.1	0.6 ± 0.5	<dl – 2.9
	Spring	118	2.3 ± 1.2 (88)	0.3 – 5.9	0.3 ± 0.3	<dl – 1.4
HAR	Whole	107	1.6 ± 0.8 (94)	0.5 – 4.5	0.1 ± 0.1	<dl – 0.7
	Summer	57	1.3 ± 0.4 (93)	0.5 – 2.5	0.1 ± 0.0	<dl – 0.2
	Autumn	50	1.9 ± 1.0 (90)	0.7 – 4..5	0.2 ± 0.2	<dl – 0.7
PM_{10} **						
EROS	Whole	500	3.9 ± 2.1 (91)	0.8 – 18.0	0.4 ± 0.4	<dl – 2.9
	Summer	116	3.0 ± 1.1 (94)	1.4 – 7.8	0.2 ± 0.1	0.1 – 1.1
	Autumn	165	3.9 ± 2.2 (89)	1.9 – 18.0	0.5 ± 0.4	0.1 – 2.9
	Winter	101	5.4 ± 2.4 (90)	2.2 – 14.3	0.6 ± 0.5	<dl – 2.9
	Spring	118	3.5 ± 1.6 (92)	0.8 – 7.4	0.3 ± 0.3	<dl – 1.5
HAR	Whole	107	2.6 ± 1.0 (96)	0.9 – 6.6	0.1 ± 0.1	<dl – 0.8
	Summer	57	2.4 ± 0.7 (96)	0.9 – 4.7	0.1 ± 0.0	<dl – 0.2
	Autumn	50	2.9 ± 1.2 (94)	1.4 – 6.6	0.2 ± 0.2	<dl – 0.8

Note: Percentage of secondary OC in brackets.

In order to evaluate the contribution of road transport to OC_{prim} and OC_{sec} at both sites, correlation analysis was applied to all data between OC_{prim} and OC_{sec} with nitrogen oxides (NO_x (NO_x = NO + NO_2)). NO_x is formed by the combustions of fuels used in power generation, domestic heating and traffic and are mainly emitted as nitric oxide (NO). NO reacts with ozone (O_3) in the atmosphere to form NO_2 known as secondary NO_2. Primary NO_2 emissions are also important and directly emitted from diesel vehicles (especially when moving slowly), and can make up as much as 25% of the total NO_x emissions from this source (AQEG, 2004). In this study, NO_x data obtained from Harwell and the Birmingham Tyburn site were used as the marker for road traffic. The relationships between OC_{prim} and OC_{sec} with NO_x were investigated and the results show a significant correlation for $PM_{2.5}$ (for Harwell, r = 0.71 and r = 0.67 for OC_{prim} and OC_{sec}, respectively and for EROS, r = 0.61 and r = 0.45 for OC_{prim} and OC_{sec}, respectively). As would be anticipated, the good relationships between OC_{prim} and NO_x were found at both sites.

With regard to OC_{sec}, these results are in agreement with local transport being the most important source of OC_{sec} as well because good correlations of OC_{sec} with NO_x were observed in this study. Therefore, the origin of OC in aerosol particle measured in these conditions (low photochemical activity, minor contribution of primary sources from OC_{bb} and OC_{bio}) may contain OC_{ff} plus complementary OC resulting probably from gas-to-particle condensation of freshly emitted anthropogenic VOCs and their oxidation products and OC_{sec} formed from VOCs emitted by vegetation, OC_{bio} and/or biomass burning, OC_{bb}.(Jones and Harrison, 2005; Gelencser, et al., 2007).

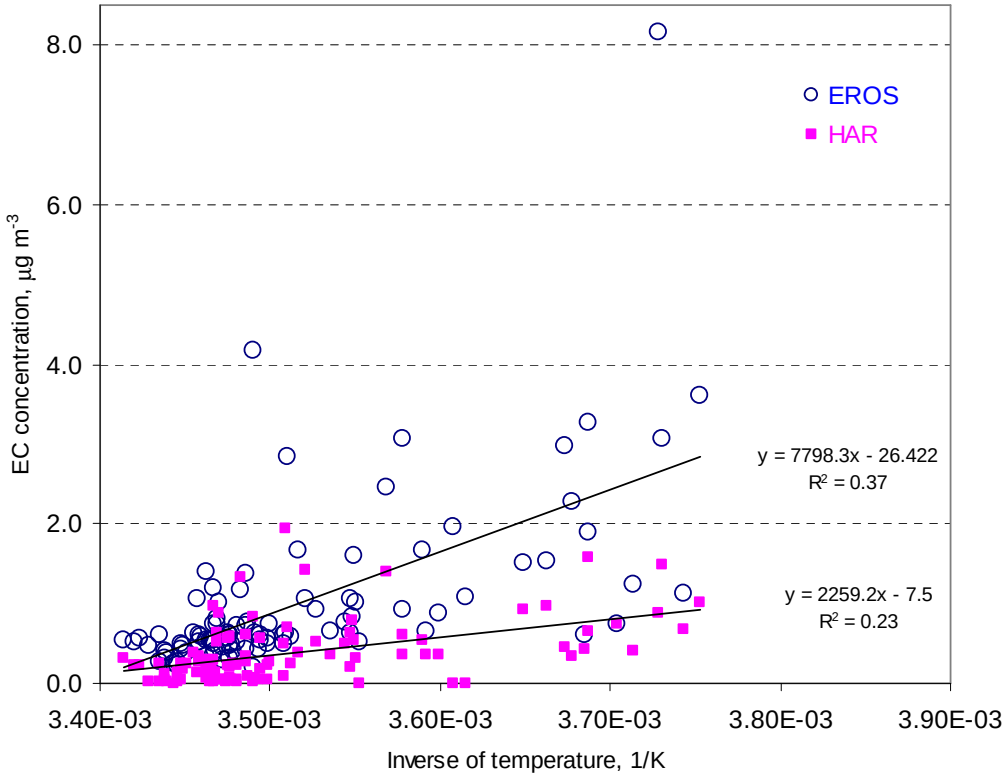

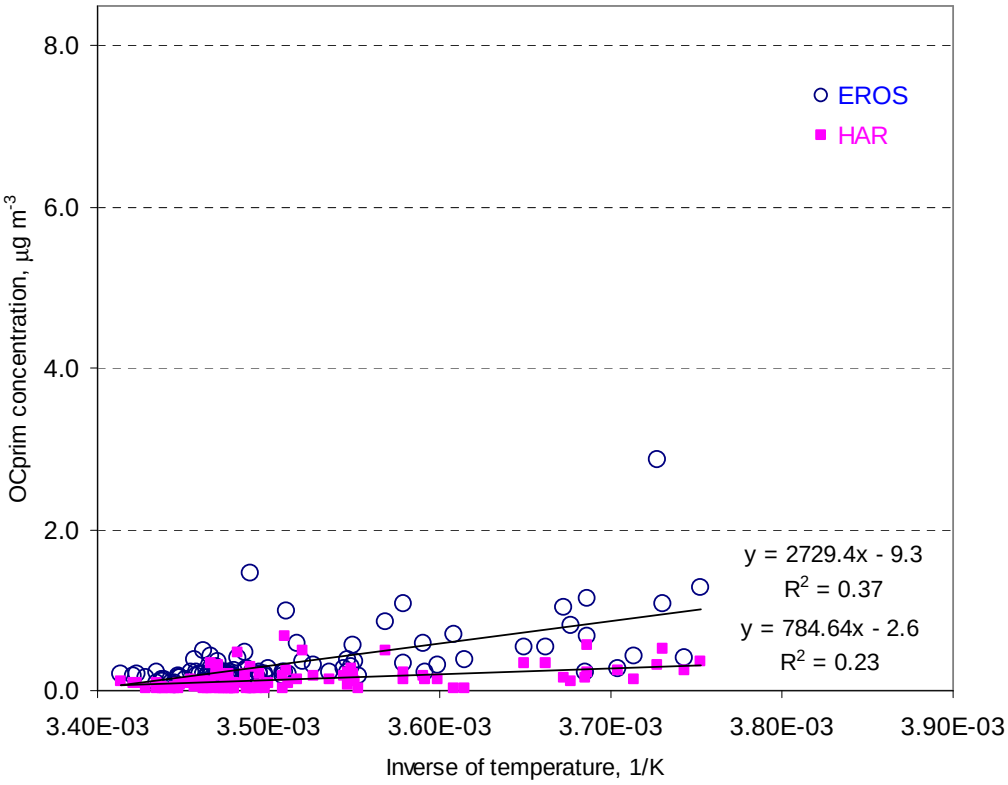

Figure 3.8 Plots of EC, OC_{prim}, OC_{sec}, sulphate and nitrate in $PM_{2.5}$ versus daily mean temperature (1/K) at EROS and HAR sites collected simultaneously

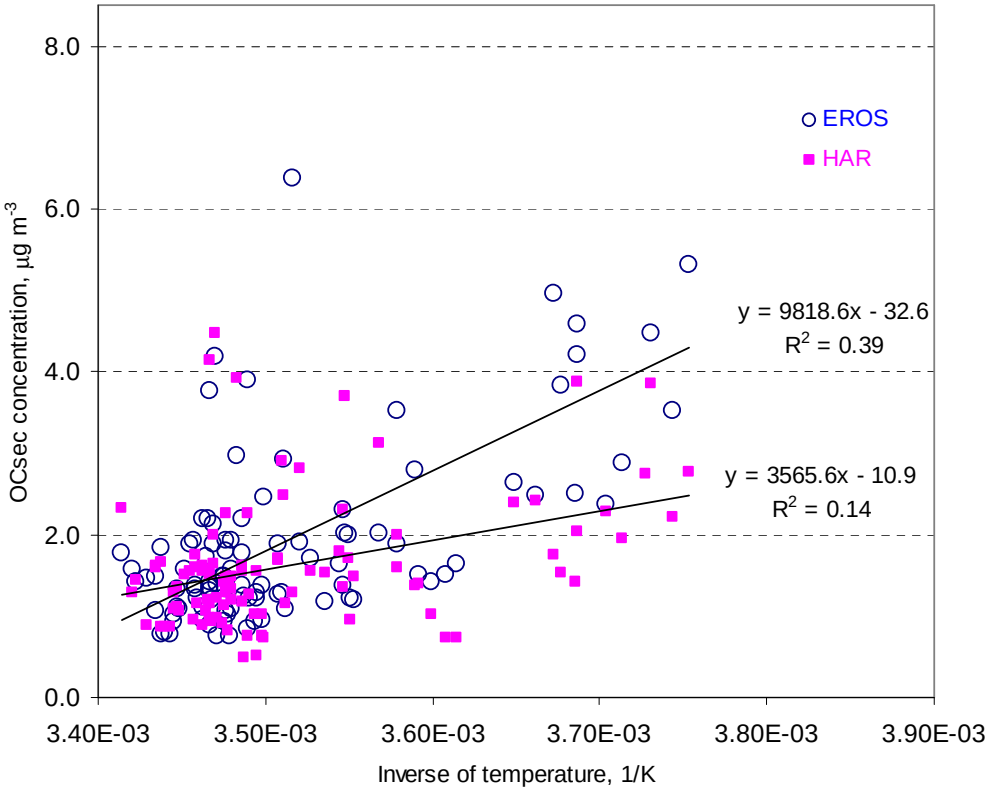

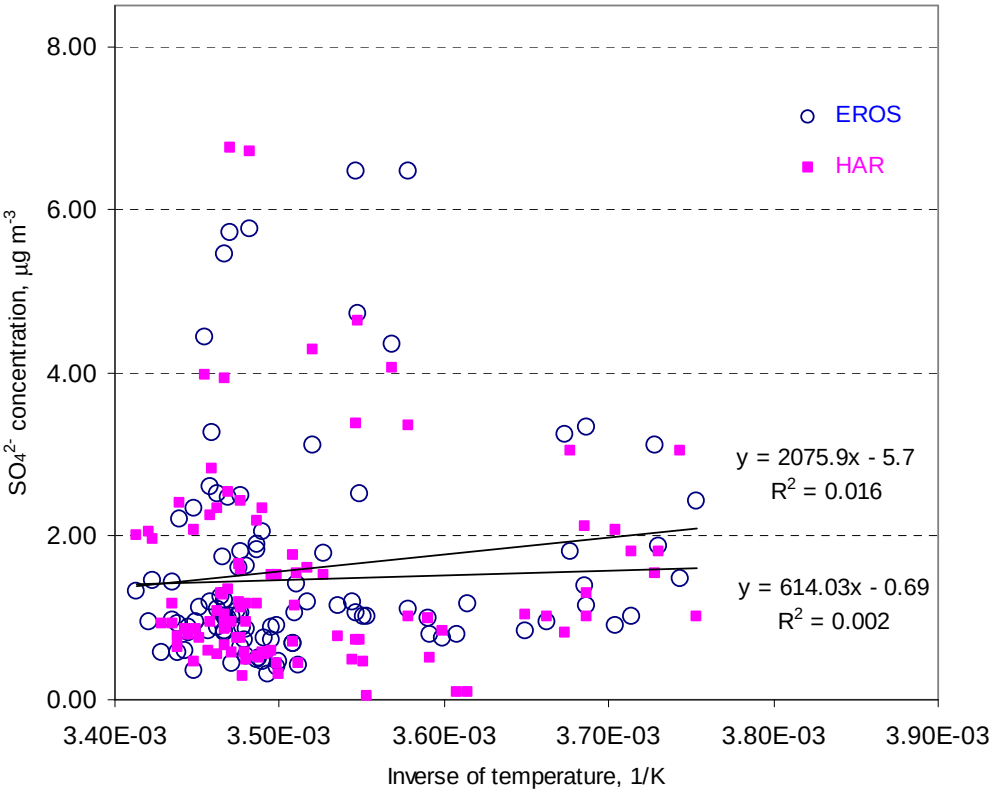

Figure 3.8 *(continued)*

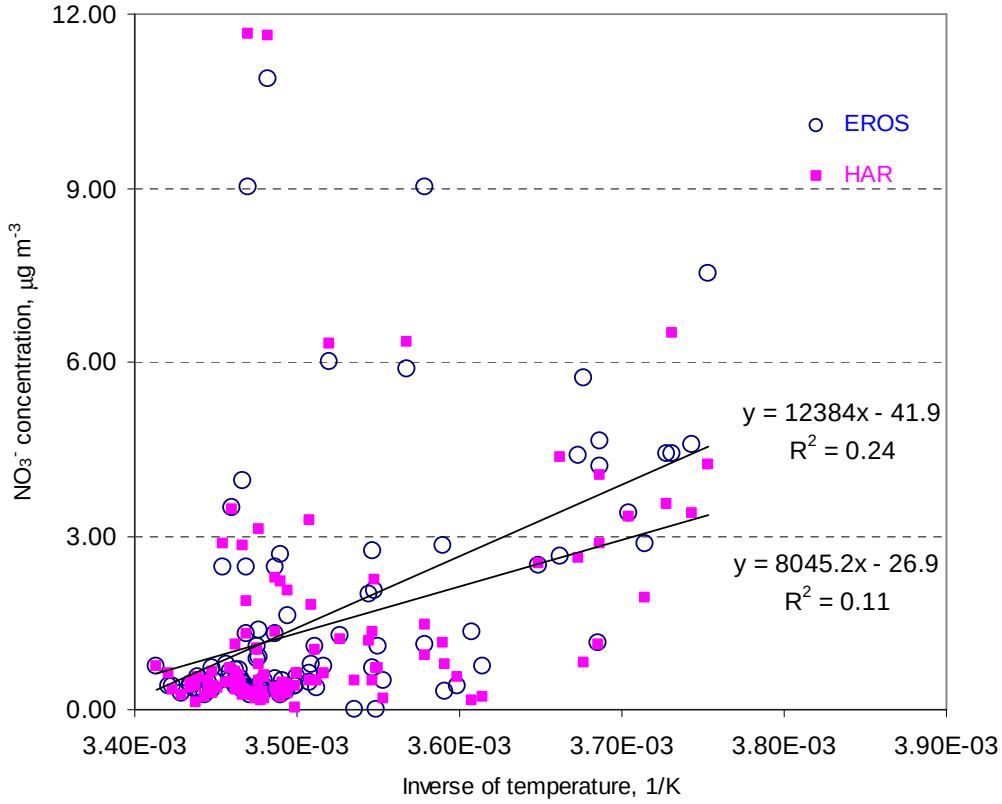

Figure 3.8 *(continued)*

The seasonal variation of secondary OC was observed from data obtained in $PM_{2.5}$ at EROS site (Figure 3.9). During the study period, the OC_{sec} concentrations varied markedly from month to month and there did not appear to strong seasonality of OC_{sec}. It needs to be cautioned for the interpretation of OC_{sec} concentrations as there were only 9, 11 and 12 air samples collected in February 2011, December 2008 and January 2009, respectively. However, it is observed that the proportions of OC_{sec} to total OC are highest in summer month for $PM_{2.5}$ and PM_{10} both in EROS and HAR sites (89% and 93% for $PM_{2.5}$ at EROS and HAR, respectively and 94% and 96% for PM_{10} at EROS and HAR, respectively) (Table 3.4). These findings are consistent with a number of studies concluding that the higher concentration of OC_{sec} favouring during period with meteorological conditions to the occurrence of photochemical activity (high temperature) (Strader et al, 1999; Dan et al., 2004; Plaza et al, 2011). It is well know that the OC_{sec} is formed from volatile organic gases by two processes. Firstly, the condensable organic compounds are produced by oxidation reaction and subsequent nucleation and condensation. Volatile organic compounds partition more into the vapour phase in summer month including the higher species of radicals for oxidation

reaction such as the hydroxyl radical (OH), nitrate radical (NO_3) and ozone (O_3) (Seinfeld and Pandis, 1998).

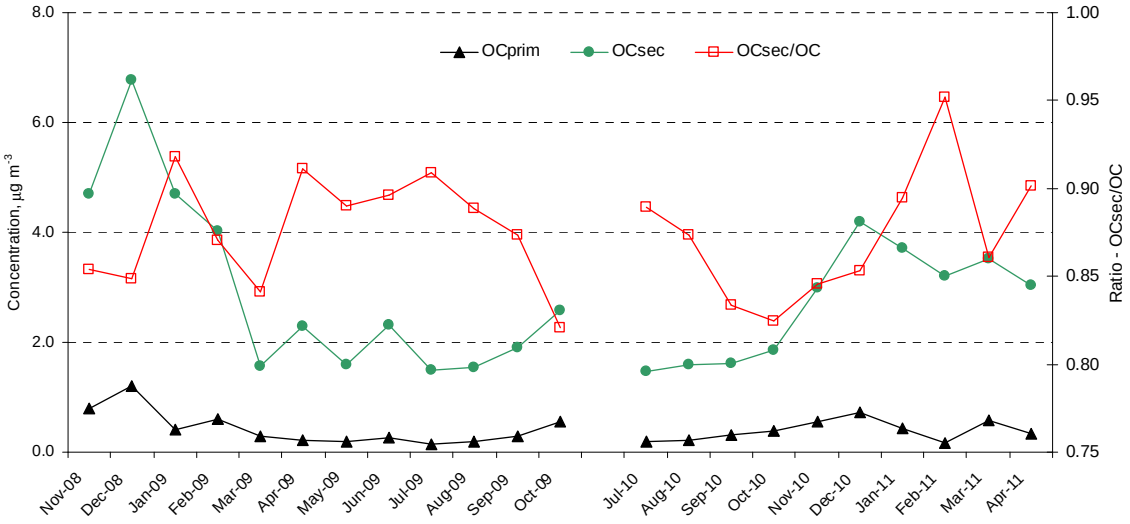

Figure 3.9 Monthly average of primary and secondary OC calculated based on OC/EC minimum ratio of 0.35 and secondary OC/OC ratio in $PM_{2.5}$ at EROS

3.3.3 Interpretation of carbonaceous aerosol between sites

Only the data collected simultaneously at EROS and HAR were used for interpreting the inter-site relationship for OC, EC, OC_{sec} and OC_{prim}. A statistical data of the carbonaceous aerosol concentration including sulphate and nitrate data at EROS and Harwell sites appear in Table 3.5. In this study, there were 100 samples collected simultaneously and OC_{prim} and OC_{sec} were calculated based on minimum ratio of OC/EC = 0.35 for both EROS and HAR sites.. The inter-site differences of the EC, OC, OC_{prim} and OC_{sec} concentrations for $PM_{2.5}$ appear 86%, 24%, 120% and 22%, respectively consistent with the differences for PM_{10} showing at 86%, 22%, 120% and 14%, respectively. It may therefore be inferred that there is a substantial local background contribution which is included very highly for EC, OC_{prim} at EROS site as showing a significant difference. On the contrary, differences are observed less than 25% for OC and OC_{sec} between EROS and Harwell sites. It is likely that OC and OC_{sec} may not be generated significantly at urban background site. Since Kolmogorov-Sminov test for EC, OC_{prim}, OC and OC_{sec} data shown that these species deviated significantly from normal distribution ($p < 0.05$) as detailed in Appendix E, the Mann-Whiney U test was applied to evaluate the significant difference between the two sites. Test results showed that

EC, OC_{prim} and OC in $PM_{2.5}$ were difference with $p < 0.05$ and OC_{sec} were observed with no difference ($p > 0.05$). All carbon compounds (EC, OC, OC_{prim} and OC_{sec}) in PM_{10} were found to be different with $p < 0.05$. However, as expected, carbonaceous aerosol concentrations show higher mean at the urban background than the rural site in all PM size ranges. The local contributions of carbonaceous compounds were determined by subtraction of rural (Harwell) concentrations from urban background concentrations and the results show in Table 3.6. This method used the same assumption as the study by Pakkanen et al. (2001) to estimate the local and long-range transport (LRT) contributions of elemental compositions to fine particle. The fine particle concentrations are considered to represent the sum of LRT and local contributions. The assumption of this method was set that the LRT of components to be similar at rural and urban background sites, and the rural site was assumed to represent purely LRT compound, consequently the contributions from local sources at the urban background site were estimated roughly as the difference between the urban background and the rural concentrations. In this assumption, the air mass backward trajectories should be investigated as for identifying a good representation of rural site (Harwell) for Birmingham (EROS) site. The air masses analysis will be discussed in the chapter 5.

As expected, EC shows a strong local contribution (0.6 μg m^{-3}) in $PM_{2.5}$ suggesting that local emission at EROS site was affected by fuel combustion as EC mostly presented in fine fraction. OC_{sec} and OC_{prim} show the lower local contribution (0.4 μg m^{-3} and 0.3 μg m^{-3}). In order to investigate the significant of local contribution to OC_{sec}, the relationship between OC_{sec} and source indicators were applied. Correlation analysis with simultaneous data between OC_{sec} and nitrate concentration in $PM_{2.5}$ showed good correlations at EROS and Harwell sites ($r = 0.62$ and $r = 0.75$, respectively). Both sites also showed a decrease in correlation with sulphate especially at EROS ($r = 0.43$ and $r = 0.66$ for EROS and Harwell, respectively). In addition to the relationship between OC_{sec} and daily mean ozone data obtained from Harwell (UK- air database) and Birmingham Tyburn for EROS site, the weak correlations were observed at both sites ($r = -0.44$ and $r = -0.37$ for EROS and Harwell, respectively). These results are strongly supportive of the good correlation between OC_{sec} and NO_x data mentioned in the previous section. It is likely that the local contribution from road transport might be an important effect to OC_{sec} with temperature dependent equilibrium between particulate and gaseous phases, as for nitrate strengthening the correlation with this ion.

Table 3.5 Statistical data of EC, OC, OC_{prim} and OC_{sec} ($\mu g\ m^{-3}$) at EROS and Harwell sites during the simultaneous period, $(OC/EC)_{min} = 0.35$

	$PM_{2.5}$		$PM_{2.5-10}$		PM_{10}	
	Mean ± S.D.	Range	Mean± S.D.	Range	Mean± S.D.	Range
EROS						
EC	1.0 ± 1.1	0.2 – 8.2	0.04 ± 0.1	<dl – 0.5	1.0 ± 1.1	0.2 – 8.3
OC	2.3 ± 1.6	0.9 – 12.1	1.2 ± 0.6	0.5 – 5.3	3.5 ± 1.8	1.6 – 13.7
OC_{prim}	0.4 ± 0.4	0.1 – 2.9	n.a	n.a	0.4 ± 0.4	0.1 – 2.9
OC_{sec}	2.0 ± 1.3	0.7 – 9.2	n.a	n.a	3.1 ± 1.5	1.4 – 10.8
Nitrate	1.61 ± 2.11	<dl – 10.88	0.63 ± 0.64	<dl – 3.29	2.25 ± 2.49	<dl – 12.49
Sulphate	1.60 ± 1.35	0.32 – 6.48	0.25 ± 0.17	<dl – 0.89	1.85 ± 1.47	0.55 – 7.37
HAR						
EC	0.4 ± 0.4	<dl – 1.9	0.03 ± 0.1	<dl – 0.5	0.4 ± 0.4	<dl – 2.2
OC	1.8 ± 0.9	0.5 – 4.8	1.0 ± 0.5	0.4 – 3.3	2.8 ± 1.1	1.0 – 7.0
OC_{prim}	0.1 ± 0.1	<dl – 0.7	n.a	n.a	0.1 ± 0.2	<dl – 0.8
OC_{sec}	1.6 ± 0.8	0.5 – 4.5	n.a	n.a	2.7 ± 1.0	0.9 – 6.6
Nitrate	1.44 ± 2.02	0.03 – 11.65	0.71 ± 0.68	<dl – 3.40	2.16 ± 2.50	0.16 – 14.75
Sulphate	1.47 ± 1.24	0.05 – 6.76	0.35 ± 0.40	<dl – 2.36	1.82 ± 1.40	0.36 – 7.53

Table 3.6 The local contributions of carbonaceous materials, sulphate and nitrate in $PM_{2.5}$, $PM_{2.5-10}$ and PM_{10}

Components	Local contribution, $\mu g\ m^{-3}$		
	$PM_{2.5}$	$PM_{2.5-10}$	PM_{10}
EC	0.6	0.01	0.6
OC	0.5	0.2	0.7
OC_{prim}	0.3	n.a	0.3
OC_{sec}	0.4	n.a	0.4
Nitrate	0.17	-0.08	0.09
Sulphate	0.13	-0.10	0.03

The reduced major axis (RMA) method is recommended to use for the regression analysis of air quality datasets in order to estimate the influence of local contribution at urban background site. This linear fit is achieved by minimising the product of the *x* and *y* deviations between the data values and fitted values (Ayers, 2001). On the contrary, the standard linear regression minimises deviations only in the *y* direction. The ionic compositions data including carbonaceous compounds of particulate matter obtained from urban background and rural site were determined the relationship by plotting the former versus the latter. The deviations between fitted and measured data value will occur in both *x* and *y* directions due to random measurement errors. Focusing on $PM_{2.5}$, Figure 3.10 shows the relationships of EC, OC, OC_{prim} and OC_{sec} between EROS and Harwell site and the

results of regression analyses are summarized in Table 3.7. In this study, a greater gradient of EC (2.72) and OC_{prim} (2.76) with a very small intercept as assumed a zero interception were observed. In addition to the high gradients of OC (1.78) and OC_{sec} (1.62), it would be interpreted that the local contributions of carbonaceous particles at urban background influence their concentrations in the same way as influence at rural site. A high gradient of EC and OC_{prim} might be based on the road transportation contributed to urban background (EROS) causing very largely of EC and calculated OC_{prim}. Moreover, the relationship for OC_{sec} shows more a reasonable fit to the $y = x$ line, it would be interpreted that the average concentrations at the two sites for OC_{sec} are broadly similar. This suggests that the selection of minimum OC/EC ratio of 0.35 to estimate OC_{prim} and OC_{sec} is appropriate and the OC appears mostly as secondary formation. It is consistent with the plot in Figure 3.11 presenting the relationship between OC difference and EC difference data collected simultaneously at EROS and Harwell. There appear only a few data scattered below minimum ratio line of OC/EC = 0.35. In order to evaluate the significant difference of OC_{sec}, the Mann-Whitney U test was applied to assess whether any significant difference of OC_{sec} between the two sites as mentioned above. The Mann-Whitney U test is a nonparametric test that can be used to analyse data from two-group independent groups design when measurement can at least be ranked or be ordered. This test evaluates the null hypothesis that two groups of sample come from the same population and therefore, because sampling was random, the two groups of scores do not differ systematically from each other. Test result indicated that OC_{sec} concentrations measured simultaneously at EROS and Harwell were no difference which accepted the null hypothesis that there was no difference between the two data sets ($p > 0.05$).

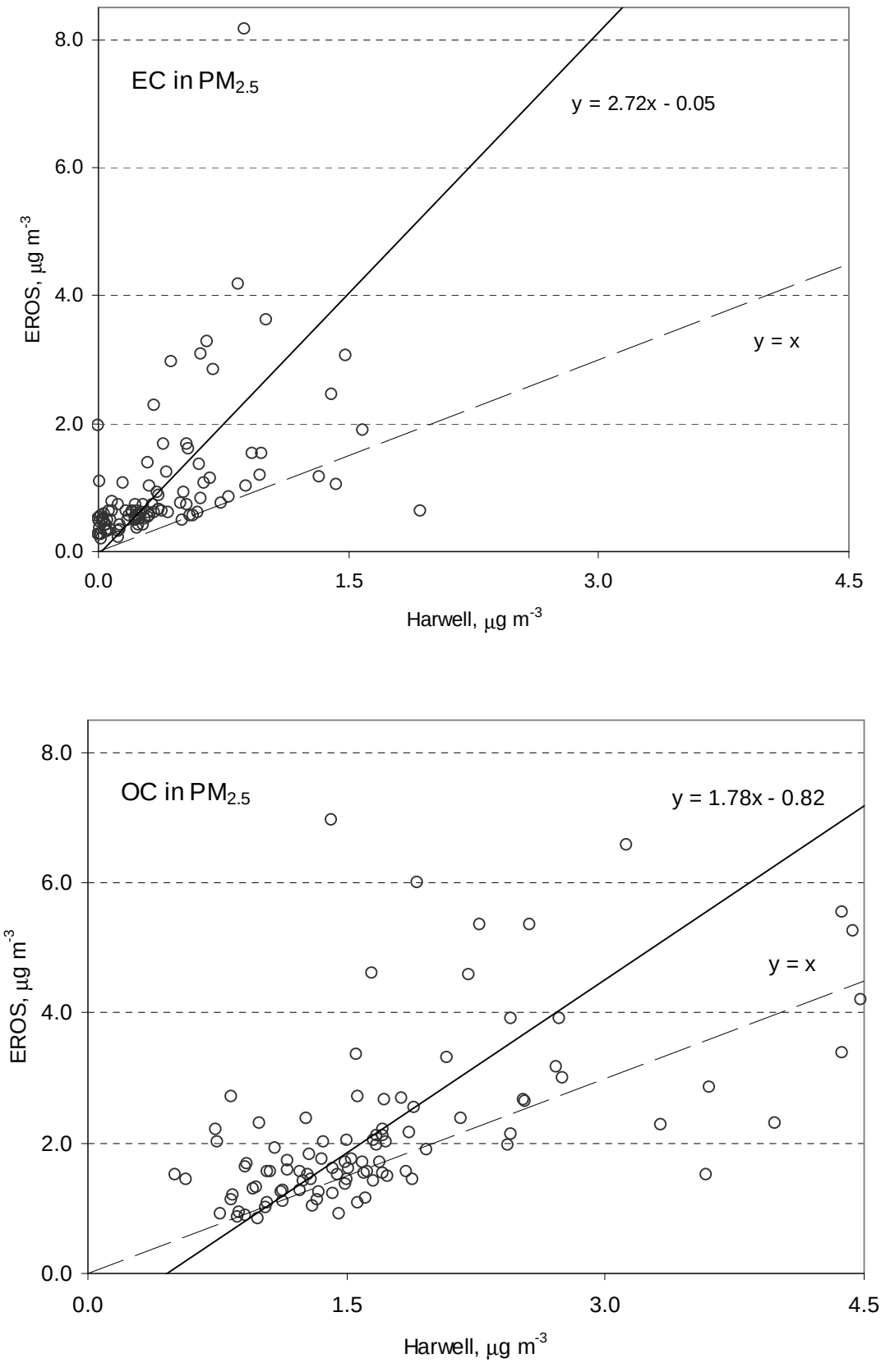

Figure 3.10 Relationships between EROS and Harwell concentrations of EC, OC, primary and secondary OC calculated by the OC/EC minimum ratio of 0.35

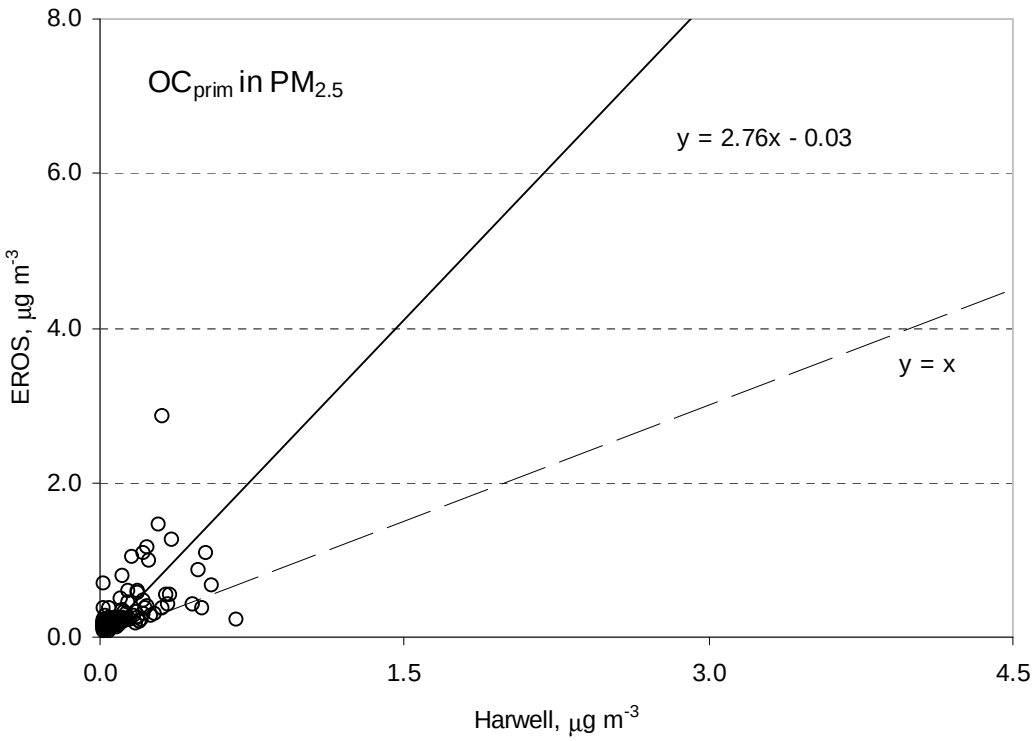

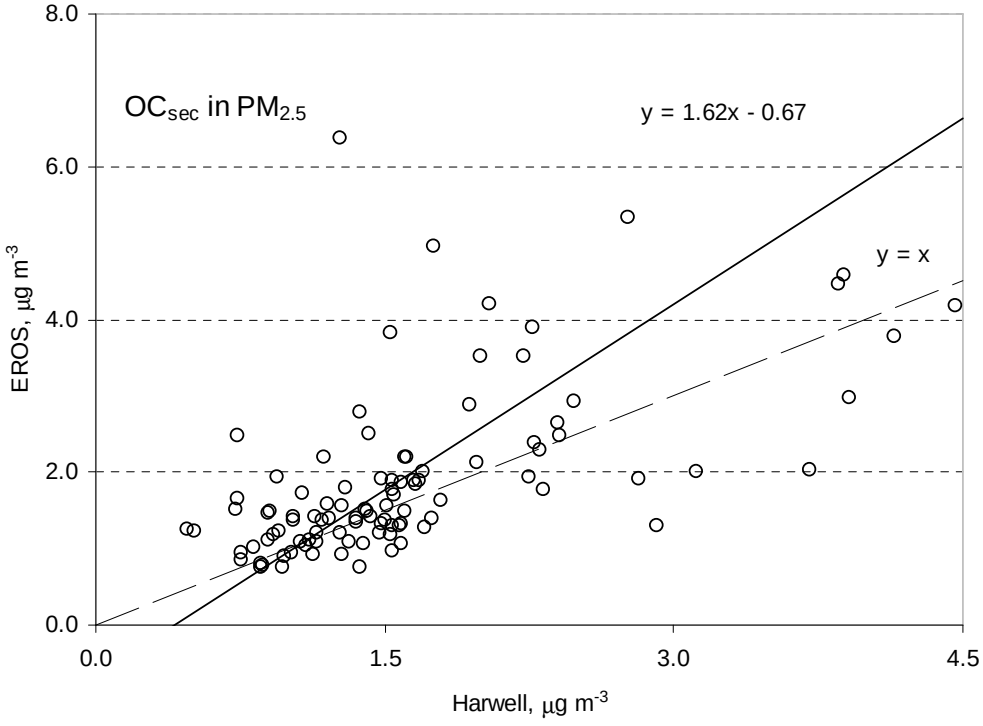

Figure 3.10 *(continued)*

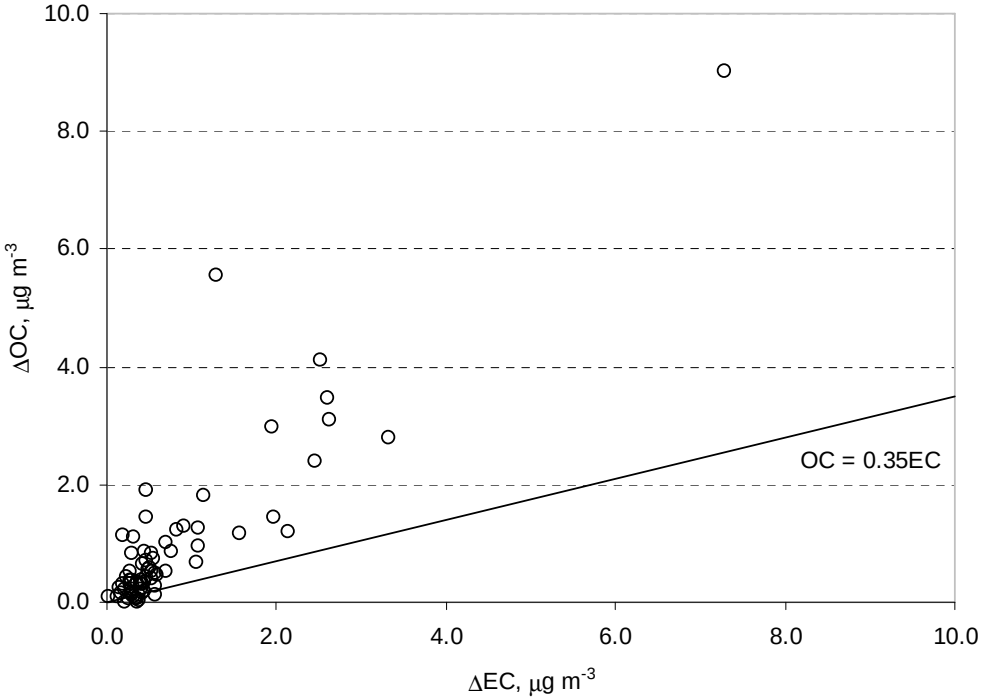

Figure 3.11 Plot of OC difference ($\Delta OC = OC_{EROS} - OC_{HAR}$) versus EC difference ($\Delta EC = EC_{EROS} - EC_{HAR}$) data taken simultaneously between EROS and Harwell

Table 3.7 Results of regression analysis of EROS (urban background) and Harwell (rural) concentrations in $PM_{2.5}$

Analyte	RMA regression
EC	$y = 2.72x - 0.05$ ($R^2 = 0.23$)
OC	$y = 1.78x - 0.82$ ($R^2 = 0.31$)
OC_{prim}	$y = 2.76x - 0.03$ ($R^2 = 0.23$)
OC_{sec}	$y = 1.62x - 0.67$ ($R^2 = 0.32$)

Note: y represents urban background (EROS) concentration of analyte in μg m^{-3}; x represents rural (HAR) concentration of analyte in μg m^{-3}.

Figure 3.12 shows the concentration data of OC_{prim} and OC_{sec} in $PM_{2.5}$ collected simultaneously. The similarity of temporal variation patterns was observed both OC_{prim} and OC_{sec} during the study period. It is clear that all OC_{prim} concentrations observed higher concentration at EROS than those at Harwell especially in November which is the coldest month as lower dispersion of primary pollutants.

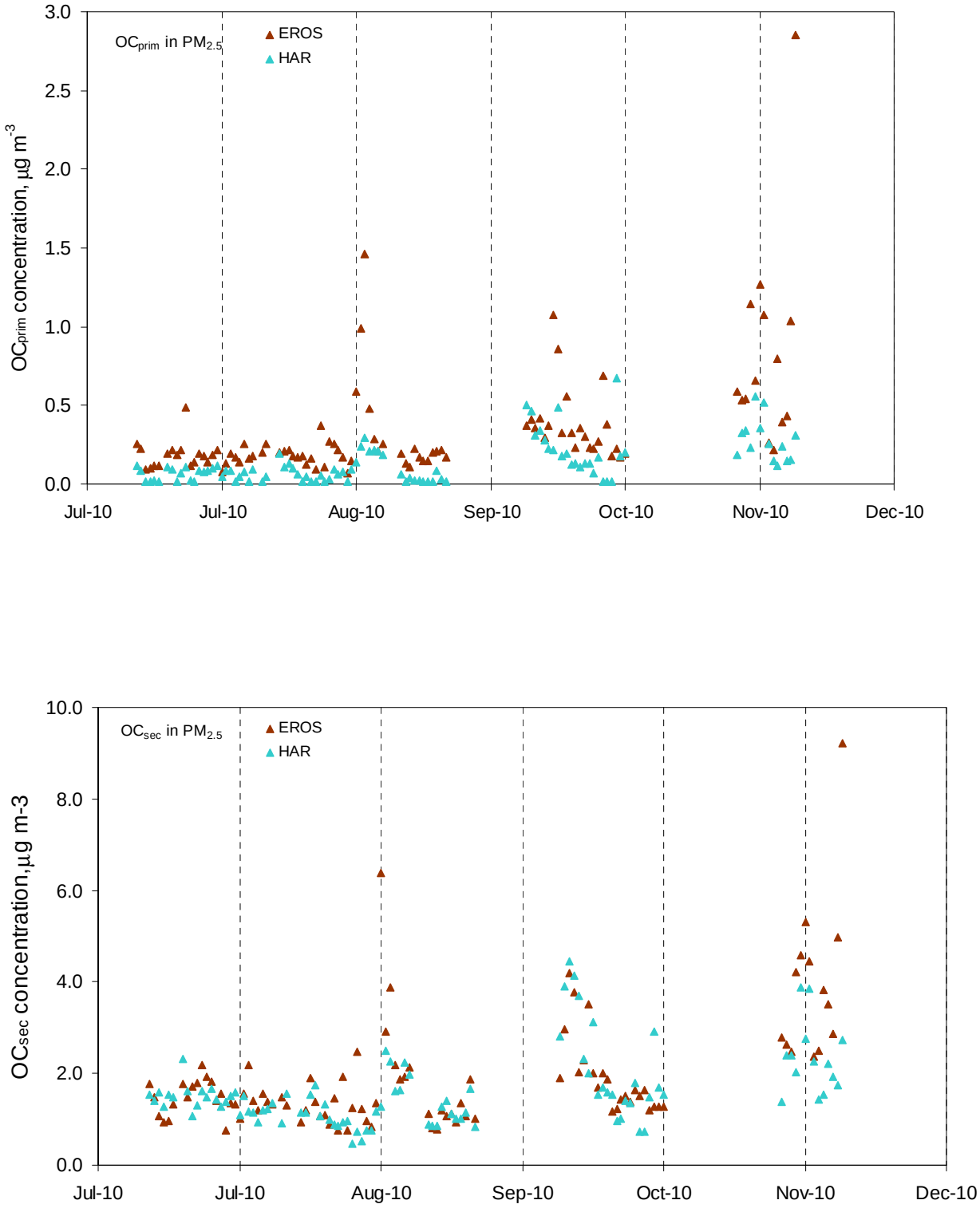

Figure 3.12 Time series of OC_{prim} and OC_{sec} concentrations in $PM_{2.5}$ measured at EROS and Harwell sites during the simultaneous period.

The correlation analysis was determined between carbonaceous species at EROS and Harwell sites in order to investigate the origin of particles. Table 3.8 shows the correlation between carbonaceous species analysed in $PM_{2.5}$, $PM_{2.5-10}$ and PM_{10} and data collected simultaneously. As OC_{prim} calculated based on OC/EC minimum ratio, the same correlation values of EC were showed in all data. The modest correlations of OC_{prim} and EC were observed between EROS and Harwell both in $PM_{2.5}$ and PM_{10} (r = 0.48 and r = 0.47 for $PM_{2.5}$ and PM_{10}, respectively). This can be attributed to the fact that OC_{prim} and EC mainly contribute from the local source especially traffic transportation. A slightly higher correlation coefficient values were seen for OC and OC_{sec} between EROS and Harwell sites, with medium correlation of OC(r = 0.55 for $PM_{2.5}$, and r = 0.44 for PM_{10}) followed by the similar correlation of OC_{sec} (r = 0.56 for $PM_{2.5}$ and r = 0.43 for PM_{10}). These findings indicate that OC and OC_{sec} concentrations measured at both sites were mainly from regional formation. Moreover, the results are strongly supportive of no difference between OC_{sec} at both sites as above significant tested. The same behaviour of OC and OC_{sec} concentrations in two sites were exhibited. This was because the compositions of OC were highly contributed by OC_{sec} ($PM_{2.5}$, 87% and 97% for EROS and Harwell; PM_{10}, 91% and 96% for EROS and Harwell, respectively). As expected, a very weak correlation of OC in coarse faction between two sites was observed (r = 0.16) indicating that the coarse particles originated from primary emissions or local sources.

Table 3.8 Inter-site correlation coefficients (r) calculated between carbonaceous species concentrations in $PM_{2.5}$, $PM_{2.5-10}$ and PM_{10}

	EC EROS	OC EROS	OC_{prim} EROS	OC_{sec} EROS
$PM_{2.5}$				
EC HAR	0.48	0.53	0.48	0.52
OC HAR	0.44	0.55	0.44	0.57
OC_{prim} HAR	0.48	0.53	0.48	0.52
OC_{sec} HAR	0.42	0.54	0.42	0.56
$PM_{2.5-10}$				
EC HAR	0.24	*0.09*	n.a	n.a
OC HAR	*-0.03*	*0.16*	n.a	n.a
OC_{prim} HAR	n.a	n.a	n.a	n.a
OC_{sec} HAR	n.a	n.a	n.a	n.a
PM_{10}				
EC HAR	0.47	0.50	0.47	0.48
OC HAR	0.34	0.44	0.34	0.45
OC_{prim} HAR	0.47	0.50	0.47	0.48
OC_{sec} HAR	0.30	0.42	0.30	0.43

Values shown in italics are not significant at $p < 0.05$ (the 95% level of significance).

3.4 Conclusions

The concentration of carbonaceous aerosol measured in $PM_{2.5}$, $PM_{2.5-10}$ and PM_{10} samples collected from two sampling sites representative of urban background (EROS) and rural (Harwell) locations has revealed some interesting and useful data for Birmingham. This is one of the most comprehensive speciation studies on OC and EC concentration in airborne particulate matter. These data clearly show that EC observed high concentrations at urban background comparing with rural site in all size ranges. Maximum EC and OC values in winter have been associated to meteorological conditions favorable to pollutant accumulation. In case of maximum EC level in winter, this has been associated to less effective dispersion process in the low temperature, and for maximum OC concentration, it could be explained by the lower atmospheric mixing depth favouring secondary organic aerosol formation and accumulation of secondary organic precursors. There are the significant problems of using the OC/EC minimum ratio to distinguish between primary and secondary OC such as the OC/EC ratio is not consistent from source to source but a number of OC/EC ratios previously studied show constant in urban background atmosphere. Those findings indicate that the minimum OC/EC ratio still uses as an effective tool to differentiate OC from primary and secondary sources. The other significant issue is some additional OC measuring as usual in urban background causing higher the OC/EC minimum ratio. This result may overestimate the primary OC from vehicle emissions and underestimates OC components from other sources especially from secondary formation. Therefore, the OC/EC minimum ratio of 0.35 have been used in accordance with the recent study by Pio et al. (2011). The selection of this minimum ratio is appropriate in this work with two reasons. Firstly, the good fit of OC_{sec} to the $y = x$ line for data collected simultaneously between EROS and Harwell sites. This is because OC_{sec} with mainly accounting for OC concentration was affected by regional contribution. Secondly, the scatter of data of OC difference and EC difference lay above the minimum ratio line of OC/EC = 0.35 for simultaneous data. Calculated OC_{prim} and OC_{sec} show a winter maximum and the strong correlation with nitrogen oxides (NO_x) at both sites suggesting that the local transport plays an important source of OC_{prim} and OC_{sec}. In this study, the behaviour of OC_{sec} is close to nitrate than that of sulphate consistent with the observation made by Harrison and Yin (2008). This indicates that the regional transport and temperature have a major influence upon OC_{sec} concentrations.

It is seen from data collected simultaneously that EC presents a significant local contribution especially in $PM_{2.5}$ and EC mostly contributed in fine fraction. The reduced major axis (RMA) analysis also reveals the local contributions of carbonaceous aerosol at EROS influence their concentrations in the same way as at Harwell site. Moreover, as significant tested, it appears that there is no difference between OC_{sec} concentration at both sites suggesting a high influence or contribution of long-lived species.

CHAPTER 4

INTERPRETATION OF ION COMPONENT COMPOSITION OF PARTICULATE MATTER

4.1 Synopsis

The samples collected from EROS and Harwell as mentioned in chapter 3.2 were mainly analysed for sulphate, nitrate, chloride and oxalate. This chapter describes the results of those chemical analyses, with comparison made between rural and urban background sites. The relationships between major components in PM were investigated and discussed to identify their sources and possible formation pathways. Focusing on oxalate aerosol, there is rarely dataset available in the UK and its precursors have not been exactly identified including its formation not well understand. The comparisons between oxalate with sulphate, nitrate and chloride were determined as their formation mechanisms have been established. Oxalate represented the most abundant water-soluble organic carbon (WSOC) in PM stated in many previous studies, therefore the analysis of WSOC in samples collected simultaneously was reported in order to better understanding oxalate sources. The possible formation pathway of oxalate by in-cloud process and potential precursors are illustrated as the important formation of secondary organic aerosols.

4.2 Particulate matter chemical components

Airborne particulate matter (PM) presents a far greater complexity than most other common air pollutants. It consists of different chemical substances and individual particles also span a wide range of sizes. Both chemical composition and size distribution can identify the sources of airborne particles, and these factors also determine the atmospheric behaviour and fate of particles as well as influencing human health effects.

Chemical composition of PM varies at different regions due to PM consists of a complex mixture of various chemical components which cloud be contributed from different pollution sources. In addition to chemical reactions in the atmosphere, long-range transport effect, removal processes and meteorological conditions, these factors result in a variation of chemical composition in atmospheric aerosol. Their components include neutral and highly soluble substances such as $(NH_4)_2SO_4$, NH_4NO_3 and NaCl through to sooty particles

composed of largely elemental carbon coated in organic compounds, and insoluble minerals such as particles of clay (Brook et al, 1997).

Airborne particles contain both major and minor components. The relative abundance of the major chemical components, termed as 'bulk chemical composition' was reported in the study of Harrison and Yin (2000) for urban areas in the UK and around the world. These major components include sulphate, nitrate, ammonium, chloride, elemental and organic carbon, crustal materials and biological materials. There are many minor chemical components present in airborne particles depending on the detection limit, sensitivity of the analytical procedure to determine their concentrations. Minor components comprise the following; trace metals (lead, cadmium, mercury, nickel, chromium, zinc and manganese) which are used in metallurgical processes or in industrial products, trace organic compounds as presented at a very low concentration even though the total mass of organic compounds comprise a significant part of the overall mass of particles.

In this study, two of the main chemical components of PM in polluted atmospheres — sulphate and nitrate — are determined the concentration in aerosol samples. There are both photochemical and heterogeneous thermal oxidation pathways from their precursor gases.

Sulphate are found as a combination of H_2SO_4, ammonium bisulphate (NH_4HSO_4), ammonium sulphate ($(NH_4)_2SO_4$) and sodium sulphate (Na_2SO_4) of marine origin (Harrison and Pio, 1983). Sulphate is mainly formed within the atmosphere by oxidation of SO_2, which is itself directly emitted from i.e. fossil fuel combustion, industrial processes, and volcanoes or produced within the atmosphere by oxidation of reduced sulphur species such as dimethyl sulphide (DMS) emitted by oceanic phytoplankton. Sulphate is expected to be present mostly in the fine fraction. The oxidation of SO_2 can occur both in gas phase (homogeneous processes) (Calvert and Stockwell, 1983) and in the aqueous phase (heterogeneous processes) in the presence of cloud, fog or aerosol droplets (Schwartz, 1987). In practice, hydroxyl radical usually plays an important oxidant in homogeneous gas phase oxidation of SO_2. The formation pathway of sulphate occurs via the following equations.

$$SO_2 + OH + M \rightarrow HSO_3 + M \qquad \text{(Equation 4.1)}$$

$$HSO_3 + O_2 \rightarrow SO_3 + HO_2 \qquad \text{(Equation 4.2)}$$

$$SO_3 + H_2O + M \rightarrow H_2SO_4 + M \qquad \text{(Equation 4.3)}$$

Where M = N_2 or O_2. Since SO_2 is a highly water-soluble gas, it partitions appreciably into the aqueous phase as the following reactions.

$$SO_2\,(g) + H_2O \leftrightarrow SO_2.H_2O \qquad \text{(Equation 4.4)}$$

$$SO_2.H_2O \leftrightarrow HSO_3^- + H^+ \qquad \text{(Equation 4.5)}$$

$$HSO_3^- \leftrightarrow SO_3^{2-} + H^+ \qquad \text{(Equation 4.6)}$$

If hydrogen peroxide and ozone are dissolved in the droplet, the sulphur dioxide is quickly oxidized to sulphuric acid.

$$H_2O_2(g) \leftrightarrow H_2O_2(aq) \qquad \text{(Equation 4.7)}$$

$$HSO_3^- + H_2O_2(aq) + H^+ \leftrightarrow SO_4^{2-} + 2H^+ + H_2O \qquad \text{(Equation4.8)}$$

$$O_3(aq) + SO_3^{2-} \leftrightarrow O_2 + SO_4^{2-} \qquad \text{(Equation 4.9)}$$

Sulphate formed from the oxidation of SO_2 is initially in the form of sulphuric acid (H_2SO_4). In gas phase, H_2SO_4 vapour can nucleate new particles under favorable conditions and can grow by condensing water vapour or in the presence of ammonia gas (NH_3), becomes neutralised as NH_4HSO_4 or $(NH_4)_2SO_4$. In aqueous phase, if ammonia is also dissolved in the droplet, H_2SO_4 is also neutralized to NH_4HSO_4 and $(NH_4)_2SO_4$. The major sources of NH_3 are from agricultural activities, for example through the use of fertilizers and the disposal of animal waste to land. Aqueous transformations rates of sulphur dioxide to sulphate are 10 to 100 times as fast as gas-phase rates.

Nitrate occurs in the atmosphere due to the formation of nitric acid, which can then form particles by reacting with ammonia or sodium chloride. It mainly found as ammonium nitrate (NH_4NO_3) produced from the reaction between gaseous nitric acid with ammonia, which is a major component of particle in fine fraction. Nitric oxide (NO) directly emitted into atmosphere converts to nitrogen dioxide (NO_2) by reaction with ozone. The major pathway to form nitric acid is reaction with hydroxyl radicals (Calvert and Stochkwell, 1983). The formation of nitric acid in daylight presents as following reaction.

$$NO_2 + OH \rightarrow HNO_3 \qquad \text{(Equation 4.10)}$$

This reaction also provides a significant loss mechanism for OH under polluted conditions. The rate of oxidation of NO_2 is faster than the rate of sulphate formation from SO_2 during the high daytime OH. At night-time the rate of production of OH drops and other mechanisms will occur as equation 4.11. This process only occurs at night as the nitrate radical is readily photolysed during the day.

$$NO_2 + O_3 \rightarrow NO_3 + O_2 \qquad \text{(Equation 4.11)}$$

NO_3 radical further reacts with NO_2 to form nitric acid by the pathways through dinitrogen pentoxide (N_2O_5). N_2O_5 is thermally unstable and decomposes back to NO_2 and NO_3, building up an equilibrium.

$$NO_3 + NO_2 \leftrightarrow N_2O_5 \qquad \text{(Equation 4.12)}$$

$$N_2O_5 + H_2O \leftrightarrow 2HNO_3 \qquad \text{(Equation 4.13)}$$

NO_3 also reacts with a number of volatile organic compounds (VOC) to form nitric acid and organic products as;

$$NO_3 + RH \rightarrow HNO_3 + R \qquad \text{(Equation 4.14)}$$

where RH is volatile organic compounds and R is organic product.

Although HNO_3, NH_4NO_3 and N_2O_5 all have relatively low volatilities compared with NO_x, they are unable to undergo homogeneous nucleation. Instead, they attach themselves to pre-existing particles to undergo heterogeneous nucleation. The particulate nitrate can produce by the reaction of HNO_3 with ammonia and sodium chloride. The coarse mode nitrate which is predominant in the marine atmosphere generate by the reaction of nitric acid and sea salt via the following equation.

$$HNO3\ (g) + NaCl\ (aq) \rightarrow NaNO_3\ (aq) + HCl\ (g) \qquad \text{(Equation 4.15)}$$

Or through nitrogen pentoxide,

$$N_2O_5\ (g) + 2NaCl\ (aq) + H_2O \rightarrow 2NaNO_3\ (aq) + 2HCl\ (g)\ \text{(Equation 4.16)}$$

Ammonium sulphate is a fairly stable compound found in particulate phase but ammonium nitrate is not. The equilibrium of gaseous ammonia and nitric acid is strongly influenced by temperature and relative humidity. Russell *et al*. (1983) show that lower temperatures and higher relative humidities favor ammonium nitrate in particulate phase.

Chloride is the other major anion in atmospheric aerosols and also analysed in this work. Contributions are also primary emissions from sea salt and also possible during the winter months by road deicing salt. These contribute mostly to chloride in coarse particles. Chloride may be also produced by secondary formation and observed in the form of ammonium chloride derived from the reaction of ammonia and hydrochloric acid (HCl) vapour emitted from combustion sources such as incinerators and power plants. In the UK, it is likely to be of modest importance due to low concentration of its precursor, HCl. Under normal atmosphere, ammonium nitrate and ammonium chloride are unstable existing in the reversible phase equilibrium with the gaseous precursors. Theses equilibrium are mainly controlled by atmospheric temperature and relative humidity.

With regard to OC_{sec} mentioned in chapter 3.3.2, some part of OC_{sec} is water-soluble because they have polar functional groups (e.g. hydroxyl, carbonyl, and carboxyl) produced by the photochemical reaction. OC_{sec} can be considered to be water-soluble organic carbon (WSOC). WSOC, therefore, represented a significant water-soluble component of the atmospheric aerosol and accounted for approximately 20% to 67% of the total particulate carbon in the atmosphere (Muller et al., 1982, Zappoli et al., 1999; Krivacsy et al., 2001; Yang et al. 2003; Wang et al., 2005; Fosco and Schmeling, 2007). Much research work has shown that WSOC had potential to act as cloud condensation nuclei (CCN) (Novakov and Penner, 1993; Yu, 2000; Mircea et al., 2002; Yao et al., 2002) and also reduced surface tension of CCN, which is one of the parameters determining cloud formation (Facchini et al., 1999). Measurement of the WSOC concentrations is necessary for quantifying the relative contribution of individual water-soluble organic components to the total WSOC mass and assessing the need for identifying additional water-soluble components. The method used for determining WSOC concentration is described in chapter 2.5.2. Only aerosol samples collected simultaneously between EROS and Harwell sites were analysed for WSOC concentrations.

The most abundant class of the identified water soluble organic compounds in the atmospheric aerosol is usually the class of the dicarboxylic acids (DCA) which can be responsible for 5 – 20% of the total WSOC in urban areas (Sempere and Kawamura, 1994). However, at rural continental sites, the fraction of DCA in the WSOC was found to be <2% (Sarvari et al., 1999). Oxalic acid and/or oxalate is the most abundant dicarboxylic acids followed by malonic and succinic acids (Kawamura and Ikushima, 1993; Kawamura and Usukura, 1993; Yao et al., 2002) and shows a strong correlation between CCN and its concentration, suggesting that it may play a role in activating CCN (Yu, 2000; Sun and Ariya, 2006). Oxalate is greatly present in particulate phase in the ambient atmosphere due to the lower volatility compared to formic and acetic acids, which are the main monocarboxylic acids (MCA) present in the gas phase (Chebbi and Carlier, 1996). Kawamura and Kaplan (1987) found that the diacids (C_2-C_{10}) were mostly associated with particles but a minor fraction of these compounds have been sampled in vapour phase. The concentrations of oxalic acid and/or oxalate range from several ng m^{-3} up to a thousand ng m^{-3} (or a few tens of pmol m^{-3} to a few tens of nmol m^{-3}) depending on location. Oxalic acid and/or oxalate was reported to constitute up to 86% of total DCA in urban PM_{10} and up to 65% of the total DCA in $PM_{2.5}$ fraction (Wang et al., 2002). Concentration of oxalic acid and/or oxalate shows seasonal variation with a maximum in summer (Kawamura and Ikushima, 1993; Sempere and Kawamura, 1994).

Currently in the UK, no work has been reported on measurement and source of oxalic acid and/or oxalate in particulate matter. Therefore, this study also intend to analyse daily aerosol samples collected both EROS and Harwell sits in order to obtain a number of oxalate concentration data. This dataset of oxalate was used in comparison with the major chemical components in ambient atmosphere. We aim to better understanding of sources and the formation pathway of oxalate in aerosol.

4.3 Atmospheric aerosol concentrations in urban background and rural sites

As appeared in Table 3.1, the results are presented in terms of the major chemical constituents in $PM_{2.5}$, $PM_{2.5-10}$ and PM_{10} at EROS and Harwell sites. The composition of PM at both sites is seen to be dominated by carbonaceous materials which are interpreted in chapter 3. The aerosol component concentrations discussed hereafter are from the measured chemical species including sulphate, nitrate, chloride and oxalate. For $PM_{2.5}$, the whole mean concentrations of sulphate with measurement uncertainties were 1.86 ± 0.06 μg m^{-3} and 1.40 ± 0.05 μg m^{-3} at EROS and Harwell, respectively. For PM_{10}, the whole mean concentrations of sulphate with measurement uncertainties were 2.13 ± 0.07 μg m^{-3} and 1.69 ± 0.06 μg m^{-3} at EROS and Harwell, respectively. The highest concentration was measured in spring, whereas the lowest was found in summer at EROS. Nitrate was present in all fractions at both sites, with a higher contribution in spring at EROS (for $PM_{2.5}$, $PM_{2.5-10}$ and PM_{10}; 4.80 ± 0.16 μg m^{-3}, 1.09 ± 0.04 μg m^{-3} and 5.88 ± 0.20 μg m^{-3}, respectively). These finding of seasonal observation both sulphate and nitrate were in agreement with the measurement at Belfast and North Kensington in the UK studied by Abdalmogith and Harrison (2006). Moreover, the concentrations of secondary aerosols at Harwell site in those report also showed similar seasonal patterns to this study with autumn higher than summer. As anticipated, the coarse ($PM_{2.5-10}$) fraction was found the highest ion component of chloride whole concentration of 0.83 ± 0.03 μg m^{-3} at EROS and the $PM_{2.5-10}$ is dominated by the chloride (the whole concentration of 0.61 ± 0.02 μg m^{-3}) at Harwell. It should be noted that chloride in fine fraction also measured high concentration at EROS (0.73 ± 0.02 μg m^{-3} for whole data), suggesting that there might be the importance of anthropogenic sources. The whole mean concentrations of oxalate with measurement uncertainties at EROS were 0.05 ± 0.002 μg m^{-3} in $PM_{2.5}$, 0.02 ± 0.001 μg m^{-3} in $PM_{2.5-10}$ and 0.06 ± 0.002 μg m^{-3} in PM_{10}. Considering the concentration level of oxalate, there observed in range with the comparison to the results reported by Khwaja (1995), Tran et al. (2000), Limbeck et al. (2001), Rohrl and Lammel (2001), Huang et al. (2006), Fosco and Schmeling (2007) and Agarwal (2010). The time series of sulphate, nitrate, chloride and oxalate in fine fraction at EROS and Harwell sites are shown in Figure 4.1. It is likely that the temporal variation of ionic species in PM was dominant comparing with the spatial variation.

(a)

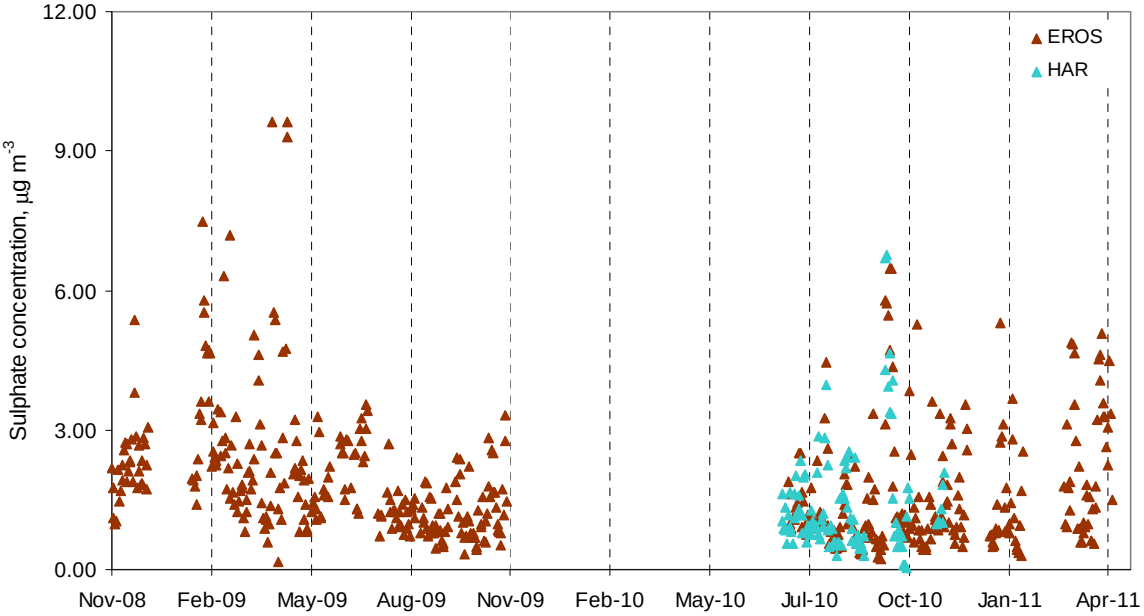

(b)

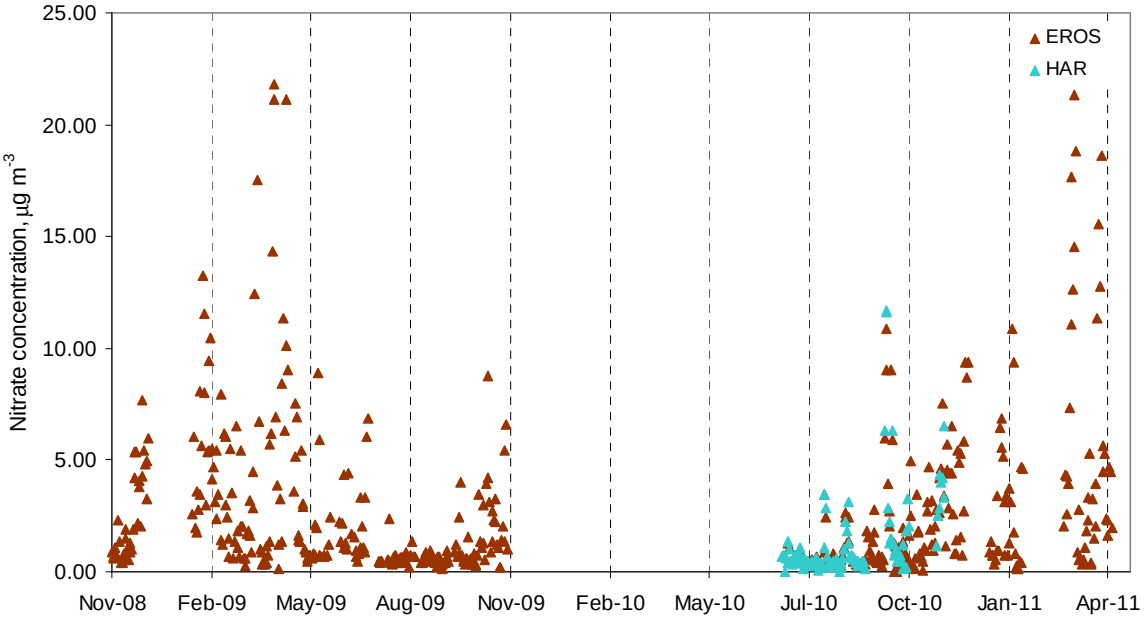

Figure 4.1 Time series of (a) sulphate, (b) nitrate, (c) chloride and (d) oxalate concentrations in $PM_{2.5}$ measured at EROS and Harwell sites

(c)

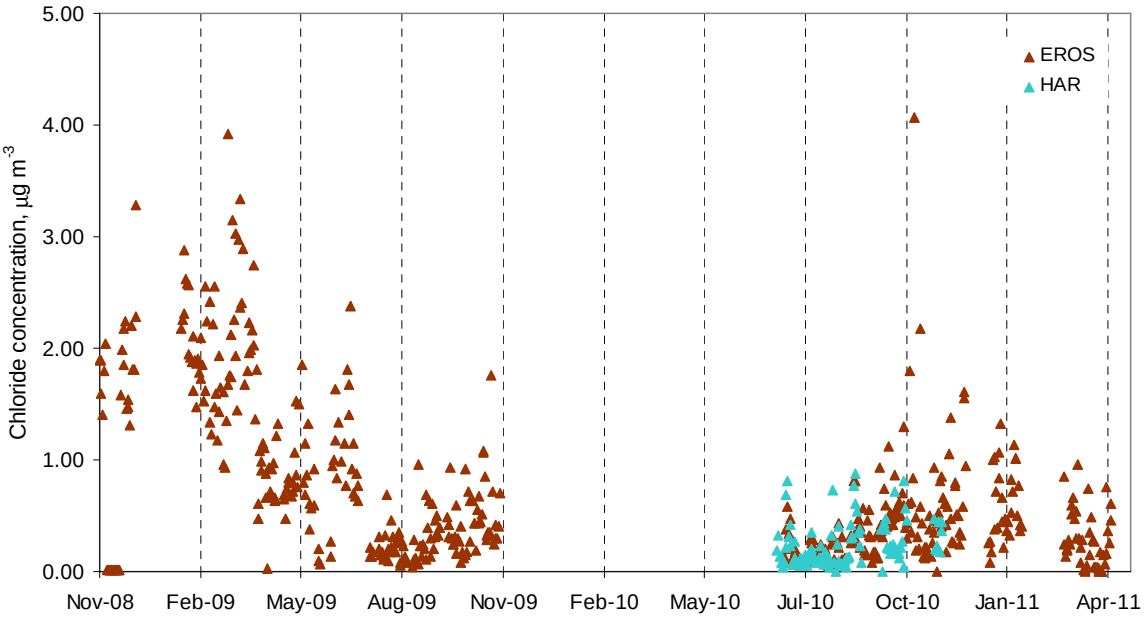

(d)

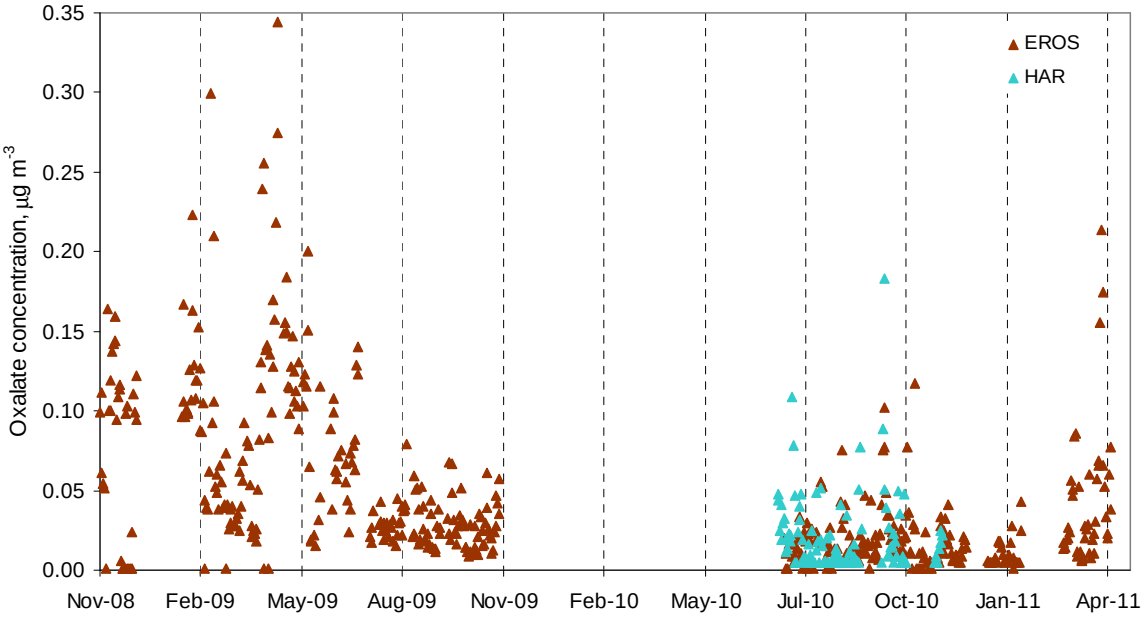

Figure 4.1 *(continued)*

As ionic components data split into four seasons during the period of November 2008 to April 2011 at EROS (Table 3.1 and Figure 3.4), the significant differences in aerosol concentration between the seasons were determined by applying the statistical test. The number of data in whole, summer, autumn, winter and spring were 500 samples, 116 samples, 165 samples, 101 samples and 118 samples, respectively. The Kruskal-Wallis nonparametric test can be used to assess whether any significant differences between *k* independent samples. It is used for comparing more than two samples. The test assumes that the measurement data are at least on an ordinal scale and that underlying variable has a continuous distribution. The null hypothesis is that the *k* samples come from the same population, or that their underlying distributions have the same average. When the Kruskal-Wallis test leads to significant results, then at least one of the samples is different from the other samples. In this data, test results indicate significant differences for each sulphate, nitrate, chloride and oxalate concentrations between the four seasons ($p \leq 0.05$). It is clear that sulphate, nitrate and chloride in fine fraction observed low in summer months suggesting the atmospheric mixing depth played an important factor on aerosol concentrations at EROS site. For chloride, the mean concentration in $PM_{2.5}$ and PM_{10} observed high in the winter and low in the summer as expected due to generally much wind speeds in winter leading to greater generation of marine aerosol. Seasonal trend for particulate oxalate does not show through so clearly but the concentration level revealed highest in spring.

4.3.1 Relationships between major component composition in PM

The correlation analysis was determined between aerosol species at EROS sites in order to investigate the origin of particles. The Pearson's correlation coefficient (r) was calculated to measure the association between two species. Table 4.1 shows the correlation between major components analysed in $PM_{2.5}$, $PM_{2.5\text{-}10}$ and PM_{10} in whole, summer, autumn, winter and spring at EROS.

Table 4.1 Correlations (*r*) calculated between analysed species in $PM_{2.5}$, $PM_{2.5-10}$ and PM_{10} at EROS during the period from November 2008 to April 2011

	SO_4^{2-}	NO_3^-	Cl^-	$C_2O_4^{2-}$	OC	EC
Whole						
$PM_{2.5}$						
NO_3^-	0.72					
Cl^-	0.31	0.19				
$C_2O_4^{2-}$	0.60	0.48	0.27			
OC	0.44	0.45	0.27	0.23		
EC	0.28	0.32	0.22	*0.07*	0.83	
OC_{sec}	0.45	0.46	0.27	0.25	0.99	0.76
$PM_{2.5-10}$						
NO_3^-	0.53					
Cl^-	0.33	-0.09				
$C_2O_4^{2-}$	0.29	0.35	*-0.05*			
OC	*0.02*	0.14	*0.06*	0.12		
EC	0.17	0.25	*0.06*	-0.09	0.50	1.00
OC_{sec}	n.a.	n.a.	n.a.	n.a.	n.a.	n.a.
PM_{10}						
NO_3^-	0.73					
Cl^-	0.12	*-0.05*				
$C_2O_4^{2-}$	0.59	0.49	0.11			
OC	0.39	0.42	*0.05*	0.17		
EC	0.29	0.33	*0.01*	*0.04*	0.83	
OC_{sec}	0.40	0.42	*0.05*	0.19	0.99	0.76
Summer						
$PM_{2.5}$						
NO_3^-	0.72					
Cl^-	0.36	0.42				
$C_2O_4^{2-}$	0.70	0.79	0.48			
OC	0.44	0.50	*0.12*	0.55		
EC	0.35	0.49	*0.03*	0.40	0.75	
OC_{sec}	0.44	0.48	*0.13*	0.54	0.99	0.67
$PM_{2.5-10}$						
NO_3^-	0.58					
Cl^-	0.46	*-0.06*				
$C_2O_4^{2-}$	0.45	0.49	*0.00*			
OC	*0.06*	*0.09*	*-0.06*	0.32		
EC	*0.11*	*0.10*	*-0.30*	0.21	0.37	1.00
OC_{sec}	n.a.	n.a.	n.a.	n.a.	n.a.	n.a.
PM_{10}						
NO_3^-	0.79					
Cl^-	*0.09*	*0.09*				
$C_2O_4^{2-}$	0.69	0.78	0.17			
OC	0.39	0.48	*-0.05*	0.50		
EC	0.38	0.55	*-0.15*	0.41	0.60	

Table 4.1 *(continued)*

	SO_4^{2-}	NO_3^-	Cl^-	$C_2O_4^{2-}$	OC	EC
OC_{sec}	0.37	0.45	*-0.03*	0.49	1.00	0.52
Autumn						
$PM_{2.5}$						
NO_3^-	0.70					
Cl^-	0.23	*0.12*				
$C_2O_4^{2-}$	0.42	*0.13*	*-0.07*			
OC	0.40	0.46	0.24	0.17		
EC	0.34	0.45	0.21	*0.06*	0.88	
OC_{sec}	0.40	0.44	0.24	0.19	0.99	0.82
$PM_{2.5-10}$						
NO_3^-	0.48					
Cl^-	0.22	-0.22				
$C_2O_4^{2-}$	0.53	0.43	*-0.06*			
OC	*-0.02*	*0.04*	0.20	*0.11*		
EC	*0.14*	0.34	*0.11*	*0.05*	0.50	1.00
OC_{sec}	n.a.	n.a.	n.a.	n.a.	n.a.	n.a.
PM_{10}						
NO_3^-	0.72					
Cl^-	*0.02*	-0.24				
$C_2O_4^{2-}$	0.48	0.27	*0.05*			
OC	0.38	0.38	*-0.02*	0.25		
EC	0.32	0.41	*-0.10*	*0.07*	0.86	
OC_{sec}	0.38	0.36	*-0.01*	0.28	0.99	0.80
Winter						
$PM_{2.5}$						
NO_3^-	0.73					
Cl^-	0.53	0.35				
$C_2O_4^{2-}$	0.58	0.38	0.66			
OC	0.45	0.54	0.39	0.28		
EC	0.31	0.40	0.36	*0.12*	0.81	
OC_{sec}	0.46	0.54	0.37	0.30	0.99	0.71
$PM_{2.5-10}$						
NO_3^-	0.39					
Cl^-	0.31	*0.03*				
$C_2O_4^{2-}$	*-0.07*	*0.18*	*-0.07*			
OC	*0.00*	*0.17*	*0.03*	0.30		
EC	0.25	0.21	*-0.05*	*-0.11*	0.65	1.00
OC_{sec}	n.a.	n.a.	n.a.	n.a.	n.a.	n.a.
PM_{10}						
NO_3^-	0.72					
Cl^-	0.20	*-0.01*				
$C_2O_4^{2-}$	0.55	0.38	0.43			
OC	0.38	0.51	*0.12*	0.26		
EC	0.33	0.44	*0.06*	*0.13*	0.82	

Table 4.1 *(continued)*

	SO_4^{2-}	NO_3^-	Cl^-	$C_2O_4^{2-}$	OC	EC
OC_{sec}	0.37	0.50	*0.13*	0.27	0.99	0.74
Spring						
$PM_{2.5}$						
NO_3^-	0.76					
Cl^-	*-0.01*	*-0.17*				
$C_2O_4^{2-}$	0.63	0.47	*-0.03*			
OC	0.57	0.68	-0.41	0.33		
EC	0.22	0.40	-0.21	*0.08*	0.67	
OC_{sec}	0.60	0.68	-0.42	0.35	0.99	0.55
$PM_{2.5-10}$						
NO_3^-	0.54					
Cl^-	0.34	*-0.13*				
$C_2O_4^{2-}$	0.33	0.22	*0.06*			
OC	*0.14*	0.39	*-0.03*	-0.32		
EC	0.27	0.42	*0.02*	-0.25	0.45	1.00
OC_{sec}	n.a.	n.a.	n.a.	n.a.	n.a.	n.a.
PM_{10}						
NO_3^-	0.75					
Cl^-	*-0.06*	-0.32				
$C_2O_4^{2-}$	0.63	0.48	*-0.15*			
OC	0.49	0.66	-0.40	0.19		
EC	0.27	0.44	-0.34	*0.07*	0.72	
OC_{sec}	0.50	0.66	-0.39	0.20	0.99	0.63

Values shown in italics are not significant at $p < 0.05$ (the 95% level of significance).

Sulphate both in $PM_{2.5}$ and PM_{10} show strong correlation with nitrate during the sampling period (for $PM_{2.5}$; $r = 0.72$, $r = 0.72$, $r = 0.70$, $r = 0.73$, $r = 0.76$ and for PM_{10}; $r = 0.73$, $r = 0.79$, $r = 0.72$, $r = 0.72$, $r = 0.75$ in whole, summer, autumn, winter and spring, respectively), whereas modest correlations are observed in coarse fraction (for $PM_{2.5-10}$; $r = 0.53$, $r = 0.58$, $r = 0.48$, $r = 0.39$ and $r = 0.54$ in whole, summer, autumn, winter and spring, respectively). The good relationships between sulphate and nitrate consistent with results reported by Arimoto et al. (1996), Hu et al. (2002), Abdalmogith and Harrison (2006) and Murillo et al. (2010). These findings could be attributed to the fact that two species undergo similar formation and removal processes in atmosphere. The weak correlations between aerosol chloride with sulphate, nitrate and oxalate in PM are consistently seen in this study together with the higher correlation coefficients observed during the winter. It is clear that the common source is expected to be marine aerosol with very much wind speed in winter.

4.3.2 Relationships between oxalate and major component composition in PM

Oxalate in $PM_{2.5}$ and PM_{10} show the modest correlation higher *r* value with sulphate (r = 0.60 and r = 0.59, respectively) than with nitrate (r = 0.48 and r = 0.49, respectively) in whole period at EROS. These results suggest that oxalate originated from similar atmospheric processes as sulphate i.e., from secondary formation. The good relationships of oxalate with sulphate consistent with results reported by Kerminen et al. (2000), Yao et al. (2003) and Yu et al. (2005). Moreover, the strong relationships of oxalate with sulphate and nitrate are also observed in summer (for $PM_{2.5}$, r = 0.70 and r = 0.79, respectively; for PM_{10}, r = 0.69 and r = 0.78, respectively). With regard to the form of oxalate in particulate phase, the semi-volatile behaviour such as in form of ammonium oxalate would expect to be appeared in oxalate particle. The good correlations between oxalate and nitrate anticipated that the temperature affected the oxalate concentration as nitrate mostly presented as ammonium nitrate which was the temperature dependence. The equilibrium between particulate nitrate and vapour phase is affected by temperature and consequently, if oxalate formed as ammonium oxalate, it may predict the observed temperature dependence behaviour of the oxalate aerosol. The further experiment of air sampling under ammonia gas atmosphere will be discussed more in chapter 6. In this study, there were weak correlations between oxalate and chloride (in whole period; r = 0.27, r = -0.05 and r = 0.11 for $PM_{2.5}$, $PM_{2.5\text{-}10}$ and PM_{10}, respectively) indicating that a contribution from sea spray or coal burning during the winter was not expected to effect on oxalate concentration. As EC is a primary pollutant derived from incomplete combustion of fuels in transportation, heating, power generation, and wood in residential heating and agriculture, the mean oxalate concentration in whole data at EROS had a very weak correlations with EC in $PM_{2.5}$, $PM_{2.5\text{-}10}$ and PM_{10} (r = 0.07, r = -0.09 and r = 0.04, respectively). These were anticipated as a result of its different production sources. The similar observation was reported by the works of Yao et al. (2004) and Yu et al. (2005), which clearly indicated a little contribution of vehicular emissions to ambient oxalic acid.

Oxalate in coarse particle show a modest correlation with nitrate and sulphate in summer (r = 0.49 and r = 0.45, respectively). Coarse oxalate probably caused via the gas-phase oxalic acid reacting with the pre-existing particles and it may also be formed by heterogeneous mechanisms with additional precursors other than oxalic acid. However, for the entire data, oxalate in coarse mode appeared the weak correlations with the other ionic species. The general assumption is that oxalate in ambient air is formed in the aqueous phase and therefore

the coarse mode oxalate can be produced by aqueous phase process. Russell and Seinfeld (1998) have also proposed that the supermicron particles can be formed by in-cloud processes. The previous studies by Dutton and Evans (1996) and Gadd (1999) stated that oxalate was a by-product of the hydrolysis of oxaloacetate from citric acid and glyoxylate via the metabolic mechanism of fungi in the soil. This could be the significant source of oxalate in coarse mode from soil particles.

Figure 4.2 to Figure 4.5 show a graphical representation of relationships between oxalate and sulphate and nitrate in $PM_{2.5}$ at EROS and Harwell sites.

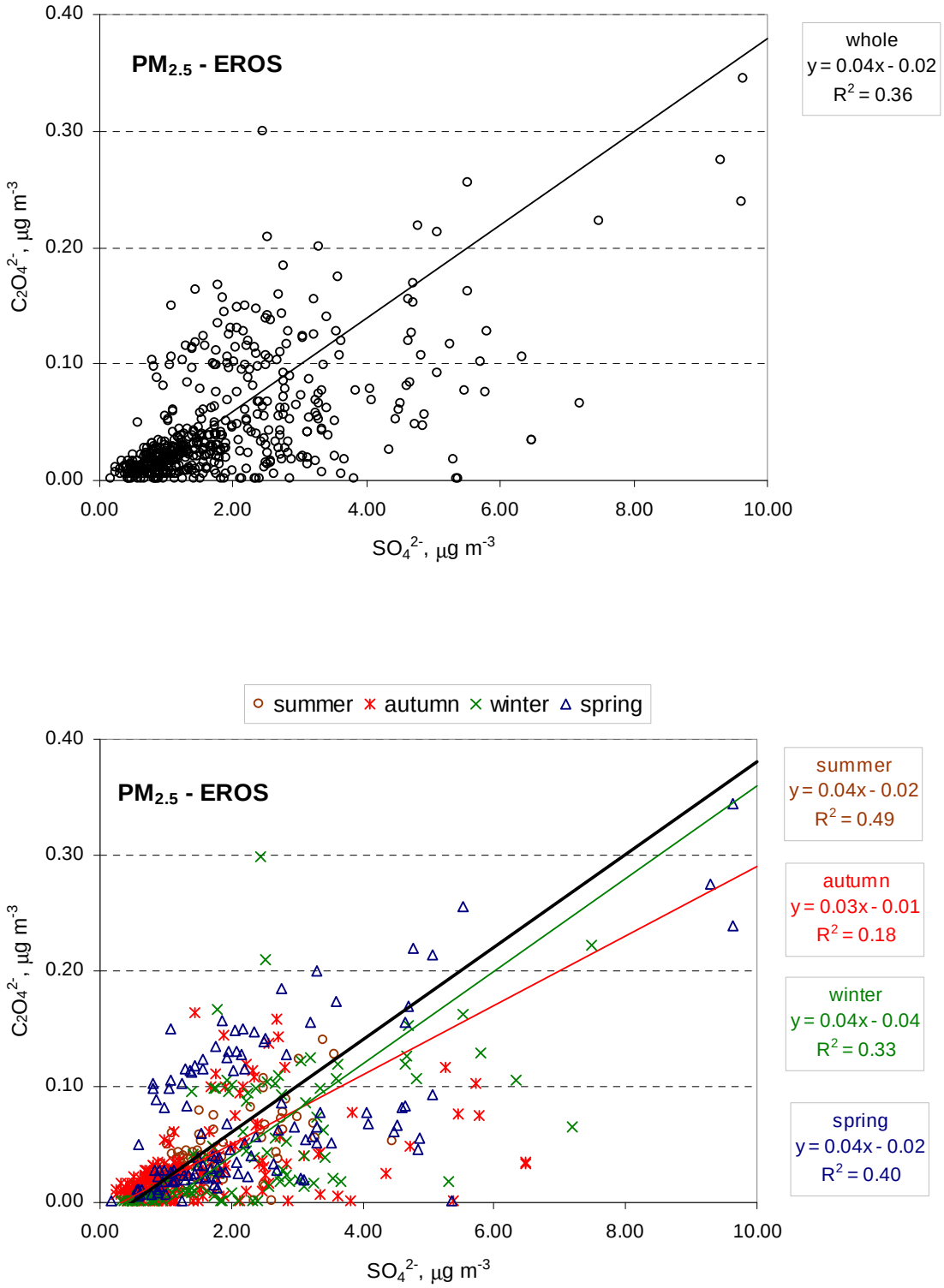

Figure 4.2 Relationship between oxalate and sulphate concentrations in $PM_{2.5}$ measured at EROS

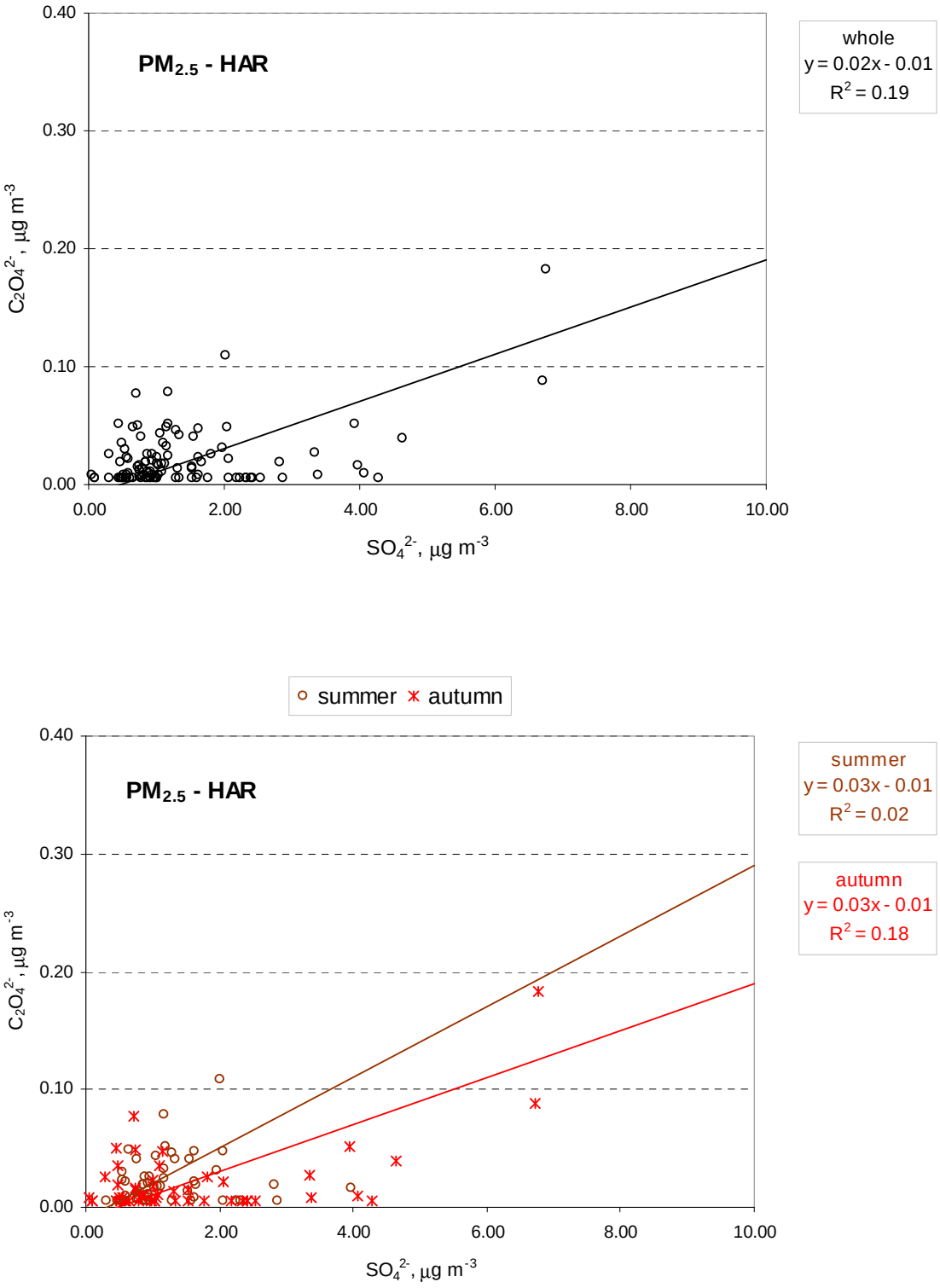

Figure 4.3 Relationship between oxalate and sulphate concentrations in $PM_{2.5}$ measured at Harwell

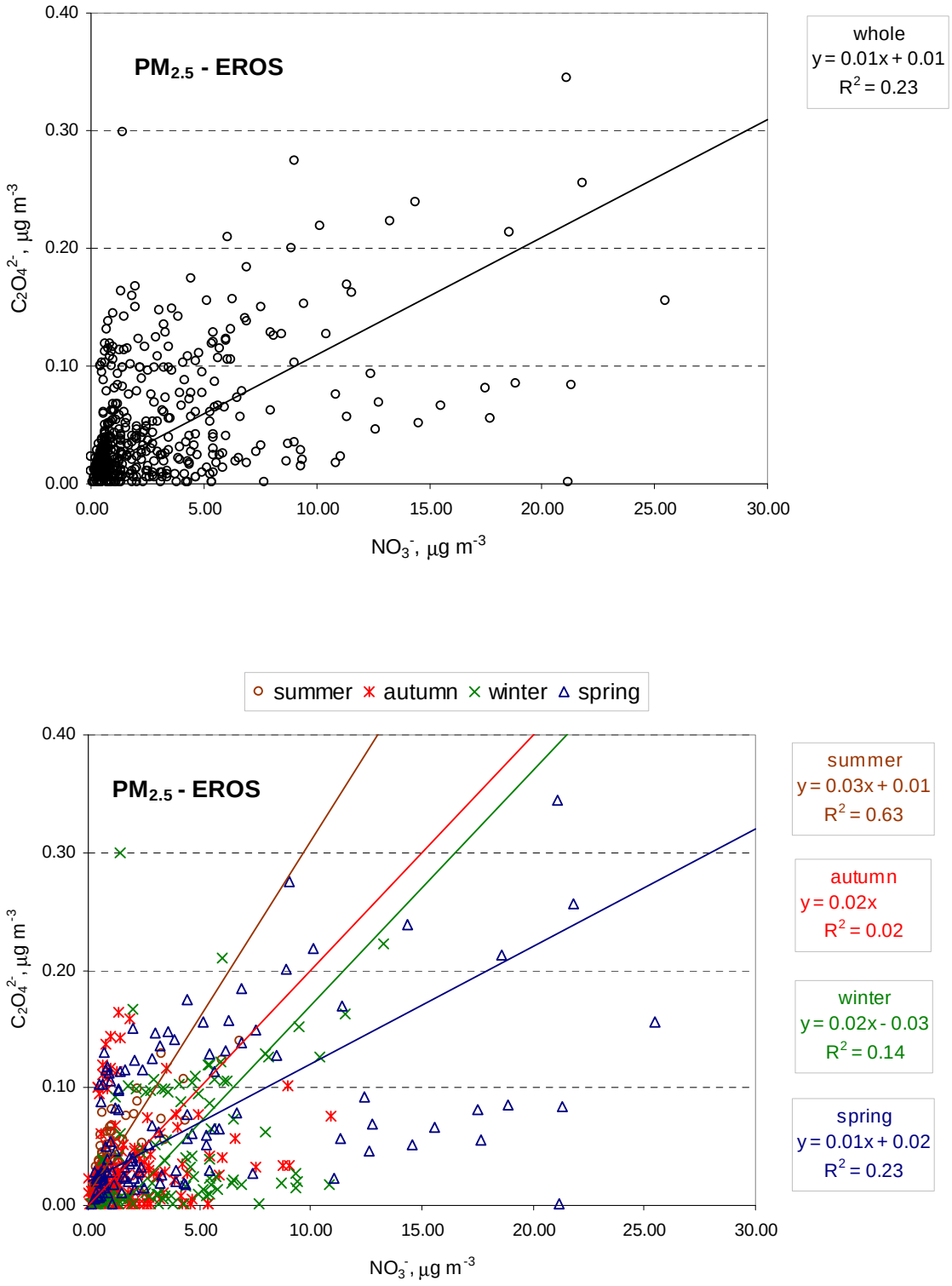

Figure 4.4 Relationship between oxalate and nitrate concentrations in $PM_{2.5}$ measured at EROS

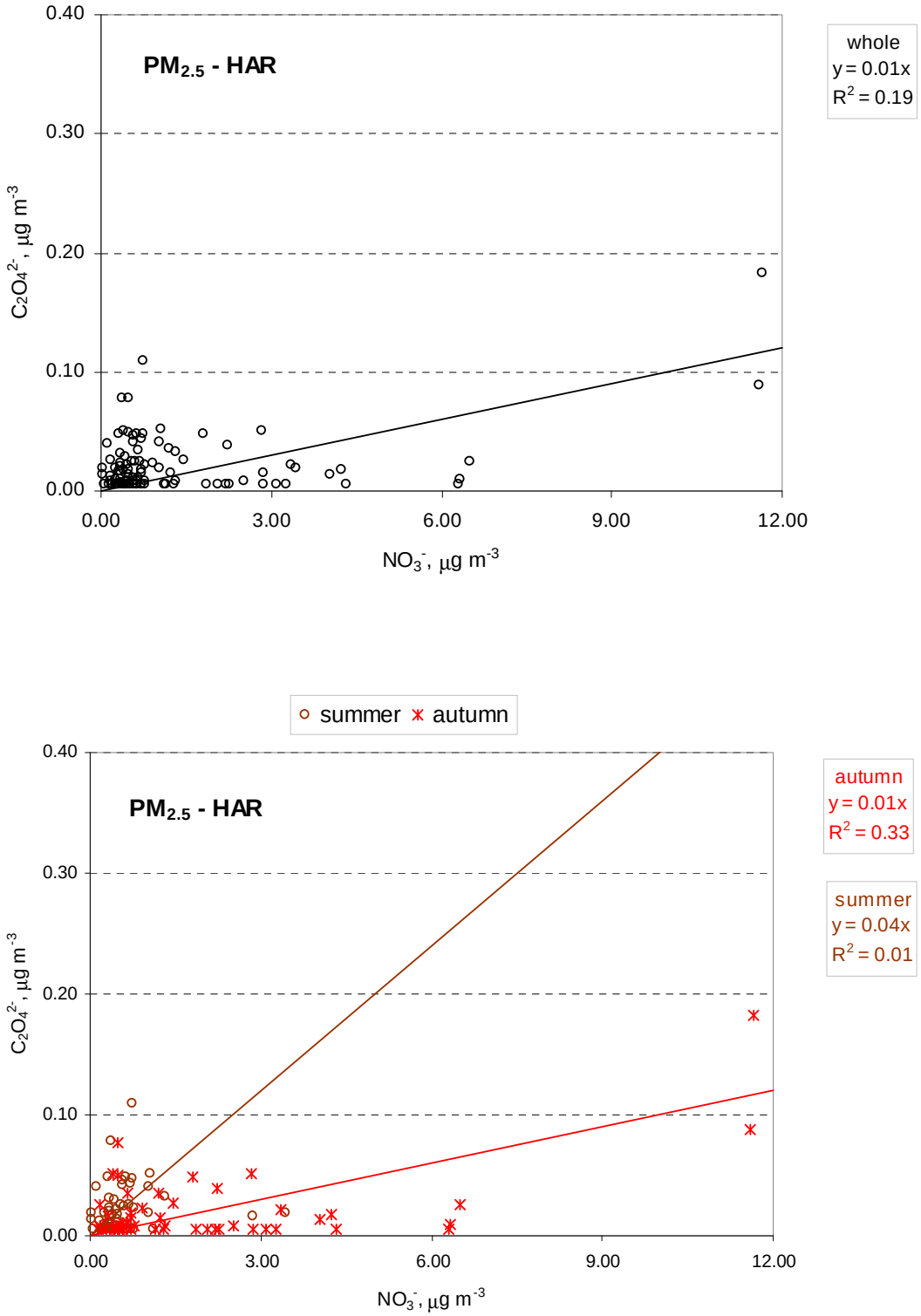

Figure 4.5 Relationship between oxalate and nitrate concentrations in $PM_{2.5}$ measured at Harwell

In order to investigate the secondary sources of oxalate aerosol, the relationships between oxalate and secondary OC are determined and the plots of oxalate versus OC_{sec} in $PM_{2.5}$ at EROS and Harwell show in Figure 4.6 and Figure 4.7, respectively. The highest regression coefficient and the modest correlation of oxalate with OC_{sec} was found in $PM_{2.5}$ at EROS (r = 0.54) during summer as the favouring of secondary OC formation by photooxidation process. This is in agreement with the study reported by Kawamura and Ikushima (1993) and Sempere and Kawamura (1994).

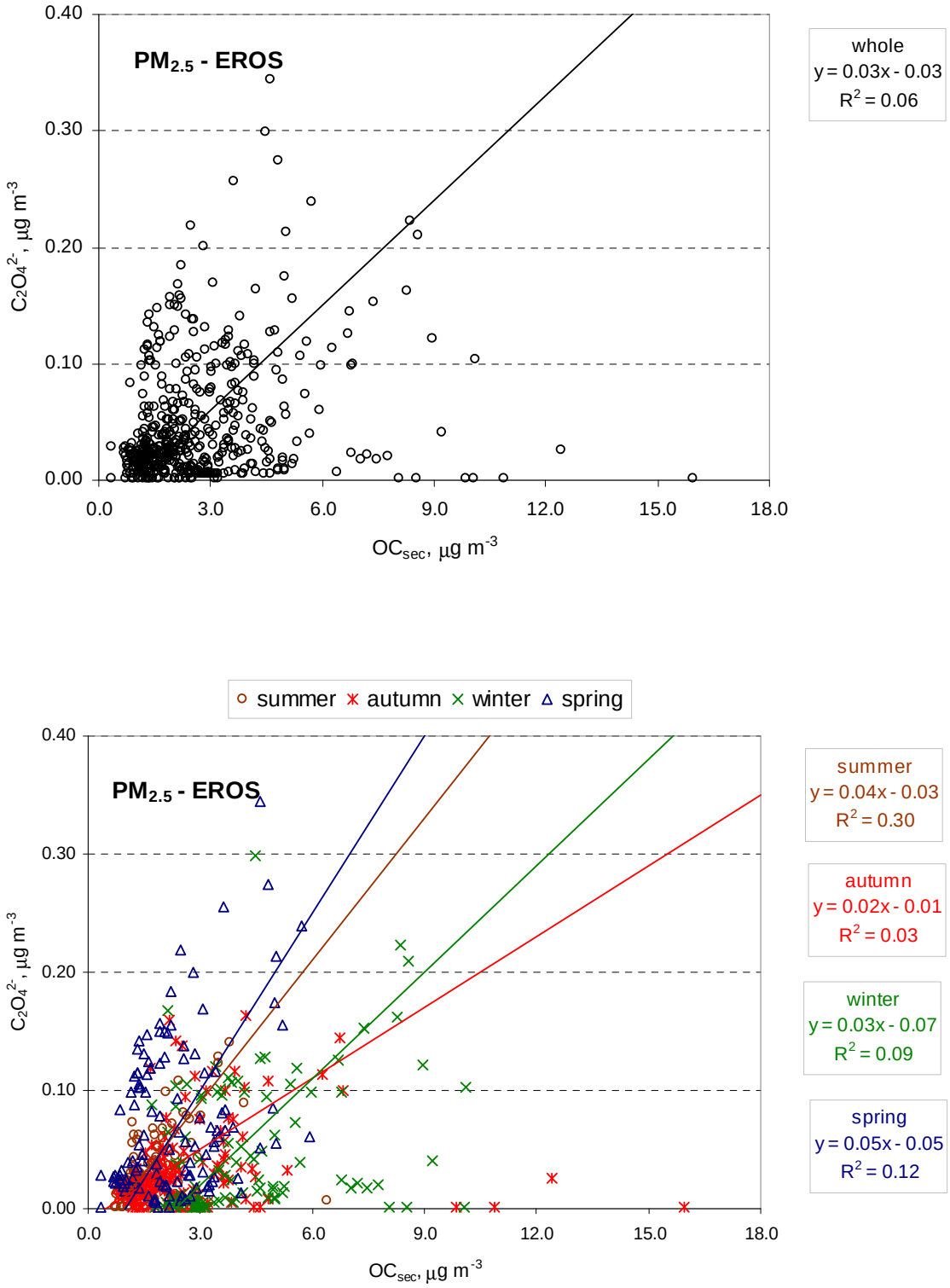

Figure 4.6 Relationship between oxalate and secondary OC concentrations in $PM_{2.5}$ measured at EROS

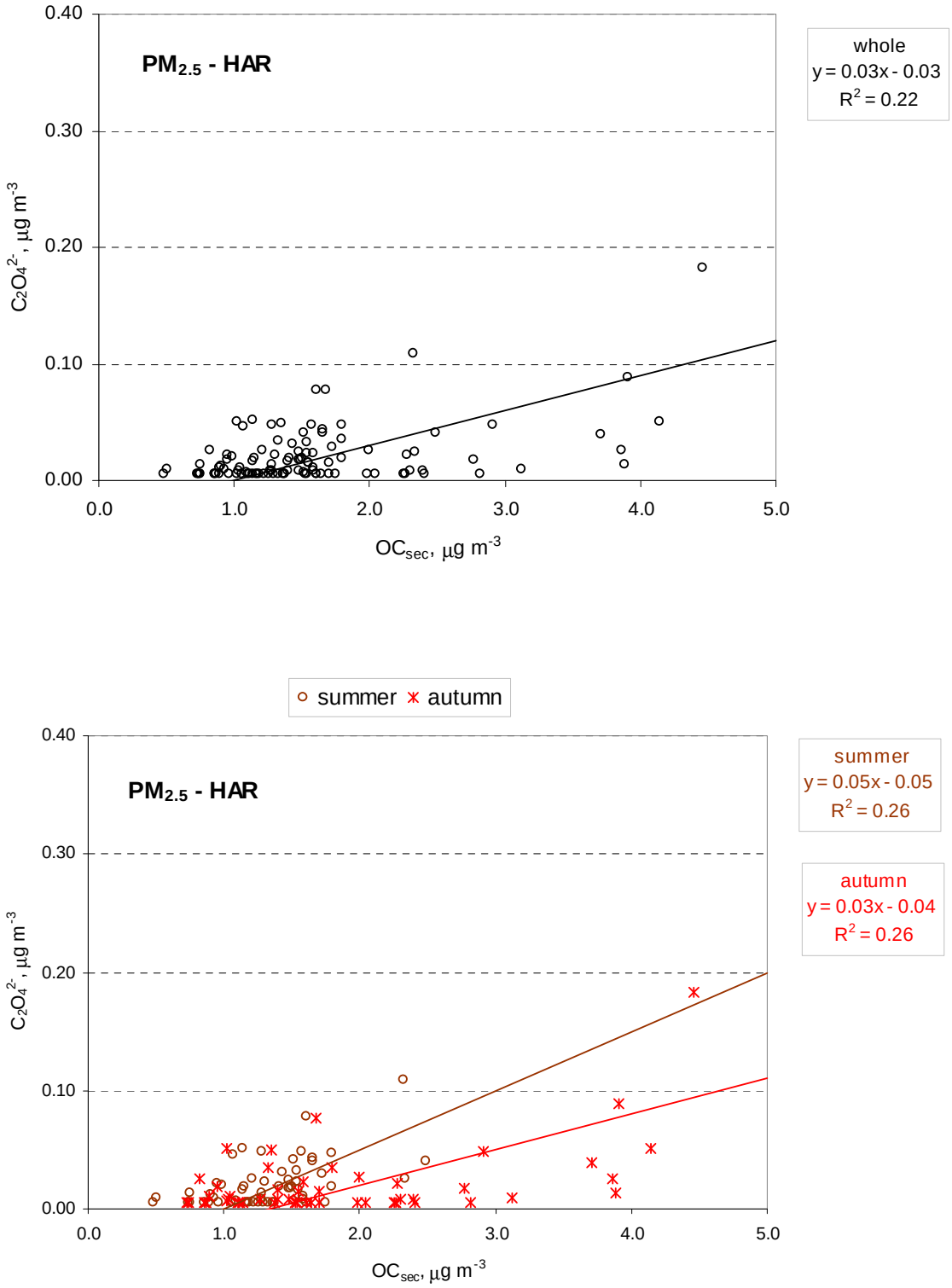

Figure 4.7 Relationship between oxalate and secondary OC concentrations in $PM_{2.5}$ measured at Harwell

4.3.3 The ratios calculated between major component composition in PM

As the fluctuation in temperature, relative humidity, meteorology, oxidant levels and the degree of long-range transport, the variations of chemical component ratios in particulate matter will be observed in different sampling sites and samples collecting period. The whole average sulphate-to-nitrate ratios at EROS were 0.68, 0.37 and 0.62 for $PM_{2.5}$, $PM_{2.5-10}$ and PM_{10}, respectively and at Harwell were 1.09, 0.39 and 0.85 for $PM_{2.5}$, $PM_{2.5-10}$ and PM_{10}, respectively (Table 4.2). In comparison between seasons, the highest SO_4^{2-}/NO_3^- ratio for $PM_{2.5}$ and PM_{10} at both sites were seen during the summer (at EROS; 1.58 and 1.08 for $PM_{2.5}$ and PM_{10}, respectively; at Harwell; 2.11 and 1.25 for $PM_{2.5}$ and PM_{10}, respectively), suggesting that the production of sulphate aerosol by photochemical oxidation of the atmosphere (aqueous oxidation) slightly reflected on its concentration but there was the significant of volatile loss of nitrate aerosol as ammonium nitrate during high temperature. Moreover, SO_4^{2-}/NO_3^- ratios were extremely high for $PM_{2.5}$ in summer (1.58 and 2.11 at EROS and Harwell, respectively), indicating that the suphate aerosol was more stable than nitrate aerosol during long-rang transport. These results also observed in the study of Abdalmogith and Harrison (2006).

The whole mean chloride-to-nitrate ratios were 0.27, 1.11 and 0.45 for $PM_{2.5}$, $PM_{2.5-10}$ and PM_{10}, respectively at EROS and were 0.18, 0.80 and 0.42 for $PM_{2.5}$, $PM_{2.5-10}$ and PM_{10}, respectively at Harwell. As expected at both sites, the Cl^-/NO_3^- ratios presented high in coarse fraction because the major source of chloride in coarse fraction mostly contributed from sea spray which can be transported from the sea to rural and urban areas (Gustafsson and Franzen, 2000). Chloride is normally associated with sodium. The average Cl^-/NO_3^- ratio is also observed high in coarse particle during the winter (1.63) causing by fast back trajectories pass over the marine atmosphere before arriving at this site (detailed in chapter 5). In addition, the contribution from coal burning in the winter would be considered.

The variations of the oxalate-to-sulphate ratio and the oxalate-to-nitrate ratio were not clearly observed in this study at EROS. For the coarse fraction, it should be noted that the $C_2O_4^{2-}/SO_4^{2-}$ ratio appeared high in summer (0.09) and oxalate did not present in winter at EROS as the observed $C_2O_4^{2-}/SO_4^{2-}$ ratio of 0, suggesting that oxalate in coarse fraction could be generated by the photochemical reaction in high temperature condition. At Harwell, the $C_2O_4^{2-}/SO_4^{2-}$ ratios in $PM_{2.5}$, $PM_{2.5-10}$ and PM_{10} revealed high during the summer (0.02, 0.17

and 0.04, respectively). In addition, the $C_2O_4^{2-}/NO_3^-$ ratios of $PM_{2.5}$, $PM_{2.5-10}$ and PM_{10} in summer were dominant values of 0.04, 0.06 and 0.05, respectively. Since Harwell is a rural site, these results indicating that the contribution of oxalate during the summer by photochemical oxidation was a significant source. The dissociation of oxalate compounds (as expected in the form of ammonium salt) in atmosphere may also play an important role to contribute its concentration during the high temperature. As nitrate in the form of ammonium nitrate represented the temperature dependence, the good correlation coefficients of oxalate with nitrate were observed in summer (Table 4.1; r = 0.79 and r = 0.78 for $PM_{2.5}$ and PM_{10}, respectively). It is likely that the rate of dissociation of aerosol nitrate was higher than particulate oxalate with evidence on the high ratios of the oxalate-to-nitrate found in airborne PM during summer.

Table 4.2 Mean SO_4^{2-}/NO_3^-, Cl^-/NO_3^-, $C_2O_4^{2-}/SO_4^{2-}$ and $C_2O_4^{2-}/NO_3^-$ ratios at the two sampling sites

	N	Mean SO_4^{2-}/NO_3^-	Ratio	Mean Cl^-/NO_3^-	Ratio	Mean $C_2O_4^{2-}/SO_4^{2-}$	Ratio	Mean $C_2O_4^{2-}/NO_3^-$	Ratio
EROS									
$PM_{2.5}$									
Whole	500	1.86/2.72	0.68	0.73/2.72	0.27	0.05/1.86	0.03	0.05/2.72	0.02
Summer	116	1.45/0.92	1.58	0.37/0.92	0.40	0.03/1.45	0.02	0.03/0.92	0.03
Autumn	165	1.57/1.75	0.90	0.53/1.75	0.30	0.03/1.57	0.02	0.03/1.75	0.02
Winter	101	2.25/3.97	0.57	1.25/3.97	0.31	0.05/2.25	0.02	0.05/3.97	0.01
Spring	118	2.32/4.80	0.48	0.93/4.80	0.19	0.07/2.32	0.03	0.07/4.80	0.01
$PM_{2.5-10}$									
Whole	500	0.28/0.75	0.37	0.83/0.75	1.11	0.02/0.28	0.07	0.02/0.75	0.03
Summer	116	0.22/0.62	0.35	0.53/0.62	0.85	0.02/0.22	0.09	0.02/0.62	0.03
Autumn	165	0.27/0.72	0.38	0.93/0.72	1.29	0.02/0.27	0.07	0.02/0.72	0.03
Winter	101	0.27/0.54	0.50	0.88/0.54	1.63	0.00/0.27	0.00	0.00/0.54	0.00
Spring	118	0.36/1.09	0.33	0.95/1.09	0.87	0.02/0.36	0.06	0.02/1.09	0.02
PM_{10}									
Whole	500	2.13/3.46	0.62	1.56/3.46	0.45	0.06/2.13	0.03	0.06/3.46	0.02
Summer	116	1.67/1.54	1.08	0.90/1.54	0.58	0.05/1.67	0.03	0.05/1.54	0.03
Autumn	165	1.82/2.44	0.75	1.45/2.44	0.59	0.04/1.82	0.02	0.04/2.44	0.02
Winter	101	2.52/4.48	0.56	2.12/4.48	0.47	0.05/2.52	0.02	0.05/4.48	0.01
Spring	118	2.67/5.88	0.45	1.87/5.88	0.32	0.09/2.67	0.03	0.09/5.88	0.02
HAR									
$PM_{2.5}$									
Whole	107	1.40/1.29	1.09	0.23/1.29	0.18	0.02/1.40	0.01	0.02/1.29	0.02
Summer	57	1.20/0.57	2.11	0.17/0.57	0.30	0.02/1.20	0.02	0.02/0.57	0.04
Autumn	50	1.62/2.10	0.77	0.30/2.10	0.14	0.02/1.62	0.01	0.02/2.10	0.01

Table 4.2 *(continued)*

	N	Mean SO_4^{2-}/NO_3^-	Ratio	Mean Cl^-/NO_3^-	Ratio	Mean $C_2O_4^{2-}/SO_4^{2-}$	Ratio	Mean $C_2O_4^{2-}/NO_3^-$	Ratio
$PM_{2.5-10}$									
Whole	107	0.30/0.76	0.39	0.61/0.76	0.80	0.02/0.30	0.07	0.02/0.76	0.03
Summer	57	0.18/0.52	0.35	0.50/0.52	0.96	0.03/0.18	0.17	0.03/0.52	0.06
Autumn	50	0.43/1.08	0.40	0.74/1.08	0.69	0.01/0.43	0.02	0.01/1.08	0.01
PM_{10}									
Whole	107	1.69/2.00	0.85	0.84/2.00	0.42	0.04/1.69	0.02	0.04/2.00	0.02
Summer	57	1.38/1.10	1.25	0.67/1.10	0.61	0.05/1.38	0.04	0.05/1.10	0.05
Autumn	50	2.04/3.02	0.68	1.04/3.02	0.34	0.03/2.04	0.01	0.03/3.02	0.01

4.4 Interpretation of ion species in PM between sites

The major ion species interested were sulphate, nitrate, chloride and oxalate measured in aerosol samples collected simultaneously. As mentioned in 4.2 about the importance of oxalate in activating CCN, its component also plays a good indicator for water-soluble organic carbon (WSOC), which is a significant portion of organic carbon as well as OC_{sec} in PM (Huang et al., 2006). In this study, water-extractable organic carbon taken by the method referred in chapter 2 is regarded as WSOC. The method efficiency was examined by the plot of all measured data of WSOC versus organic carbon in fine fraction (both at EROS and Harwell) showing the good correlation with R^2 of 0.86 (Figure 4.8). Typically, WSOC constitute a substantial fraction of OC and account for 20 – 80% of particulate OC (Saxena and Hildemann, 1996). Consequently, the completion of procedure for water extracted should be evaluated by the good relationship observed between OC and WSOC in aerosol samples. The percentage contributions of WSOC to OC at EROS and Harwell were 75% and 72%, respectively. It is likely that the formation mechanism of WSOC can be suggested for the secondary pathway with discussions later in comparison with OC_{sec}.

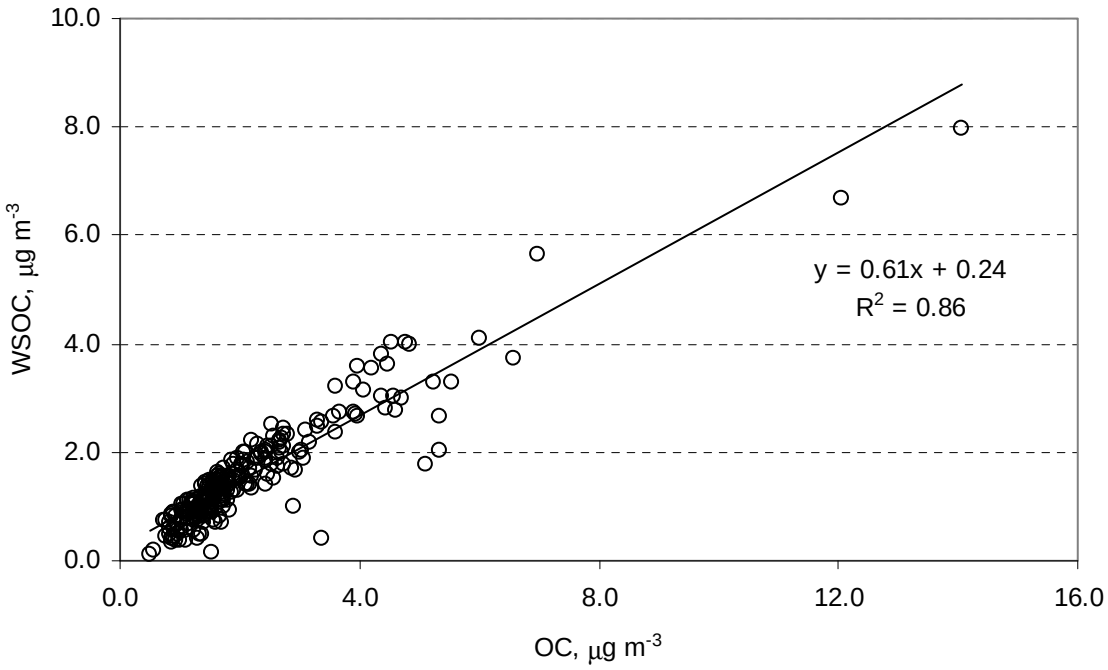

Figure 4.8 Plot of all data of WSOC versus organic carbon concentrations measured at EROS and Harwell

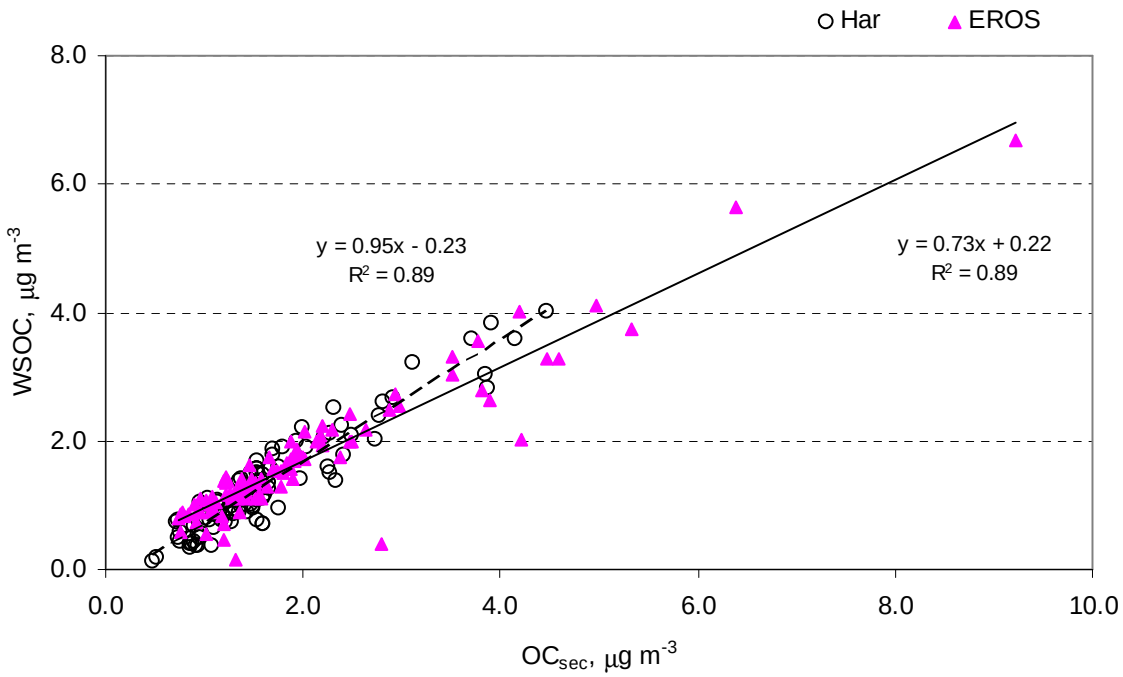

Figure 4.9 Relationships between WSOC and secondary organic carbon concentrations in $PM_{2.5}$ measured at EROS and Harwell

The concentration data of major anionic species including OC_{sec} and WSOC in $PM_{2.5}$, $PM_{2.5-10}$ and PM_{10} at EROS and Harwell sites appear in Table 4.3 in term of mean and range. With regard to fine fraction, the inter-site differences of SO_4^{2-}, NO_3^-, Cl^-, $C_2O_4^{2-}$, OC_{sec} and WSOC are 8%, 11%, 26%, 0%, 22% and 27%, respectively. For PM_{10}, the inter-site differences of SO_4^{2-}, NO_3^-, Cl^-, $C_2O_4^{2-}$ and OC_{sec} are 2%, 4%, 3%, 29% and 14%, respectively. The Mann-Whitney U test was applied in order to evaluate the significant difference between the two sites. Test results indicated that SO_4^{2-}, NO_3^-, $C_2O_4^{2-}$ and OC_{sec} concentrations measured in $PM_{2.5}$ simultaneously at EROS and Harwell were no difference with $p > 0.05$. There were the differences of Cl^- and WSOC concentrations in fine particle between the two sites ($p < 0.05$). The same calculation in order to quantify the influence of local contribution on secondary aerosol formation was applied by subtraction of Harwell concentrations representing rural site from EROS concentrations representing urban background site (as mentioned in 3.3.3). The results of local contribution show in Table 4.4. The lower local contributions were observed in fine sulphate, nitrate and chloride in this study (0.13 μg m^{-3}, 0.17 μg m^{-3} and 0.08 μg m^{-3}, respectively), suggesting that the secondary formations by oxidation in atmosphere mostly effected in these species. There is no difference mean concentration of oxalate in $PM_{2.5}$ between both sites. This finding is strongly supportive the formation of oxalate by photochemical transformations of precursors in the atmosphere with long-lived species. Backward air trajectories arriving at both sites are determined in the following chapter in order to investigate the reflection of regional contribution.

The mean concentrations of WSOC in $PM_{2.5}$ at EROS and Harwell sites are 1.7 ± 1.0 μg m^{-3} and 1.3 ± 0.8 μg m^{-3}, respectively. The ratios of WSOC-to-secondary OC at both site do not show significant difference and present high percentage contributions to OC_{sec} (0.9 ± 0.2 and 0.8 ± 0.2 for EROS and Harwell, respectively) including the very good correlations between WSOC and OC_{sec} within sampling site ($r = 0.94$ for $PM_{2.5}$ at both sites) (Table 4.6). The relationships between WSOC and OC_{sec} at EROS and Harwell sites are plotted in Figure 4.9 with the good R^2 of 0.89. In addition, modest correlations of WSOC with sulphate and nitrate are observed at EROS ($r = 0.45$ and $r = 0.58$, respectively) and WSOC showed strong relationships with sulphate and nitrate at Harwell site ($r = 0.69$ and $r = 0.79$, respectively). These suggest that WSOC substances mainly occur by the secondary formation in the atmosphere especially in rural site, consistent with the study by Yang et al. (2005) and Sullivan et al. (2004). Basically, OC_{sec} components are water soluble because the oxidation reactions leading to their formation given polar functional groups i.e. hydroxyl, carbonyl and

carboxyl, to the secondary organic carbons. WSOC formation for the secondary pathway can be suggested as homogeneous photooxidation from VOC precursors and heterogeneous oxidation in the presence of clouds and fog (Huang et al., 2006). The local contribution of WSOC is observed in the concentration of 0.4 μg m^{-3} in this work. It is likely a combined result of more aged aerosols and probably higher contributions of biomass burning aerosols at the sampling sites as also stated by Yang et al. (2005). Although, it is recognised that emission from biomass burning include a large portion of soluble organic compounds (Schauer, et al., 2001, Mayol-Bracero et al., 2002, Park et al., 2006), there were quite low concentration of potassium (0.11 μg m^{-3} with approximately 6% to WSOC) at EROS, a tracer for biomass burning (Hu, 2011). Thus, the other sources of local WSOC should be considered (i.e. biogenic emission sources) as well.

Table 4.3 Statistical data of sulphate, nitrate, chloride, oxalate, secondary OC and WSOC (μg m^{-3}) concentrations including the ratio of $WSOC/OC_{sec}$ at EROS and Harwell sites measured simultaneously

	$PM_{2.5}$		$PM_{2.5-10}$		PM_{10}	
	Mean ± S.D.	Range	Mean± S.D.	Range	Mean± S.D.	Range
EROS						
SO_4^{2-}	1.60 ± 1.35	0.32 – 6.48	0.25 ± 0.17	<dl – 0.89	1.85 ± 1.47	0.55 – 7.37
NO_3^-	1.61 ± 2.11	<dl – 10.88	0.63 ± 0.64	<dl – 3.29	2.25 ± 2.50	<dl – 12.49
Cl^-	0.35 ± 0.27	<dl – 1.29	0.61 ± 0.51	0.08 – 2.79	0.96 ± 0.67	0.16 – 3.38
$C_2O_4^{2-}$	0.02 ± 0.02	<dl – 0.10	0.01 ± 0.01	<dl – 0.05	0.03 ± 0.02	<dl – 0.12
OC_{sec}*	2.0 ± 1.3	0.7 – 9.2	n.a	n.a	3.1 ± 1.5	1.4 – 10.8
WSOC	1.7 ± 1.0	0.1 – 6.7	n.a	n.a	n.a	n.a
$WSOC/OC_{sec}$	0.9 ± 0.2	0.1 – 1.2	n.a	n.a	n.a	n.a
HAR						
SO_4^{2-}	1.47 ± 1.24	0.05 – 6.76	0.35 ± 0.40	<dl – 2.36	1.82 ± 1.40	0.36 – 7.53
NO_3^-	1.44 ± 2.02	0.03 – 11.65	0.71 ± 0.68	<dl – 3.40	2.16 ± 2.50	0.19 – 14.75
Cl^-	0.27 ± 0.23	<dl – 1.22	0.66 ± 0.60	0.04 – 3.17	0.93 ± 0.80	0.09 – 4.39
$C_2O_4^{2-}$	0.02 ± 0.03	<dl – 0.18	0.02 ± 0.02	<dl – 0.05	0.04 ± 0.03	<dl – 0.19
OC_{sec}*	1.6 ± 0.8	0.5 – 4.5	n.a	n.a	2.7 ± 1.0	0.9 – 6.6
WSOC	1.3 ± 0.8	0.1 – 4.0	n.a	n.a	n.a	n.a
$WSOC/OC_{sec}$	0.8 ± 0.2	0.2 – 1.1	n.a	n.a	n.a	n.a

* Secondary organic carbon calculated based on the ratio of $(OC/EC)_{min}$ = 0.35

Table 4.4 The local contributions of sulphate, nitrate, chloride, oxalate, OC_{sec} and WSOC in $PM_{2.5}$, $PM_{2.5-10}$ and PM_{10} calculated based on mean differences concentration between EROS and Harwell during the simultaneous period (EROS conc. – HAR conc.)

Components	Local contribution, μg m^{-3}		
	$PM_{2.5}$	$PM_{2.5-10}$	PM_{10}
SO_4^{2-}	0.13	-0.10	0.03
NO_3^-	0.17	-0.08	0.09
Cl^-	0.08	-0.05	0.03
$C_2O_4^{2-}$	0	-0.01	-0.01
OC_{sec}	0.4	n.a.	0.4
WSOC	0.4	n.a.	n.a.

Regression analysis of ion species in $PM_{2.5}$ obtained from EROS and Harwell data was run using the reduced major axis (RMA) regression. The relationships between the urban background (EROS) concentration and the rural (Harwell) concentration were plotted (Figure 4.10) and the results of regression analyses are summarized in Table 4.5. In this data, the regression coefficients (R^2) of sulphate and nitrate in fine particle show high value of 0.67 and 0.70, respectively. On the contrary, the low values of regression coefficient of chloride, oxalate, WSOC and OC_{sec} were observed in range from 0.20 to 0.32.

Sulphate in fine mode showed the zero intercept with a gradient close to 1.0 indicating that the regional contributions by long-range transport and photochemical oxidation in the atmosphere play an important factor on its concentration. In addition, there was the same local sulphate both in EROS and Harwell sites. For nitrate in $PM_{2.5}$, it is clear that the higher local nitrate concentration was found at urban background to rural area as the intercept value of 0.11 in agreement with the local fine nitrate contribution of 0.17 μg m^{-3}. This finding suggests that the nitrate increment probably arises from anthropogenic sources in the conditions of high conversion of nitric acid vapour to nitrate aerosol. As mentioned in the previous chapter, the road traffic might be the related source as NO_x showing a significant correlation with EC at EROS site, consequently, HNO_3 is the primary chemical sink for NO_x in urban environments. With regard to chloride, oxalate and WSOC, the intercept values of chloride, oxalate and WSOC in fine fraction were low (0.05 μg m^{-3}, 0.01 μg m^{-3} and 0.01 μg m^{-3}, respectively) indicating that any local chloride, oxalate and WSOC contributions at EROS are similar to those at Harwell site.

(a)

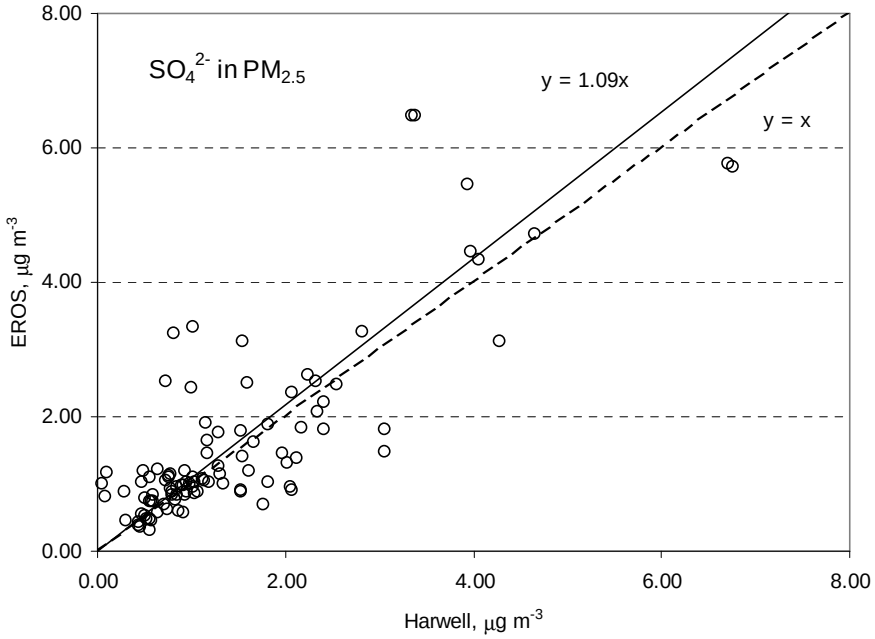

(b)

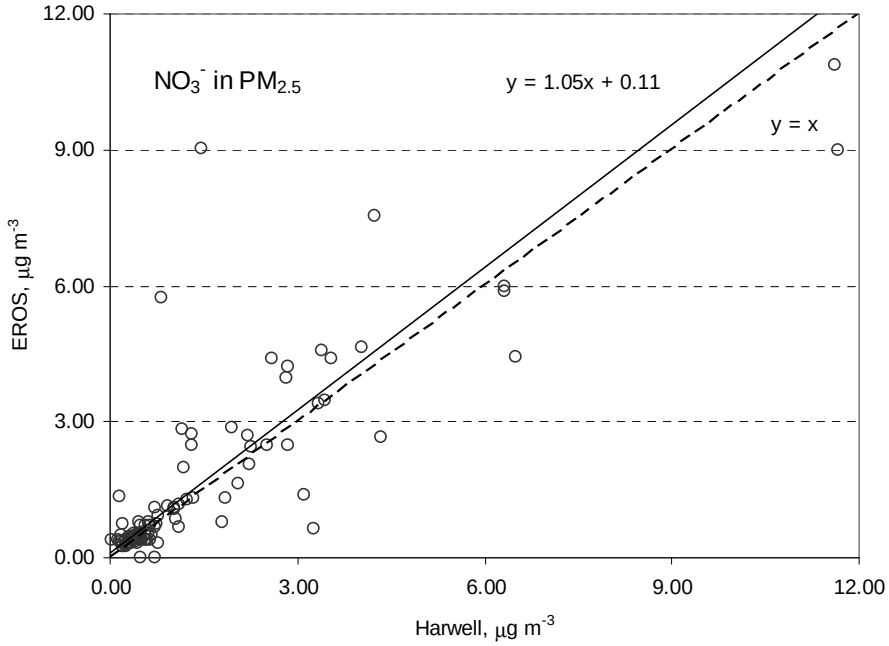

Figure 4.10 Relationships between EROS and Harwell concentrations of (a) sulphate, (b) nitrate, (c) chloride, (d) oxalate and (e) WSOC during the simultaneous period

(c)

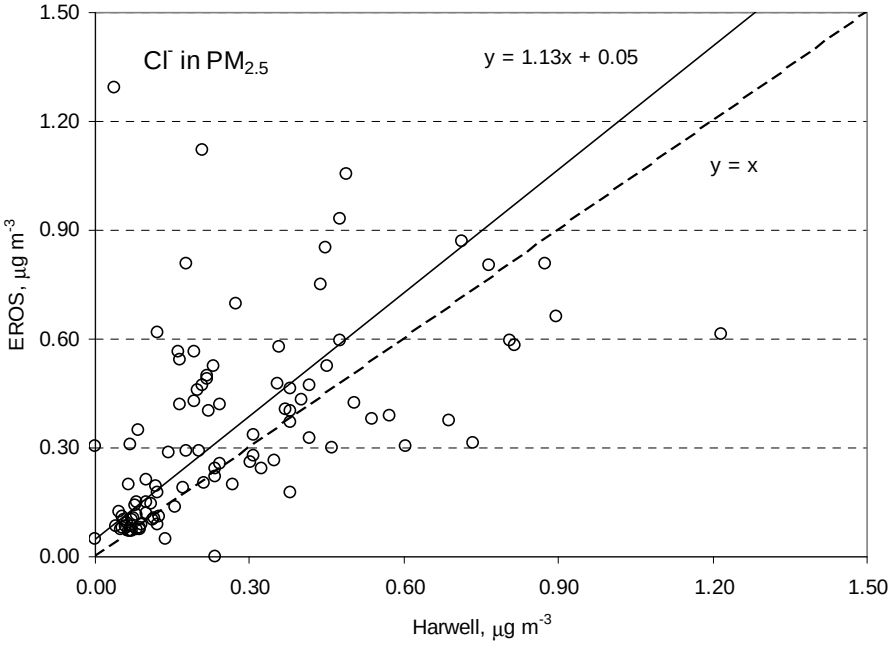

(d)

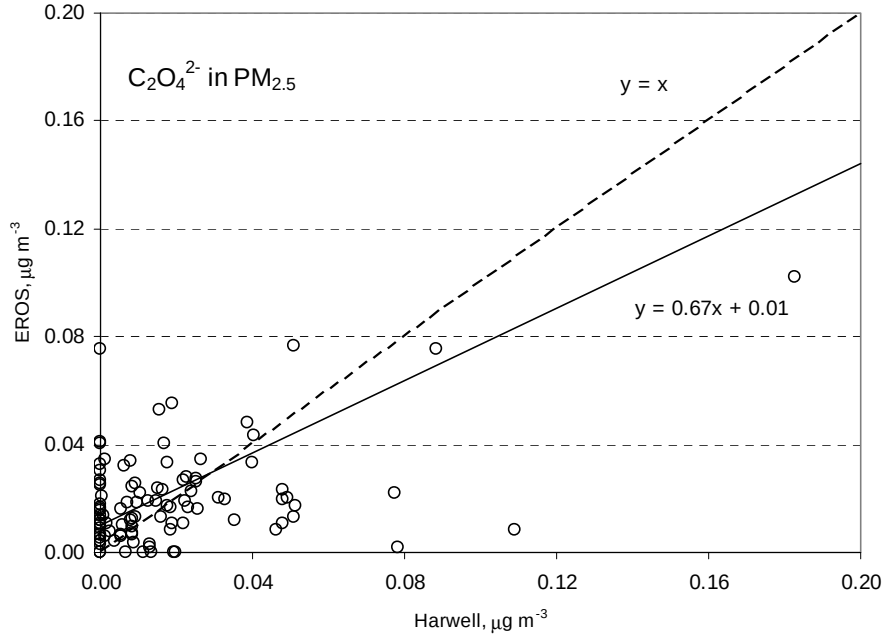

Figure 4.10 *(continued)*

(e)

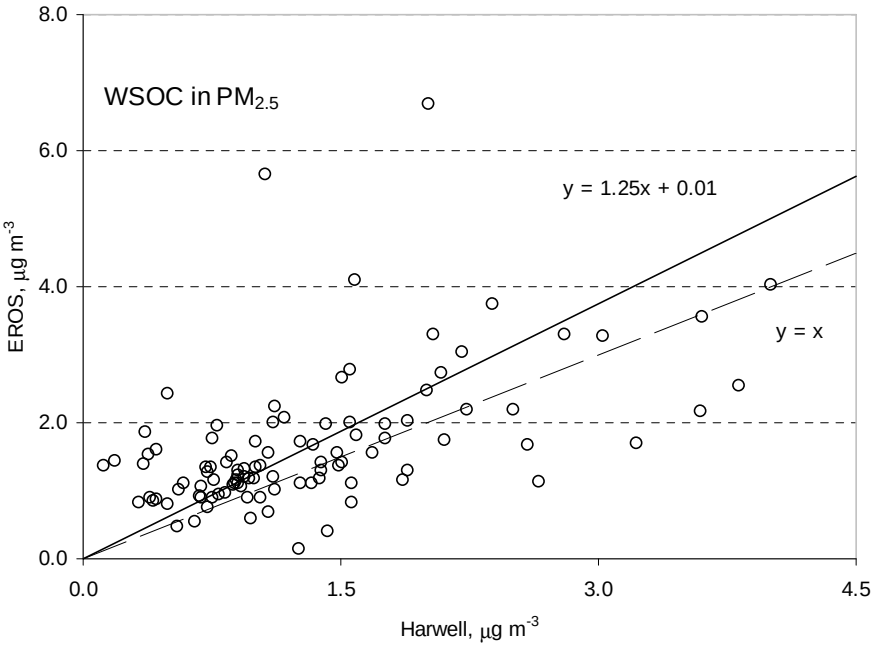

Figure 4.10 *(continued)*

Table 4.5 Results of regression analysis of EROS (urban background) and Harwell (rural) concentrations of ion components in $PM_{2.5}$

Analyte	RMA regression
Sulphate	$y = 1.09x$ ($R^2 = 0.67$)
Nitrate	$y = 1.05x + 0.11$ ($R^2 = 0.70$)
Chloride	$y = 1.13x + 0.05$ ($R^2 = 0.27$)
Oxalate	$y = 0.67x + 0.01$ ($R^2 = 0.20$)
WSOC	$y = 1.25x + 0.01$ ($R^2 = 0.27$)
OC_{sec}	$y = 1.62x - 0.67$ ($R^2 = 0.32$)

Note: y represents urban background (EROS) concentration of analyte in μg m^{-3}; x represents rural (HAR) concentration of analyte in μg m^{-3}

4.4.1 Seasonal behaviour of ion species

It is advantage to have a look at the seasonal behaviour of major ion species from data collected simultaneously. Figure 4.11 shows daily data of (a) sulphate, (b) nitrate, (c) chloride, (d) oxalate and (e) WSOC concentration in fine particle observed simultaneously at EROS and Harwell. As appeared in time series, each of these ions presents quite similar temporal variation patterns between EROS (urban background) and Harwell (rural). This indicates the dominance of long-range transport and meteorological conditions over the local sources in determining the concentration of these secondary aerosols. This is also supported by the quite low local contribution value of these compound already showed in Table 4.4.

(a)

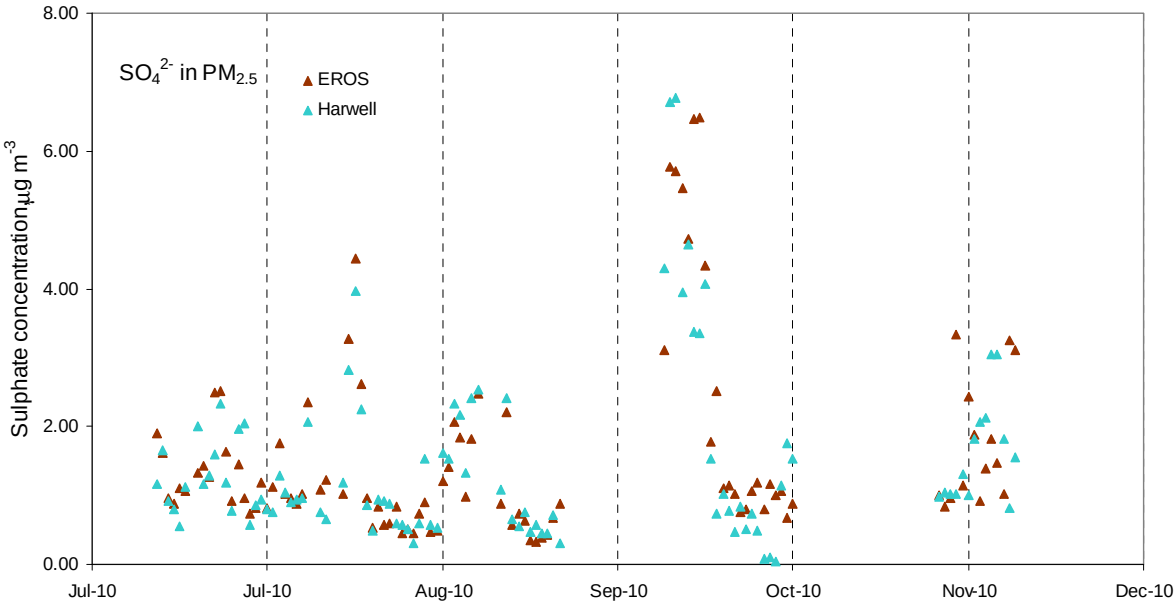

Figure 4.11 Time series of (a) sulphate, (b) nitrate, (c) chloride, (d) oxalate and (e) WSOC concentrations in $PM_{2.5}$ measured simultaneously at EROS and Harwell sites

(b)

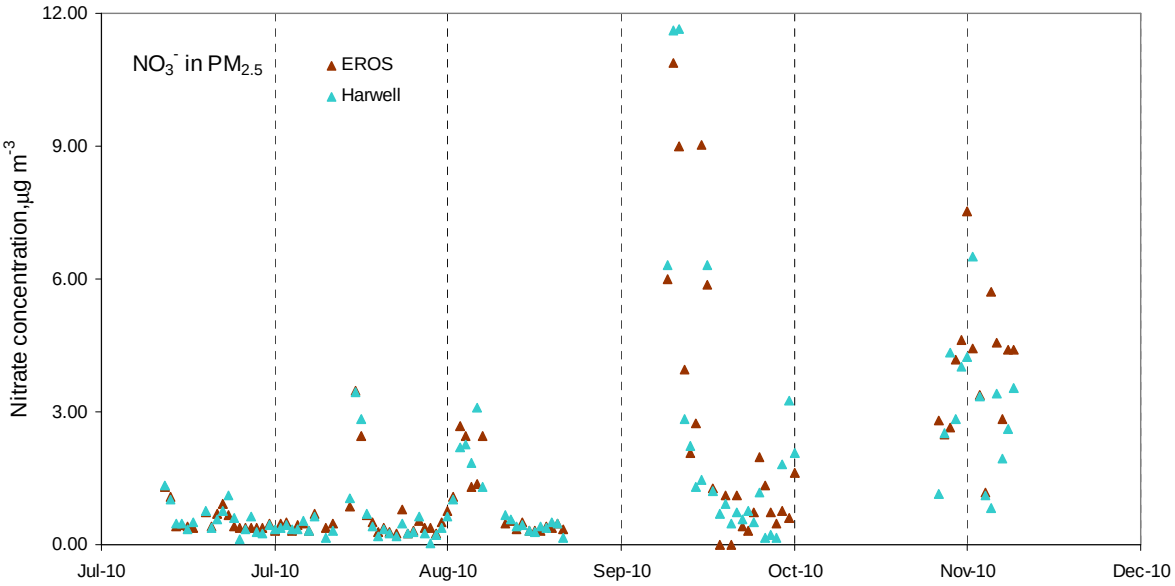

(c)

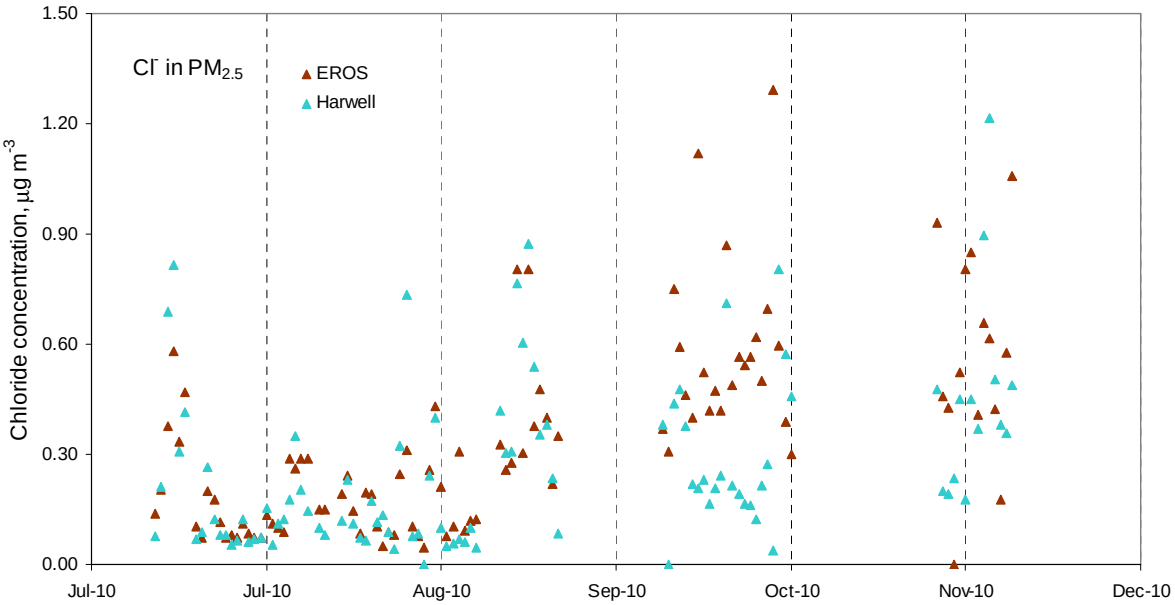

Figure 4.11 *(continued)*

(d)

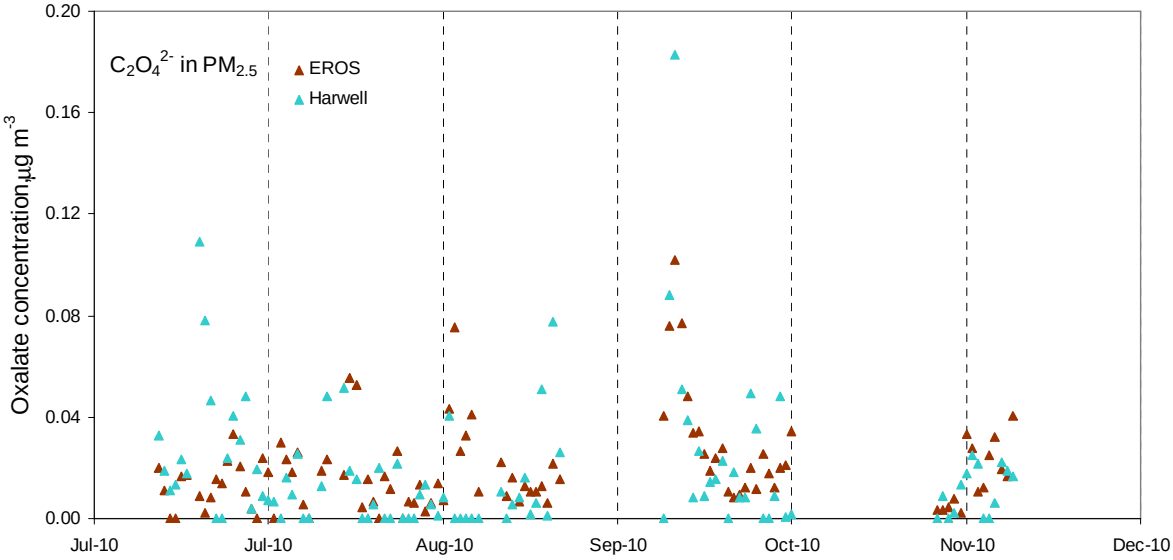

(e)

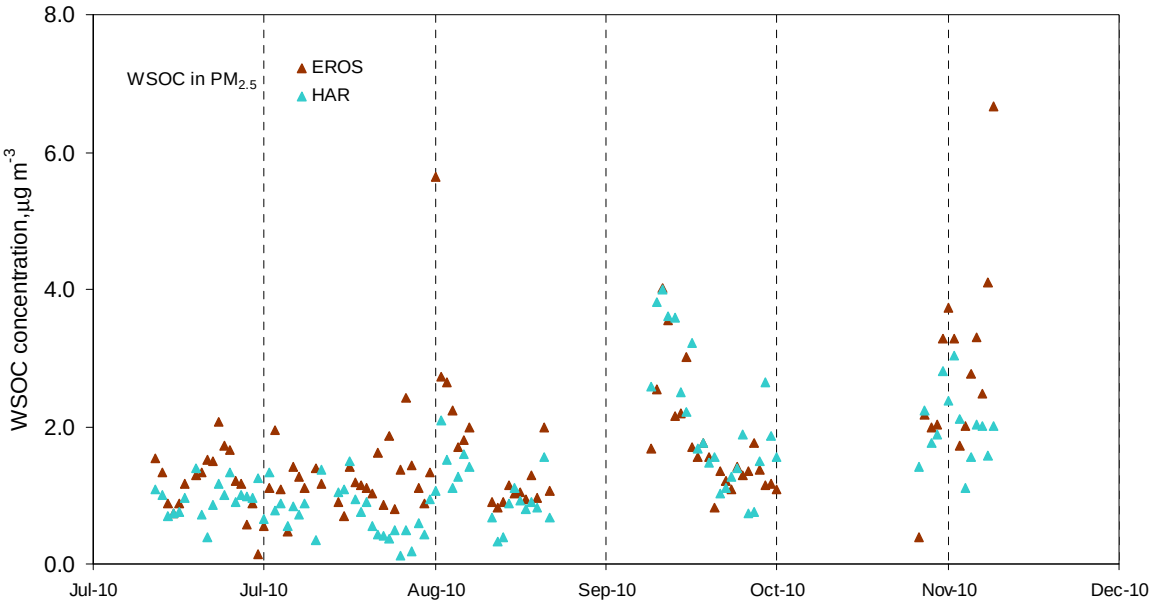

Figure 4.11 *(continued)*

4.4.2 Implication of relationships between oxalate and major component composition between sites

As mentioned in 4.3.2 about the relationships between oxalate and ion species in PM, hereafter the data collected simultaneously between EROS and Harwell will be included in order to better understanding the sources and formation pathways of oxalate in atmospheric particles. Since major inorganic species are not the same category as oxalate, the concurrent measurement of WSOC concentrations can be provided the convenient reference for oxalate. This also includes the study of relationship between oxalate and secondary organic carbon as also in the same category. The plots of oxalate concentrations with WSOC and OC_{sec} at EROS and Harwell show in Figure 4.12 and Figure 4.13, respectively. Table 4.6 shows the correlation between aerosol species analysed in $PM_{2.5}$, $PM_{2.5-10}$ and PM_{10} collected simultaneously at both sites. Oxalate in fine faction showed the modest correlation with WSOC and OC_{sec} within sampling site (at EROS, r = 0.42 and r = 0.37, respectively; at Harwell, r = 0.42 and r = 0.46, respectively). Furthermore, the intra-site relationship of oxalate concentration in $PM_{2.5}$ with WSOC appeared higher correlation (r = 0.61). It is likely that oxalate play an important indicator and/or contributor to WSOC species as referred in many studies (Huang et al., 2006; Yu et al., 2005 and Yang et al., 2005). Despite the intra-site correlation coefficient of oxalate and OC_{sec} in $PM_{2.5}$ also appeared higher value (r = 0.58), oxalate seems not a good indicator for OC_{sec} causing from the weak correlation shown in whole data of $PM_{2.5}$ (500 samples) at EROS site (r = 0.25 as in Table 4.1).

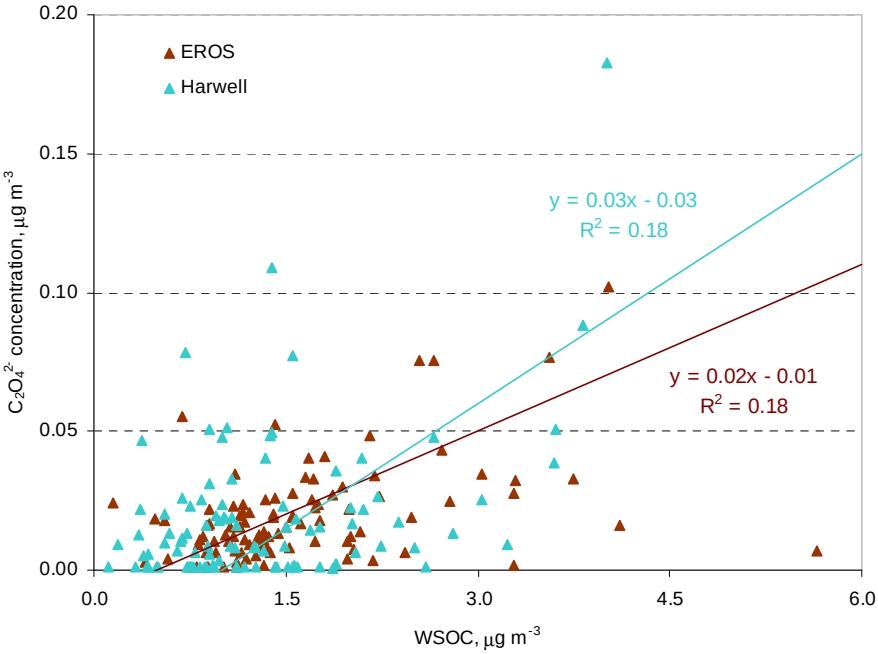

Figure 4.12 Relationship between oxalate and WSOC concentrations in $PM_{2.5}$ measured simultaneously at EROS and Harwell

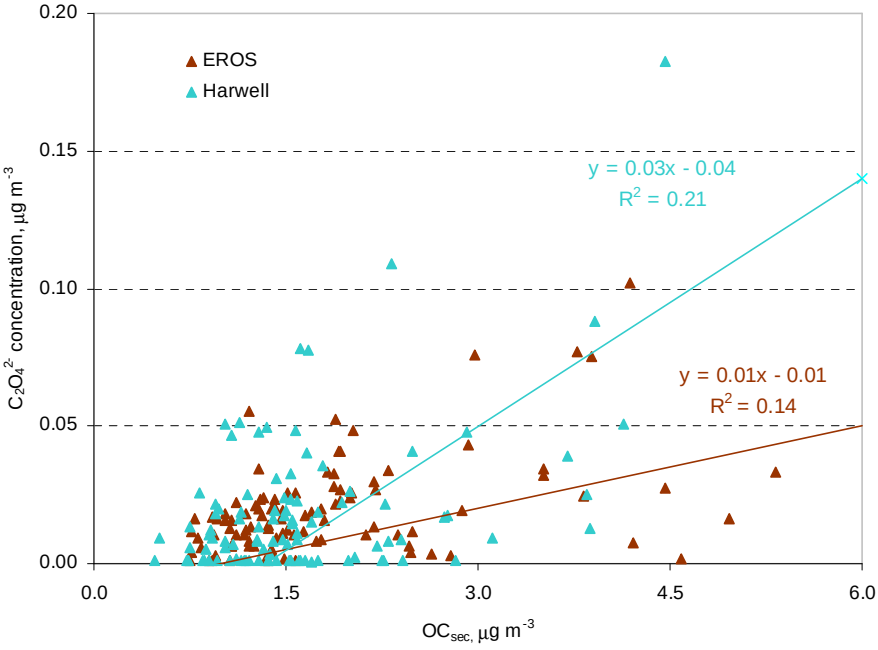

Figure 4.13 Relationship between oxalate and secondary OC concentrations in $PM_{2.5}$ measured simultaneously at EROS and Harwell

Table 4.6 Intra- and inter-site correlation coefficients of aerosol species in $PM_{2.5}$, $PM_{2.5-10}$ and PM_{10} calculated from samples measured simultaneously

	SO_4^{2-} EROS	NO_3^- EROS	Cl^- EROS	$C_2O_4^{2-}$ EROS	OC_{sec} EROS	WSOC EROS	SO_4^{2-} HAR	NO_3^- HAR	Cl^- HAR	$C_2O_4^{2-}$ HAR	OC_{sec} HAR
$PM_{2.5}$											
NO_3^- EROS	0.72										
Cl^- EROS	0.21	0.39									
$C_2O_4^{2-}$ EROS	0.65	0.59	*0.11*								
OC_{sec} EROS	0.43	0.62	0.34	0.37							
WSOC EROS	0.45	0.58	0.31	0.42	0.94						
SO_4^{2-} HAR	0.82	0.72	0.06	0.71	0.33	0.37					
NO_3^- HAR	0.60	0.84	0.25	0.64	0.48	0.47	0.76				
Cl^- HAR	*-0.07*	*0.11*	0.52	*-0.04*	*0.10*	*0.07*	*0.04*	*0.06*			
$C_2O_4^{2-}$ HAR	0.32	0.32	0.04	0.45	*0.14*	0.20	0.42	0.43	*-0.09*		
OC_{sec} HAR	0.63	0.71	0.30	0.58	0.56	0.55	0.68	0.79	*0.11*	0.46	
WSOC HAR	0.67	0.75	0.40	0.61	0.52	0.52	0.69	0.79	*0.14*	0.42	0.94
$PM_{2.5-10}$											
NO_3^- EROS	0.57										
Cl^- EROS	*0.17*	*-0.18*									
$C_2O_4^{2-}$ EROS	0.66	0.49	*-0.09*								
SO_4^{2-} HAR	0.22	*0.14*	0.21	*0.11*							
NO_3^- HAR	0.54	0.86	*-0.13*	0.47	-		*0.13*				
Cl^- HAR	*0.05*	-0.25	0.63	*-0.08*	-	-	0.40	-0.23			
$C_2O_4^{2-}$ HAR	-0.23	*0.07*	-0.35	*-0.09*	-	-	-0.27	*-0.01*	-0.42	1.00	-
PM_{10}											
NO_3^- EROS	0.79										
Cl^- EROS	*-0.07*	*-0.06*									
$C_2O_4^{2-}$ EROS	0.73	0.72	*-0.09*								
OC_{sec} EROS	0.40	0.58	*-0.04*	0.31							
SO_4^{2-} HAR	0.80	0.78	*-0.04*	0.73	0.35						
NO_3^- HAR	0.67	0.86	*-0.01*	0.71	0.48	-	0.76				
Cl^- HAR	*-0.14*	*-0.08*	0.68	*-0.16*	*-0.03*	-	0.03	*-0.16*			
$C_2O_4^{2-}$ HAR	0.25	0.19	-0.30	0.35	*0.01*	-	0.31	0.28	-0.35		
OC_{sec} HAR	0.61	0.68	*0.02*	0.60	0.43	-	0.68	0.77	*-0.10*	0.44	1.00

Values shown in italics are not significant at $p < 0.05$ (the 95% level of significance)

Oxalate shows the strong correlation with sulphate and nitrate between sites (for $PM_{2.5}$, r = 0.71 and r = 0.64, respectively; for PM_{10}, r = 0.73 and r = 0.71, respectively). Similar higher correlation values of oxalate with sulphate than nitrate in $PM_{2.5}$ and PM_{10} are seen for intra-site as mentioned in the whole data at EROS (Table 4.1). These findings indicate that the elevated oxalate aerosol could be formed by secondary formation and affected by regional contribution. The dominant formation pathway of oxalate could be attributed the in-cloud process as same as in-cloud sulphate formation. The further study on the measurement of size distribution of oxalate in comparison with the other major components revealed that the dominant oxalate in droplet mode was similar to the sulphate droplet mode (as detailed later in chapter 6). This result suggests the activation of condensation mode of oxalate particles to

form fog or cloud droplets followed by aqueous-phase chemistry and cloud/fog evaporation (Meng and Seinfeld, 1994; Kerminen and Wexler, 1995). In addition, oxalate and sulphate are expected to have similar removal rate via wet deposition as both are highly water-soluble. Typically, the formation pathways of sulphate are well- investigated as a number of previous studies (Seinfeld and Pandis, 1998). The heterogeneous pathway through in-cloud process by aqueous oxidants can rate 10 to 100 times as fast as gas-phase. This process requires the presence of clouds and clouds are discrete events. Therefore, the relative contribution of the heterogeneous pathway depends on the frequency and duration of clouds. The production rate of sulphate from the in-cloud pathway can be expressed as the equation below (Yu et al., 2005);

$$P_{sulphate} = f k_{cloud} k_{SO_2}^{H} [O_x][SO_2] \qquad \text{(Equation 4.17)}$$

where f is the frequency of cloud events

k_{cloud} is the rate constant of SO_2 oxidation

$k_{SO_2}^{H}$ is the Henry's law constant of SO_2

$[O_x]$ is the oxidant concentration in the cloud that is responsible for oxidation of aqueous S(IV) into sulphate

$[SO_2]$ is the gaseous SO_2 concentration

The recent modeling research by Myriokefalitakis et. al (2011) on a 3-D modeling study revealed that the in-cloud global oxalate net chemical production was calculated to be about 21-31 Tg yr^{-1} with almost 79% originating from biogenic hydrocarbon precursors, mainly isoprene. The possible formation pathway of oxalate in PM via isoprene shows in Figure 4.14 as in-cloud isoprene chemistry. In this study, the direct emissions from road transportation and incomplete combustion of fossil fuels do not play an important source of oxalate causing from the very weak correlations with EC observed as mentioned in 4.3.2. Isoprene (biogenic source) emitted from plants and trees, (Taalman, 1996; Borbon et al., 2001) may be expected as the potential source of oxalate in ambient air. This could be supported by the weak correlation coefficients between oxalate and OC_{sec} (r = 0.25 and r = 0.19 in $PM_{2.5}$ and PM_{10}, respectively for the entire data at EROS), which is originated mainly from anthropogenic sources. However, there were the modest correlations of oxalate and OC_{sec} during the

summer (r = 0.54 and r = 0.49 in $PM_{2.5}$ and PM_{10}, respectively for the entire data at EROS), indicating that the significant sources of anthropogenic precursors would be considered.

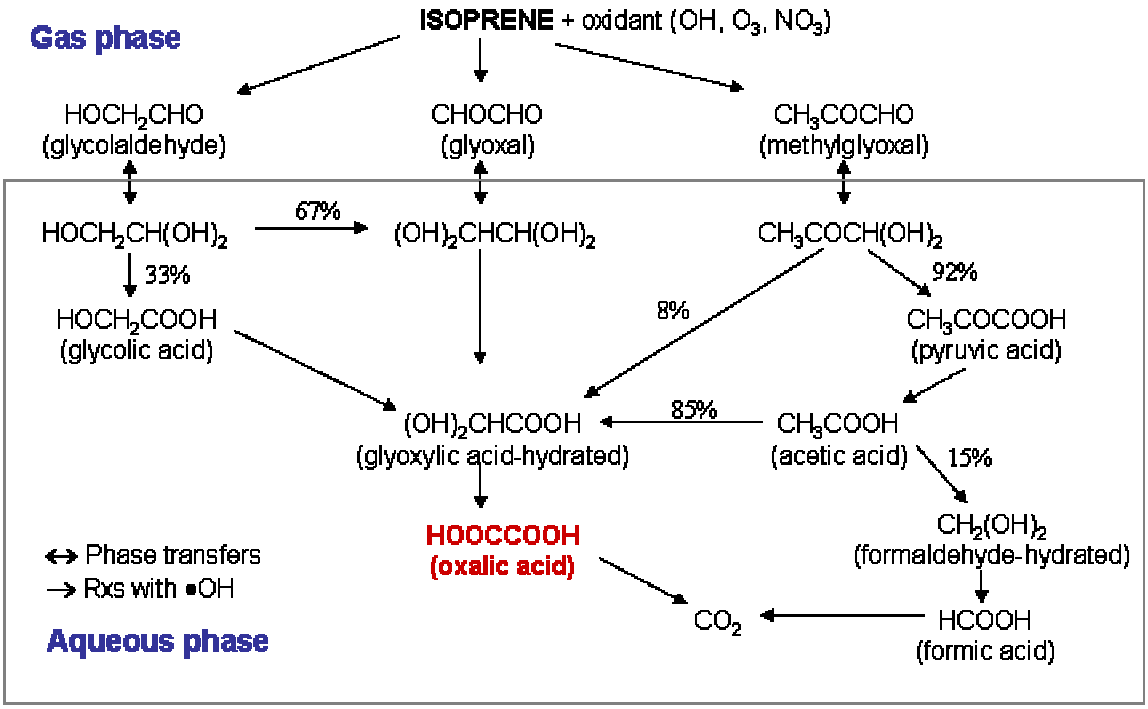

Figure 4.14 In-cloud isoprene chemistry for the formation of hygroscopic organic acids: glycolic acid, glyoxylic acid, pyruvic acid, and oxalic acid. (source: Lim et al., 2005)

Similar to suphate formation mechanism, the production rate of oxalate through in-cloud processes can be approximated as (Yu et al., 2005);

$$P_{oxalate} = f k'_{cloud} k_X^H \left[O'_X\right][X] \qquad \text{(Equation 4.18)}$$

where f is the frequency of cloud events

k'_{cloud} is the oxidation rate constant leading to oxalate formation

k_X^H is the Henry's law constant of precursor X

$\left[O'_X\right]$ is the oxidant concentration in the cloud that is responsible for oxidation of X to oxalate

$[X]$ is the gaseous concentration of precursor X

Oxalate formation by in-cloud chemistry was also investigated in the marine atmosphere by Warneck (2003). The proposed precursors for the formation were acetylene and ethene via glyoxal and glycolaldehyde, respectively (Figure 4.15). On the contrary, the precursors of C_2 difunctional compounds in urban background and rural environments may be more complicated, therefore, the potential precursor would be considered for the other compounds (i.e. aromatic hydrocarbons, cyclic olefins and aldehydes) as proposed by Kawamura et al. (1996). Oxalic acid can be produced in the atmosphere as a result of secondary photochemical reaction of anthropogenic aromatic hydrocarbons i.e. benzene and toluene and their oxidation intermediates i.e. glyoxal and methylglyoxal.

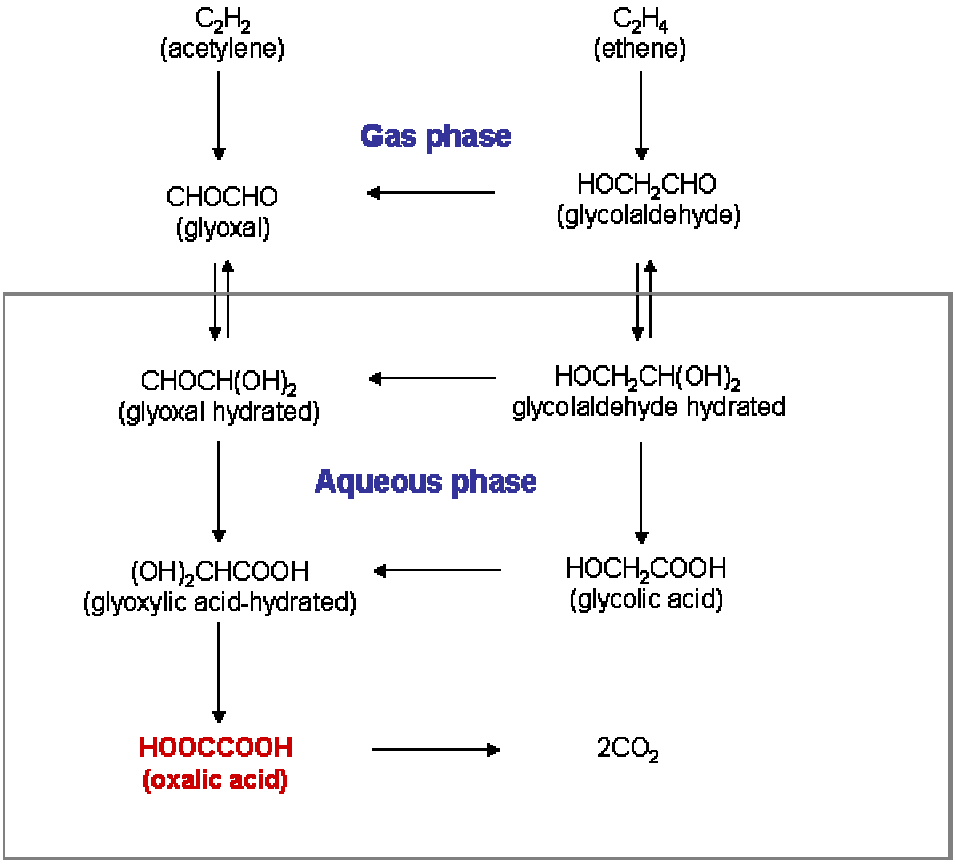

Figure 4.15 Flow chart for the in-cloud formation of oxalic acid from acetylene and ethene as precursors (source: Warneck, 2003)

4.5 Conclusions

The determination of chemical composition of ionic species including carbonaceous materials (as discussed in chapter 3) in PM samples collected from EROS and Harwell provide the better understanding of their sources in the UK. Moreover, this study reveals and focuses on the new data series of oxalate concentration in the atmosphere. The discussion data were based on the aerosol samples measured in urban background (EROS) during November 2008 to April 2011 and rural (Harwell) sites during July 2010 to December 2010. The studies of local contribution of ionic species were calculated based on mean differences concentration between sites collected simultaneously (EROS conc. – HAR conc.). The results show a minor local contribution of WSOC, OC_{sec}, sulphate, nitrate and chloride in $PM_{2.5}$ (0.4 μg m^{-3}, 0.4 μg m^{-3}, 0.13 μg m^{-3}, 0.17 μg m^{-3} and 0.08 μg m^{-3}, respectively). There is no difference in mean concentration for oxalate in fine fraction suggesting that oxalate formation by photooxidation of precursors in the atmosphere with long-lived species. The strong correlation between sulphate and nitrate is consistent with previous studies indicates the fact that two species undergo similar formation and removal processes in atmosphere. For chloride, the results strongly support the common source from marine aerosol with the weak correlation observed with other species. The seasonal behaviour of sulphate, nitrate, chloride and oxalate show a dominant temporal variation over the spatial variation. In addition, the same patterns of time series appear between EROS and Harwell for simultaneous data. These findings indicate the important of long-rang transport on the contribution to the secondary aerosols. Particulate oxalate reveals not clear a seasonal pattern but the concentration show highest in spring. The study on the ratio of sulphate-to-nitrate indicates the stability of sulphate higher than nitrate because SO_4^{2-}/NO_3^- ratios were extremely high for $PM_{2.5}$ in summer. The formation of sulphate by photooxidation in the atmosphere (aqueous oxidation) slightly reflects on its concentration but there was the significant of volatile loss of nitrate aerosol as ammonium nitrate during the summer.

In this study, the whole mean concentrations with measurement uncertainties of oxalate are from 0.02 ± 0.001 μg m^{-3} to 0.06 ± 0.002 μg m^{-3} at urban background and from 0.02 ± 0.001 μg m^{-3} to 0.04 ± 0.001 μg m^{-3} at rural site. These concentration levels are in range with a number of studies in the past. The relationships of oxalate with major chemical composite provide the useful information on its formations and sources. Oxalate shows a good correlation with sulphate suggesting that its formation pathway could be from similar

atmospheric processes. The significant correlation between oxalate and nitrate especially in summer can be interpreted as that oxalate formed in PM is affected by temperature in the same way as nitrate. This is strongly supported by the $C_2O_4^{2-}/NO_3^-$ ratio observed high during the summer. The weak relationship between oxalate and chloride indicate little contribution from marine aerosol or coal burning in winter on oxalate concentration. Since oxalate is believed as the most abundant species of WSOC, this study confirms that oxalate plays an important indicator and contributor to WSOC with the significant correlation of both species observed. The dominant formation pathway of oxalate could be demonstrated as the in-cloud process and the potential precursor from biogenic sources i.e. isoprene emitted mainly from plants and trees may contribute oxalate particle at EROS and Harwell site. However, this seems unlikely to be the main source as this would produce a pronounced seasonality which is not observed. The study of relationships between oxalate and OC_{sec} in $PM_{2.5}$ and PM_{10} showed the weak correlations for the whole data. A modest correlation of oxalate and OC_{sec} were observed during the summer. This finding indicates the important of precursors originated from anthropogenic sources. The further analysis of air mass backward trajectories discussed in chapter 5 will provide the evidence of long-range transport as expected the important formation pathway. Future work is also suggested to investigate the sources of oxalate aerosol from precursors such as aromatic hydrocarbons, cyclic olefins and aldehydes.

CHAPTER 5

A TRAJECTORY ANALYSIS OF LONG-RANGE TRANSPORT OF MAJOR AEROSOL SPECIES AT EROS AND HARWELL SITES

5.1 Synopsis

Backward air mass trajectories were determined as diagnostic tools for interpreting the long-rang transport (LRT) of major secondary aerosols in this study. This is because the temporal variability of atmospheric particulate matter concentrations at the sampling sites highly involved to the history of the airflows arriving at the sites. HYSPLIT_4 model available on NOAA Laboratory website was used for calculation of backward trajectories. This model is a complete system for calculating simple trajectories to complex dispersion and deposition simulations using either puff or particle approaches (Draxler and Hess, 1997). Calculations perform by using previously gridded meteorological data from archive data field. The meteorological data used have been downloaded from Air Resource Laboratory (ARL) archives. The cluster analysis was used to group the back trajectories into homogeneous groups depending on direction and speed of transport in order to minimise errors associated with individual trajectory. The time period for generating the trajectories was performed for the whole dataset at EROS and the simultaneous data of air sampling between EROS and Harwell sites. In this study, 3-day back trajectories arriving at both sites were calculated. At Harwell site representing the rural area, it is expected that the major contribution to the concentrations of major atmospheric components was from regional sources associated with the LRT and the contribution to PM is slightly affected by the primary sources. Significant differences of major chemical composition in PM between clusters were analysed by using nonparametric statistics. A seasonal pattern is also discussed for the back trajectories arriving at EROS for the whole period (500 trajectories). Each individual chemical component in $PM_{2.5}$ is represented by box-whisker plots in each cluster in order to clearly show the influence of their sources by air mass transport paths.

5.2 Overview of air mass back trajectories

Trajectories are known as the paths of infinitesimally air parcels and represent as the curves denoting successive three-dimensional positions in time of the air parcels (Dutton, 1986; Stohl, 1998). As air parcels followed either forward or backward in time, there are two types

of trajectories that are forward trajectories and back trajectories. Trajectories have been used for study dynamical behaviour in the atmosphere including meteorology, climatology, environmental sciences. The major application of trajectory analysis of air parcels is to investigate the transport processes of air pollutants. Back trajectories obtained from trajectory models, which computed based on archived meteorological data, provide an advantage on identification of source regions of pollutants. It is well know that the accuracy of an individual trajectory depends on the temporal and spatial resolution of meteorological data, measurement errors, analysis errors and by any simplifying assumptions used in the trajectory model (Brankov, et al., 1998). Errors in the individual trajectories could be minimised by cluster analysis which will be discussed later.

Currently, the HYSPLIT_4 (Hybrid Single-Particle Lagrangian Inegrated Trajectory) model (Draxler and Hess, 1997, 1998) is a complete system that can be used to calculating trajectories and air concentration for analytical studies including the atmospheric transport and dispersion of pollutants. The method of model calculation is a hybrid between the Lagrangian approach, which uses a moving frame of reference as the air parcels flow from their origin, and the Eulerian approach, which uses a fixed three-dimensional grid as a frame of reference. The minimum requirements of meteorological data for HYSPLIT model are the horizontal wind components, temperature, height, pressure and the pressure at the surface. Trajectories (the integrated advection term of a particle) are calculated from the mean of the three-dimensional velocity vectors for the initial-position $P(t)$ and the first-guess position $P'(t+\Delta t)$. The velocity vectors are linearly interpolated in both space and time. The first guess position shows as following equation (Draxler and Hess, 1998);

$$P'(t+\Delta t) = P(t) + V(P,t)\Delta t \qquad \text{(Equation 5.1)}$$

And the final position is given by

$$P(t+\Delta t) = P(t) + 0.5\left[V(P,t) + V(P',t+\Delta t)\right]\Delta t \qquad \text{(Equation 5.2)}$$

where $P'(t+\Delta t)$ and $P(t+\Delta t)$ are the first-guess and the final positions of a particle or puff, respectively, $P(t)$ is the initial-position of a particle or puff, $V(P,t)$ and $V(P',t+\Delta t)$ are the average of the three-dimensional velocity vectors for a particle or puff at the initial and the

first-guess positions, respectively, Δt is the integration time step which can vary during the simulation. A more detailed description of the equations, algorithms and meteorological data is reported by Draxler and Hess (1998).

5.2.1 Meteorological data

Meteorological data for the calculation of trajectories are downloaded from the National Oceanic and Atmospheric Administration (NOAA)'s Air Resources Laboratory (ARL) archives. The operational system used for calculation is the Global Data Assimilation System (GDAS) run at the U.S. National Weather Service's National Centers for Environmental Prediction (NCEP). The meteorological data include basic fields such as the u- and v-wind components, temperature, and humidity. NCEP's GDAS is run 4 times a day e.g. at 00, 06, 12, and 18 UTC. Model output is for the analysis time and 3h, 6h, and 9h forecasts. ARL saves the successive analyses and 3h forecast, four times each day to produce a continuous data archive. The ARL archiving program produces a 3 hourly, global, 1 degree latitude longitude dataset on pressure surfaces. The data are put into weekly files and made available online as GDAS1. GDAS1 data are shown as the files called gdas1.*mmmyy.w#*, where *mmm* is the month (e.g. jul) and *yy* is the year (05) and # refer to:

= 1 → days 1 -7
= 2 → days 8 – 14
= 3 → days 15 – 21
= 4 → days 22 – 28
= 5 → days 29 – rest of the month

5.3 Calculation of trajectories and cluster analysis

In the present study, air parcel trajectories arriving at EROS and Harwell sites during the sampling period at 12:00 h GMT (500 metre above ground level (a.g.l)) were computed for each day by using HYSPLIT_4 model. These trajectories are consistent with the time of changing the filters for 24h sampling period overall this work. Each of the trajectories comprised 72h back trajectories ending at each site. The back trajectories with a timescale of 72h are appropriate for the lifetime of secondary aerosol species to describe the long-rang transport (Wojcik and Chang, 1997).

In order to minimise the uncertainty of individual trajectories associated by the resolution and accuracy of the meteorological data and by any simplifying assumptions used in the trajectory model (Stohl, 1998), a cluster analysis was applied in many studies (Buchanan et al., 2002; Abdalmogith and Harrison, 2005; Borge et al., 2007; Baker, 2010). Cluster analysis is a multivariate statistical technique, which groups the individual trajectories into a smaller number of clusters, where the errors in the individual trajectories trend to average out. The objective is to maximise between-group variance and to minimise within-group variance (Dorling, 1992). All back trajectories are used as the clustering variables. The calculation process of clustering starts by the spatial variance (*SV*) computed between each endpoint (*k*) along trajectory (*j*) with its cluster (*i*) as the following equation (Air Resources Laboratory, 2011);

$$SV_{i,j} = \sum_k (P_{j,k} - M_{i,k})^2 \qquad \text{(Equation 5.3)}$$

Where the sum is taken over then number of endpoints along the trajectory and *P* and *M* are the position vectors for the individual trajectory and its cluster mean trajectory, respectively. The cluster spatial variance (*CSV*) is then just the sum of the spatial variance of all trajectories within its cluster;

$$CSV_i = \sum_j SV_{i,j} \qquad \text{(Equation 5.4)}$$

And the total spatial variance (*TSV*) is the sum of the *CSV* over all clusters:

$$TSV = \sum_i CSV_{j,k} \qquad \text{(Equation 5.5)}$$

The clustering process describes more in Air Resources Laboratory, 2011. Basically, the ideal final number of clusters would be prior to the point of TSV rise significantly. The recommended criterion for the percentage change of TSV according to HYSPLIT_4 software calculation in order to pairing of different clusters is indicated by at least 30% of TSV (or 20% of TSV in the case of no identification of appropriated final number of clusters). The maximum is arbitrarily set to 20 clusters.

5.4 Atmospheric boundary layer

Once air pollution is emitted into the atmosphere, chemical, physical and meteorological factors determine how it is distributed. The location of air pollution sources with referring to local, regional, and global air circulation patterns influences how efficiently pollutants are transported and dispersed. The winds transport air both horizontally and vertically. Vertical transport is important when considering atmospheric long-range transport because pollutants distributed to higher altitudes usually encounter stronger winds that provide rapid transport to distant locations. Atmospheric stability, controlled by how temperature varies with height, determines whether vertical transport will be slow or rapid.

Pollutant transport occurs in the lowest two layers of the atmosphere — the troposphere and stratosphere (National Research Council, 2009). Most weather phenomena that affect pollutant transport occur in the troposphere, which extends from the surface to approximately 18 km in the tropics and approximately 8 km near the poles. The boudndary layer is the lowest part of the atmosphere and its behaviour is directly influenced by its contact with a planetary surface. The working definition of the boundary layer provided by Garratt (1992) (cited in Barlow, 2009) is the layer of air directly above the Earth's surface in which the effects of the surface (heating and cooling, friction) are felt directly on time scales less than a day, and in which significant fluxes of momentum, heat or matter are carried by turbulent motions on a scale of the order of the depth of the boundary layer or less. The boundary layer is approximately 1 – 2 kilometres deep and above boundary layer is the "free atmosphere". The vertical structure of the boundary layer is denoted by variations of temperature, moisture and wind speed. Table 5.1 shows the characteristics of the boundary layer and free troposphere. Air movements within the boundary layer are strongly influenced by energy inputs from the surface and most of the energy in the Sun's rays reaches the surface. Both shortwave and longwave radiation are absorbed at the surface. By day the energy due to the net radiation is used in different processes i.e. evaporation of surface moisture into vapour. The diurnal cycle of heating and cooling of the surface causes distinct changes in boundary layer structure.

Table 5.1 Comparison between the boundary layer and the free troposphere characteristics (modified from Stull, 1950)

Property	Boundary layer	Free troposphere
- Turbulence	Almost continuously turbulent over its whole depth	More seldom turbulent, mostly in clouds and near the jet stream
- Friction	Large dissipation, large friction at surface	Small dissipation, “friction” in gravity waves
- Mixing	Strong mixing daytime and rapid turbulent mixing in the vertical and horizontal, weaker at night	Weak mixing, small molecular diffusion. Often rapic horizontal transport by mean wind
- Winds	Large vertical variation, near logarithmic profile at surface, ageostrophic flow across isobars	Near geostrophic wind, small vertical variation, thermal wind balance
- Vertical transport	Turbulent transport dominates	Transport by mean vertical wind, small in synoptic systems, locally larger with convection

The atmosphere’s vertical temperature profile plays the dominant role in controlling whether and how quickly an air pollutant will be dispersed upward from its point of emission. Large lapse rates (change of temperature with height), especially those near the surface on a sunny day, are associated with atmospheric instability, which promotes turbulence. On the other hand, small lapse rates near the surface denote stability that suppresses vertical motion. Layers containing temperature inversions (a negative lapse rate) are very stable, greatly inhibiting vertical transport and promoting the accumulation of pollutants. Inversions in the troposphere can occur when the surface is colder than the overlying air and in subsiding air, which occurs in regions of high pressure.

The stratosphere is a permanently stable region, with a near zero lapse rate between 11 and 20 km and increasingly negative (stable) rates above. As a result of this stability pollutants injected into the stratosphere tend to remain there for much longer periods than in the troposphere.

With regard to the calculation of trajectories, three-day backward trajectories arriving at noon (500 metre above ground level (a.g.l)) at EROS and Harwell were generated by HYSPLIT_4 model. The arrival elevation and time were chosen because the optimum profiles of potential temperature, wind and specific humidity within the boundary layer appeared in a well-mixed layer. This is because air mass trajectories did not maintain the same height for the duration of the back trajectory due to vertical motion and often vary considerably from the receptor height selected. Consequently, each back trajectory generated for the same location and time but with different receptor heights may show significantly different air flow patterns for part

of or the entire trajectory. Air sampling performed at ground level was strongly affected by the ability of atmosphere to disperse of pollutants as related to vertical atmospheric motion. By day the surface layer, typically 100 – 200 m thick, occupies the lowest 10% of the boundary layer (Barlow, 2009). This layer is unstable because the potential temperature decreases with height. Thermals are driven by the surface heating but their action is to cause the rest of the boundary layer to be a well-mixed layer. There is little or no wind shear within the well-mixed layer. Specific humidity within the mixed layer shows a similar profile to temperature except that air above the boundary layer is much drier. On the contrary, the weaker mixing of air appears at night time. During the air mass transport, changes of pollutant concentrations are also affected by secondary formation, precipitation, wet and dry deposition. 72h back trajectories are suitable for lifetime of secondary pollutants to study the long-range transport (Wojcik and Chang, 1997).

After clustering analysis of all back trajectories, each group of trajectories represents a distinct transport pathway bringing air masses into sampling sites. The transport frequency associated with a pathway is defined as the percentage of trajectories in that grop.

5.5 Results and discussion

5.5.1 Whole dataset at EROS

The daily midday back trajectories arriving at EROS during the sampling period between November 2008 to April 2011 were 500 trajectories generated by HYSPLIT_4 model. The average of 3-day back trajectories of each cluster is calculated from its trajectories members. The result of the cluster analysis of the trajectories is presented in Figure 5.1. This graph shows the change in total spatial variance with number of clusters. The average back trajectories for five clusters at EROS are observed as 31.24% change in TSV when reducing the number of clusters from five to four, indicating five clusters for this period. Diagram showing the individual trajectories which combined to make up each cluster are available in Appendix C. These five clusters are shown in Figure 5.2. In this study, they have been labeled according to their overall wind speed and direction; cluster 1 – the fast south westerly accounted for 22% of the total trajectories, cluster 2 – the north westerly accounted for 21% of the total trajectories, cluster 3 – the slow southerly accounted for 19% of the total trajectories, cluster 4 – the fast westerly accounted for 9% of the total trajectories, cluster 5 – the slow easterly accounted for 29% of the total trajectories. The highest number of

trajectories was from the slow easterly airflow (cluster 5) whilst the lowest number of trajectories was from the fast westerly airflow (cluster 4). Cluster 5 occurred more frequently during autumn and spring (Figure 5.3). The fastest maritime represented in cluster 4 occurred predominantly both in the winter and autumn months and less during the summer. Many of trajectories during summer grouped in the slow southerly airflow (cluster 3) whilst many of winter time trajectories were accounted significantly both in cluster 2 and cluster 5.

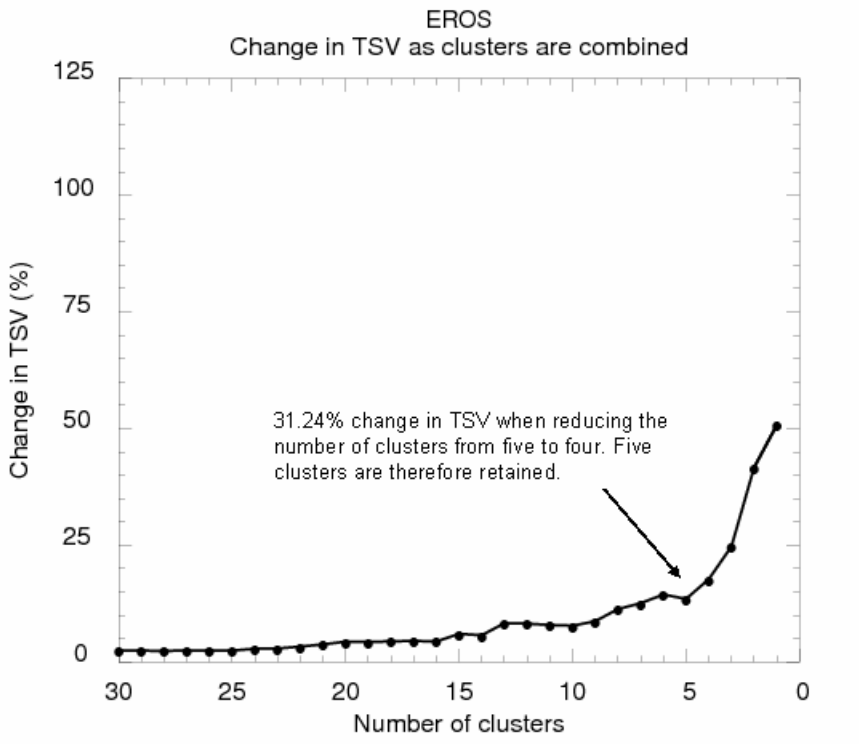

Figure 5.1 The percent change in total spatial variance with cluster number for the clustering of trajectories arriving at EROS from November 2008 to April 2011

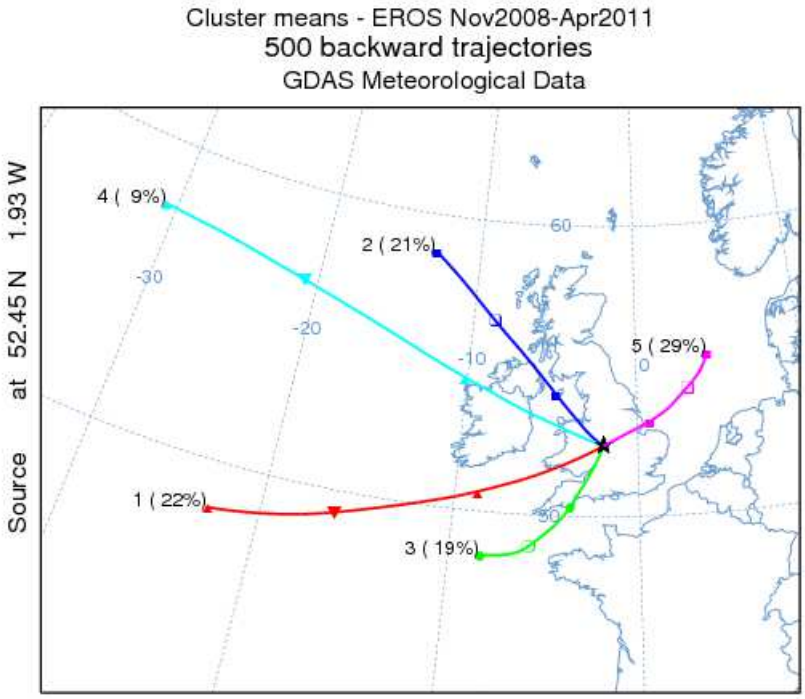

Figure 5.2 Average 3-day back trajectory for the main trajectory clusters arriving at EROS from November 2008 to April 2011. Symbols denote the location of the air parcel every 24 hours. (Individual trajectories contributing to each cluster are presented in Appendix C)

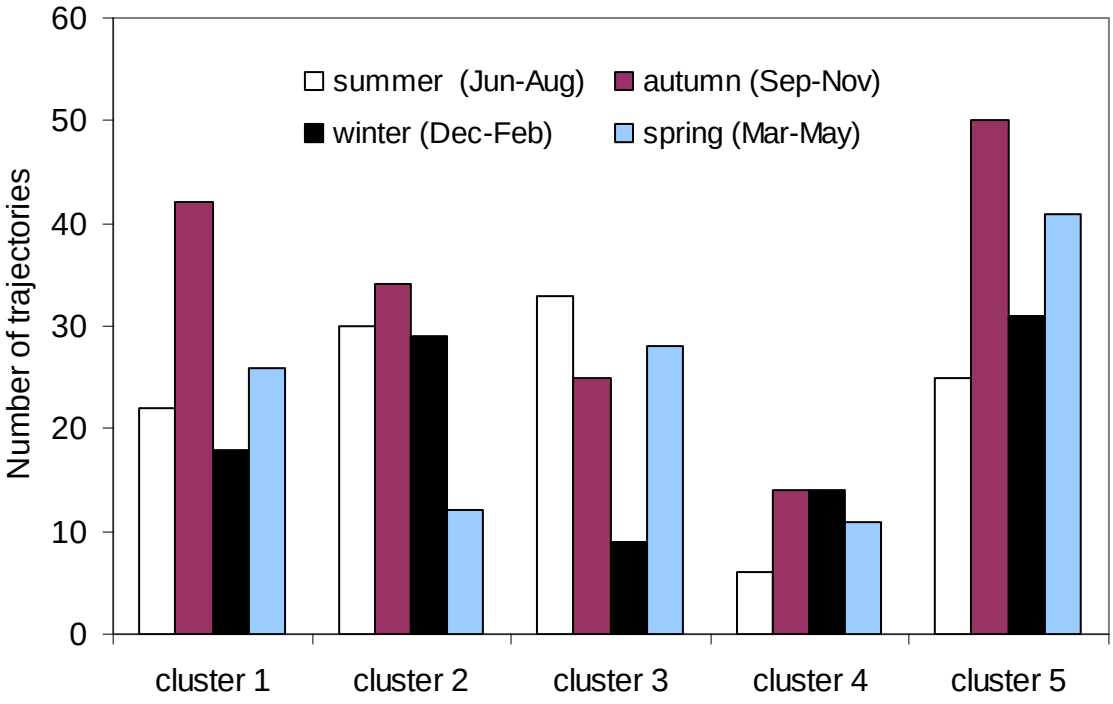

Figure 5.3 Seasonal number of trajectories analysed for each cluster at EROS

When major chemical composition of PM are analysed following air mass cluster type, differences in concentration are also observed. Table 5.2 presents the average concentration of sulphate, nitrate, chloride, oxalate, OC, EC, primary and secondary OC in fine fraction for all trajectory clusters arriving at EROS site. This site represents an urban background with the aerosol components comprising the sum of local contribution and the LRT. The estimation of local contribution for aerosol species was calculated in chapter 3 and chapter 4 by using the data collected simultaneously between EROS and Harwell (rural site). The concentrations of chemical components analysed at Harwell were assumed purely representing the LRT. The further interpretation of LRT for simultaneous data between both sites will be presented in the following section.

For the whole data at EROS, the slow easterly (cluster 5) and the slow southerly (cluster 3) airflows appeared significantly for chemical components in PM. The highest concentrations of ionic species associated with cluster 5 except chloride concentration. This result indicates that for urban background site (EROS, Birmingham), the concentrations of major aerosol species associated with the LRT of pollutants emitted from Eastern European sources are consistent with the study reported by Baker (2010), Abdalmogith and Harrison (2005) and Buchanan (2002). The low atmospheric mixing depth could be contributed the high concentration of OC and OC_{sec} in cluster 5 affecting by the lower mean temperature of 8 ^{o}C (Table 5.3). Moreover, EC concentration is elevated with cluster 5, indicating that the poor dispersion of pollutants associated in trajectories with the low temperature. As anticipated, the fastest maritime cluster 4 originated from Atlantic ocean appears the highest chloride concentration of 1.12 ± 0.98 μg m^{-3}. The Kruskal-Wallis non-parametric technique was also used to test the significant of inter-cluster variation in the concentrations of major component composition in $PM_{2.5}$. This technique tests the null hypothesis that sample clusters have been drawn from the same population. If the test leads to the rejection of null hypothesis, it is interpreted that major components in aerosols collected at the sampling site are influenced by the LRT air masses arriving at this site, which are shown by the clusters (Moody and Galloway, 1988). At EROS, the test results indicate significant differences ($p < 0.05$) in major component concentrations among clusters of air back trajectories arriving at this site, then LRT affected to aerosol concentration by transport paths.

Table 5.2 Average concentrations (± S.D.) of major chemical components in $PM_{2.5}$ by trajectory clusters at EROS for the entire dataset

$PM_{2.5}$	*n*	Concentration, μg m^{-3}							
		SO_4^{2-}	NO_3^-	Cl^-	$C_2O_4^{2-}$	OC	EC	OC_{prim}	OC_{sec}
Cluster 1	108	1.30±1.04	1.18±2.21	0.79±0.78	0.03±0.03	2.3±1.6	0.8±0.8	0.3±0.3	2.0±1.4
Cluster 2	105	1.59±0.99	2.04±2.20	0.69±0.72	0.04±0.04	3.3±2.4	1.3±1.2	0.4±0.4	2.8±2.0
Cluster 3	95	1.63±0.93	2.08±2.20	0.52±0.59	0.05±0.05	2.5±1.3	0.9±0.6	0.3±0.2	2.2±1.2
Cluster 4	45	1.49±1.14	1.40±1.49	1.12±0.98	0.05±0.05	2.6±2.0	0.9±0.8	0.3±0.3	2.3±1.8
Cluster 5	147	2.71±1.76	5.16±5.07	0.74±0.65	0.06±0.06	3.9±2.4	1.5±1.3	0.5±0.5	3.4±2.1

OC_{sec} calculated based on $(OC/EC)_{min}$ of 0.35

Table 5.3 Average ratios of SO_4^{2-}/NO_3^-, Cl^-/NO_3^-, $C_2O_4^{2-}/SO_4^{2-}$, $C_2O_4^{2-}/NO_3^-$ and $C_2O_4^{2-}/OC_{sec}$ by trajectory clusters including meteorological data (± S.D.) at EROS for the entire dataset

	SO_4^{2-}/NO_3^-	Cl^-/NO_3^-	$C_2O_4^{2-}/SO_4^{2-}$	$C_2O_4^{2-}/NO_3^-$	$C_2O_4^{2-}/OC_{sec}$	Temperature (°C)	Relative humidity (%)
Cluster 1	1.10	0.66	0.02	0.02	0.01	11 ± 4	81 ± 9
Cluster 2	0.78	0.34	0.02	0.02	0.01	9 ± 6	79 ± 9
Cluster 3	0.78	0.25	0.03	0.02	0.02	12 ± 5	81 ± 8
Cluster 4	1.06	0.80	0.03	0.04	0.02	8 ± 4	79 ± 9
Cluster 5	0.53	0.14	0.02	0.01	0.02	8 ± 6	81 ± 10

The sulphate-to-nitrate ratio was observed to be low from slow easterly (cluster 5) airflow (Table 5.3). This finding was quite similar to the study reported by Abdalmogith and Harrison (2005) as possibly expecting the reflection of the high NO_x/SO_2 emission ratios originating from Western Europe. Baker (2010) indicated that sulphur dioxide in Europe associated high with easterly airflows originated from coal and oil fired power stations and heavy industry with emissions via tall stacks. The additional contribution of NO_x by local traffic emissions was also from the LRT transportation associated with this continental airflow. Under high NO_x condition, a low SO_4^{2-}/NO_3^- ratio was revealed since a decrease in OH radical levels, an inhibition of the peroxide formation pathways and the consequent decrease in the formation of sulphate (Stein and Lamb, 2003). The possible reason of lower SO_4^{2-}/NO_3^- ratio includes the presence of high particulate nitrate in form of NH_4NO_3 during the low temperature. This was because the winter trajectories accounted in cluster 5 more than summer trajectories (Figure 5.3) and consequently, the lower mean temperature was observed in this cluster (8 °C). The behaviour of temperature dependence of nitrate in aerosol was evident that cluster 5 also revealed the lowest ratios of Cl^-/NO_3^- and $C_2O_4^{2-}/NO_3^-$ (0.14 and 0.01, respectively). The concentration of nitrate associated with cluster 1 was observed low (1.18 μg m^{-3}) with the cluster mean temperature of 11 °C. It is likely that the dissociation of ammonium nitrate plays an important influence on nitrate concentration because the

highest ratio of SO_4^{2-}/NO_3^- was also observed in cluster 1 (1.10). The fast moving maritime trajectories (cluster 4) normally observed in winter showed the dominant ratio of Cl^-/NO_3^-.

For the oxalate ratios to sulphate, nitrate and secondary OC, they represented by the less dependence upon cluster. In this work, it could be noted that oxalate in fine fraction associated more with the long maritime cluster 4 ($C_2O_4^{2-}/SO_4^{2-}$, $C_2O_4^{2-}/NO_3^-$ and $C_2O_4^{2-}/OC_{sec}$ for 0.03, 0.04 and 0.02, respectively). These findings supported the significance of the LRT of oxalate which could be generated by its formation pathway in the marine atmosphere (Warneck, 2003) and the results are in consistent with the study of air mass back trajectories identifying the potential source areas of diacids produced by involving marine biogenic emission (Salvador et al., 2010). In order to evaluate the significance of the marine source contribute to oxalate concentration in terrestrial environment, the more seasonal data of oxalate are needed and this point will be more discussion later. However, these findings could be attributed the effect from lower mean temperature (8 ^oC) associated with cluster 4 and consequently, oxalate as expected in form of semi-volatile specie favoured to account in particulate phase. Despite cluster 5 exhibited the low mean temperature (8 ^oC), the oxalate ratios to sulphate, nitrate and OC_{sec} were still observed low comparing with the oxalate ratios in cluster 4. This finding could be explained by the fact that the contributions of pollutants (sulphate, nitrate and OC_{sec}) from marine sources are much lower than the terrestrial environment. In this study, the slow easterly (cluster 5) airflow coming from eastern part of the UK before arriving at EROS are observed the highest concentrations of suphate, nitrate and OC_{sec} with the relative higher concentrations than oxalate and consequently the low oxalate ratios to these species were obtained.

The graphical illustrations of chemical components in aerosol in each cluster are shown by box-whisker plots. The plots of major components in $PM_{2.5}$ for the whole data at EROS by the clusters are presented in Figure 5.4. The middle line and open circle in the box represent the median and the mean in that cluster, respectively. The box ends represents the 25^{th} and 75^{th} percentiles of their concentrations. The whiskers show the minimum and maximum concentrations in that cluster. These plots show the dominant aerosol transport with the slow easterly airflow (cluster 5) contributing the high concentrations of SO_4^{2-}, NO_3^-, $C_2O_4^{2-}$, OC, EC, OC_{prim} and OC_{sec}. Overall, the little polluted trajectories at EROS are associated with the fast south westerly and slow southerly airflows in cluster 1 and 3, respectively.

(a)

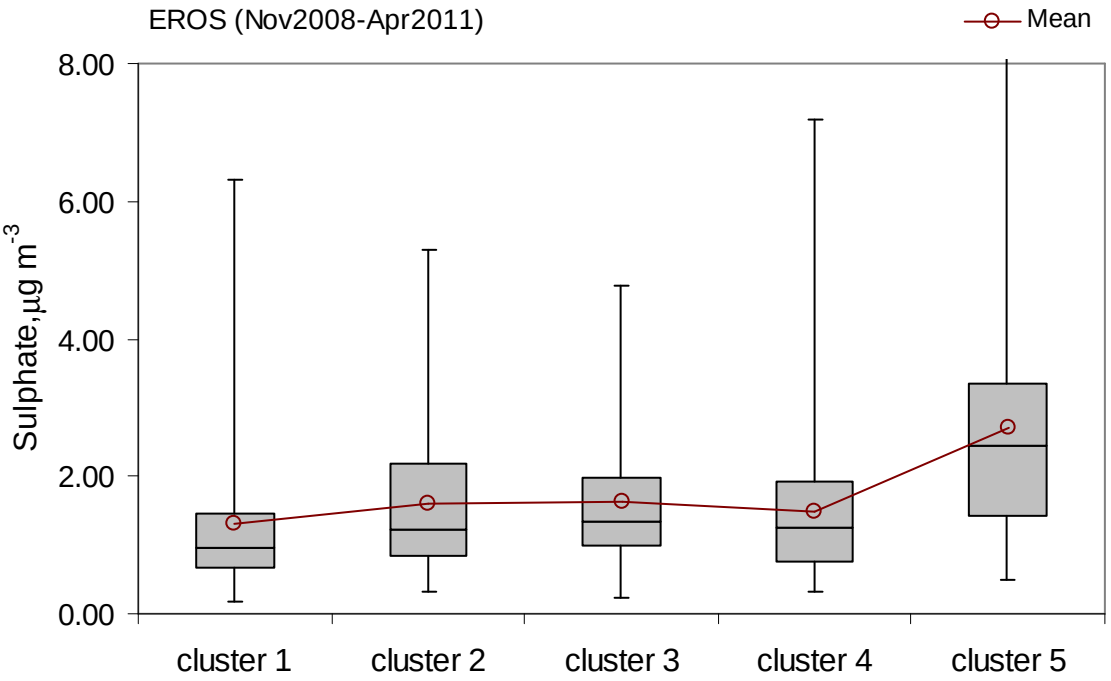

(b)

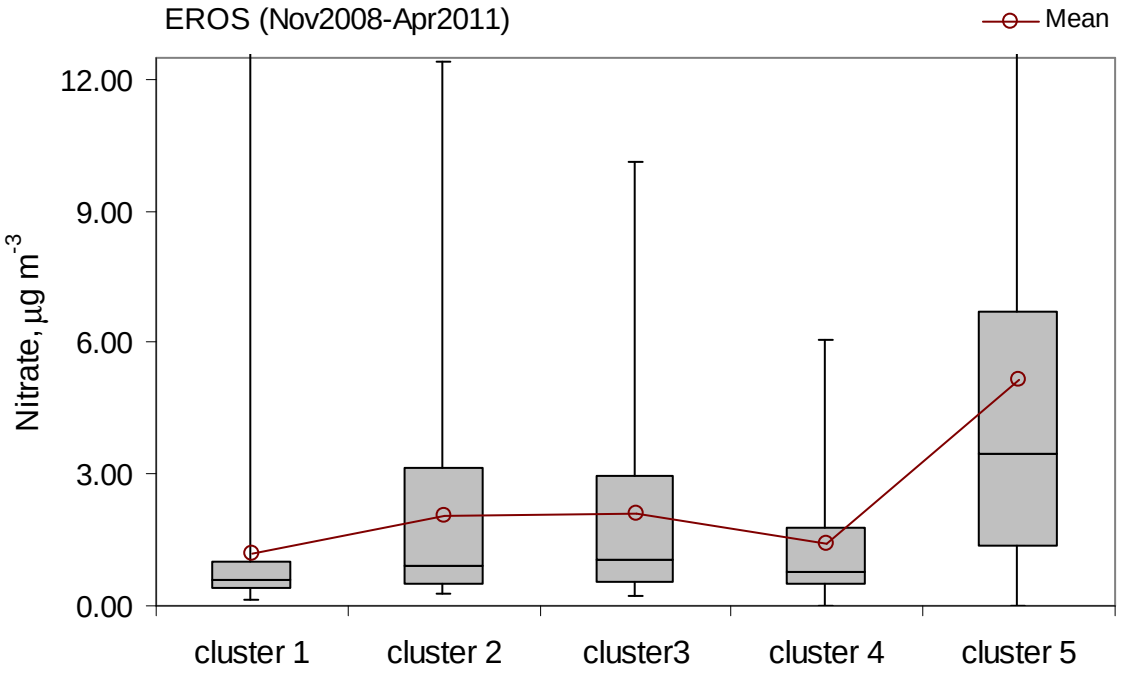

Figure 5.4 Box-whisker plots of major components in $PM_{2.5}$ at EROS by clusters for the whole dataset; (a) sulphate, (b) nitrate, (c) chloride, (d) oxalate, (e) OC, (f) EC, (g) OC_{prim} and (h) OC_{sec}

(c)

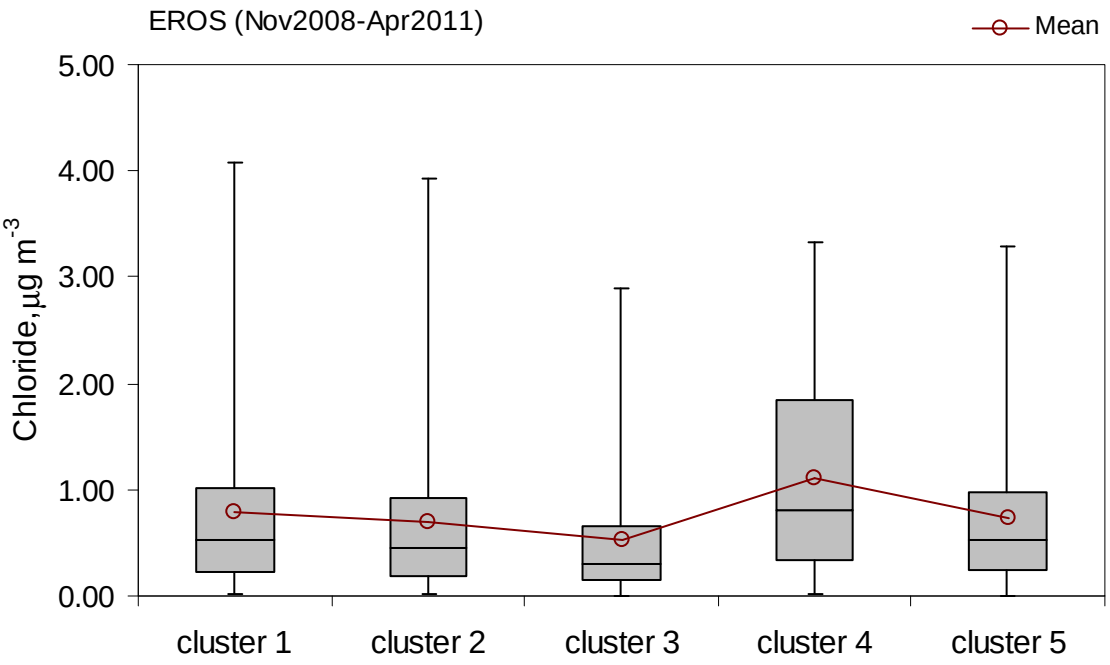

(d)

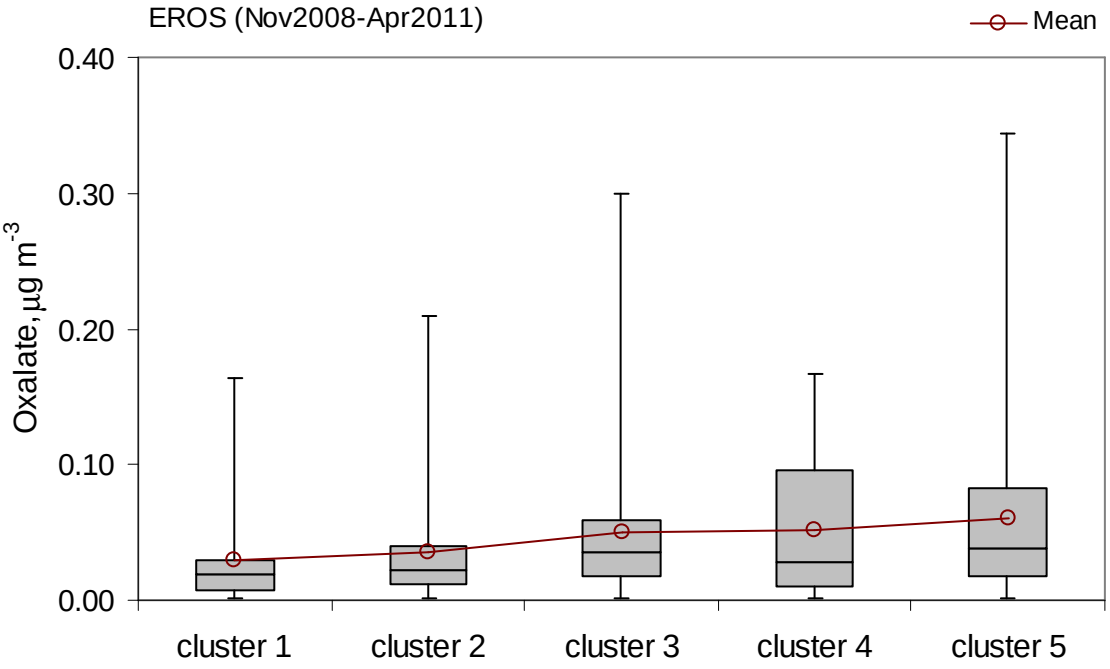

Figure 5.4 *(continued)*

(e)

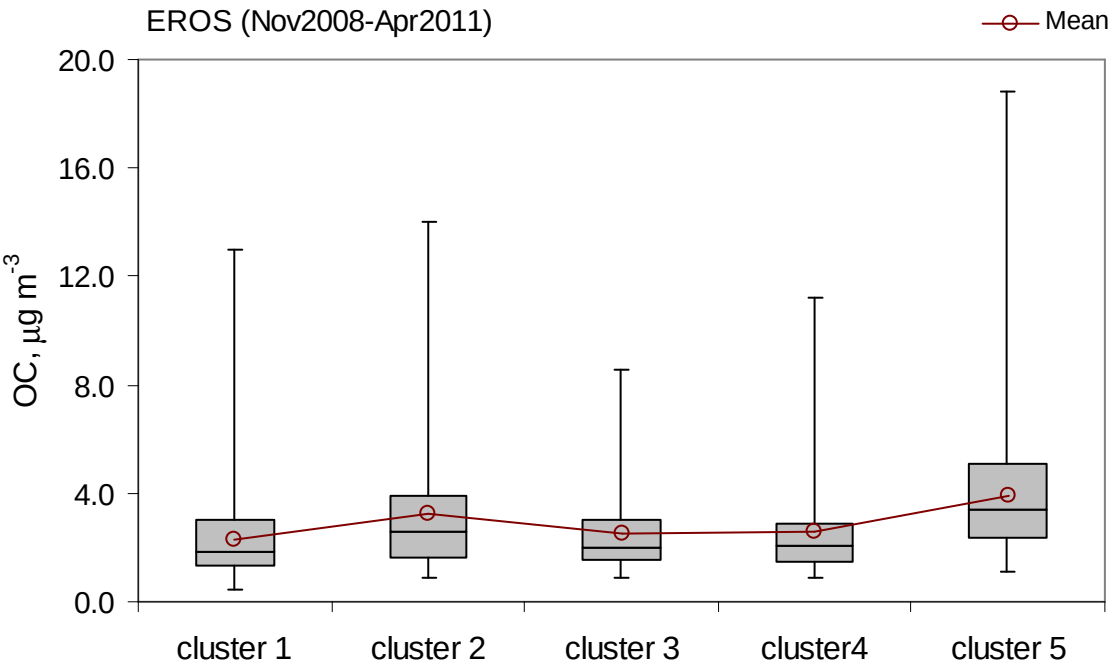

(f)

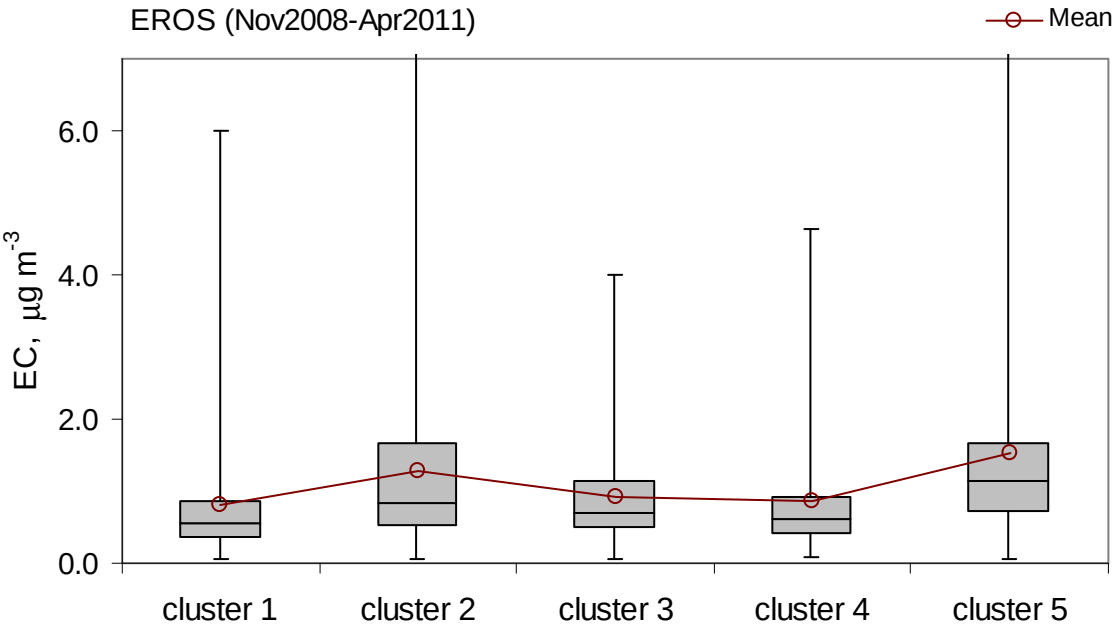

Figure 5.4 *(continued)*

(g)

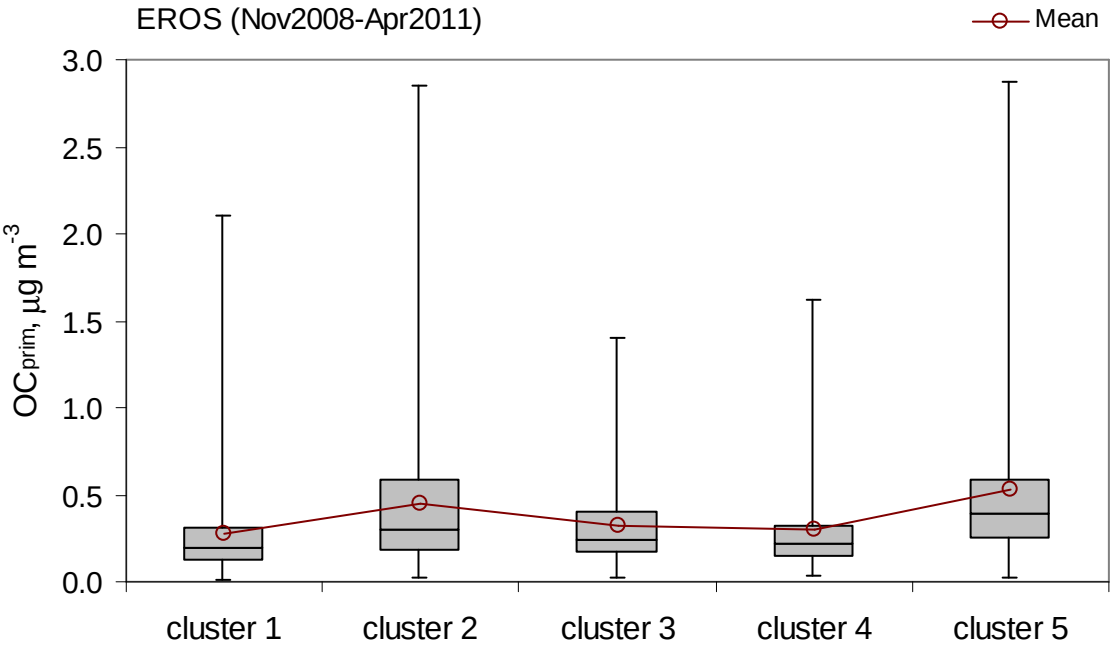

(h)

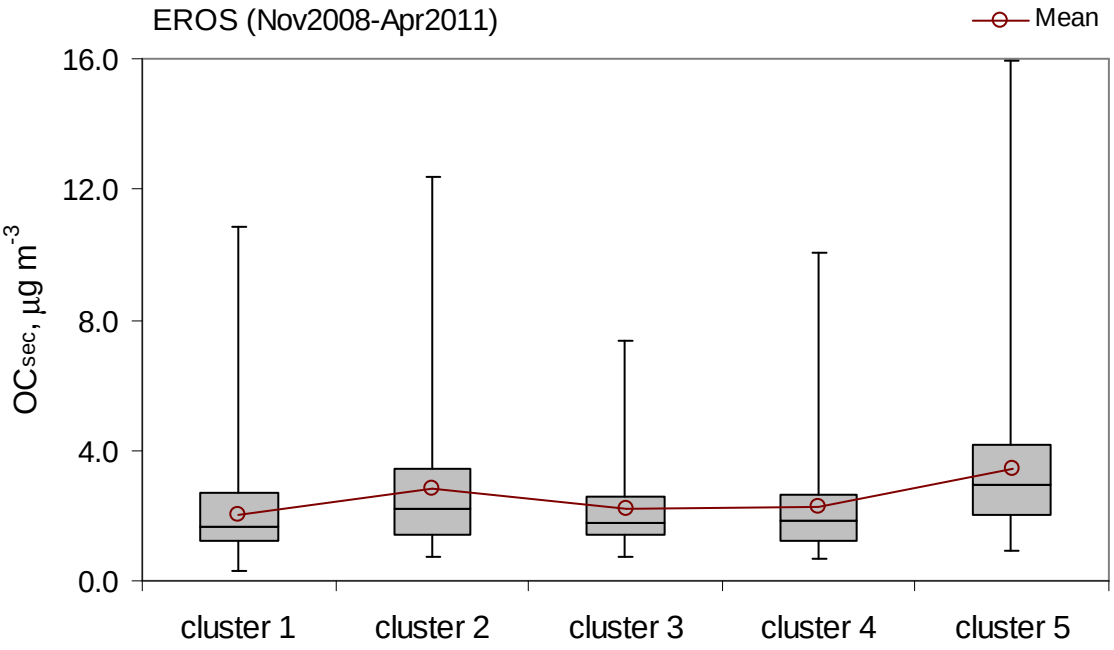

Figure 5.4 *(continued)*

5.5.2 Seasonal variation

In order to investigate seasonal patterns, the whole data set between November 2008 and April 2011 at EROS was split into four seasons; summer (Jun – Aug), autumn (Sep – Nov), winter (Dec – Feb) and spring (Mar – May). The cluster analysis was tested to each of the seasons and the mean trajectories are shown in Figure 5.5. The numbers of trajectories generated in accordance with the sampling time in each season were 116, 165, 101 and 118 trajectories for summer, autumn, winter and spring, respectively. In the summer, there were significant air flow coming both from north westerly (cluster 4 and cluster 7 with 16% and 8% of total trajectories, respectively) and from south westerly (cluster 8 and cluster 9 with 9% and 14% of total trajectories, respectively). The slow air mass back trajectories observed within UK (cluster 2 with 10% of total trajectories) during summer months. The southerly (cluster 5), northerly (cluster 1) and easterly (cluster3) air flows accounted for 14%, 9% and 8% of the data, respectively. The slow westerly and slow easterly airflows were outstanding and accounted for 24% and 18% of data during the spring, respectively. In summary, there was no clear seasonal trends of air mass back trajectories representing by cluster analysis. These airflows have been registered throughout the year and it should be noted that the westerly trajectories both fast and slow airflows were the most frequent at the UK passing over the marine atmosphere.

Table 5.4 represents the mean concentrations of aerosol components in $PM_{2.5}$ by cluster in each season. At EROS, it is clear that the easterly airflow contributed the highest concentrations of chemical composition for summer (cluster 3), autumn (cluster 7) and spring (cluster 5, 8). During the winter, the higher concentrations were observed with very slow southerly airflow (cluster 5) than easterly airflow (cluster 8). The chloride observed highest in winter with the fast maritime airflow trajectories (cluster 4) causing by the very much wind speed comparing with the fast maritime in other seasons.

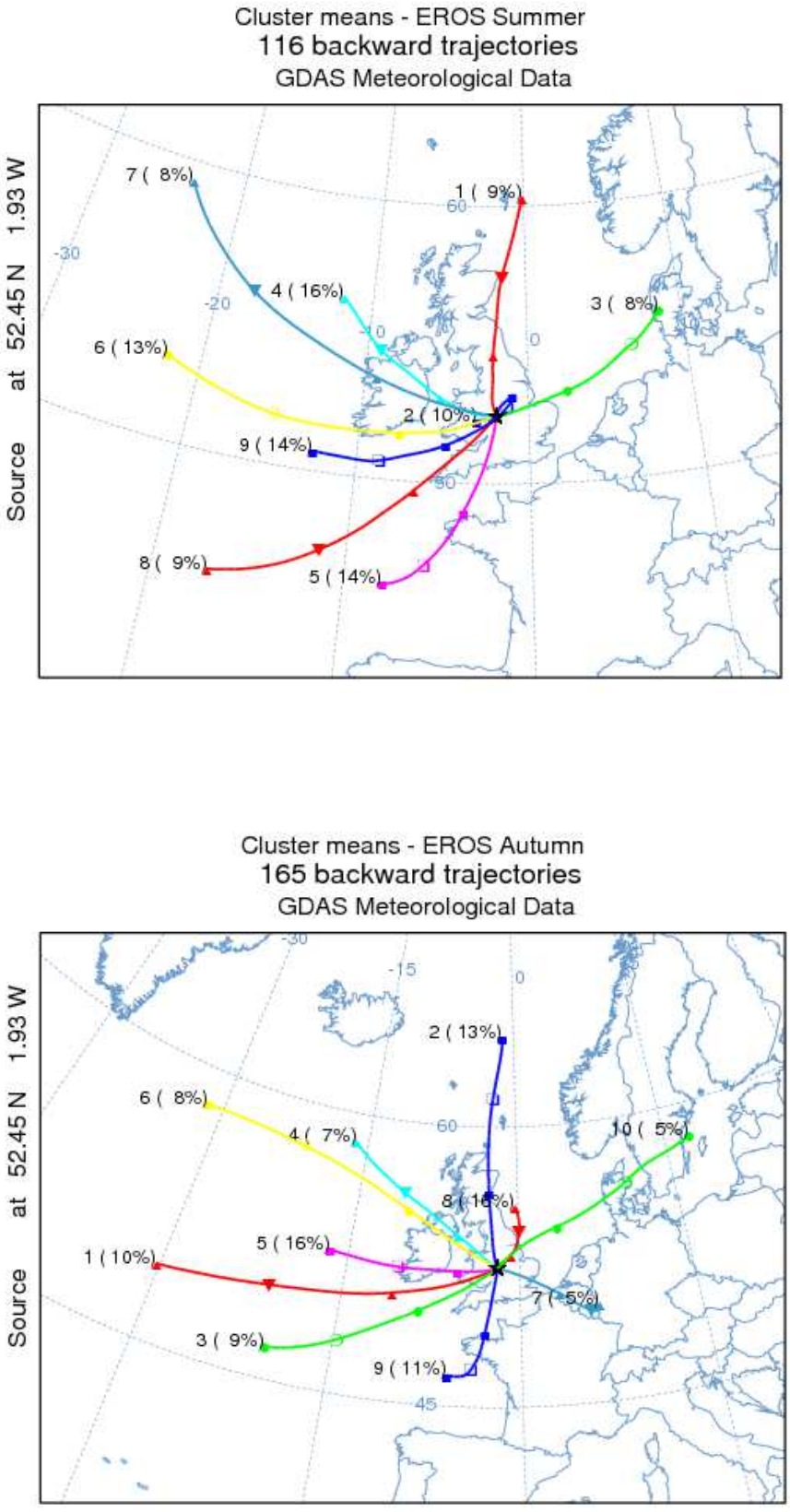

Figure 5.5 Average 3-day back trajectories for the main trajectory clusters in each season arriving at EROS. Symbols denote the location of the air parcel every 24 hours. (Individual trajectories contributing to each cluster are presented in Appendix C)

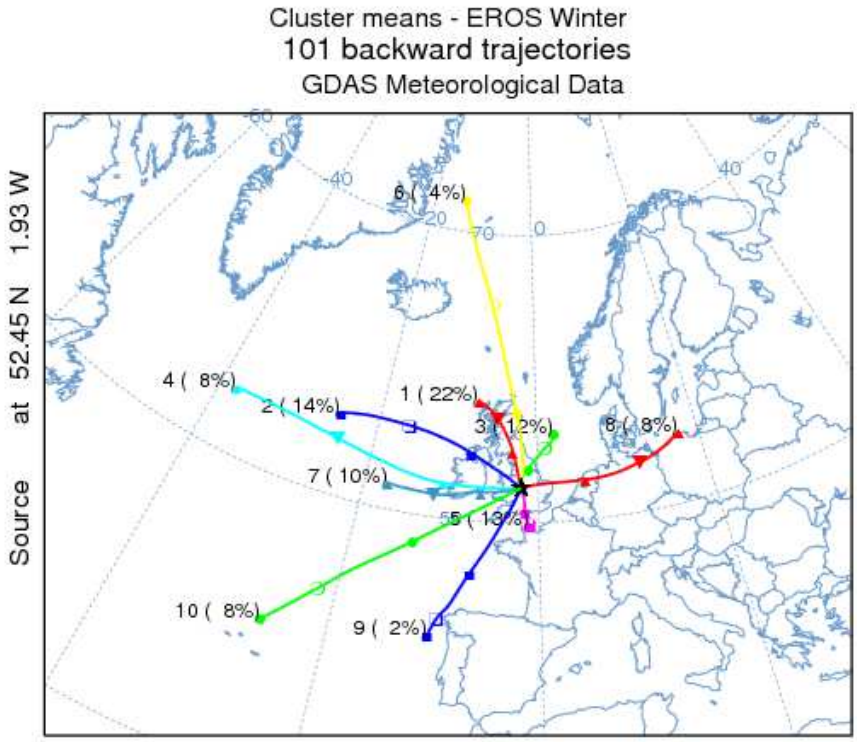

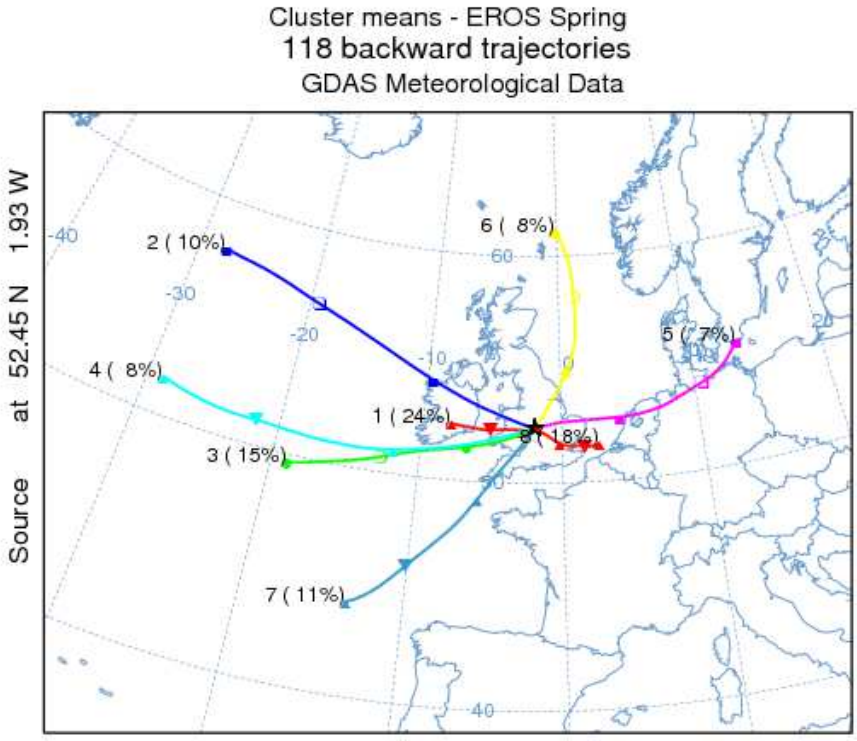

Figure 5.5 *(continued)*

Table 5.4 Average concentrations (± S.D.) of major chemical components in $PM_{2.5}$ by trajectory clusters in each season at EROS (Box-whisker plots of each component by clusters in each season detailed in Appendix D)

$PM_{2.5}$	*n*	Concentration, μg m^{-3}								T	RH
		SO_4^{2-}	NO_3^-	Cl^-	$C_2O_4^{2-}$	OC	EC	OC_{prim}	OC_{sec}	(^oC)	(%)
Summer											
Cluster 1	11	1.65±0.81	1.00±0.67	0.22±0.25	0.03±0.03	2.9±1.7	1.0±0.7	0.3±0.3	2.5±1.6	14±2	71±9
Cluster 2	12	1.99±0.92	1.84±2.01	0.44±0.38	0.06±0.04	2.3±1.0	0.7±0.3	0.2±0.1	2.0±0.9	15±2	79±7
Cluster 3	9	2.66±0.97	2.39±1.84	0.85±0.49	0.07±0.04	2.3±1.0	0.8±0.4	0.3±0.1	2.0±0.9	14±3	79±9
Cluster 4	18	1.41±0.77	0.67±0.48	0.34±0.36	0.03±0.02	1.8±0.6	0.5±0.2	0.2±0.1	1.7±0.6	16±2	73±6
Cluster 5	16	1.14±0.30	0.57±0.18	0.30±0.42	0.03±0.01	1.6±0.4	0.5±0.2	0.2±0.1	1.4±0.4	16±2	83±9
Cluster 6	15	1.25±0.64	0.67±0.74	0.48±0.66	0.02±0.02	1.4±0.3	0.4±0.1	0.1±0.0	1.3±0.3	16±2	76±4
Cluster 7	9	0.79±0.33	0.46±0.20	0.50±0.36	0.02±0.01	1.4±0.4	0.4±0.2	0.1±0.1	1.3±0.4	14±1	71±2
Cluster 8	10	1.09±0.37	0.44±0.12	0.24±0.27	0.02±0.01	1.4±0.3	0.4±0.1	0.1±0.1	1.3±0.2	17±2	79±5
Cluster 9	16	1.37±0.57	0.78±0.50	0.14±0.06	0.03±0.02	2.0±0.5	0.7±0.3	0.2±0.1	1.7±0.4	16±2	75±5
Autumn											
Cluster 1	16	1.29±1.21	0.85±0.86	1.13±0.99	0.03±0.04	2.2±1.0	0.8±0.4	0.3±0.2	1.9±0.9	11±3	82±4
Cluster 2	21	1.32±0.81	1.36±1.18	0.68±0.56	0.03±0.04	3.1±1.8	1.6±1.0	0.5±0.4	2.5±1.5	6±4	79±7
Cluster 3	15	1.23±0.90	0.99±1.20	0.58±0.48	0.03±0.04	2.1±1.3	1.1±1.0	0.4±0.3	1.7±1.0	13±3	83±5
Cluster 4	11	0.95±0.38	0.97±0.59	0.41±0.28	0.02±0.03	4.2±3.8	2.0±1.6	0.7±0.6	3.5±3.3	10±3	80±7
Cluster 5	27	1.15±0.86	1.35±1.30	0.34±0.36	0.02±0.02	2.8±2.2	1.3±1.1	0.4±0.4	2.3±1.9	10±4	83±7
Cluster 6	14	1.47±0.99	0.75±0.51	0.28±0.30	0.06±0.06	2.1±0.9	0.8±0.3	0.3±0.1	1.9±0.8	10±3	80±6
Cluster 7	9	2.97±2.16	4.14±3.82	0.32±0.23	0.05±0.04	3.4±1.3	1.1±0.5	0.4±0.2	3.0±1.2	10±5	86±6
Cluster 8	26	2.31±1.61	3.13±2.48	0.61±0.56	0.03±0.02	4.3±3.7	2.1±1.9	0.7±0.7	3.6±3.1	9±5	83±9
Cluster 9	18	1.46±0.86	1.83±1.65	0.36±0.26	0.03±0.02	2.5±1.1	1.1±0.4	0.4±0.2	2.1±1.0	11±2	87±6
Cluster 10	8	2.07±1.36	2.73±1.32	0.43±0.19	0.03±0.03	3.5±1.5	1.4±0.8	0.5±0.3	3.0±1.3	6±7	88±6
Winter											
Cluster 1	22	2.36±1.09	4.21±2.17	1.19±0.75	0.04±0.05	5.4±2.7	2.3±1.7	0.8±0.6	4.6±2.2	1±4	88±4
Cluster 2	14	1.97±1.64	2.82±2.09	1.21±0.82	0.03±0.03	4.4±2.4	1.3±1.2	0.5±0.4	4.0±2.1	4±3	86±5
Cluster 3	12	2.45±0.88	5.58±2.67	1.52±0.91	0.05±0.04	6.3±3.0	2.9±1.5	1.0±0.5	5.3±2.5	-1±4	90±5
Cluster 4	8	2.46±1.16	3.43±1.53	2.18±0.44	0.10±0.05	4.4±2.4	1.4±1.4	0.5±0.5	3.9±2.0	3±3	87±4
Cluster 5	13	3.68±1.62	7.52±3.33	1.43±0.53	0.11±0.08	6.1±1.9	1.8±1.2	0.6±0.4	5.5±1.8	1±6	90±5
Cluster 6	4	1.34±0.72	3.45±2.17	0.97±0.90	0.03±0.04	4.3±1.7	1.5±1.1	0.5±0.4	3.8±1.5	0±3	87±5
Cluster 7	10	2.43±1.68	3.16±2.38	1.29±0.78	0.06±0.05	4.4±1.9	1.4±0.8	0.5±0.3	3.9±1.7	6±3	87±10
Cluster 8	8	2.71±2.02	3.91±2.33	0.99±0.72	0.05±0.06	3.9±1.5	1.3±0.6	0.4±0.2	3.4±1.3	-1±2	83±9
Cluster 9	2	0.74	0.95	0.32	0.01	3.3	0.9	0.3	3.0	5	88
Cluster 10	8	0.61±0.21	0.49±0.27	0.71±0.41	0.002±0.002	3.1±0.3	0.3±0.3	0.1±0.1	3.0±0.3	9±2	85±8
Spring											
Cluster 1	28	2.36±1.12	4.96±4.47	0.86±0.74	0.08±0.06	2.8±0.9	1.1±0.6	0.4±0.2	2.4±0.8	8±3	74±7
Cluster 2	12	1.49±0.70	1.40±1.52	1.91±1.23	0.04±0.03	1.7±1.1	0.6±0.5	0.2±0.2	1.5±0.9	8±2	71±7
Cluster 3	18	1.45±0.72	1.45±1.10	1.02±0.91	0.05±0.04	2.0±1.0	0.7±0.6	0.2±0.2	1.7±0.9	9±2	78±7
Cluster 4	9	1.70±1.42	2.83±6.88	1.54±0.72	0.04±0.05	1.3±0.6	0.3±0.1	0.1±0.0	1.2±0.6	10±2	75±5
Cluster 5	8	5.53±3.41	10.41±6.68	1.01±0.50	0.17±0.11	4.1±1.2	1.0±0.8	0.4±0.3	3.7±1.2	10±2	83±9
Cluster 6	9	1.95±1.27	1.82±1.23	0.95±0.65	0.05±0.05	2.2±0.9	0.6±0.3	0.2±0.1	2.0±0.8	9±3	68±6
Cluster 7	13	1.29±0.60	2.09±1.95	0.36±0.28	0.06±0.05	2.1±0.6	0.6±0.2	0.2±0.1	1.9±0.6	10±3	80±7
Cluster 8	21	3.32±1.37	11.07±6.70	0.43±0.36	0.10±0.07	4.1±1.5	1.4±1.1	0.5±0.4	3.6±1.3	10±3	74±9

With regard to the sources of oxalate in aerosol, oxalate was found high concentrations for the air mass trajectories coming from continental airflows and was generally associated with high sulphate and nitrate concentrations (cluster 3, 7, 5 and 5 in summer, autumn, winter and spring, respectively), suggesting that marine precursors for production of oxalate were not very important. Since there was no obvious strong seasonality in oxalate concentrations at this site, the precursors from anthropogenic sources may be considered more than biogenic isoprene.

5.5.3 Cluster analysis for simultaneous data between EROS and Harwell

As mentioned in 5.5.1, it is useful to evaluate the air mass back trajectories in order to know the LRT paths of aerosol composition in air samples collected simultaneously between EROS and Harwell. There were 100 back trajectories computed by HYSPLIT_4 during 12 Jul to 6 Dec 2010 and the cluster analysis was applied to each of the site locations. Figure 5.6 shows the change in total spatial variance with number of clusters at EROS and Harwell. The mean back trajectories for nine clusters were represented at both sites as change in TSV when reducing the number of clusters from nine to eight (49.87% and 33.48% for EROS and Harwell, respectively), indicating nine clusters for this sampling period. The clustering results were quite similar at EROS and Harwell (Figure 5.7), despite some minor cluster differences from the very slow easterly airflow (cluster 1) accounted for 12% of the data for EROS and not for Harwell including the slow southerly airflow (cluster 2) accounted for 8% of the data for Harwell and not for EROS. In comparison the clustering data of Harwell with the study by Abdalmogith and Harrison (2005), the clustering paths in this study yielded mostly the same direction as during the period of 2002 - 2003 data. The fast easterly flows were registered at both sites (cluster 9) and accounted for 3% and 5% of the data for EROS and Harwell, respectively. The significant slow westerly airflows were seen in this period (cluster 4 accounted for 25% of the trajectories and cluster 1 accounted for 16% of the trajectories for EROS and Harwell, respectively). Meteorological scenarios favouring the transport of air masses from the northern part passing over the UK before arriving at EROS and Harwell also appeared during this period with the slow and fast airflows accounted between 8% to 15% of the data (cluster 7, 8 and cluster 6, 7 for EROS and Harwell, respectively).

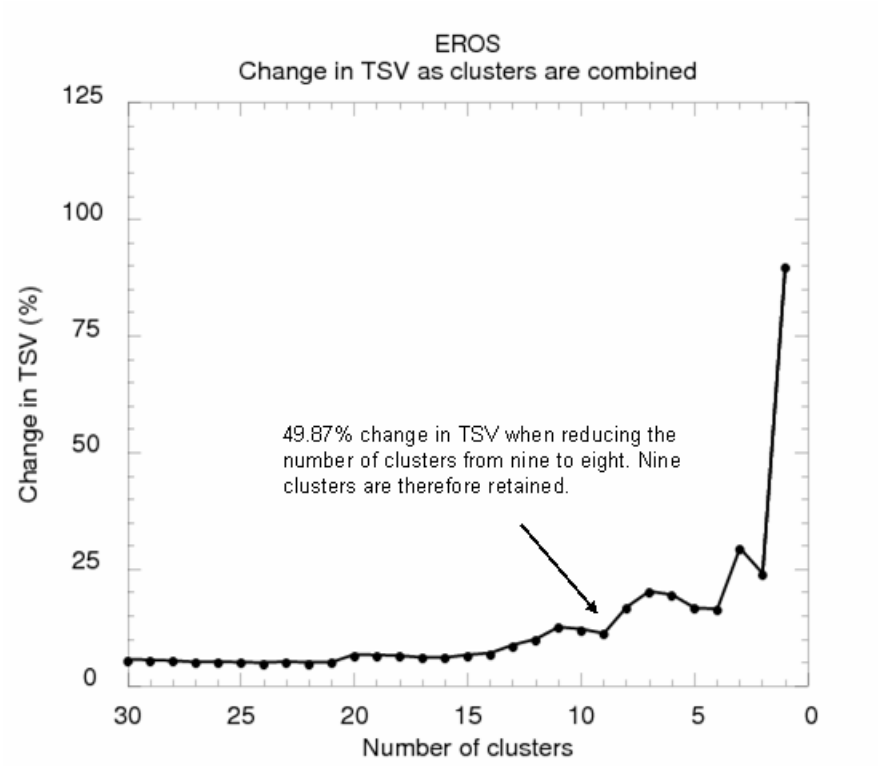

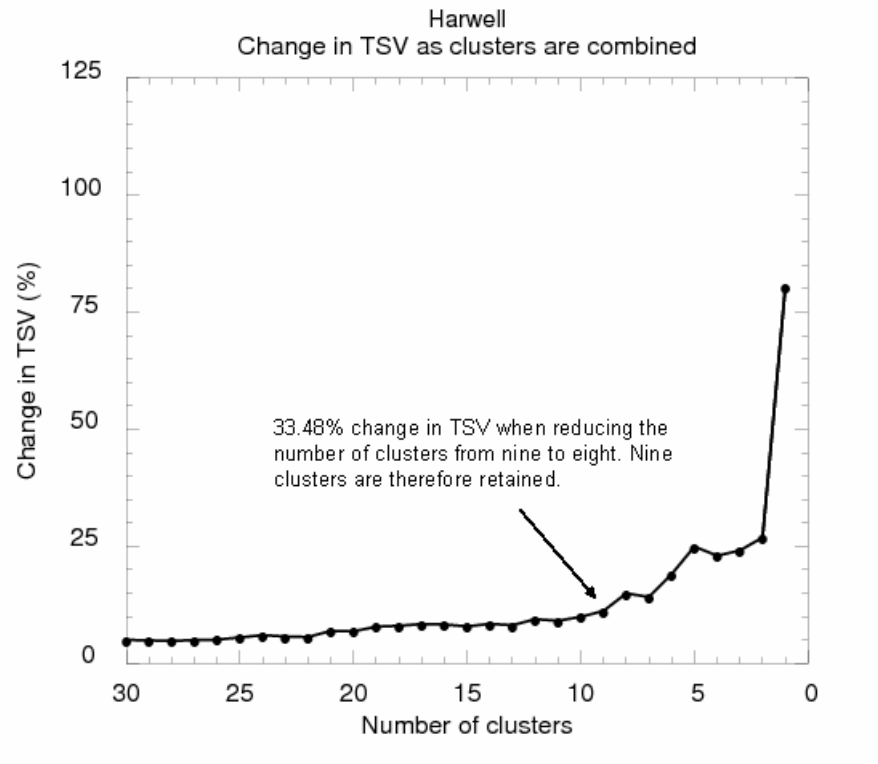

Figure 5.6 The percent changes in total spatial variance with cluster number for the clustering of trajectories arriving at EROS and Harwell during the period of simultaneous air sampling (12 July 2010 to December 2010)

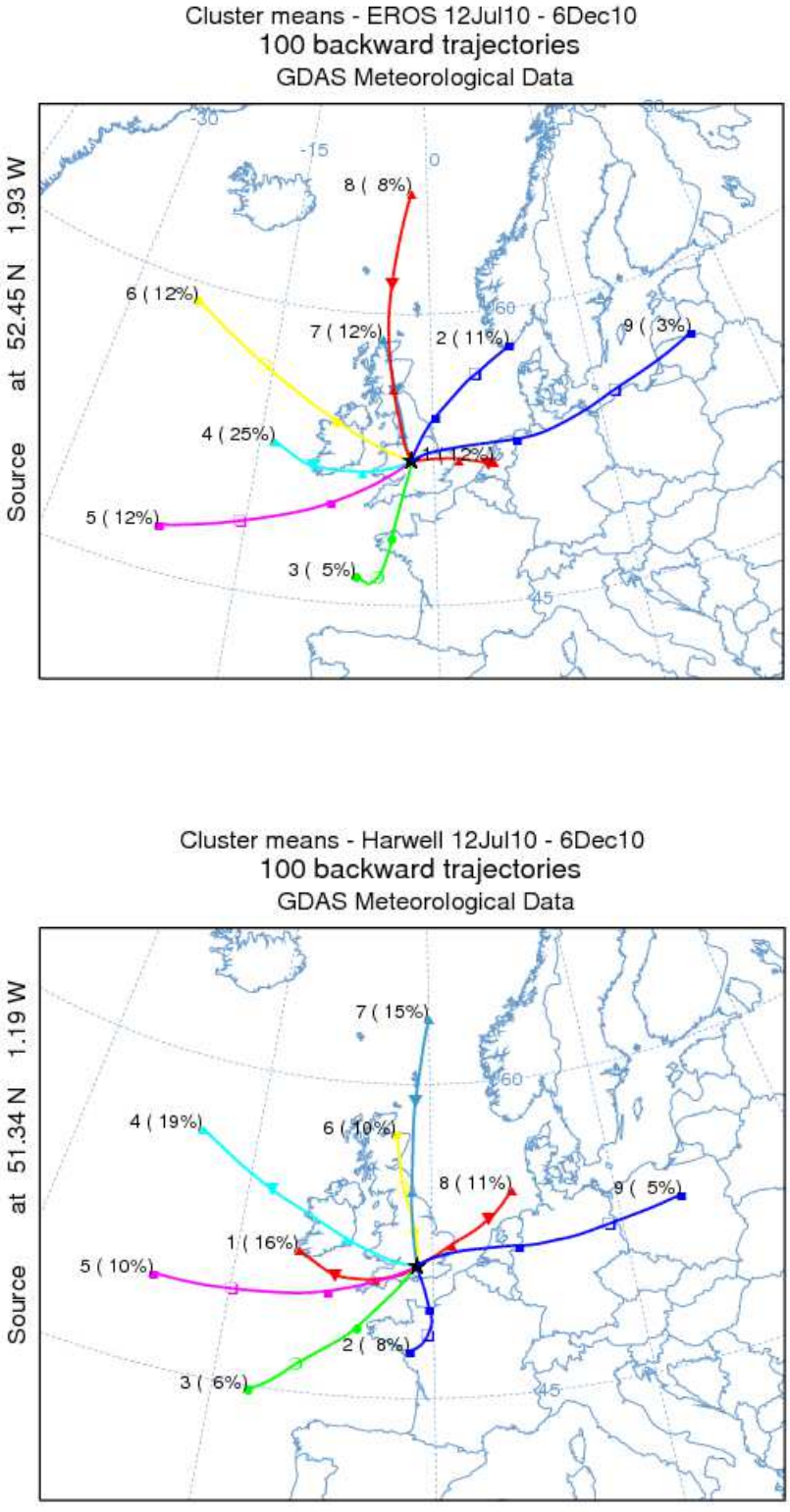

Figure 5.7 Average 3-day back trajectories for the main trajectory clusters arriving at EROS and Harwell during the period of simultaneous air sampling (12 July 2010 and December 2010). Symbols denote the location of the air parcel every 24 hours. (Individual trajectories contributing to each cluster are presented in Appendix C)

Table 5.5 summarises the average concentration of chemical components in $PM_{2.5}$ for clusters arriving at EROS and Harwell during the period of simultaneous sampling. As the local contribution calculated by the subtraction of the LRT from urban background concentration, the assumption of this method also included the formation of secondary aerosol species by photochemical oxidation contributed insufficiently for local formation of ion species to influence the analysed concentrations appreciably. For EROS, the local contribution to the major chemical components in fine fraction dominated for carbonaceous particles (EC, OC, OC_{prim}, OC_{sec} and WSOC for 0.6 μg m^{-3}, 0.5 μg m^{-3}, 0.3 μg m^{-3}, 0.4 μg m^{-3} and 0.4 μg m^{-3}, respectively) as presented in chapter 3 (Table 3.6) and chapter 4 (Table 4.4). The low local contributions were observed for nitrate, sulphate, chloride in this study (0.17 μg m^{-3}, 0.13 μg m^{-3} and 0.08 μg m^{-3}, respectively). There was mostly influence of regional contribution for oxalate in ambient air as a zero value obtained from mean concentration difference between the two sites during the simultaneous period.

With regard to Harwell represented purely LRT, the fast easterly (cluster 9) and the slow southerly (cluster 2) airflows contribute the significant concentration of chemical composition levels. Nitrate and sulphate concentrations associated with the slow southerly airflow and the fast easterly airflow, respectively appeared the highest concentrations. (4.25 μg m^{-3} and 3.17 μg m^{-3} for nitrate and sulphate, respectively). This transport path of cluster 2 also dominantly contributed the highest concentration of oxalate in fine fraction (0.06 μg m^{-3}). These findings indicate that the secondary aerosols could be transported from the polluted urban in Western Europe, mainly during the autumn. For oxalate at Harwell, the biogenic emissions from vegetation especially isoprene could be the important precursor in associated with southerly trajectories as stated by Legrand et al. (2007). Their study confirmed the role of isoprene on the contribution of oxalic acid since the high estimated isoprene emissions in Europe especially in the east flank of France (Simpson et al., 1995) with the isoprene emissions of 1.5 to 2.5 tons km^{-2} yr^{-1}. However, the sources of oxalate from the other anthropogenic precursors would be considered because the slow southerly trajectory did not contribute for the highest oxalate concentration at EROS site as later discussion.

Although the large concentration of chloride associated with the fast maritime airflows coming form Atlantic ocean (cluster 4, 5), it should be noted that the highest chloride concentration was from the continental air masses with the fast easterly trajectory (cluster 9).

This finding indicates the important sources of chloride in fine fraction originated from urban and industrial regions passing over Europe.

Table 5.5 Average concentrations (± S.D.) of major chemical components in $PM_{2.5}$ by trajectory clusters arriving at EROS and Harwell during the period of simultaneous air sampling

$PM_{2.5}$	*n*	Aerosol Concentration, μg m^{-3}									
		SO_4^{2-}	NO_3^-	Cl^-	$C_2O_4^{2-}$	OC	EC	OC_{prim}	OC_{sec}	WSOC	WSOC/ OC_{sec}
EROS											
Cluster 1	12	2.83±2.00	3.18±3.34	0.27±0.22	0.04±0.03	2.8±1.3	1.1±1.0	0.4±0.3	2.4±1.0	2.2±0.9	0.92
Cluster 2	11	2.28±1.72	2.91±2.21	0.44±0.23	0.02±0.01	3.3±1.8	1.5±1.0	0.5±0.4	2.8±1.4	2.2±1.0	0.79
Cluster 3	5	1.46±0.94	1.85±2.36	0.49±0.46	0.02±0.02	1.7±0.5	0.6±0.3	0.2±0.1	1.4±0.4	1.3±0.3	0.93
Cluster 4	25	1.00±0.40	0.56±0.51	0.21±0.15	0.01±0.01	1.6±0.6	0.5±0.2	0.2±0.1	1.4±0.5	1.2±0.6	0.86
Cluster 5	12	1.04±0.65	0.45±0.17	0.30±0.22	0.01±0.01	1.3±0.3	0.5±0.1	0.2±0.0	1.2±0.3	1.1±0.2	0.92
Cluster 6	12	0.84±0.35	0.56±0.52	0.42±0.25	0.01±0.01	1.5±0.3	0.6±0.2	0.2±0.1	1.3±0.2	1.2±0.2	0.92
Cluster 7	12	2.50±1.65	2.46±2.81	0.42±0.38	0.02±0.01	3.6±3.0	2.1±2.2	0.7±0.8	2.9±2.3	2.5±1.6	0.86
Cluster 8	8	1.10±0.95	1.60±1.42	0.44±0.27	0.01±0.01	3.2±2.0	1.5±0.9	0.5±0.3	2.7±1.8	1.9±1.6	0.70
Cluster 9	3	1.37±0.45	3.43±2.28	0.56±0.13	0.02±0.01	3.3±1.1	1.2±0.9	0.4±0.3	2.9±0.8	2.2±0.5	0.76
Harwell											
Cluster 1	16	0.85±0.36	0.49±0.30	0.13±0.08	0.02±0.02	1.2±0.3	0.1±0.1	0.1±0.0	1.2±0.3	0.8±0.4	0.67
Cluster 2	8	3.02±2.58	4.25±4.96	0.21±0.19	0.06±0.07	2.7±1.3	0.6±0.5	0.2±0.2	2.4±1.2	2.1±1.3	0.88
Cluster 3	6	1.09±0.66	0.36±0.14	0.23±0.24	0.004±0.005	1.0±0.3	0.1±0.1	0.03±0.02	1.0±0.4	0.5±0.2	0.50
Cluster 4	19	0.82±0.43	0.53±0.41	0.35±0.26	0.01±0.01	1.3±0.4	0.2±0.1	0.1±0.0	1.3±0.4	1.0±0.5	0.77
Cluster 5	10	1.10±0.63	0.83±0.97	0.40±0.29	0.02±0.02	1.6±0.8	0.3±0.6	0.1±0.2	1.5±0.6	1.2±0.7	0.80
Cluster 6	10	1.89±1.11	2.20±1.96	0.20±0.14	0.02±0.02	2.3±0.8	0.6±0.4	0.2±0.1	2.1±0.6	1.8±0.7	0.86
Cluster 7	15	1.03±0.69	1.32±1.33	0.22±0.12	0.01±0.02	1.5±0.6	0.4±0.3	0.1±0.1	1.4±0.6	1.3±0.5	0.93
Cluster 8	11	2.27±0.96	2.10±0.78	0.24±0.25	0.01±0.01	2.2±0.6	0.7±0.4	0.2±0.1	2.0±0.4	1.7±0.5	0.85
Cluster 9	5	3.17±1.13	2.07±1.08	0.67±0.37	0.02±0.02	2.8±1.3	0.6±0.3	0.2±0.1	2.6±1.2	2.4±1.2	0.92

Concerning the secondary OC transport paths at Harwell, OC_{sec} formed in the atmosphere dominantly associated with easterly airflow (cluster 8, 9) including the slow southerly (cluster 2) and the northerly airflows (cluster 6). The slow and fast trajectories coming from northern and eastern part of UK before arriving EROS were influence on OC_{sec} concentrations (cluster 1, 2, 7, 8 and 9). The similar observations appeared for the transport paths of WSOC as mainly produced by secondary formation stated in the previous chapter. Kruskal-Wallis non-parametric tests indicates no significant difference ($p > 0.05$) in ratio of WSOC/OC_{sec} among clusters arriving at EROS but significant difference is observed at Harwell site. This could be evident the important secondary source of WSOC associated with the LRT arriving EROS site. As seen in Table 5.5, WSOC also associated with the clusters containing significant of OC at both sites (cluster 1, 2, 7 and 9 for EROS and cluster 2, 6 and 9 for Harwell). This is because a large fraction of OC is water soluble and it contains the more oxygenated and polar fraction of particulate organic carbon.

For EC and primary OC concentrations, they were expected the local contribution rather than the LRT as EC was formed during the incomplete combustion and a good indicator for primary source. The highest concentration of EC was observed dominantly in association with northerly airflow (cluster 7) for EROS, whilst the easterly airflow (cluster 8) made the significant contribution to EC concentration at Harwell. A similar pattern was seen for OC_{prim} as its concentration calculated based on the minimum ratio of 0.35 (OC_{prim} = 0.35 × EC). Since both clusters were the slow moving airflows, it seems likely the airmasses to be associated with low local wind speeds and low mixing depths associated with the cold conditions which would lead to poor dispersion of local urban emissions. This is evidenced by the highest concentrations of EC and OC_{prim} associated with cluster 3 during the winter moth for EROS site.

In comparison between dataset collecting in this period with the whole data at EROS, the major chemical composition in $PM_{2.5}$ associated with the airflows mainly from Western Europe which is industrialized European continent (cluster 1, 2, and 9). The significant northerly trajectories passing over the UK before arriving EROS also contributed the high concentrations of atmospheric pollutants. The westerly airflows (cluster 4, 5 and 6) were observed low major component concentrations similar to the results obtained from whole EROS data. The oxalate concentration revealed the highest concentration with the slow easterly airflow (cluster 1) from continental Europe in consistent with the continental air masses (cluster 2) affecting its concentration at Harwell during this period. These results could be attributed the fact that the regional contribution of oxalate concentration in fine fraction coming from continental airflows at both sites. Similarly, Salvador et al. (2010) observed the source of oxalic and other diacids from central Europe before arriving France and Germany (Puy de Dome-PDD and Schauinsland-SIL sampling sites, respectively).

The box-whisker plots of chemical composition of $PM_{2.5}$ for simultaneous data between EROS and Harwell by the clusters are presented in Figure 5.8 and Figure 5.9. The pattern of oxalate in Figure 5.9 looks very similar to that for nitrate but rather different from sulphate. This finding could be attributed the fact that oxalate exhibit the same behaviour as nitrate aerosol mostly found in form of NH_4NO_3 which is a temperature dependent species. On the other hand, sulphate in form of $(NH_4)_2SO_4$ is more stable in ambient air. As expected, the patterns of WSOC were similar to that for OC_{sec} and OC at both sites, it could be confirmed

that WSOC mostly formed by secondary formation and WSOC accounted for the significant fraction of OC in atmospheric particle.

(a)

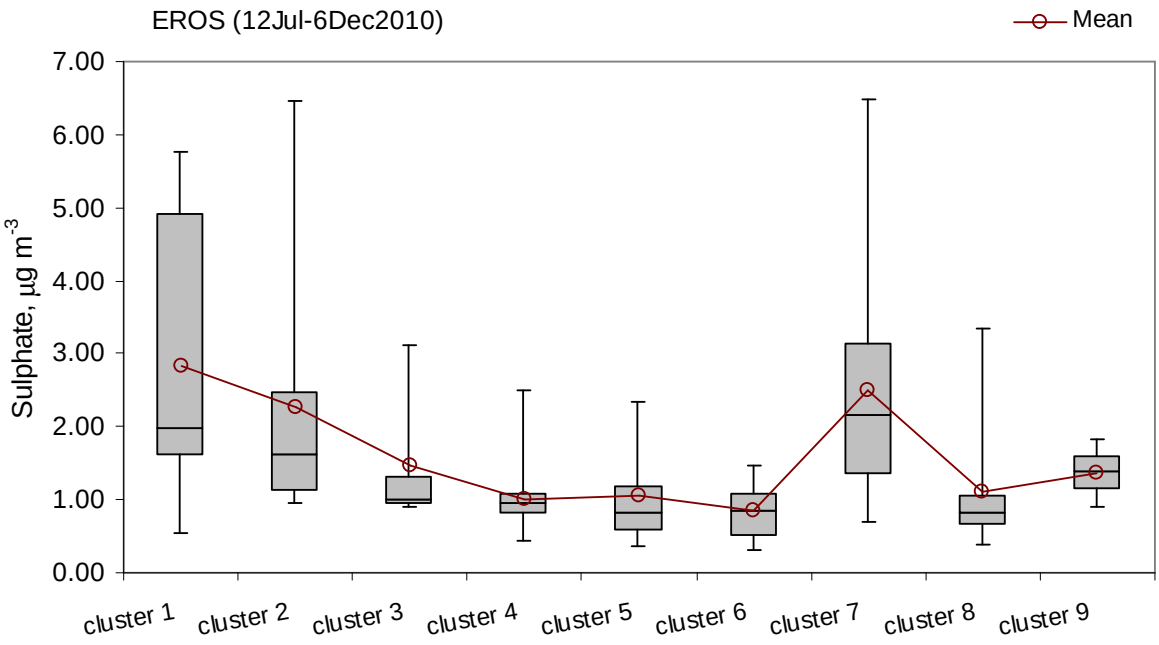

(b)

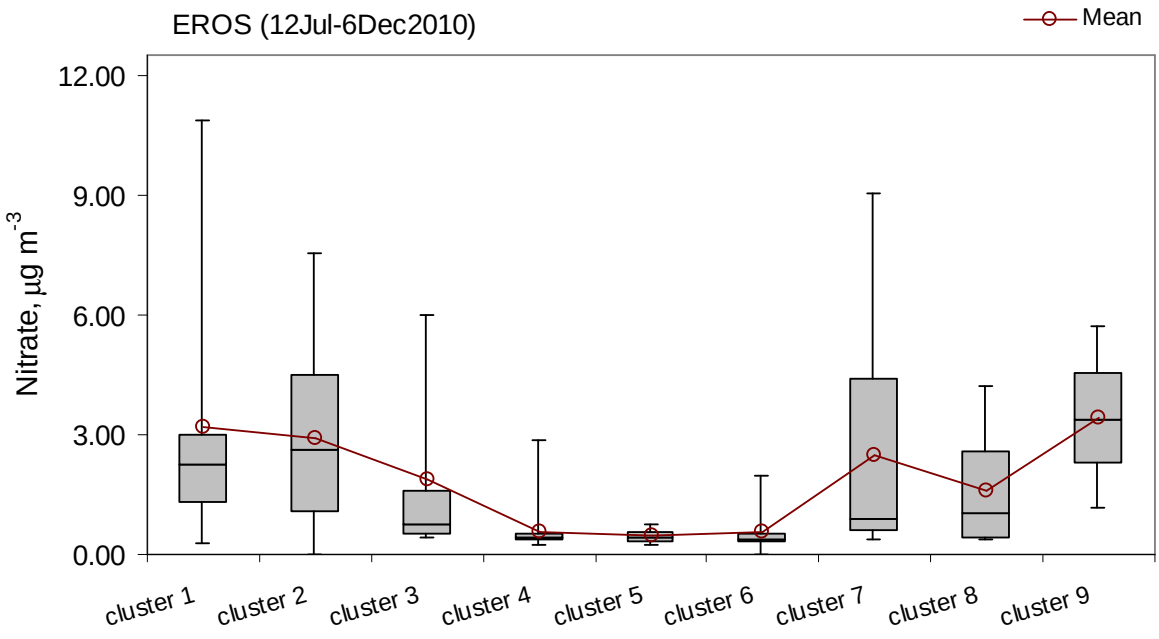

Figure 5.8 Box-whisker plots of major components in $PM_{2.5}$ at EROS by clusters during the simultaneous air sampling with Harwell; (a) sulphate, (b) nitrate, (c) chloride, (d) oxalate, (e) OC, (f) EC, (g) OC_{prim}, (h) OC_{sec}, (i) WSOC and (j) $WSOC/OC_{sec}$

(c)

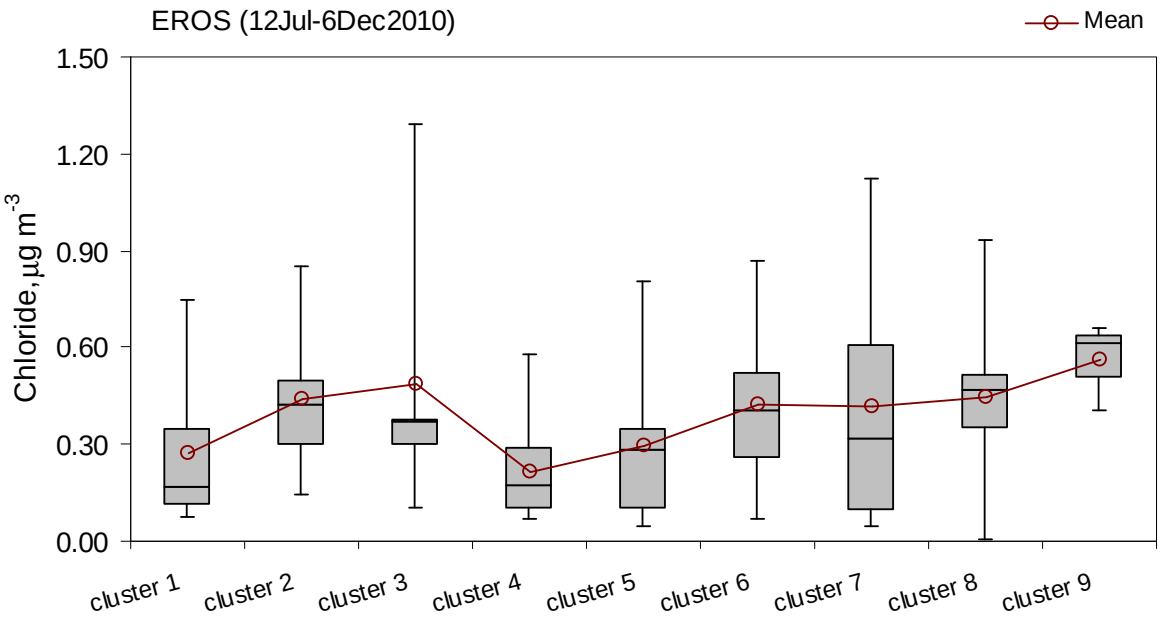

(d)

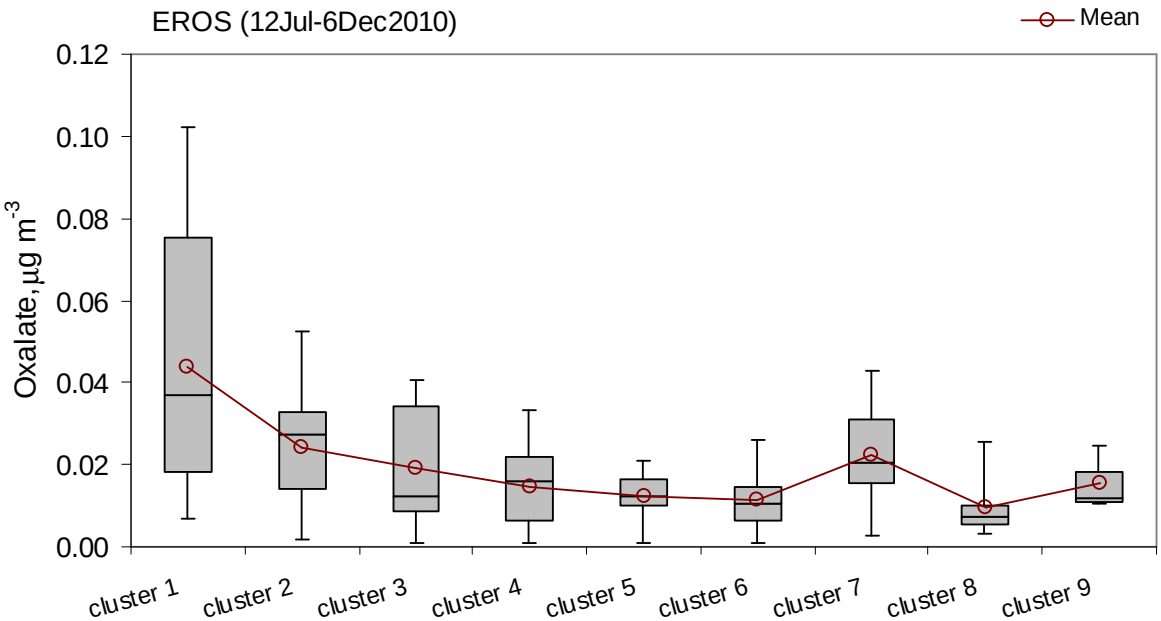

Figure 5.8 *(continued)*

(e)

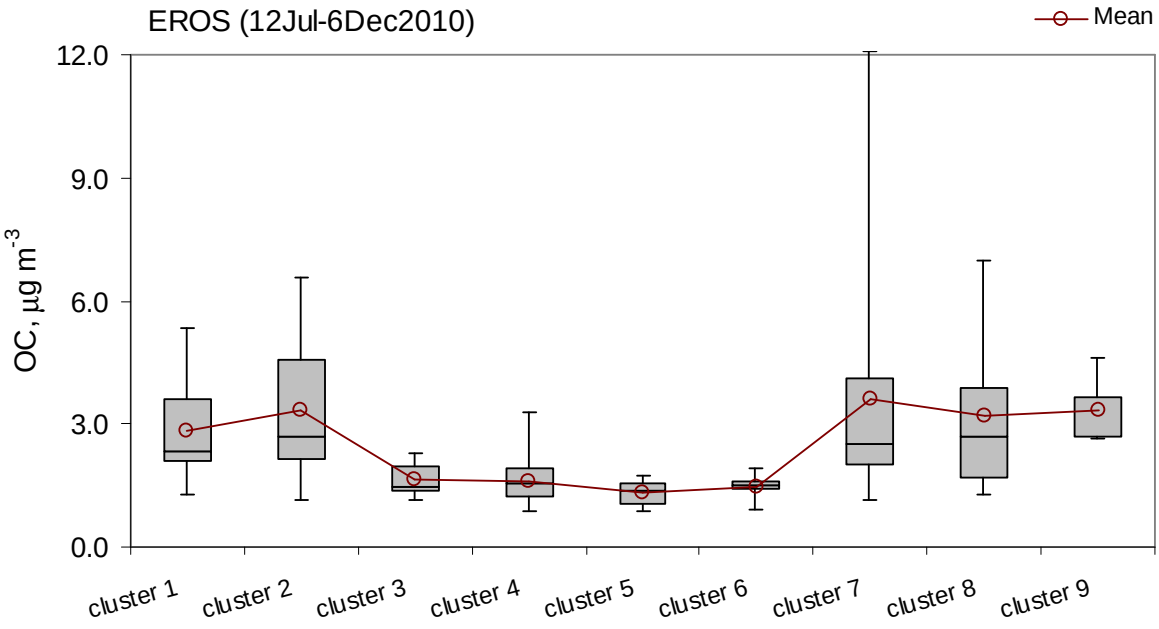

(f)

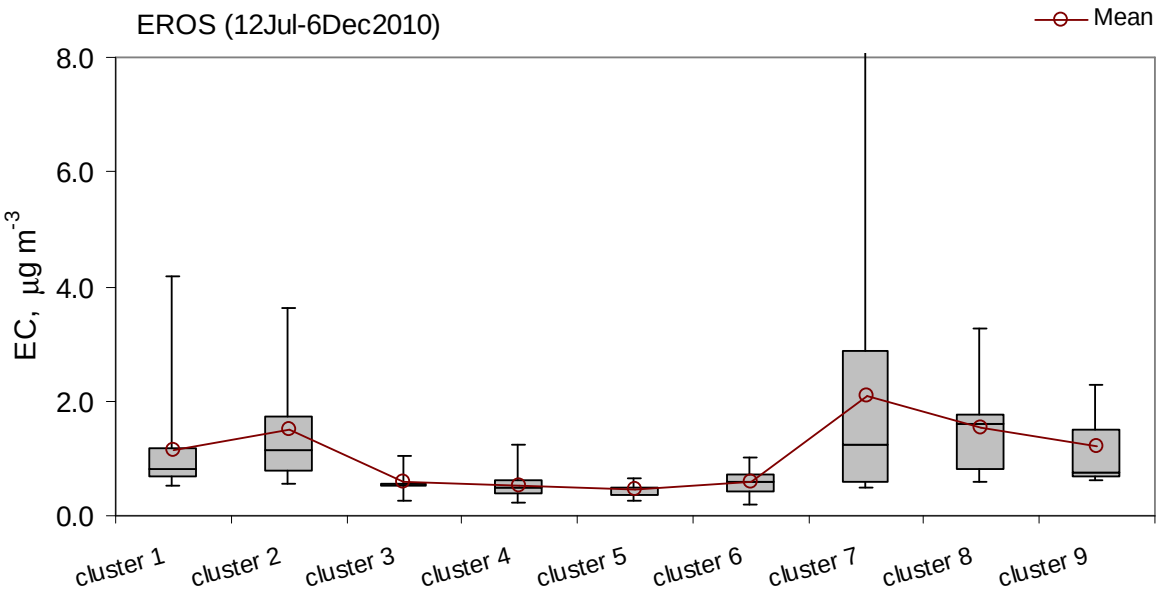

Figure 5.8 *(continued)*

(g)

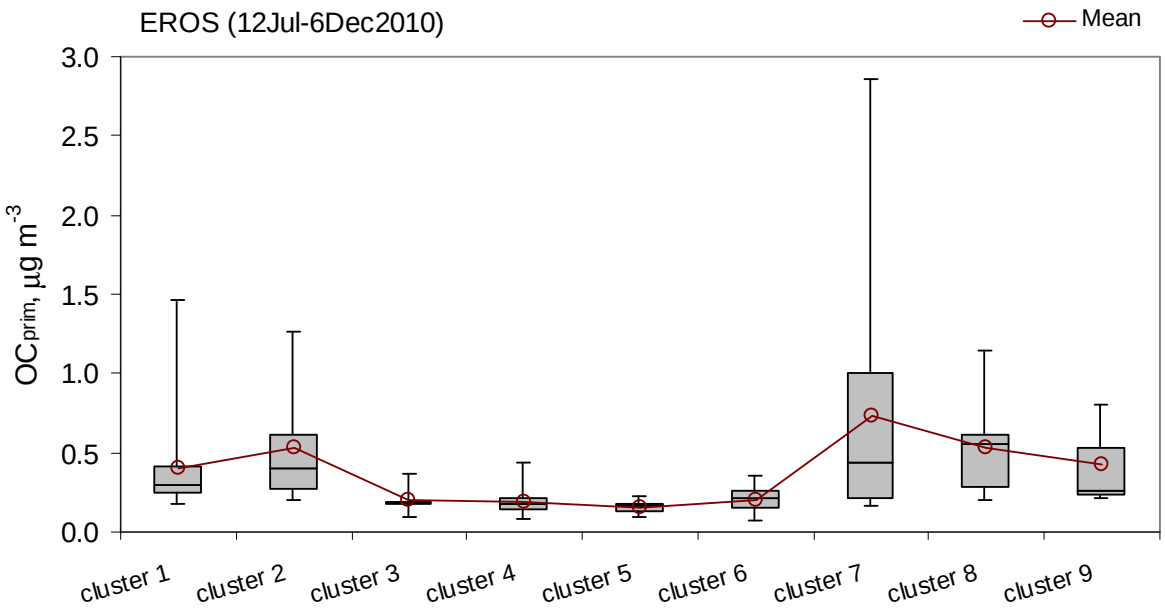

(h)

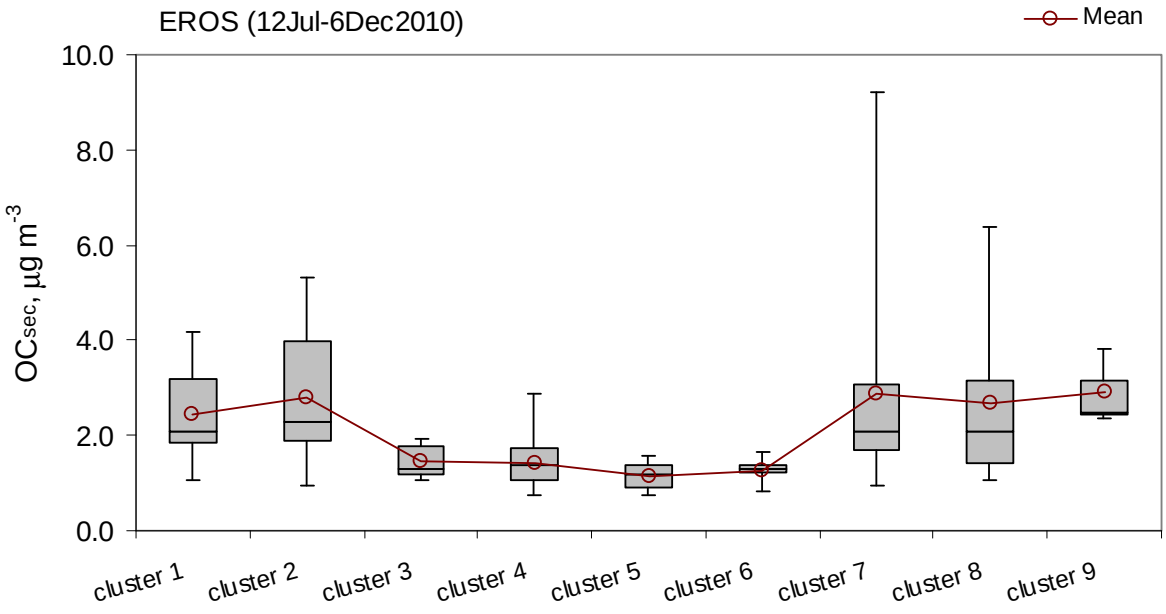

Figure 5.8 *(continued)*

(i)

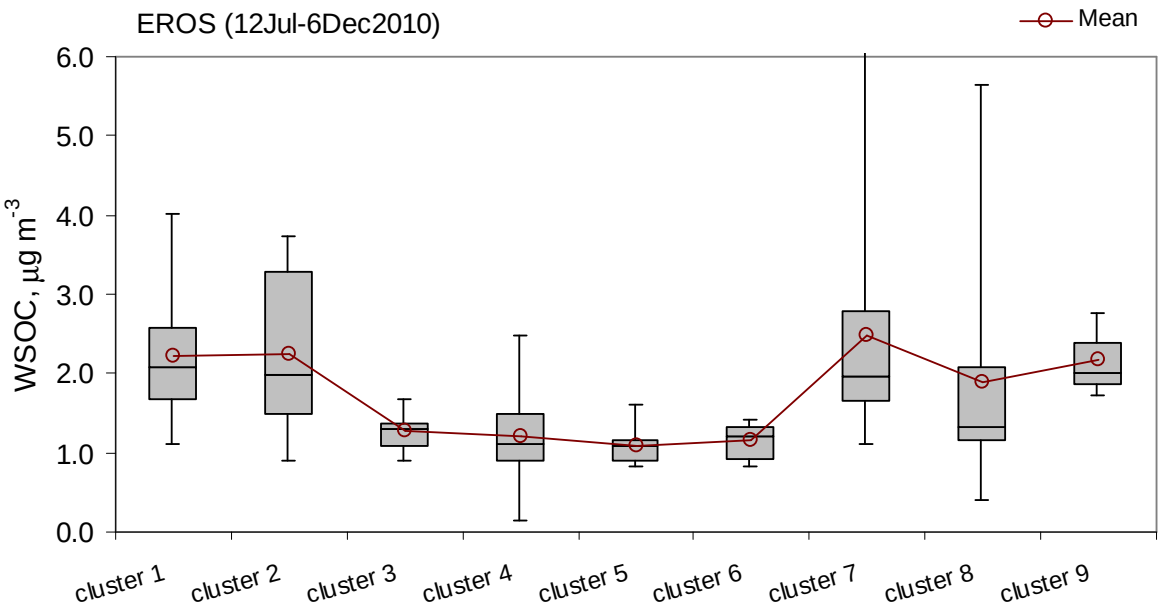

(j)

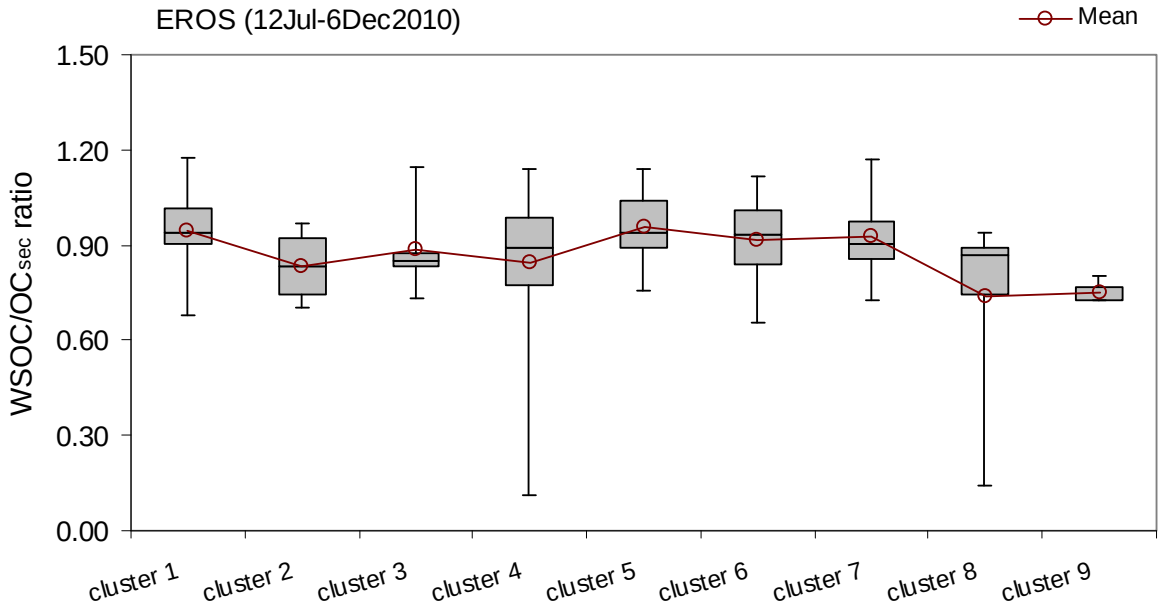

Figure 5.8 *(continued)*

(a)

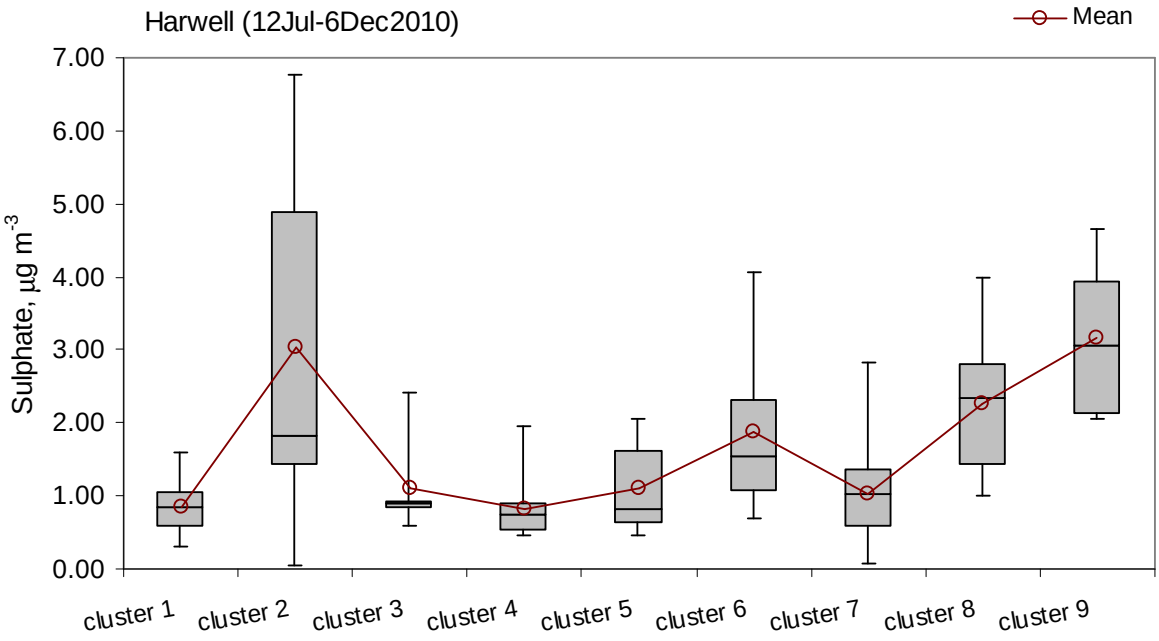

(b)

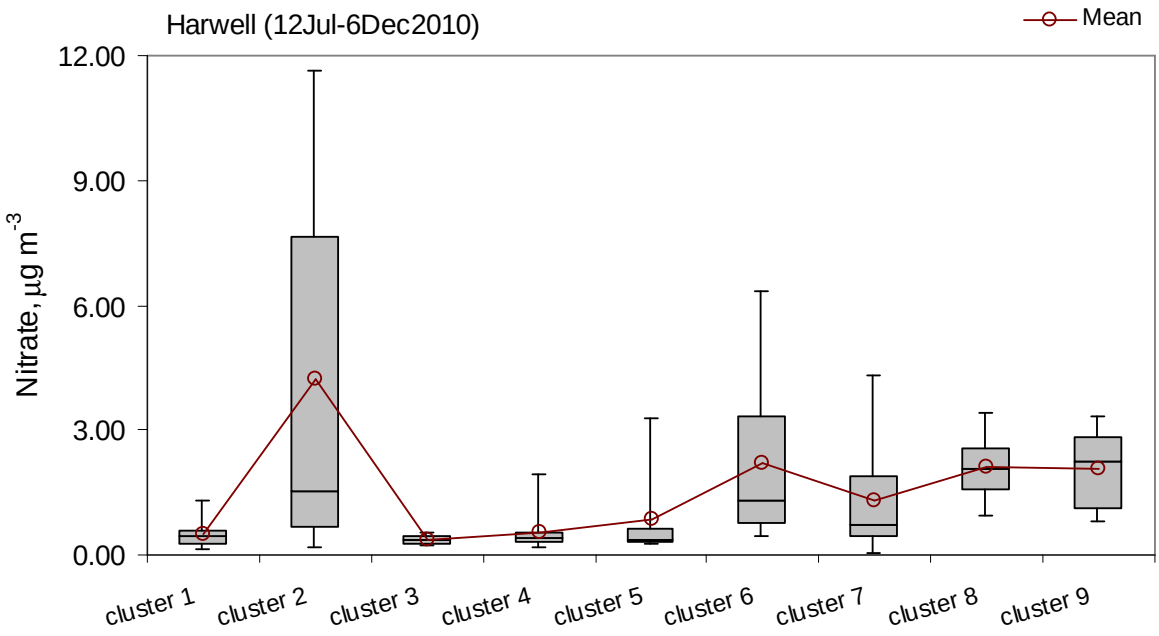

Figure 5.9 Box-whisker plots of major components in $PM_{2.5}$ at Harwell by clusters during the simultaneous air sampling with EROS; (a) sulphate, (b) nitrate, (c) chloride, (d) oxalate, (e) OC, (f) EC, (g) OC_{prim}, (h) OC_{sec}, (i) WSOC and (j) $WSOC/OC_{sec}$

(c)

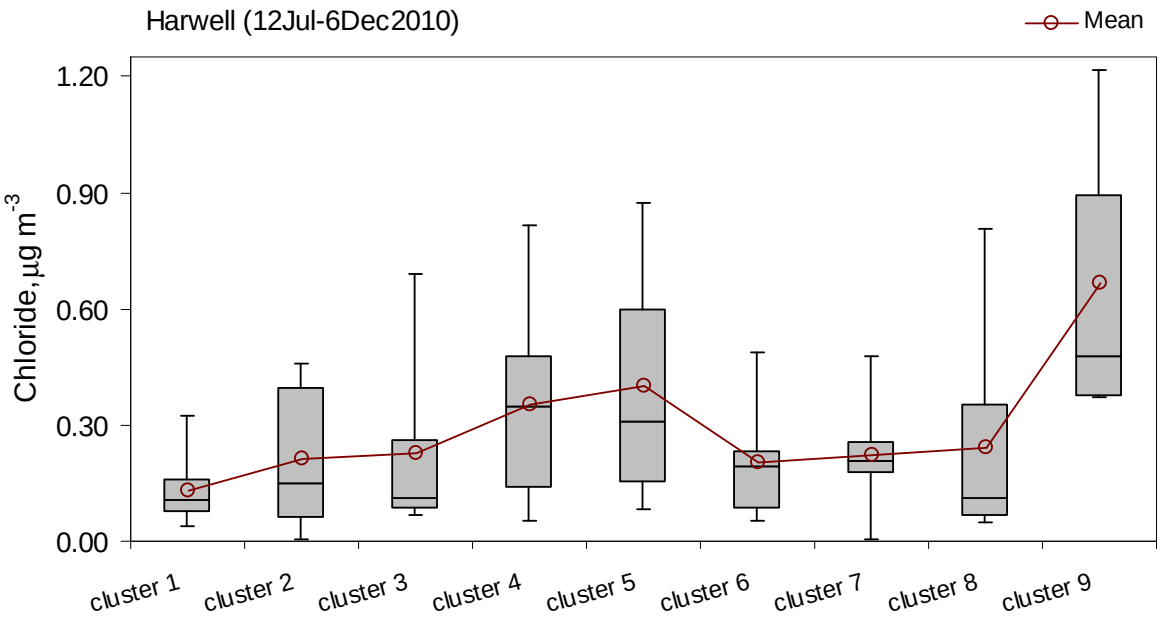

(d)

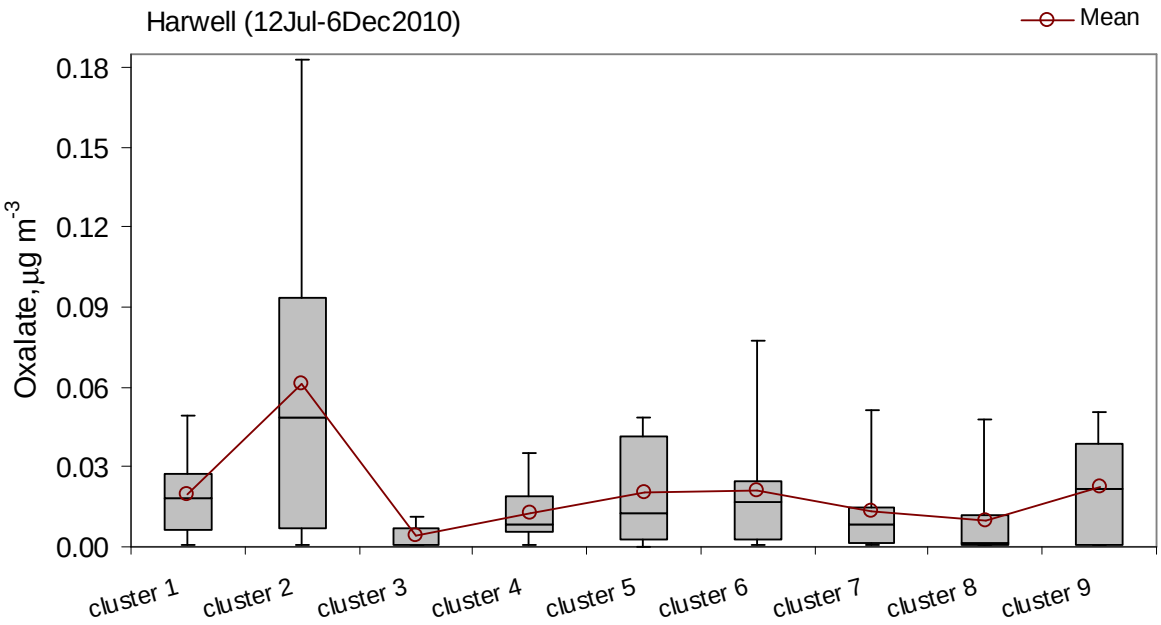

Figure 5.9 *(continued)*

(e)

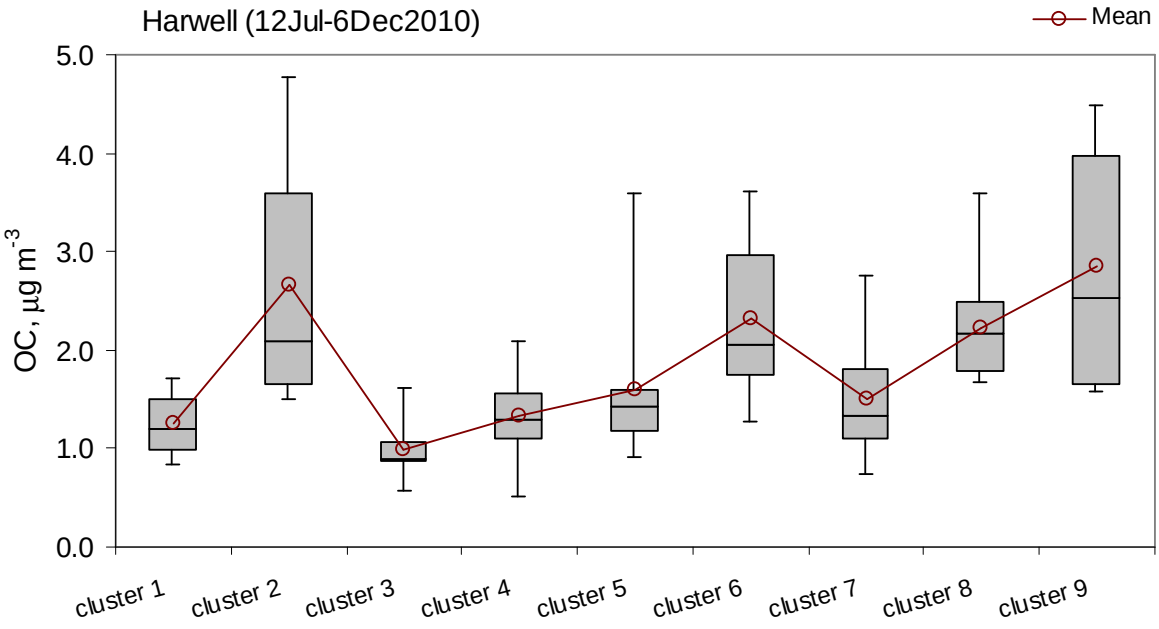

(f)

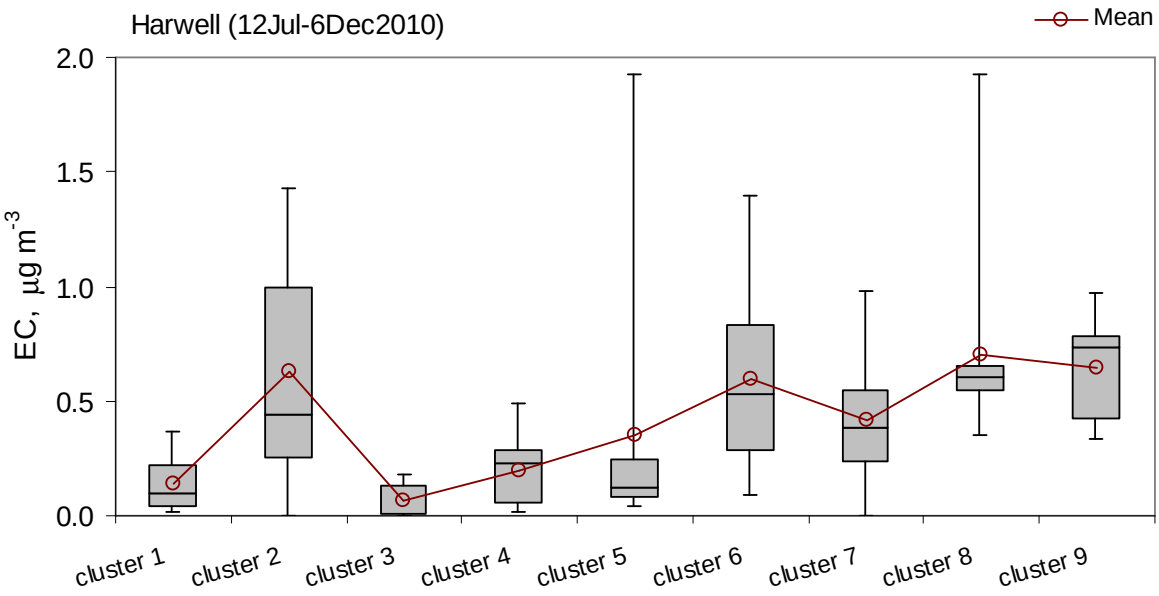

Figure 5.9 *(continued)*

(g)

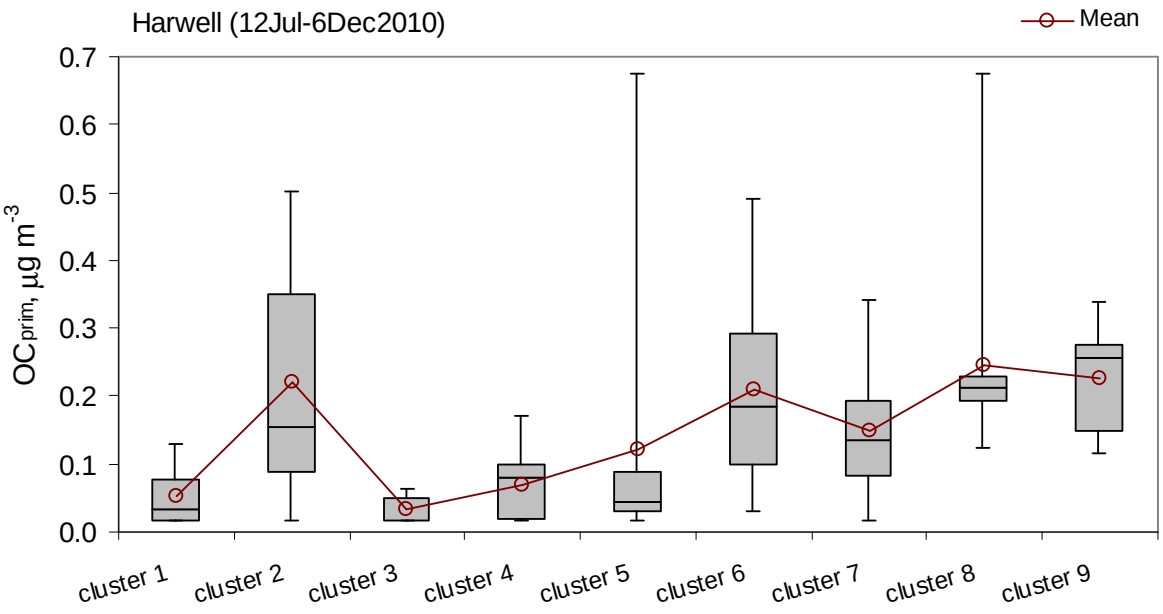

(h)

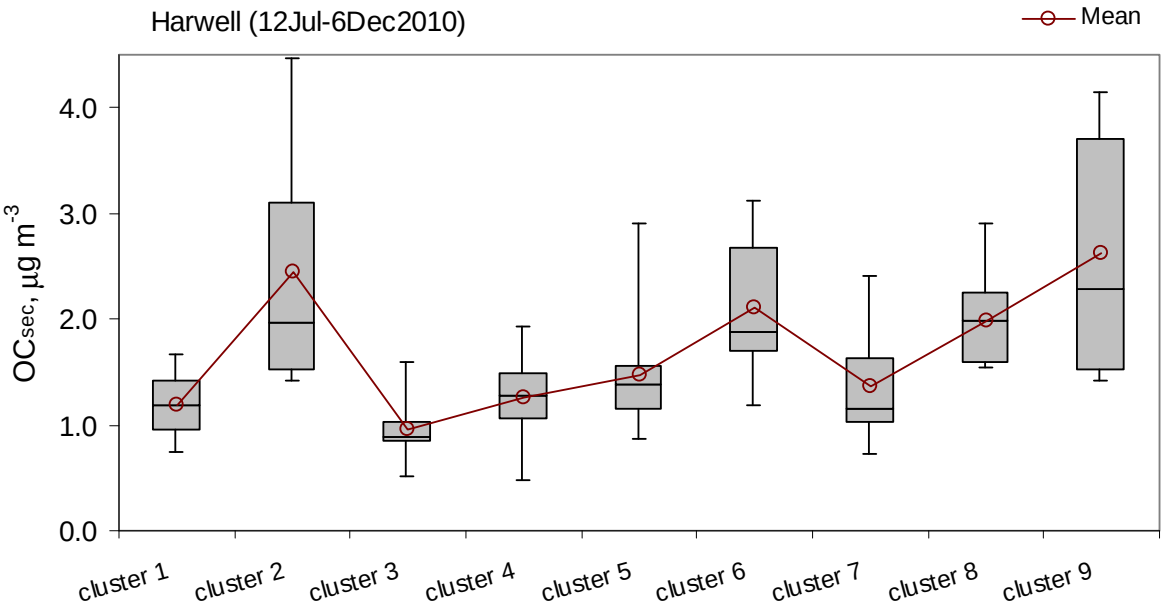

Figure 5.9 *(continued)*

(i)

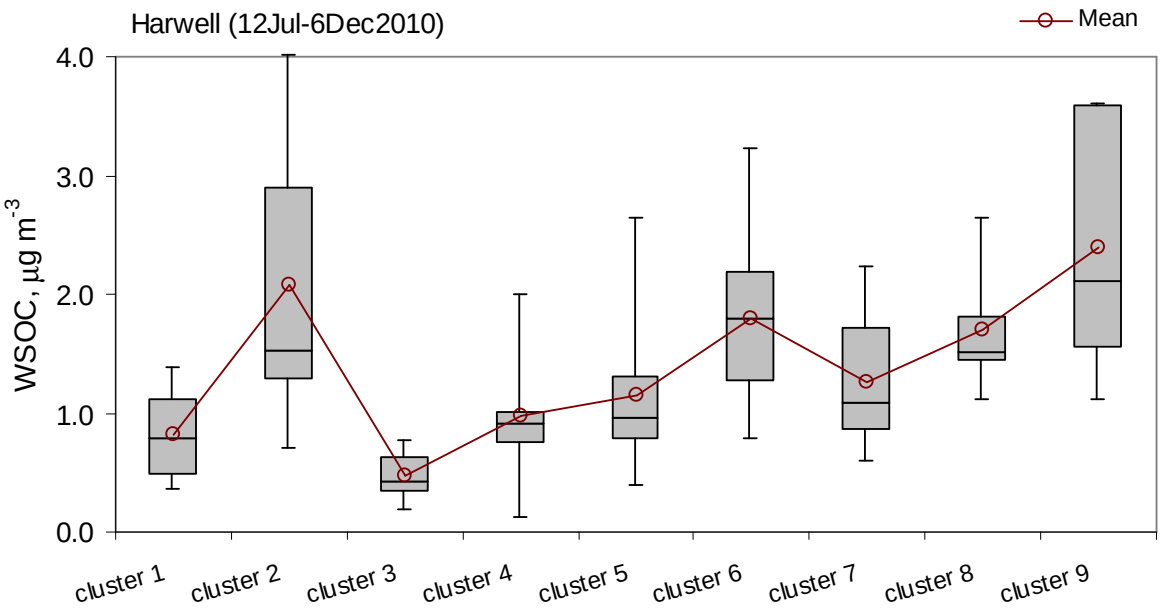

(j)

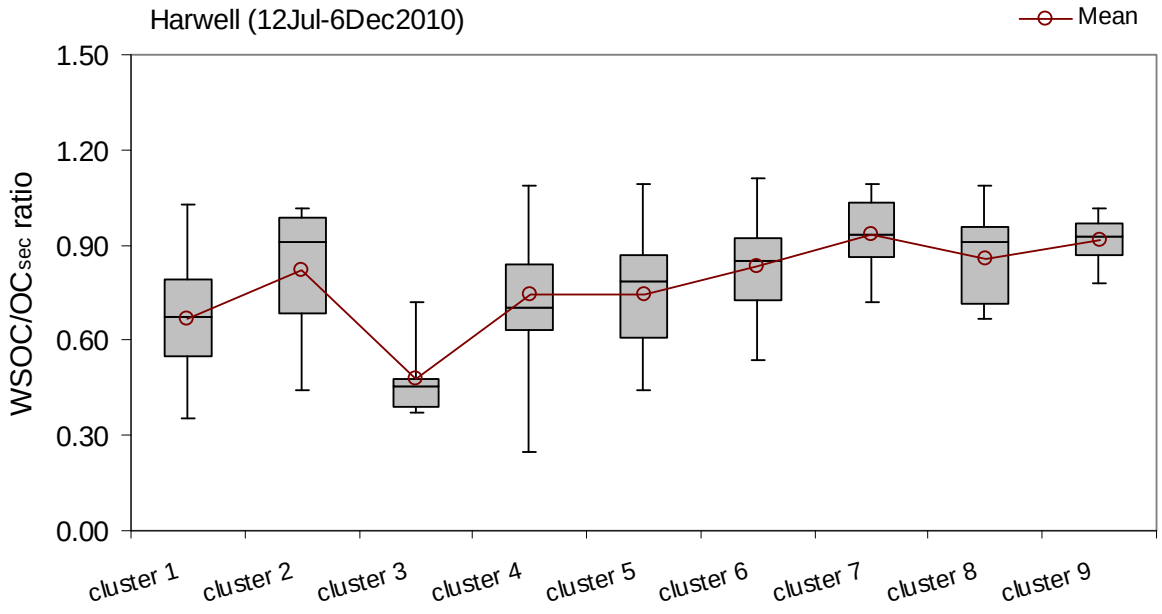

Figure 5.9 *(continued)*

5.6 Conclusions

The air mass back trajectories arriving at EROS and Harwell sites provide the effective evidence in the sources of airborne particulate matter by long-rang atmospheric transport. HYSPLIT_4 model available online at NOAA website used for the calculation of air mass back trajectories arriving at both sites. Application of cluster analysis in order to groups the similar trajectories showed the major five distinct clusters at EROS for the whole data and nine clusters at both EROS and Harwell for simultaneous data during this sampling period. At EROS, the slow-easterly airflow accounted for the highest trajectories of the data with more frequent during the autumn. Overall, the westerly airflows arriving EROS are the most frequent trajectories during this sampling period. These comprised the north westerly, westerly and south westerly and accounted for 21%, 9% and 22% of the data, respectively. The highest potential source regions of major chemical components of $PM_{2.5}$ were emitted from European mainland regions rather than westerly airflows at this site.

As the calculation of local contribution mentioned in the previous chapter, the sum of local and regional contribution on the chemical composition of $PM_{2.5}$ in urban background (EROS) would be considered, whilst the purely LRT affecting the rural site (Harwell) was assumed. The back trajectories arriving at EROS and Harwell during the simultaneous sampling time were clustered and consequently the clustering analysis revealed the significant nine main air mass transports at both sites. The LRT pathways of high major component (SO_4^{2-}, NO_3^-, Cl^-, $C_2O_4^{2-}$, EC, OC, OC_{prim}, OC_{sec} and WSOC) concentrations at both sites were from continental Europe (easterly and southerly air flows) which is polluted urban and industrial regions with many of precursor sources compared to the westerly trajectories with mostly passing over marine atmosphere. Although chloride commonly associated with air mass trajectories passing over marine atmosphere, it should be noted that there was an important anthropogenic sources contributed to fine chloride as shown in this study.

With focusing on oxalate concentration, cluster analysis of air mass trajectories indicates that the dominant sources of oxalate were observed to be associated with airmasses originating from continental air flows consist with the other pollutants (sulpphate, nitrate, OC, EC and OC_{sec}). As repoted by Legrand et al. (2007), diacids which dominated by oxalate were not only related to the LRT from continents but also to marine biogenic emissions from phytoplankton. The contributions of oxalate by the long maritime trajectories yielded the

small ratios of $C_2O_4^{2-}/SO_4^{2-}$, $C_2O_4^{2-}/NO_3^-$ and $C_2O_4^{2-}/OC_{sec}$ for the whole data at EROS (500 trajectories). In addition, there were observed the weak correlation between oxalate and chloride commonly generated from sea spray (as mentioned in chapter 4), indicating the insignificant sources of oxalate from marine atmosphere. At EROS and Harwell sites, this could conclude that the sources of anthropogenic precursors for oxalate formation are more likely than biogenic sources because there was the lack of strong seasonality in oxalate concentration observed in this study. It should be noted that the secondary formations of oxalate in atmosphere play an important contribution to particulate oxalate as the weak relationships observed for oxalate with EC, which is a good indicator of primary origins of incomplete combustion from the burning of carbonaceous materials including emission from fuel combustion.

CHAPTER 6

INTERPRETATION OF SIZE DISTRIBUTIONS OF MAJOR COMPONENTS IN AIRBORNE PARTICULATE MATTER

6.1 Synopsis

In this chapter, the size distributions of anionic and cationic species in ambient aerosols at EROS are presented. The analysed species were sulphate, nitrate, chloride, oxalate, sodium, potassium, ammonium, total carbon and PM mass. The measurement and interpretation of size distributions of major component composition in PM are useful in order to the overall understanding their origins and formation mechanisms. The modes of aerosol size distribution were defined according to the size-segregated configuration of the MOUDIs, therefore, collected aerosol particles were divided into four modes; a nuclei mode with particle diameters less than 0.175 μm, a condensation mode with particle diameters between 0.175 μm and 0.325 μm, a droplet mode with particle diameters between 0.325 μm and 1.8 μm and a coarse mode with particle diameters between 1.8 μm and 18 μm. The distinction of size fractions between fine and coarse particles was defined by MOUDI's cut point of 1.8 μm. Many of the studies have indicated that atmospheric particles most presented as ammonium neutralised forms such as $(NH_4)_2SO_4$, NH_4HSO_4, NH_4NO_3, NH_4Cl, $(NH_4)_2SO_4 \cdot 2NH_4NO_3$, $(NH_4)_2SO_4 \cdot 3NH_4NO_3$ etc. (Harrison and Jones, 1995; Allen, 1989; Yin and Harrison, 2008). In order to study the effect of ammonia gas on aerosol particles, the direct comparison of air samplings was carried out between aerosols collected by the MOUDI with and without NH_3 gas supply. The concentrations and mass size distributions of component composition of atmospheric particles collected by both systems were determined and investigated. To author's knowledge, studies and data on the size distributions of oxalate are limited within the UK. Hence, the discussions on oxalate concentration and its size distribution including the neutralised form in atmospheric particles were emphasized in comparison with data of inorganic aerosol species.

6.2 Size distributions of ionic species in atmospheric aerosols

Airborne particulate matter is commonly characterised by its size, more precisely by aerodynamic diameter. The aerodynamic diameter is defined as the diameter of the unit density (ρ_p = 1 g cm^{-3}) sphere that has the same settling velocity as the particle being measured (Hinds, 1999). For example, a particle with an aerodynamic of 1 micrometre will exhibit the same inertial properties as a sphere with a diameter of 1 micrometre and a density of 1 g cm^{-3} – irrespective of the actual size, shape or density of the particle. PM in the ambient atmosphere have diameters spanning the entire range within the definition of an aerosol. Whitby (2007) remarked the simplification size distribution model called the Whitby trimodal model. The model described the particle size distributions consisting of a nucleation or Aitken mode (0.005 μm < D_p < 0.1 μm), an accumulation mode (0.1 μm < D_p < 2.0 μm), and a coarse mode (D_p > 2.0 μm). Each mode was fitted by a lognormal function. Whitby separated the particles into two main fractions; fine particle with diameters less than 2 μm and coarse particles with diameters of more than 2 μm. Currently, legislative air quality objectives are defined in term of PM_{10} and $PM_{2.5}$ that fractions of particles with an aerodynamic diameter below 10 μm and 2.5 μm, respectively. Therefore, the trimodal size distribution is represented and modified as; nucleation or Aitken mode, below approximately 0.1 μm in diameter; accumulation mode (0.1 μm < D_p < 2.5 μm), and the coarse mode (2.5 μm < D_p < 10 μm). With regard to fine fraction, the particle size classification is also divided into the fine (D_p < 2.5 μm) and ultrafine (D_p < 0.1 μm) fractions. The latter is focused because these small particles might penetrate the issue in the deep lung, leading to the respiratory health effects (Hughes et al., 1998; Pakkanen et al., 2001). The typical particle size distribution of aerosols is shown in Figure 6.1.

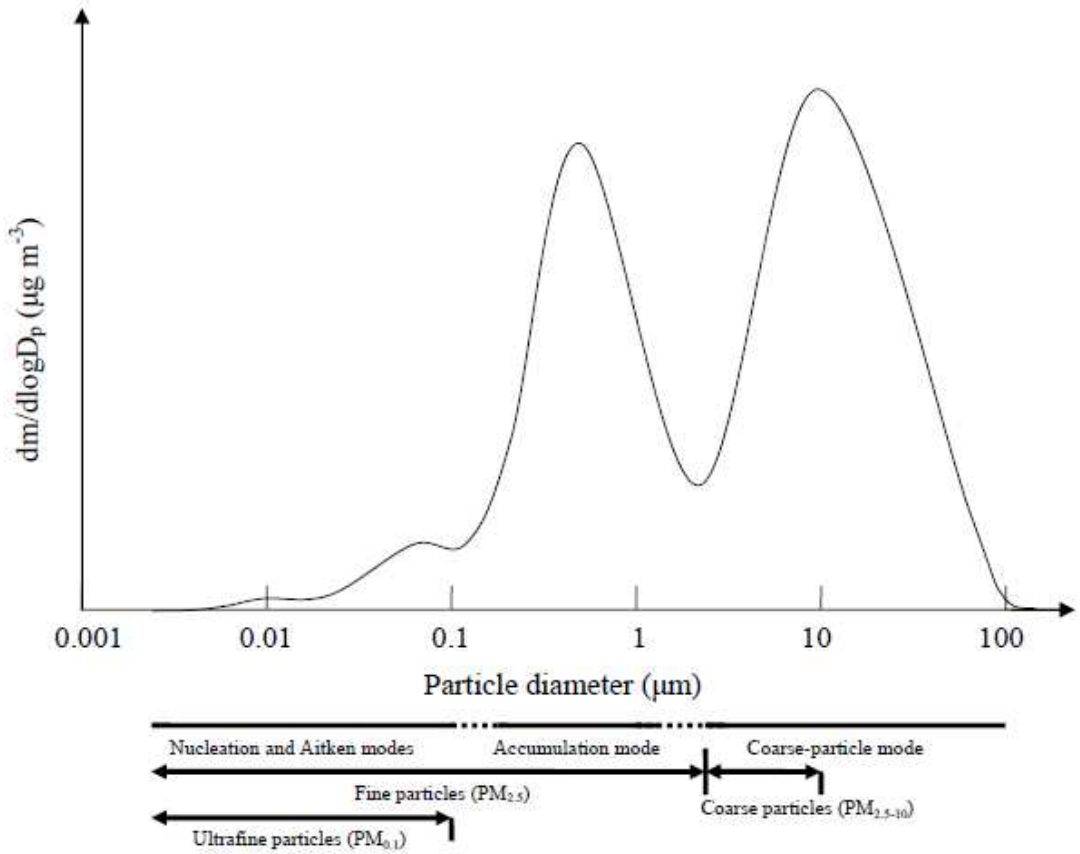

Figure 6.1 Mass size distribution of airborne particulate matter in urban atmosphere (source : modified from U.S.EPA, 2012)

Each mode in the mass size distributions of aerosols has different major sources, formation pathways and chemical composition. The size distribution is changed in the atmosphere by the mechanisms of new particle formation (gas to particle by photochemical oxidation of precursors), following by growth (coagulation and condensation), evaporation and removal (diffusion, settling, impaction, washout and rainout) (Hinds, 2001). An increase in the particle size occurs through coagulation and condensation of aerosol particles. Coagulation is the growth process of aerosol from the collision of particles whilst particle condensation occurs when more vapor molecules arrive on their particle's surface. Evaporation is the reverse process changing the size and results in a net loss of molecules and reduction of airborne particles.

Nucleation or Aitken mode consists gases and vapors emitted directly into atmosphere and particles produced in the atmosphere by gas-to-particle conversion. This mode is usually found near the sources so that the greatest numbers of particles originate in the nucleation mode. These particles coagulate rapidly with each other and in particular with the particles in

accumulation mode. Nuclei particles can also grow by condensation of vapour on their surface, or by cloud processing during transport from source locations. Due to ultrafine particles rapidly diffuse and undergo agglomeration ending up in the accumulation mode, most of them have a short lifetime in the atmosphere probably form minutes to hours. Moreover, these particles may serve as nuclei for the production of cloud droplets and may be discharged from the ambient air as rain droplets.

The accumulation mode comprises mainly combustion particles (i.e. anthropogenic emissions), smog particles and the growth nuclei-mode particles that have coagulated with accumulation-mode particles. Smog particles are aerosols formed in the atmosphere by the presence of sunlight on vapors (Baron and Willeke, 2001). The nuclei and accumulation modes together constitute fine particles ($PM_{2.5}$). The accumulation mode may have two submodes: a condensation mode with the mass median aerodynamic diameters (MMAD) of 0.2 ± 0.1 μm and a droplet mode with MMAD of 0.7 ± 0.2 μm (John et al., 1990). The condensation mode was formed and growth by condensation of gases either directly of indirectly through coagulation with nuclei mode particles. The rate of growth of particles in condensation mode declines with increasing particle size. The droplets are formed by the growth of hygroscopic condensation-mode particles.

Coarse particles are attributed to sea salts or atmospheric particles produced via abrasion mechanisms (e.g. dust from the wind-driven erosion of soils or released biogenic particles). These particles are readily removed by gravitational settling at appreciable rated or impaction on surfaces as their large size. The residence time in the atmosphere is only from hours to days. The separating line between coarse and fine particles is the saddle point between 1 and 3 μm. Coarse fraction may be accounted for various concentrations in airborne particulate matter depending on area conditions. In the UK urban areas, the major sources of coarse particles are a re-suspended road dusts, windblown soils and sea spray particles (QUARG, 1996).

6.3 Measurement of aerosol size distributions at EROS

In this study, size-segregated aerosol samples were colleted by two Micro Orifice Uniform Deposit Impactors (MOUDI) at EROS. One MOUDI was supplied by ammonia gas with a concentration of 52.08 ppm cylinder (NH_3 in synthetic air). The other one was operated to

collect the air samples under a normal instrumental procedure as detailed in chapter 2. The sampling was conducted over fifteen periods from 23 November 2010 to 24 January 2011 (Table 6.1). Because of the instrument problem, there were only three sampling periods which the aerosol samples were collected simultaneously by both MOUDIs (P1-P9, P2-P10 and P6-P14). Totally 15 sets of samples were collected at this site. Eight sets of 72h samples were obtained by MOUDI supplied with NH_3 gas and seven sets of 72h samples were collected by MOUDI with usual operation. More detailed information of meteorological parameters and analysed species is also given in Table 6.1.

Table 6.1 Summary of air sampling conditions by MOUDI and chemical analysis of aerosol samples at EROS

Period	Sampling date	Sampling volume (m^3)	Temperature (^oC)			Relative humidity (%)			Instrument	Analytes
			Max	Min	Mean	Max	Min	Mean		
P1*	23 – 26/11/10	123.5	7	-5	1 ± 2	100	65	86 ± 2	MOUDI with NH_3 supply	SO_4^{2-}, NO_3^-, Cl^-, $C_2O_4^{2-}$, Na^+, NH_4^+, K^+, PM_{mass}, TC
P2*	26 – 29/11/10	125.3	3	-10	-3 ± 2	100	65	91 ± 3		
P3	30/11 – 3/12/10	124.4	1	-8	-2 ± 1	100	80	92 ± 2		
P4	7 – 10/12/10	117.6	7	-12	-2 ± 5	100	74	88 ± 5		
P5	14 – 17/12/10	118.4	7	-5	1 ± 3	100	64	88 ± 5		
P6*	11 – 14/01/11	115.8	13	1	7 ± 3	100	76	91 ± 3		
P7	14 – 17/01/11	116.2	12	2	8 ± 1	100	76	89 ± 4		
P8	18 – 21/01/11	118.0	7	-5	1 ± 2	100	65	90 ± 3		
P9*	23 – 26/11/10	123.5	7	-5	1 ± 2	100	65	86 ± 2	MOUDI without NH_3 supply	SO_4^{2-}, NO_3^-, Cl^-, $C_2O_4^{2-}$, Na^+, NH_4^+, K^+, PM_{mass}, TC
P10*	26 – 29/11/10	125.3	3	-10	-3 ± 2	100	65	91 ± 3		
P11	3 – 6/12/10	121.7	4	-9	-2 ± 4	100	80	95 ± 2		
P12	10 – 13/12/10	116.9	8	-5	3 ± 3	100	76	89 ± 6		
P13	17 – 20/12/10	116.4	-1	-15	-7 ± 3	100	64	91 ± 6		
P14*	11 – 14/01/11	111.5	13	1	7 ± 3	100	76	91 ± 3		
P15	21 – 24/01/11	116.6	7	-4	2 ± 2	100	65	87 ± 3		

* both MOUDIs were sampling simultaneously
Meteorology data available from: www.wunderground.com

The primary objectives of this experiment are;

- To better understanding the formation mechanisms and sources of ionic species in ambient aerosols by interpretation of particle size distributions.
- To characterise and quantify the particle mass and chemical composition of PM samples in each size range.
- To study the effect of ammonia gas concentration whether to stabilise the semi-volatile species in atmospheric particulate matter when air samples were collected under the ammonia gas atmosphere.

With regard to the form of inorganic chemical constituents in aerosol particles, ammonia originated from primarily biological source readily dissolves in aqueous particles and neutralises sulphate, nitrate and chloride, which are usually observed as ammonium sulphate ($(NH_4)_2SO_4$), ammonium nitrate (NH_4NO_3) and ammonium chloride (NH_4Cl) in atmosphere (Yin et al., 2010; Yin and Harrison, 2008; Harrison et al., 2003; Zhuang et al., 1999). At EROS site, Yin et al. (2010) indicated that the most significant sources of $PM_{2.5}$ were ammonium salts (sulphate plus nitrate) contributing about 52.6% in summer and 33.7% in winter. The instrument designed for ammonia gas feeding during the air sampling is expecting to produce more substantial neutralisation of ammonium salt aerosol particles. Hence, the excess ammonia in the concentration of 50 ppb (at final mixing) was accurately supplied and controlled for the MOUDI during the sampling (chapter 2.2.2). The reactions of ammonia gas to form ammonium salts are presented as following equations (Kitto and Harrison, 1992; Allen et al., 1989; McCulloch et al., 1998);

In gas phase;

$$H_2SO_4(g) + 2NH_3(g) \rightarrow (NH_4)_2SO_4(aq,s) \quad \text{(Equation 6.1)}$$

$$HNO_3(g) + NH_3(g) \leftrightarrow NH_4NO_3(aq,s) \quad \text{(Equation 6.2)}$$

$$HCl(g) + NH_3(g) \leftrightarrow NH_4Cl(aq,s) \quad \text{(Equation 6.3)}$$

In aqueous phase by dissolved ammonia;

$$H_2SO_4(aq) + 2NH_4OH(aq) \rightarrow (NH_4)_2SO_4(aq,s) + 2H_2O \quad \text{(Equation 6.4)}$$

$$HNO_3(aq) + NH_4OH(aq) \leftrightarrow NH_4NO_3(aq,s) + H_2O \quad \text{(Equation 6.5)}$$

$$HCl(aq) + NH_4OH(aq) \leftrightarrow NH_4Cl(aq,s) + H_2O \quad \text{(Equation 6.6)}$$

Moreover, the study of particulate oxalate, which was a dominant WSOC species of aerosol, was emphasized in this work. The mass size distribution of oxalate is also important evidence to investigate its formation pathway. Lefer and Talbot (2001) reported the similarity of the size distribution between oxalate and ammonium and proposed that ammonium oxalate aerosol may be directly formed from the gaseous precursors (heterogeneous production) that were ammonia and oxalic acid. With the same assumption of form of oxalate aerosol and the neutralisation reaction of oxalate by ammonia gas, the air samples obtained from MOUDI with NH_3 gas supplied were analysed and expected to yield high concentration of particulate oxalate. The reactions of ammonia to form ammonium oxalate salt in gas and aqueous phases are shown below.

$$H_2C_2O_4(g) + 2NH_3(g) \leftrightarrow (NH_4)_2C_2O_4(aq) \quad \text{(Equation 6.7)}$$

$$H_2C_2O_4(aq) + 2NH_4OH(aq) \leftrightarrow (NH_4)_2C_2O_4(aq) + 2H_2O \quad \text{(Equation 6.8)}$$

In this study, collected aerosol particles were divided into four modes of size distributions according to the restriction of the MOUDI size configuration; *a nuclei mode* with particle diameters less than 0.175 μm, *a condensation mode* with particle diameters between 0.175 μm and 0.325 μm, *a droplet mode* with particle diameters between 0.325 μm and 1.8 μm and *a coarse mode* with particle diameters between 1.8 μm and 18 μm. Since MOUDI does not have a 2.5 μm cutoff point, the cut size of 1.8 μm is defined as the cutoff point to separate the fine and coarse particles. Therefore, PM in fine and coarse fractions represented the sum of species with diameter below 1.8 μm and above 1.8 μm, respectively.

In order to evaluate the measurement data obtained from MOUDI experiment, the measurement uncertainties of ionic component data were investigated and estimated to be included systematic and analytical errors. Since K^+ and Na^+ are the non-volatile species and do not neutralise by ammonia gas, their concentrations measured from the two systems should be observed in identical value. In this experiment, there were slightly differences in concentrations of both species found in samples collected in both samplers with and without NH_3. The concentrations of Na^+ were 0.53 μg m^{-3} and 0.55 μg m^{-3} in aerosol samples taken with and without NH_3, respectively and the concentrations of K^+ were 0.08 μg m^{-3} and 0.07 μg m^{-3} in aerosol samples taken with and without NH_3, respectively. These findings are indicative of sampling and analytical variability. For the measurement of K^+, many samples

observed below the detection limit, therefore the estimation of experiment uncertainty in this system was estimated based on Na^+ species. The error value of 5% from Na^+ concentration was one of additional parameter for the calculation of ionic measurement uncertainty as detailed in Appendix A. The expanded uncertainty of the measurement of ionic species (SO_4^{2-}, NO_3^-, Cl^-, $C_2O_4^{2-}$, K^+, Na^+ and NH_4^+) was 6.6%.

Table 6.2 summarises the major components concentration of aerosol into nuclei, condensation, droplet and coarse modes. Each mode represents the sum concentration of species in defined stage ranges. For particle mass, PM_{mass} in nuclei modes are not reported due to the technical problem in gravimetric analysis. After sampling, the quartz fibre filters in the back-up stage were damage at the edge when unscrewing the cover to remove them, so this resulted in the loss of filter mass. With regard to total carbon (TC), there are not data available for TC in some periods (P6, P7, P8, P14 and P15) due to the air samples collected on Teflon filters were not able to analyse by thermal optical transmission technique. For other periods, aerosol samples were collected onto Al foil substrates in order to investigate their PM_{mass}, chemical components including carbonaceous materials in atmospheric particles. The analytical method used described in chapter 2. Only TC data reported by thermal optical transmission (TOT) analysis in this case because the analyser was not able to split TC into OC and EC when measuring samples taken by aluminium substrates. A red-light laser, which is used to monitor transmittance of the filter, cannot pass through the Al foils and consequently the software does not calculate the split time between OC and EC.

With regard to aerosol samples taken by MOUDI under normal conditions (P9 – P15), SO_4^{2-} concentrations by modes of size distribution were in range of 0.07 – 2.62 μg m^{-3}. There is clear that the lowest concentration observed in nuclei mode and the highest concentration presented in droplet mode accounting for 4.1% and 50.0% of the total suphate concentration, respectively for the whole data (Table 6.3). Nitrate in four modes were observed in the concentration range from 0.04 μg m^{-3} to 2.66 μg m^{-3}. Mean NO_3^- fraction for entire data contributions to total nitrate concentration were 4.3%, 37.2%, 52.0% and 6.6% for nuclei, condensation, droplet and coarse modes, respectively. The sea salt ions Na^+ and Cl^- were dominate in coarse mode and contribute to their total concentrations for 40.4% and 45.8%, respectively. Although sea salt ions commonly observed in coarse particle, they may exist as nanoparticles, evidenced by the presence of Na^+ and Cl^- in the nuclei mode at 19.0% and 9.2%, respectively, of their total concentrations. These indicate the significance of

anthropogenic sources. At this site, $C_2O_4^{2-}$, NH_4^+ and K^+ also found mainly in accumulation (condensation + droplet) mode and the concentrations in four modes of distribution were in range 0.001 – 0.073 μg m^{-3}, 0.00 – 0.54 μg m^{-3} and 0.00 – 0.05 μg m^{-3} for $C_2O_4^{2-}$, NH_4^+ and K^+, respectively. Total carbon (TC) which was the sum of OC and EC were found in range from 0.2 μg m^{-3} to 3.8 μg m^{-3} within four modes of size distribution.

Table 6.2 Four modes of size distribution in concentrations of anions, cations, TC and PM_{mass} of aerosol at EROS

Period	Modes of size distributions*	Aerosol concentration, μg m^{-3} (±6.6%)								
		SO_4^{2-}	NO_3^-	Cl^-	$C_2O_4^{2-}$	Na^+	$NH4^+$	K^+	TC	PM_{mass}
with NH_3										
P1	Nuclei	0.10	0.17	0.01	0.003	0.05	0.04	0.01	1.2	n.a.
	Condensation	0.89	1.42	0.17	0.005	0.01	0.30	0.03	1.9	5.22
	Droplet	1.44	1.05	0.32	0.007	0.23	0.21	0.01	1.7	4.67
	Coarse	0.66	0.23	0.62	0.004	0.41	0.03	0.02	0.4	4.21
P2	Nuclei	0.15	0.24	0.03	0.003	0.05	0.07	0.01	1.4	n.a.
	Condensation	1.05	2.25	0.31	0.007	0.01	0.51	0.03	3.0	8.54
	Droplet	2.42	2.26	0.43	0.008	0.11	0.72	0.04	2.4	10.20
	Coarse	0.76	0.22	0.56	0.004	0.33	0.03	0.01	0.3	3.75
P3	Nuclei	0.11	0.12	0.02	0.002	0.05	0.03	0.00	1.1	n.a.
	Condensation	1.24	1.36	0.21	0.005	0.00	0.39	0.02	1.3	4.98
	Droplet	1.64	1.32	0.56	0.006	0.37	0.32	0.03	0.8	5.26
	Coarse	0.98	0.22	0.73	0.002	0.43	0.05	0.02	0.2	3.01
P4	Nuclei	0.19	0.18	0.02	0.002	0.06	0.05	0.00	1.3	n.a.
	Condensation	1.18	1.81	0.34	0.005	0.02	0.46	0.03	2.8	7.65
	Droplet	2.24	1.23	0.44	0.005	0.20	0.32	0.02	1.7	6.34
	Coarse	0.86	0.19	0.69	0.004	0.43	0.03	0.02	0.3	3.71
P5	Nuclei	0.08	0.01	0.01	0.000	0.07	0.01	0.00	1.0	n.a.
	Condensation	0.86	1.06	0.16	0.004	0.03	0.27	0.03	1.3	3.78
	Droplet	1.40	1.58	0.33	0.005	0.13	0.31	0.03	1.0	5.03
	Coarse	0.22	0.15	0.33	0.002	0.15	0.02	0.03	0.4	2.00
P6	Nuclei	0.11	0.03	0.02	0.002	0.07	0.00	0.00	n.a.	n.a.
	Condensation	1.18	0.35	0.02	0.005	0.01	0.14	0.00	n.a.	2.16
	Droplet	1.12	0.43	0.18	0.005	0.16	0.08	0.00	n.a.	2.36
	Coarse	0.69	0.08	0.24	0.001	0.14	0.02	0.00	n.a.	1.70
P7	Nuclei	0.06	0.02	0.02	0.003	0.05	0.01	0.00	n.a.	n.a.
	Condensation	0.70	0.16	0.03	0.019	0.01	0.06	0.02	n.a.	2.13
	Droplet	1.21	0.67	1.61	0.020	0.89	0.12	0.02	n.a.	5.89
	Coarse	1.19	0.18	1.61	0.004	0.81	0.05	0.01	n.a.	5.35
P8	Nuclei	0.12	0.10	0.03	0.004	0.06	0.03	0.00	n.a.	n.a.
	Condensation	1.10	1.84	0.34	0.013	0.03	0.51	0.03	n.a.	8.34
	Droplet	3.16	2.63	0.79	0.016	0.27	0.91	0.05	n.a.	11.93
	Coarse	1.22	0.35	0.95	0.002	0.56	0.05	0.02	n.a.	5.30

Table 6.2 *(continued)*

Period	Modes of size distributions*	Aerosol concentration, μg m^{-3} (±6.6%)								
		SO_4^{2-}	NO_3^-	Cl^-	$C_2O_4^{2-}$	Na^+	$NH4^+$	K^+	TC	PM_{mass}
without NH_3										
P9	Nuclei	0.11	0.09	0.02	0.003	0.10	0.01	0.00	1.4	n.a.
	Condensation	1.17	0.77	0.03	0.009	0.06	0.23	0.03	1.6	4.57
	Droplet	0.93	0.39	0.20	0.005	0.22	0.05	0.00	0.7	2.77
	Coarse	0.10	0.04	0.40	0.001	0.33	0.02	0.00	0.2	3.07
P10	Nuclei	0.21	0.08	0.40	0.003	0.29	0.02	0.00	1.7	n.a.
	Condensation	1.30	1.93	0.08	0.013	0.01	0.34	0.05	3.0	8.65
	Droplet	2.62	1.77	0.19	0.011	0.11	0.41	0.01	2.2	8.82
	Coarse	0.17	0.09	0.40	0.004	0.25	0.02	0.01	0.3	3.83
P11	Nuclei	0.18	0.07	0.02	0.002	0.11	0.05	0.03	1.2	n.a.
	Condensation	1.22	0.86	0.03	0.006	0.00	0.20	0.01	2.0	4.89
	Droplet	2.44	2.02	0.15	0.010	0.09	0.53	0.01	1.5	7.95
	Coarse	0.07	0.09	0.19	0.002	0.11	0.05	0.00	0.2	1.50
P12	Nuclei	0.15	0.06	0.04	0.002	0.00	0.00	0.00	1.1	n.a.
	Condensation	1.05	0.20	0.03	0.008	0.06	0.13	0.02	1.4	3.20
	Droplet	1.36	1.53	0.71	0.012	0.47	0.21	0.00	1.6	6.53
	Coarse	0.38	0.14	0.65	0.006	0.38	0.03	0.00	0.4	3.07
P13	Nuclei	0.09	0.05	0.01	0.002	0.00	0.00	0.03	1.4	n.a.
	Condensation	0.83	2.66	0.17	0.022	0.01	0.54	0.04	3.8	10.17
	Droplet	1.18	2.46	0.34	0.032	0.11	0.25	0.05	2.2	9.10
	Coarse	0.22	0.24	0.21	0.007	0.14	0.00	0.05	0.5	3.25
P14	Nuclei	0.03	0.04	0.04	0.000	0.09	0.01	0.01	n.a.	n.a.
	Condensation	0.59	0.09	0.01	0.029	0.00	0.10	0.01	n.a.	1.95
	Droplet	0.27	0.12	0.13	0.015	0.13	0.02	0.00	n.a.	1.36
	Coarse	0.08	0.05	0.13	0.005	0.07	0.00	0.00	n.a.	1.58
P15	Nuclei	0.06	0.04	0.01	0.001	0.05	0.01	0.01	n.a.	n.a.
	Condensation	0.80	1.20	0.04	0.040	0.01	0.34	0.03	n.a.	7.39
	Droplet	1.76	2.05	0.25	0.073	0.28	0.25	0.02	n.a.	9.47
	Coarse	0.23	0.33	0.39	0.020	0.26	0.02	0.01	n.a.	2.67

* Nuclei mode represents the sum of species concentrations in sizes below 0.175 μm
* Condensation mode represents the sum of species concentrations in sizes between 0.175 μm and 0.325 μm
* Droplet mode represents the sum of species concentrations in sizes between 0.325 μm and 1.8 μm
* Coarse mode represents the sum of species concentrations in sizes between 1.8 μm and 18 μm

6.3.1 Contribution of aerosol particles by ammonia experiment

Table 6.3 shows fraction contributions of aerosol species in each size mode for the whole and simultaneous datasets as well as their mean concentrations.

Table 6.3 Mean fraction contributions of aerosol species in different size modes for the whole and simultaneous datasets

	MOUDI with NH_3						MOUDI without NH_3					
	Fraction contributions in each mode (%)					Concentration* (nmol m^{-3}) (±6.6%)	Fraction contributions in each mode (%)					Concentration* (nmol m^{-3}) (±6.6%)
	Nuclei	Conden.	Droplet	Coarse	Fine		Nuclei	Conden.	Droplet	Coarse	Fine	
Whole												
SO_4^{2-}	3.0	28.0	47.4	21.6	78.4	39.5	4.1	38.9	50.0	7.0	93.0	29.2
NO_3^-	3.5	40.4	48.1	8.0	92.0	48.2	4.3	37.2	52.0	6.6	93.4	44.9
Cl^-	1.7	14.5	36.6	47.2	52.8	42.8	9.2	7.7	37.3	45.8	54.2	21.2
$C_2O_4^{2-}$	11.1	34.5	39.7	14.7	85.3	0.3	6.8	39.2	41.7	12.3	87.7	0.6
Na^+	9.7	2.6	35.3	52.4	47.6	33.7	19.0	3.2	37.4	40.4	59.6	23.3
NH_4^+	3.7	44.3	45.4	6.6	93.4	42.7	3.0	53.8	39.4	3.8	96.2	30.5
K^+	3.6	35.9	36.2	24.3	75.7	2.0	20.3	58.3	13.2	8.3	91.7	1.6
TC	24.7	39.6	29.0	6.7	93.3	*5.1*	25.2	40.5	28.5	5.7	94.3	*5.7*
PM_{mass}	n.a **	34.3	41.1	24.6	75.4	*15.44*	n.a **	38.1	41.6	20.3	79.7	*15.11*
Simultaneous data												
SO_4^{2-}	3.4	30.3	46.0	20.3	79.7	36.7	4.2	47.2	43.0	5.5	94.5	26.3
NO_3^-	4.7	44.7	43.5	7.1	92.9	47.0	7.5	46.5	38.7	7.4	92.6	29.4
Cl^-	2.5	14.3	33.3	49.9	50.1	27.4	17.8	5.1	30.2	47.0	53.0	19.1
$C_2O_4^{2-}$	14.9	32.2	37.2	15.6	84.4	0.2	9.4	50.0	31.1	9.5	90.5	0.4
Na^+	11.9	2.0	32.3	53.8	46.2	22.9	28.2	8.1	28.7	35.0	65.0	24.1
NH_4^+	8.7	46.7	39.7	4.9	95.1	39.8	3.1	51.2	36.7	6.0	94.0	22.8
K^+	12.7	38.1	29.4	19.8	80.2	2.0	19.0	42.9	19.0	19.0	81.0	1.0
TC	21.4	39.4	33.2	6.0	94.0	*6.2*	29.8	41.3	24.3	4.6	95.4	*5.6*
PM_{mass}	n.a **	36.6	38.8	24.6	75.4	*14.27*	n.a **	41.5	31.9	26.6	73.4	*12.20*

* Concentration calculated from mean of the sum of species concentrations in all size ranges during the sampling period. TC and PM_{mass} were in unit of $\mu g\ m^{-3}$

** All exposed back-up filters (QMA filter) were damaged and loosen at the edge when unscrewing to remove from the filter base cover. Therefore, the PM mass was not measured by gravimetric analysis.

*** Fine fraction is defined by the cut point below 1.8 μm

In comparison between air sampling under the normal condition and under ammonia supply, the mean concentrations of SO_4^{2-}, NO_3^-, Cl^- and NH_4^+ revealed the lower values in samples collected under normal condition than those samples collected under NH_3 atmosphere for the entire data (Table 6.3). This finding can be attributed the fact that ammonia gas neutralises the anionic aerosol species to form ammonium salts as $(NH_4)_2SO_4$, NH_4NO_3 and NH_4Cl in particulate matter. On the contrary, particulate oxalate observed high concentration in the samples collected under normal atmosphere (0.6 nmol m^{-3} and 0.3 nmol m^{-3} in air samples collected without and with NH_3, respectively for the entire data). This finding will be

discussed later in comparison with data collected simultaneously. There was higher mean concentration of TC (5.7 μg m^{-3}) in aerosol collected under normal condition than those (5.1 μg m^{-3}) in aerosol collected under ammonia gas experiment for the whole data. PM_{mass} showed high concentration in samples taken under NH_3 gas atmosphere (15.44 μg m^{-3} and 15.11 μg m^{-3} for samples collected with NH_3 supply and without NH_3, respectively).

Focusing on the data collected simultaneously by both MOUDIs, there were 3 datasets obtained from ammonia experiment (P1, P2 and P6) and normal air sampling (P9, P10 and P14). Figure 6.2 shows the major component concentrations in aerosols by modes of size distributions for the samples collected simultaneously under NH_3 atmosphere and normal conditions. The mean concentrations and fraction contributions of chemical components for simultaneous data also summarised in Table 6.3. It is clear that SO_4^{2-}, NO_3^-, $C_2O_4^{2-}$, NH_4^+, K^+, TC and PM_{mass} accounted much higher in fine fraction than in coarse particle both in samples with and without ammonia gas supply. The accumulation modes (condensation + droplet) were the dominant size distributions for these species. There were significant contributions in coarse fraction for Na^+ and Cl^- commonly originated from sea spray in samples taken from both systems. For samples taken under NH_3 supply; there were 53.8% and 49.9% contribution to their total concentrations in coarse mode for Na^+ and Cl^-, respectively. In addition, the contribution of 35.0% and 47.0% for coarse mode Na^+ and Cl^-, respectively were observed in the samples collected in normal condition. The important anthropogenic sources of Cl^- showing significantly in the fine fraction accounted for 50.1% and 53.0% for data with and without ammonia systems, respectively.

In principle, after NH_3 emitted into the atmosphere, NH_3 may undergo conversion to NH_4^+ aerosol. The rate of this conversion, which is mostly unknown, depends on the regional impact of NH_3 emissions (McCulloch, 1998). The conversion of NH_3 to NH_4^+ aerosol is affected by the concentration of acids in the ambient air especially HNO_3 and HCl as shown in Equation 6.1 – 6.6. Two common volatile inorganic aerosol species are NH_4NO_3 and NH_4Cl and the equilibrium constants based on Equation 6.2 and 6.3 are $K_n = [NH_3][HNO_3]$ and $K_c = [NH_3][HCl]$, where K_n and K_c are the equilibrium concentration products of ammonium nitrate and ammonium chloride, respectively (Allen et al., 1989). Since equilibrium constant is temperature and humidity dependent, the measured concentrations of gases would change during the sampling periods depending on temperature and humidity. For example, at mean ambient RH above the deliquescence RH, the measured concentration of

NH_3 and/or HNO_3 is present in the gas phase more than those predicted by theoretical calculation.

There were no data analysed for the concentrations of acid gases in this experiment, then the calculation of equilibrium/dissociation constants was not tested. The effect of NH_3 gas supply during air sampling (50ppb ≈ 2.235 μmol m^{-3}) on the chemical component composition was investigated by calculation of the difference between the concentrations of component species in aerosol collected under NH_3 atmosphere and the normal condition. In NH_3 system, NH_3 gas was continually supplied in constant rate in order to maintain the atmospheric equilibrium between gaseous and aerosol phases. Table 6.4 presents the contribution concentration of chemical composition in fine (particle diameter < 1.8 μm) and coarse (particle diameter between 1.8 μm to 18 μm) fractions in this experiment.

PM_{mass} were measured higher during the sampling under NH_3 atmosphere (1.68 μg m^{-3} and 0.39 μg m^{-3} for fine and coarse fraction, respectively). Sulphate, nitrate and chloride both in fine and coarse mode were also found the higher concentration in aerosols during the experiment taken under NH_3 atmosphere. The contribution concentrations were 0.006 μmol m^{-3}, 0.018 μmol m^{-3} and 0.004 μmol m^{-3} for SO_4^{2-}, NO_3^- and Cl^-, respectively in fine fractions and were 0.006 μmol m^{-3}, 0.002 μmol m^{-3} and 0.005 μmol m^{-3} for SO_4^{2-}, NO_3^- and Cl, respectively in coarse fraction. These findings could be attributed the fact that the productions of ammonium salts ($(NH_4)_2SO_4$, NH_4NO_3, NH_4Cl) were highly generated and stabilised in air particles. It is possible to calculate concentration of NH_3 which was used for stabilising aerosol salts as $2[SO_4^{2-}]$, $[NO_3^-]$ and $[Cl^-]$ where all concentrations are in unit of μmol m^{-3}. The results show that concentration of NH_3 used were 0.012 μmol m^{-3} (0.204 μg m^{-3}), 0.018 μmol m^{-3} (0.306 μg m^{-3}) and 0.004 μmol m^{-3} (0.068 μg m^{-3}) for SO_4^{2-}, NO_3^- and Cl^-, respectively in fine fractions. The NH_4^+ in fine fraction was found significant contribution (0.018 μmol m^{-3}), suggesting that excess NH_4^+ may react with other anionic species to form the stable particle in fine mode.

With regard to particulate oxalate, there were no concentration contributions of particulate oxalate observed in both fine (-0.0002 μmol m^{-3}) and coarse (0 μmol m^{-3}) fractions during the simultaneous sampling period. If particulate oxalate is expecting in form of ammonia salt in ambient air and behaves as volatile compound like NH_4NO_3 and NH_4Cl, it should be

observed high concentration in ammonia atmosphere. Since oxalate shows a significant correlation with nitrate which is the temperature dependent specie, especially in summer at EROS (r = 0.79) as mentioned in chapter 4, this can be interpreted as that oxalate form in PM is affected by temperature. This discordant result which found more oxalate concentration in samples without NH_3 addition might be indicative of an analytical measurement uncertainty including errors from air sampling by the MOUDI. In this work, the uncertainty of the determination of ionic species by IC method was estimated around 6.6% as shown in Appendix A. There were 3 samples collected simultaneously between the two systems in this study. Each of the samples also observed high oxalate in samples taken without NH_3 supply. Thus, the analytical uncertainty had only a minor influence on oxalate analysis. Alternatively, the physical and chemical atmospheric processes for oxalate formation would be considered in this case. An excess of NH_3 might contribute the formation of oxalate in gas phase by the reaction with various oxalate precursors. This was not clear in this experiment because oxalate in gas phase was not measured. Additionally, the lower concentration of oxalate in sample taken under NH_3 atmosphere in freezing cold temperature during this experiment could be described as well by thermodynamic of aerosols as discussed in section of oxalate size distribution.

As expected for TC, there were the contributions of 0.3 μg m^{-3} and 0.1 μg m^{-3} in fine and coarse particles, respectively, suggesting that ammonia gas may stabilise some semi-volatile organic carbon species in the atmosphere. Particulate mass of aerosol samples collected under NH_3 gas were observed higher than those in normal condition with the contributions of 1.68 μg m^{-3} and 0.39 μg m^{-3} in fine and coarse fractions, respectively.

It was also observed from ammonia experiment that contributions of ammonium salt species are lower than computed value approximately 2.235 μmol m^{-3} (50 ppb). This would be possible from the kinetic limitations in the formation/evaporation of aerosol particles and timescale for re-equilibrium the gas-aerosol system. The variation of atmospheric conditions especially diurnal cycle of temperature and humidity during the sampling periods (72h) may disturb the equilibrium including the organics formation coating at the surface of aerosol droplets delaying the achievement of equilibrium relationships. All factors will invalidate thermodynamically calculated concentrations. Furthermore, there might have rarely or insufficiently acid gases (precursor's emission/formation) to form ammonium salts at this site. In addition, there might be also the presence of other nitrate and chloride containing species,

which are less volatile than NH_4NO_3 and NH_4Cl. Some parts of fine nitrate and chloride might be formed as non-volatile salts such as Ca^{2+}, Mg^{2+}, K^+ or Na^+ salts.

Table 6.4 Contributions of major components in aerosol as the difference between air samples collected with and without ammonia atmosphere ($conc._{with} - conc._{without}$)

Component	Contribution concentration μmol m^{-3}	
	Fine*	Coarse**
SO_4^{2-}	0.006	0.006
NO_3^-	0.018	0.002
Cl^-	0.004	0.005
$C_2O_4^{2-}$	-0.0002	0
NH_4^+	0.018	0
TC	*0.3*	*0.1*
PM_{mass}	*1.68*	*0.39*

* Fine fraction is defined by the cut point below 1.8 μm.

** Coarse fraction is defined by the cut point between 1.8 μm to 18 μm

TC and PM_{mass} were in unit of μg m^{-3}

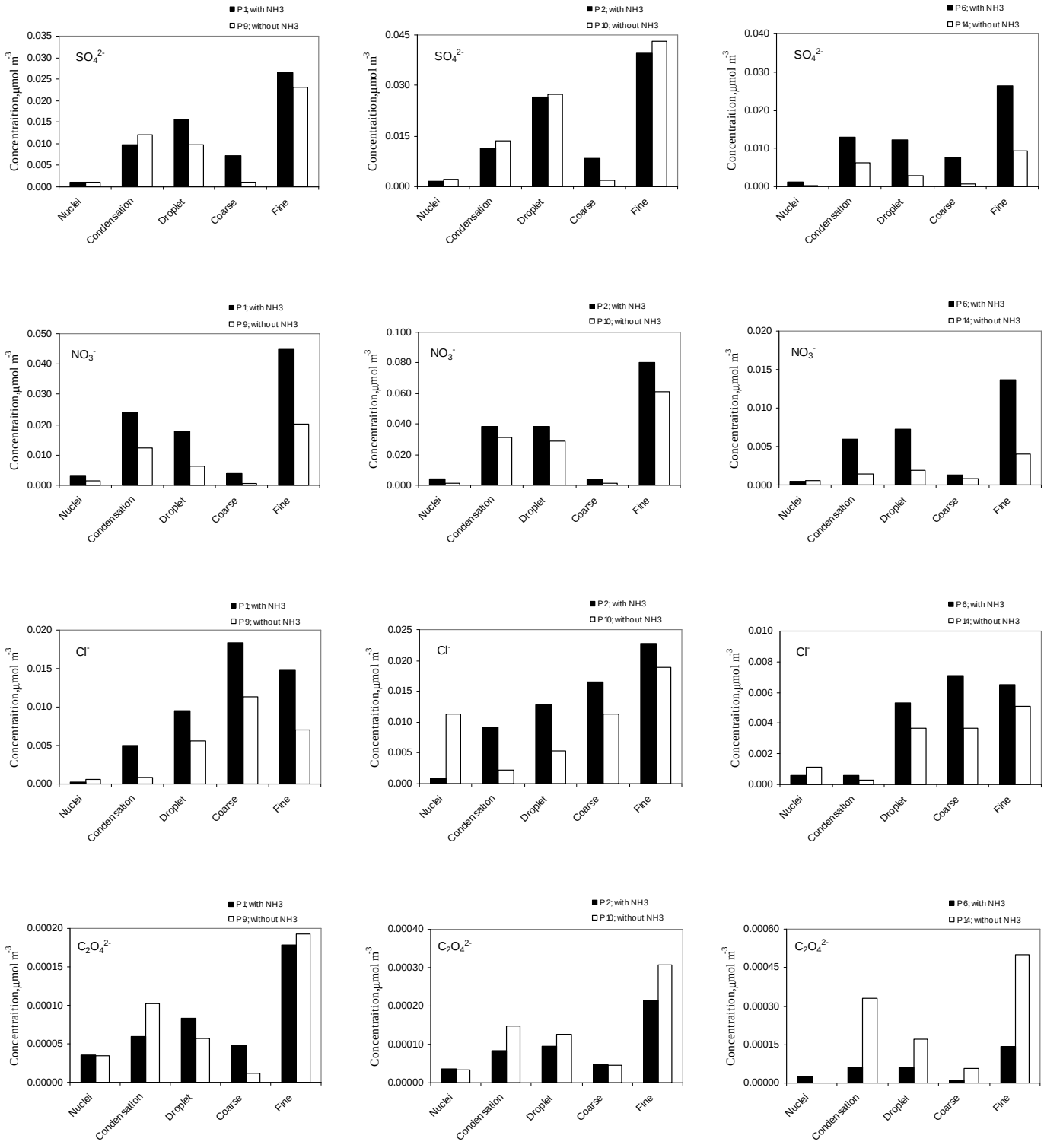

Figure 6.2 Major component composition by modes during the periods of samples collected simultaneously with (P1, P2 and P6) and without (P9, P10 and P14) NH_3 gas supply

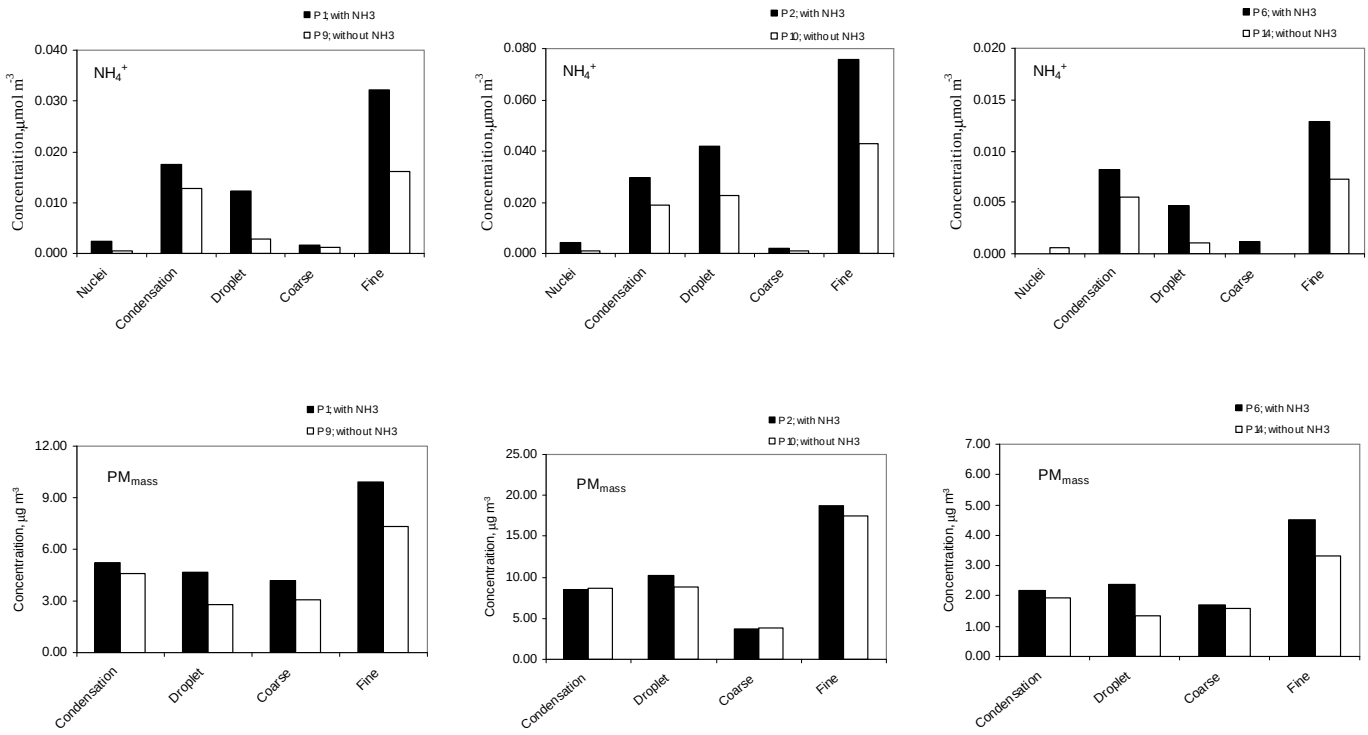

Figure 6.2 *(continued)*

6.4 Size distributions of inorganic ions

In order to study the formation pathways and sources of chemical components in PM, the measured mass size distributions of inorganic species in aerosol samples collected by MOUDI without ammonia gas atmosphere were investigated and results show in Figure 6.3. The comparisons of mean size distributions of major components in the samples taken with and without ammonia gas for the whole and simultaneous period also present in Figure 6.4 (a) – (e).

Chloride and sodium

The average mass size distributions of chloride and sodium revealed bimodal mode (Figure 6.3 and Figure 6.4 (c), (e)). The first peak in fine mode appeared at 0.4 μm – 0.5 μm and the second coarse mode mostly dominated with a concentration peak around 2.0 μm – 6.0 μm. In comparison with size distribution data available within research group (Figure 6.5), chloride size distribution showed the same structure with two peaks as data obtained from Marylebone road (MR) and Regents College (RC) representing roadside and background sites,

respectively. The very strong correlation between Na^+ and Cl^- in coarse mode (r = 0.98) was observed for the whole data (Figure 6.6) indicating the common contribution, especially in coarse mode of sea spray, which can be transported from the sea to rural and urban areas (Gustafsson and Franzen, 2000). As chloride is normally associated with sodium, a significant correlation between Na^+ and Cl^- in fine fraction also observed in nuclei (r = 0.95) and droplet (r = 0.91) mode, indicating the presence of sea spray in these modes of size distribution. However, fine mode chloride was observed dominantly in aerosol samples collected under NH_3 atmosphere as same as the mass size distribution of NH_4^+ in fine mode (0.4 μm – 0.5 μm), suggesting that chloride is more likely to be formed and stabilised as ammonium chloride in fine particles. The contribution of particulate chloride in aerosol particle was observed clearly from plot of mean size distribution of chloride during the simultaneous sampling period (Figure 6.4(c)). The occurrence of chloride in fine mode probably contributed from the local emissions affecting its concentration by anthropogenic sources such as waste incineration, local HCl emissions, the resuspension of sea salt deposited on roads or other paved areas (Kaneyasu et al., 1999; Clarke et al., 1999). In addition, chloride depletion associated with coarse particle may occur at EROS site then it could be enhanced the fine mode chloride. Loss of chloride from particulates may be ascribed to reaction of H_2SO_4 and HNO_3 with NaCl to produce gaseous HCl as follows (Parmar et. al., 2001):

$$H_2SO_4(g) + 2NaCl(aq) \rightarrow Na_2SO_4(aq) + 2HCl(g) \qquad \text{(Equation 6.9)}$$

$$HNO_3(g) + NaCl(aq) \rightarrow NaNO_3(aq) + HCl(g) \qquad \text{(Equation 6.10)}$$

The relationships of Na^+ and Cl^- with SO_4^{2-} both in nuclei and coarse mode showed the significant and higher value of correlation than those with NO_3^- (for Na^+ with SO_4^{2-}; r = 0.54 and r = 0.80 for nuclei and coarse mode, respectively; for Cl^- with SO_4^{2-}; r = 0.51 and r = 0.81 for nuclei and coarse mode, respectively), suggesting that the reaction of NaCl favoured with H_2SO_4 when the air masses travelling before arriving at the site.

Potassium

The mass size distribution of potassium was dominated by peaking around 0.4 μm – 0.5 μm in the droplet mode and a minor peak observed in coarse mode (4.0 μm – 5.0 μm) (Figure 6.3, 6.4 (e)). K^+ is one of the most important and abundant nutrient elements of plants and

therefore, K^+ in fine particles can serve as an effective tracer for biomass burning aerosols (Yamasoe et al., 2000). Fresh biomass burning particles mostly found in the size range of 0.1 μm – 0.5 μm (Remer et al, 1998; Kleeman et al., 1999) in agreement with data observed within range in this study. The formation mechanism of K^+ in the droplet mode could be regarded fresh and cloud-processed biomass burning aerosols (Huang et al., 2006). Furthermore, Hsieh (2008) suggested the possible source of K^+ from agricultural waste burning with the indicative of relationship between K^+ and NH_4^+. At EROS site, there is low potential of this source with the modest correlation coefficients of K^+ and NH_4^+ (r = 0.59 and r = 0.46 for condensation and droplet modes, respectively).

A small coarse mode presented for K^+ at this site peaked over the coarse mode of sea salt particles (Na^+ and Cl^-), indicating the contribution by sea spray to K^+ could be ignored. In consistent with the study of relationship between K^+ with Na^+ and Cl^- in coarse mode, it was found that the insignificant correlations were observed at this site (r = -0.48 and r = -0.44 for correlation coefficients of K^+ with Na^+ and Cl^-, respectively). At EROS, soil particles would be considered to be the important source of K^+ in coarse mode as K^+ is also a constituent of soil.

Ammonium

The mass size distributions of ammonium are presented in Figure 6.3 and Figure 6.4 (d). Ammonium size distribution exhibited a dominant peak in the 0.4 μm – 0.5 μm range for both samples collected with and without NH_3 atmosphere. A small peak around 1.0 μm – 2.0 μm was observed in some sampling periods (P13 and P15), indicating that the fine mode of ammonium probably overlaid the coarse mode when the experiment set by NH_3 feeding as appeared only one dominant peak in fine mode (Figure 6.4 (d)). As expected, the higher mean concentration of particulate ammonium was seen in the aerosol samples collected under NH_3 atmosphere in comparison to air samples obtained by normal condition (44.8 nmol m^{-3} and 30.5 nmol m^{-3} for samples taken simultaneously with and without NH_3 supply, respectively) (Table 6.3). The mean size distribution of NH_4^+ was clearly shown the high concentration in samples taken under ammonia atmosphere during the simultaneous period (Figure 6.4 (d)). The major peak of NH_4^+ in droplet mode displayed a similar distribution to sulphate, nitrate and chloride, suggesting that the productions of ammonium salts ($(NH_4)_2SO_4$, NH_4NO_3 and NH_4Cl) generated in this size range. The stability of these ammonium salts are different and

depend on temperature and relative humidity. $(NH_4)_2SO_4$ is the most stable while NH_4Cl is the most volatile, therefore NH_4^+ favours to react with particulate sulphate (Parmar et al., 2001). This behaviour is supported by the study of correlations of NH_4^+ with SO_4^{2-}, NO_3^- and Cl^- in droplet mode and the results showed the very strong relationships of NH_4^+ with SO_4^{2-} and NO_3^- (r = 0.90 and r = 0.80, respectively) (Figure 6.6). The insignificant correlation of NH_4^+ and Cl- was found in aerosol droplet (r = 0.08).

A small fraction of ammonium was also observed in the coarse fraction with the average contributions of 6.6% and 3.8% to total ammonium concentration for the whole data with and without NH_3 atmosphere, respectively (Table 6.3). For the simultaneous data, the coarse ammonium accounted for 4.9% and 6.0% to total ammonium concentration in aerosol samples collected with and without NH_3 supply, respectively. When excess NH_3 gas was available, the potential formation of ammonium salts of sulphate and nitrate in coarse particle may be found in this condition as the small peaks of sulphate and nitrate exhibited around 1.0 μm – 2.0 μm (Figure 6.4 (a), (b)).

Sulphate

Sulphate had a predominant concentration peak in the droplet mode (0.4 μm – 1.0 μm) both in samples taken under ammonia and normal atmosphere (Figure 6.3, 6.4 (a)). The condensation modes may contribute and observed dominantly in this study during period of P6, P9 and P14 for the concentrations of 1.18 μg m^{-3}, 1.17 μg m^{-3} and 0.59 μg m^{-3}, respectively (Table 6.2). Most of the sulphate size distribution exhibited the high concentration values of droplet mode and consequently it overlaid the condensation mode. The highest concentration of sulphate in droplet mode occurred in the samples collected under NH_3 atmosphere (3.16 μg m^{-3} during the P8), suggesting that sulphate aerosol in forms of ammonium salts such as ammonium sulphate ($(NH_4)_2SO_4$), ammonium bisulphate (NH_4HSO_4), triammonium sulphate ($(NH_4)_3HSO_4)_2$), Metal ammonium sulphate ($(NH_4)_2SO_4.MSO_4$: (M = metal)) may be favour to produce in aerosol particle in this condition. It is clear that the ammonia gas has little effect on stabilising sulphate aerosol, which is non-volatile specie at atmospheric conditions, as the mean size distribution of sulphate during simultaneous period observed the same pattern with slightly difference in concentration (Figure 6.4 (a)). In contrast, nitrate and fine particulate chloride which are volatile species observed higher concentration in samples taken simultaneously (Figure 6.4

(b), (c)). The average size distribution of sulphate at EROS showed a similar pattern to those sulphate in aerosol samples taken at MR and RC sites (Figure 6.5). Sulphate size distributions have been investigated in the past studies so that its formation mechanisms and size distribution characteristics are fairly well understood (Kerminen and Wexler, 1995; Meng and Seinfeld, 1994; Seinfeld and pandas, 1998; Zhuang et al., 1999).

Sulphate can be originated by both primary and secondary sources (Yamasoe et al., 2000; Herner et al., 2006; Guo et al., 2010). Biomass burning such as wood burning and meat cooking was a dominant contributor for particulate sulphate at the size range around 0.1 μm in diameter (Kleeman et al., 1999). The nucleation mode of sulphate (Dp < 0.175 μm) accounted to sulphate concentration less than 5% in both air sampling with and without NH_3 atmosphere. In addition, there was not significant correlation between SO_4^{2-} and K^+, a good tracer for biomass burning, in nuclei mode (r = 0.46 in Figure 6.6) observed in this work. These results indicate that a contribution of direct sulphate emission by biomass burning could not be effected on aerosol sample at EROS site. Particulate sulphate in the size range of 0.32 μm – 0.6 μm can be emitted directly by gasoline-powered vehicles (Kleeman et al., 2000). The dominate peak of sulphate observed in droplet mode between 0.4 μm and 1.0 μm and some samples (P1, P3, P7, P9 and P14) clearly appeared at particle size range of 0.4 μm – 0.5 μm, suggesting that primary sulphate emission would be considering as the primary sulphate sources during these period. Parmar et. al. (2001) stated that the occurrence of SO_4^{2-} particles in the size range of 0.7 μm – 1.6 μm cannot be explained by primary emission, gas-phase nucleation or condensation, such as in the case of smaller diameters. Growth of the condensation mode particles and evaporation of large droplets may form these particles.

For sulphate formed by secondary sources, the condensation mode of sulphate as H_2SO_4 vapour was firstly produced by homogeneous gas phase photochemical oxidation of SO_2 followed by gas-to-particle conversion. For the droplet mode, in-cloud process was suggested to be the dominant pathway (Kerminen and Wexler, 1995; Meng and Seinfeld, 1994). The possible formation pathway for sulphate was generated through the following chemical reactions;

$$SO_2(g) + H_2O \leftrightarrow SO_2 \cdot H_2O \qquad \text{(Equation 6.11)}$$

$$SO_2 \cdot H_2O \leftrightarrow HSO_3^- + H^+ \qquad \text{(Equation 6.12)}$$

$$H_2O_2(g) \leftrightarrow H_2O_2(aq) \quad \text{(Equation 6.13)}$$

$$HSO_3^- + H_2O_2(aq) + H^+ \leftrightarrow SO_4^{2-} + 2H^+ + H_2O \quad \text{(Equation 6.14)}$$

Sulphate in coarse particles can be contributed by sea salt particles and photochemical reaction of SO_2 to generate higher amounts of sulphuric acid which reacted with sodium and calcium containing particles such as soil particles (Pakkanen, 1996). In this data, the mass size distribution of Na^+ showed dominant peak in coarse mode at 2.0 μm – 6.0 μm and the strong correlation between SO_4^{2-} and Na^+ in coarse mode was observed (r = 0.80). This finding is consistent with the previous study by Zhao and Gao (2008), suggesting that sulphate could occur as sea salt sulphate (Na_2SO_4). However, the low concentration of coarse sulphate and contribution of sulphate in the coarse mode (whole data; 21.6% and 7.0% for sample with and without NH_3 supply as in Table 6.3) indicates that the reaction of sulphuric acid and sea spray particles was slow or the reaction time of sea salt sulphate was short (equation 6.7). In case of aerosol sample under NH_3 atmosphere, the excess of NH_3 could be attributed the fact that $(NH_4)_2SO_4$ in coarse particle generated in this condition with the contribution of coarse particle around 20.3% to total sulphate for simultaneous data. This was evident by the average size distribution of SO_4^{2-} in coarse mode clearly observed for the samples taken under NH_3 atmosphere (Figure 6.4 (a)). In addition, the moderate correlation between SO_4^{2-} and NH_4^+ in coarse mode (r = 0.59) was found in this experiment.

Nitrate

The mass size distribution of nitrate exhibited two modes, with a droplet mode in the size range of 0.4 μm – 0.5 μm (P9, P10, P13 and P15) and a coarse mode in the size range of 1.8 μm – 3.1 μm appeared during P9 and P14 (Figure 6.3, 6.4 (b)). The mean nitrate concentrations were 50.6 nmol m^{-3} and 44.9 nmol m^{-3} in samples collected under NH_3 atmosphere and without NH_3, respectively for the entire data. For simultaneous data between experiment with and without NH_3 supply, the aerosol nitrate in the concentrations of 49.3 nmol m^{-3} and 29.4 nmol m^{-3}, respectively were observed. Most of particulate nitrate accounted in fine mode more than 90% of total nitrate in both experiment. These findings indicate the combination of NO_3^- and NH_4^+ in fine fraction as both particles exhibited the dominant peaks in droplet mode. The possible two pathways have been suggested to explain the formation of nitrate in the accumulation mode; in-cloud processes and condensation of its precursors onto pre-existing particles (Zhuang et al., 1999; Herner et al., 2006). In this study,

droplet mode nitrate and sulfate showed a strong correlation with r = 0.73, suggesting that their formation mechanisms may be the same. In the presence of clouds, rain or moist aerosol surfaces, the heterogeneous pathway for production of nitrate from NO_2 involving the heterogeneous hydrolysis of dinitrogen pentoxide (N_2O_5) on the surface of aqueous aerosol particles (Riemer et al., 2003).

$$N_2O_5 + H_2O \xrightarrow{aerosol} 2HNO_3 \qquad \text{(Equation 6.15)}$$

For the condensation mechanism, after NH_4NO_3 predominantly produced by the photochemical transformation of NO_x in the gas-phase, the condensation of NH_4NO_3 onto hygroscopic sulphate particles would be favoured to contribute nitrate in fine mode. It is clear that NH_4NO_3 which is highly volatile particle, can be stable and found higher concentration in aerosol samples collected under ammonia gas supply as NH_4NO_3 in the atmosphere exists in reversible phase equilibrium with gaseous HNO_3 and NH_3.

The average mass size distribution of nitrate in the samples collected without NH_3 supply exhibited a small peak in coarse fraction (Figure 6.4 (b)). For the other sampling period, coarse nitrate may be overlaid by fine nitrate fraction with showing the very high concentration. The presence of coarse mode nitrate was clearly observed in the average mass size distribution of nitrate for the samples taken without NH_3 atmosphere (P9 and P14). Coarse mode nitrate is mainly formed through the reactions of nitric acid onto existing coarse particles such as $NaNO_3$ and $Ca(NO_3)_2$ (Pakkanen, 1996). The mass size distribution of nitrate in coarse mode was in the corresponding peak with sodium in this work. However, the correlation of NO_3^- and Na^+ in coarse mode was shown insignificant relationship (r = 0.42), suggesting that the low contribution from sea salt particles effected on particulate nitrate in coarse fraction (Equation 6.10). Coarse mode nitrate accounted equally to total nitrate around 7% both in aerosol samples collected with and without NH_3 atmosphere, indicating that coarse nitrate as NH_4NO_3 salts did not generate more under NH_3 atmosphere. In addition, the relationship between NH_4^+ and NO_3^- in coarse mode observed insignificant correlation coefficient (r = 0.31). Coarse nitrate originated by reaction between nitric acid and crustal particles which are from suspended soil and road dust, and dust from construction and demolition sites, especially in form of $Ca(NO_3)_2$ or primary emissions by local traffic would be considering at EROS site.

Compared to nitrate size distribution in other locations, the tri-modal pattern in nitrate size distribution was observed at Marylebone road (roadside) and Regents College (background) (Figure 6.5). The difference in size distribution suggests that the formation pathway should be not the same way. The variation of the nitrate in aerosol was mainly driven by fluctuation in temperature, relative humidity, meteorology, oxidant levels and the degree of long-range transport. As appeared the peak in nuclei mode at these two sites, this indicated that nuclei mode gas-to-particle conversion occurred to form primary nitrate particles during that period.

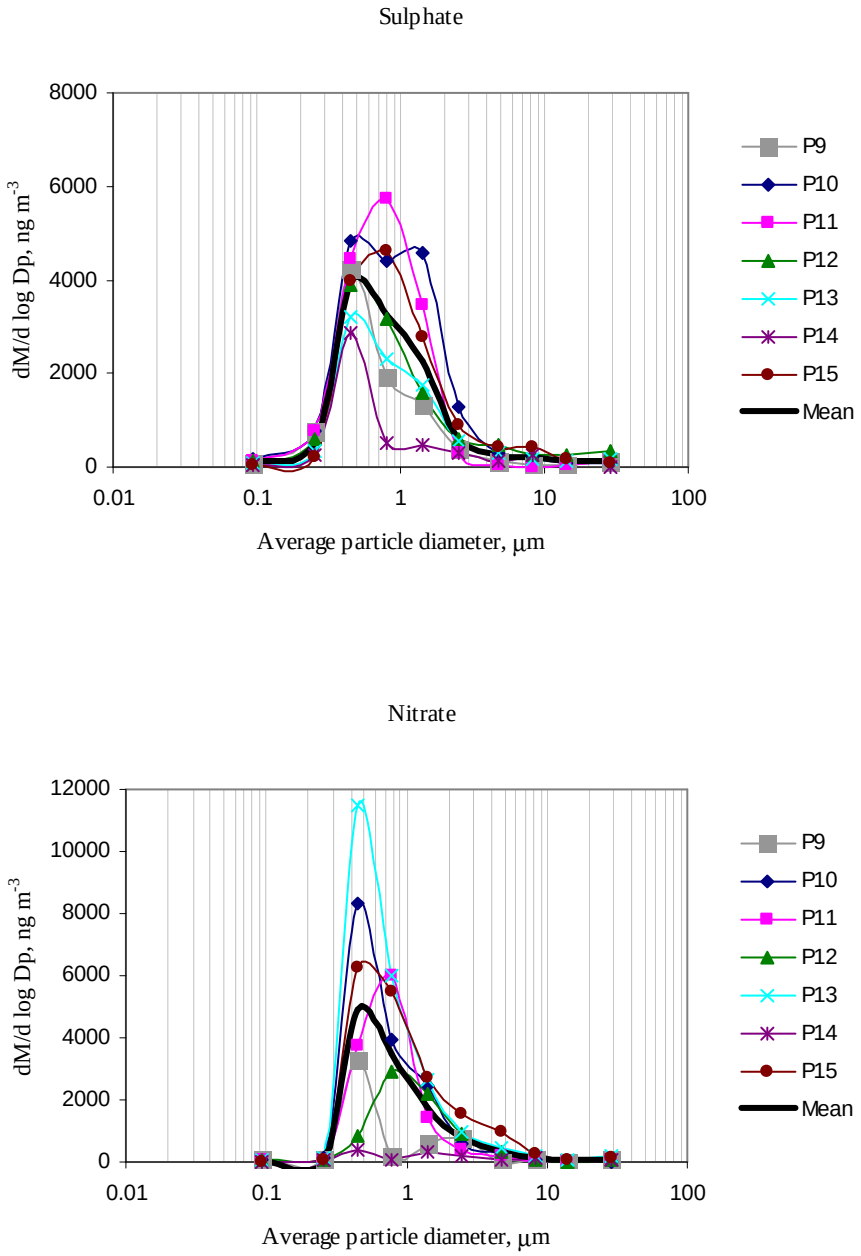

Figure 6.3 Size distributions of chemical species in aerosol samples collected with MOUDI operated under normal conditions for all periods

Chloride

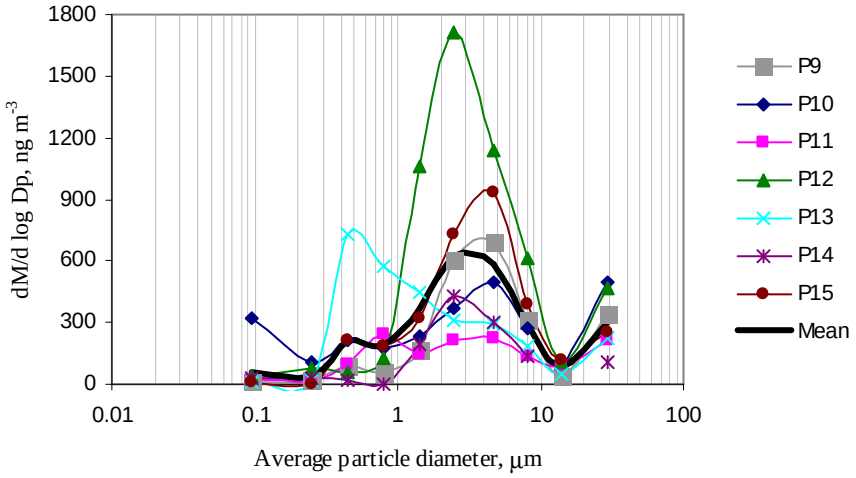

Sodium

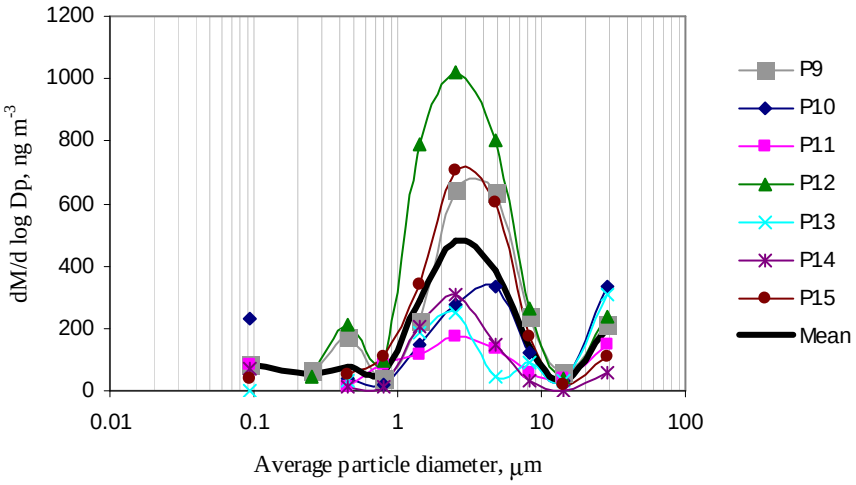

Figure 6.3 *(continued)*

Ammonium

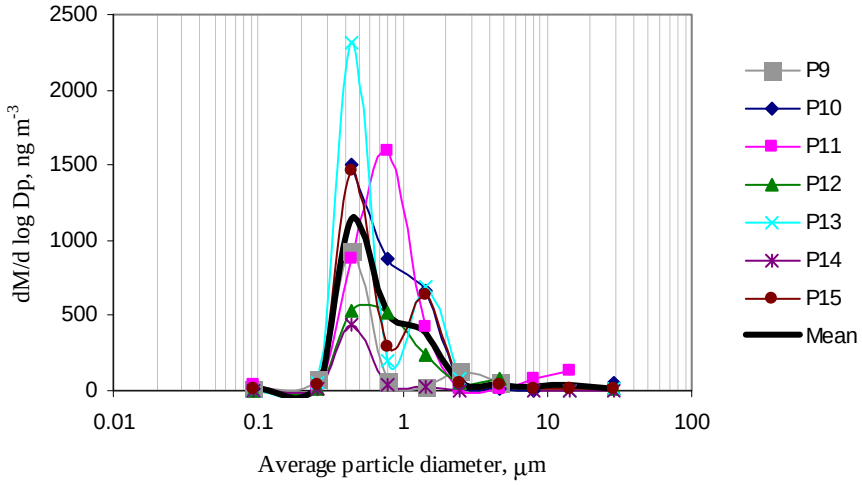

Potassium

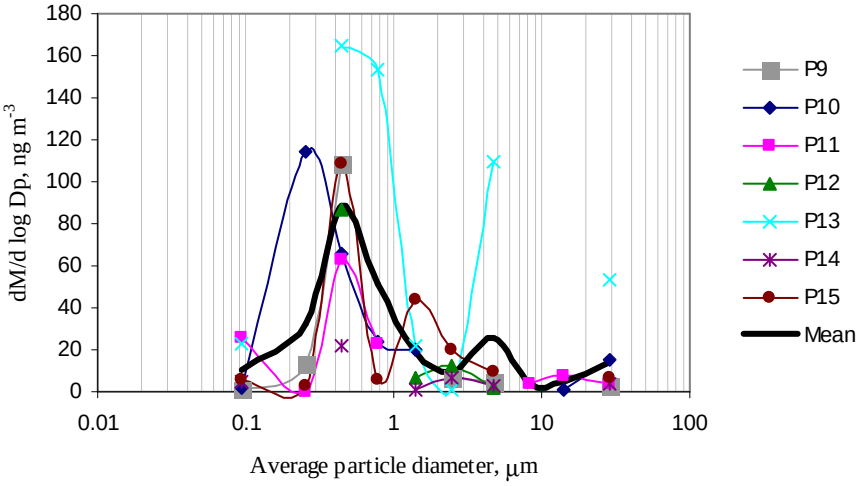

Figure 6.3 *(continued)*

(a)

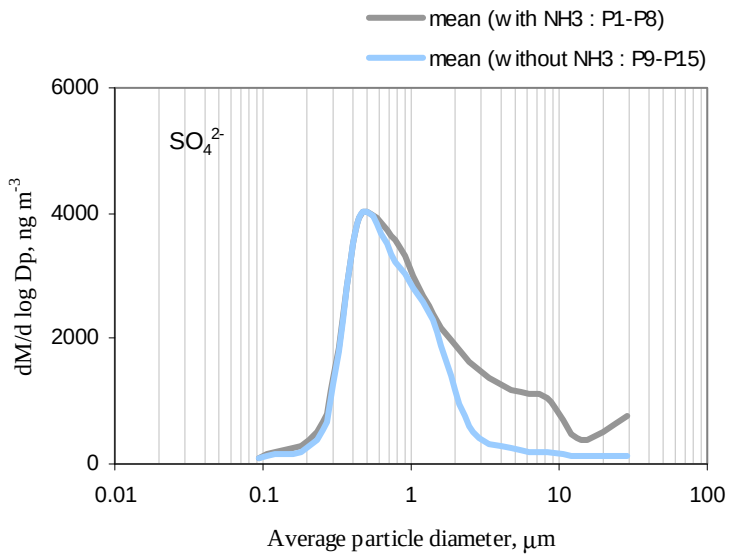

(b)

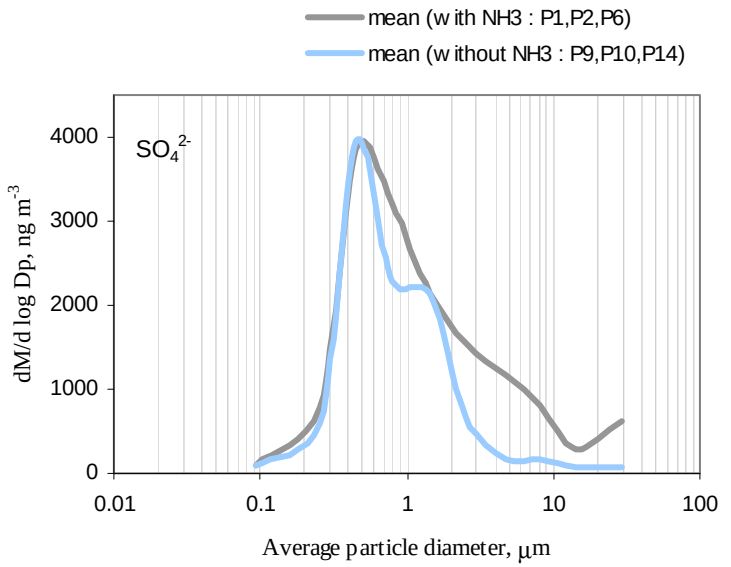

Figure 6.4 (a) Comparisons of mean size distributions of sulphate during the air sampling with and without NH_3 supply for (a) the whole period and (b) the simultaneous period (with NH_3 – mean of P1, P2 and P6; without NH_3 – mean of P9, P10 and P14)

(a)

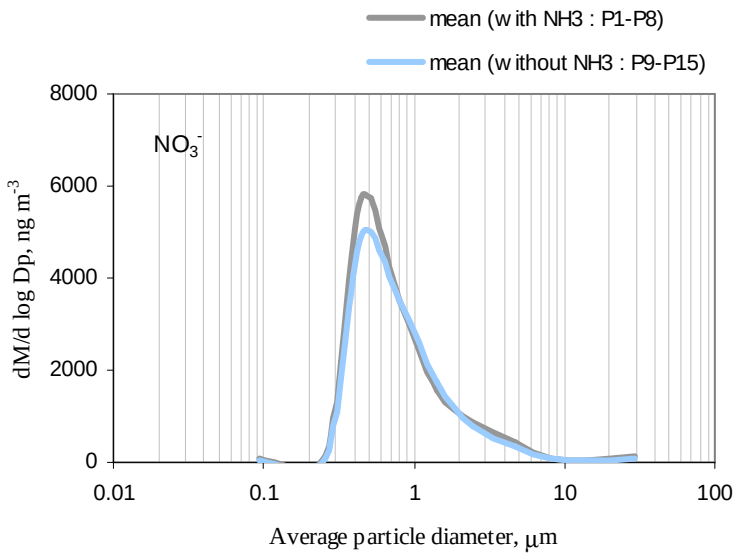

(b)

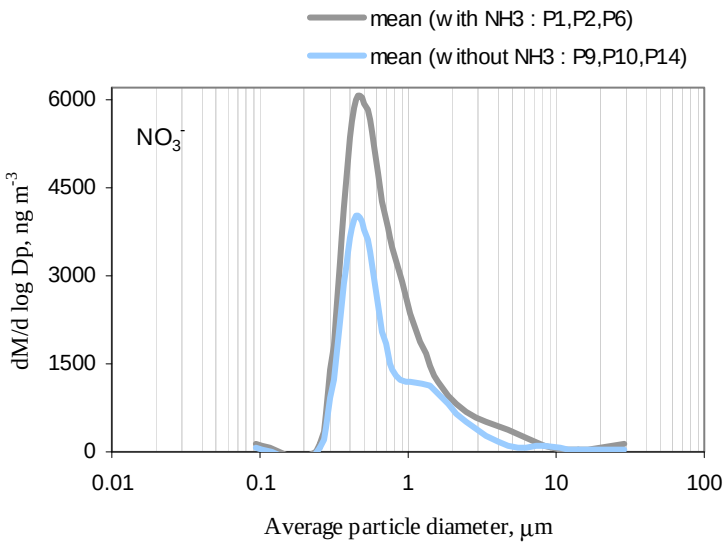

Figure 6.4 (b) Comparisons of mean size distributions of nitrate during the air sampling with and without NH_3 supply for (a) the whole period and (b) the simultaneous period (with NH_3 – mean of P1, P2 and P6; without NH_3 – mean of P9, P10 and P14)

(a)

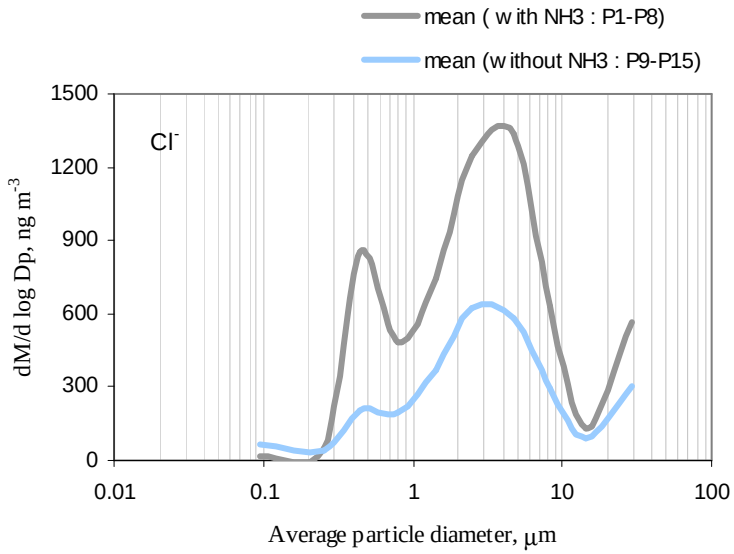

(b)

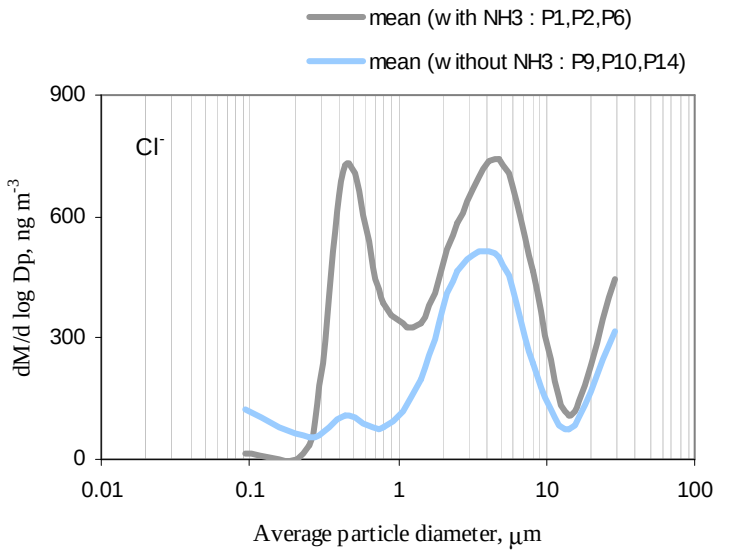

Figure 6.4 (c) Comparisons of mean size distributions of chloride during the air sampling with and without NH_3 supply for (a) the whole period and (b) the simultaneous period (with NH_3 – mean of P1, P2 and P6; without NH_3 – mean of P9, P10 and P14)

(a)

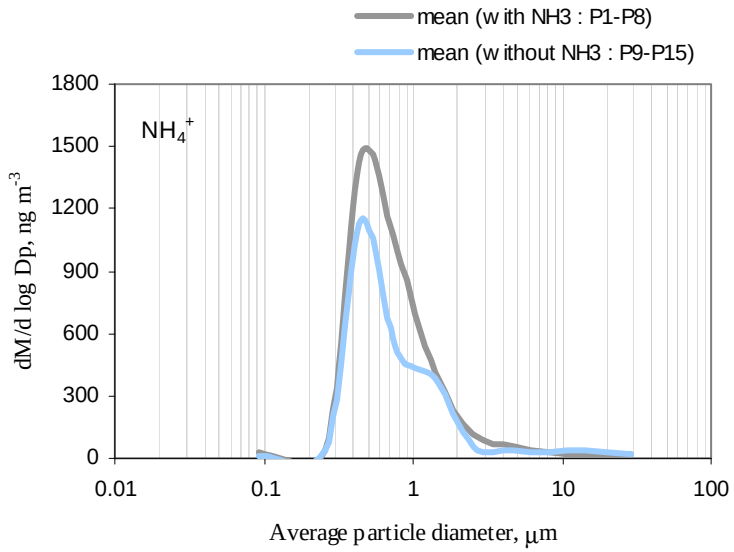

(b)

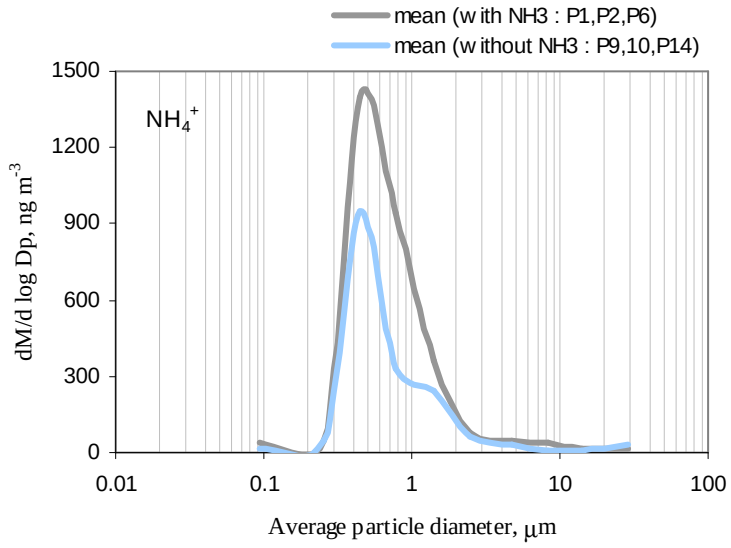

Figure 6.4 (d) Comparisons of mean size distributions of ammonium during the air sampling with and without NH_3 supply for (a) the whole period and (b) the simultaneous period (with NH_3 – mean of P1, P2 and P6; without NH_3 – mean of P9, P10 and P14)

(a)

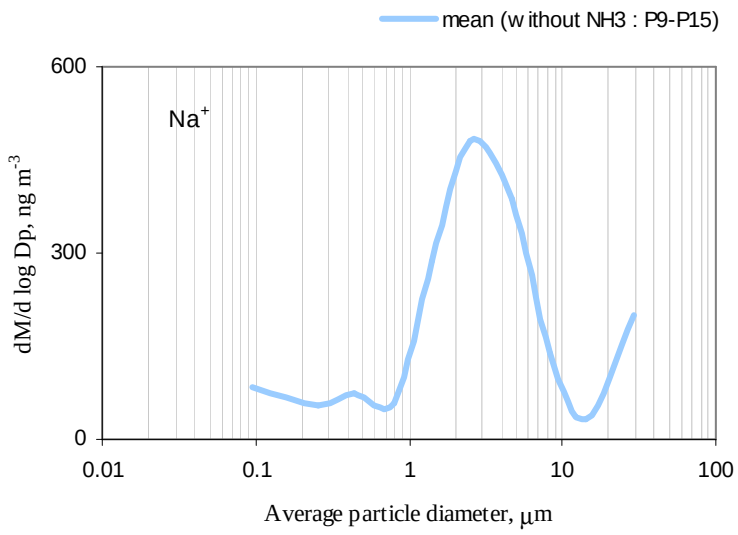

(b)

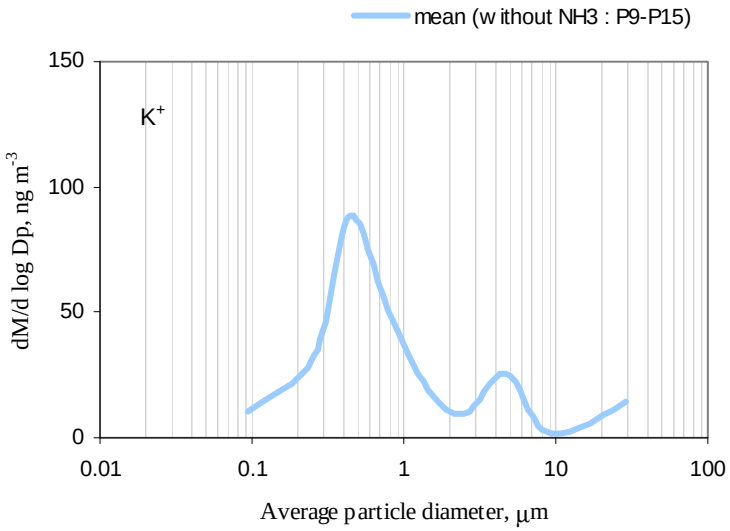

Figure 6.4 (e) Mean size distributions of sodium and potassium during the air sampling without NH_3 supply for the whole period

(a)

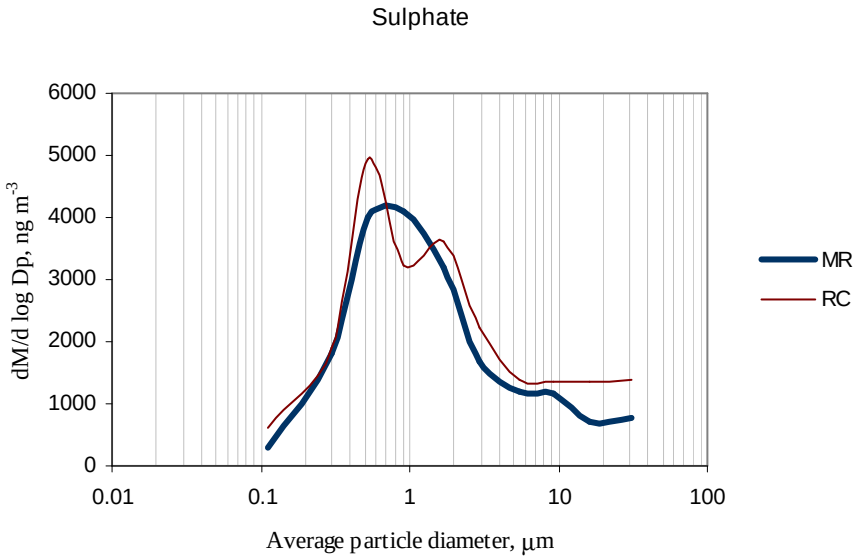

(b)

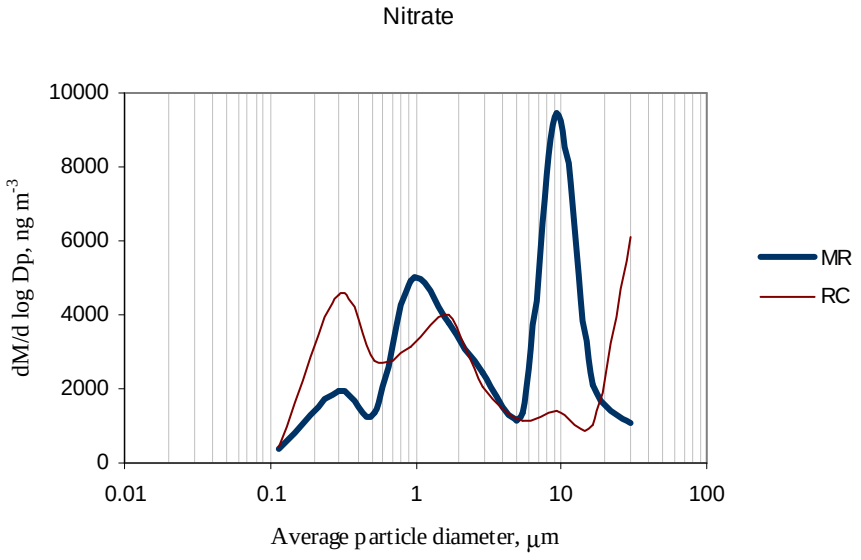

Figure 6.5 Mean size distributions of (a) sulphate, (b) nitrate, (c) chloride and (d) oxalate measure at Marylebone road (MR) and Regents College (RC) sites during March 2007

(c)

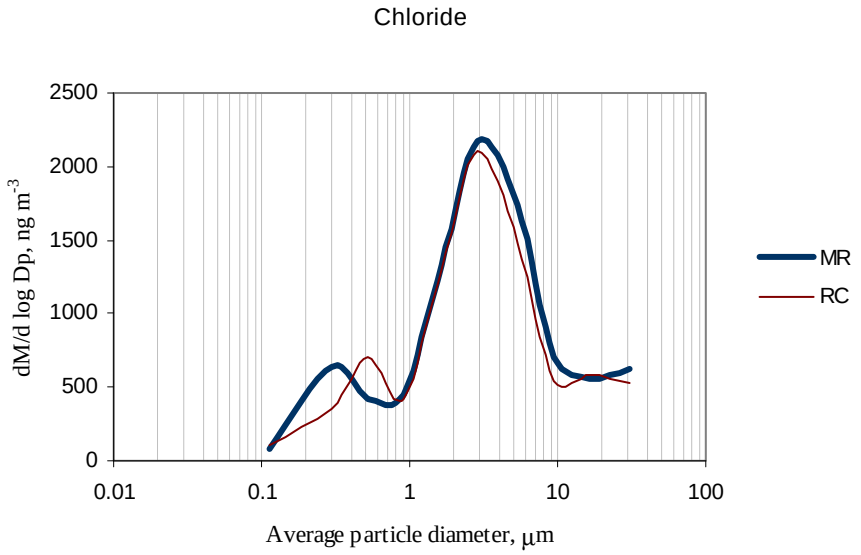

(d)

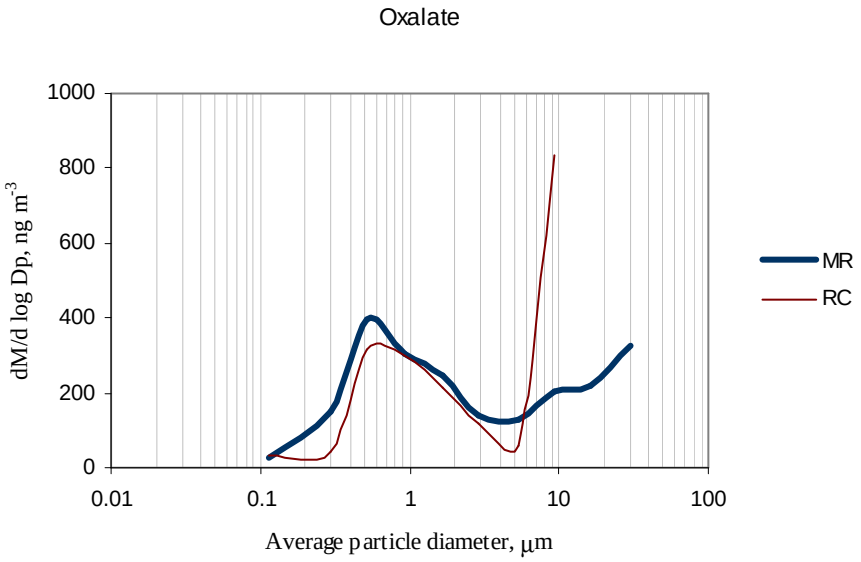

Figure 6.5 *(continued)*

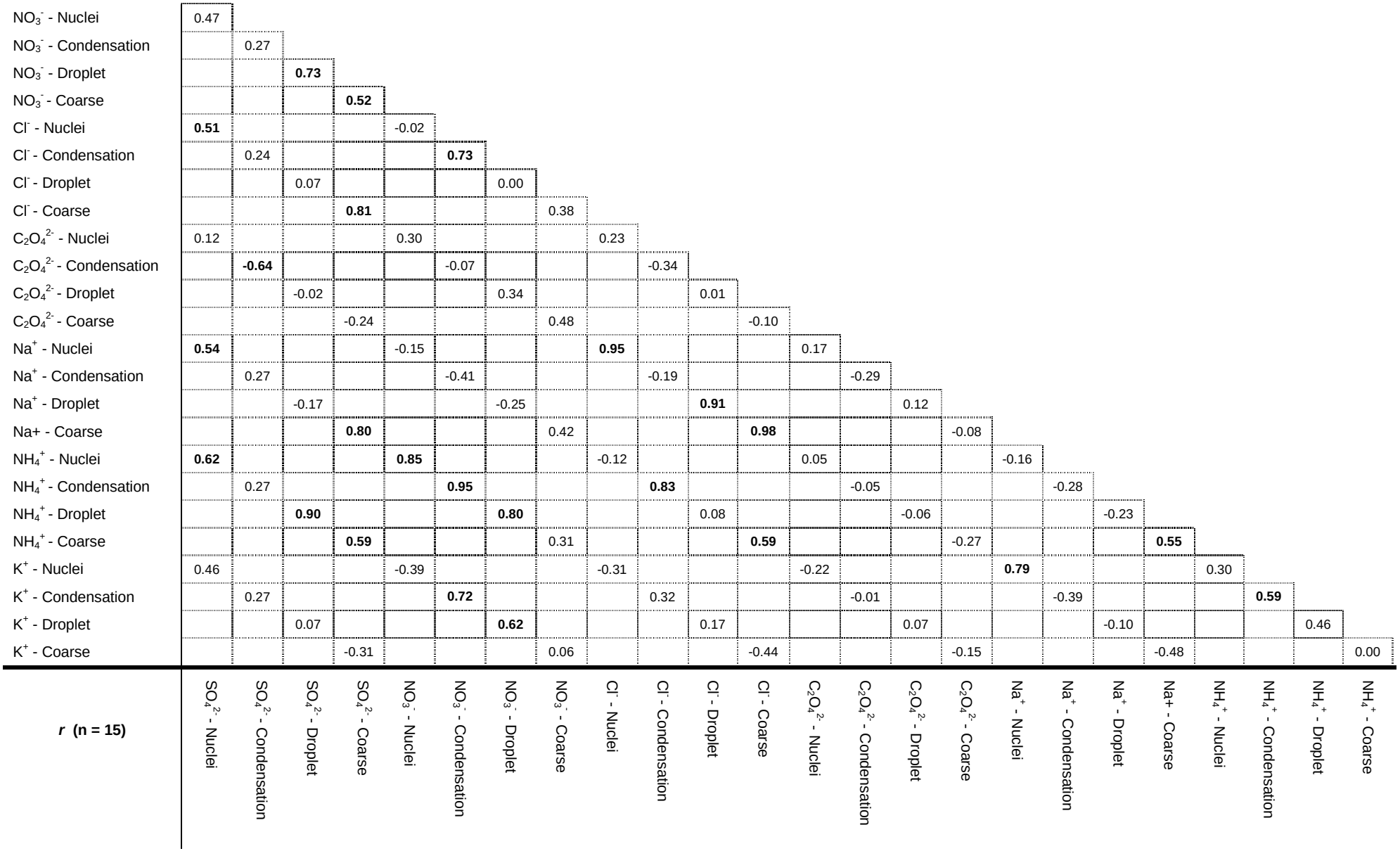

r (n = 15)	SO_4^{2-} - Nuclei	SO_4^{2-} - Condensation	SO_4^{2-} - Droplet	SO_4^{2-} - Coarse	NO_3^- - Nuclei	NO_3^- - Condensation	NO_3^- - Droplet	NO_3^- - Coarse	Cl^- - Nuclei	Cl^- - Condensation	Cl^- - Droplet	Cl^- - Coarse	$C_2O_4^{2-}$ - Nuclei	$C_2O_4^{2-}$ - Condensation	$C_2O_4^{2-}$ - Droplet	$C_2O_4^{2-}$ - Coarse	Na^+ - Nuclei	Na^+ - Condensation	Na^+ - Droplet	Na+ - Coarse	NH_4^+ - Nuclei	NH_4^+ - Condensation	NH_4^+ - Droplet	NH_4^+ - Coarse
NO_3^- - Nuclei	0.47																							
NO_3^- - Condensation		0.27																						
NO_3^- - Droplet			**0.73**																					
NO_3^- - Coarse				**0.52**																				
Cl^- - Nuclei	**0.51**				-0.02																			
Cl^- - Condensation		0.24				**0.73**																		
Cl^- - Droplet			0.07				0.00																	
Cl^- - Coarse				**0.81**				0.38																
$C_2O_4^{2-}$ - Nuclei	0.12				0.30				0.23															
$C_2O_4^{2-}$ - Condensation		**-0.64**				-0.07				-0.34														
$C_2O_4^{2-}$ - Droplet			-0.02				0.34				0.01													
$C_2O_4^{2-}$ - Coarse				-0.24				0.48				-0.10												
Na^+ - Nuclei	**0.54**				-0.15				**0.95**				0.17											
Na^+ - Condensation		0.27				-0.41				-0.19				-0.29										
Na^+ - Droplet			-0.17				-0.25				**0.91**				0.12									
Na+ - Coarse				**0.80**				0.42				**0.98**				-0.08								
NH_4^+ - Nuclei	**0.62**				**0.85**				-0.12				0.05				-0.16							
NH_4^+ - Condensation		0.27				**0.95**				**0.83**				-0.05				-0.28						
NH_4^+ - Droplet			**0.90**				**0.80**				0.08				-0.06				-0.23					
NH_4^+ - Coarse				**0.59**				0.31				**0.59**				-0.27				**0.55**				
K^+ - Nuclei	0.46				-0.39				-0.31				-0.22				**0.79**				0.30			
K^+ - Condensation		0.27				**0.72**				0.32				-0.01				-0.39				**0.59**		
K^+ - Droplet			0.07				**0.62**				0.17				0.07				-0.10				0.46	
K^+ - Coarse				-0.31				0.06				-0.44				-0.15				-0.48				0.00

Values shown in bolds are significant at $p < 0.05$ (the 95% level of significance).

Figure 6.6 Correlation coefficient matrix among the measured ionic components by modes of size distribution

6.5 Size distribution of oxalate

Oxalate was the most abundant dicarboxylic acid in atmospheric aerosols. In most of the samples, the mass size distribution displayed bimodal structure consisting one submicron mode and one supermicron mode. Few samples exhibited a complex structure which included additional submicron and supermicron modes such as samples collected during P10 and P15. The size distribution of oxalate exhibited the dominant mode peaking at 0.4 μm – 0.5 μm and the small coarse mode (1.0 μm – 2.0 μm) (Figure 6.7 and 6.9). The size distributions of oxalate were similar to the results measured in the previous study at Marylebone road and Regent College sites (Figure 6.5). In comparison its size distribution with major anionic species in PM (sulphate, nitrate and chloride), oxalate size distributions were similar to those of sulphate both in samples taken with NH_3 and without NH_3 atmosphere (Figure 6.8). Reference with the relationships of major components in aerosols discussed in chapter 4, the good relationship between $C_2O_4^{2-}$ and SO_4^{2-} in fine fraction ($PM_{2.5}$) was found at this site for the samples collected by Partisol Plus air samplers (500 samples). These can be attributed to the fact that the formation pathway of oxalate in 0.4 μm – 0.5 μm was dominated by in-cloud processes as same as sulphate in droplet mode. This was in agreement with Yao et al. (2002) concluded that oxalate in 0.32 μm – 0.54 μm and sometimes shifted to 0.54 μm – 1.0 μm was produced by in-cloud processes. Other studies also reported that suphate in the droplet mode has been attributed to in-cloud processes (Meng and Seinfeld, 1994; Kerminen and Wexler, 1995; Yu et al., 2005).

In principle, sulphate and oxalate are chemically distinct since one is an inorganic compound and the other is an organic compound. This means that their precursors are basically different. Oxalate has been found in aerosol in various environments. The possible sources include from primary emission of vehicular transportation (Kawamura and Kaplan, 1987), biomass burning (Narukawa et al., 1997), biogenic activity (Kawamura, 1996; Jones, 1998) and plant emission which do not emit oxalic acid directly, but isoprene could be the important precursor (Lim et al., 2005). Oxalate concentrations in PM appeared various levels based on the spatial and temporal characteristics. In the previous section of this work, aerosol samples were collected simultaneously at EROS and Harwell representing urban background and rural sites, respectively. Although there was found some effect from road traffic contributed to aerosol composition at EROS site, the mean oxalate concentration in $PM_{2.5}$ (0.02 μg m^{-3}) was the same as those samples taken from Harwell. In addition, there was a poor correlation

between oxalate and EC, a primary pollutant derived from incomplete combustion of fuels in transportation, observed in the whole data at EROS. It is clear that vehicle exhausts do not play the important source for oxalate in ambient air. Moreover, this is also supported by the results obtained from previous study in our research group. Those measurements were carried out by the analysis of aerosol samples collected simultaneously at Marylebone road and Regents College representing roadside and background roadside sites, respectively during March 2007. The mean concentrations of oxalate were similar at two sites (0.35 μg m^{-3} in $PM_{2.5}$). This conclusion on less contribution of vehicular emissions to ambient oxalate is consistent with the reported by Yu et al. (2005), Yao et al. (2004) and Poore (2000). Despite the same peak of K^+ and oxalate in droplet mode (0.4 μm – 0.5 μm), oxalate by modes of size distribution revealed the insignificant correlation with K^+ which was an indicator of biomass burning in atmospheric particles (Figure 6.6). Therefore, primary biomass burning was not a significant source of oxalate in fine fraction.

For the secondary formation of oxalate, Kawamura et al., (1996) and Kalberer et al., (2001) stated that the condensation mode oxalate was from the photochemical formation in the gas phase by the reaction of organic compounds with photochemical oxidants such as OH free radicals and O_3 to form gaseous oxalic, followed by its condensation onto existing particles. If gas-particle condensation is main process to form oxalate, the highest concentration of condensation mode (0.175 μm – 0.325 μm) should be found in the samples at this site. On the contrary, the results showed the highest concentration of oxalate in droplet mode, suggesting that the condensation mode oxalate-containing particles were activated and became the droplet mode particles due to cloud processing. A further proposed mechanism of formation of oxalic acid is from isoprene by in-cloud oxidation processes (Lim et al. 2005).

In coarse mode, oxalate was found in the smaller concentration than that in the fine mode during all sampling periods (Table 6.2). For the entire data, oxalate in coarse mode accounted range from 12% to 15% of total oxalate for the samples collected both with and without NH_3 supply. There were no significant correlations observed between cationic species and oxalate in coarse mode in this study. Similarities in coarse mode size distribution with sodium (2.0 μm – 6.0 μm), suggest the possibility of formation within, or uptake of gaseous oxalate by sea salt particles. Alternatively, Russell and Seinfeld (1998) have proposed that supermicron particles can be formed by in-cloud processes. It should be noted that coarse mode oxalate may form from soil particles since oxalic acid also present in the soil. Oxalate is a by-product

of the hydrolysis of oxaloacetate from citric acid and glyoxylate via the metabolic mechanism of fungi in the soil (Dutton and Evans, 1996; Gadd, 1999).

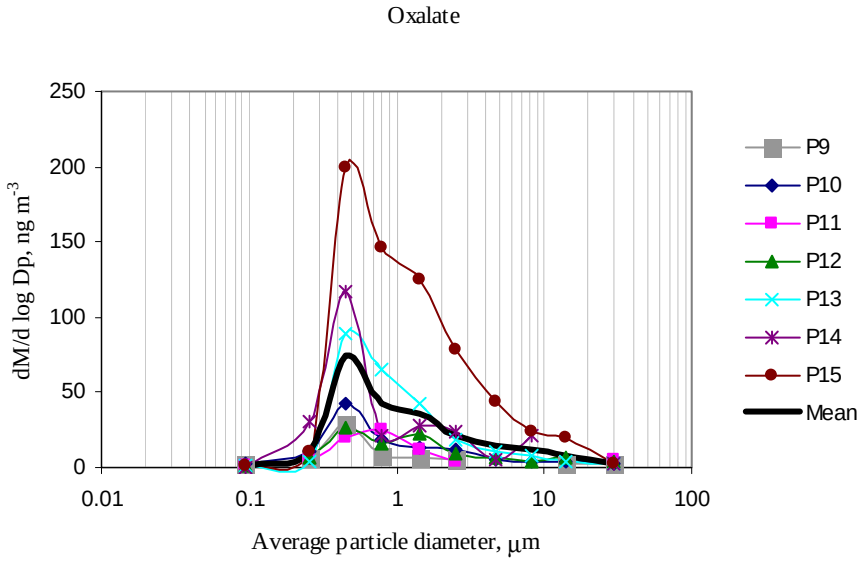

Figure 6.7 Size distributions of oxalate in aerosol samples collected with MOUDI operated under normal conditions for all period

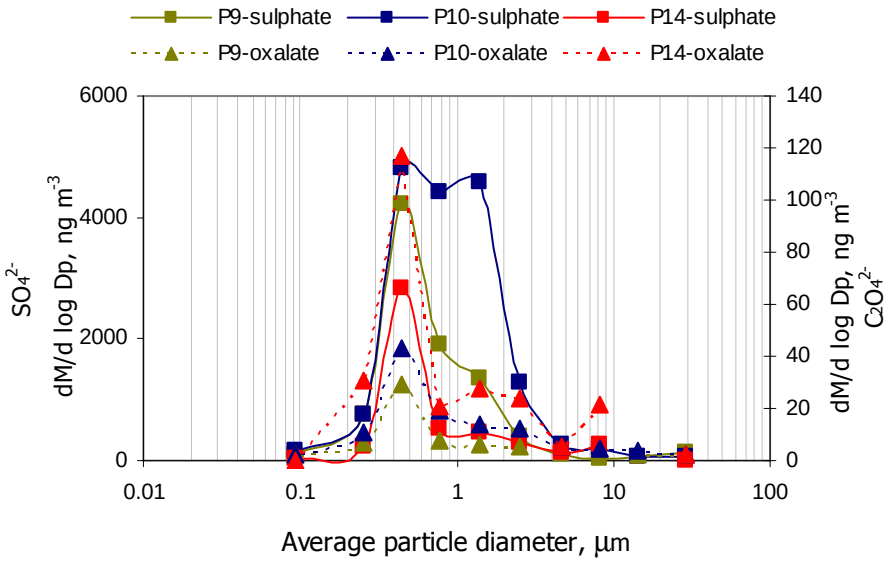

Figure 6.8 Size distributions of sulphate and oxalate in aerosol samples collected during the simultaneous period

(a)

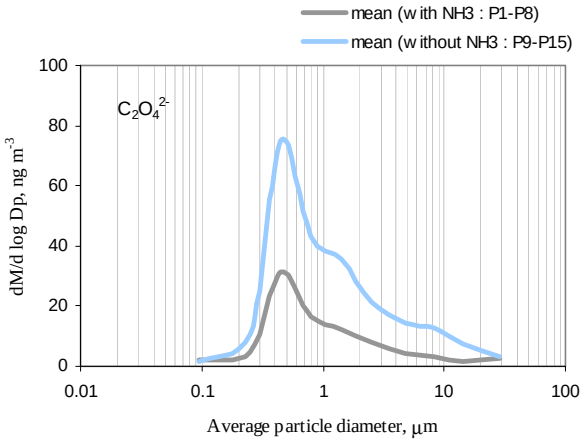

(b)

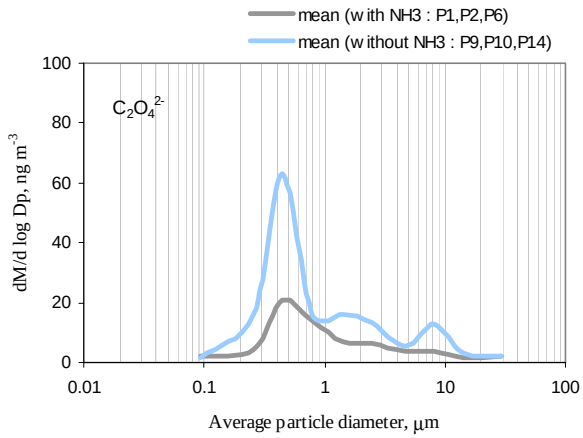

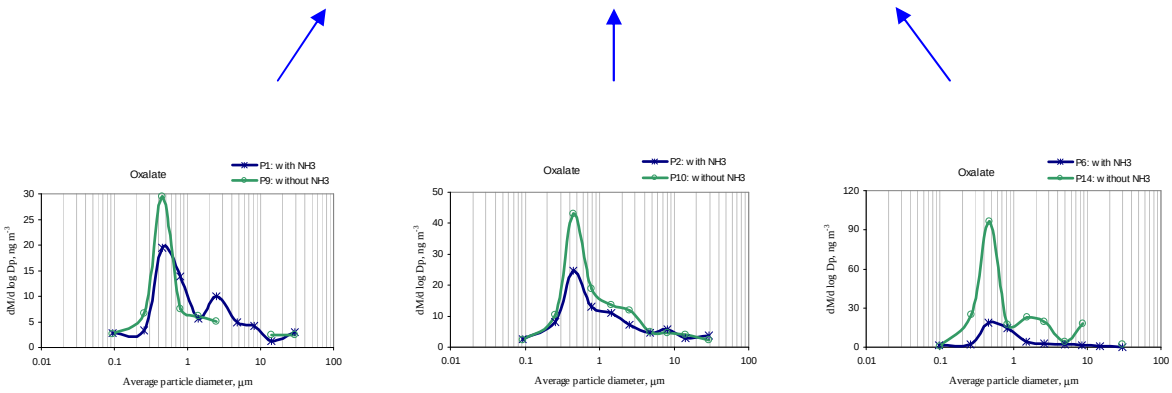

Figure 6.9 Comparisons of mean size distributions of oxalate during the air sampling with and without NH_3 supply for (a) the whole period and (b) the simultaneous period (with NH_3 – mean of P1, P2 and P6; without NH_3 – mean of P9, P10 and P14)

With regard to aerosol samples taken simultaneously under NH_3 atmosphere and normal conditions, particulate oxalate mainly accounted in fine fraction in both experiment with 84.4% and 90.5% to total oxalate, respectively. There was a difference in the average oxalate concentration observed between samples obtained by the two MOUDI systems (Table 6.3). The increment of oxalate was determined by the subtraction of component concentration under normal sampling from component concentration under NH_3 atmosphere (-0.0002 μmol m^{-3} and 0 μmol m^{-3} in fine and coarse fractions, respectively). Mass size distributions of oxalate in aerosols collected simultaneously by both MOUDIs are demonstrated in Figure 6.9. Oxalate in droplet mode exhibited the dominant peak around 0.4 μm – 0.5 μm with the minor coarse mode.

If ammonium oxalate is expecting to present and stabilise by ammonia gas atmosphere in aerosol phase, the higher concentration may observe in samples collected in NH_3 atmosphere as same as nitrate and chloride particles causing by equilibrium condition. The contribution of oxalate in ammonia experiment appeared discordant value comparing with concentrations of particulate nitrate and chloride. Although concentrations of the oxalic acid in gas phase were not measured in this work, the atmospheric aerosol equilibrium may describe according to the hypothesis of thermodynamic of aerosols (Seinfeld and Pandis, 1998). It may be anticipated that the ambient gas-aerosol system will be at equilibrium if the rates of change of the concentrations of gaseous species are slow compared with the characteristic times for diffusion of these species to the particles and for equilibrium within the particle. In this sampling conditions with high relative humidity and freezing cold temperature, ammonium oxalate form exhibited as solid $(NH_4)_2C_2O_4$ (non-deliquescence). For solid-phase aerosol particles, the equilibrium concentration of aerosol species is constants and does not change as species are transferred to the aerosol phase. In comparison with atmospheric inorganic salts (NH_4NO_3, NH_4Cl – deliquescent species), the equilibrium concentrations of these salts will increase as condensation proceeds, and equilibration between the two phases will be accelerated. Moreover, the timescales to approach equilibrium condition in aqueous aerosols are shorter for the order of a fraction of a second than in solid aerosol particles. Therefore, in case of ammonium oxalate salt, the characteristic time for mass transfer to and form oxalate aerosol was likely longer than rate of change of gaseous species concentration so there might rarely be oxalate equilibrium in this sampling condition. The preceding analysis suggests that under conditions of low aerosol mass concentrations, low temperatures and large particle sizes, the timescale can be on the order of several hours or even days and the aerosol phase

may not be in equilibrium with the gas phase (Seinfeld and Pandis, 1998). Consequently, excessive ammonia gas during air sampling does not effect on oxalate salts concentration in atmospheric aerosol. The thermodynamic equilibrium between gas- and particle-phase depends on the ambient temperature, relative humidity and chemical composition of particles and gases.

In comparison between ammonium salts of oxalate and nitrate with the latter represented the temperature dependence specie, nitrate concentration in aerosol taken under NH_3 gas was observed higher than those samples taken with normal system (0.018 μmol m^{-3} in fine particle). The discordant measurement result was seen in aerosol oxalate with negative difference in concentration of -0.0002 μmol m^{-3} in fine particle. However, the correlation analysis of oxalate and nitrate showed the moderate relationships at this site (r = 0.48, r = 0.35 and r = 0.49 for $PM_{2.5}$, $PM_{2.5\text{-}10}$ and PM_{10}, respectively for the whole Partisol data) and the strong correlations were observed during summer (r = 0.79 and r = 0.78 for $PM_{2.5}$ and PM_{10}, respectively for the whole Partisol data as mentioned in chapter 4). It is likely that oxalate aerosol exhibited the temperature dependence including oxalic acid is typically the lowest molecular weight dicarboxylic acids in atmosphere with vapour pressure of 3.5×10^{-5} mmHg at 30 ^{o}C. The feature of NH_4NO_3 probably explains by its hygroscopic properties. Even though Allen et al. (1989) reported that the good equilibrium formation of NH_4NO_3 was found at ambient temperature above *ca* 5 ^{o}C and at RH below about 80% and in the other cases higher NH_3 and HNO_3 concentration was measure in the gas phase. The meteorology data during this sampling period shown in Table 6.1, there were only P6, P7 and P14 with the ambient temperature over 5 ^{o}C. The results found that particulate nitrate still appeared higher concentration in atmospheric aerosol collected under NH_3 atmosphere. This is because NH_4NO_3 is deliquescent and can form solution droplets at RH 62% (at 25 ^{o}C), and therefore in this air sampling condition of very high humidity and freezing cold temperature, NH_4NO_3 can grow in the droplet fractions. In contrast, ammonium oxalate is not deliquescent under these conditions. This is also strongly supported by the relationships study as shown in Figure 6.6. The good correlation coefficients between NO_3^- and NH_4^+ in fine mode were observed but there were no significant correlations between $C_2O_4^{2-}$ and NH_4^+ in this study.

6.6 Conclusions

The study on the mass size distributions of major components in aerosols in term of the direct comparison between samples collected with and without NH_3 provided the useful information about the sources and formation pathway of aerosol species. Measurement results indicated that the systematic and analytical errors were observed by the difference of concentration data of K^+ and Na^+ analysed in both samplers with and without ammonia gas supply. Since both species are the non-volatile components, the concentrations would expect to be identical in samples both with and without ammonia. Thus experimental uncertainty was estimated based on these results. Particulate NO_3^-, Cl^- and NH_4^+ were present in higher concentrations in the samples taken under NH_3 atmosphere. On the contrary, there was high oxalate concentration observed in samples taken under normal condition. Since oxalate shows a significant correlation with nitrate which is the temperature dependent species, especially in summer at EROS as mentioned in chapter 4, this can be interpreted as that oxalate form in PM is affected by temperature. This discordant data might also be indicative of the analytical and sampling errors by the two systems. However, the lower concentration of oxalate in samples collected under ammonia might be described by physical and chemical atmospheric processes for oxalate formation in gas phase affected the formation of oxalate in particulate phase. There was not clear explanation in this experiment because there was no data of components in gas phase. Sulphate was the dominant inorganic species contributed in the concentration of 3.79 μg m^{-3} and 2.80 μg m^{-3} for samples collected with and without NH_3, respectively for the whole data. As expected, there was little effect of ammonia gas to stablise particulate sulphate as ammonium sulphate represented non-volatile specie in atmosphere. Its mass size distribution dominated broadly in droplet mode peaking at 0.55 μm. suggesting in-cloud processes were the significant formation pathway following many previous studies. Coarse mode sulphate was contributed from sea spray to form sea salts sulphate (Na_2SO_4). Since ammonium also appeared in coarse mode during some sampling periods, ammonium sulphate could be contributed in coarse mode sulphate even in NH_3 experiment. Under ammonia sampling condtions, it was not clearly observed ammonium in coarse particle because this may be overlaid by fine ammonium fraction.

Nitrate size distributions were bimodal with a droplet mode peaking at 0.4 μm – 0.5 μm and a coarse mode peaking at 1.8 μm – 3.1 μm. The secondary photochemical formation was expected in the droplet mode via the condensation of NH_4NO_3 onto the surface of existing

particles such as sulphate particle. NH_4NO_3 was firstly produced by the photochemical oxidation of NO_x in gas phase and neutralised by gaseous ammonia and consequently the condensation of NH_4NO_3 proceeded. The high contribution of nitrate in droplet mode was observed in the samples collected under NH_3 atmosphere, indicating that the stable ammonium nitrate was found in aerosol particles in this condition. Coarse mode nitrate could be formed through the reactions of nitric and crustal particles at this site or a minor contribution of primary nitrate emissions by local traffic.

Chloride and sodium which are commonly contributed by sea salt aerosol were investigated and both components revealed bimodal mode of size distribution. The coarse mode was dominant with a concentration peak around 2.0 μm – 6.0 μm and fine mode appeared at 0.4 μm – 0.5 μm. The findings suggest that the influence of sea spray and anthropogenic emissions including the process of chloride depletion may affect at EROS site. Chloride in fine mode as expected to be present as ammonium chloride was stablise and observed higher concentration in aerosol particles collected under NH_3 gas.

Oxalate had similar formation pathway as sulphate with a dominant peak at 0.4 μm – 0.5 μm. The formation mechanism of particulate oxalate could be attributed to in-cloud processes. As oxalate did not appear any peak in nucleation mode which were particles formed mostly by gas-to-particle conversion and usually found near the sources, there was less important of primary oxalate sources in atmosphere. The evidences of this also support by the weak correlations of oxalate with EC and K^+ which are good indicator of primary combustion sources and biomass burning, respectively. Coarse mode oxalate probably caused by the contribution of biological processes. The equilibrium phase of particulate oxalate and gaseous phase in expected form of ammonium salts ($(NH_4)_2C_2O_4$) was different from the semi-volatile species such as NH_4NO_3 and NH_4Cl. This was because the concentration of oxalate did not increase in aerosol samples collected under NH_3 atmosphere. On the contrary, the other major components were observed higher concentrations when air sampling experiment taken under NH_3 supply. This might be explained by the difference in physical and chemical atmospheric processes for oxalate formation. In addition, NH_3 system may contribute the formation of oxalate in gas phase which did not measure in this experiment. In overall, ammonia gas does not affect the size distribution patterns of component species but it rather influences the contribution on their modes concentration of the semi-volatile species in ambient air.

CHAPTER 7
CONCLUSIONS AND RECOMMENDATIONS FOR FURTHER WORK

7.1 Conclusions

In this study, comprehensive studies of chemical and physical properties of airborne particulate matter have been presented. It is clear that airborne particulate matter originated from many sources depending on location and meteorological conditions. Understanding both chemical and physical properties of PM is highly valuable for evaluation of the sources and formation pathways. The measurements of PM have been conducted at the Elms Road Observatory Site (EROS) located in the University of Birmingham and Harwell (HAR) located in the Harwell Science Centre. These two sites represent an urban background and rural area, respectively. Data analysed from Harwell was mainly used for comparison of major chemical components of PM collected simultaneously with EROS. Daily aerosol samplings have been employed for collecting of fine ($PM_{2.5}$) and coarse ($PM_{2.5-10}$) particles. The concentration data of PM_{10} were also calculated based on the sum of fine and coarse fractions. The major chemical composition of SO_4^{2-}, NO_3^-, Cl^-, $C_2O_4^{2-}$, OC, WSOC and EC in PM were analysed according to analytical methods described in chapter 2. Particle size distribution data in this study have been obtained from the experiment designed for studying the effect of ammonia gas to stabilise semi-volatile aerosol species.

Concentration composition for carbonaceous materials, which consisted mainly of particulate organic and elemental carbon, measured in all samples collected at both sites. The mean concentrations with measurement uncertainties of EC measured ranged from 0.4 ± 0.03, 0.2 ± 0.01 and 0.4 ± 0.03 μg $m^{-3}$for $PM_{2.5}$, $PM_{2.5-10}$ and PM_{10}, respectively at the rural site to 1.1 ± 0.08, 0.2 ± 0.01 and 1.2 ± 0.09 μg m^{-3} for $PM_{2.5}$, $PM_{2.5-10}$ and PM_{10}, respectively for the whole data at the urban background. The mean concentrations with measurement uncertainties of OC measured ranged from 1.7 ± 0.12, 1.0 ± 0.07 and 2.8 ± 0.20 μg $m^{-3}$for $PM_{2.5}$, $PM_{2.5-10}$ and PM_{10}, respectively for the whole data at the rural site to 3.0 ± 0.22, 1.3 ± 0.09 and 4.3 ± 0.31 μg m^{-3} for $PM_{2.5}$, $PM_{2.5-10}$ and PM_{10}, respectively at the urban background. These data clearly show that OC and EC observed higher concentrations at urban background than those at rural area. Maximum EC and OC values in winter have been associated to meteorological conditions favourable to pollutant accumulation. In case of maximum EC

concentration, this has been associated to less effective dispersion process in the low temperature, and for maximum OC concentration, it could be explained by the lower atmospheric mixing depth favouring secondary organic aerosol formation and accumulation of secondary organic precursors. The sources of carbonaceous particles can be qualitatively evaluated by finding the relationship between OC and EC concentrations. The OC/EC minimum ratio of 0.35 has been used to distinguish between primary and secondary OC according to research recently reported by Pio et al. (2011). This ratio was used to determine values of OC_{prim} and OC_{sec} in PM. With focusing on $PM_{2.5}$, the mean OC_{sec} concentrations (± S.D.) were 2.6 ± 1.8 μg m^{-3} and 1.6 ± 0.8 μg m^{-3} for the whole data at EROS and Harwell, respectively. The mean OC_{prim} concentrations (± S.D.) were 0.4 ± 0.4 μg m^{-3} and 0.1 ± 0.1 μg m^{-3} for the whole data at EROS and Harwell, respectively. Calculated OC_{prim} and OC_{sec} show a winter maximum and the strong correlation with nitrogen oxides (NO_x) at both sites suggesting that the local transport plays an important source of OC_{prim} and OC_{sec}. In this study, the behaviour of OC_{sec} is closer to nitrate than that of sulphate, consistent with the observation made by Harrison and Yin (2008). This indicates that regional transport and temperature have a major influence upon OC_{sec} concentrations. The local contributions of carbonaceous compounds were roughly calculated by subtraction of rural (Harwell) concentrations from urban background (EROS) concentrations in aerosol samples collected simultaneously. It was found that EC, especially in $PM_{2.5}$, exhibited a strong local contribution (0.6 μg m^{-3}), suggesting that local emission at EROS was affected by fuel combustions as EC mostly associated in fine particles. The local contributions of OC_{prim} and OC_{sec} in $PM_{2.5}$ were 0.3 μg m^{-3} and 0.4 μg m^{-3}, respectively. The good correlations between OC_{sec} with NO_x and NO_3^- which are indicators for road traffic and temperature dependent specie as NH_4NO_3, respectively, indicate that OC_{sec} may be affected by local contribution from road transport with temperature dependent equilibrium of OC_{sec} in particulate phase and gaseous phase. The reduced major axis (RMA) regression analysis also reveals the local contributions of carbonaceous aerosol at EROS influence their concentrations in the same way as at Harwell site. Moreover, as significant tested, it appears that there is no difference between OC_{sec} concentration at both sites suggesting a high influence or contribution of long-lived species.

For ionic component composition in PM, SO_4^{2-}, NO_3^- and Cl^- are basically required analysed species in fine fraction under the directive on ambient air quality and cleaner air for Europe. The whole mean concentrations with measurement uncertainties of sulphate, nitrate and

chloride were 1.86 ± 0.06 μg m^{-3} 2.72 ± 0.09 μg m^{-3} and 0.73 ± 0.02 μg m^{-3}, at EROS respectively and were 1.40 ± 0.05 μg m^{-3} 1.29 ± 0.04 μg m^{-3} and 0.23 ± 0.01 μg m^{-3}, at Harwell, respectively. Oxalate also measured at both sites and whole mean concentrations with measurement uncertainties were 0.05 ± 0.002 μg m^{-3} and 0.02 ± 0.001 μg m^{-3} at EROS and Harwell, respectively. The calculated local contributions of ionic species were also estimated from the differences concentration in PM collected simultaneously between two sites. Water-soluble organic carbon (WSOC), which is a significant group of OC_{sec}, represents mostly in the atmospheric aerosol as the secondary formation by photochemical oxidation. The results show slightly local contribution of WSOC, OC_{sec}, sulphate, nitrate and chloride in $PM_{2.5}$ (0.4 μg m^{-3}, 0.4 μg m^{-3}, 0.13 μg m^{-3}, 0.17 μg m^{-3} and 0.08 μg m^{-3}, respectively). There is no difference in mean concentration for oxalate in fine fraction suggesting that oxalate formation by photochemical oxidation of precursors in the atmosphere with long-lived species. The seasonal behaviour of sulphate, nitrate, chloride and oxalate show a dominant temporal variation over the spatial variation. In addition, the same patterns of time series appear between EROS and Harwell for simultaneous data. These findings indicate the important of long-rang transport on the contribution to the secondary aerosols. Particulate oxalate reveals no clear seasonal pattern but the concentration show highest in spring. The study on the ratio of sulphate-to-nitrate indicates the stability of sulphate higher than nitrate because SO_4^{2-}/NO_3^- ratios were extremely high for $PM_{2.5}$ in summer. This could be interpreted that formation of sulphate by photooxidation in the atmosphere (aqueous oxidation) slightly reflects on its concentration but there was more volatile loss of nitrate aerosol as ammonium nitrate during the high temperature. As expected at both sites, the Cl^-/NO_3^- ratios were high in the coarse fraction because the major source of chloride in coarse fraction mostly contributed from sea spray which can be transported from the sea to rural and urban areas (Gustafsson and Franzen, 2000). The average Cl^-/NO_3^- ratio in coarse particle is also observed high during the winter probably causing by the high wind speed blowing pass the marine origin.

The relationships and size distributions of major ionic species were investigated in order to identify the sources and formation pathways of their components. With regard to the size distribution study, the air sampler designed for collecting aerosol particles under ammonia atmosphere was employed at EROS site as well as the aim of studying the effect of ammonia gas to stabilise the semi-volatile species in ambient air. The results for anionic species can be summarised as follows;

Sulphate - the strong correlation between sulphate and nitrate (as observed both in $PM_{2.5}$ and PM_{10} at EROS) in consistent with previous studies indicates the fact that two species undergo similar formation and removal processes in atmosphere. When the regression analysis was applied for simultaneous data between the two sites, sulphate in fine mode showed the zero intercept with a gradient close to 1.0 indicating that the regional contributions by long-range transport and photochemical oxidation in the atmosphere play an important factor on its concentration. Sulphate was the dominant inorganic species: 3.79 μg m^{-3} and 2.80 μg m^{-3} for samples collected with and without NH_3, respectively for the whole data. Its mass size distribution dominated broadly in droplet mode peaking at 0.55 μm, suggesting that in-cloud processes were the significant formation pathway following many previous studies. As expected, there was little effect of ammonia gas to stabilise particulate sulphate as ammonium sulphate represented non-volatile specie in atmosphere. Coarse mode sulphate was contributed from sea spray to form sea salts sulphate (Na_2SO_4). Under the condition of excess NH_3 gas during air sampling, ammonium sulphate could be contributed in coarse mode sulphate.

Nitrate – the results of the reduced major axis (RMA) regression show that the higher local nitrate concentration in $PM_{2.5}$ was found at urban background to rural area as the intercept value of 0.11 consistent with the local fine nitrate contribution of 0.17 μg m^{-3} calculated from the difference concentration of simultaneous data. This finding suggests that the nitrate increment probably arises from anthropogenic sources in the conditions of high conversion of nitric acid vapour to nitrate aerosol. Nitrate size distributions were bimodal with a droplet mode peaking at 0.4 μm – 0.5 μm and a coarse mode peaking at 1.8 μm – 3.1 μm. The secondary photochemical formation was expected in the droplet mode via the condensation of NH_4NO_3 onto the surface of existing particles such as sulphate particle. NH_4NO_3 was firstly produced by the photochemical oxidation of NO_x in gas phase and neutralized by gaseous ammonia and consequently the condensation of NH_4NO_3 proceeded. The high contribution of nitrate in droplet mode was observed in the samples collected under NH_3 atmosphere, indicating that the stable ammonium nitrate was found in aerosol particles in this condition. Coarse mode nitrate could be formed through the reactions of nitric and crustal particles at this site or a minor contribution of primary nitrate emissions by local traffic.

Chloride - the results of relationship study strongly support a common source from marine aerosol with the weak correlation observed with other species (sulphate, nitrate, oxalate).

Chloride and sodium which are commonly contributed by sea salt aerosol were investigated and both components revealed bimodal mode of size distribution. The coarse mode was dominant with a concentration peak around 2.0 μm – 6.0 μm and fine mode appeared between 0.4 μm and 0.5 μm. The findings suggest that the influence of sea spray and anthropogenic emissions including the process of chloride depletion may affect at EROS site. The appearance of anthropogenic sources for chloride was shown by air mass trajectory analysis. Chloride concentration associated with back trajectories coming from Europe mainland revealed high concentration during simultaneous sampling period (100 daily samples) between the two sites. Chloride in fine mode as expected to be present as ammonium chloride was stabilised and observed higher concentration in aerosol particles collected under NH_3 gas.

Oxalate – these are the dominant dicarboxylic acids observed in aerosol particles. The whole mean concentrations with measurement uncertainties of oxalate are from 0.02 ± 0.001 μg m^{-3} to 0.06 ± 0.002 μg m^{-3} at urban background and from 0.02 ± 0.001 μg m^{-3} to 0.04 ± 0.001 μg m^{-3} at rural site. These concentration levels are in range with a number of studies in the past as shown in Table 1.6 and there are very similar at the urban and rural sites. The relationships of oxalate with major chemical composite provide useful information on its formations and sources. Oxalate shows a good correlation with sulphate, suggesting that oxalate originates from similar atmospheric processes as sulphate i.e., from secondary formation. The significant correlation between oxalate and nitrate especially in summer can be anticipated that temperature may influence the oxalate concentration as it does for nitrate through the ammonium nitrate dissociation. Oxalate exhibited the weak correlations with EC in $PM_{2.5}$, $PM_{2.5\text{-}10}$ and $_{PM10}$ in the whole dataset. This was anticipated from its regional distribution and reflects an insignificant contribution to oxalate from primary combustion sources. Moreover, a poor correlation between oxalate and potassium, a tracer for biomass burning, was observed in the fine fraction at EROS suggesting that primary biomass burning or rapid formation in biomass burning plumes was also not a major source of the oxalate. The weak relationship between oxalate and chloride indicate a little contribution from marine aerosol or coal burning in winter on oxalate concentration. Oxalate in $PM_{2.5}$ shows a significant correlation with secondary OC in summer, suggesting the important of photochemical contribution to oxalate aerosol. Furthermore, it should be noted that there was no significant difference in fine oxalate collected simultaneously between EROS and Harwell

sites, indicating the significant sources of secondary oxalate formation by precursors with long-lived species.

Oxalate had similar size distribution to sulphate with dominant mode peaked at 0.4 μm – 0.5 μm, suggesting that oxalate and sulphate may have similar formation pathways. Kawamura et al., (1996) and Kalberer et al., (2001) concluded that the condensation mode oxalate was from the photochemical formation in the gas phase by the reaction of organic compounds with photochemical oxidants such as OH free radicals and O_3 to form gaseous oxalic acid, followed by its condensation onto existing particles. If gas-particle condensation were the main process to form oxalate, the highest concentrations should be found in the condensation mode (0.175 μm – 0.325 μm). On the contrary, the results showed the highest concentration of oxalate in the droplet mode, suggesting that condensation mode oxalate-containing particles were activated and became droplet mode particles due to cloud processing. A further proposed mechanism of formation of oxalic acid is from isoprene by in-cloud oxidation processes (Lim et al. 2005).

Oxalate in the coarse mode accounted for 12% to 15% of total oxalate for the samples collected by cascade impactor. There were no significant correlations observed between cationic species and oxalate in the coarse mode. Similarities in coarse mode size distribution with sodium (2.0 μm – 6.0 μm), suggest the possibility of formation within, or uptake of gaseous oxalate by sea salt particles. Alternatively, Russell and Seinfeld (1998) have proposed that supermicron particles can be formed by in-cloud processes.

In ammonia experiment, oxalate salt as expected in form of $(NH_4)_2C_2O_4$ show discordant results to inorganic atmospheric salts such as NH_4NO_3, $(NH_4)_2SO_4$ and NH_4Cl. The measurement observed that concentration of oxalate did not increase in aerosol samples collected under NH_3 atmosphere. On the contrary, the other major components were observed higher concentrations when air sampling experiment taken under NH_3 supply especially nitrate and chloride salts in fine particle. It should be noted that this experiment was observed the systematic and analytical errors by showing the difference of concentration data of K^+ and Na^+ in both samplers with and without ammonia. Since both species are the non-volatile components, the concentrations would expect to be identical in the two samplers. However, the discordant result of oxalate might be from the difference of physical and chemical atmospheric processes for oxalate formation in gas phase which did not measure in this

experiment. In addition, behaviour of oxalate could also be explained by the hypothesis of thermodynamic of aerosols (Seinfeld and Pandis, 1998). $(NH_4)_2C_2O_4$ which is non-deliquescence, exhibits as solid phase aerosol particles during high relative humidity and freezing cold temperature but NH_4NO_3 and NH_4Cl which are deliquescent species, show as aqueous aerosols. The time scales of NH_4NO_3 and NH_4Cl to approach equilibrium condition in aerosols are shorter than in solid aerosol particles as $(NH_4)_2C_2O_4$. In overall, ammonia gas does not affect the size distribution patterns of component species but it rather influence on the contribution on their modes concentration. The principal role of NH_3 is to neutralising acidic substances which are directly emitted or produced in the atmosphere and excess NH_3 gas could stabilise the semi-volatile species in particulate phase.

The further analysis of air mass back trajectories arriving at EROS and Harwell sites provided the effective evidence in the sources of airborne particulate matter by long-range atmospheric transport. Cluster analysis was applied in order to group similar trajectories for the whole dataset and simultaneous data between the two sites. The LRT pathways of high major component (SO_4^{2-}, NO_3^-, Cl^-, $C_2O_4^{2-}$, EC, OC, OC_{prim}, OC_{sec} and WSOC) concentrations at both sites were from continental Europe (easterly and southerly air flows) which is polluted urban and industrial regions with many of precursor sources compared to the westerly trajectories with mostly passing over marine atmosphere.

Focusing on oxalate concentration, trajectory cluster analysis of oxalate indicates the highest concentrations of oxalate were found to be associated with airmasses originating over the European mainland consistent with the behaviour of sulphate, nitrate and secondary organic carbon. It should, however, be noted that the elevation of oxalate in the continental trajectory is less than that for sulphate, nitrate or secondary organic carbon and the inter-site correlation between the urban EROS and rural Harwell sites is less strong for oxalate than for sulphate and nitrate. This is interpreted as oxalate having a number of secondary sources through different reaction pathways, depending upon different precursors which react at different rates, consequently leading to less spatial homogeneity than for sulphate and nitrate which have predominantly single precursor compounds. A significant source of biogenic emissions from vegetation especially isoprene, could be a potential precursor associated with continental trajectories as stated by Legrand et al. (2007). Their study confirmed the role of isoprene as a precursor of oxalic acid associated with the high estimated isoprene emissions in Europe especially in the east flank of France (Simpson et al., 1995). This seems unlikely to

be the main source, however, as this would produce a pronounced seasonality which is not observed. Thus, at EROS and Harwell sites, this could conclude that the sources of anthropogenic precursors for oxalate formation are more likely than biogenic isoprene. This research does not clearly identify the precursors of oxalate in atmospheric particles but the information about spatial and temporal variations, correlations with other chemical components and size distributions provide the useful behaviour of oxalate in atmosphere.

7.2 Recommendations for further work

There are some recommendations for further work as following;

- The studies of chemical and physical properties of airborne particulate matter should be performed in more different types of sampling locations such as urban, kerbside, industrial areas in order to make various factors of comparison and represent the good data source for the UK. The knowledge of properties of aerosol would help in designing a better legislation with the objective of limiting air pollution and climate change. Moreover, there is not clear about the precursors of particulate oxalate in this study, concentration data of chemical composition in PM obtained in difference locations can be used for study the relationships between oxalate with other components in order to confirm its sources and maybe identify its important precursors.
- Because there are many chemical components in aerosols affecting human health and climate, the further aerosol chemical composition analysis would be recommended for example elemental species (silicon (Si), aluminium (Al), iron (Fe), titanium (Ti), manganese (Mn), nickel (Ni), copper (Cu), zinc (Zn), lead (Pb) etc.), organic species (PAHs, acids, alkanes, alkenes, aldehydes, ketones, phenols etc.). These data will be useful because their composition impact the size, density, volatility, reactivity and toxicity of the particles.
- With regard to particulate oxalate in atmosphere, this study is expecting that oxalate in PM should be presented as ammonium salts as same as the form of inorganic species (NH_4SO_4, NH_4HSO_4, NH_4NO_3, NH_4Cl). It would be useful to apply the specific and reliable analytical methods to identify the form of oxalate in aerosol for example high performance liquid chromatography (HPLC) or gas chromatography (GC) combined with mass spectrometry (MS). Commercially

available chemistry databases would allow the identification of unknown compounds present in the aerosol samples.

- It was difficult to identify the equilibrium concentrations between gaseous and aerosol phases in the study of effect of ammonia gas on stabilising the semi-volatile species since there were no data of concentration in gaseous phase. The air sampling system with denuders is recommended for the further work. Denuders are often used as part of, or immediately behind, size-selective inlets to remove gases that might interfere with the aerosol sampling, or to quantify the concentrations of gaseous species that are precursors to secondary aerosols. The experiment should be also conducted in different conditions such as in summer, spring, autumn and winter. This is because the fluctuation of chemical components in aerosol particles depends on the meteorological conditions (i.e. temperature, humidity, wind speed). Measurements and records of meteorological data especially temperature and relative humidity at the sampling sties should be performed. A number of samples collected simultaneously from the systems with and without ammonia gas supply were recommended in order to obtain the reliable and accurate results.
- According to quality assurance and quality control (QA/QC) in the measurement and chemical characterization of aerosol particles, the development and use of standard reference materials (SRM) in this field would be focused in order to evaluate the measurement results for national traceability. There are some SRMs produced by the National Institute of Standards and Technology such as urban dust (SRM1649b), air particulate on filter media (SRM2783 and 8785) and ultra fine test dust (SRM8632). Inter-laboratory comparison programme for the measurement of aerosol particles should be conducted regularly and carried out by reference or national laboratory to monitor and maintain the quality of analysed data obtained from network and individual laboratory to be national acceptance.

REFERENCES

Abdalmogith, S.S. and Harrison, R.M. (2006) An analysis spatial and temporal properties of daily sulfate, nitrate and chloride concentrations at UK urban and rural sites. **Journal of Environmental Monitoring,** 8: 691 – 699.

Abdalmogith, S.S., Harrison, R.M. (2005) The use of trajectory cluster analysis to examine the long-range transport of secondary inorganic aerosol in the UK. **Atmospheric Environment,** 39: 6686 – 6695.

Agarwal, S., Aggarwal, S.G., Okuzawa, K., Kawamura, K. (2010) Size distributions of distributions of dicarboxylic acids, ketoacids, α-dicarbonyls, sugars, WSOC, OC, EC and inorganic ions in atmospheric particles over Northern Japan: implication for long-rang transport of Siberian biomass burning and East Asian polluted aerosols. **Atmospheric Chemistry and Physics,** 10: 5839 – 5858.

Air Resources Laboratory (2011) HYSPLIT Tutorial [online]. Available from: *www.arl.noaa.gov/HYSPLIT_workshop.php* [Accessed 2 August 2011].

Allen, A.G., Harrison, R.M. and Erisman, J.W. (1989) Field measurements of the dissociation of ammonium nitrate and ammonium chloride aerosols. **Atmospheric Environment,** 23: 1591 – 1599.

Allen, A.G., Harrison, R.M., Erisman, J.W. (1989) Field measurements of the dissociation of ammonium nitrate and ammonium chloride aerosols. **Atmospheric Environment,** 23: 1591 – 1599.

Alves, C., Pio, E., Campos, E., Barbebo, P. (2007) Size distribution of atmospheric particulate ionic at a coastal site in Portugal. **Quim Nova**, 30: 1938 – 1944.

AQEG (2004) Nitrogen Dioxide in the United Kingdom. Defra, London.

AQEG (2005) Particulate matter in the UK: Summary. Defra, London.

Arimoto, R., Duce, R.A., Savoie, D.L. (1996) Relationships among aerosol constituents from Asia and the North Pacific during PEM-West. **Journal of Geophysical Research,** 101: 2011 – 2023.

Arsene, C., Olariu, R.L, Zarmpas, P., Kanakidou, M., Mihalopoulos, N. (2011) Ion composition of coarse and fine particles in lasi, north-eastern Romania: Implications for aerosols chemistry in the area. **Atmospheric Environment,** 45: 906 – 916.

Ayers, G.P. (2001) Comment on regression analysis of air quality data. **Atmospheric Environment,** 35: 2423 – 2425.

Baker, J. (2010) A cluster analysis of long range air transport pathways and associated pollutant concentrations within the UK. **Atmospheric Environment,** 44: 563 – 571.

Barlow, J. (2009) “Boundary layer meteorology and atmospheric dispersion.” In Hewitt, C.N. and Jackson, A.V. **Atmospheric Science for Environmental Scientists.** Oxford: Wiley-Blackwell. pp. 218 – 242.

Baron, P.A. and Willeke, K. (2001) **Aerosol measurement principles, techniques, and applications.** 2nd ed. New York, John Wiley & Sons.

Bauer, H., Kasper-Giebl, A., Loflund, M., Giebl, H., Hitzenberger, R., Zibuschka, F., Puxbaum, H. (2002) The contribution of bacteria and fungal spores to the organic carbon content of cloud water, precipitation and aerosols. **Atmospheric Research,** 64: 109 – 119.

Belle, G.V., (2008) **Statistical rules of thumb.** 2nd ed. New Jersey, John Wiley & Sons.

Biswas, K. F., Ghauri, B. M., Husain, L. (2008) Gaseous and aerosol pollutants during fog and clear episodes in South Asian urban atmosphere. **Atmospheric Environment,** 42: 7775 – 7785.

Borbon, A., Fontaine, H., Veillerot, M., Locoge, N., Galloo, J,C., Guillermo, R. (2001) An investigation into the traffic-related fraction of isoprene at an urban location. **Atmospheric Environment,** 35: 3749 – 3760.

Borge, R., Lumbreras, J., Vardoulakis, S., Kassomenos, P., Rodriguez, E. (2007) Analysis of long-range transport influences on urban PM10 using two-stage atmospheric trajectory clusters. **Atmospheric Environment,** 41: 4434 – 4450.

Brankov, E., Rao, S.T., Porter, P.S. (1998) A Trajectory-clustering-correlation methodology for examining the long-range transport of air pollutans. **Atmospheric Environment,** 32: 1525 – 1534.

Brook JR, Dann TF, Burnett RT (1997) The relationship among TSP, PM_{10}, $PM_{2.5}$, and inorganic constituents of atmospheric particulate matter at multiple Canadian locations, **Journal of the Air & Waste Management Association,** 47: 2-19.

Buchanan, C.M., Beverland, I.J., Heal, M.R. (2002) The influence of weather-type and long-range transport on air particle concentration in Edinburgh, UK. **Atmospheric Environment,** 36: 5343 – 5354.

Calvert, J.G. and Stockwell, W.R. (1983) Acid generation in the troposphere by gas-phase chemistry. **Environmental Science and Technology,** 17: 428A – 443A.

Cavalli, F., Viana, M., Yttri, K.E., Genberg, J. and Putaud, J.P. (2010) Toward a standardized thermal-optical protocol for measuring atmospheric organic and elemental carbon: the EUSAAR protocol. **Atmospheric Measurement Techniques,** 3: 79-89.

Cecinato, A., Amati, B., Palo, V.D., Marino, F., Possanzini, M. (1999) Determination of short-chain organic acids in airborne aerosols by ion chromatography. **Chromatographia,** 50: 670 – 672.

Chebbi, A. and Carlier, P. (1996) Carboxylic acids in the troposphere, occurrence, sources, and sinks: a review. **Atmospheric Environment**, 30 (24): 4233 – 4249.

Chow, J.C., Watson, J.G., Fujita, E.M., Lu, Z., Lawson, D.R. (1994) Temporal and Spatial Variations of $PM_{2.5}$ and PM_{10} Aerosol in the southern California Air Quality Study. **Atmospheric Environment,** 28: 2016 – 2080.

Chow, J.C., Watson, J.G., Lu. Z., Lowenthal, D.H., Frazier, C.A., Solomon, P.A., Thuillier, R.H., Magliano, K. (1996). Descriptive analysis of $PM_{2.5}$ and PM_{10} at regionally representative locations during SJVAQSrAUSPEX. **Atmospheric Environment,** 30: 2079 – 2112.

Clarke, A.G., Azadi-Boogar, G.A., Andrews, G.E. (1999) Particle size and chemical composition of urban aerosols. **The Science of the Total Environment,** 235: 15 – 24.

Dabek-Zlotorzynska, E. and McGrath, M. (2000) Determination of low-molecular-weight carboxylic acids in the ambient air and vehicle emission: a review. **Fresenius' Journal of Analytical Chemisrty**, 367: 507-518.

Deng, C., Zhuang, G., Huang, K., Li, J., Zhang, R., Wang, Q., Sun, Y., Guo, Z., Wang, Z. (2010) Chemical characterization of aerosols at the summit of Mountain Tai in the middle of central east China. **Atmospheric Chemistry and Physics Discussions,** 10: 20975 – 21021.

Dorling, S.R., Davies, T.D., Pierce, C.E. (1992) Cluster analysis: a technique for estimating the synoptic meteorological controls on air and precipitation chemistry- method and applications. **Atmospheric Environment,** 26A: 2575 – 2581.

Draxler, R.R. and Hess, G.D. (1997) Description of the HYSPLIT_4 modelling system. **NOAA Technical Memorandum ERL ARL-224**, December, 24pp.

Draxler, R.R. and Hess, G.D. (1998) An overview of the HYSPLIT_4 modelling system for trajectories, dispersion, and deposition. **Australian Meteorological Magazine**, 47: 295 – 308.

Dutton, J.A. (1986) The ceaseless wind. An introduction to the theory of atmospheric motion. Dover, New York.

Dutton, M.V. and Evans, C.S. (1996) Oxalate production by fungi: its role in pathogenicity and ecology in the soil environment. **Canadian Journal of Microbiology**, 42: 881 – 895.

Eldred, R.A., Cahill, T.A., Floccini, R.G. (1997) Composition of $PM_{2.5}$ and PM_{10} aerosols in the IMPROVE network. **Journal of the Air & Waste Management Association,** 47: 194 – 203.

Ervens, B., Feingold, F., Frost, G.J., Kreidenweis, S.M. (2004) A modeling study of aqueous production of dicarboxylic acids:1. Chemical pathways and speciated organic mass production. **Journal of Geophysical Research – Atmospheres,** 109: D15205.

Facchini, M.C., Mircea, M., Fuzzi, S., Charlson, R.J. (1999) Cloud albedo enhancement by surface-active organic solutes in growing droplets. **Nature,** 401: 257 – 259.

Falkovich, A.H., Graber, E.R., Schkolnik, G., Rudich, Y., Maenhaut, W., Artaxo, P. (2004) Low molecular weight organic acids in aerosol particles from Rondonia, Brazil, during the biomass-burning, transition and wet periods. **Atmospheric Chemistry and Physics Discussions,** 4: 6867-6907.

Finlayson-Pitts, B.J. and Pitts, J.N. (1986) **Atmospheric Chemistry: Fundamentals and Experimental Techniques**. New York, John Wiley and Sons.

Fitz, D.R. (1990) Reduction of the positive organic artifact on quartz filters. **Aerosol Science and Technology,** 12(1): 142 – 148.

Fosco, T. and Schmeling, M. (2007) Determination of water-soluble atmospheric aerosols using ion chromatography. **Environmental Monitoring and Assessment,** 130: 187-199.

Gadd, G.M. (1999) Fungal production of citric and oxalic acid: importance in metal speciation, physiology and biogeo-chemical processes. **Advances in Microbial Physiology,** 41: 47 – 92.

Graham, B., Mayol-Bracero, O.L., Guyon, P., Roberts, G.C., Decesari, S., Facchini, M.C., Artaxa, P., Maenhaut, W., Koll, P., Andreae, M.O. (2002) Water-soluble organic compounds in biomass buring aerosols over Amazonia. **Journal of Geophysical Research,** 107: 8047.

Guo, S., Hu, M., Wang, Z.B., Slanina, J., Zhao, Y.L. (2010) Size-resolved aerosol water-soluble ionic compositions in the summer of Beijing: implication of regional secondary formation. **Atmospheric Chemistry and Physics**, 10: 947 – 959.

Gustafsson, M.E.R. and Franzen, L.G. (2000) Inland transport of marine aerosols in southern Sweden. **Atmospheric Environment,** 34: 313 – 325.

Harrison, R.M. and Jones, M. (1995) The chemical composition of airborne particles in the UK atmosphere. **The Science of the Total Environment,** 168: 195 – 214.

Harrison, R.M. and Kitto, A.M.N. (1992) Estimation of the Rate Constant for the Reaction of Acid Sulphate Aerosol with NH3 Gas from Atmospheric Measurements. **Journal of Atmospheric Chemistry,** 15: 133 – 143.

Harrison, R.M. and Mora, S.J. (1996) **Introductory chemistry for the environmental sciences.** 2nd ed. Cambridge, Cambridge University Press.

Harrison, R.M. and Pio C.A. (1983) Major ion chemical composition and chemical associations in inorganic atmospheric aerosols. **Environmental Science and Technology,** 17: 169-174.

Harrison, R.M. and Pio, C.A. (1983) Major ion chemical composition and chemical associations in inorganic atmospheric aerosols **Environmental Science & Technology,** 17: 169 – 174.

Harrison, R.M. and Yin, J. (2000) Particulate matter in the atmosphere: which particle properties are important for its effects on health?. **The Science of the Total Environment,** 249: 85 – 101.

Harrison, R.M. and Yin, J. (2008) Sources and processes affecting carbonaceous aerosol in central England. **Atmospheric Environment,** 42: 1413-1423.

Harrison, R.M., Deacon, A.R., Jones, M.R., Appleby, R.S. (1997) Sources and processes affecting concentrations of PM10 and PM2.5 in Birmingham, UK. **Atmospheric Environment,** 31: 4103 – 4117.

Harrison, R.M., Jones, A.M. and Lawrence, R.G. (2003) A pragmatic mass closure model for airborne particulate matter at urban background and roadside sites. **Atmospheric Environment,** 37: 4927-4933.

Harrison, R.M., Laxen, D., Moorcroft, S., Laxen, K. (2012) Process affecting concentrations of fine particulate matter ($PM_{2.5}$) in the UK atmosphere. **Atmospheric Environment,** 46: 115 – 124.

He, N. and Kawamura, K. (2010) Distributions and diurnal changes of low molecular weight organic acids and α-dicarbonyls in suburban aerosols collected at Mangshan, North China, **Geochemical Journal**, 44: e17 – e22.

Hegg, D.A., Gao, S., Jonsson, H. (2002) Measurements of selected dicarboxylic acids in marine cloud water. **Atmospheric Research,** 62: 1–10.

Herner, J.D., Ying, Q., Aw, J., Gao, O., Chang, D.P.Y., Kleeman, M. (2006) Dominant mechanisms that shape the airborne particle size and composition in central California. **Aerosol Science and Technology,** 40: 827–844.

Hinds, W. C. (1999) **Aerosol Technology: properties, behavior, and measurement of airborne particles.** 2nd ed. New York, John Wiley & Sons.

Hinds, W.C. (2001) "Physical and chemical changes in the particulate phase." In Baron, P.A. and Willeke, K. 2nd ed. **Aerosol measurement principles, techniques, and applications,** New York, John Wiley & Sons.

Ho, K.F., Ho, S.S.H., Lee, S.C., Kawamura, K., Zou, S.C., Cao, J.J., Xu, H.M. (2011) Summer and winter variations of dicarboxylic acids, fatty acids and benzoic acid in $PM_{2.5}$ in Pearl Delta River Region, China. **Atmospheric Chemistry and Physics,** 11: 2197 – 2208.

Hsieh, L.-Y., Chen, C.-L., Wan, M.-W., Tsai, Y.I. (2008) Speciation and temporal characterization of dicarboxylic acids in $PM_{2.5}$ during a PM episode and a period of non-episodic pollution. **Atmospheric Environment,** 42: 6836–6850.

Hu, L. (2011) *personal communication*. Division of Environmental Health and Risk Management, School of Geography, Earth and Environmental Sciences, University of Birmingham. The United Kingdom

Hu, M., He, L.Y., Zhang, Y.H., Wang, M., Kim, Y.P., Moon, K.C. (2002) Seasonal variation of ionic species in fine particles at Qingdao, China. **Atmospheric Environment,** 36: 5853 – 5859.

Huang, X.F. and Yu, J.Z. (2007) Is vehicle exhaust a significant primary source of oxalic acid in ambient aerosols? **Geophysical Research Letters,** 34: L02808.

Huang, X.F., Hu, M., He, L.Y., Tang, X.Y., (2005) Chemical characterization of water-soluble organic acids in $PM_{2.5}$ in Beijing, China. **Atmospheric Environment,** 39: 2819 – 2827.

Huang, X.F., Yu, J.Z., He, L.Y., Yuan, Z. (2006) Water-soluble organic carbon and oxalate in aerosols at a coastal urban site in China: Size distribution characteristics, sources, and formation mechanisms. **Journal of Geophysical Research,** 111: D22212.

Hughes, L.S., Cass, G.R., Gone, J., Ames, M., Olmez, I. (1998) Physical and chemical characterization of atmospheric ultra fine particles in the Los Angles area. **Environmental Science and Technology,** 32: 1153 – 1161.

Ion, A.C., Vermeylen, R., Kourtchev, I., Cafmeyer, J., Chi, X., Gelencser, A., Maenhaut, W., Claeys, M. (2005) Polar organic compounds in rural PM2.5 aerosols from K-puszta, Hungary, during a 2003 summer field campaign: Sources and diel variations. **Atmospheric Chemistry and Physics,** 5: 1805 – 1814.

Jacobson, M.C., Hansson, H-C, Noone, K.J., Charlson, R.J. (2000) Organic atmosphere aerosols: review and state of the science. **Reviews of Geophysics,** 38: 267 – 294.

Jaffrezo, J.-L., Aymoz, G., Cozic, J. (2005) Size distribution of EC and OC in the aerosol of Alpine valleys during summer and winter. **Atmospheric Chemistry and Physics,** 5: 2915 – 2925.

Jaffrezo, J-L, Davidson, C.I., Kuhns, H.D., Bergin, M.H., Hillamo, R., Maenhaut, W., Kahl, J.W., Harris, J.M. (1998) Biomass burning signatures in the atmosphere of central Greenland. **Journal of Geophysical Research,** 103: 31067 – 31078.

JCGM 100:2008 (2010) "GUM 1995 with minor corrections: Evaluation of measurement data – Guide to the expression of uncertainty in measurement" [online] Available from: *http://www.bipm.org/utils/common/documents/jcgm/JCGM_100_2008_E.pdf* [Accessed 20 March 2012].

John, W. (2001) "Size distribution characteristics of aerosols." In Baron, P.A. and Willeke, K. 2nd ed. **Aerosol measurement principles, techniques, and applications,** New York, John Wiley & Sons.

John, w., Wall, S.M., Ondo, J.L, Winklmayr, W. (1990) Modes in the size distributions of atmospheric inorganic aerosol. **Atmospheric Environment,** 24: 2349 – 2359.

Jones, D.L. (1998) Organic acids in the rhizosphere – a critical review. **Plant Soil**, 205: 25 – 44.

Kalberer, M., Seinfeld, J.H., Yu, J.Z., Cocker, D.R., Morrical, B., Zenobi, R. (2001) Composition of SOA from cyclohexene oxidation and involved heterogeneous reactions. **Journal of Aerosol Science,** 32: s907 – s908.

Kaneyasu, N., Yoshikado, H., Mizuno, T., Sakamoto, K., Soufuku, M. (1999) Chemical forms and sources of extremely high nitrate and chloride in winter aerosol pollution in Kanto plain of Japan. **Atmospheric Environment,** 33: 1745–1756.

Karthikeyan, S. and Balasubramanian, R. (2005) Rapid extraction of water soluble organic compounds from airborne particulate matter. **Analytical Sciences,** 21: 1505 – 1508.

Kawamura, K. and Ikushima, K. (1993) Seasonal changes in the distribution of dicarboxylic acids in the urban atmosphere. **Environmental Science and Technology,** 27: 2227 – 2235.

Kawamura, K. and Kaplan, I.R. (1987) Motor exhaust emissions as a primary source for dicarboxylic acids in Los Angeles ambient air. **Environmental Science and Technology,** 21: 105-110.

Kawamura, K. and Usukura, K. (1993) Distributions of low molecular weight dicarboxylic acids in the North Pacific aerosol samples. **Journal of Oceanography**, 49: 271 – 283.

Kawamura, K., Barrie, L.A., Toom-Sauntry, D. (2010) Intercomparison of the measurements of oxalic acid in aerosols by gas chromatography and ion chromatography. **Atmospheric Environment,** 44: 5316 – 5319.

Kawamura, K., Kasukabe, H., Barrie, L.A. (1996) Source and reaction pathways of dicarboxylic acids, ketoacids and dicarbonyls in arctic aerosols: One year of observations. **Atmospheric Environment,** 30: 1709 – 1722.

Kerminen, V.M and Wexler, A.S. (1995) Growth laws for atmospheric aerosol particle: an examination of the bimodality of the accumulation mode. **Atmospheric Environment,** 29: 3263 – 3275.

Kerminen, V.M., Aurela, M., Hillamo, M., Virkkula, R. (1997) Formation of particulate MSA: deductions from size distribution measurements in Finnish Arctic. **Tellus,** 49B: 159 – 171.

Kerminen, V.M., Teinila, K., Hillamo, R., Makela, T. (1999) Size-segregated chemistry of particulate dicarboxylic acids in the Arctic atmosphere. **Atmospheric Environment,** 33: 2089 – 2100.

Kerminent, V.M., Ojanen, C., Pakkanen, T., Hillamo, R., Aurela, M., Merilainen, J. (2000) Low-molecular-weight dicarboxylic acids in an urban and rural atmosphere. **Journal of Aerosol Science,** 31: 349 – 362.

Khwaja, H.A. (1995) Atmospheric concentrations of carboxylic acids and related compounds at a semiurban site. **Atmospheric Environment,** 29: 127 – 139.

Kirchstetter, T.W,, Corrigan, C.E., Novakov, T. (2001) Laboratory and field investigation of the adsorption of gaseous organic compounds onto quartz filters. **Atmospheric Environment,** 35: 1663 – 1671.

Kiss, G., Gelencser, A., Krivacsy, Z., Hlavay, J. (1997) Occurrence and determination of organic pollutants in aerosol, precipitation, and sediment samples collected at Lake Balaton. **Journal of Chromatography,** A 774: 349 – 361.

Kitto, A.M.N. and Harrison, R.M. (1992) Processes affecting concentrations of aerosol strong acidity at sites in eastern England. **Atmospheric Environment,** 26A: 2389 – 2399.

Kleeman, M.J., Schauer, J.J., Cass, G.R. (1999) Size and composition distribution of fine particulate matter emitted from wood burning, meat charbroiling and cigarettes. **Environmental Science and Technology,** 33: 3516 – 3523.

Kleeman, M.J., Schauer, J.J., Cass, G.R. (2000) Size and composition distribution of fine particulate matter emitted from motor vehicles. **Environmental Science and Technology,** 34 (7): 1132–1142.

Krivacsy, Z., Gelencser, A., Kiss, G., Meszaro, E.O., Molnar, A, Hoffer, A., Meszaro T., Sarvari, Z., Temesi, D., Varga, B., Baltensperger, U., Nyeki, S., Weingartner, E. (2001) Study on the chemical character of water soluble organic compounds in fine atmospheric aerosol at the Jungfrajoch. **Journal of Atmospheric Chemistry**, 39: 235 – 259.

Kundu, S., Kawamura, K., Andreae, T. W., Hoffer, A., Andreae, M. O. (2010) Molecular distributions of dicarboxylic acids, ketocarboxylic acids and _-dicarbonyls in biomass burning aerosols: implications for photochemical production and degradation in smoke layers. **Atmospheric Chemistry and Physics,** 10: 2209 – 2225.

Kundu, S., Kawamura, K., Lee, M., Andreae, T. W., Hoffer, A., Andreae, M. O.(2010) Comparison of Amazonian biomass burning and East Asian marine aerosols: Bulk organics, diacids and related compounds, water-soluble inorganic ions, stable carbon and nitrogen isotope ratios. **Low Temperature Science,** 68: 89 – 100.

Laden, F., Schwartz, J., Speizer, F.E., Dockery, D.W. (2006) Reduction in fine particulate air pollution and mortality: extended follow-up of the Harvard Six Cities study. **American Journal of Respiratory and Critical Care Medicine,** 173: 667 – 672.

Lefer, B.L. and Talbot, R.W. (2001) Summertime measurements of aerosol nitrate and ammonium at a northeastern U.S. site. **Journal of Geophysical Research,** 106: 20365 – 20378.

Legrand, M., Preunkert, S., Oliveira, T., Pio, C.A., Hammer, S., Gelencser, A., Kasper-Giebl, A., Laj, P. (2007) Origin of $C_2 - C_5$ dicarboxylic acids in the European atmosphere inferred from year-round aerosol study conducted at a west-east transect. **Journal of Geophysical Research,** 112: D23S07.

Lim, H.J., Carlton, A.G., Turpin, B.J. (2005) Isoprene forms secondary organic aerosol through cloud processing: model simulations. **Environmental Science and Technology,** 39: 4441 – 4446.

Limbeck, A. and Puxbaum, H. (1999) Organic acids in continental background aerosols. **Atmospheric Environment**, 33: 1847 – 1852.

Limbeck, A., Kraxner, Y., Puxbaum, H. (2005) Gas to particle distribution of low molecular weight dicarboxylic acids at two different sites in central Europe (Austria). **Journal of Aerosol Science**, 36: 991 – 1005.

Limbeck, A., Puxbaum, H., Otter, L., Scholes, M.C. (2001) Semivolatile behavior of dicarboxylic acids and other polar organic species at a rural background site (Nylsvley, RSA). **Atmospheric Research,** 35: 1853 – 1862.

Matsumoto, K., Nagao, I., Tanaka, H., Miyaji, H., Iida, T., Ikebe, Y. (1998) Seasonal characteristics of organic and inorganic species and their size distributions in atmospheric aerosols over the northwest Pacific Ocean. **Atmospheric Environment**, 32 (11): 1931 – 1946.

Matthias-Maser, S. and Jaenicke, R. (1994) Examination of atmospheric bioaerosol particles with radii > 0.2 μm. **Journal of aerosol Science,** 25: 1605 – 1613.

Matthias-Maser, S. and Jaenicke, R. (2000) The size distribution of primary biological aerosol particles in the multiphase atmosphere. **Aerobiological,** 16: 207 – 210.

Mayol-Bracero, O., Guyon, P., Graham, B., Roberts, G., Andreae, M.O., Decesari, S., Facchini, M.C., Fuzzi, S., Artaxo, P. (2002) Water soluble organic compounds in biomass burning aerosols over Amazonia: 2. Apportionment of the chemical composition and importance of the polyacidic fraction. **Journal of Geophysical Research,** 107: 8091.

McCulloch, R.B., Few, G.S., Murray, G.C., Aneja, V.P. (1998) Analysis of ammonia, ammonium aerosols and acid gases in the atmosphere at a commercial hog farm in eastern North Carolina, USA. **Environment Pollution,** 102: 263 – 268.

Meng, Z. and Seinfeld, J.H. (1994) On the source of the submicrometer droplet mode of urban and regional aerosols. **Aerosol Science and Technology,** 20: 253 – 265.

Mircea, M.A., Facchini, M.C., Decesari, S., Fuzzi, S., Charlson, R.J. (2002) The influence of the organic aerosol component on CCN supersaturation spectra for different aerosol types. **Tellus,** 54B: 74 – 81.

Miyazaki, Y., Aggarwal, S. G., Singh, K., Gupta, P. K., Kawamura, K. (2009) Dicarboxylic acids and water-soluble organic carbon in aerosols in New Delhi, India, in winter: Characteristics and formation processes. **Journal of Geophysical Research,** 114: D19206,

Mochida, M., Umemoto, N., Kawamura, K., Uematsu, M. (2003) Bimodal size distribution of C2-C4 dicarboxylic acids in the marine aerosols. **Geophysical Research Letters,** 30: 1672.

Moody, J.L., Galloway, J.N. (1988) Quantifying the relationship between atmospheric transport and the chemical composition of precipitation on Bermuda. **Tellus,** 40B: 463 – 479.

Morris, K.J. (1995) "Modern Microscopic Methods of Bioaerosol Analysis." In Cox, C.S. and Wathes, C.M. **Bioaerosols Handbook**, CRC Press: pp. 285 – 316.

Mueller, P.K., Fung, K.K., Heisler, S.L., Grosjean, D., Hidy, G.M. (1982) Atmospheric particulate carbon observations in urban and rural areas of the United States. In Wolff, G.T., Klimisch, R.L. (EDs.), **Particulate Carbon – Atmospheric Life Cycle.** Plenum Press, New York, pp. 343 – 370.

Müller, K. (1999) A three year study of aerosol in northwest Saxony (Germany), **Atmospheric Environment,** 33: 1679-1685.

Murillo, J.H., Marin, J.F.R., Roman, S.R., Martinez, R.G. (2010) Sulfate, nitrate and chloride in PM_{10} in the city of San Jose, Costa Rica: 2004-2006. **Atmosfera**, 23: 83 – 94.

Myriokefalitakis, S., Tsigaridis, K., Mihalopoulos, N., Sciare, J., Nenes, A., Kawamura, K., Segers, A., Kanakidou, M. (2011) In-cloud oxalate formation in the global troposphere: a 3-D modeling study. **Atmospheric Chemistry and Physics,** 11: 5761 – 5782.

Na, K., Sawant, A.A., Song, C. and Cocker III, D.R. (2004) Primary and secondary carbonaceous species in the atmosphere of Western Riverside County, Califonia. **Atmospheric Environment,** 38: 1345 – 1355.

National Research Council (2009) **Global sources of local pollution: An assessment of long-range transport of key air pollutants to and from the United States.** The national academies press.

Narukawa, M., Kawamura, K., Li, S.M., Bottenheim, J.W. (2002) Dicarboxylic acids in the Arctic aerosols and snowpacks collected during ALERT 2000. **Atmospheric Environment,** 36: 2491 – 2499.

Narukawa, M., Kawamura, K., Takeuchi, N., Nakajima, T. (1999) Distribution of dicarboxylic acids and carbon isopotic compositions in aerosols from 1997 Indonesian forest fires. **Geophysical Research Letters,** 26: 3101 – 3104.

Niemi, J.V., Saarikoski, S., Aurela, M., Tervahattu, H., Hillamo, R., Westphal, D.L., Aarnio, P., Koskentalo, T., Makkonen, U., Vehkamaki, H., Kulmala, M. (2009) Long-range transport episodes of fine particles in southern Finland. **Atmospheric Environment,** 43: 1255 – 1264.

Norton, R.B., Roberts, J.M., Huebert, B.J. (1983) Tropospheric oxalate. **Geophysical Research Letters**, 10: 517 – 520.

Novakov, T. and Penner, J.E. (1993) Large contribution of organic aerosols to cloud-condensation-nuclei concentrations. **Nature,** 365: 823-826.

NPL (2007) Report DQL-AS 037, CPEA 28: Airborne particulate concentrations and numbers in the United Kingdom (phase 2); Estimation of measurement uncertainty in network data, pp 1 – 20.

NTP (2011) Report on Carcinogens, Twelfth Edition. National Toxicology Program. P247.

Official Journal (2008) Directive 2008/50/EC of the European Parliament and the Council of 21 May 2008 on ambient air quality and cleaner air for Europe. **Official Journal of the European Union** [online] Available form; *http://eur-lex.europa.eu/LexUriServ/LexUriServ.do?uri=OJ:L:2008:152:0001:0044:EN:PDF* [Accessed 20 March 2012].

Pakkanen, T.A. (1996) Study of formation of coarse particle nitrate aerosol. **Atmospheric Environment,** 30: 2475–2482.

Pakkanen, T.A., Kerminen, V.M., Korhonen, C.H., Hillamo, R.E., Aarnio, P., Koskentalo, T., Maenhaut., W. (2001a) Urban and rural ultrafine ($PM_{0.1}$) particles in the Helsinki area. **Atmospheric Environment,** 35: 4593 – 4607.

Pakkanen, T.A., Kerminen, V.M., Korhonen, C.H., Hillamo, R.E., Aarnio, P., Koskentalo, T., Maenhaut, W. (2001b) Use of atmospheric elemental size distributions in estimation aerosol sources in the Helsinki area. **Atmospheric Environment,** 35: 5537 – 5551.

Park, S.S., Bae, M.S., Schauer, J.J., Kim, Y.J., Cho, S.Y., Kim, S.J. (2006) Molecular composition of $PM_{2.5}$ organic aerosol measured at an urban site of Korea during the ACE-Asia campaign. **Atmospheric Environment,** 40: 4182 - 4198.

Parmar, R.S., Satsangi, G.S., Kumari, M., Lakhani, A., Srivastava, S.S., Prakash, S. (2001) Study of size distribution of atmospheric aerosol at Agra. **Atmospheric Environment,** 35: 693 – 702.

Pasquill, F. (1961) The estimation of the dispersion of wind borne material. **Meteorological Magazine**, 90: 34 – 49.

Pavuluri, C. M., Kawamura, K., Swaminathan, T.(2010) Water-soluble organic carbon, dicarboxylic acids, ketoacids, and α-dicarbonyls in the tropical Indian aerosols. **Journal of Geophysical Research,** 115: D11302.

Pio, C., Cerqueira, M., Harrison, R.M., Nunes, T., Mirante, F., Alves, C., Oliveira, C. de la Campa, A.S., Artinano, B., Matos, M. (2011) OC/EC ratio observations in Europe: Re-thinking the approach for apportionment between primary and secondary organic carbon. **Atmospheric Environment,** doi:10.1016/j.atmosenv.2011.08.045.

Poore, M. W. (2000) Oxalic acid in $PM_{2.5}$ particulate matter in California. **Journal of the Air & Waste Management Association,** 50: 1874 – 1875.

Putaud, J-P., Raes, F., Dingenen, R.V., Bruggemann, E., Facchini, M-C., Decesari, S., Fuzzi, S., Gehrig, R., Huglin, C., Laj, P., Lorbeer, G., Maenhaut, W., Mihalopoulos, N., Muller, K. Querol, X., Rodriguez, S., Schneider, J., Spindler, G., Brink, H., Torseth, K., Wiedensohle, A. (2004) A European aerosol phenomenology – 2: chemical characteristics of particulate matter at kerbside, urban, rural and background sites in Europe. **Atmospheric Environment,** 38: 2579 – 2595.

Putaud, J-P., Van Dingenen, R., Alastuey, A., Bauer, H., Birmili, W., Cyrys, J., Flentje, H., Fuzzi, S., Gehrig, R., Hansson, H.C., Harrison, R.M., Herrmann, H., Hitzenberger, R., Huglin, C., Jones, A.M., Kasper-Giebl, A., Kiss, G., Kousa, A., Kuhlbusch, T.A.J., Loschau, G., Maenhaut, W., Molnar, A., Moreno, T., Pekkanen, J., Perrino, C., Pitz, M., Puxbaum, H., Querol, X., Rodriguez, S., Salma, I., Schwarz, J., Smolik, J., Schneider, J., Spindler, G., ten Brink, H., Tursic, J., Viana, M., Wiedensohler, A., Raes, F. (2010) A European Aerosol Phenomenology – 3: Physical and Chemical Characteristics of Particulate Matter from 60 Rural, Urban, and Kerbside Sites Across Europe, **Atmospheric Environment,** 44: 1308 – 1320.

Qin, Y., Chan, C.K., Chan, L.Y. (1997) Characteristics of chemical compositions of atmospheric aerosols in Hong Kong: spatial and seasonal distributions. **Science of the Total Environment,** 206: 25 – 37.

QUARG (1996) Airborne particulate matter in the United Kingdom. **Third Report of the Quality of Urban Air Review Group,** Department of the Environment, London.

Rebecca, J.K., Mason Jr., R.M., Heilig, C.M., Neas, L.M., Dockery, D.W. (2000) Is daily mortality associated specifically with fine particles? Data reconstruction and replication of analyses. **Journal of the Air & Waste Management Association,** 50: 1215 – 1222.

Remer, L.A., Kaufman, B.N., Holben, A., Thompson, M., McNamara, D. (1998) Biomass burning aerosol size distribution and modeled optical properties. **Journal of Geophysical Research,** 103: 31879 – 31891.

Riemer, N., Vogel, H., Vogel, B, Schell, B., Ackermann, I., Kessler, C. Hass, H. (2003) Impact of the heterogeneous hydrolysis of N2O5 on chemistry and nitrate aerosol formation in the lower troposphere under photosmog conditions. **Journal of Geophysical Research,** 108: 4144.

Rohrl, A. and Lammel, G. (2001) Low-molecular weight dicarboxylic acids and glyoxylic acids: seasonal and air mass charactheristics. **Environmental Science and Technology,** 35: 95 – 101.

Russell, A.G., McRae, G.J., Cass, G.R. (1983) Mathematical modeling of the formation and transport of ammonium nitrate aerosol. **Atmospheric Environment,** 17: 949 – 964.

Russell, L.M. and Seinfeld, J.H. (1998) Size and composition-resolved externally mixed aerosol model. **Aerosol Science and Technology,** 28: 403 – 416.

Saarnio, K., Aurela, M., Timonen, H., Saarikoski, S., Teinila, K.,Makela, T., Sofiev, M., Koskinen, J., Aalto, P. P., Kulmala, M., Kukkonen, J., Hillamo, R. (2010) Chemical composition of fine particles in fresh smoke plumes from boreal wild-land fires in Europe. **Science of the Total Environment,** 408: 2527– 2542.

Salvador, P., Artinano, B., Pio, C., Afonso, J., Legrand, M., Puxbaum, H., Hammer, S. (2010) Evaluation of aerosol sources at European high altitude background sites with trajectory statistical methods. **Atmospheric Environment,** 44: 2316 – 2329.

Sarvari, Zs., Krivacsy, Z., Baltensperger, U., Nyeki, S., Weingartner, E., Wessel, S., Jennings, S. G. (1999) Low-molecular weight carboxylic acids in atmospheric aerosol at different European sites. **Journal of Aerosol Science,** 30: S261–S262.

Saxena, P. and Hildemann, L.M. (1996) Water-soluble organics in atmospheric particles: A critical review of the literature and application of thermodynamics to identify candidate compounds. **Journal of Atmospheric Chemistry,** 24: 57 – 109.

Schauer, J.J., Kleeman, M.J., Cass, G.R., Simoneit, B.R.T. (2001) Measurement of emissions from air pollution sources. 3. C1-C29 organic compounds from fireplace combustion of wood. **Environmental Science and Technology,** 35: 1716 - 1728.

Schmidl, C., Marr, I. L. Caseiro, A., Kotianova, P., Berner, A., Bauer, H., Kasper-Giebl, A., Puxbaum, H. (2008) Chemical characterization of fine particle emissions from wood stove combustion of common woods growing in mid-European Alpine regions. **Atmospheric Environment,** 42: 126 – 141.

Schwartz, J., Dockery, D.W., Neas, L.M. (1996) Is daily mortality associated specifically with fine particles? **Journal of the Air & Waste Management Association,** 46: 927 – 939.

Schwartz, S.E. (1987) “Aqueous-phase reactions in clouds.” In John, R.W. and Gordon, G.E. **American chemical society, symposium series, the chemistry of acid rain: source and atmospheric processes**, Washington, D.C.

See, W.S., Balasubramaanian, R., Rianawati, E., Karthikeyan, S., Streets, D. (2007) Characterization and source apportionment of particulate matter ≤ 2.5 μm in Sumatra, Indonesia, during a recent peat fire episode. **Environmental Science and Technology,** 41: 3488 – 3494.

Seinfeld, J.H. and Pandis, S.N. (1998) **Atmospheric chemistry and physics from air pollution to climate change.** New York: John Wiley & Sons, Inc.

Seinfeld, J.H. and Pankow, J.F. (2003) Organic atmospheric particulate material. **Annual Review of Physical Chemistry,** 54: 121 – 140.

Sempere, R. and Kawamura K. (1994) Comparative distribution of dicarboxylic acids and related polar compounds in snow, rain, and aerosols from urban atmosphere. **Atmospheric Environment,** 28: 449 – 459.

Sempere, R. and Kawamura K. (1996) Low molecular weight dicarboxylic acids and related polar compounds in the remote marine rain samples collected from western Pacific. **Atmospheric Environment,** 30: 1609 – 1619.

Simpson, S., Guenther, A., Hewitt, C.N., Steinbrecher, R. (1995), Biogenic emissions in Europe: 1. Estimates and uncertainties. **Journal of Geophysical Research,** 100: 22,875–22,890.

Smekens, A., Godoi, R.H.M., Berghmans, P., Van Grieken, R. (2005) Characterization of soot emitted by domestic heating, aircraft and cars using diesel or biodiesel. **Journal of Atmospheric Chemistry,** 52: 45 – 62.

Smith, D.J.T., Harrison, R.M., Luhana, L., Pio, C.A., Castro, L.M., Tariq, M.N., Hayat, S., Quraishi, T. (1996) Concentrations of particulate airborne polycyclic aromatic hydrocarbons and metals collected in Lahore, Pakistan. **Atmospheric Environment,** 30: 4031 – 4040.

Solomon, S.,Qin, D., Manning, M., Chen, Z., Marquis, M., Averyt, K.B., Tignor, M., Miller, H.L. (2007) **Climate Change 2007: The Physical Science Basis** [online]. Cambridge University Press. Available from IPCC. [online] Available from: *http://www.ipcc.ch/publications_and_data/publications_ipcc_fourth_assessment_report_wg1_report_the_physical_science_basis.htm* [Accessed 20 March 2012].

Souza, S.R., Vasconcellos, P.C., Carvalho, L.R.F. (1999) Low molecular weight carboxylic acids in an urban atmosphere: Winter measurement in Sao Paulo City, Brazil. **Atmospheric Environment,** 33: 2563 – 2574.

Statutory Instruments (2010) The Air Quality Standards Regulations 2010. **2010 No.1001 Environmental Protection**. [online] Available form; *http://www.legislation.gov.uk/uksi/2010/1001/pdfs/uksi_20101001_en.pdf* [Accessed 20 March 2012].

Stein, A. and Lamb, D. (2003) Empirical evidence for the low- and high-NO_x photochemical regimes of sulfate and nitrate formation. **Atmospheric Environment** 37, 3615 – 3625.
Stockwell, W.R. and Calvert, J.G. (1983) The mechanism of the HO-SO_2 reaction. **Atmospheric Environment,** 17: 2231 – 2235.

Stohl, A. (1998) Computation, accuracy and applications of trajectories - a review and bibliography. **Atmospheric Environment,** 32: 947 – 966.

Stone, E. A., Hedman, C. J., Zhou, J., Mieritz, M., Schauer, J.J. (2010) Insights into the nature of secondary organic aerosol in Mexico City during the MILAGRO experiment 2006. **Atmospheric Environment,** 44: 312 – 319.

Strader, R., Lurmann, F., Pandis, S.N. (1999) Evaluation of secondary organic aerosol formation in winter. **Atmospheric Environment,** 33: 4849 – 4863.

Stull, R.B. (1950) **An introduction to boundary layer meteorology.** Dordrecht; London: Kluwer Academic Publishers.

Sullivan, A.P., Weber, R.J., Clements, A.L., Turner, J.R., Bae, M.S., Schauer, J.J. (2004) A method for on-line measurement of water-soluble organic carbon in ambient aerosol particles: results from an urban site. **Geophysical Research Letter,** L13105.

Sun, J. M. and Ariya, P. A. (2006) Atmospheric organic and bio-aerosols as cloud condensation nuclei (CCN): A review. **Atmospheric Environment,** 40: 795 – 820.

Sunset Laboratory Inc. (2004) **A Guide to running and maintaining the sunset laboratory OCEC analyser,** February, 2.

Swietlicki, E., Puri, S., Hansson, H.C., Edner, H. (1996) Urban air pollution source apportionment using a combination of aerosol and gas monitoring techniques. **Atmospheric Environment,** 30: 2795 – 2809.

Taalman R. (1996) Isoprene: Background and issues. **Toxicology,** 113: 242 – 246.

Thorpe, A. and Harrison, R.M. (2008) Source and properties of non-exhaust particulate matter from road traffic: a review. **Science of the Total Environment,** 400: 270 – 282.

Tran, N.K., Steinberg, S.M., Johnson, B.J. (2000) Volatile aromatic hydrocarbons and dicarboxylic acid concentrations in air at an urban site in the Southwestern US. **Atmospheric Environment,** 34: 1845 – 1852.

U.S. EPA. (1996) EPA-452_R-96-013. Review of the Ambient Air Quality Standard for Particulate Matter: Policy Assessment of Scientific and Technical Information. **OAQPS Staff Paper,** Research Triangle Park. North Carolina

U.S. EPA (2006) EPA QA/G-9S; Data quality assessment: Statistical methods for practitioners. United States. [online] Available from: *http://www.epa.gov/quality/qs-docs/g9s-final.pdf* [Accessed 20 March 2012].

U.S. EPA (2009) EPA/600/R-08/139F Integrated Science Assessment for Particulate Matter (Final Report). **U.S. Environmental Protection Agency,** Washington, DC.

U.S. EPA (2012) BCES: Module 3 – Characteristics of particles. United States. [online] Available from: *http://www.epa.gov/apti/bces/module3/index.htm* [Accessed 20 March 2012].

Wang, G., Niu, S., Liu, C., Wang, L. (2002) Identification of dicarboxylic acids and aldehydes of PM10 and PM2.5 aerosols in Nanjing, China. **Atmospheric Environment,** 36: 1941 – 1950.

Wang, G., Xie, M., Hu, S., Gao, S., Tachibana, E., Kawamura,K. (2010) Dicarboxylic acids, metals and isotopic compositions of Cand N in atmospheric aerosols from inland China: implications for dust and coal burning emission and secondary aerosol formation. **Atmospheric Chemistry and Physics,** 10: 6087 – 6096.

Wang, Y., Zhuang, G., Chen, S., An, Z., Zhen, A. (2007) Characteristics and sources of formic, acetic and oxalic acids in $PM_{2.5}$ and PM_{10} aerosols in Beijing, China. **Atmospheric Research,** 84: 169 – 181.

Wang, Y., Zhuang, G., Tang, A., Yuan, H., Sun, Y., Chen, S., Zheng, A. (2005) The ion chemistry and the source of $PM_{2.5}$ aerosol in Beijing. **Atmospheric Environment,** 39: 3771 – 3784.

Wang, Y., Zhuang, G., Tang, A., Yuan, H., Sun, Y., Chen, S., Zheng, A. (2005) The ion chemistry and the source of $PM_{2.5}$ aerosol in Beijing. **Atmospheric Environment,** 39: 3771– 3784.

Warneck, P. (2003) In-cloud chemistry opens pathway to the formation of oxalic acid in the marine atmosphere. **Atmospheric Environment,** 37: 2423 – 2427.

Watts, S. and Halliwell (1996) **Essential environmental science; Methods & Techniques**, London, TJ Press (Padstow) Ltd.

Whitby, K.T. (2007) The physical characteristics of sulfur aerosols. **Atmospheric Environment,** 41: S25 – S49.

Wojcik, G.S., Chang, J.S. (1997) A re-evaluation of sulfur budgets, lifetimes, and scavenging ratios for eastern north America. **Journal of Atmospheric Chemistry,** 26: 106 – 145.

Yamasoe, M. A., Artaxo, P., Miguel, A. H., Allen, A. G. (2000) Chemical composition of aerosol particles from direct emissions of vegetation fires in the Amazon Basin: water-soluble species and trace elements. **Atmospheric Environment,** 34: 1641 – 1653.

Yang, H., Li, Q., Yu, J.Z. (2003) Comparison of two methods for the determination of water-soluble organic carbon in atmospheric particles. **Atmospheric Environment,** 37: 865-870.

Yang, H., Yu, J.Z., Ho, S.S.H., Xu, J., Wu, W.S., Wan, C.H., Wang, X., Wang, X., Wang, L., (2005) The chemical composition of inorganic and carbonaceous materials in $PM_{2.5}$ in Nanjing, China. **Atmospheric Environment,** 39: 3735 – 3749.

Yang, L. and Yu, L. (2008) Measurements of oxalic acid, oxalates, malonic acid, and malonates in atmospheric particulates. **Environmental Science and Technology,** 42(24): 9268-9275.

Yao, X, Fang, M., Chan, C.K., Ho, K.F., Lee, S.C. (2004) Characterization of dicarboxylic acids in PM2.5 in Hong Kong. **Atmospheric Environment,** 38: 963 – 970.

Yao, X., Chan, C.K., Fang, M., Cadle, S., Chan, T., Mulawa, P., He, K.,Ye, B. (2002) The water-soluble ionic composition of PM2.5 in Shanghai and Beijing, China. **Atmospheric Environment,** 36: 4223 – 4234.

Yao, X., Fang, M., Chan, C.K. (2002) Size distribution and formation of dicarboxylic acid in atmospheric particles. **Atmospheric Environment,** 36: 2099 – 2107.

Yao, X., Fang, M., Chan, C.K. (2002) Size distributions and formation of dicarboxylic acids in atmospheric particles. **Atmospheric Environment,** 36: 2099 – 2107.

Yao, X., Lau, A.P.S., Fang, M., Chan, C.K., Hu, M. (2003) Size distributions and formation of ionic species in atmospheric particulate pollutants in Beijing, China: 2-dicarboxylic acids. **Atmospheric Environment,** 37: 3001 – 3007.

Yin, J. (2002) Monitoring of airborne particulate mass and number concentrations in the UK atmosphere. **Thesis,** University of Birmingham.

Yin, J. and Harrison, R.M. (2008) Pragmatic mass closure study for PM1.0, PM2.5 and PM10 at roadside, urban background and rural sites. **Atmospheric Environment,** 42: 980 – 988.

Yin, J., Harrison, R.M., Chen, Q., Rutter, A. and Schauer, J.J. (2010) Source apportionment of fine particles at urban background and rural sites in the UK atmosphere. **Atmospheric Environment,** 44: 841 – 851.

Yu, J.Z., Huang, X.F., Xu, J., Hu, M. (2005) When aerosol sulfate goes up, so does oxalate: implication for the formation mechanisms of oxalate. **Environmental Science and Technology,** 39: 128 – 133.

Yu, S. (2000) Role of organic acids (formic, acetic, pyruvic and oxalic) in the formation of cloud condensation nuclei (CCN): A review. **Atmospheric Research,** 53: 185 – 217.

Yuan, H., Wang, Y., Zhuang, G. (2004) MSA in Beijing aerosol. **Chinese Science Bulletin,** 49: 1020 – 1025.

Zappoli, S., Andracchio, A., Fuzzi, S., Facchini, M.C., Gelencse, A., Kiss, G., Krivacsy, Z., Molnar, A. Meszaros, E., Hansson, H.C., Rosman, K., Zebuhr, Y. (1999) Inorganic, organic and macromolecular components of fine aerosol in different areas of Europe in relation to their water solubility. **Atmospheric Environment,** 33: 2733 – 2743.

Zhang, Q., Jimenez, J. L., Canagaratna, M. R., Allan, J. D., Coe, H., Ulbrich, I., Alfarra, M. R., Takami, A., Middlebrook, A. M., Sun, Y. L., Dzepina, K., Dunlea, E., Docherty, K., DeCarlo, P. F. , Salcedo, D., Onasch, T., Jayne, J. T. , Miyoshi, T., Shimono, A., Hatakeyama, S., Takegawa, N., Kondo, Y., Schneider, J., Drewnick, F., Borrmann, S., Weimer, S., Demerjian, K., Williams, P., Bower, K., Bahreini, R., Cottrell, L., Griffin, R. J., Rautiainen, J., Sun, J. Y., Zhang, Y. M., and Worsnop, D. R. (2007) Ubiquity and dominance of oxygenated species in organic aerosols in anthropogenically-influenced Northern Hemisphere midlatitudes, **Geophysical Research Letter,** 34: L13801.

Zhao, Y. and Gao, Y. (2008) Mass size distribution of water-soluble inorganic and organic ions in size-segregated aerosols over metropolitan Newark in the US east coast. **Atmospheric Environment,** 42: 4063 – 4078.

Zhuang, H., Chan, C.K., Fang, M., Wexler, A.S. (1999) Size distribution of particulate sulfate, nitrate, and ammonium at a coastal site in Hong Kong. **Atmospheric Environment,** 33: 843 – 853.

Zlotorynska, E.D., McGrath, M. (2000) Determination of low-molecular-weight carboxylic acids in the ambient air and vehicle emissions: a review. **Journal of Analytical Chemistry,** 367: 507 – 518.

Zlotorzynska, E.D. and McGranth, M. (2000) Determination of low-molecular-weight carboxylic acids in the ambient air and vehicle emissions: a review. **Journal of Analytical Chemistry,** 367: 507-518.

APPENDIX A

ESTIMATION OF MEASUREMENT UNCERTAINTY

Calculation of the measurement uncertainties associated with analysed data

The objective of estimation of measurement uncertainties associated with analysed data is to compare results from similar measurements, or the same system over time (method reproducibility and repeatability). The uncertainties of the results can be calculated in accordance with NPL report (2007) and JCGM 100:2008 (2010). In general, the result of a measurement is only an approximation or estimate of the value of the measurand and therefore, is complete only when accompanies by a statement of the uncertainty of that estimate. The uncertainty components basically divide into two categories based on their method of evaluation; a Type A and a Type B are associated with errors arising from random effects and know systematic effects, respectively. There are three important terms used in this calculation as following;

Standard uncertainty – uncertainty of the result of a measurement expressed as a standard deviation.

Combined standard uncertainty - standard uncertainty of the result of a measurement when that result is obtained from the values of a number of other quantities, equal to the positive square root of a sum of terms, the terms being the variances or covariances of these other quantities weighted according to how the measurement result varies with changes in these quantities.

Expanded uncertainty – quantity defining an interval about the result of a measurement that may be expected to encompass a large fraction of the districution of values that could reasonably be attributed to the measurand.

Organic carbon, elemental carbon and total carbon (OC, EC and TC)

The analytical method used to determine OC, EC and TC was detailed in chapter 2. The overall measurement equation for concentrations of OC, EC and TC in the ambient air is:

$$c_{air} = \frac{m}{V_{air}} \qquad \text{(Equation A.1)}$$

where c_{air} is the concentration of carbon fraction in the ambient air, μg m^{-3}, m is the mass of carbon on a filter, μg, V_{air} is the volume of air sample, m^{-3}

Partisol 2025 as mentioned in chapter 2 utilises a PM-10 inlet operating at 16.7 l min^{-1} (1 m^3 h^{-1}) to provide the initial D_{50} particle size cut-off at a 10 micron diameter. The virtual impactor is located after the inlet and two separate flow controllers maintain the coarse particle stream at 1.7 l min^{-1} and the fine particle stream at 15 l min^{-1}.

Then, the concentration of carbon in fine particle ($PM_{2.5}$) can be calculated as;

$$c_{PM_{2.5}} = \frac{m_f}{V_f} \qquad \text{(Equation A.2)}$$

where $c_{PM_{2.5}}$ is the concentration of carbon in fine particle in the ambient air, μg m^{-3}, m_f is the mass of carbon on the filter of fine fraction, μg, V_f is the volume of air sample in the fine particle steam, m^{-3}

and, the concentration of carbon in coarse particle ($PM_{2.5-10}$) can be calculated as;

$$c_{PM_{2.5-10}} = \frac{m_c}{V_t} - (\frac{V_c}{V_t}) \times c_{PM_{2.5}} \qquad \text{(Equation A.3)}$$

where $c_{PM_{2.5-10}}$ and $c_{PM_{2.5}}$ are the concentrations of carbon in coarse and fine particles in the ambient air, respectively, μg m^{-3}, m_c is the mass of carbon on the filter of coarse fraction, μg, V_c is the volume of air sample in the coarse particle steam, m^{-3}, V_t is the total volume of air sample, m^{-3}

The uncertainty of measurement can be estimated with the following equation;

for the concentration of carbon in $PM_{2.5}$

$$\frac{u(c_{PM_{2.5}})}{c_{PM_{2.5}}} = \sqrt{\left[\frac{u(m_f)}{m_f}\right]^2 + \left[\frac{u(V_f)}{V_f}\right]^2} \qquad \text{(Equation A.4)}$$

for the concentration of carbon in $PM_{2.5\text{-}10}$

$$\frac{u(c_{PM_{2.5-10}})}{c_{PM_{2.5-10}}} = \sqrt{\left[\frac{u(m_c)}{m_c}\right]^2 + \left[\frac{u(V_c)}{V_c}\right]^2 + \left[\frac{u(V_t)}{V_t}\right]^2 + \left[\frac{u(C_{PM_{2.5}})}{C_{PM_{2.5}}}\right]^2} \qquad \text{(Equation A.5)}$$

- Uncertainty in the mass of carbon analysed by carbon aerosol analyser (Sunset Laboratory) were from repeatability, sensitivity, calibration of instrument by sucrose standard solutions. The acceptance criterion for the accuracy of analyser run by standards was calculated within 5%. The repeatability of measurement calculated from the standard deviation of total carbon in same sample filter was within 0.07 μg m^{-3} (1.5%) based on air volume of a nominal PM fine fraction collected 24h sampling period.

  Calibration standards of sucrose solutions were prepared from the stock sucrose solution in concentration of 4.2 g. l^{-1} (analytical laboratory grade). Three standard solutions were used to calibrate the instrument in concentration of 0.42, 0.85 and 2.12 g. l^{-1} during every month and the QC solution was run every time before performing routine analysis.

- Uncertainty in the volume of particle steam includes uncertainties of flow controller, temperature and pressure correction. This has been reduced and estimated with a flow calibration during the routine audit round. The expanded uncertainty for measurements of analyser flow is taken to be ± 3% (NPL report, 2007). Flow rate is multiplied by time (assume uncertainty is negligible) to calculate the volume of particle stream.

- Uncertainties due to sampling and storage are not included.

The measurement uncertainty of OC, EC and TC analysis was;

	Distribution	Standard uncertainty
Repeatability	Normal	1.5
Accuracy of analyser	Rectangular	$5/\sqrt{3}$
Flow	Normal	3/2
Combined standard uncertainty		3.6%
Expanded uncertainty (k = 2)		7.2%

With regard to WSOC determination, aerosol carbon analyser was used to quantify this component by measuring OC in samples before and after water extracted. The differences of OC content represent WSOC in aerosol samples. The uncertainties of measurement results were consistent with OC, EC and TC analysis. The extraction efficiency was also investigated by plot of relationships between WSOC and OC showing the good correlation as mentioned in chapter 4.

Ionic species

Ion chromatography was used to analyse ionic components (sulphate, nitrate, chloride, oxalate, sodium, potassium, ammonium) in PM. Partisol 2025 sampler was used for collection of samples both fine and coarse fractions.

The mixed anion standard solutions were prepared from standard solutions of sulphate, nitrate, chloride and oxalate and mixed cation standard solutions were prepared from standard solutions of sodium, ammonium and potassium. The ranges of concentrations for each ion species are given as follow;

Species	Concentration, μg ml^{-1}	
	Minimum	Maximum
Sulphate	2.0	20.0
Nitrate	2.0	20.0
Chloride	2.0	10.0
Oxalate	0.2	1.0

Sodium	0.2	1.0
Ammonium	2.0	20
Potassium	0.2	1.0

There were five concentration level of mixed calibration standards measured during every analysis and they were used to relate the sample peak area to concentration of the ions the extracted solution.

Then, the mass of the ion species on the exposed filter can be calculated as;

$$m_i = c_i \times V \times \frac{A_f}{A_e} \qquad \text{(Equation A.6)}$$

where m_i is the mass of the ion on the exposed filter, μg, c_i is the concentration of the ion in the extracted solution, μg ml^{-1}, V is the volume of the extracted solution, ml, A_f is the area of exposed filter, cm^2, A_e is the area of the extracted filter, cm^2

The overall measurement equation for ionic species concentrations in the ambient air is;

$$C_i = \frac{m_i}{V_{air}} \qquad \text{(Equation A.7)}$$

where C_i is the concentration of the ionic specie in the ambient air, μg m^{-3}, m_i is the mass of the ion on the exposed filter, μg, V_{air} is the volume of air sample, m^{-3}

The concentrations of the ionic species both in fine and coarse particle were calculated based on the volume of each particle steam. The concentrations in coarse particle was also corrected by fine particle concentration in the carrier flow as same as the calculation of carbon concentrations in PM mentioned above.

The uncertainty of measurement can be estimated with the following equation;

$$\frac{u(C_i)}{C_i} = \sqrt{\left[\frac{u(m_i)}{m_i}\right]^2 + \left[\frac{u(V_{air})}{V_{air}}\right]^2} \qquad \text{(Equation A.8)}$$

- Uncertainties in the mass of the ionic species analysed by IC were from repeatability, sensitivity, linearity of calibration standards, instrument accuracy. Chromeleon software was used to generate the calibration curve including ionic species concentrations. The accuracy of the generation of this line and uncertainty of identification of peaks and accurate integration should be further investigated. The preparation of the calibration standards series was done volumetrically by calibrated micro pipettes. Moreover, the uncertainties from stock standard solutions associated with gravimetric and volumetric preparation.

  The overall uncertainty of the ion mass could be estimated by the replication measurement of calibration standards yielded the repeatability of 0.5% (based on air volume of a nominal PM fine fraction collected 24h sampling period).
- The extraction efficiency of the sonication process was also investigated by the study of recoveries presented in chapter 2. Since the remained filters after carbon analysis were all extracted by DDW, there was not be able to replicate extraction in this study.

- Uncertainty in the volume of particle steam includes uncertainties of flow controller, temperature and pressure correction. This has been reduced and estimated with a flow calibration during the routine audit round. The expanded uncertainty for measurements of analyser flow is taken to be ± 3% (NPL report, 2007). Flow rate is multiplied by time (assume uncertainty is negligible) to calculate the volume of particle steam.

- Uncertainties due to sampling and storage are not included for Partisol data.

The measurement uncertainty of ion analysis by IC was;

	Distribution	Standard uncertainty
Repeatability	Normal	0.5
Flow	Normal	3/2
Combined standard uncertainty		1.6%
Expanded uncertainty (k = 2)		3.2%

As mentioned in chapter 2, the recoveries of the analysis of anionic species were studied by spiking of standard solution onto QMA filters and spiked filters were extracted by water in the same procedure as aerosol samples. The uncertainty of recovery was estimated to be 0.5%. Then the expanded uncertainty of ions measurement including recovery was calculated to be 3.4%.

In case of aerosol sampling by MOUDI with ammonia experiment, the measurement uncertainties due to systematic and analytical errors were investigated. Since K^+ and Na^+ which are the non-volatile components observed slightly differences in concentration during the simultaneous sampling period between the two MOUDIs, the error value was estimated around 5%. For the measurement of K^+, many samples observed below the detection limit, therefore the estimation of error value in this experiment was estimated based on Na^+ species. The calculation of the measurement uncertainty of ionic data shows as follow;

	Distribution	Standard uncertainty
Repeatability	Normal	0.5
Flow	Normal	3/2
Sampling and analytical errors	Rectangular	$5/\sqrt{3}$
Combined standard uncertainty		3.3%
Expanded uncertainty (k = 2)		6.6%

Particulate matter mass

Mass of particulate matter is determined by gravimetric analysis. Only samples which were collected on PTFE and aluminium foil substrates by MOUDI sampler are measured for mass concentration in ambient air. This gravimetric method is described in chapter 2.

The overall measurement equation is;

$$PM_{mass} = \frac{\Delta m}{V_{air}} \qquad \text{(Equation A.9)}$$

Where PM_{mass} is the mass concentration of particulate matter, μg m^{-3}, Δm is the mass difference of the PM on the filer before and after sampling, μg, V_{air} is the volume of air sample, m^{-3}

The uncertainty of measurement can be estimated with the following equation;

$$\frac{u(PM_{mass})}{PM_{mass}} = \sqrt{\left[\frac{u(\Delta m)}{\Delta m}\right]^2 + \left[\frac{u(V_{air})}{V_{air}}\right]^2} \qquad \text{(Equation A.10)}$$

- Uncertainties in the mass of PM determined by gravimetry were from repeatability, sensitivity, linearity and readability of microbalance. The filters were weighed at least three times and consequently the mean values were used to calculate the mass difference. The repeatability was obtained by the ten replicated weighing of filter, estimated to be 0.6%.

- Uncertainty in the volume of air based on the efficiency of pump used and calibrated rotameter was used to measure the air flow rate. The accuracy of flow is taken to be 1.25%. Flow rate is multiplied by time (assume uncertainty is negligible) to calculate the volume of ambient air.

The measurement uncertainty of PM_{mass} analysis was;

	Distribution	Standard uncertainty
Repeatability	Normal	0.6
Flow	Rectangular	$1.25/\sqrt{3}$
Combined standard uncertainty		0.9%
Expanded uncertainty (k = 2)		1.8%

APPENDIX B

CALCULATION OF CONCENTRATION OF AMMONIA GAS SUPPLY

Calculation of the concentration of ammonia gas use in cylinder

In the experiment of air sampling with ammonia gas, the target NH_3 supplied concentration is ***50 ppb*** in total air flow in order to exceed its concentration over the average concentrations of major ionic species in atmospheric particles at EROS site. According to the specifications of MOUDI sampling flow rate, the total air flow of 30 L min^{-1} should be operated during air sampling.

If a mixing ratio of NH_3 gas is based on a dilution of one percent (1 : 100), the flow rate of NH_3 will control around 0.3 L min^{-1}. The expected NH_3 concentration is 50 ppb in total air flow so there need NH_3 in a concentration of ; $50 \text{ ppb} \times 100 = 5 \text{ ppm}$

The certified NH_3 standard (NH_3 in synthetic air) concentration of 52.08 ppm (uncertainty less than 5%) was used in this study in order to supply enough amounts during the sampling period. ***The flow rate of NH_3 was controlled at 0.03 L min^{-1}***.

Calculation of the concentration of ammonia gas during the air sampling

Convert 50 ppb NH_3 into μg m^{-3} (for example @ 0 ^oC and 761 torr)

17 g NH_3 occupy 22.41 L at STP

17 g NH_3 occupy $22.41 \times \frac{273}{273} \times \frac{760}{761}$ L = 22.39 L @ 0 ^oC and 761 torr

50 ppb NH_3 is 5×10^{-8} L. $L^{-1} = 5 \times 10^{-5}$ L. m^{-3}

so 5×10^{-5} L NH_3 at 20 ^oC and 750 torr contain $17 \times \frac{5 \times 10^{-5}}{22.39}$ g = 38 μg NH_3

$\therefore$ NH_3 concentration = 38 μg m^{-3} = 2.235 μmol m^{-3}

Calculation of the flow Reynolds number

To ensure that the ammonia is reasonably well mixed with the air coming into the MOUDI, the flow Reynolds number, a dimensionless number, that characterised gas flow through a pipe was also calculated

$$\text{Flow Reynolds number} = \frac{\rho V d}{\eta} = \quad 6.6\,Vd \ \ (@\ 20\ ^{o}\text{C}) \qquad \text{(Equation B.1)}$$

Where ρ = the density of air

η = the coefficient of viscosity

V = the relative flow velocity in cm s^{-1}

d = the diameter of tube in cm

In this experiment, the air sample was taken at the air flow rate of 30 L min^{-1} in the tube of inner diameter less than 1 cm.

Then, the velocity of the air relative to the tube was calculated as;

$$V = \frac{Q}{A}$$

Where

$$Q = \frac{30\,(L/\min) \times 1000\,(cm^3/L)}{60\,(s/\min)} = 500 \quad cm^3/s$$

and A is the cross-sectional area of the tube,

$$A = \frac{\pi d^2}{4} = \frac{\pi}{4} = 0.79\ cm^2$$

$$V = \frac{500}{0.79}\frac{cm^3/s}{cm^2} = 632.91\,cm/s$$

Substituting gives

Flow Re = $6.6\,Vd$ = 6.6 x 632.91 x 1 = 4177.21

(The flow in the tube is turbulent for higher Re than 4000)

APPENDIX C

AIR MASS BACK TRAJECTORIES

CLUSTER ANALYSIS OF AIR MASS BACK TRAJECTORIES ARRIVING AT EROS FOR THE WHOLE PERIOD (November 2008 – April 2011)

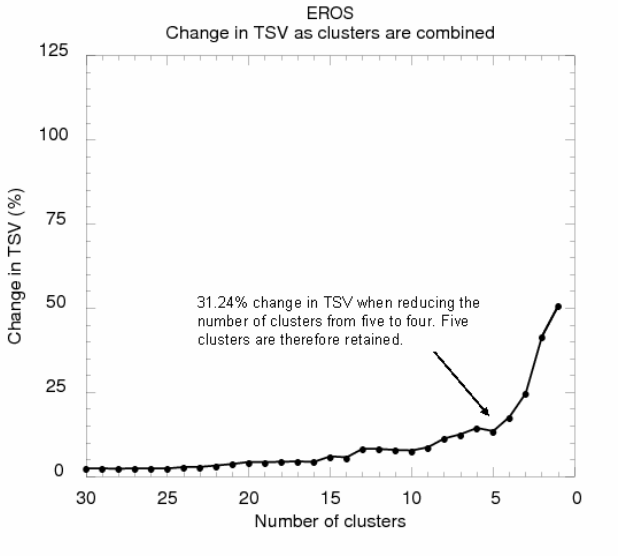
EROS
Change in TSV as clusters are combined
Change in TSV (%)
125
100
75
50
25
0
31.24% change in TSV when reducing the number of clusters from five to four. Five clusters are therefore retained.
30
25
20
15
10
5
0
Number of clusters

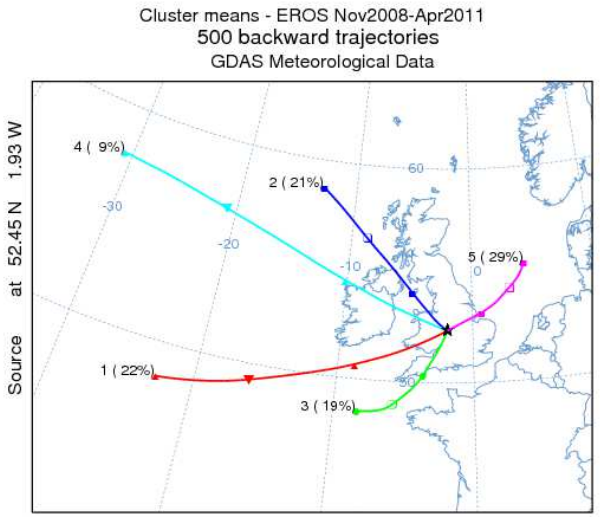
Cluster means - EROS Nov2008-Apr2011
500 backward trajectories
GDAS Meteorological Data
Source ★ at 52.45 N 1.93 W
4 (9%)
2 (21%)
5 (29%)
1 (22%)
3 (19%)

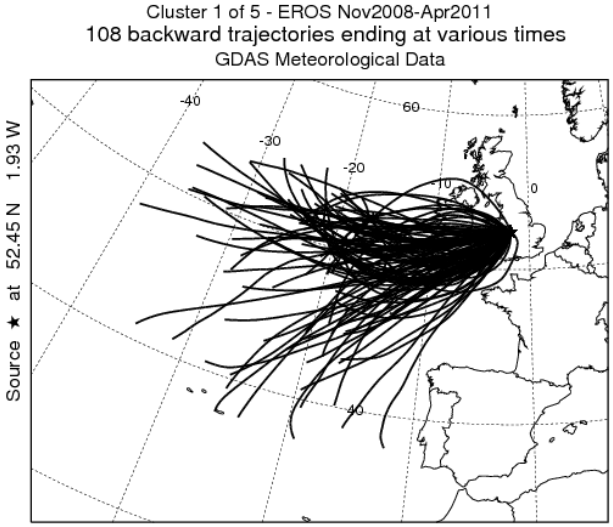
Cluster 1 of 5 - EROS Nov2008-Apr2011
108 backward trajectories ending at various times
GDAS Meteorological Data
Source ★ at 52.45 N 1.93 W

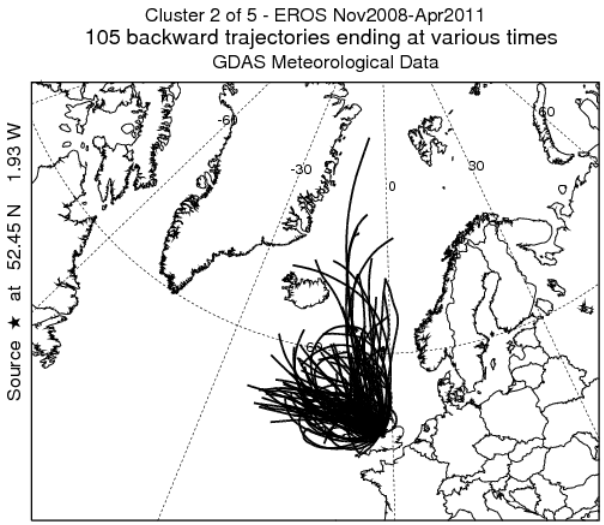
Cluster 2 of 5 - EROS Nov2008-Apr2011
105 backward trajectories ending at various times
GDAS Meteorological Data
Source ★ at 52.45 N 1.93 W

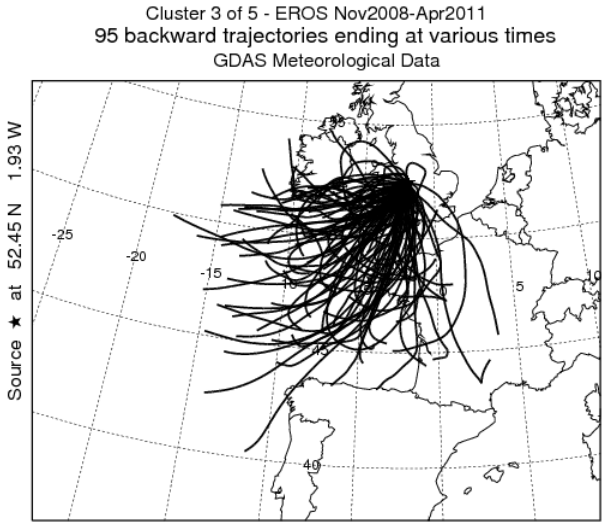
Cluster 3 of 5 - EROS Nov2008-Apr2011
95 backward trajectories ending at various times
GDAS Meteorological Data
Source ★ at 52.45 N 1.93 W

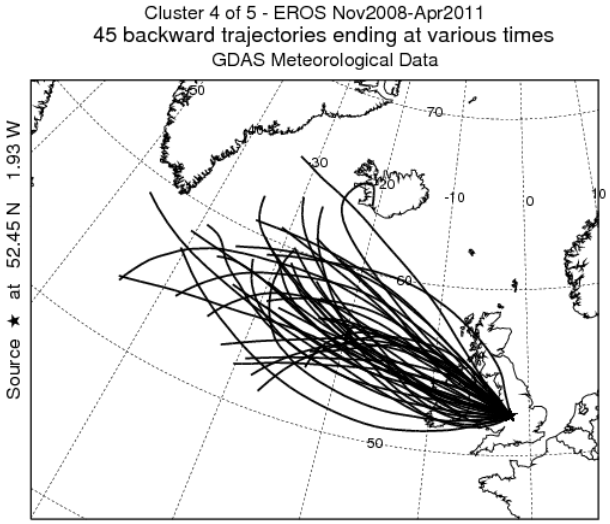
Cluster 4 of 5 - EROS Nov2008-Apr2011
45 backward trajectories ending at various times
GDAS Meteorological Data
Source ★ at 52.45 N 1.93 W

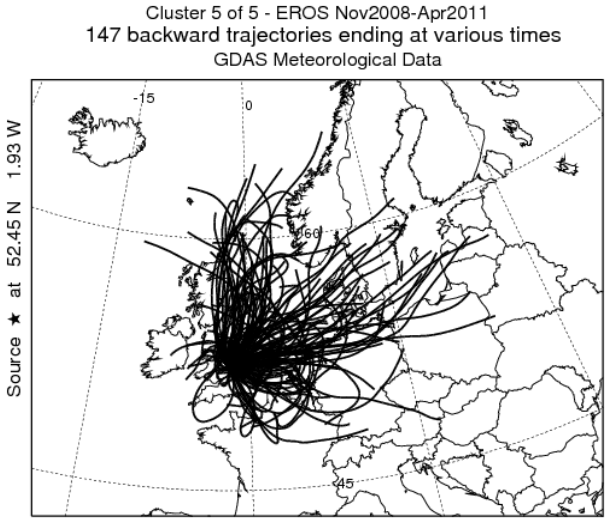
Cluster 5 of 5 - EROS Nov2008-Apr2011
147 backward trajectories ending at various times
GDAS Meteorological Data
Source ★ at 52.45 N 1.93 W
-15
0
60
45

CLUSTER ANALYSIS OF AIR MASS BACK TRAJECTORIES ARRIVING AT EROS DURING SUMMER

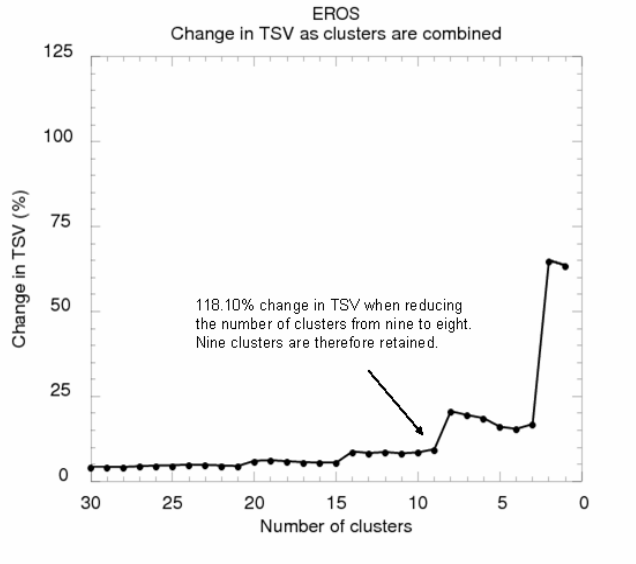
EROS
Change in TSV as clusters are combined
Change in TSV (%)
Number of clusters
118.10% change in TSV when reducing
the number of clusters from nine to eight.
Nine clusters are therefore retained.

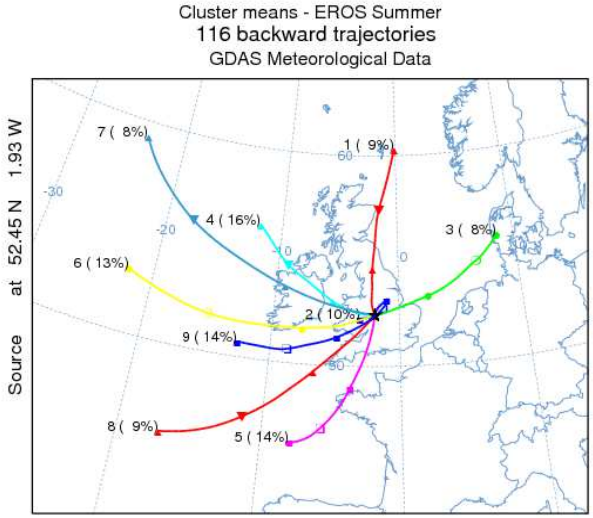
Cluster means - EROS Summer
116 backward trajectories
GDAS Meteorological Data
Source ★ at 52.45 N 1.93 W
7 (8%)
1 (9%)
4 (16%)
3 (8%)
6 (13%)
2 (10%)
9 (14%)
8 (9%)
5 (14%)

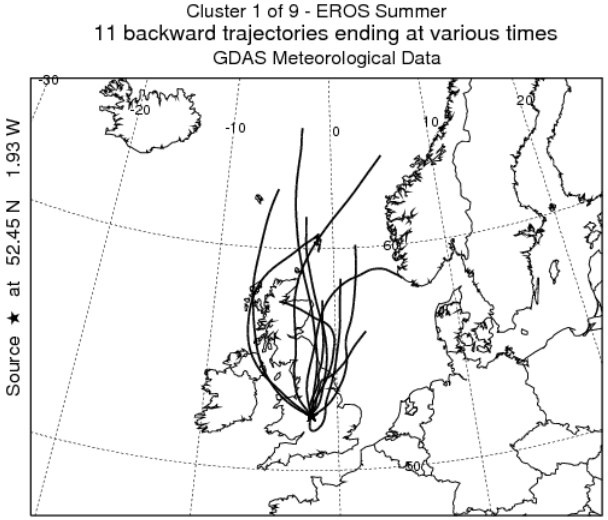
Cluster 1 of 9 - EROS Summer
11 backward trajectories ending at various times
GDAS Meteorological Data
Source ★ at 52.45 N 1.93 W

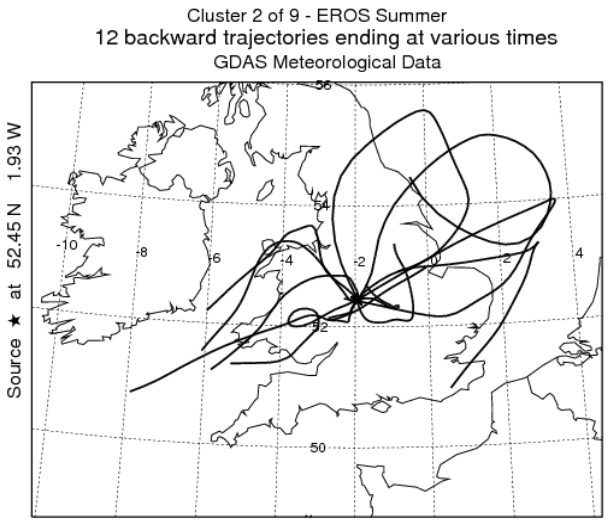
Cluster 2 of 9 - EROS Summer
12 backward trajectories ending at various times
GDAS Meteorological Data
Source ★ at 52.45 N 1.93 W

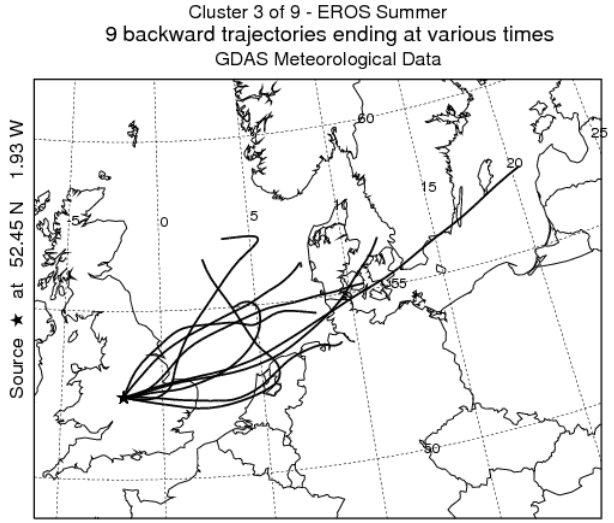
Cluster 3 of 9 - EROS Summer
9 backward trajectories ending at various times
GDAS Meteorological Data
Source ★ at 52.45 N 1.93 W

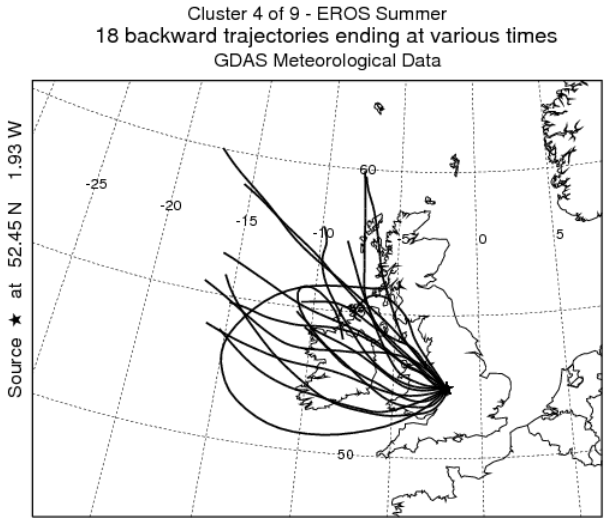
Cluster 4 of 9 - EROS Summer
18 backward trajectories ending at various times
GDAS Meteorological Data
Source ★ at 52.45 N 1.93 W

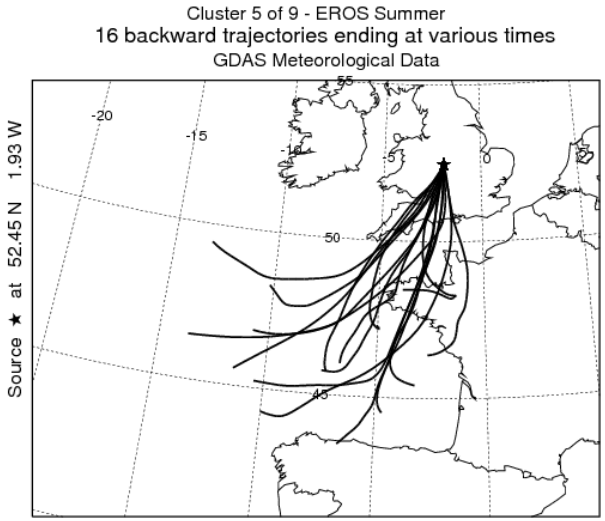
Cluster 5 of 9 - EROS Summer
16 backward trajectories ending at various times
GDAS Meteorological Data
Source ★ at 52.45 N 1.93 W

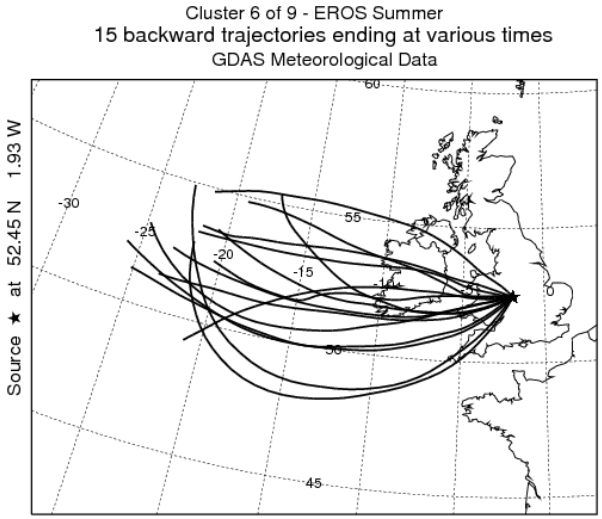
Cluster 6 of 9 - EROS Summer
15 backward trajectories ending at various times
GDAS Meteorological Data
Source ★ at 52.45 N 1.93 W

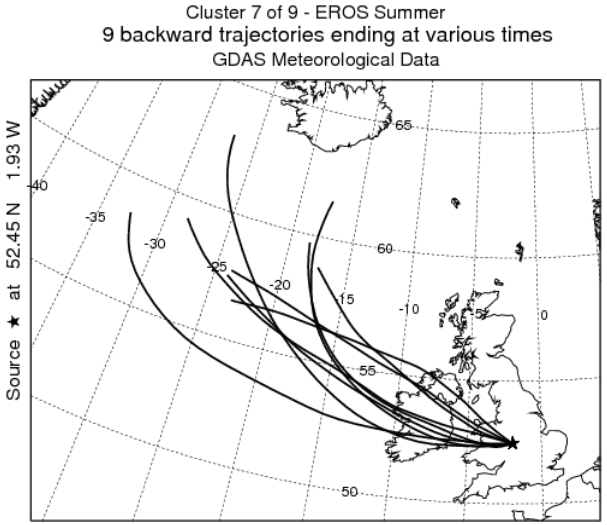
Cluster 7 of 9 - EROS Summer
9 backward trajectories ending at various times
GDAS Meteorological Data
Source ★ at 52.45 N 1.93 W

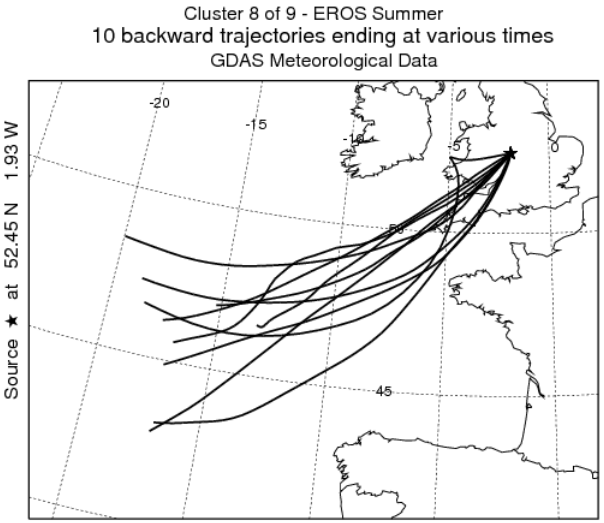
Cluster 8 of 9 - EROS Summer
10 backward trajectories ending at various times
GDAS Meteorological Data
Source ★ at 52.45 N 1.93 W

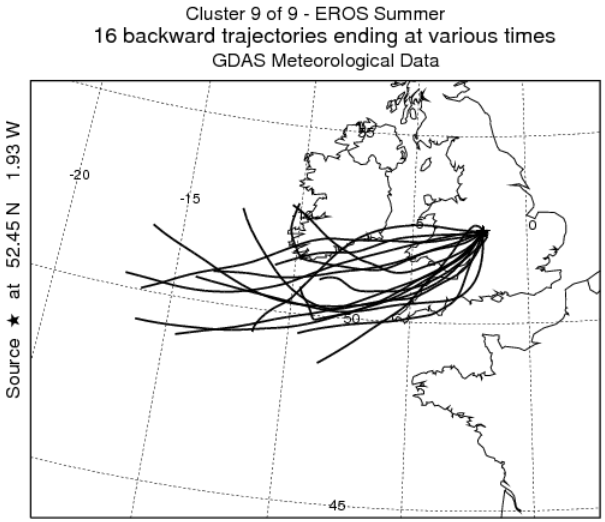
Cluster 9 of 9 - EROS Summer
16 backward trajectories ending at various times
GDAS Meteorological Data
Source ★ at 52.45 N 1.93 W

CLUSTER ANALYSIS OF AIR MASS BACK TRAJECTORIES ARRIVING AT EROS DURING AUTUMN

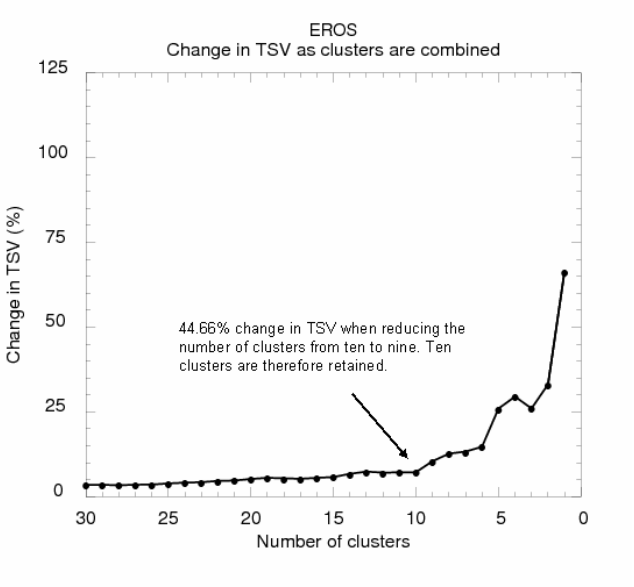
EROS
Change in TSV as clusters are combined
Change in TSV (%)
125
100
75
50
25
0
30
25
20
15
10
5
0
Number of clusters
44.66% change in TSV when reducing the number of clusters from ten to nine. Ten clusters are therefore retained.

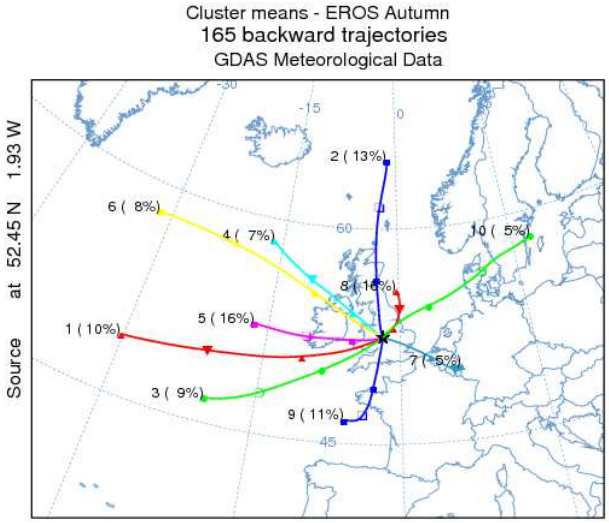
Cluster means - EROS Autumn
165 backward trajectories
GDAS Meteorological Data
Source ★ at 52.45 N 1.93 W
2 (13%)
6 (8%)
4 (7%)
10 (5%)
8 (16%)
1 (10%)
5 (16%)
7 (5%)
3 (9%)
9 (11%)

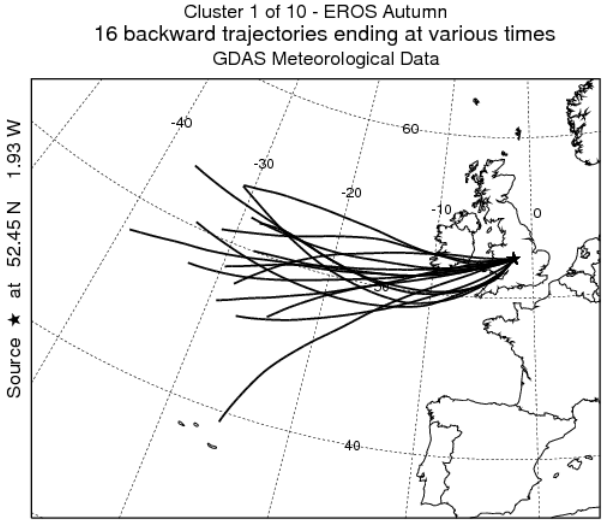
Cluster 1 of 10 - EROS Autumn
16 backward trajectories ending at various times
GDAS Meteorological Data
Source ★ at 52.45 N 1.93 W

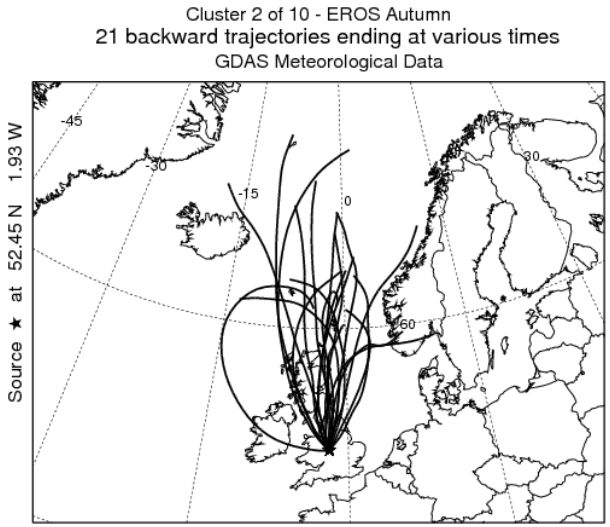
Cluster 2 of 10 - EROS Autumn
21 backward trajectories ending at various times
GDAS Meteorological Data
Source ★ at 52.45 N 1.93 W

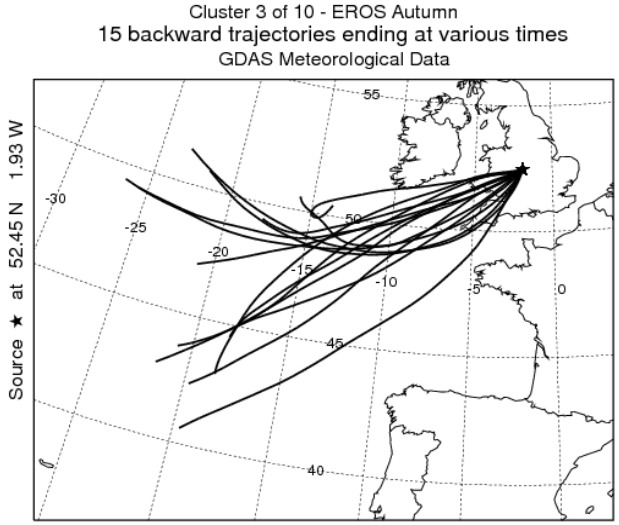
Cluster 3 of 10 - EROS Autumn
15 backward trajectories ending at various times
GDAS Meteorological Data
Source ★ at 52.45 N 1.93 W

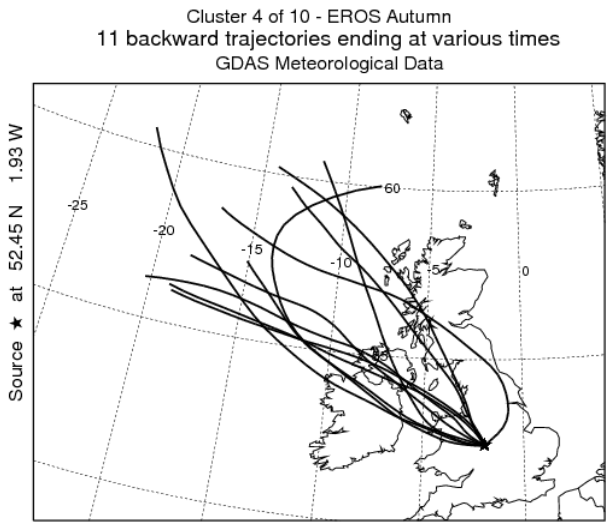
Cluster 4 of 10 - EROS Autumn
11 backward trajectories ending at various times
GDAS Meteorological Data
Source ★ at 52.45 N 1.93 W

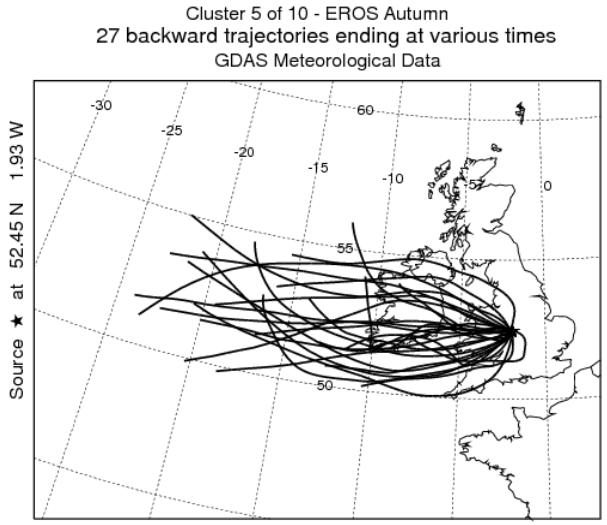
Cluster 5 of 10 - EROS Autumn
27 backward trajectories ending at various times
GDAS Meteorological Data
Source ★ at 52.45 N 1.93 W

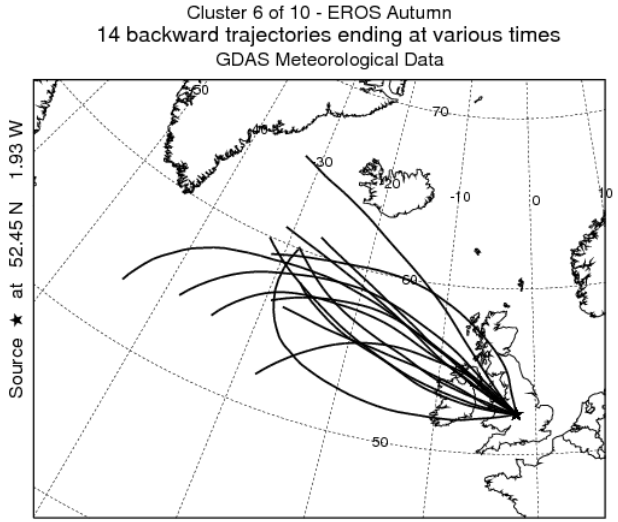
Cluster 6 of 10 - EROS Autumn
14 backward trajectories ending at various times
GDAS Meteorological Data
Source ★ at 52.45 N 1.93 W

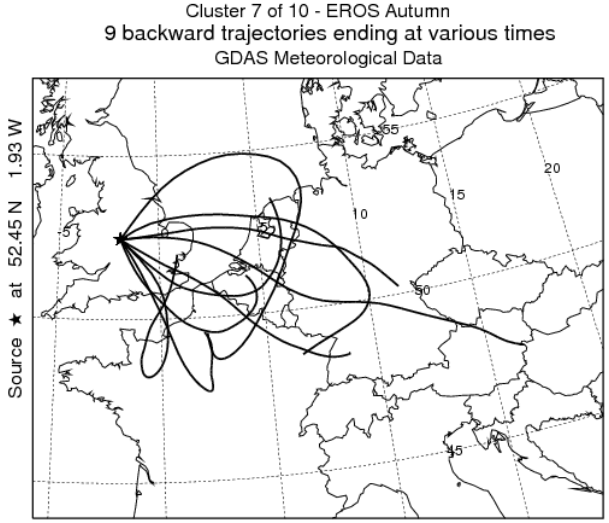
Cluster 7 of 10 - EROS Autumn
9 backward trajectories ending at various times
GDAS Meteorological Data
Source ★ at 52.45 N 1.93 W

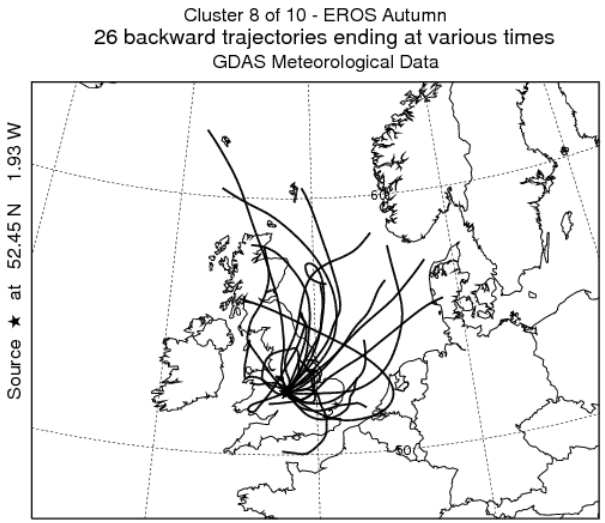
Cluster 8 of 10 - EROS Autumn
26 backward trajectories ending at various times
GDAS Meteorological Data
Source ★ at 52.45 N 1.93 W

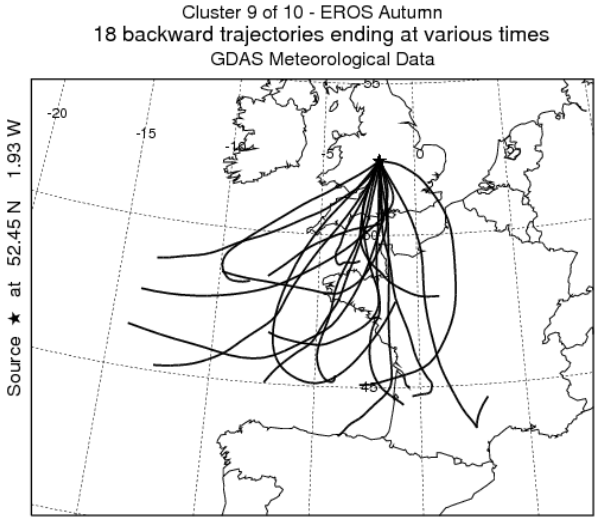
Cluster 9 of 10 - EROS Autumn
18 backward trajectories ending at various times
GDAS Meteorological Data
Source ★ at 52.45 N 1.93 W

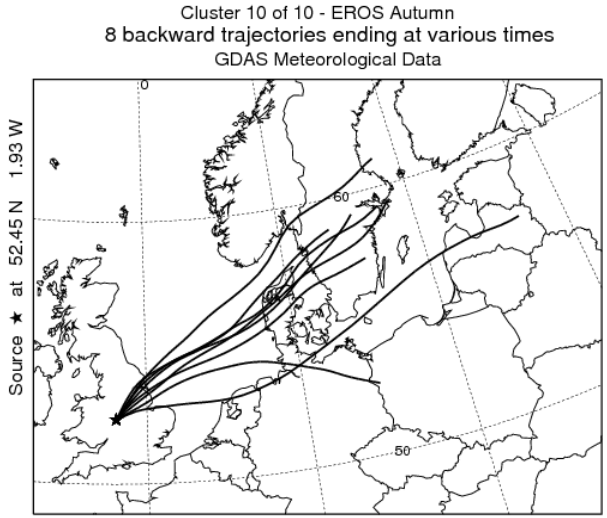
Cluster 10 of 10 - EROS Autumn
8 backward trajectories ending at various times
GDAS Meteorological Data
Source ★ at 52.45 N 1.93 W

CLUSTER ANALYSIS OF AIR MASS BACK TRAJECTORIES ARRIVING AT EROS DURING WINTER

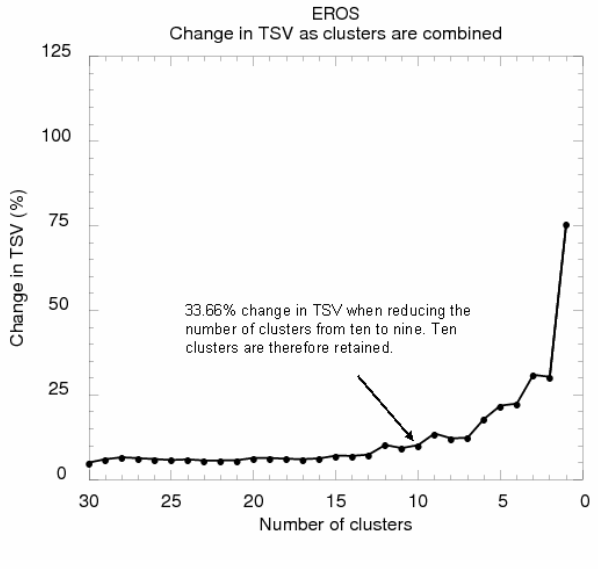
EROS
Change in TSV as clusters are combined
Change in TSV (%)
125
100
75
50
25
0
30
25
20
15
10
5
0
Number of clusters
33.66% change in TSV when reducing the number of clusters from ten to nine. Ten clusters are therefore retained.

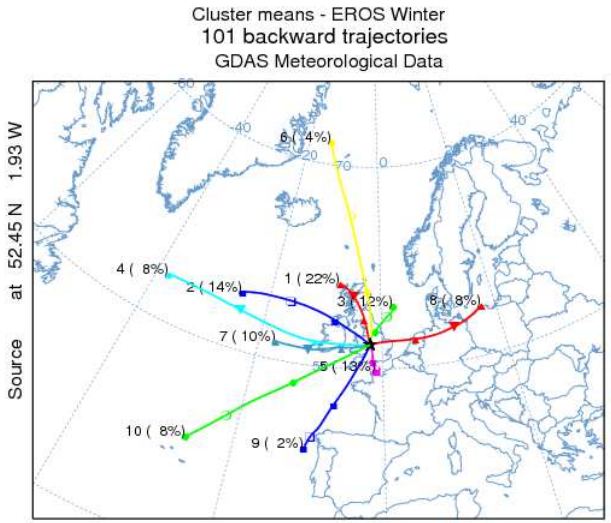
Cluster means - EROS Winter
101 backward trajectories
GDAS Meteorological Data
Source at 52.45 N 1.93 W
6 (4%)
4 (8%)
2 (14%)
1 (22%)
3 (12%)
8 (8%)
7 (10%)
5 (13%)
10 (8%)
9 (2%)

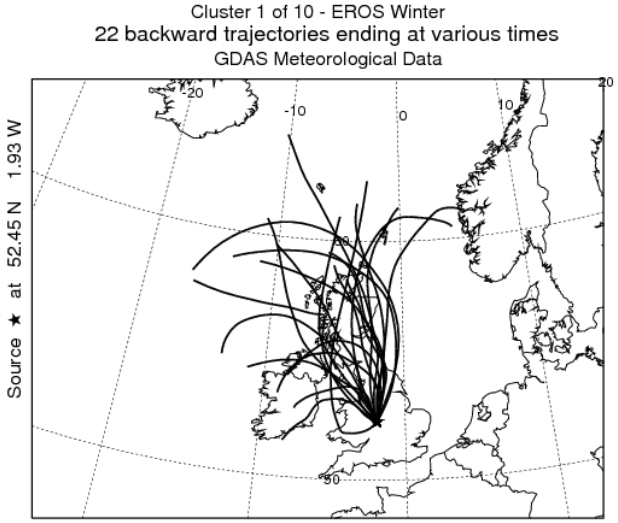
Cluster 1 of 10 - EROS Winter
22 backward trajectories ending at various times
GDAS Meteorological Data
Source ★ at 52.45 N 1.93 W

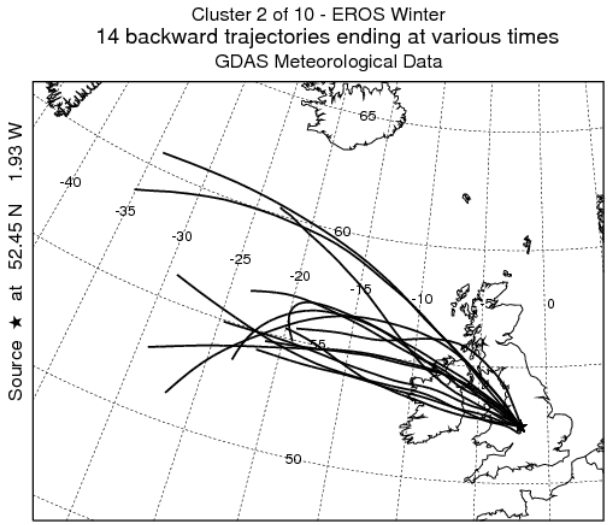
Cluster 2 of 10 - EROS Winter
14 backward trajectories ending at various times
GDAS Meteorological Data
Source ★ at 52.45 N 1.93 W

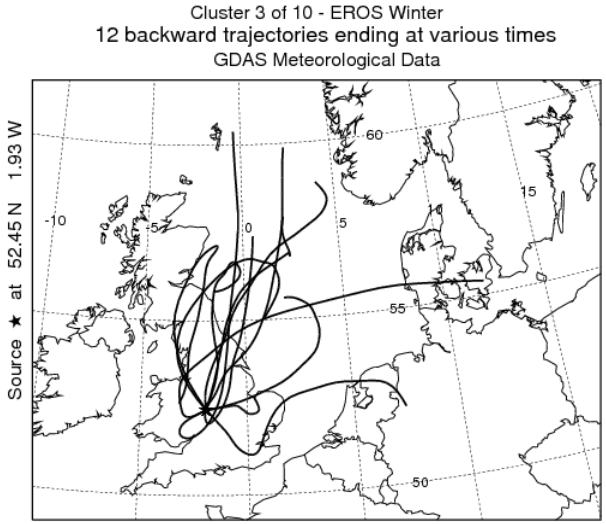
Cluster 3 of 10 - EROS Winter
12 backward trajectories ending at various times
GDAS Meteorological Data
Source ★ at 52.45 N 1.93 W

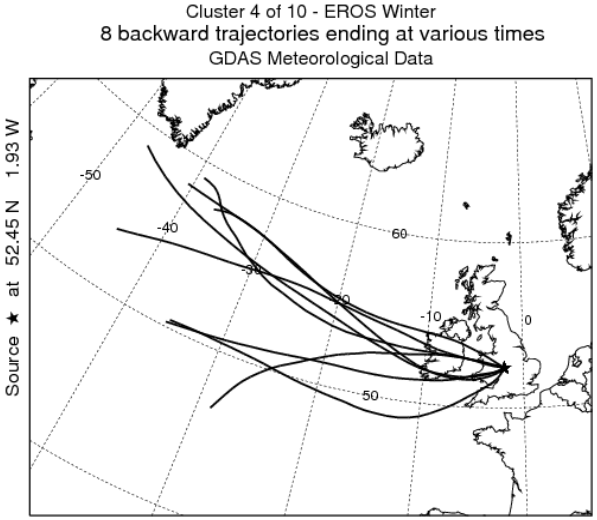
Cluster 4 of 10 - EROS Winter
8 backward trajectories ending at various times
GDAS Meteorological Data
Source ★ at 52.45 N 1.93 W

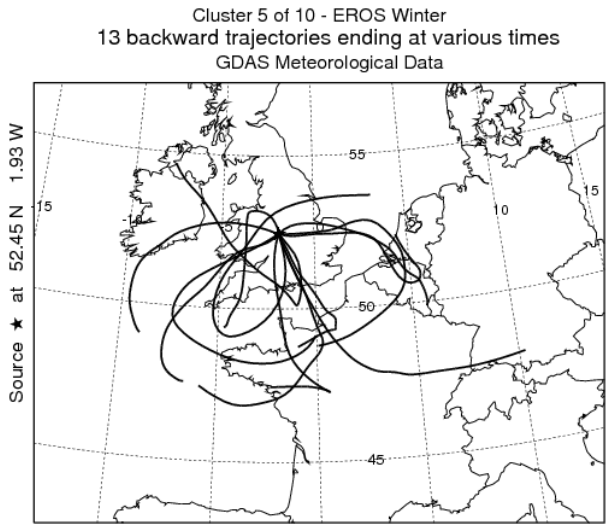
Cluster 5 of 10 - EROS Winter
13 backward trajectories ending at various times
GDAS Meteorological Data
Source ★ at 52.45 N 1.93 W

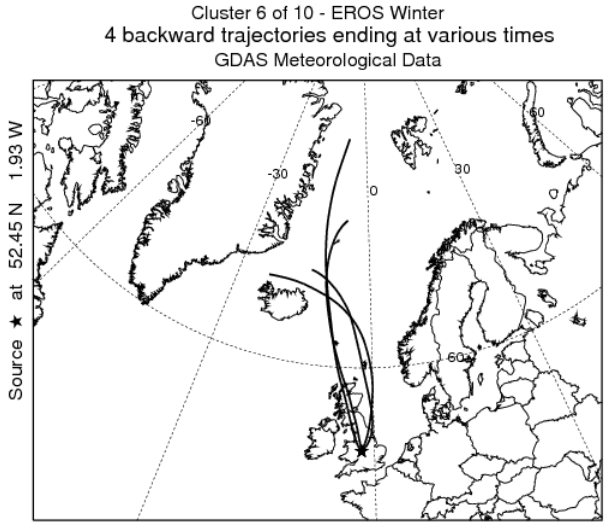
Cluster 6 of 10 - EROS Winter
4 backward trajectories ending at various times
GDAS Meteorological Data
Source ★ at 52.45 N 1.93 W

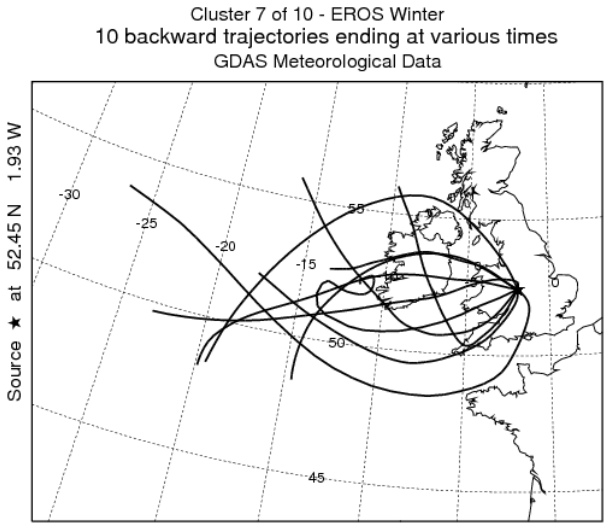
Cluster 7 of 10 - EROS Winter
10 backward trajectories ending at various times
GDAS Meteorological Data
Source ★ at 52.45 N 1.93 W

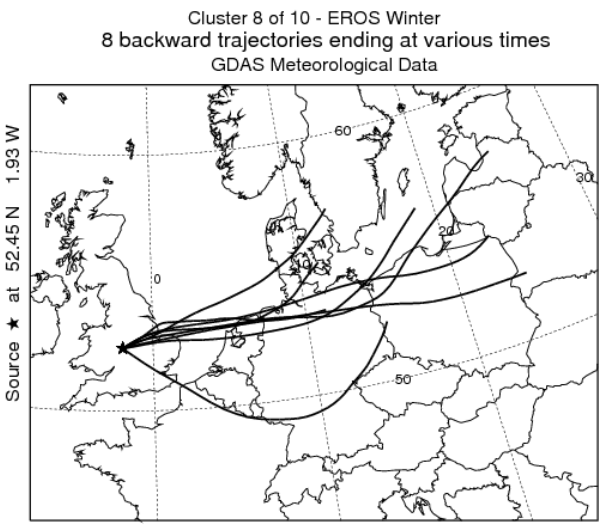
Cluster 8 of 10 - EROS Winter
8 backward trajectories ending at various times
GDAS Meteorological Data
Source ★ at 52.45 N 1.93 W

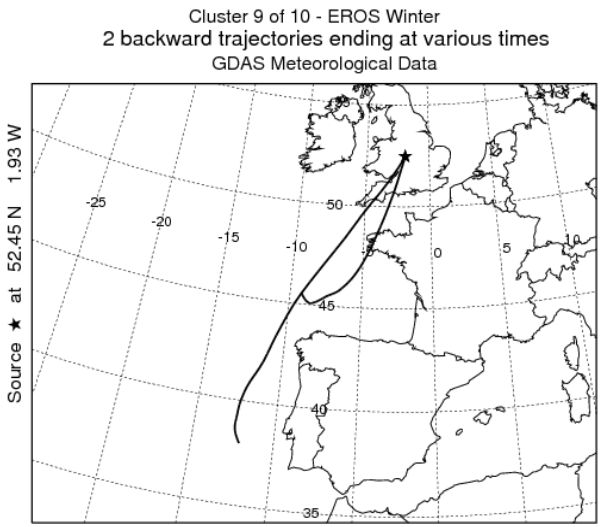
Cluster 9 of 10 - EROS Winter
2 backward trajectories ending at various times
GDAS Meteorological Data
Source ★ at 52.45 N 1.93 W

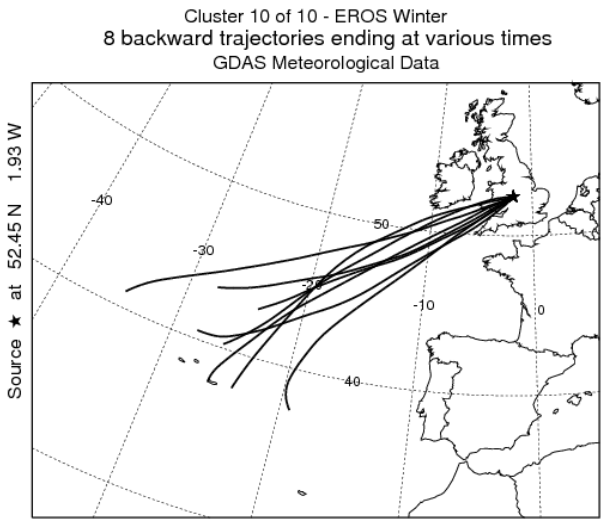
Cluster 10 of 10 - EROS Winter
8 backward trajectories ending at various times
GDAS Meteorological Data
Source ★ at 52.45 N 1.93 W

CLUSTER ANALYSIS OF AIR MASS BACK TRAJECTORIES ARRIVING AT EROS DURING SPRING

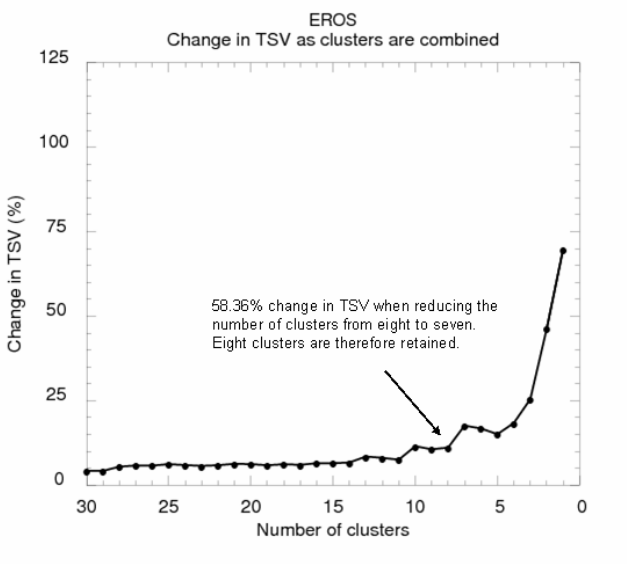
EROS
Change in TSV as clusters are combined
Change in TSV (%)
Number of clusters
58.36% change in TSV when reducing the number of clusters from eight to seven. Eight clusters are therefore retained.

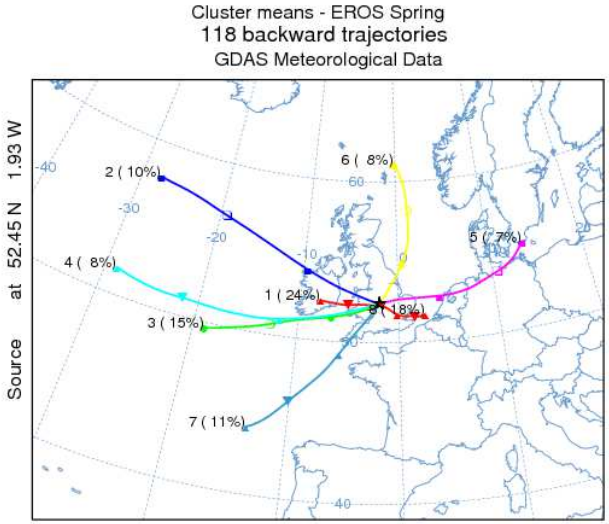
Cluster means - EROS Spring
118 backward trajectories
GDAS Meteorological Data
Source ★ at 52.45 N 1.93 W
1 (24%)
2 (10%)
3 (15%)
4 (8%)
5 (7%)
6 (8%)
7 (11%)
8 (18%)

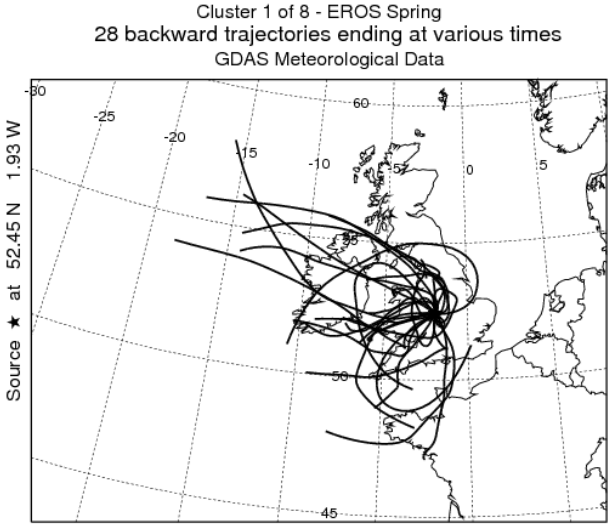
Cluster 1 of 8 - EROS Spring
28 backward trajectories ending at various times
GDAS Meteorological Data
Source ★ at 52.45 N 1.93 W

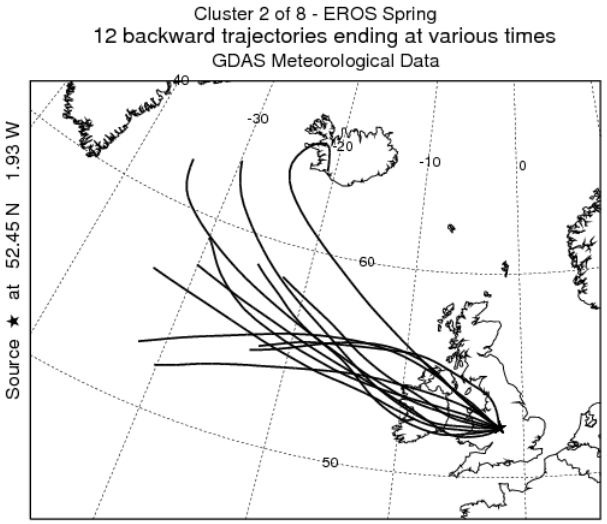
Cluster 2 of 8 - EROS Spring
12 backward trajectories ending at various times
GDAS Meteorological Data
Source ★ at 52.45 N 1.93 W

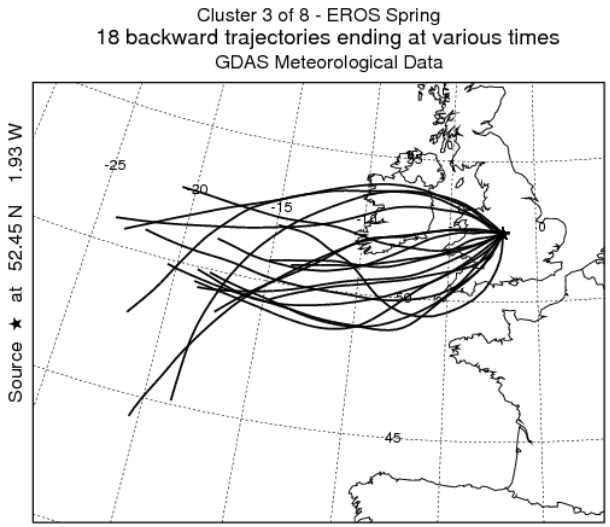
Cluster 3 of 8 - EROS Spring
18 backward trajectories ending at various times
GDAS Meteorological Data
Source ★ at 52.45 N 1.93 W

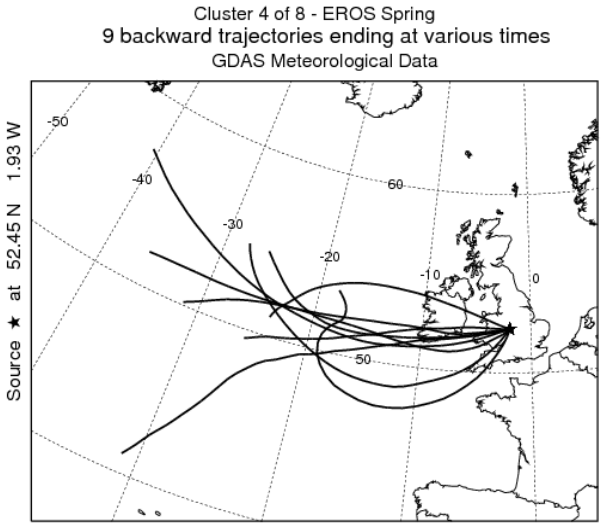
Cluster 4 of 8 - EROS Spring
9 backward trajectories ending at various times
GDAS Meteorological Data
Source ★ at 52.45 N 1.93 W

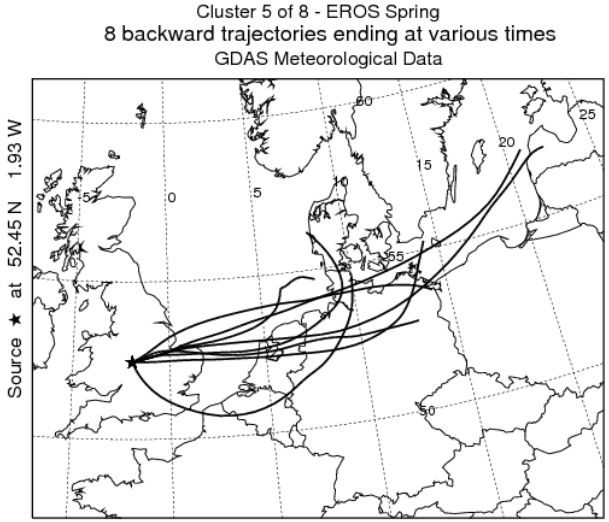
Cluster 5 of 8 - EROS Spring
8 backward trajectories ending at various times
GDAS Meteorological Data
Source ★ at 52.45 N 1.93 W

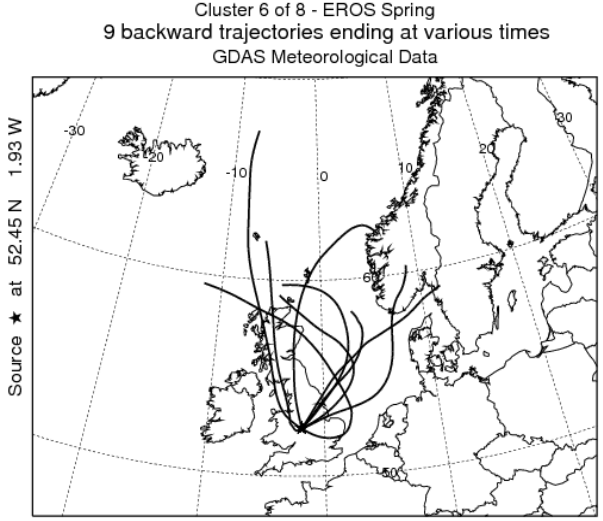
Cluster 6 of 8 - EROS Spring
9 backward trajectories ending at various times
GDAS Meteorological Data
Source ★ at 52.45 N 1.93 W

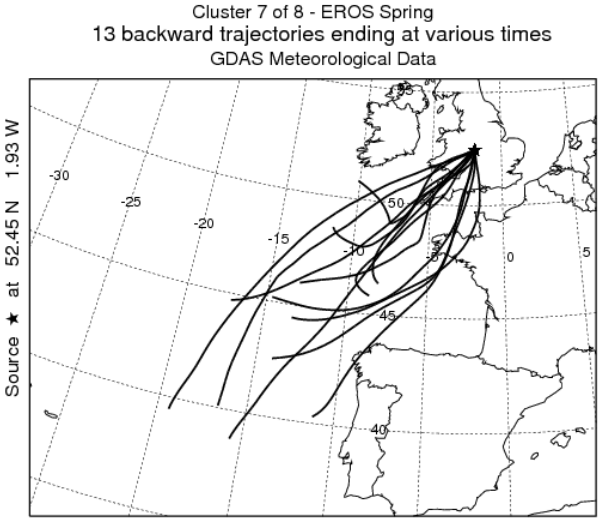
Cluster 7 of 8 - EROS Spring
13 backward trajectories ending at various times
GDAS Meteorological Data
Source ★ at 52.45 N 1.93 W

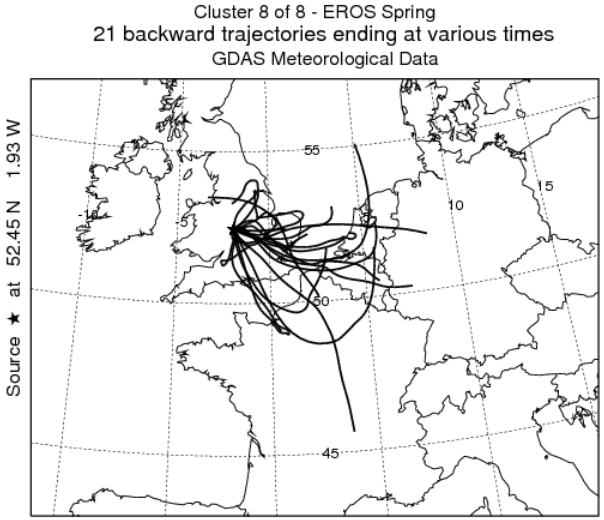
Cluster 8 of 8 - EROS Spring
21 backward trajectories ending at various times
GDAS Meteorological Data
Source ★ at 52.45 N 1.93 W

CLUSTER ANALYSIS OF AIR MASS BACK TRAJECTORIES ARRIVING AT EROS DURING THE PERIOD OF SIMULTANEOUS SAMPLING WITH HARWELL (12 July – 6 December 2010)

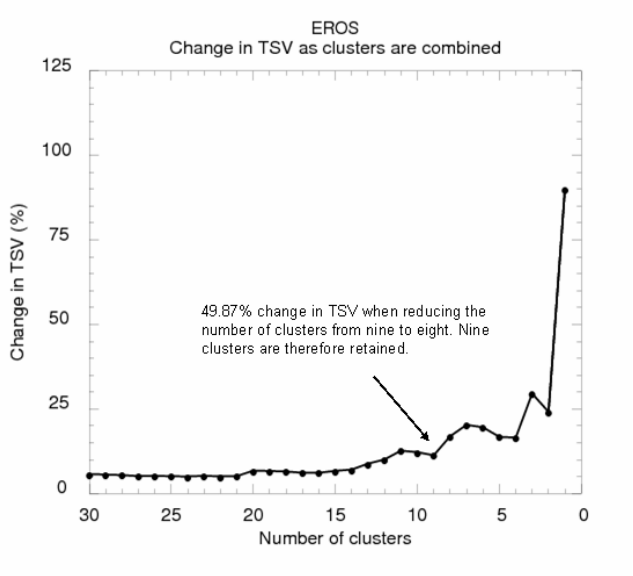
EROS
Change in TSV as clusters are combined
Change in TSV (%)
Number of clusters
49.87% change in TSV when reducing the number of clusters from nine to eight. Nine clusters are therefore retained.

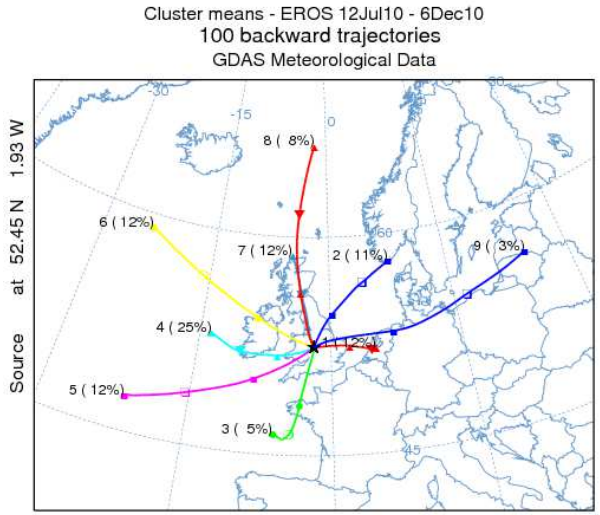
Cluster means - EROS 12Jul10 - 6Dec10
100 backward trajectories
GDAS Meteorological Data
Source ★ at 52.45 N 1.93 W
8 (8%)
6 (12%)
7 (12%)
2 (11%)
9 (3%)
4 (25%)
1 (29%)
5 (12%)
3 (5%)

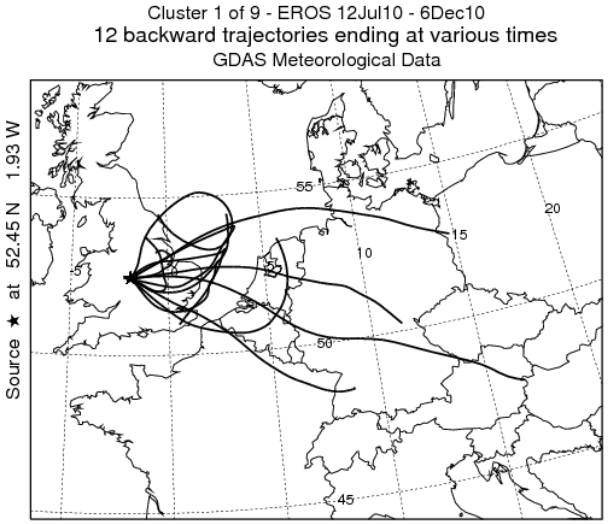
Cluster 1 of 9 - EROS 12Jul10 - 6Dec10
12 backward trajectories ending at various times
GDAS Meteorological Data
Source ★ at 52.45 N 1.93 W

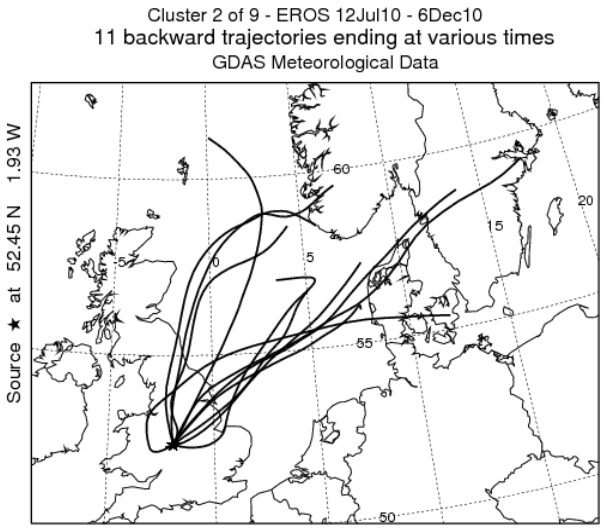
Cluster 2 of 9 - EROS 12Jul10 - 6Dec10
11 backward trajectories ending at various times
GDAS Meteorological Data
Source ★ at 52.45 N 1.93 W

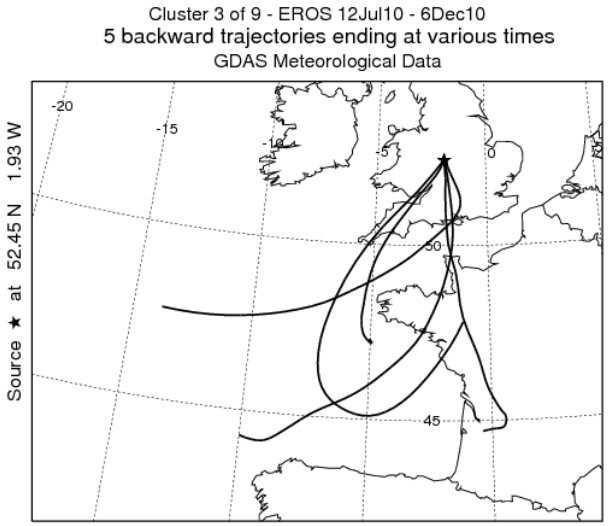
Cluster 3 of 9 - EROS 12Jul10 - 6Dec10
5 backward trajectories ending at various times
GDAS Meteorological Data
Source ★ at 52.45 N 1.93 W

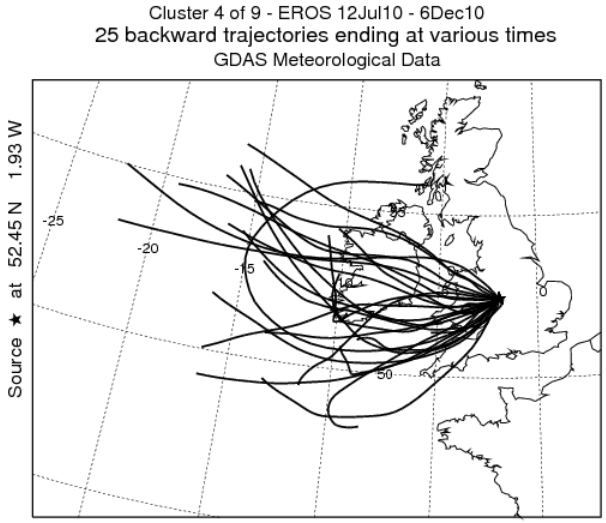
Cluster 4 of 9 - EROS 12Jul10 - 6Dec10
25 backward trajectories ending at various times
GDAS Meteorological Data
Source ★ at 52.45 N 1.93 W

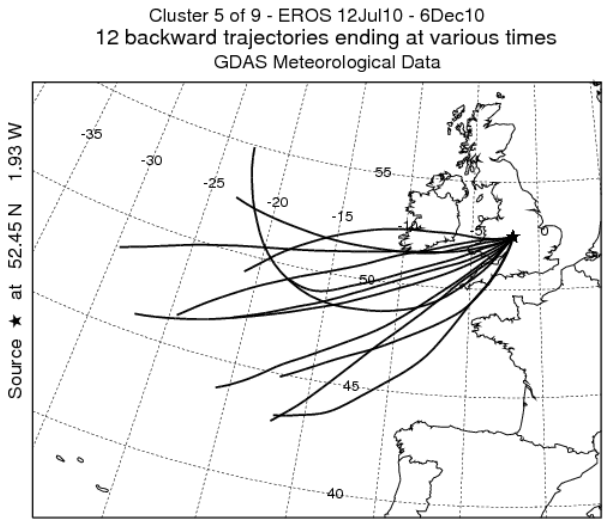
Cluster 5 of 9 - EROS 12Jul10 - 6Dec10
12 backward trajectories ending at various times
GDAS Meteorological Data
Source ★ at 52.45 N 1.93 W

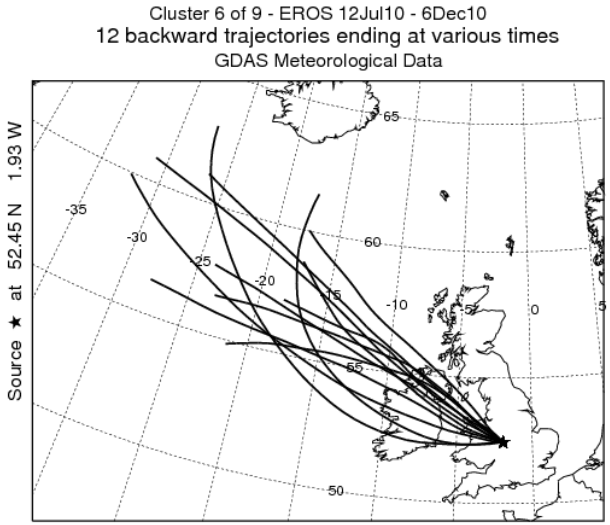
Cluster 6 of 9 - EROS 12Jul10 - 6Dec10
12 backward trajectories ending at various times
GDAS Meteorological Data
Source ★ at 52.45 N 1.93 W

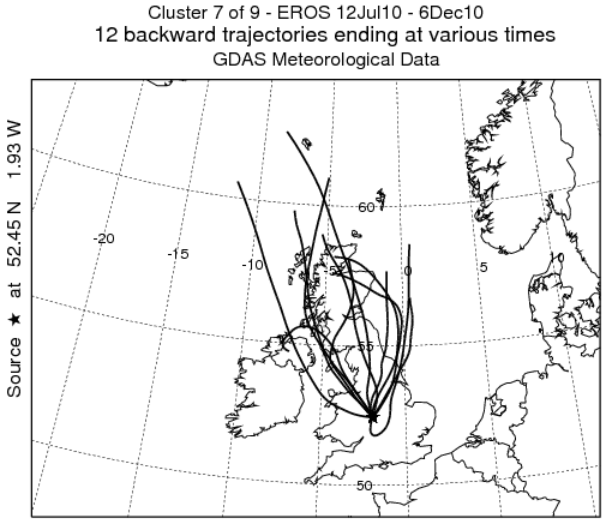
Cluster 7 of 9 - EROS 12Jul10 - 6Dec10
12 backward trajectories ending at various times
GDAS Meteorological Data
Source ★ at 52.45 N 1.93 W

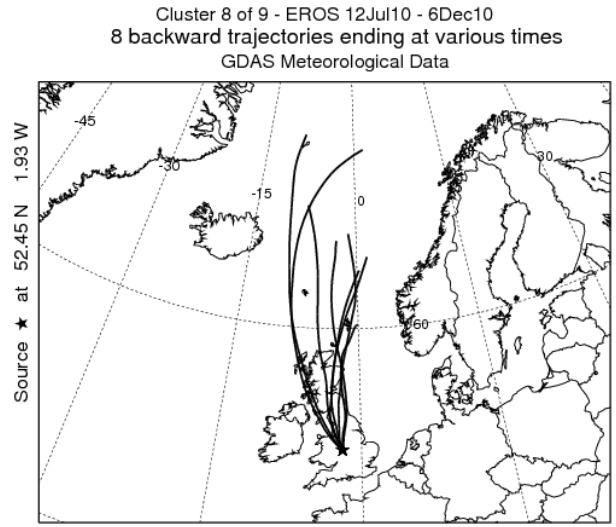
Cluster 8 of 9 - EROS 12Jul10 - 6Dec10
8 backward trajectories ending at various times
GDAS Meteorological Data
Source ★ at 52.45 N 1.93 W

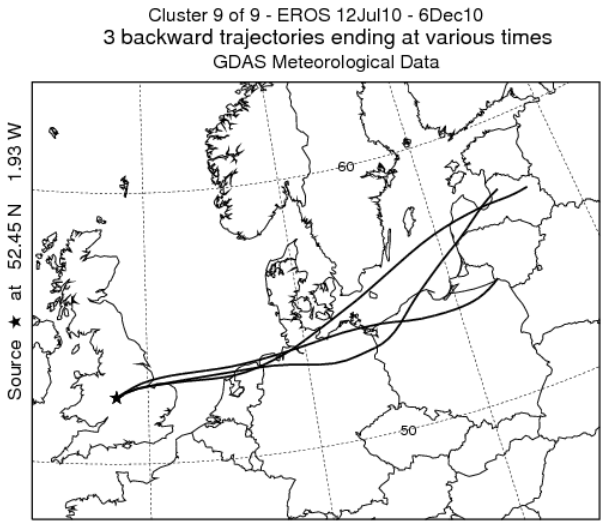
Cluster 9 of 9 - EROS 12Jul10 - 6Dec10
3 backward trajectories ending at various times
GDAS Meteorological Data
Source ★ at 52.45 N 1.93 W

CLUSTER ANALYSIS OF AIR MASS BACK TRAJECTORIES ARRIVING AT HARWELL DURING THE PERIOD OF SIMULTANEOUS SAMPLING WITH EROS (12 July – 6 December 2010)

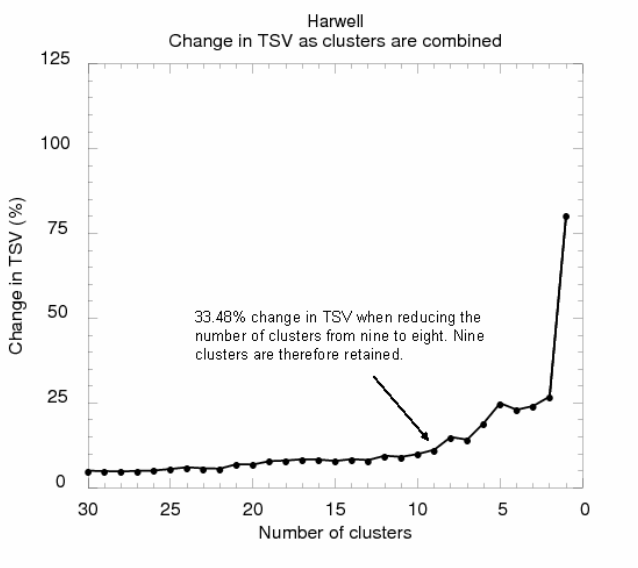
Harwell
Change in TSV as clusters are combined
Change in TSV (%)
Number of clusters
33.48% change in TSV when reducing the number of clusters from nine to eight. Nine clusters are therefore retained.

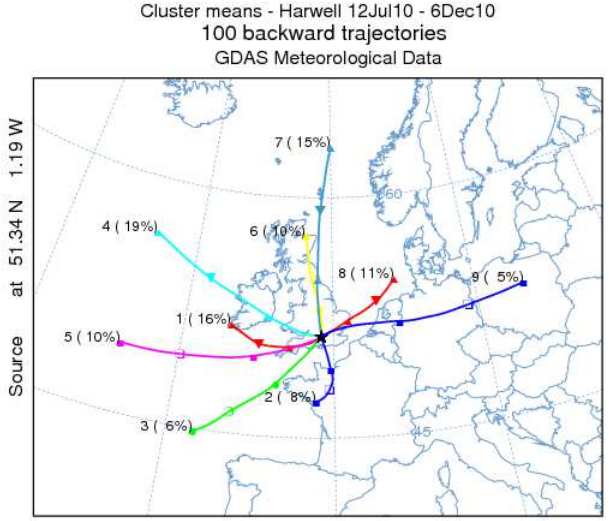
Cluster means - Harwell 12Jul10 - 6Dec10
100 backward trajectories
GDAS Meteorological Data
Source ★ at 51.34 N 1.19 W
7 (15%)
4 (19%)
6 (10%)
8 (11%)
9 (5%)
1 (16%)
5 (10%)
2 (8%)
3 (6%)

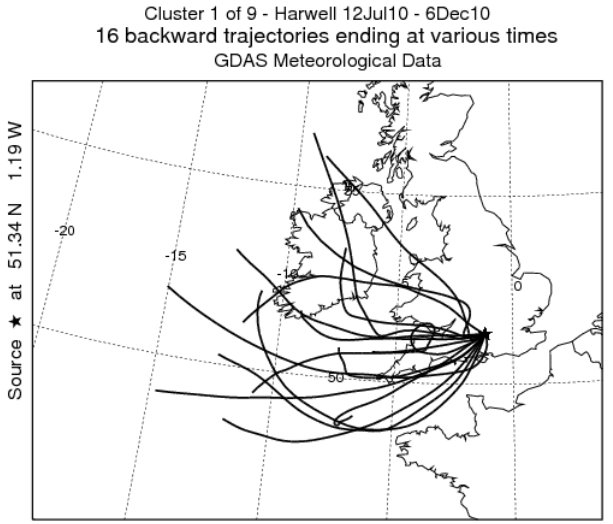
Cluster 1 of 9 - Harwell 12Jul10 - 6Dec10
16 backward trajectories ending at various times
GDAS Meteorological Data
Source ★ at 51.34 N 1.19 W

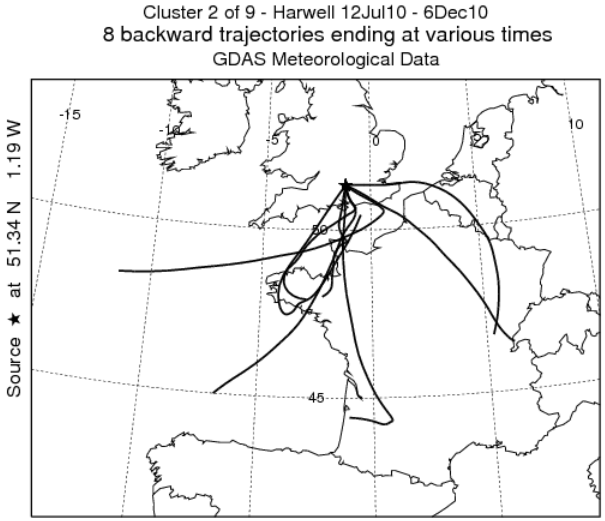
Cluster 2 of 9 - Harwell 12Jul10 - 6Dec10
8 backward trajectories ending at various times
GDAS Meteorological Data
Source ★ at 51.34 N 1.19 W

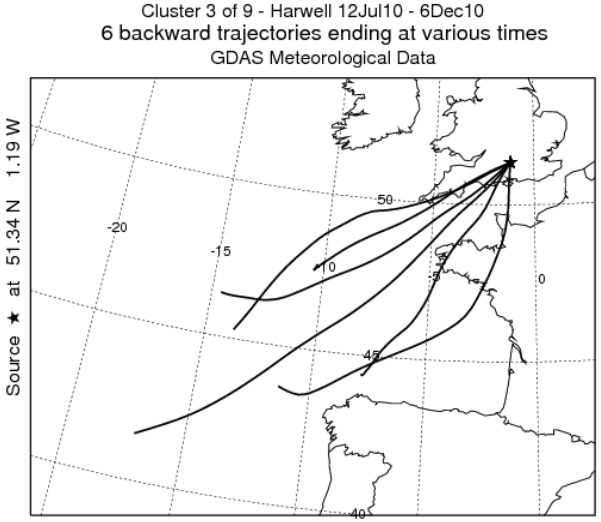
Cluster 3 of 9 - Harwell 12Jul10 - 6Dec10
6 backward trajectories ending at various times
GDAS Meteorological Data
Source ★ at 51.34 N 1.19 W

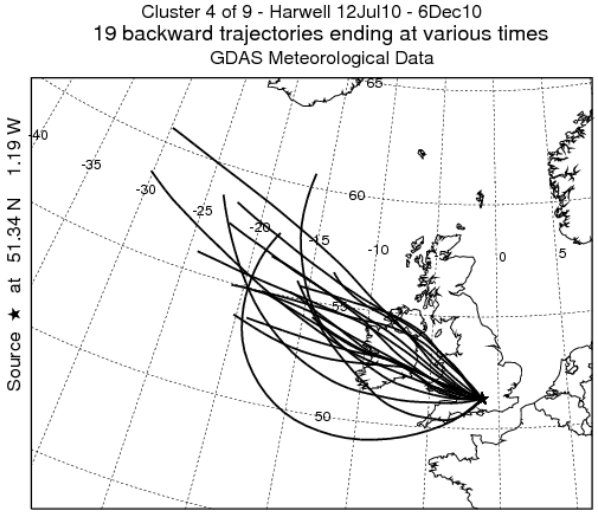
Cluster 4 of 9 - Harwell 12Jul10 - 6Dec10
19 backward trajectories ending at various times
GDAS Meteorological Data
Source ★ at 51.34 N 1.19 W

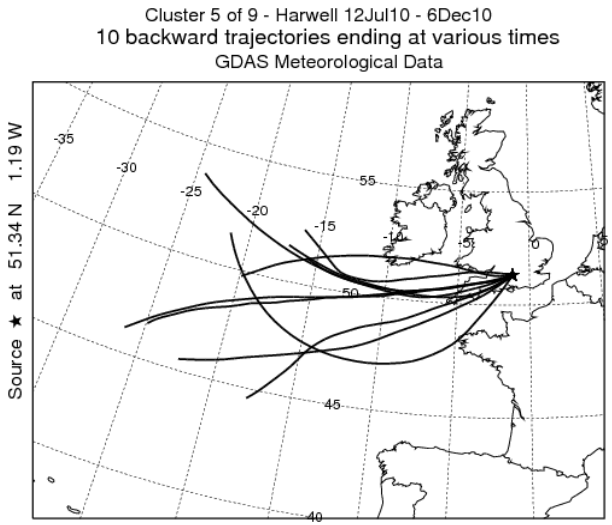
Cluster 5 of 9 - Harwell 12Jul10 - 6Dec10
10 backward trajectories ending at various times
GDAS Meteorological Data
Source ★ at 51.34 N 1.19 W

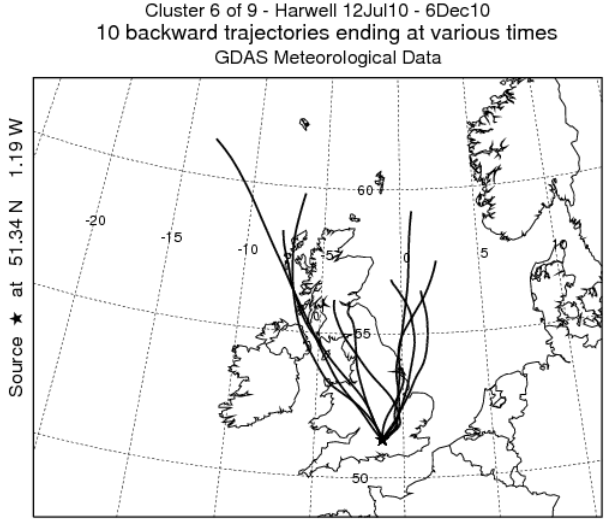
Cluster 6 of 9 - Harwell 12Jul10 - 6Dec10
10 backward trajectories ending at various times
GDAS Meteorological Data
Source ★ at 51.34 N 1.19 W

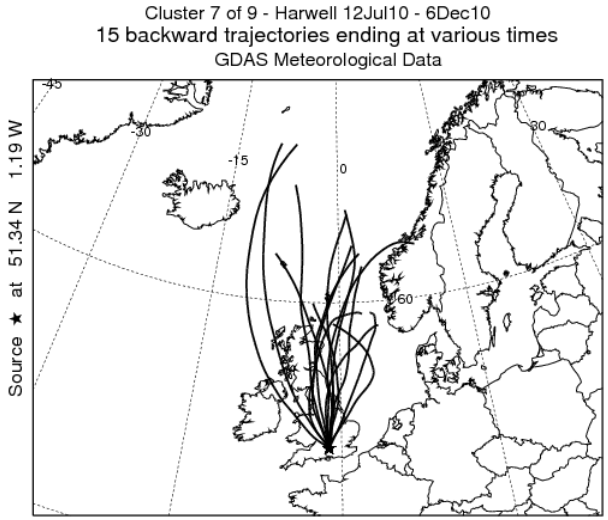
Cluster 7 of 9 - Harwell 12Jul10 - 6Dec10
15 backward trajectories ending at various times
GDAS Meteorological Data
Source ★ at 51.34 N 1.19 W

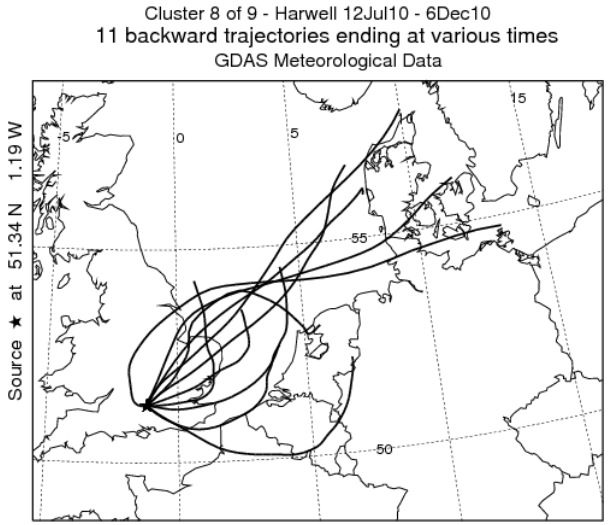
Cluster 8 of 9 - Harwell 12Jul10 - 6Dec10
11 backward trajectories ending at various times
GDAS Meteorological Data
Source ★ at 51.34 N 1.19 W

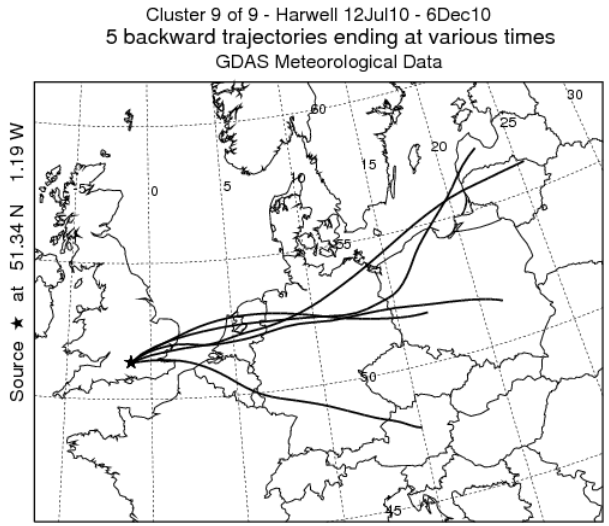
Cluster 9 of 9 - Harwell 12Jul10 - 6Dec10
5 backward trajectories ending at various times
GDAS Meteorological Data
Source ★ at 51.34 N 1.19 W

APPENDIX D
BOX-WHISKER PLOTS OF MAJOR COMPONENTS IN $PM_{2.5}$ BY CLUSTERS IN EACH SEASON AT EROS

SUMMER

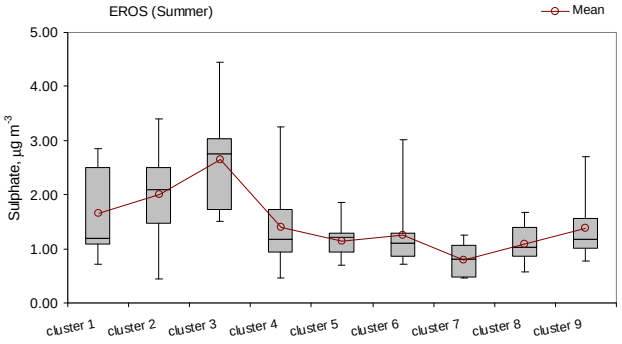

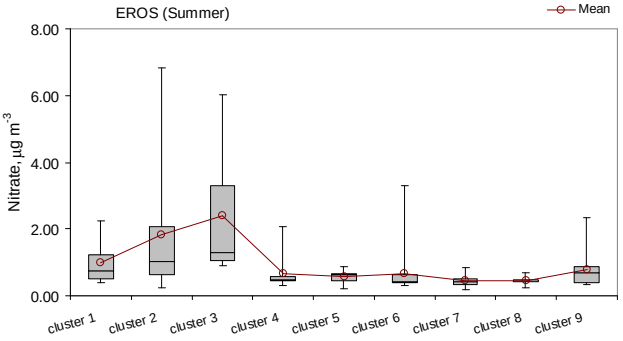

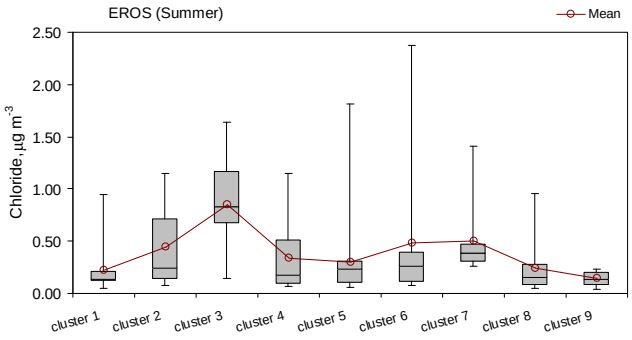

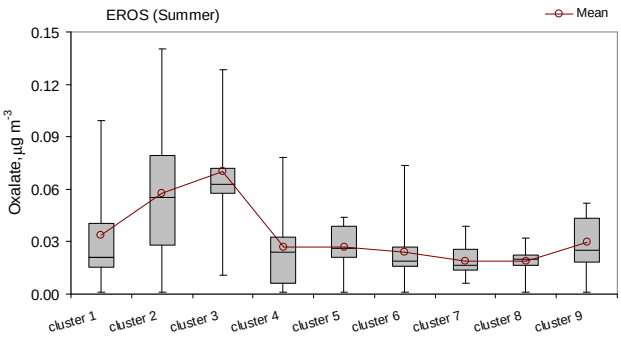

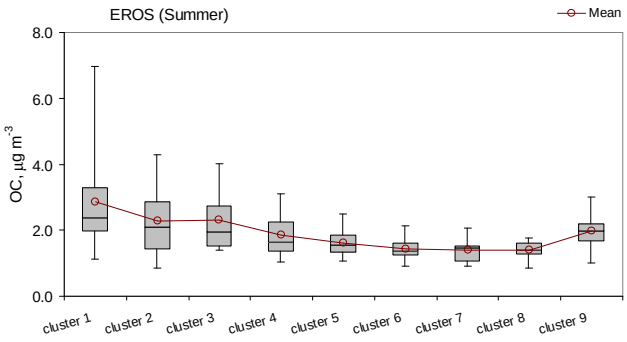

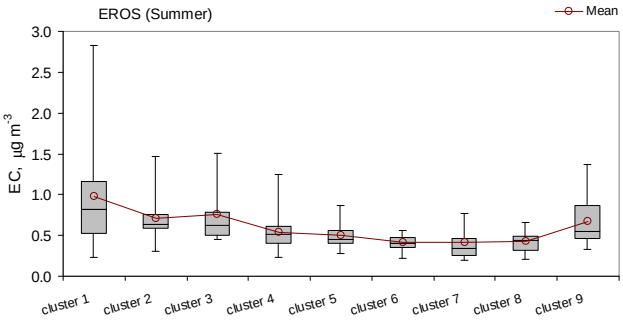

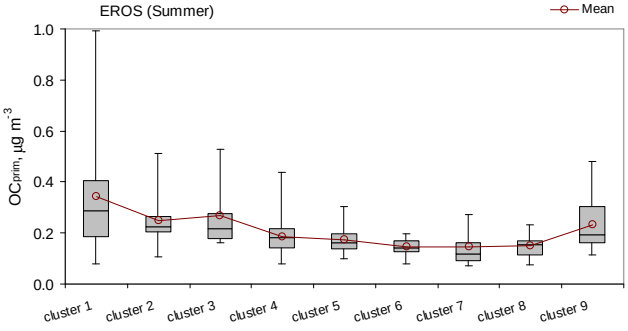

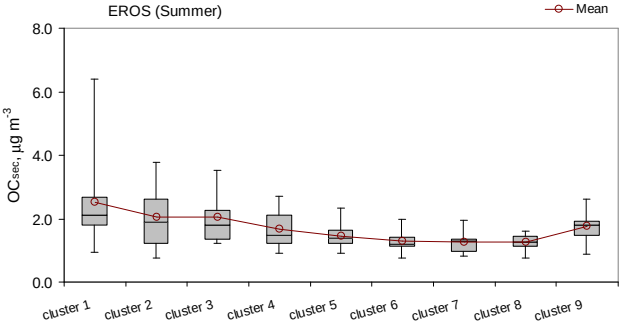

AUTUMN

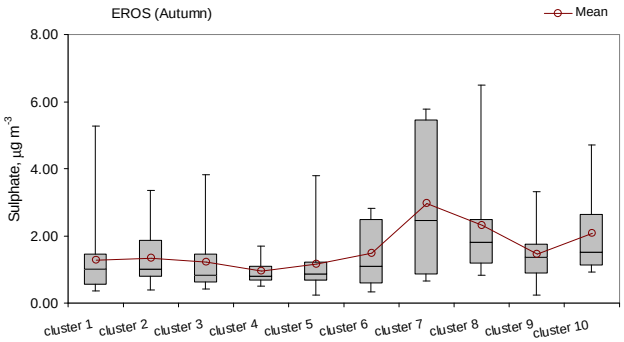
EROS (Autumn)
Mean
Sulphate, µg m-3
8.00
6.00
4.00
2.00
0.00
cluster 1
cluster 2
cluster 3
cluster 4
cluster 5
cluster 6
cluster 7
cluster 8
cluster 9
cluster 10

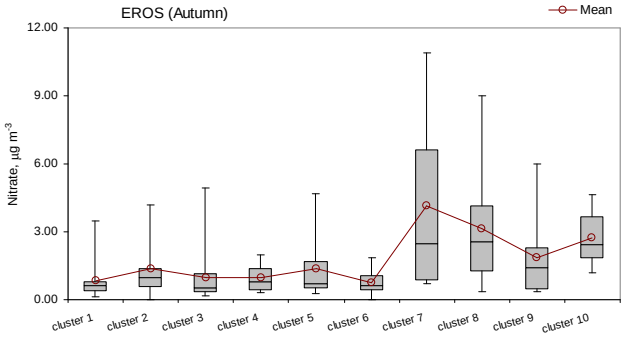
EROS (Autumn)
Mean
Nitrate, µg m-3
12.00
9.00
6.00
3.00
0.00
cluster 1
cluster 2
cluster 3
cluster 4
cluster 5
cluster 6
cluster 7
cluster 8
cluster 9
cluster 10

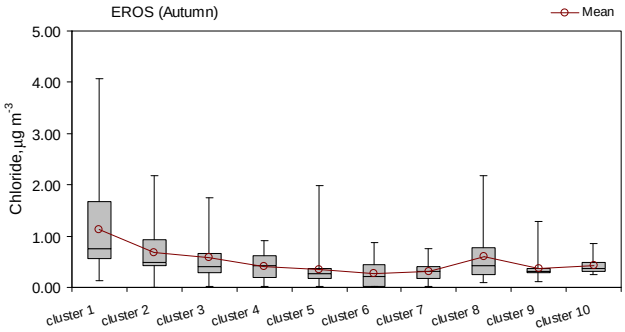
EROS (Autumn)
Mean
Chloride, µg m-3
5.00
4.00
3.00
2.00
1.00
0.00
cluster 1
cluster 2
cluster 3
cluster 4
cluster 5
cluster 6
cluster 7
cluster 8
cluster 9
cluster 10

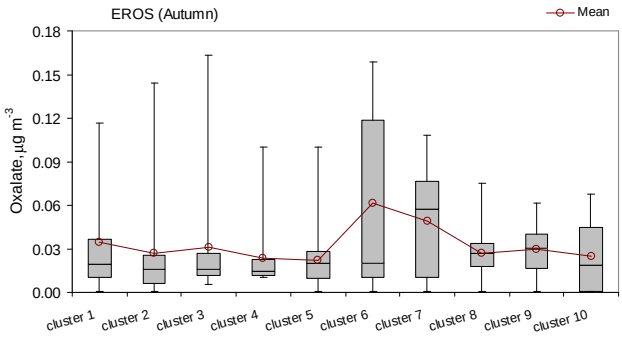
EROS (Autumn)
Mean
Oxalate, µg m-3
0.18
0.15
0.12
0.09
0.06
0.03
0.00
cluster 1
cluster 2
cluster 3
cluster 4
cluster 5
cluster 6
cluster 7
cluster 8
cluster 9
cluster 10

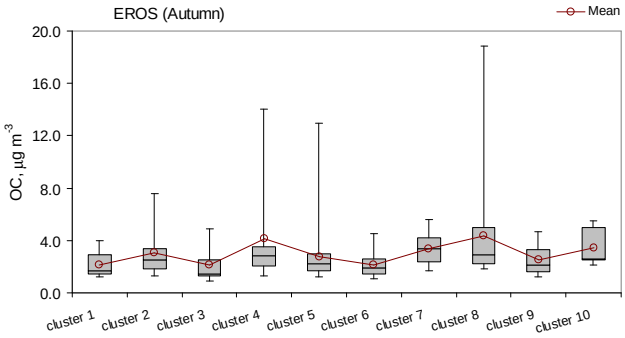
EROS (Autumn)
Mean
OC, µg m-3
20.0
16.0
12.0
8.0
4.0
0.0
cluster 1
cluster 2
cluster 3
cluster 4
cluster 5
cluster 6
cluster 7
cluster 8
cluster 9
cluster 10

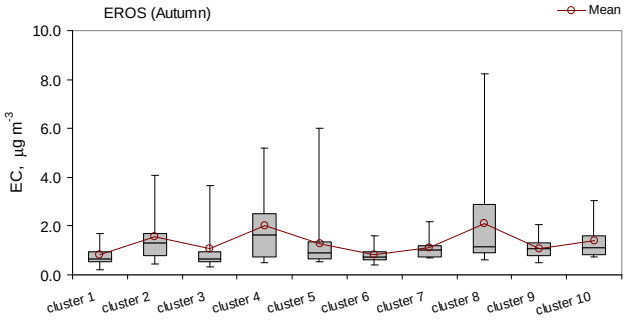
EROS (Autumn)
Mean
EC, µg m-3
10.0
8.0
6.0
4.0
2.0
0.0
cluster 1
cluster 2
cluster 3
cluster 4
cluster 5
cluster 6
cluster 7
cluster 8
cluster 9
cluster 10

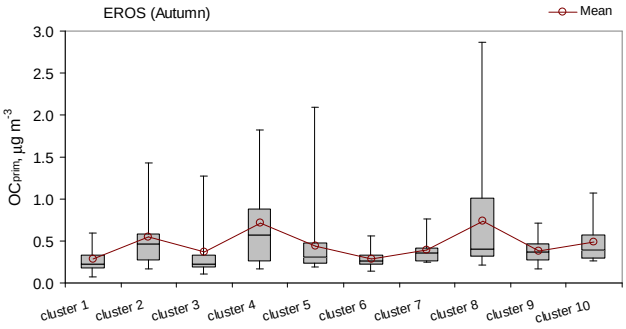
EROS (Autumn)
Mean
OCprim, µg m-3
3.0
2.5
2.0
1.5
1.0
0.5
0.0
cluster 1
cluster 2
cluster 3
cluster 4
cluster 5
cluster 6
cluster 7
cluster 8
cluster 9
cluster 10

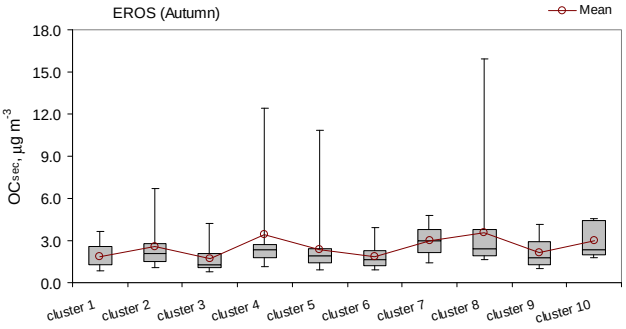
EROS (Autumn)
Mean
OCsec, µg m-3
18.0
15.0
12.0
9.0
6.0
3.0
0.0
cluster 1
cluster 2
cluster 3
cluster 4
cluster 5
cluster 6
cluster 7
cluster 8
cluster 9
cluster 10

WINTER

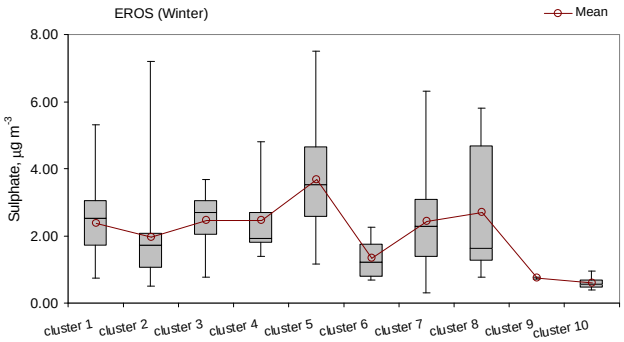
EROS (Winter)
Mean
Sulphate, µg m-3
8.00
6.00
4.00
2.00
0.00
cluster 1
cluster 2
cluster 3
cluster 4
cluster 5
cluster 6
cluster 7
cluster 8
cluster 9
cluster 10

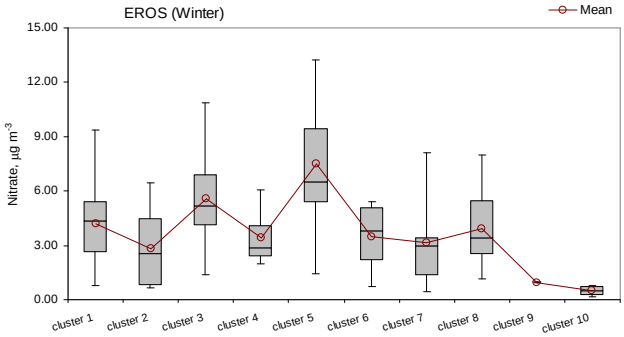
EROS (Winter)
Mean
Nitrate, µg m-3
15.00
12.00
9.00
6.00
3.00
0.00
cluster 1
cluster 2
cluster 3
cluster 4
cluster 5
cluster 6
cluster 7
cluster 8
cluster 9
cluster 10

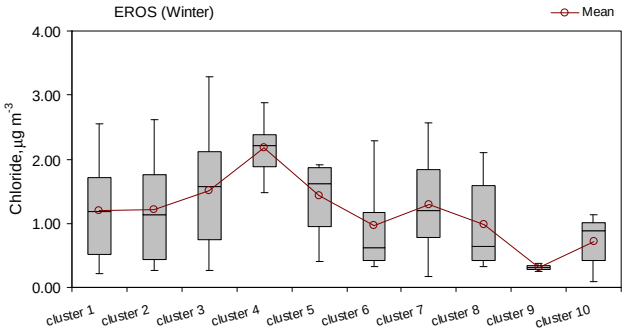
EROS (Winter)
Mean
Chloride, µg m-3
4.00
3.00
2.00
1.00
0.00
cluster 1
cluster 2
cluster 3
cluster 4
cluster 5
cluster 6
cluster 7
cluster 8
cluster 9
cluster 10

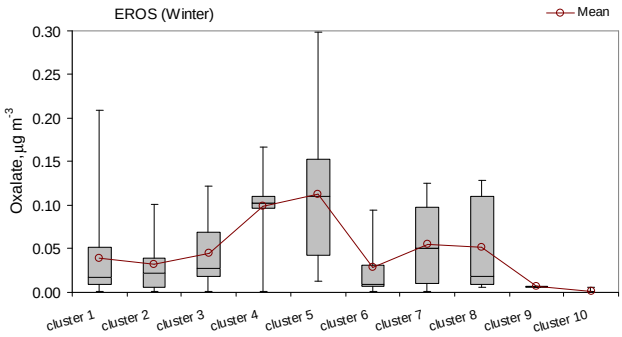
EROS (Winter)
Mean
Oxalate, µg m-3
0.30
0.25
0.20
0.15
0.10
0.05
0.00
cluster 1
cluster 2
cluster 3
cluster 4
cluster 5
cluster 6
cluster 7
cluster 8
cluster 9
cluster 10

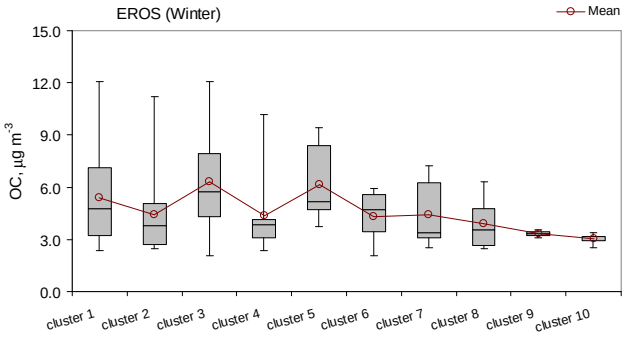
EROS (Winter)
Mean
OC, µg m-3
15.0
12.0
9.0
6.0
3.0
0.0
cluster 1
cluster 2
cluster 3
cluster 4
cluster 5
cluster 6
cluster 7
cluster 8
cluster 9
cluster 10

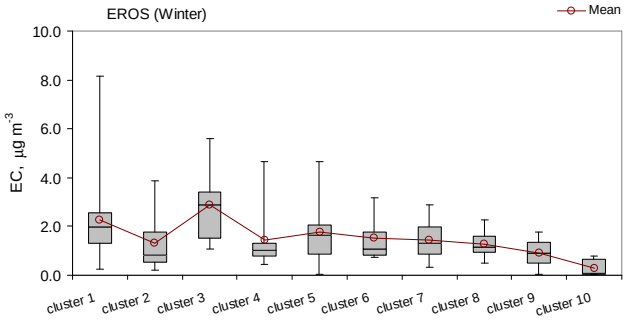
EROS (Winter)
Mean
EC, µg m-3
10.0
8.0
6.0
4.0
2.0
0.0
cluster 1
cluster 2
cluster 3
cluster 4
cluster 5
cluster 6
cluster 7
cluster 8
cluster 9
cluster 10

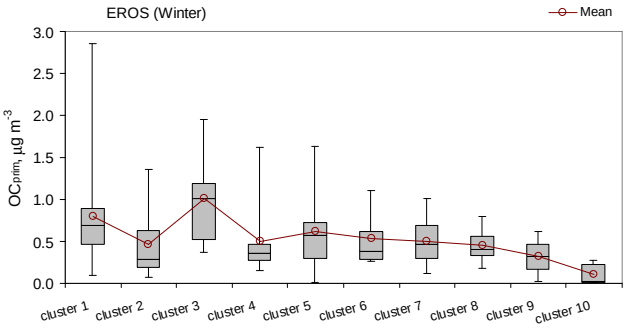
EROS (Winter)
Mean
OCprim, µg m-3
3.0
2.5
2.0
1.5
1.0
0.5
0.0
cluster 1
cluster 2
cluster 3
cluster 4
cluster 5
cluster 6
cluster 7
cluster 8
cluster 9
cluster 10

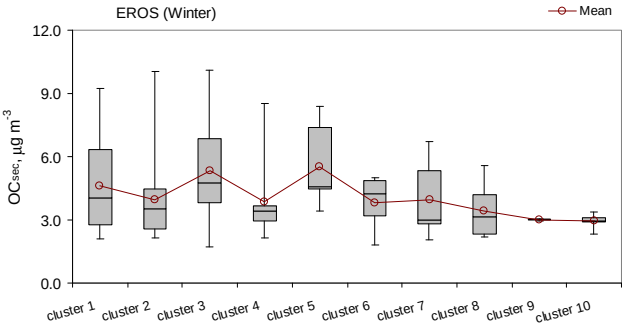
EROS (Winter)
Mean
OCsec, µg m-3
12.0
9.0
6.0
3.0
0.0
cluster 1
cluster 2
cluster 3
cluster 4
cluster 5
cluster 6
cluster 7
cluster 8
cluster 9
cluster 10

SPRING

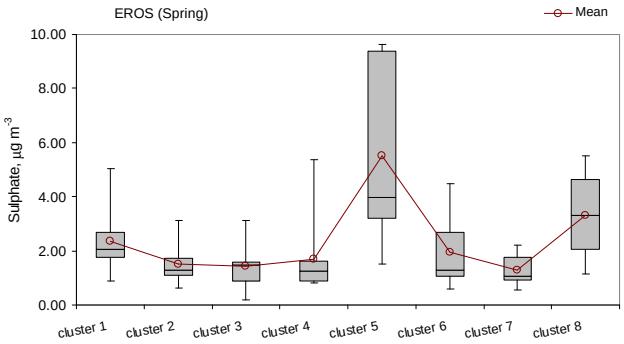
EROS (Spring)
Mean
Sulphate, µg m-3
10.00
8.00
6.00
4.00
2.00
0.00
cluster 1
cluster 2
cluster 3
cluster 4
cluster 5
cluster 6
cluster 7
cluster 8

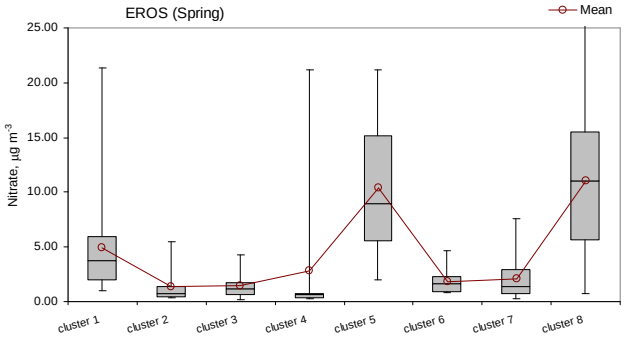
EROS (Spring)
Mean
Nitrate, µg m-3
25.00
20.00
15.00
10.00
5.00
0.00
cluster 1
cluster 2
cluster 3
cluster 4
cluster 5
cluster 6
cluster 7
cluster 8

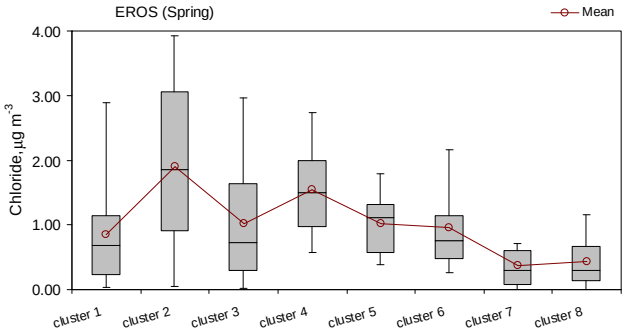
EROS (Spring)
Mean
Chloride, µg m-3
4.00
3.00
2.00
1.00
0.00
cluster 1
cluster 2
cluster 3
cluster 4
cluster 5
cluster 6
cluster 7
cluster 8

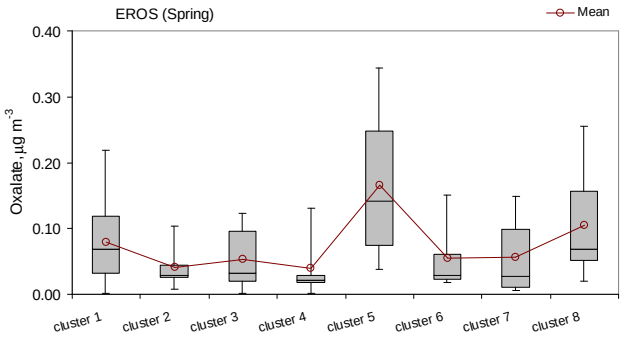
EROS (Spring)
Mean
Oxalate, µg m-3
0.40
0.30
0.20
0.10
0.00
cluster 1
cluster 2
cluster 3
cluster 4
cluster 5
cluster 6
cluster 7
cluster 8

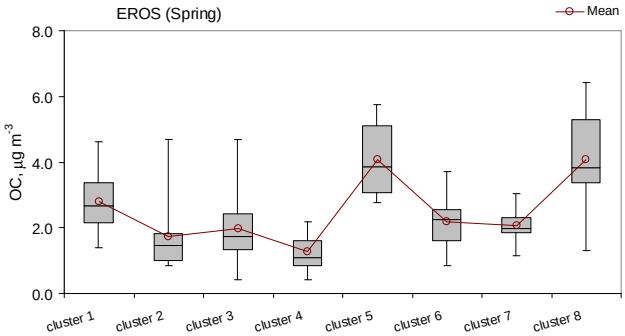
EROS (Spring)
Mean
OC, µg m-3
8.0
6.0
4.0
2.0
0.0
cluster 1
cluster 2
cluster 3
cluster 4
cluster 5
cluster 6
cluster 7
cluster 8

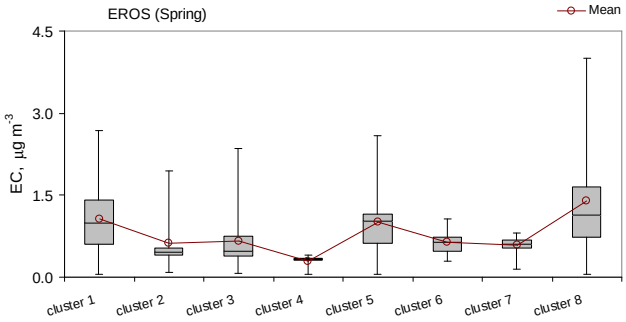
EROS (Spring)
Mean
EC, µg m-3
4.5
3.0
1.5
0.0
cluster 1
cluster 2
cluster 3
cluster 4
cluster 5
cluster 6
cluster 7
cluster 8

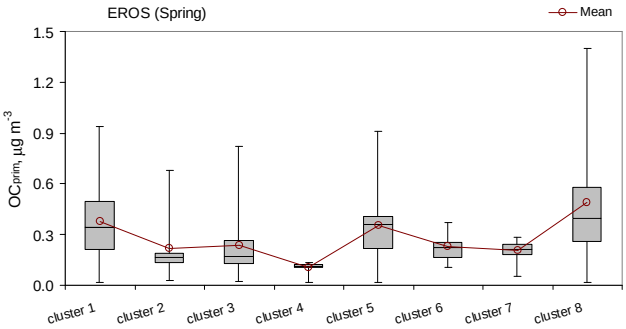
EROS (Spring)
Mean
OCprim, µg m-3
1.5
1.2
0.9
0.6
0.3
0.0
cluster 1
cluster 2
cluster 3
cluster 4
cluster 5
cluster 6
cluster 7
cluster 8

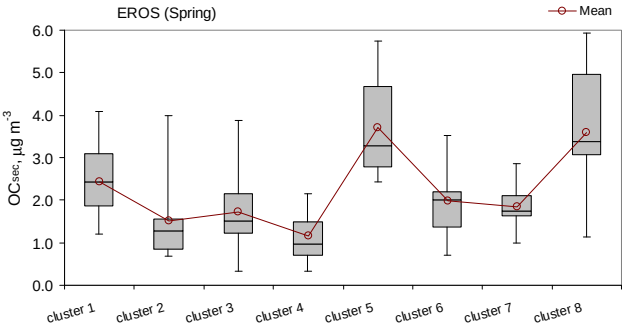
EROS (Spring)
Mean
OCsec, µg m-3
6.0
5.0
4.0
3.0
2.0
1.0
0.0
cluster 1
cluster 2
cluster 3
cluster 4
cluster 5
cluster 6
cluster 7
cluster 8

APPENDIX E
THE KOLMOGOROV-SMIRNOV TEST

Tests of Normality

Component	Kolmogorov-Smirnov		
	Statistic	df	Sig.
EROS			
$PM_{2.5}$			
OC	.168	500	.000
EC	.203	500	.000
Oxalate	.236	500	.000
Nitrate	.234	500	.000
Sulphate	.139	500	.000
Chloride	.167	500	.000
OC_{pri}	.231	500	.000
OC_{sec}	.152	500	.000
$PM_{2.5-10}$			
OC	.168	500	.000
EC	.431	500	.000
Oxalate	.203	500	.000
Nitrate	.192	500	.000
Sulphate	.136	500	.000
Chloride	.133	500	.000
PM_{10}			
OC	.161	500	.000
EC	.196	500	.000
Oxalate	.181	500	.000
Nitrate	.210	500	.000
Sulphate	.142	500	.000
Chloride	.134	500	.000
OC_{pri}	.227	500	.000
OC_{sec}	.142	500	.000
HARWELL			
$PM_{2.5}$			
OC	.219	107	.000
EC	.245	107	.000
Oxalate	.294	107	.000
Nitrate	.286	107	.000
Sulphate	.204	107	.000
Chloride	.186	107	.000
OC_{pri}	.284	107	.000
OC_{sec}	.213	107	.000

Component	Kolmogorov-Smirnov		
	Statistic	df	Sig.
$PM_{2.5-10}$			
OC	.193	107	.000
EC	.506	107	.000
Oxalate	.213	107	.000
Nitrate	.198	107	.000
Sulphate	.270	107	.000
Chloride	.139	107	.000
PM_{10}			
OC	.151	107	.000
EC	.249	107	.000
Oxalate	.158	107	.000
Nitrate	.253	107	.000
Sulphate	.194	107	.000
Chloride	.140	107	.000
OC_{pri}	.292	107	.000
OC_{sec}	.142	107	.000